

**Synthesis and Evaluation of a Novel Series of
 β -Diketones and Related Compounds as
Anticancer Agents**

Al-ameen Abubakar Mohammed

**School of Science Engineering and Environment
University of Salford, Greater Manchester, UK**

**Submitted in Partial fulfilment of the Requirements of the
Degree of Doctor of Philosophy**

May 2021

Table of contents

List of figures.....	v
List of tables.....	ix
Acknowledgements.....	x
Abstract.....	xii
List of abbreviations.....	xiii
Chapter One.....	2
1.0 Introduction:.....	2
1.1 Basis of cancer at a molecular level:.....	3
1.1.1 Gene alteration:.....	3
1.1.2 Oncogenes:.....	4
1.1.3 Angiogenesis and tumour metastasis:.....	5
1.1.4 Tumour suppressor genes:.....	7
1.1.5 Cell-cycle-related defects and carcinogenesis:.....	8
1.1.6 Senescence and its connection with tumourigenesis:.....	9
1.2 Therapeutic approaches in cancer diagnosis:.....	11
1.2.1 Gene therapy.....	11
1.2.2 Immunotherapy.....	12
1.2.3 Photodynamic therapy.....	13
1.2.4 Hormone therapy.....	15
1.3 Chemotherapy.....	16
1.3.1 Alkylating agents.....	17
1.3.1.1 Antimetabolites.....	20
1.3.1.2 Topoisomerase-interacting agents.....	20
1.3.1.3 Kinase inhibitors.....	22
1.3.1.4 Proteasome inhibitors.....	23
1.3.1.5 Platinum analogues.....	25
1.3.2 Antimitotic agents:.....	28
1.4 Colchicine binding site inhibitors (CBSI) reported before 2019.....	35
1.4.1 Combretastatins A-4 (CA-4).....	35
1.4.2 Successful modifications of CA-4 stilbenoid double bond.....	37
1.4.3 Chalcone analogues of CA-4.....	38

1.4.4 Phenstatin CA-4 analogues	40
1.5 β -Diketones as inhibitors of the colchicine binding site and Wnt / β -catenin pathway ...	42
1.5.1 Naturally occurring β -diketones as anticancer agents	43
1.5.2 β -Diketones as inhibitors of tubulin polymerisation	45
1.5.3 Curcumin and modulation of Wnt / β -catenin pathway leading to cancer.....	47
1.6 Overview on synthesis of β -diketones:.....	53
1.7 Aims and objectives	56
Chapter two	59
2.0 Materials and Methods.....	59
2.1 Synthesis and purification of 1,3-diketones	59
2.1.1 Synthesis of 1,3-diketones, benzoyl thiourea and intermediates:.....	61
2.1.2 Synthesis of β -diketones:.....	67
1-(3-Fluoro-4-methoxyphenyl)-3-(3,4,5-trimethoxyphenyl) propane-1,3-dione (4)	67
1,3-Bis(3,4,5-trimethoxyphenyl) propane-1,3-dione (5)	68
1-(3,4-Dimethylphenyl)-3-(3,4,5-trimethoxyphenyl) propane-1,3-dione (6).....	69
1-(3,4-Dimethoxyphenyl)-3-(3,4,5-trimethoxyphenyl) propane-1,3-dione (7)	70
1-(4-Methoxyphenyl)-3-(3,4,5-trimethoxyphenyl) propane-1,3-dione (8)	71
1-(2-Bromophenyl)-3-(3,4,5-trimethoxyphenyl) propane-1,3-dione (9).....	72
1-(4-Methoxyphenyl)-3-(4-(trifluoromethyl(phenyl)propane-1,3-dione (10).....	73
1-(4-Bromophenyl)-3-(3,4,5-trimethoxyphenyl) propane-1,3-dione (11).....	74
1,3-Bis(3,4,5-trimethoxyphenyl) propane-1,3-dione (12)	75
4-(3-oxo-3-(3,4,5-trimethoxyphenyl) propanoyl) benzonitrile (13)	76
1-(2,5-Dimethylphenyl)-3-(3,4-dimethoxyphenyl) propane-1,3-dione (14).....	77
4-(3-(3,4-Dimethoxyphenyl)-3-oxopropanoyl)benzonitrile (15)	78
1-(3,4-Dimethoxyphenyl)-3-(3-fluoro-4-methoxyphenyl)propane-1,3-dione (16)	79
1-(3-Fluoro-4-methoxyphenyl)-3-(4-methoxyphenyl) propane-1,3-dione (17)	80
1-(3-Chloro-4-fluorophenyl)-3-(3,4-dimethoxyphenyl) propane-1,3-dione (18)	81
1-(3-fluoro-4-methoxyphenyl)-3-(4-methoxyphenyl) propane-1,3-dione (19).....	82
1-(3,4-Difluorophenyl)-3-(3,4-dimethoxyphenyl)propane-1,3-dione (20)	83
1-(3-Bromo-4-methylphenyl)-3-(4-methoxyphenyl) propane-1,3-dione (21).....	84
1-(2,4-Dimethoxyphenyl)-3-(3,4,5-trimethoxyphenyl) propane-1,3-dione (22).....	85
1-(2,4-Dimethoxyphenyl)-3-(3-fluoro-4-methoxyphenyl)propane-1,3-dione (23)	86
1,3-Bis(3-fluoro-4-methoxyphenyl)propane-1,3-dione (24)	87

3-(3,4-Dichlorophenyl)-1-(3,4,5-trimethoxyphenyl)-1,3-propanedione (25).....	88
1-(3,4-Dichlorophenyl)-3-(3-fluoro-4-methoxyphenyl)-1,3-propanedione (26)	89
1-(3,4-Dichlorophenyl)-3-(3,4-dimethoxyphenyl)-1,3-propanedione (27).....	90
1-(3,4-Dichlorophenyl)-3-(4-methoxyphenyl)-1,3-propanedione (28).....	91
3-(3-Chloro-4-fluorophenyl)-1-(3,4,5-trimethoxyphenyl)-1,3-propanedione (29).....	92
1-(3-Chloro-4-fluorophenyl)-3-(3-fluoro-4-methoxyphenyl) propane-1,3-dione (30)	93
1-(3,4-Dimethoxyphenyl)-3-(3-iodo – 4-methyl)-1,3-propanedione (31)	94
1-(3-Chloro-4-methylphenyl)-3-(3,4-dimethoxyphenyl)propane-1,3-dione (32).....	95
1-(3-Bromo-4-methylphenyl)-3-(3,4-dimethoxyphenyl)propane-1,3-dione (33)	96
1-(3-Bromo-4-methylphenyl)-3-(3,4,5-trimethoxyphenyl) propane-1,3-dione (34).....	97
1-(3-Iodo-4-methylphenyl)-3-(3,4,5-trimethoxyphenyl)propane-1,3-dione (35)	98
1-(3-Chloro-4-methylphenyl)-3-(3,4,5-trimethoxyphenyl) propane-1,3-dione (36)	99
1-(4-(Trifluoromethyl)phenyl)-3-(3,4,5-trimethoxyphenyl)propane-1,3-dione (37)	100
1-[3-(tert-Butyldimethylsilyloxy)phenyl]ethanone (38)	101
(Z)-1-(3-((tert-Butyldimethylsilyloxy)-4-methoxyphenyl)-3-hydroxy-3-(3,4,5- trimethoxyphenyl)prop-2-en-1-one (39)	102
BENZOYL THIOUREA ANALOGUES	103
N-((4-(trifluoromethyl)phenyl)carbamothioyl)benzamide (40)	103
4-Methoxy-N-((4-methoxyphenyl)carbamothioyl)benzamide (41).....	104
4-Methoxy-N-((4-(trifluoromethyl)phenyl)carbamothioyl)benzamide	105
N-((4-methoxyphenyl)carbamothioyl)-4-(trifluoromethyl)benzamide (43).....	106
3,4,5-Trimethoxy-N-((4-methoxyphenyl)carbamothioyl)benzamide (45)	108
N-((2,3-Dihydrobenzo[b][1,4]dioxin-6-yl)carbamothioyl)-3,4,5-trimethoxybenzamide (46).....	109
N-((2,4-Dimethoxybenzyl)carbamothioyl)-3,4,5-trimethoxybenzamide (47)	110
N-((3-Chloro-4-fluorophenyl)carbamothioyl)-3-fluoro-4-methoxybenzamide (48).....	111
3,4,5-Trimethoxy-N-((3,4,5-trimethoxyphenyl)carbamothioyl)benzamide (49).....	112
3,4,5-Trimethoxy-N-((3,4,5-trimethoxybenzyl)carbamothioyl)benzamide (50)	113
3,4,5-Trimethoxy-N-((4-(trifluoromethyl)phenyl)carbamothioyl)benzamide (51)	114
3,4,5-Trimethoxy-N-((4-(trifluoromethyl)phenyl)carbamothioyl)benzamide (52)	115
3,4,5-Trifluoro-N-((3,4,5-trimethoxyphenyl)carbamothioyl)benzamide (53)	116
N-((4-Hydroxyphenyl)carbamothioyl)-3,4,5-trimethoxybenzamide (54)	117
N-((2-Bromophenyl)carbamothioyl)-3,4,5-trimethoxybenzamide (55)	118
N-((3-Hydroxy-4-methoxyphenyl) carbamothioyl)-3,4,5-trimethoxybenzamide (56)	119
N-(H-hydroxy-4-methoxyphenyl)carbamothioyl)-3,4,5-trimethoxybenzamide (57)	120

N-((2-Bromophenyl)carbamothioyl)-3-fluoro-4-methoxybenzamide (58).....	121
3-Fluoro-N-((3-fluoro-4-methoxyphenyl)carbamothioyl)-4-methoxybenzamide (59)	122
2.2 Biological activity of β -diketones	123
2.2.1 Cell lines profiles and culture tips:.....	123
2.2.2 Cell conditioning maintenance	125
2.2.3 Cell viability	126
2.2.4 Ligand Docking Studies	128
Chapter three.....	130
3.0 Results and discussion	130
3.1 Synthesis and characterisation of β -diketones:.....	130
3.1.1 Optimisation of reaction parameters (temperature and base equivalents):.....	132
3.1.2 Effect of reaction time on irradiation under microwave.....	133
3.1.3 Attempted synthesis of β -diketones mimicking combretastatin-A4.....	134
3.1.4 Attempted thionation of β -diketones.....	138
3.1.5 Position of the enolic protons on the proton NMR:	139
3.1.4 NMR couplings of fluorinated β -diketones:.....	141
3.2 Discussion of biological activity of β -diketones	144
3.2.1 Effects of β -diketones on cancer cells.....	144
3.2.2 Assessment of some substituted β -diketones and benzoyl thiourea on leukaemia cells	172
Chapter four.....	178
4.0 Molecular docking of β -diketone in the colchicine binding site.....	178
4.1 Protein preparation:	178
4.1.1 Generation of Grid in the receptor site:	178
4.2 Ligand preparation:.....	178
4.3 Glide Extra precision (XP) ligand docking:	179
4.3.1 Discussion of docking result.....	179
Chapter Five	184
Conclusions and future prospect	184
References	188
Appendix	207
Chemical Spectra of compounds	207

List of figures

Figure 1: depicting chromosomal instability, obtained from (Vargas-Rondón, Villegas and Rondón-Lagos, 2017)	3
Figure 2: Structure of Ginsenoside (left) and Chloramphenicol (right)	6
Figure 3: Different stages of cancer progression, taken from (Fidler, 2003).....	7
Figure 4: Structures of reported drug targets with antitumour activity	9
Figure 5: The role of TERT related pathways (β -catenin and NF- κ B) in relation to cancer, diagram obtained from (Bajaj et al., 2020)	10
Figure 6: Telomerase inhibitors derived from polyphenols.	11
Figure 7: Mechanism of photodynamic therapy (PDT), adapted from (Agostinis et al., 2011).....	13
Figure 8: Tetrapyrrole based photosensitizers used in PDT, (Bonneau and Vever-Bizet, 2008).....	14
Figure 9: Mode of action in PDT, obtained from (Castano, Mroz and Hamblin, 2006)	14
Figure 10: Structure of tamoxifen	15
Figure 11: Structures of some steroidal and non-steroidal inhibitors.....	16
Figure 12: Clinically approved steroidal and non-steroidal antiandrogen drugs for prostate cancer.....	16
Figure 13: Structures of guanine, adenine, cytosine, and thymine (from left to right)	17
Figure 14: Types of interactions between alkylating agents and DNA.	18
Figure 15: Disruption of hydrogen bond interaction due to alkylation in the DNA	19
Figure 16: Modified hybrids of nitrogen mustards.....	19
Figure 17: Camptothecin and Topotecan used as topoisomerase inhibitors.....	21
Figure 18: Topoisomerase II drugs that interact with the DNA.....	21
Figure 19: Structure of a biologically active derivative of curcumin	22
Figure 20: Structure of combretastatin CA-4	23
Figure 21: Chemical structures of some clinically approved HIV protease inhibitors	24
Figure 22: Active protease inhibitors in chemotherapy	24
Figure 23: DNA interacting with different platinum drugs. Obtained from (Muggia et al., 2015).....	25
Figure 24: Glutathione reduces the activity of platinum drugs.....	26
Figure 25: Structure of FDA approved platinum (II) drugs	26
Figure 26: Structural geometry of platinum (II) drugs.....	27
Figure 27: Structure of naphthalimide, a potent DNA intercalator and target for cancer therapy	27
Figure 28: Prodrug and dual activity of platinum (IV) tethered with naphthalimide (Nap) at the axial position. Obtained from (Wang et al., 2018b).....	28
Figure 29: Dimensional structure of microtubule with (+) and (-) represented in green and red. Obtained from (Janke and Chloë Bulinski, 2011)	29
Figure 30: Assembly of α and β -tubulins from dimers to form microtubules. Obtained from (Barbier et al., 2019).....	29
Figure 31: Structure of colchicine.....	30
Figure 32: Structures of microtubule stabilizing agents.....	31

Figure 33: Interaction of taxane (green) with oxetane ring with Thr276 (blue) of β -tubulin within a binding distance of 3.0 Å. (1JFF- β -tubulin retrieved from PDB). The coloured broken lines represent the site of interaction between residue and the taxane ligand.....	32
Figure 34: Structural scaffold of a vinca alkaloids (highlighted red)	32
Figure 35: 2D and 3D representation of vinblastine (vinca alkaloid) interaction with both α and β -chain of tubulin.	33
Figure 36: Hydrogen bond interaction of colchicine with microtubule. Adapted from (Li et al., 2017)	34
Figure 37: Structural features of colchicine and important substituents.....	35
Figure 38: Isomers of CA-4. cis on the left and the trans-isomer on the right.	36
Figure 39: Imidazole and pyrazine analogue of CA-4 showing decreased activity in 5 and 6-membered ring. ...	37
Figure 40: Different linker modification with R and R' denoting atom or functional group at different positions of the ring	38
Figure 41: Structure of E-1-(4'-hydroxyphenyl)-but-1-en-3-one	39
Figure 42: Chalcone analogues bearing electron withdrawing groups	39
Figure 43: structure of first synthesised 1,3-diarylchalcone with tubulin inhibiting property in HeLa cells	39
Figure 44: Modified diaryl chalcone bearing CA-4 moieties.....	40
Figure 45: Diaryl-chalcones bearing methyl and phosphate moieties	40
Figure 46: Structure of potentially active phenstatin.....	41
Figure 47: Active groups that contribute to activity of phenstatin with CBS	42
Figure 48: α -Alkenylated analogue of β -diketone used as intermediate to heterocyclic compounds	42
Figure 49: β -Diketone (left) used as intermediate to synthesis of substituted pyrazoles (right)	43
Figure 50: β -diketone as intermediate for synthesis of chromones pyrimidines and pyridines	43
Figure 51: Structure of curcumin.....	44
Figure 52: Structure of Taxol	44
Figure 53: Curcumin activity in modulating cell different stages of cycle progression. Obtained from (Sa and Das, 2008)	45
Figure 54: 2D diagram of curcumin interaction in the CBS (Docking score and -6.8 and -7.7)	46
Figure 55: 3D-structure of curcumin interacting in the CBS.....	46
Figure 56: Inhibition and stimulation of transcription of Wnt / β -catenin signalling pathway, adapted from (Cooper, 2019).....	47
Figure 57: Different wnt / β -catenin bathways targetted by curcumin to inhibit cancer progression. Adapted from (Milad et al., 2020).....	51
Figure 58: (Left) 3D representation of curcumin interacting with amino acid residues of Dvl2 (PDB ID: 3CBY)..	52
Figure 59: Replacement of the olefinic length of curcumin chain in β -diketone	56
Figure 60: Haemocytometer reading plate. Obtained from Invitrogen Cell culture basics Handbook.	126
Figure 61: Substitution of fluorine or trifluoromethyl at position numbered 1, 2 or 3.....	141
Figure 62: Coupling of carbon in the trifluoromethyl group (CF ₃) and aromatic ipso carbon.....	143
Figure 63: IC ₅₀ of β -diketones tested on A204 cell line. 0 indicate compounds with undetermined activity. ...	148

Figure 64: IC ₅₀ of β-diketones tested on A549 cell lines. 0 indicate compounds with undetermined activity...	149
Figure 65: IC ₅₀ of β-diketones tested on HeLa cell line. 0 indicate compounds with undetermined activity. ...	150
Figure 66: IC ₅₀ of β-diketones tested on HepG2 cell line. 0 indicate compounds with undetermined activity. ...	151
Figure 67: IC ₅₀ of β-diketones tested on U2OS cell line.....	152
Figure 68: IC ₅₀ of benzoyl thiourea tested on A204 cell line. 0 indicate compounds with undetermined activity.	156
Figure 69: IC ₅₀ of benzoyl thiourea tested on A549 cell line. 0 indicate compounds with undetermined activity.	157
Figure 70: IC ₅₀ of benzoyl thiourea tested on HeLa cell line. 0 indicate compounds with undetermined activity.	158
Figure 71: IC ₅₀ of benzoyl thiourea tested on HepG2 cell line. 0 indicate compounds with undetermined activity.....	159
Figure 72: IC ₅₀ of benzoyl thiourea tested on U2OS cell line 0 indicate compounds with undetermined activity.	160
Figure 73: Sensitivity of the most active BDKT analogues on A204 cells	161
Figure 74: improvement of β-diketone activity on A204 by changing the positions of methoxy groups on the aromatic ring	162
Figure 75: BTU analogues with activity of A204 showing IC ₅₀ values below 4 μM.....	163
Figure 76: Inhibitory effect of the most active compounds tested on A549 cells.....	165
Figure 77: Trend in activity of compound by modification of ring substituents	165
Figure 78: Sensitivity of 31, 32 and 33 bearing halogen groups on A549 cells	166
Figure 79: Slight improvement in the activity of β-diketone and benzoyl thiourea series bearing the same substituents in their rings tested on A549 cells.....	167
Figure 80: Analogue BTU-12 (49) bearing methoxy substituents have better activity on A549 (IC ₅₀ = 7.41 μM) than BDKT-3 (5) (IC ₅₀ = 35.69 μM) with the same substituent.	168
Figure 81: Comparison between structure activity of BTU and BDKT series bearing the same ring substituents.....	168
Figure 82: Activity of β-diketones bearing nitrile group.....	169
Figure 83: HeLa and HepG2 treated with BDKT-7 (9) showing the least value among the BDKT series	170
Figure 84: Chart showing the lowest IC ₅₀ values of U2OS cells treated with 9 , 8 , 46 and 43	171
Figure 85: IC ₅₀ of β-diketones and benzoyl thiourea treated with acute lymphoblastic leukaemia (CCFR-CEM and MOLT-4) and chronic myeloid leukaemia (K562) cell lines.....	175
Figure 86: 3D view of BDKT-41 (31), BDKT-42 (32) and BDKT-44(34) docking in the binding site of tubulin (PDB ID: 1SA0). Interactions shown with coloured broken lines. The orange circles points to the essential amino acid residue cys241 that binds with the ligand molecules. This interaction is present in many active antimicrotubular agents reported from literature.	180
Figure 87: Refined tubulin crystal structure (PDB:1sa0) showing colchicine binding site on chain B. The encircled region is an interaction with Cys241, an essential interaction in most anti-microtubular drugs.....	181

List of Schemes

Scheme 1: Protein kinase catalysed phosphorylation of amino acids, obtained from (Müller, 2009)	5
Scheme 2: Synthetic steps for the synthesis of phenstatin (Pettit et al., 2000).....	41
Scheme 3: A modified Claisen condensation of ketones to a β -diketone using potassium tert-butoxide as a base.	53
Scheme 4: Optimisable Baker-Venkataraman conversion of aromatic esters to β -diketones.....	54
Scheme 5: Baker-Venkataraman rearrangement of phenylbenzoate to β -diketone using DMSO as solvent	54
Scheme 6: Isolation of aromatic esters from aromatic acetophenone and carboxylic acid	55
Scheme 7: Rearrangement of aromatic ester into β -diketone.	55
Scheme 8: Modified Baker-Venkataraman synthesis of β -diketone bearing alkyl and aryl groups from DBU and pyridine.	55
Scheme 9: A modified route to preparation of β -diketone using THF as solvent	56
Scheme 10: Reduction and ring opening of MTT to formazan	127
Scheme 11: Claisen condensation of ketone and ester to form β -diketone	130
Scheme 12: Resonance stabilised formation of enolate ion	130
Scheme 13: Mechanism of formation of β -diketone	131
Scheme 14: Equilibrium of β -diketone in the basic medium.....	131
Scheme 15: Synthesis of β -diketones.....	132
Scheme 16: Microwave assisted synthesis of β -diketones:	133
Scheme 17: Proposed synthesis of CA-4 analogue of β -diketone	134
Scheme 18: Product during the first attempted synthesis of CA4- analogue of β -diketone.....	135
Scheme 19: Ester group at ortho-position is essential for baker-Venkataraman rearrangement	136
Scheme 20: Formation of product fails when ester group is at meta-position from ketone ($R = OCH_3$ at position 3, 4, and 5).....	136
Scheme 21: Formation of silyl-protected β -diketone.....	137
Scheme 22: Mechanism of pyran protected ester	137
Scheme 23: Proposed thionation of β -diketones.....	138
Scheme 24: Proposed mechanism for the thionation of β -diketones with Lawessons reagent, (Polshettiwar and Kaushik, 2006)	139

List of tables

Table 1: FDA approved monoclonal antibodies	13
Table 2: Wnt / β -catenin pathway targets currently in different stages of clinical trials	48
Table 3: Yields of optimisation of β -diketones with different reaction conditions.	132
Table 4: Attempted microwave assisted synthesis of β -diketone:.....	134
Table 5: $^1\text{H-NMR}$ Chemical shifts of enolic protons in prepared β -diketones.....	140
Table 6: Chemical shifts of some fluoro-substituted β -diketones.....	142
Table 7: IC_{50} values of synthesised benzoyl thiourea (BTU) series determined by MTT assay after 120 hours of drug exposure. The experiments were carried out in triplicates.....	144
Table 8: IC_{50} values of synthesised benzoyl thiourea (BTU) series determined by MTT assay after 120 hours of drug exposure. The experiments were carried out in triplicates.....	153
Table 9: Cytotoxicity some selected β -diketone and benzoyl thiourea analogues tested against multiple leukaemia cell lines.....	173
Table 10: Different types of interactions exhibited by BDKT-41 (31) and BDKT-42 (32).....	181

Acknowledgements

First and foremost, I thank Allah SWT for giving me courage support and guidance through the PhD academic ladder; and may abundant blessings be upon his prophet Muhammad SAW. This journey through the PhD at the University of Salford has given me the opportunity to meet people who have directly or indirectly contributed toward accomplishing my goals.

I would like to thank my supervisor, Dr John Hadfield for his support, guidance, and presence in urgent time of need, especially when dealing with difficult experiments in the laboratory. His advice and approach to troubleshooting reactions has contributed to my skills of working in the organic chemistry laboratory. I would also like to appreciate the support of Dr Patricia Ragazzon, Dr David Greensmith and Dr Ian Goodhead for their motivation and guidance under their supervision.

My appreciation also goes to the lecturers in the school of science, engineering, and environment. I would like to thank Dr Roderick Elder, Dr Ian Podmore, Dr Jim Wilkinson and Dr Steve Rossington for contributing opinions and suggestion related to my research. Dr David Pye has inspired me greatly toward furthering my skills in molecular modelling. Indeed, meeting these people at Cockcroft building was an opportunity that widened my understanding of chemistry.

Working on the 3rd floor of Cockcroft building (Room-307) would have been boring without the Lee Harman. His friendly and supportive presence at Cockcroft building has made my work in the lab very exciting. Lee, if you are reading this page, I want you to know that I mean what I said, thank you.

I owe Kirit Amin a huge debt of gratitude for strengthening my foundation in elucidating molecules using different NMR techniques. Openheartedly, he developed and broadened my logic in tackling complicated spectra elucidated in this thesis, especially spectra molecules bearing fluorine atoms. With the newly installed 600 MHz equipment, I wish I could be given enough time to gain from the pool of your experience with more advanced NMR techniques.

I would like to thank Helen Bradshaw for her understanding, kindness toward postgraduate researchers especially in difficult times when they need assistance with facilities at Cockcroft building. Despite Helen's busy schedule, her commitment to supporting students request within her capacity is always assured, thank you Helen.

I am lucky to meet with Dr Muna Abubaker, who trained me and guided me through the cell culture work. Indeed, her patience, support, and eagerness in assisting students has inspired me to screen large number of compounds in the limited time I was given after the Covid-19 lockdown.

Being a student at the University of Salford has given me an opportunity to meet colleagues who have made my journey on the research ladder more exciting. Like a toddler, I walked into Lab 307, I met Amjed Malullah and Natalie Barnes to hold my hands and walk on my feet. Amjed has helped with refreshing most of my laboratory skills, words cannot express my token of appreciation for their support and encouragement. The friendly presence of Babatunde Adegbulugbe, Joseph Dobiecki-Davies and Aaron Breski all working in Lab 307 has made it an exciting place that I will miss after completion.

The atmosphere at PGR study room 217 gave me the privilege to meet smiley Maria Morlan, Laura Bretell, Eljelani, Jessica Kevill, Basmah Allarakia, Natasha Hadgraft, Flaviane Souza, Assem Elshenshani, Dominic West and Izuchika Nduka. Meeting these people and some their names not mentioned here was an opportunity to share and exchange inspiring ideas to keep me going on the journey. Also, special thanks to my research colleague, Muhammad Ali for his utmost support and I believe our friendship will have no boundaries.

My deepest gratitude to the management of petroleum trust development fund (PTDF) for sponsoring my studies financially throughout the entire duration of my PhD programme at the University of Salford. An immense thanks to Alhaji Balarabe Ahmad for his kind support for the entirety of my postgraduate journey from MSc through PhD. I am truly indebted for his encouragement and guide toward my ambition in chemistry, thank you for shaping my path.

Finally, I appreciate the support of my family, mum, wife, brothers and sisters for bearing the patience and concern during the prolonged period of stay in the UK and the Covid-19 global pandemic. I look forward to reconnecting with you soon, thank you for tolerating my absence for this entire period.

Abstract

β -Diketones are 1,3-dicarbonyl compounds containing two carbonyl compounds separated by a methylene carbon. This functional diketo group is found in natural sources and can be synthesised in the laboratory. They serve as a synthetic intermediate to medicinally important compounds such as flavonoids. The aim of this thesis is focused on the synthesis and cytotoxic evaluation of novel series of β -diketones bearing different substituents. 30 novel β -diketones and 19 benzoyl thiourea analogues have been synthesised, characterised, and tested for activity on 6 different cancer cell lines. All the β -diketones synthesised appeared as the enolic tautomer, with chemical shifts ranging between 16.25 ppm – 17.15 ppm. The synthesised compounds were tested on lung adenocarcinoma (A549), human bone osteosarcoma cells (U2OS) and three different human myeloid leukaemia cells: K-562, MOLT-4 and CCRF-CEM. An MTT-assay was carried out on the compounds to enable determine their activity. Among the cell lines tested with both series of β -diketones (BDKT) and benzoylthiourea (BTU), the A204 cells have shown greater sensitivity at a lower IC_{50} s at micromolar range than the remaining cell lines. Unlike the other cell lines, the IC_{50} values of the BDKT series ranged from 3.61 μ M to 23.82 μ M. **31**, **32** and **34** and **30** have the best activity with IC_{50} s 3.61 μ M, 3.63 μ M and 3.78 μ M and 3.87 respectively. Whereas A204 compounds treated BTU series showed lower IC_{50} values ranging from 3.39 μ M to 9.36 μ M, suggesting greater activity than the BDKT series. The most active compounds (with lower IC_{50} values < 4 μ M) among the BTU series include **55** (3.39 μ M), **56** (3.65 μ M), **61** (3.75 μ M) **60** (3.76 μ M), and **53** (3.97). Molecular docking result analysis of the active compounds: **31**, **32** and **34** from the BDKT series have revealed that the presence of halogen groups in the molecules is contributing to its activity. Also, of significant activity in **31,32** and **33** is the bonding interaction with cys241 amino acid residue located in the tubulin binding site. This interaction site is common for most microtubule inhibitors such as colchicine, combretastatin-A4 and curcumins.

List of abbreviations

Å	Armstrong
Ad	Adenovirus
ALT	Alternative Lengthening of Telomere
ATP	Adenosine Triphosphate
BDKT	Beta-diketone
BRCA-1	Breast cancer type 1 susceptibility protein
BRCA-2	Breast cancer type 2 susceptibility protein
BTU	Benzoylthiourea
C	Coulomb
CBSI	Colchicine binding site inhibitors
CDK	Cyclin Dependent Kinase
CDKI	Cyclin Dependent Kinase Inhibitors
CIN	Chromosomal Instability
DNA	Deoxyribonucleic acid
DVL	Dishevelled
EDG	Electron Donating Group
EGFR	Epidermal growth factor
EWG	Electron Withdrawing Group
FDA	Food and Drug Administration
GF	Growth Factor
GPC3	Glypican 3 protein
GSK	Glycogen synthase kinase
GTP	Guanosine triphosphate
HER-2	Human Epidermal Growth factor receptor-2
HIF-1	Hypoxia induced factor-1
HIV	Human immunodeficiency virus
HOMO	Highest Occupied Molecular Orbital
hTERT	human Telomerase reverse transcriptase
IC ₅₀	Inhibitory Concentration
IFN	Interferons

IL	Interleukins
LDA	Lithium Diisopropyl amine
LiHMDS	Lithium Hexamethyldisilane
LUMO	Lowest unOccupied Molecular Orbital
MAP	Mitogen activated pathway
MDA	Microtubule Disrupting Agent
MAPK	Mitogen activated pathway
mRNA	Messenger Ribonucleic Acid
MSI	Microsatellite instability
MTA	Microtubule targeting agents
NIH	National institutes of health
NK	Natural Killer
NP	Nanoparticles
PDGF	Platelet Derived Growth Factor
PDT	Photo dynamic therapy
RNA	Ribonucleic Acid
ROS	Reactive Oxygen Specie
ROS	Reactive Oxygen Species
SAR	Structure Activity Relationship
SOD	Superoxide dismutase
TGF β	Transforming Growth Factors
THF	Tetrahydrofuran
TK	Tyrosine Kinase
UCN-01	7-hydroxystaurosporine
UPP	Ubiquitin-proteasome pathway
VEGFR	Vascular Epidermal Growth Factor
WHO	World Health Organization

CHAPTER ONE

Introduction

Chapter One

1.0 Introduction:

Cancer rises as an uncontrollable growth which occurs in cells and can be recognized by rapid structural and functional alteration in cell development that varies from normal cell activities (Kesikli and Guler, 2015). Cancer is the term used to describe this condition, derived from the Latin for “crab” having claws that enables it to move to neighbouring tissues in a living body (McKinnell *et al.*, 2006). Cell proliferation and continuity is generally controlled by the genes in the form of DNA, which resides in the nucleus of a cells. These genes (constituting characters and traits) are transferred by parents to the offspring in a well-organised pattern. Cancer emerges as a result of uncontrollable growth and abnormal behaviour of these cells in the body (Kierszenbaum and Tres, 2016). Main causes of all cancers known today results from the damage in DNA, which result in abnormal cell division (Vogelstein and Kinzler, 2004). Clinically, cancer can be either a benign neoplasm (Greek, *neos*, new; *plasma*, things formed) or a malignant neoplasm. The benign cancer is a massive growth of abnormal cells in a localized region within the body, which gradually moves into the lymphatic vessels. Sometimes, a tumour can grow and cause blockage by compression of adjacent organ (e.g. tumour that affects the brain stem) or it can lead to obstruction of the intestine (Kierszenbaum and Tres, 2016). In malignant tumours, abnormal cells develop from the originating tissue and then flow into the lymphatic vessels. They get transported to other parts of the body to establish colonies also known as secondary metastasis (Stephens and Aigner, 2009). Malignant tumours are the major cause of death in cancer patients as compared to benign tumours which tend to localize in a certain region (NIH, 2020).

Cancers can be further classified into three depending on the region from which they originate, these are: carcinomas, sarcomas, and leukaemia (Bielenberg and Zetter, 2015). Carcinoma affects the epithelial cells, this includes the layers such as the intestinal tracts, the stomach and mouth. This type of malignancy constitutes about 80-90% of cancer cases in the western world (Cancer Classification | SEER Training, 2020). Sarcoma is the cancer that affects connective tissues of bones and cartilages, cases of this type of cancer is not common in humans. Leukaemia contributes about 8% of cases in cancer fatalities, it affects the ‘blood-forming-cells’ and cells that are responsible for immunity (Cooper, 2019).

1.1 Basis of cancer at a molecular level:

1.1.1 Gene alteration:

Gene alteration is an integral factor that leads to most malignancies in human cancers at different stages and occurs because of the variation in the genetic sequence and is considered one of the hallmarks of cancer. This variation takes place in different forms (Negrini, Gorgoulis and Halazonetis, 2010). The most common one is known as chromosomal instability (CIN). This happens when a large portion of chromosome undergoes change in number of chromosomes (aneuploidy) or structural rearrangement (Tanaka and Hirota, 2016). About 70-90% of reported cancer cases emerge from this type of instability (Weaver and Cleveland, 2006). Confirmed cases of cancer is the result of CIN which is related with mutations in DNA repair genes (Figure 1). The mutational changes favours cells to adapt to stressful and cytotoxic conditions. This type of instability is one of the primary targets in most anticancer research. The mechanism of CIN is not clearly understood but many studies attribute the mechanism to division and duplication that occurs during the process of mitosis (Vargas-Rondón, Villegas and Rondón-Lagos, 2017).

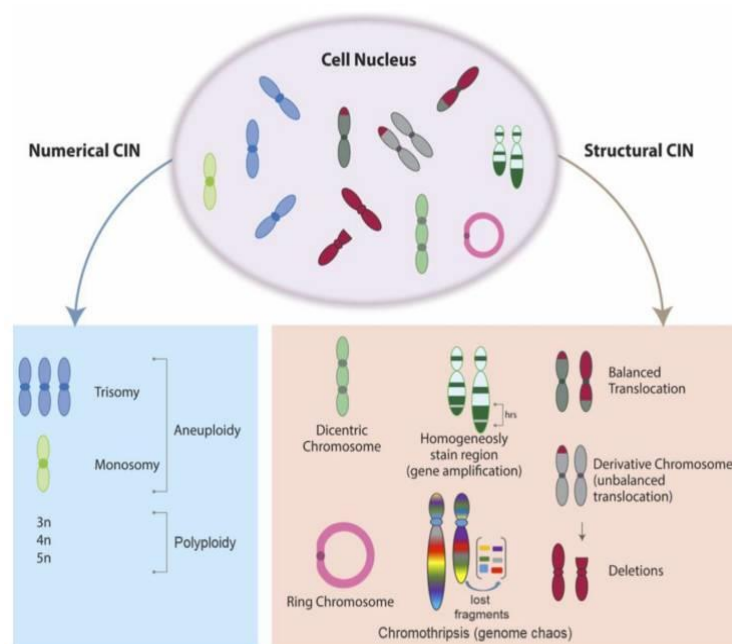


Figure 1: depicting chromosomal instability, obtained from (Vargas-Rondón, Villegas and Rondón-Lagos, 2017)

Microsatellite instability (MSI), another form of genetic instability, occurs when addition or deletion of a few nucleotides takes place. As mentioned above, the primary cause of microsatellite instability occurs when the DNA repair mechanism that is responsible for

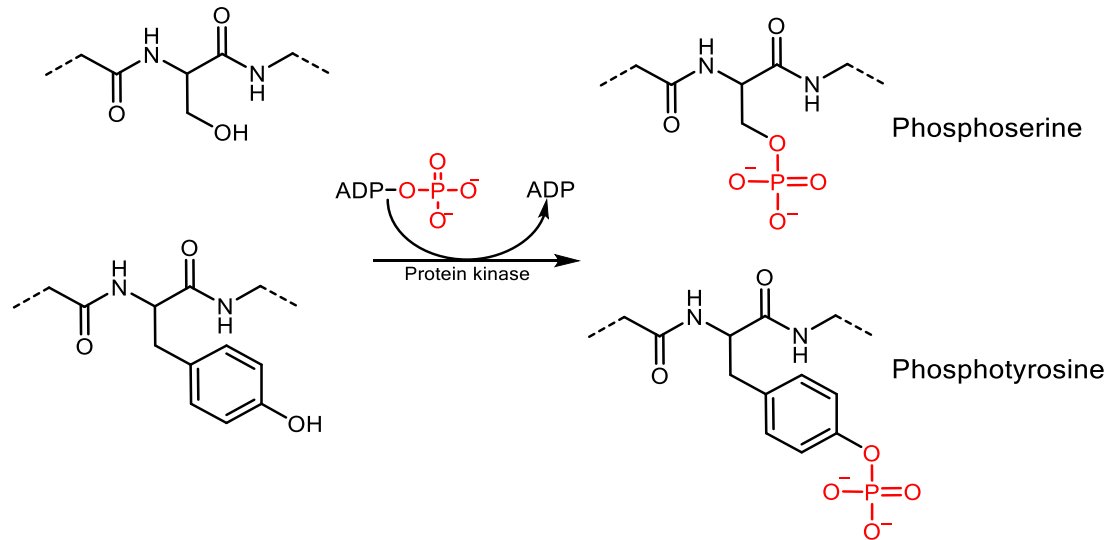
detection and correction is not functional (Baudrin, Deleuze and How-Kit, 2018). About 15-20% MSI have been identified in cases related to colorectal cancer and with minor cases being confirmed as gastric, liver, and ovarian cancer (Baudrin, Deleuze and How-Kit, 2018; Ionov *et al.*, 1993).

1.1.2 Oncogenes:

Oncogenes refers to mutated genes that are formed from normal cellular proteins, the proto-oncogenes. This gene encodes the essential regulatory proteins required by blocking the sequence required for normal transformation; thus, leading to aberration in cell cycle process (Papoutsoglou and Moustakas, 2020). Alterations that take place in the sequence can be addition, insertion between two genes, deletion or by changing the position of chromosomes location to a different environment (chromosomal translocation) (Kierszenbaum and Tres, 2016). The formation of oncogenic products takes place through different pathways depending on the regulatory function involved. Among the prominent functions used by oncogenes include growth factors, growth factor receptors, signal transduction and transcription factors (Labazi and Phillips, 2003; Kierszenbaum and Tres, 2016).

Oncogenes take advantage of growth factor proteins (mitogens) to induce abnormal cell proliferation. These growth factors are supplied by the rough endoplasmic reticulum and then transferred to the membranous outer surface of the cell, before being activated by enzymes. Some of these growth factors for instance, the platelet-derived growth factors (PDGF) are released by platelets to enable coagulation (Goustin *et al.*, 1986). Growth factor receptors are transmembrane proteins that bind to ligands (which are essentially growth factors) to enable them to pass to the intracellular space. They are also collectively grouped as tyrosine kinase receptors, with the same protein structural features made up of three important domains. This includes the extracellular domain that binds with ligands; the transmembrane and the tyrosine kinase (TK) domain (Vargas-Rondón, Villegas and Rondón-Lagos, 2017). About 10% of cancers related to proteins are caused by kinases. These molecules are capable of phosphorylating different amino acids (Scheme 1) such as serine and threonine, and therefore, tumours related to protein kinases are classified according to the amino acid that they phosphorylate. For instance, threonine protein kinase, tyrosine kinase. When a growth factors (GFs) bind one of these TK domains, it forms a dimer that phosphorylate and activate

the mitogen activated pathway (MAPKs) also known as the MAP kinase cascade (Wagener, Stocking and Muller, 2017).



Scheme 1: Protein kinase catalysed phosphorylation of amino acids, obtained from (Müller, 2009)

Examples of these receptors include epidermal growth factor receptors (EGFR) and vascular endothelial growth factor receptors (VEGFR, required for growing blood vessels) are examples of receptors that can initiate oncogenesis in cells (Goustin *et al.*, 1986).

1.1.3 Angiogenesis and tumour metastasis:

Angiogenesis is a process associated with formation of new blood vessels. These new vessels enable the supply of neighbouring tissues with oxygen and nutrients. It also helps with adequate supply of nutrients to wounds that require healing. Earlier studies have shown that angiogenesis could be a major contributor of cancer growth (tumour angiogenesis), as new blood vessels are rapidly formed from preexisting vessel so that tumour cells can have access to an oxygen supply and nutrients for growth and replication (Folkman, 1971; Bielenberg and Zetter, 2015). Eventually, tumour cells accumulate and become deficient in oxygen until an equilibrium is attained between proliferation and apoptosis. Recent progress have been made on the fact that tumour cells may be hypoxic, and the information about the important roles played by the vascular growth factor receptors (VEGF) and their inhibitors such as bevacizumab has provided clinical approaches to treat patients with cancer (Hsu *et al.*, 2019). This approach has proved an effective inhibitor against tumour genesis. Yet, despite the

progress, some tumour cells tend to be resistant to such drugs by growing further until it metastasises (McKinnell *et al.*, 2006).

However, the challenge is linked to the fact that hypoxia due to oxygen deprivation in the tumour environment is associated with cellular response that expresses hypoxia induced factor-1 (HIF-1). HIF-1 is a transcription factor that initiates the activity of genes involved in angiogenesis and migration (Gilkes and Semenza, 2013). Most recent studies have shown that ginsenoside and autophagy-inducing-chloramphenicol (Figure 2) proved as a potent inhibitor of HIF-1 with increased level of hypoxia in lung and gastric cancer cells (Li and Qu, 2019; Hsu *et al.*, 2019).

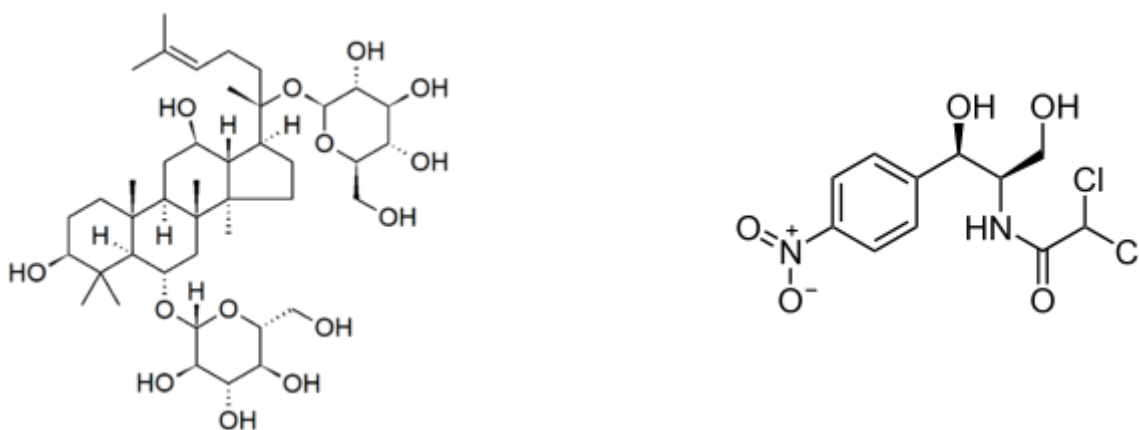


Figure 2: Structure of Ginsenoside (left) and Chloramphenicol (right)

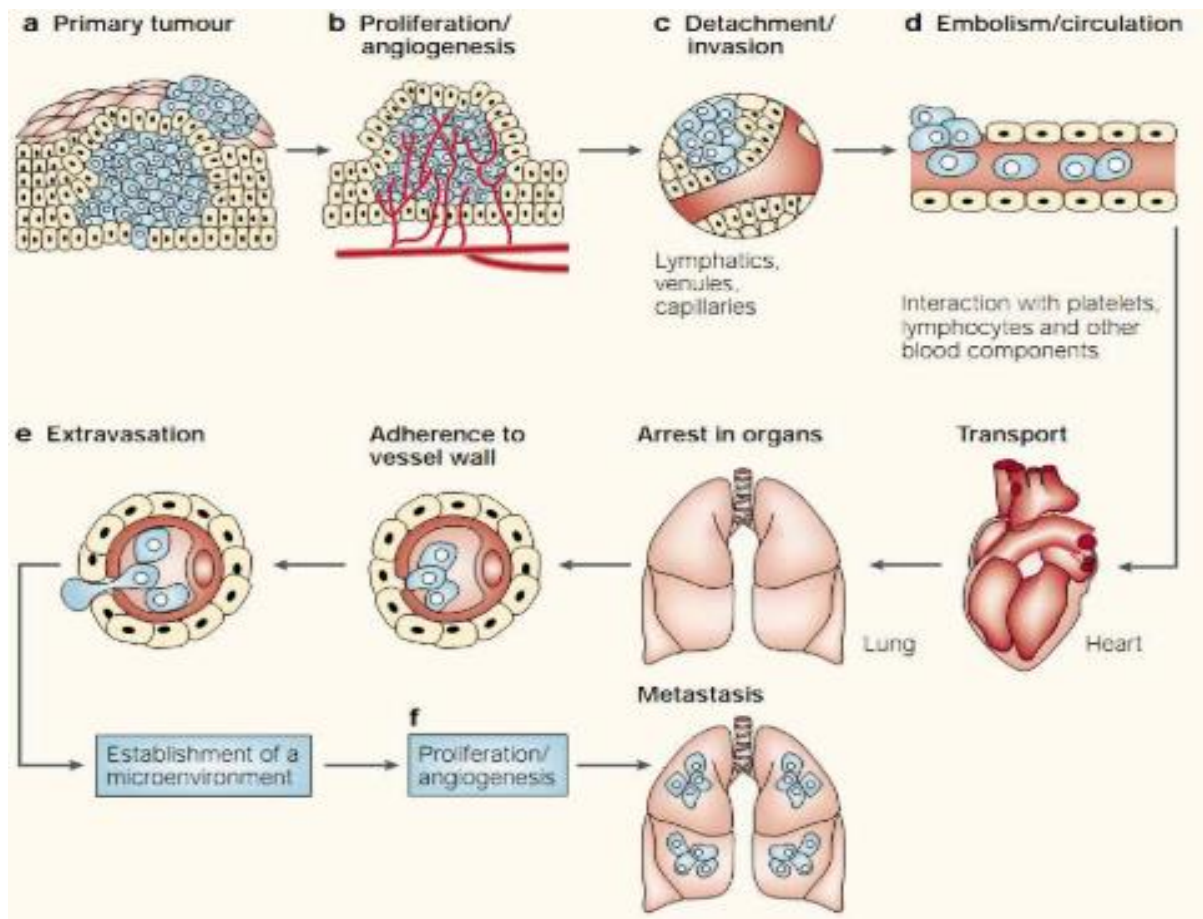


Figure 3: Different stages of cancer progression, taken from (Fidler, 2003)

1.1.4 Tumour suppressor genes:

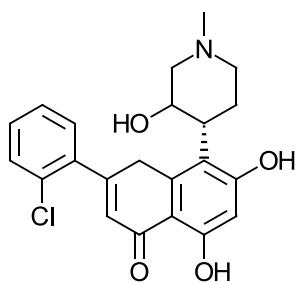
Tumour suppressor genes belong to an important class of cellular proteins that control and inhibit the growth of abnormal cells. Absence or reduction in the activity of these proteins can lead to uncontrolled growth of abnormal cells that may lead to carcinogenesis (Swanson, Kim and Glucksman, 2013; Stephens and Aigner, 2009).

p53 is a tumour suppressor gene, also referred to as the “guardian of the genome”, is an important gene that halts the cell cycle by inducing senescence (loss of ability to grow) or activating of apoptosis. About 50% of cancer manifestation in patients is due to defects from p53 (Lu, 2012). Another group of tumour suppressor genes are the BRCA1 and BRCA2 related with breast cancer and ovarian cancer. About 20-30% of women with breast cancer can be attributed to the mutated version of the BRCA1 and BRCA2. They play an active role in suppressing the estrogen-dependent transcription pathways that controls the replication of epithelial cells in the breast (Mehrgou and Akouchekian, 2016).

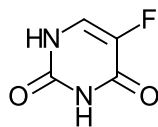
1.1.5 Cell-cycle-related defects and carcinogenesis:

Cell-cycle related tumours are sometimes related to defects in regulation and deregulation of cyclin dependent kinase (CDK) and its inhibitor (CDKI). The genome in humans is reported to encode about 21 different CDKs, however, seven among these have a direct relation with cell cycle progression (Sánchez-Martínez *et al.*, 2015). Mutation in CDK is also attributed to many cancer conditions, as the mutation in these proteins could improve their resistance to inhibitors that regulates their functionality. (Wagener, Stocking and Muller, 2017). Under physiological conditions, however, cell cycle can be controlled by the proteins that encode cyclin dependent kinase inhibitors (CDKI). CDKI is required as a checkpoint to control cell cycle progression, by inhibiting growth factors such as TGF β (transforming growth factors) and stress signals like reactive oxygen species (ROS). Cell-cycle related factors leading to cancer is prevalent in lung, colon, and breast cancer in women. Absence of these mutations in patients is an important marker in tumour patients. Higher concentrations of CDKI infers good prognosis. Many cancer cases show active mutations of genes encoded for CDK4 and CDK6 and these mutations are significantly resistant to CDKI (Wagener, Stocking and Muller, 2017; Tsihlias, Kapusta and Slingerland, 1999).

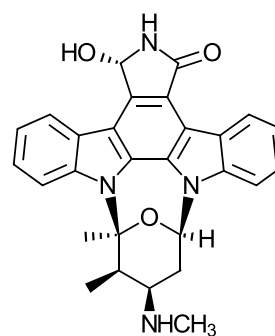
The functional differences underlying cell cycle activities between normal cells and cancer cells can be explored as a medicinal target. Tumour cells compromise the cell cycle checkpoints and increases the rate of proliferation at a faster rate and by targeting the proteins involved in the mechanism will represent a potential drug target (Bonelli *et al.*, 2014). Recently, many drug targets have been reported to show activity on tumour cells in different phases of the cell cycle. For instance, an analogue of a base nucleotide, 5-fluorouracil (5-FU) blocked the replication of DNA in S phase; flavopiridol inhibited CDK activity at checkpoint. 7-Hydroxystaurosporine (UCN-01) has shown a greater activity on many cell lines (**Figure 4**). It affects cell cycle progression from G1 phase to S phase. UCN-01 activity is linked with CDK inhibition and in combination with tamoxifen, it has revealed potent clinical activity on breast cancer (Bonelli *et al.*, 2014; Wagener, Stocking and Muller, 2017).



Flavopiridol



5-fluorouracil



7-Hydroxystaurosporine

Figure 4: Structures of reported drug targets with antitumour activity

1.1.6 Senescence and its connection with tumourigenesis:

Normal cells generally undergo replication for a limited number of times and then undergo a self-destructing mechanism referred to as senescence. A normal fibroblast cell has earlier been reported to replicate about 40-60 times (Hayflick limit) before it self-destructs (Lee and Lee, 2019). However, loss telomeric DNA resulting from degradation and partial replication in immortal cells is balanced by telomere elongation (Harley, Futcher and Greider, 1990). The enzyme DNA telomerase extends the required nucleotide sequence of several kilobases of TTAGGG repeats. This telomeric end serves as a clock counter that maintains the lifetime and integrity of cells. The mechanism of senescence is therefore expected to take place when the integrity of cell is no longer assured due to shortening in length of the telomere (Kierszenbaum and Tres, 2016).

Large number of studies have reported the presence of higher proportion of telomerase in cancer tests than normal cells (Shay *et al.*, 2001). While telomere plays a key role in regulating cancer from evolving, the enzyme, telomerase reverse transcriptase (hTERT) is linked to the higher telomerase activity that is major contributor of immortality in tumour cells (Shay *et al.*, 2001; Blackburn, 2005). The TERT activity is due to the expression of two proliferative genes Wnt/ β -catenin (Hoffmeyer *et al.*, 2012; Zhong *et al.*, 2020) and NF- κ B that can be mutated. This is responsible for deregulation of TERT activity (Perkins, 2012). Hence, the TERT mechanism proceeds to restore telomeres by activating an alternative lengthening of telomere (ALT) which overcomes the replication problem and preserves the length of telomere with unrestricted and unlimited replication that may result in abnormal proliferation (**Figure 5**) (Bajaj *et al.*, 2020).

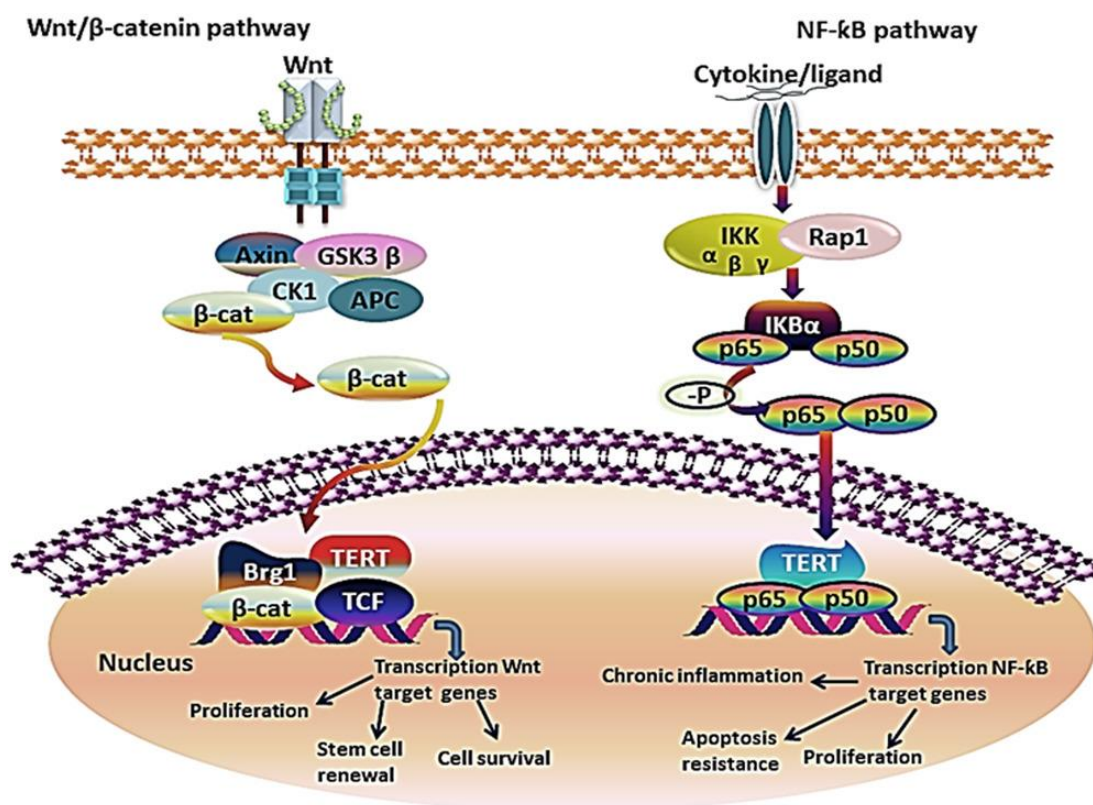


Figure 5: The role of TERT related pathways (β -catenin and NF- κ B) in relation to cancer, diagram obtained from (Bajaj et al., 2020)

Owing to the expression of telomerase in varieties of cancers and the high activity of telomerase in abnormal cells (Prasad, Pal and Mohammad, 2020), targeting the hTERT with potency and selectivity to healthy cells has become an important approach to inhibiting telomerase activity in cancer cells.

Depending on the structural orientation and presence of susceptible binding pocket in the target, many approaches have been established ranging from nucleotide inhibitors to development of vaccines (Ruden and Puri, 2013) and G-quadruplex stabilisers (Burger et al., 2005).

Moreover, polyphenols such as resveratrol and curcumins (**Figure 6**) have been reported to be effective telomerase inhibitors in cancerous cells (Bajaj et al., 2020).

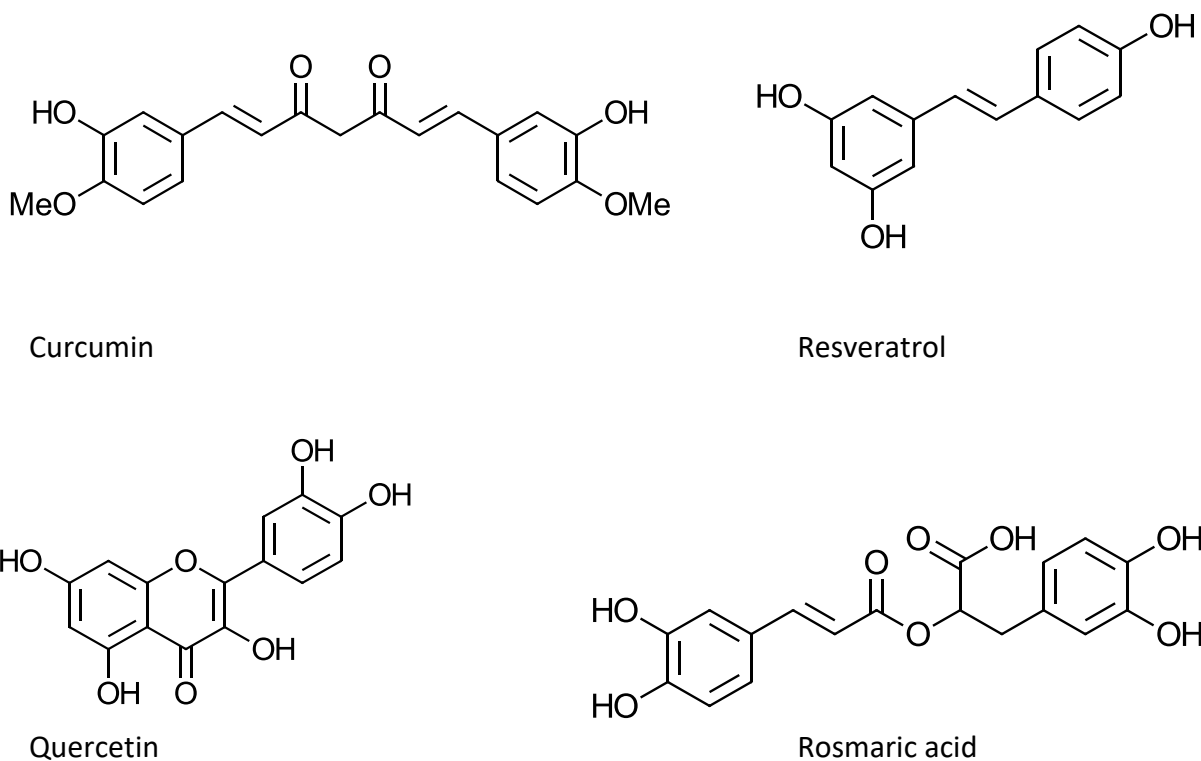


Figure 6: Telomerase inhibitors derived from polyphenols.

1.2 Therapeutic approaches in cancer diagnosis:

Cancer therapeutics has been one of the major concerns among medical communities throughout history. No one approach is considered a milestone treatment, rather combined methods are considered for different cases depending on the nature and complexity of the disease. For instance, a surgical approach for removal of tumour has evolved a long time ago, yet, it remains a valuable option to patients with solid tumours detected at late stage (Arruebo *et al.*, 2011). Furthermore, the current emergence and advancement in technology is contributing to the present therapies administered to patients. Whereas gene therapy has offered promising alternatives to curing cancer by targeting cancer cells at a genetic level. Most clinicians today, frequently consider the use of chemotherapy and radiotherapy as the method of choice in modern medicine.

1.2.1 Gene therapy

This therapy involves introducing a DNA or RNA to the target to stabilise or restore the gene functionality. The technique requires a delivery vector that ensures reaching the target. Adenoviruses (Ad) is one of the clinically used vectors for encapsulation and delivery of gene

materials(Lee *et al.*, 2017), however, it is generally expensive and difficult to manufacture. Other delivery shuttles include recombinant proteins, organic cations and inorganic nanoparticles (Pucci, Martinelli and Ciofani, 2019).

The mode of action in gene therapy requires inserting a gene called antisense version of mRNA obtained from the target gene (oncogene). The antisense is a flipped version of the RNA which blocks the synthesis of protein for the oncogene by hybridising with the produced mRNA which undergoes degradation that results in apoptosis (Brown, 2016).

1.2.2 Immunotherapy

Immunotherapy is a suitable alternative and is recommended for different stages of cancer by increasing the immune system of patients against tumour cell progression, and is now considered an important hallmark in cancer therapy (Esfahani *et al.*, 2020). Immunotherapy has now transformed the area of oncology as it prolonged the survival rate of many patients, a preferred clinical choice in diagnostics and presumably, will be opening a plethora of novel combinations in decades to come (Waldman, Fritz and Lenardo, 2020). One of the interesting mechanisms in immunotherapy is by mediation of cytokines to activate different signalling molecules directly or indirectly.

However, the toxicity in this method is significantly low as some cells can gradually overcome the effect and resist the immune response (Disis, 2014). Employing cytokines characterised with direct tumour activity remains a subject of research in many institutes. Cytokines that affect tumour cells indirectly is currently in practice clinically. Interleukins-2 (IL-2) and interferon- α (IFN- α) are examples of approved products by FDA. These immunomodulatory cytokines act on target cells by activating T-cells and natural killer (NK) and are widely used as a successful alternative in treating metastatic stage melanoma and renal cell carcinoma (Dong and Markovic, 2018; Disis, 2014).

Table 1: FDA approved monoclonal antibodies

Drug	Target	Immunological relevance	FDA-approved indication
Bevacizumab	VEGF-A	Significant toward angiogenesis and inhibition of apoptosis	Colorectal cancer and cervical cancer
Ramucirumab	VEGFR2	VEGF2 receptor plays role in angiogenesis and inhibition of apoptosis	Gastric and colorectal cancer
Trastuzumab	HER2	Controls cell growth and angiogenesis	Gastrointestinal cancer and breast cancer

Adapted from (Dong and Markovic, 2018)

1.2.3 Photodynamic therapy

Photodynamic therapy (PDT) is a clinically approved technique used in treating solid and malignant tumour cells by a source of light directed on tumours at a certain wavelength in the presence of photosensitive compounds. PDT is simple to apply, and because of its selective cytotoxic activity, has been used to patients with early-stage cancer and conditions that are not surgically operable (**Figure 7**) (Agostinis *et al.*, 2011).

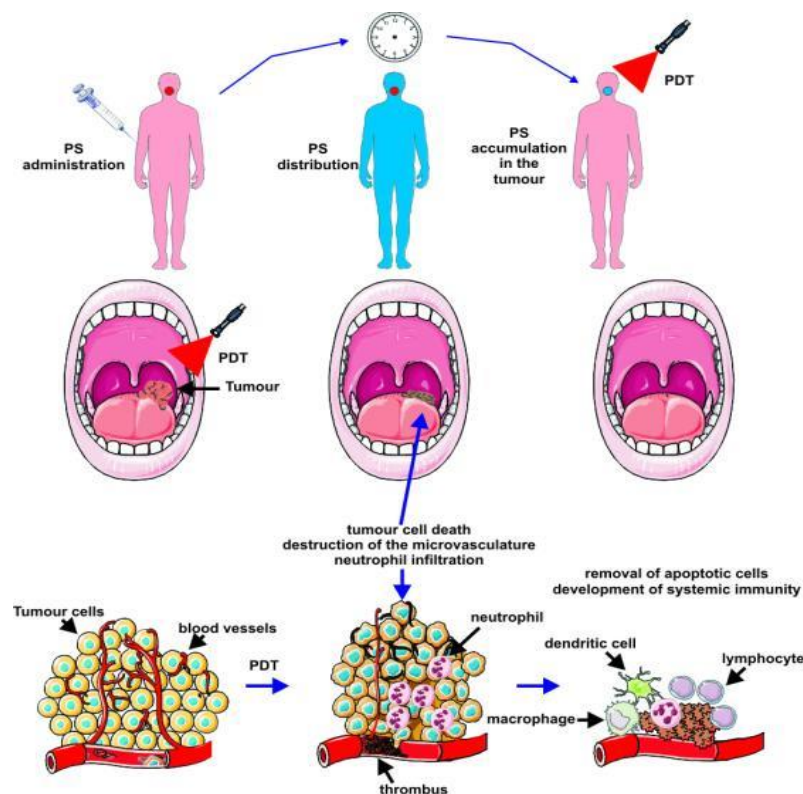


Figure 7: Mechanism of photodynamic therapy (PDT), adapted from (Agostinis *et al.*, 2011)

Moreover, PDT is considered to have fewer side effects with no recurring complications of intrinsic resistance mechanisms as the mode of action in this therapy is mainly necrosis or apoptosis. Because it is a safer technique its application is also evident in cosmetics. Three integral steps are required to ensure proper administration of PDT in cancer treatment. A photosensitizing agent with good light absorbing properties such as monomeric or dimeric tetrapyrrole (**Figure 8**); a critical absorption wavelength of the photosensitizer and *in situ* generation of an energetic oxygen (in a singlet state 1O_2). Singlet unstable oxygen has an opposite spin of electron pair that is energetically favourable to react.

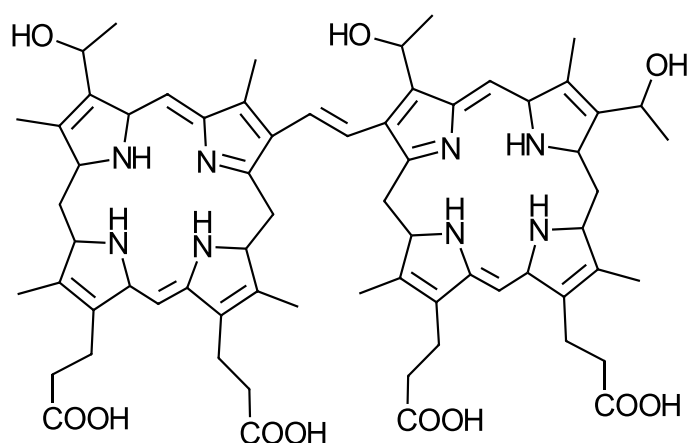


Figure 8: Tetrapyrrole based photosensitizers used in PDT, (Bonneau and Vever-Bizet, 2008)

Tumour damaging effect in the process depends on the concentration of the photosensitizer, generation of excited oxygen and the rate interval between the light source and the photosensitizer also known as fluence rate.

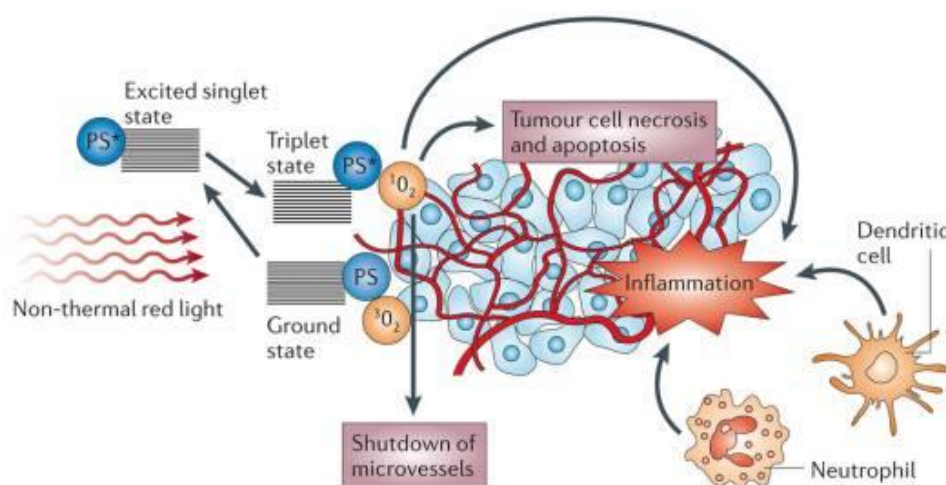


Figure 9: Mode of action in PDT, obtained from (Castano, Mroz and Hamblin, 2006)

The injected photosensitizer is typically activated by light irradiation of 800-1200 nm to initiate a photochemical reaction that generates a singlet oxygen specie ($^1\text{O}_2$). The oxygen species causes an irreversible damage to the tumour cells exposed, thus leading to apoptosis or necrosis (**Figure 9**) (Castano, Mroz and Hamblin, 2006). Nanoparticle based (NP) photosensitizers have been used recently to improve and enhance efficient delivery to the tumour site (Wilson, 2006).

1.2.4 Hormone therapy

Hormone therapy is a treatment that inhibits the development of cancer by targeting hormones through surgical means or with the aid of drugs. The mode of action in this therapy is to block the production of hormones that cause cancer or by the altering the functional activity of the hormone to render it inactive. Most cancers affecting glands such as breast cancer, prostate cancer and ovarian cancer is caused by disruption in hormones and the glands that produce it (Simpkins, Garcia-Soto and Slingerland, 2013).

Hormonal agents administered to breast cancer patients is increasing in the market, however, the commonly used drugs include aromatase inhibitors and tamoxifen. These drugs (**Figure 10**) act by inhibiting the estrogen receptors, thus weakening the tumour activity. An annual study for duration of 5 years on tamoxifen administered to breast cancer patients reduced recurring cases by about 40% (Trialists, 2015) and mortality rate by 34% (Abraham and Staffurth, 2020).

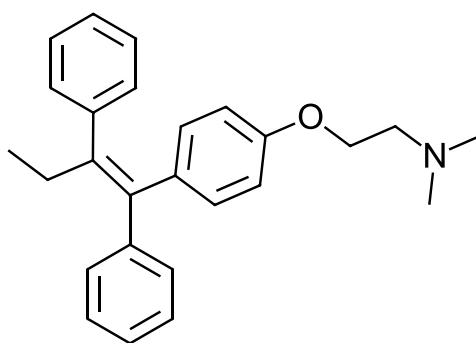


Figure 10: Structure of tamoxifen

Clinically approved steroidal and non-steroidal inhibitors administered to breast cancer patients include exemestane, letrozole and anastrozole(**Figure 11**) (Fusi *et al.*, 2014).

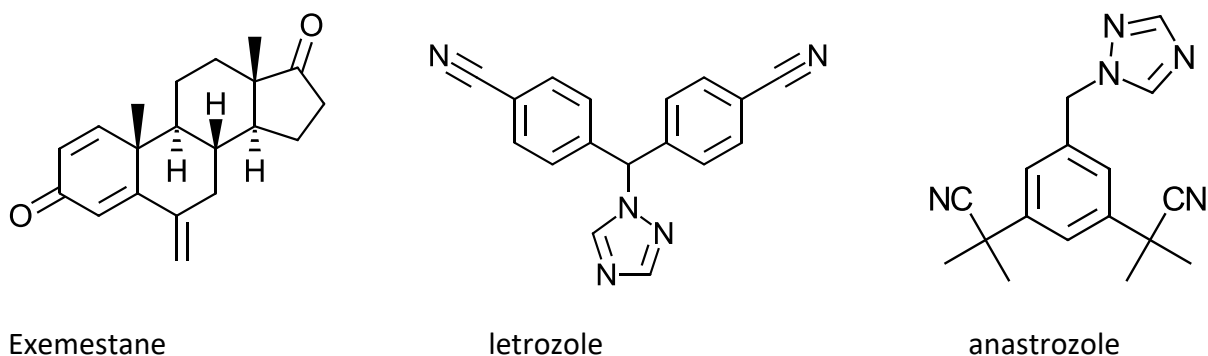


Figure 11: Structures of some steroidal and non-steroidal inhibitors

Anti-androgen drugs are administered to male patients with prostate cancer, as the drugs are capable of blocking androgen receptors that regulate genes associated with cell development of prostate cells, and hence leading to cancer progression (**Figure 12**). Bicalutamide and cyproterone acetate are two of the among clinically approved antiandrogens for patients with prostate cancer (Hejmo *et al.*, 2020).

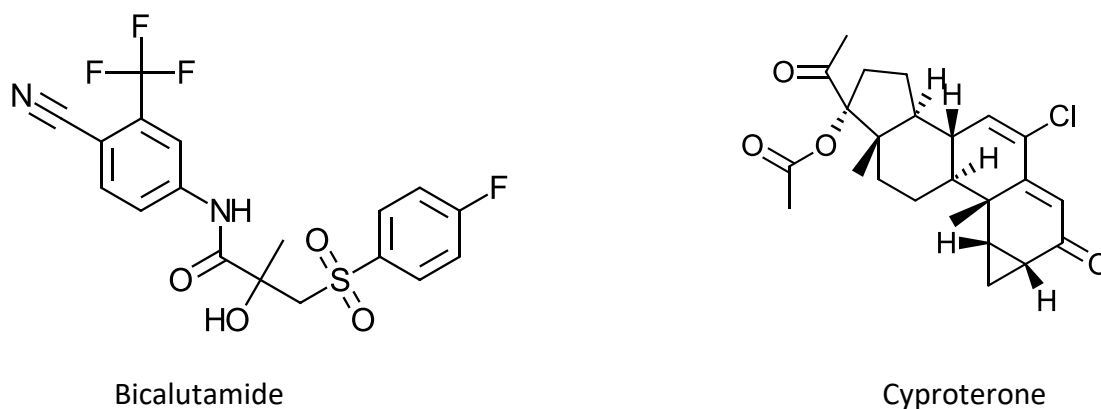


Figure 12: Clinically approved steroidal and non-steroidal antiandrogen drugs for prostate cancer

1.3 Chemotherapy

Chemotherapy refers to the use of drugs that are used in treating different types of cancer. Hundreds of drugs are clinically approved which are administered as a single drug or in combination with other drugs to enhance the success of the therapy. Furthermore, an increasing number of cancer therapeutic targets such as tyrosine kinase (TK), proteasome

inhibitors, gene therapy, vaccines have been developed recently and a new generation of chemotherapeutic drugs continue to emerge. Chemotherapeutic drugs are initially identified in the laboratory through a series of successive experiments and tests on cell lines and animals. They undergo successive phases of clinical trials to ascertain their efficacy as a successful drug candidate (Kesikli and Guler, 2015). Chemotherapeutic agents can be classified into two major categories based on the structure activity of relationship (SAR) of the agents and the mode of action within the cell cycle.

1.3.1 Alkylating agents

Alkylating agents refers to group of compounds that covalently interact with the macromolecules through an alkyl group. Commonly known alkylating agents interact with DNA to disrupt the activity of cellular process. Alkylating agents attack DNA in a nucleophilic or electrophilic fashion depending on the specie in the molecule and the bases present in the DNA (Burney, 2011). However, nucleophilic oxygen and nitrogen atoms present in the nucleoside bases are regarded to be of therapeutic use (Avendaño and Menéndez, 2015b). The process is primarily an electrostatic interaction between the two sites (ligand and the receptor): an overlap of the high occupied molecular orbital (HOMO) of the receptor site with lower unoccupied molecular orbital (LUMO) of the ligand site.

The interaction of alkylating agents with the DNA results in different steric changes by preventing DNA from replication and transcription. The main site exposed for alkylation in the DNA are the nitrogen atoms present at different positions of the bases (**Figure 13**). The reactivity of alkylating agents with N atoms in the bases depends on their increase in nucleophilicity (N7 of guanine > N1 of adenine > N3 of cytosine > N3 of thymine) (Oronsky *et al.*, 2012).

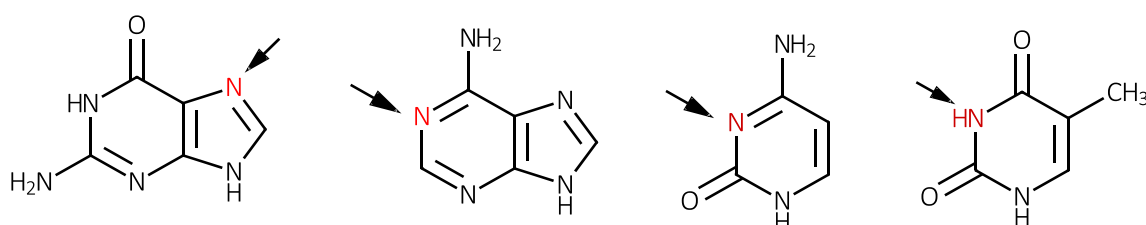


Figure 13: Structures of guanine, adenine, cytosine, and thymine (from left to right)

Mode of interactions in alkylating drugs

The primary target of all alkylating drugs is DNA (Burney, 2011); and their cytotoxic effect can be determined based on their mode of interaction with the target and the reaction kinetics involved in drug metabolism (Huang and Li, 2013). Many alkylating drugs can link two complementary DNA strands (inter-strand crosslinking, **Figure 14**), while some bind to single strand at two different points (intrastrand crosslinking). Some alkylators bind to DNA at one end with a different molecule, e.g protein at another end. It has been reported that compounds that form interstrand crosslinking are more cytotoxic than those interacting through intrastrand and with proteins. Cisplatin and its analogues targets DNA and form both inter and intrastrand DNA adducts which makes it one of the most effective alkylating drugs (Avenidao and Menendez, 2015).

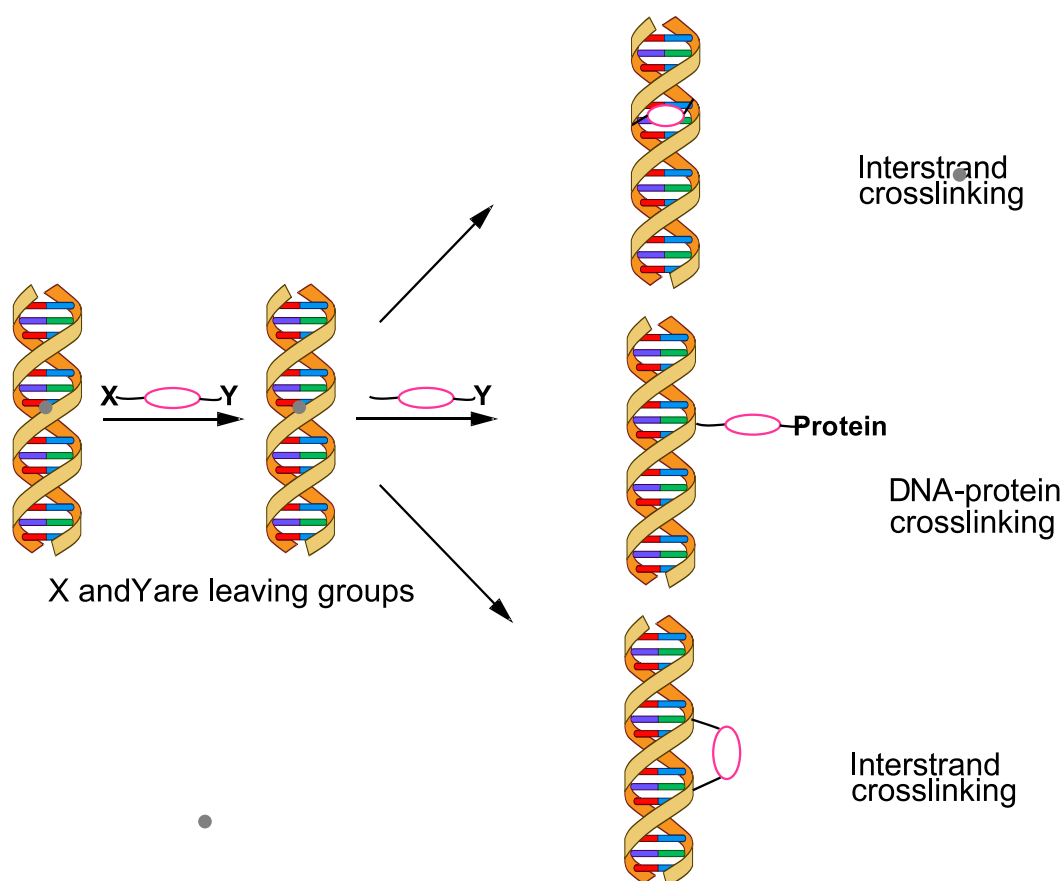


Figure 14:Types of interactions between alkylating agents and DNA.

Nitrogen mustards

Nitrogen mustards are highly reactive bio-alkylating agents discovered during World War II when its effect was observed to cause lymphoid and myeloid suppression. Their high

reactivity is attributed to the formation of a highly unstable aziridinium cation that reacts with the nucleophilic sites on the DNA (**Figure 15**). The high reactivity also results from disruption in the hydrogen bond interaction occurring between two adjacent DNA bases e.g. The DNA base pairs between guanine and cytosine (also known as the Watson-Crick bases pairs) can be affected by the tautomeric effect of cytosine. This is caused by the presence of the alkyl group at the N7 position (**Figure 15**) that generates a partial positive charge at the carbonyl center at the purine site, hence making it electron deficient (Cleaves, 2011).

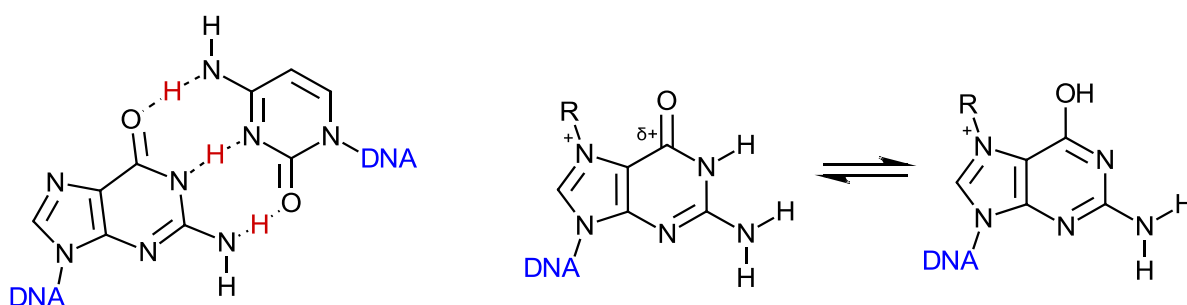


Figure 15: Disruption of hydrogen bond interaction due to alkylation in the DNA

Higher toxicity associated with nitrogen mustards toward normal cells encouraged the development of varieties of hybrids which include aromatic nitrogen mustards, fatty nitrogen mustard and amide nitrogen mustards (**Figure 16**). These hybrids have shown significant clinical effects, yet toxicity and solubility remained a prevailing clinical disadvantage. A recent study reveals that cyclophosphamide, a heterocyclic nitrogen mustards is toxic and is clinically used for lung, ovarian and breast cancer (Chen *et al.*, 2018b).

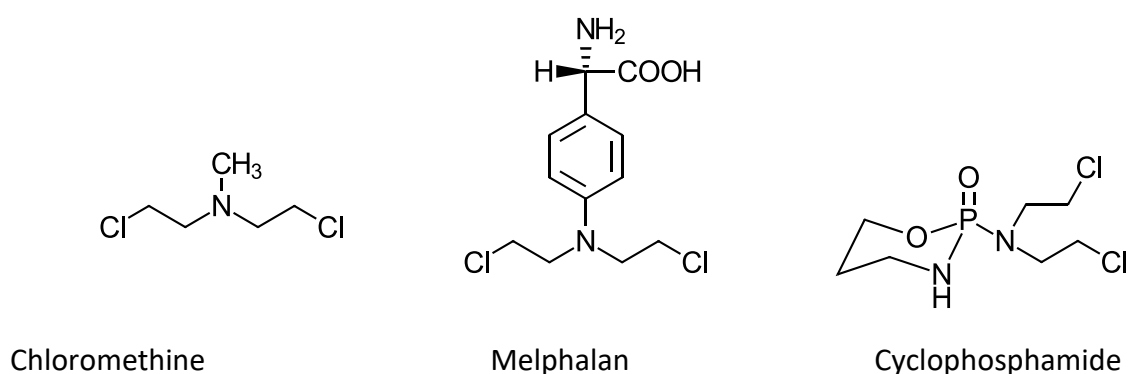


Figure 16: Modified hybrids of nitrogen mustards

1.3.1.1 Antimetabolites

Antimetabolites are naturally occurring compounds or their synthetic analogues, capable of interfering with the metabolic reactions within a cellular environment, mainly through interaction with enzymes (Avenidaño and Menéndez, 2015a). A notable feature of antimetabolites is their ability to competitively interact with binding sites of enzymes in rapidly dividing cancerous cells. Also, this property makes them a good target in the chemotherapeutics. Also, most clinically approved antimetabolites have different mechanisms of action on DNA. This include blocking the synthesis of pyrimidines and blocking the pathway to synthesis of DNA polymerase. However, disadvantage of this group of compounds in chemotherapy is their lack of specificity, as they interact with metabolic processes in normal cells which may cause side effects. Nevertheless, antimetabolites remain one of the essential areas in chemotherapy with current ongoing research (Tassinari *et al.*, 2017; Logan *et al.*, 2020).

1.3.1.2 Topoisomerase-interacting agents

Topoisomerases are the enzymes that maintain the 3-dimensional integrity of the DNA and regulates the winding and unwinding process during transcription and replication, to ensure the functional stability of the genomic system. Two types of topoisomerases are known in both prokaryotes and eukaryotes, they are: topoisomerase I and topoisomerase II. Their function depends on the number of strands they break and ligate. Topoisomerase I break a single DNA strand and then allows it to pass through the unbroken strand. Whereas topoisomerase II breaks both DNA strands. During the process, however, the topology of the DNA remains intact with no loss in DNA fragments. As a result, cells cannot replicate without the role played by topoisomerases which makes it an important target for cancer.

The mode of action in drugs that target topoisomerase is related with the enzymatic activity of “topoisomerase suppressors” and camptothecins (abbreviated CPT), an alkaloid isolated from the bark *Camptoteca acuminata* (originated from China), interacts by limiting the activity of topoisomerase. However, despite its potency, it has solubility problems.

Improved analogues of CPT have been synthesised to overcome the difficulties associated with solubility. Topotecan (abbreviated CPT-11) is a clinically approved drug to address this problem and has been used for various cancer including ovarian and lung cancer (**Figure 17**).

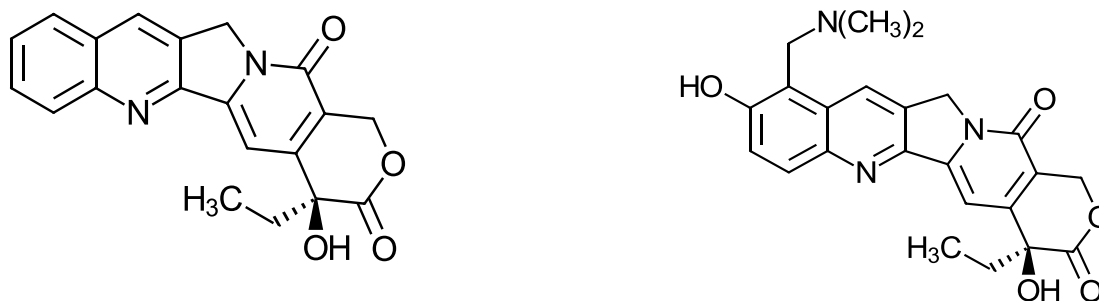
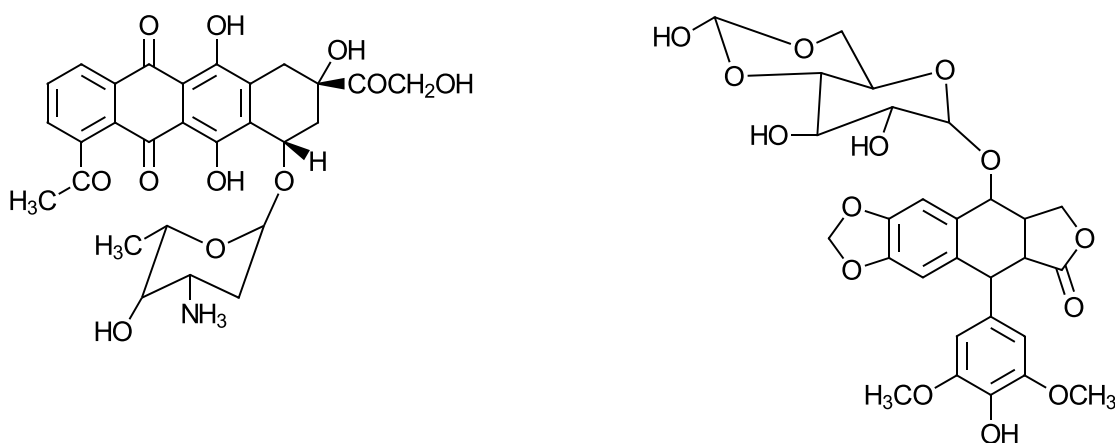


Figure 17: Camptothecin and Topotecan used as topoisomerase inhibitors

Some drugs primarily target (intercalate) to the enzymes-DNA complex after cleavage (**Figure 18**). Most of the topoisomerase II inhibitors belong to this group and because of their direct mode interaction with complex domain of the DNA, they are described as “topoisomerase poisons”.



Doxorubicin

Etoposide

Figure 18: Topoisomerase II drugs that interact with the DNA

Clinically approved drugs in this group include Doxorubicin and Etoposide which bind to the DNA-topoisomerase II complex after cleavage thus stabilising the activity of the enzyme. Some analogues of these compounds have other inhibition mechanisms and have not yet been fully identified (Marinello, Delcuratolo and Capranico, 2018).

1.3.1.3 Kinase inhibitors

Protein kinases consist of vast number of proteins that catalyse the transfer of a phosphate group from phosphates with higher energy, a process also commonly known as phosphorylation. It involves reduction of adenosine triphosphate (ATP) to an adenosine diphosphate along with transfer of energy during the process. It is the basis through which energy is exchanged such that the life cycle of a cell depends on it. As a result, many studies have revealed that distortion in the activity of kinase activity is related to the activation of protooncogenic pathways that lead to uncontrolled proliferation of cells and manifestation of cancer. About 2000 protein kinases have been recognized in nature, ranging from unicellular to multicellular organisms (Manning *et al.*, 2002). More than 500 kinase genes were identified with 90 of these genes existing in human genes as receptor and non-receptor kinases (Metibemu *et al.*, 2019).

Protein kinases have become an important target in cancer chemotherapy. This is because many cases of cancer activation have revealed the overexpression of enzymes that are directly or indirectly related to oncogenesis (Pericles, 2012). About 16 PTKs have been marked as important therapeutic targets in cancer chemotherapy depending on their structural and binding functionality, along with their localization on the cellular membrane. Recently, the naturally occurring β -diketone, curcumin has been reported to be an essential receptor tyrosine kinase inhibitor and responsible for targeting cancer by inhibiting autophosphorylation and transphosphorylation in p185neu tyrosine kinase receptor and inhibition of proliferation in breast cancer cells (Hong, Spohn and Hung, 1999).

A more recent study revealed that curcumin (**Figure 19**) is also effective in deregulation of HER-2 oncoproteins in breast cancer cells. The mechanism of its action is to block signal transduction pathways associated expression of cancer. This includes the PI3K/Akt, MAPK, and NF- κ B. (Lai *et al.*, 2012).

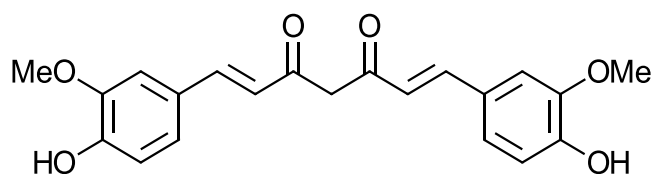


Figure 19: Structure of a biologically active derivative of curcumin

The structural features that determine the activity of curcumin is the presence of methoxy and phenolic groups attached to the ring. These two groups describe the anticancer and antioxidant activity and can be compared with compounds such as the anti-vascular agent combretastatin A-4 (**Figure 20**) that bear the same groups on one of its aromatic rings (Golonko *et al.*, 2019).

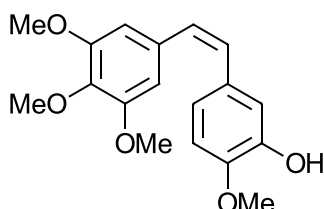


Figure 20: Structure of combretastatin CA-4

Furthermore, the structural flexibility emerging from the unsaturated bonds in curcumin enables it to freely interact with different proteins. The β -carbonyl group is useful in reducing metal toxicity in many most metal complexes (Busse *et al.*, 2001).

1.3.1.4 Proteasome inhibitors

Proteasomes also known as proteolytic enzymes are agents that aid in degradation and regulation of misfolded proteins by breaking them down into peptides and amino acids. They are high molecular weight proteins (2.4 MDa) comprising of 60 subunits, constituting almost 2% of proteins located within the cytoplasm of cells and are involved in many cellular processes related to cell progression (Adams, 2004). In eukaryotes, alteration in their structural conformation due to genetic and environmental factors can lead to varieties of abnormalities including cancer (Giovanni and David, 2005). About 80% of protein is being degraded through the ubiquitin proteasome pathway (UPP) into polypeptide units (Crawford, Walker and Irvine, 2011).

Protease inhibitors constitute many FDA approved drugs for HIV therapy and about 26 of these drugs are clinically administered (Lv, Chu and Wang, 2015; Rakashanda and Amin, 2013). The main effect of these drugs is by imitating the proteasome active site where the hydroxyl group of the inhibitor interacts with the carboxylic site on the protein. The presence of a hydroxyl in these molecules commonly represents one of the active groups in most HIV-inhibitors available on the market (**Figure 21**).

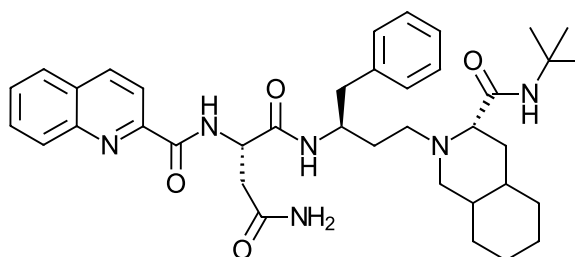
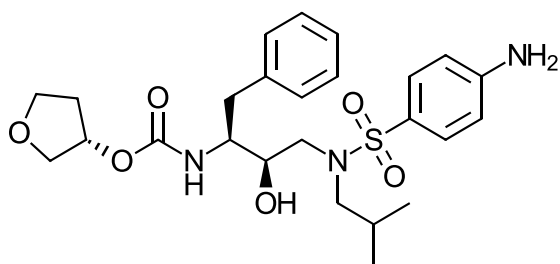
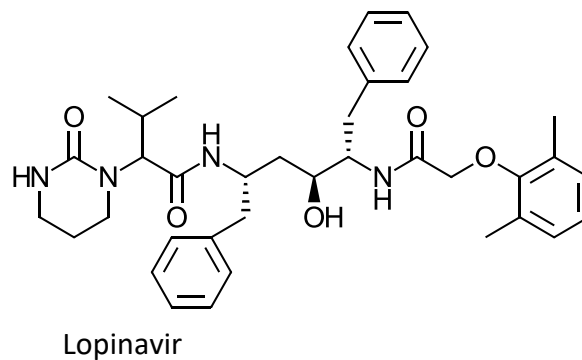
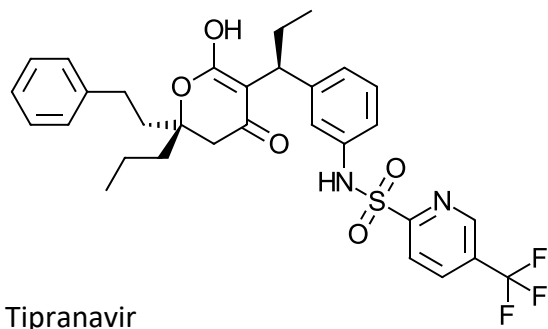


Figure 21: Chemical structures of some clinically approved HIV protease inhibitors

Recently, proteases have also become an important target in cancer as they control and regulate cell cycle processes (cell progression and apoptosis) that lead to cancer. Cellular pathways such as p-53, nuclear factor NF-kB and the cyclins can be targeted by proteasome inhibitors through blocking their activity and thus leading to cellular death (Adams, 2004). The full details of how the mechanism of this process leads to cellular death is not yet fully understood (Giovanni and David, 2005).

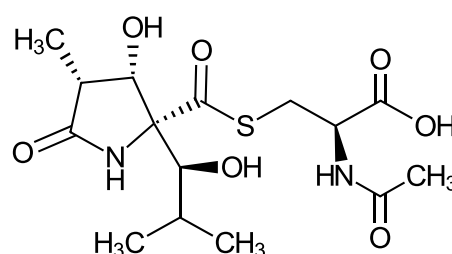
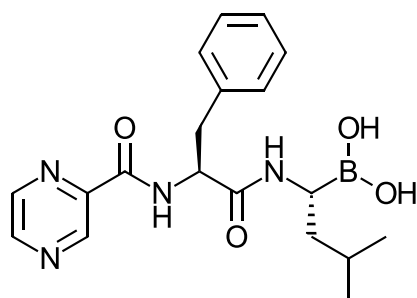


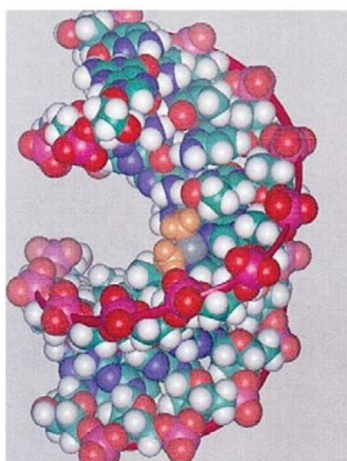
Figure 22: Active protease inhibitors in chemotherapy

The approval of bortezomib (**Figure 22**) by FDA as the first protease inhibitor has prompted the development of novel protease inhibitors with clinical applications in treatment of malignancies such as myeloma and cell lymphoma (Korubo *et al.*, 2017).

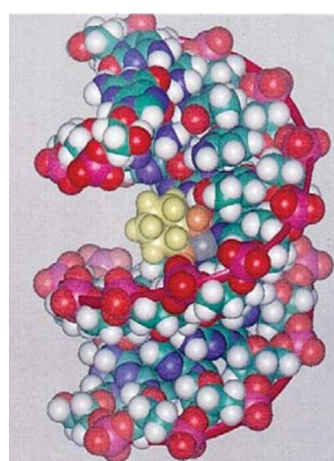
The mode of action in bortezomib is by reversibly binding to 26S catalytic domain thus blocking the activity of $\beta 2$ /trypsin and $\beta 1$ /caspase. Likewise, lactacystin has been tested *in vitro* to induce cellular death at a minimal concentration of about 5 μ M thus qualifying it as a useful PI candidate (Chabner and Longo, 2019). High cost of isolating bortezomib and the other protease inhibitors has discouraged the production and diversion to other alternative drugs (Trezza *et al.*, 2020).

1.3.1.5 Platinum analogues

Platinum-related drugs constitute one of the oldest and most effective anticancer drugs with an outstanding mechanism of action and have been administered to combat different types of cancer. The first generation of platinum drugs, cisplatin, was approved for the first time by the food drug administration (FDA) for treating lung, ovarian, colorectal, bladder and testicular cancers (Yu *et al.*, 2020). Since the approval of cisplatin as an anticancer drug in the past 40 years, over 150,000 platinum compounds have been explored and documented in chemical abstract databases (Angel and Consuelo, 2009; Sarkar, 2017).



(a) Cisplatin-DNA



(b) Oxaliplatin-DNA

Figure 23: DNA interacting with different platinum drugs. Obtained from (Muggia *et al.*, 2015)

One of the interesting applications of platinum drugs is their affinity to bind and bend the DNA chain (**Figure 23**) leading to cell cycle arrest and apoptosis. Third generation platinum drugs like oxaliplatin further block the major groove and by interacting with many sites in the DNA, and hence show greater activity (Muggia *et al.*, 2015).

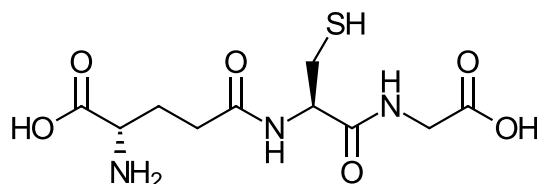


Figure 24: Glutathione reduces the activity of platinum drugs

Toxicity and drug resistance due to high reactivity with scavenging species such as glutathione transferase and metallothionein (**Figure 24**) (Zhou *et al.*, 2020; Si and Lang, 2018) remain one of the main setbacks that led to the development of second and third generation of platinum (II) drugs (Raymond *et al.*, 2002; De Luca *et al.*, 2019). Considering the 23 platinum drugs in clinical trials, only carboplatin and oxaliplatin analogues (**Figure 25**) of the 2nd and 3rd generation platinum (II) have been clinically approved (Wheate *et al.*, 2010). Considering the enhanced toxicity problems above with cisplatin, research on the mechanism of resistance of these drugs has continued for the past four decades (Zhou *et al.*, 2020).

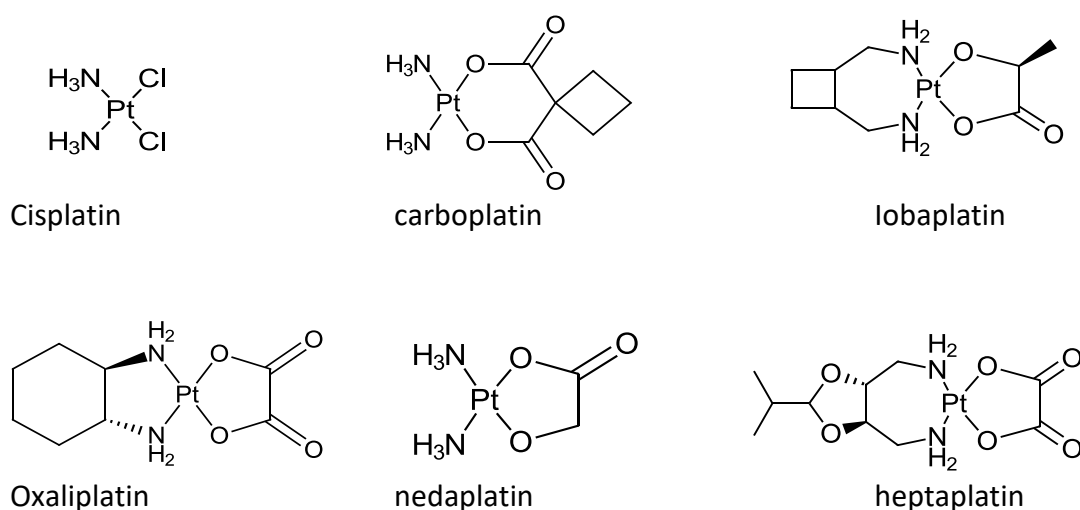


Figure 25: Structure of FDA approved platinum (II) drugs

Current and ongoing research to overcome the drawbacks associated with the square planar platinum (II) analogues is the emerging interest in inert platinum (IV) bearing two extra ligands at the axial positions (**Figure 26**). The oxidative addition of two ligands kinetically controls

unintended extracellular interactions with plasma proteins before reaching the tumour cell environment, and hence makes it more effective in reaching its target (Karmakar *et al.*, 2019; Browning *et al.*, 2017).

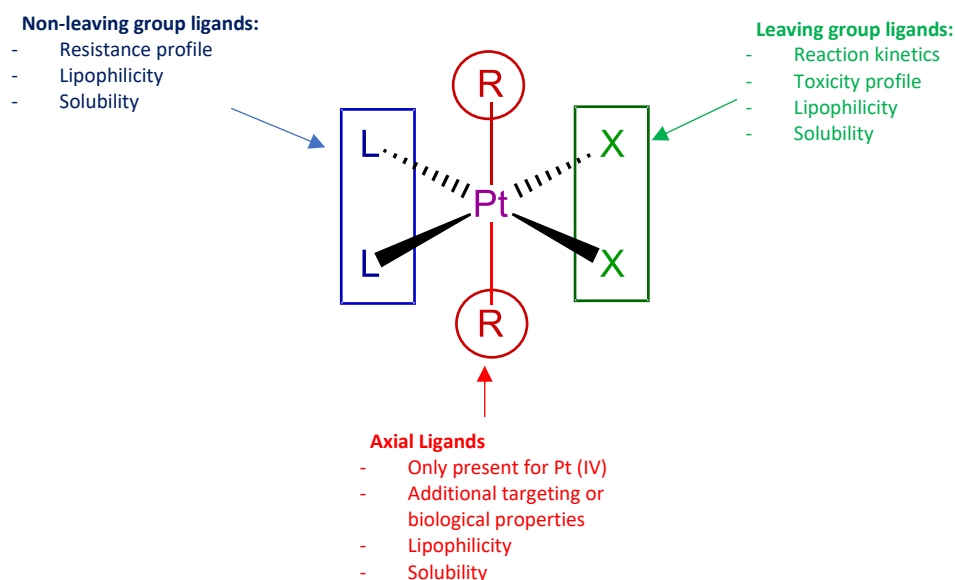


Figure 26: Structural geometry of platinum (II) drugs

The structural geometry of platinum (IV) compound from the axial position offers an excellent physicochemical property that platinum (II) compounds cannot provide. Almost all platinum (IV) compounds explored have enhanced lipophilicity and solubility which makes them suitable for tethering with active ligands with wider activity for many biological targets.

Furthermore, owing to their advantage as stable compounds compared to platinum (II), they express minimal side effects (as they are not prone for interaction with many proteins); and their axial ligands can be linked with pharmacologically active ligands, leading to a dual activity with the same or different target within the tumour microenvironment (Browning *et al.*, 2017; Wang *et al.*, 2018b).

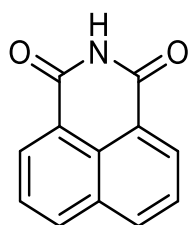


Figure 27: Structure of naphthalimide, a potent DNA intercalator and target for cancer therapy

Naphthalimides (**Figure 27**) are fused aromatic compounds which effectively interacts with the DNA. Owing to its conjugated structure, it can form different interactions (H-bond, Van der Waals) and hence is considered as a suitable DNA intercalator. In a recent report, platinum (IV) tethered at the O- axial bonds with naphthalimide (**Figure 28**) can provide a suitable strategy for dually active compounds for targeting cancer as compared to platinum (II) compounds (Wang *et al.*, 2018b).

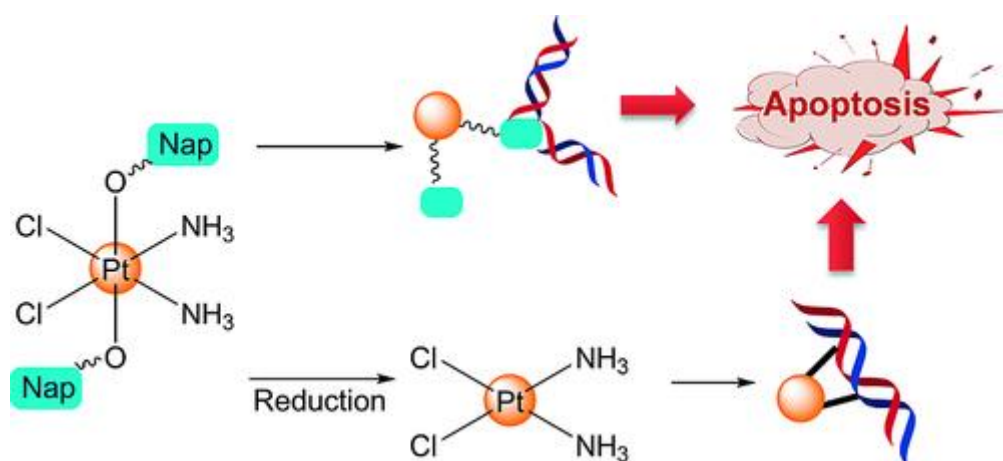


Figure 28: Prodrug and dual activity of platinum (IV) tethered with naphthalimide (Nap) at the axial position. Obtained from (Wang *et al.*, 2018b)

1.3.2 Antimitotic agents:

1.3.2.1 Structural orientation of tubulins and microtubules:

Microtubules and the microtubular proteins represent an essential part in the formation of the mitotic spindle, which plays a significant role during mitosis (Gupta and Bhattacharyya, 2003). The microtubules consist of tubulin dimers identified as α and β tubulins, with each subunit arranged in a longitudinally ordered fashion termed as the protofilaments (**Figure 29**). Tubulins are 55 kDa sized proteins coded by 23 genes of the human genome. Collectively, tubulins form subfamilies of six, the alpha (α), beta (β), gamma (γ), delta (δ), epsilon (ϵ) and zeta (ζ) tubulin (Findeisen *et al.*, 2014; Hu *et al.*, 2020). The two subfamilies, α and β are more common in eukaryotic cells and form heterodimers that undergo polymerisation leading to microtubules (Schwarzerová *et al.*, 2019).

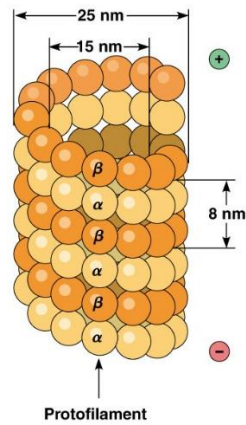


Figure 29: Dimensional structure of microtubule with (+) and (-) represented in green and red. Obtained from (Janke and Chloë Bulinski, 2011)

Dimers formed from α and β -tubulins form oligomers that lead to the formation of a protofilament (**Figure 30**) with thirteen of these protofilaments assemble in a vertical manner forming a cylindrical hollow space that forms the microtubule (Barbier *et al.*, 2019).

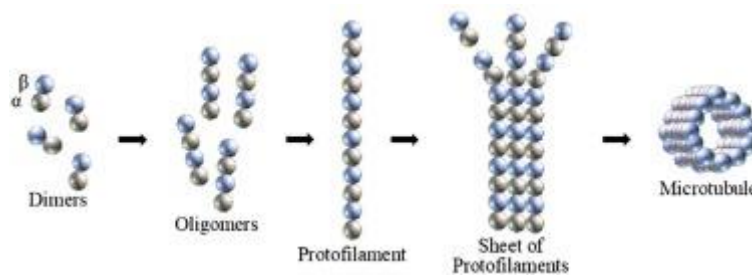


Figure 30: Assembly of α and β -tubulins from dimers to form microtubules. Obtained from (Barbier *et al.*, 2019)

The interior diameter of microtubule is approximately 15 nm and 25 nm from the exterior (Huang *et al.*, 2020). The vertically elongated structure of the microtubule have polar ends; one end being positive representing the phase of growth and elongation, and negative end that enables contraction, a process called dynamic instability (Kierszenbaum and Tres, 2016).

During the polymerisation process, both alpha and beta tubulins are bound to two guanine triphosphate (GTP) molecules, through the GTP binding sites on the subunits, with one site irreversible and trapped and not actively hydrolysable. The second molecule is bound to the site of the beta tubulin exposed on the surface, hence easily hydrolyses to GDP (Kaur *et al.*, 2014). Evidence has shown that the kinetic property of tubulin to polymerize and depolymerize is largely dependent on factors including temperature, concentration of local

tubulin dimers favoured by energy in the form of GTP (Huzil, Ludueña and Tuszynski, 2006), the driving factor that controls the polymeric assembly of microtubules (Sontag, Staley and Erickson, 2005). As a result, different anti-mitotic agents have different binding capacities with tubulin and could develop resistance that render such drugs ineffective (Kumbhar *et al.*, 2020). Alteration in the dynamic equilibrium of microtubules is an important target for development of cancer drugs (He *et al.*, 2020). Microtubule targeting agents (MTA) disrupt the formation of mitotic spindles which arrests cells in the G2/M phase (the phase in which cells physically separate into two newly formed cells).

1.3.2.2 Microtubule targeting agents (MTA)

A large number of microtubule targeting agents (MTA) and microtubule disrupting agents (MDA) have been derived from natural products and synthetic sources; with some isolated from marine products such as marine sponges (Gupta *et al.*, 2019) and plant algae (Steinmetz and Prota, 2018). As mentioned earlier, MTA / MDA destabilize the assembly of microtubules leading to cell arrest at the G2/M phase. The first drug molecule that was known to have inhibiting activity on tubulin is colchicine (**Figure 31**) (Warda *et al.*, 2020). Currently, x-ray crystallography studies has revealed 6 binding sites in tubulin have been identified as important MTA targets and their molecular mechanisms reveals their exciting activities in anticancer research (Coulup and Georg, 2019).

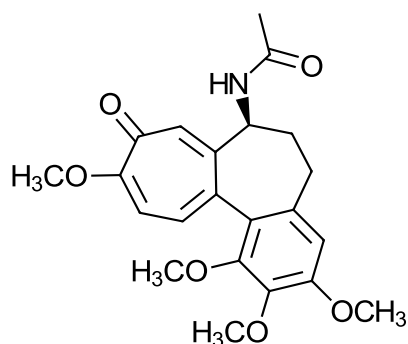


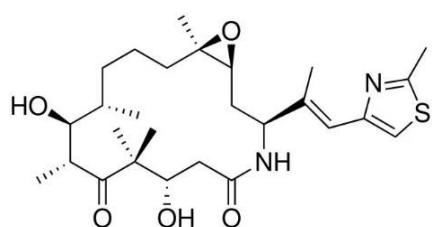
Figure 31: Structure of colchicine

Early discovery in their activity from natural sources provided an abundant means of obtaining MTAs with bioactive properties on a larger scale and only a few were synthesised and modified to improve their activity. Many types of MTA analogues have been designed, explored, and used as medication against different types of cancer for many years. Yet, a common problem associated with these compounds is that patients undergoing treatment

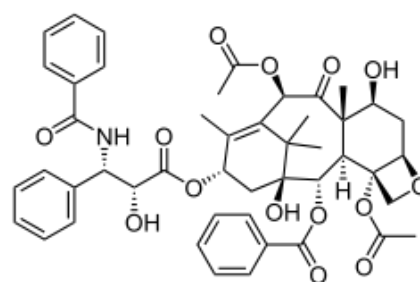
with these drugs develop resistance and toxicities that lead to peripheral malfunctions in the nervous system (Gupta *et al.*, 2019).

1.3.2.4 Tubulin associated ligands and their binding agents

Microtubule targeting agent can be classified into two groups depending on their mode of action as stabilisers or destabilisers of tubulin. Epothilones and taxanes such as paclitaxel, and docetaxel are well known microtubule stabilisers and can catalyse the polymerisation of microtubules. Evidence from a previous clinical study revealed that epothilones and taxanes (**Figure 32**) share a common tubulin binding site. The conclusion of the study also suggests that epothilones show greater activity than taxanes by stabilising microtubule and inducing apoptosis (Forli, 2014).



An epothilone analogue (Ixabepilone)



Taxane (paclitaxel)

Figure 32: Structures of microtubule stabilizing agents

Colchicine and vinca-alkaloids on the other hand are well known as effective destabilizing agents as they can hinder the polymerisation of microtubules (Mirzaei *et al.*, 2020). In addition, colchicine can also act as an antiangiogenic agent and cause disruption of tumour vasculature which is not present in the other binding agents (Li *et al.*, 2017).

1.3.2.5 Taxane binding site

The taxane binding site is located at the β -domain of the tubulin. They share a common similarities with the epothilone binding site and much interest is focused on finding a pharmacophore that targets both sites (Gupta *et al.*, 2003). Different amino acid residues in the receptor site of the tubulin are susceptible for interaction with ligands within a bond distance of 6 Å. The cyclic structure that contributes to taxane activity is the polar oxetane ring (**Figure 33**). The ring is in proximity with the amino acids Pro274, Leu27 (not shown) and Thr276 within a binding distance of 2.0 – 3.0 Å. Thr276 interacts effectively with oxygen in the oxetane ring as shown in Fig 32. It is in believed to be in close range to form hydrogen

bond interaction with the hydroxyl group directly attached to the alicyclic ring neighbouring the oxetane moiety (Löwe et al., 2001).

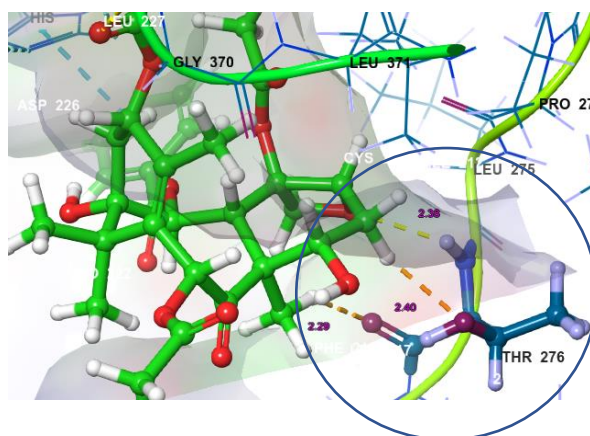


Figure 33: Interaction of taxane (green) with oxetane ring with Thr276 (blue) of β -tubulin within a binding distance of 3.0 Å. (1JFF- β -tubulin retrieved from PDB). The coloured broken lines represent the site of interaction between residue and the taxane ligand.

1.3.2.6 Vinca alkaloid binding site

Like the taxane molecular structure, vinca alkaloids also consist of a complex structure with molecular weights to more than 800 g mol^{-1} and appreciable number of electronegative groups present within their structural scaffolds (**Figure 34**). Analogues of this natural product demonstrate their activity by stabilising the microtubules in cancerous cells (Huzil, Ludueña and Tuszynski, 2006).

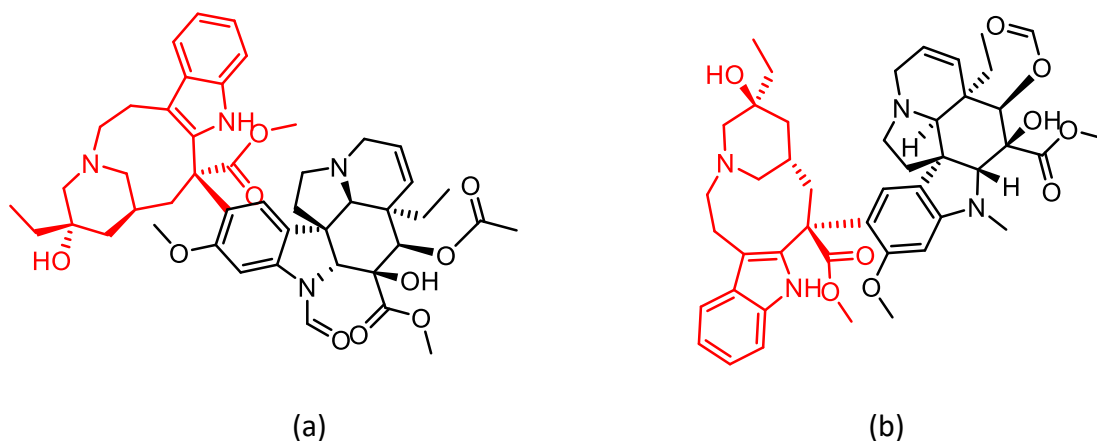


Figure 34: Structural scaffold of a vinca alkaloids (highlighted red)

In vitro and *in vivo* studies on different vinca alkaloids have revealed the formation of different metabolites. Owing to the presence of active functional groups attached to the complex structure. Currently, about 35 different metabolites with molecular weights between 350 to 830 gmol⁻¹ have been elucidated and their adverse drug reactions such as hydroxylation, hydrolysis, demethylation and N-demethylation have been documented (Chagas and Alisaraie, 2019). As a result, vinblastine and related alkaloids interact with different protein receptors and cause clinical side effects in cancer patients.

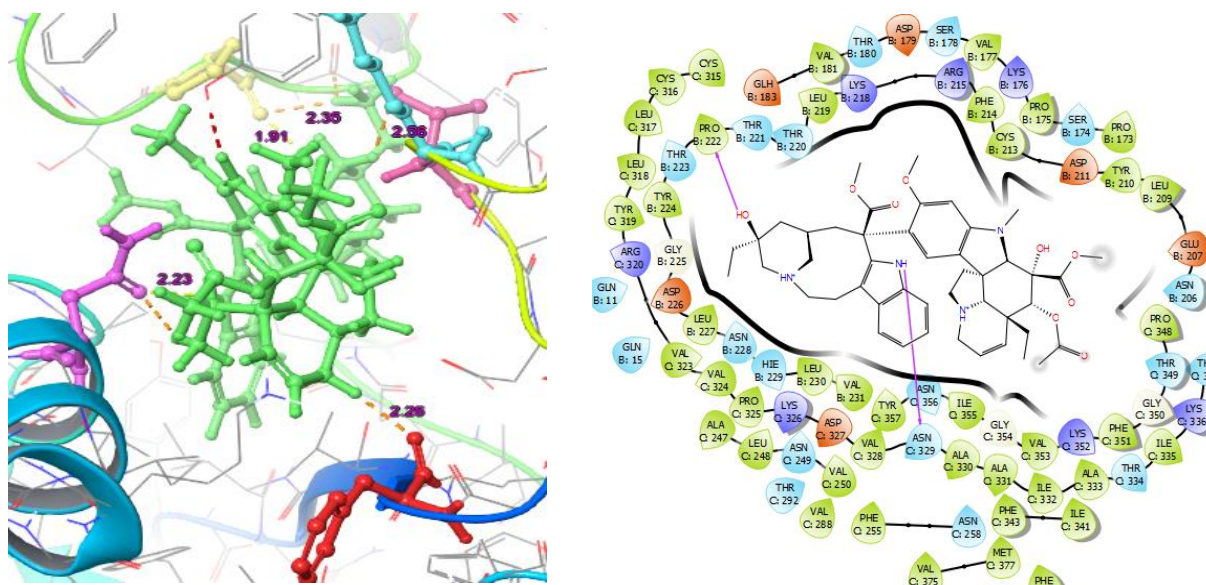


Figure 35: 2D and 3D representation of vinblastine (vinca alkaloid) interaction with both α and β -chain of tubulin.

The image on the right is a 2D depicts the hydroxyl and amine groups present in catharanthine scaffold interacting with Pro222 and Asn329.

Molecular docking analysis reveals that vinca alkaloids interact with residues in both α -tubulin and β -tubulin. The catharanthine moiety in these molecules (coloured red) is the major contributor to the activity of vinca alkaloids (Huzil, Ludueña and Tuszynski, 2006). Most vinca alkaloids including the ones in (Figure 35) form a hydrogen bond interaction with residues Asn329 (purple, 2.23 Å) and Phe351 (red, 2.26 Å) on the α -tubulin, and a strong interaction with β -tubulin residues at Pro222 (yellow, 1.91 Å), Val177 (pink, 2.56 Å). Other interactions of vinca alkaloids in tubulin include the residues of α -subunits at Ser178, Asp179 and Tyr210 (Chagas and Alisaraie, 2019; Torin Huzil *et al.*, 2010).

1.3.2.7 Structural features of Colchicine binding site

The water-soluble colchicine molecule was extracted from a toxic meadow saffron plant, (botanical name *Colchicum autumnale*). Many studies have explored inhibitors that target the colchicine binding site on tubulin. Colchicine has a simple structure compared to the other tubulin sites targeted by enormously complex ligands. Structural conformation of colchicine appears like a butterfly (Yingge *et al.*, 2020) that perfectly fits into one of the binding pockets in the colchicine domain (**Figure 36**).

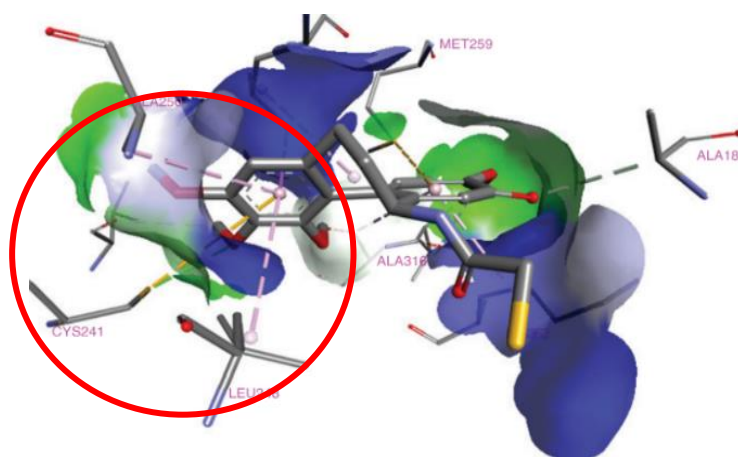


Figure 36: Hydrogen bond interaction of colchicine with microtubule. Adapted from (Li *et al.*, 2017)

From X-ray diffraction studies, it has been reported that the trimethoxy phenyl moieties (assigned as ring A) in the structure is bonded to the Cys241 amino acid residue through a hydrogen bonding. The carbonyl group on the seven-membered ring of the colchicine also interacts through a hydrogen bond with Val α 181 (Li *et al.*, 2017; Ravelli *et al.*, 2004).

The trimethoxy phenyl group in the molecule is essential. Replacing one of the groups with a bulky substituent result in loss of activity (Yingge *et al.*, 2020). However, a study has shown that the replacement of the substituents with a different groups (**Figure 37**) has presented an improved activity than expected (Torin Huzil *et al.*, 2010).

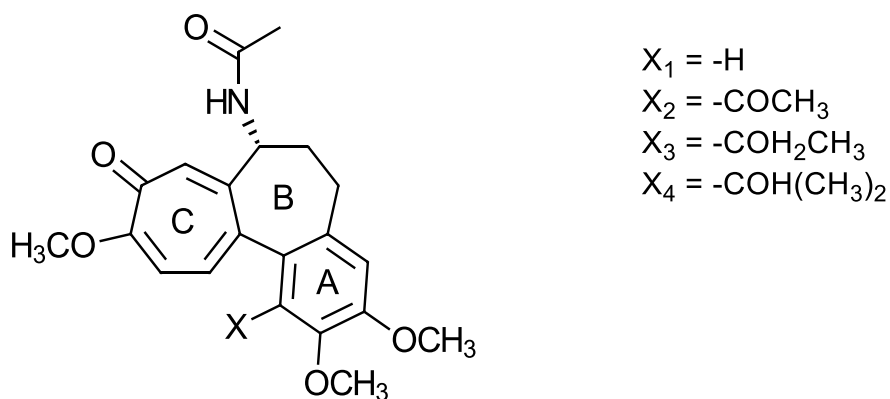


Figure 37: Structural features of colchicine and important substituents

Extensive studies on the microtubule inhibitors that target the colchicine binding site bearing aliphatic moieties have been reviewed in studies (Luduena and Roach, 1991). They emphasized that the colchicine binding pocket is rich with nucleophilic groups attached to the amino acid residues which are attracted to alkyl groups in ligands. Ligands bearing aromatic rings or substituted with larger alkyl groups (X_4 from **Figure 37**) tend to interact better and hence more aliphatic substitution will infer a greater hydrophobic interaction (Legault *et al.*, 2000).

Owing to the high toxicity of colchicine, effort of many research concentrated on modifying the colchicine scaffold by replacing ring B (**Figure 37**) with a different bridge / linker (Lu *et al.*, 2012). Ring C has also been replaced with an aromatic ring bearing different substituents. Many analogues targeting the colchicine binding site have been synthesised and tested for activity. The methoxy groups were retained in the aromatic system to identify a pharmacophore with similar activities in the colchicine binding site (Niu *et al.*, 2014). Recently synthesised combretastatin analogues have been proposed to be among the best targets of the colchicine binding site and have demonstrated a binding capacity of about 78 % relative to colchicine (Zheng *et al.*, 2014).

1.4 Colchicine binding site inhibitors (CBSI) reported before 2019

1.4.1 Combretastatins A-4 (CA-4)

Combretastatins (CA-4) belongs to a member of naturally occurring stilbenes isolated for the first-time by Pettit *et. al* in 1989. It is extracted from the bark of the bush willow tree botanically known as *Combretum caffrum*, which more often grows near a riverbank in the

Eastern province of South Africa. CA-4 is an active anti-cancer agent with a simplified structural scaffold that can be easily modified for improved solubility and therapeutic activity. The IC₅₀ of CA-4 is in the nanomolar range for many cancer cell lines (Nainwal *et al.*, 2019). Approximately, over a thousand of CA-4 analogues have been synthesised and have shown cytotoxic effects on cancerous cell lines, thus making CA-4 to qualify as a lead compound in cancer research. Due to its structural flexibility, CA-4 can exist in two geometric configurations: *cis*-stilbene and *trans*-stilbene (**Figure 38**).

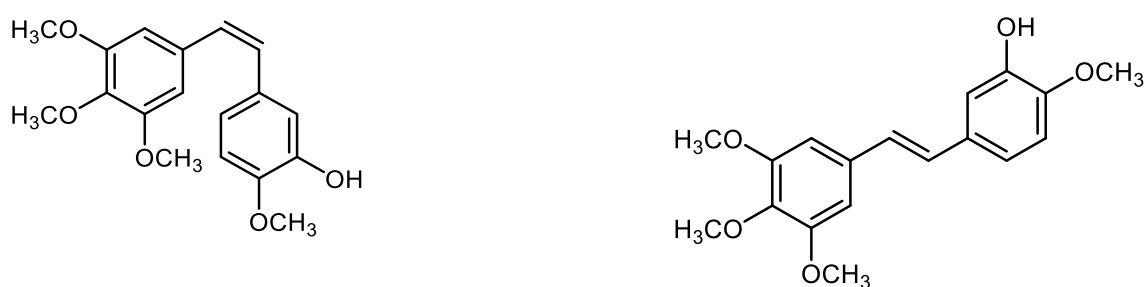


Figure 38: Isomers of CA-4. *cis* on the left and the *trans*-isomer on the right.

The *cis*-configuration is biologically active and interacts strongly with colchicine binding site (CBS) on tubulin. However, some factors such as heat, light, prolonged storage and metabolism in the cell environment can isomerize *cis*-configuration to a thermodynamically favourable *trans*-configuration (Ibrahim *et al.*, 2021). Bioactivity of CA-4 drastically falls when the configuration changes from *cis* to *trans* and therefore, limited efforts have been made to synthesise the *trans*-isomer of CA-4 (McLoughlin and O'Boyle, 2020). Hence, almost all the synthesised analogues aimed at targeting cancer is focused on the *cis*-isomer analogues.

Considering the structure activity relationship (SAR) of colchicine with CA-4, three essential features are expected to be the major contributors of CA-4 as an effective tubulin inhibitor. These features include:

1. substitution of three methoxy groups on ring A at positions 3, 4, and 5;
2. Hydroxyl at position-3 on ring B can be subject for modifications with a different group (e.g a halogen);
3. retaining the *cis*-orientation that links the two aromatic rings.

1.4.2 Successful modifications of CA-4 stilbenoid double bond

Modifying a lead compound in order to improve its bioactivity without altering the structural scaffold is regarded as one of the important elements in identifying new drugs. These modifications can be three to six-membered cyclic or heterocyclic rings which replace the olefinic bond in CA-4 (Harrold and Zavod, 2018; Hadfield *et al.*, 2005) or they can be a straight chain alkyls or units bearing electron withdrawing groups such as carbonyls, dicarbonyl and thiourea (Gomtsyan, 2012).

A number of CA-4 analogues bearing different groups have been prepared with the aim of replacing the ethylene bridge without changing the configuration of the original molecule (McLoughlin and O'Boyle, 2020). To date, CA-4 analogues bearing pyrrole, thiazole, imidazole, and oxazole have been prepared and their bioassays reveals an enhanced solubility. It is believed that modifying the stilbene bonds can play significant role than just a linker, as it can allow insertion of active groups that can interact with the CBS (Tron *et al.*, 2006).

However, in some cases, linkers with 3-membered atoms and six membered atoms may tend to result in decreased activity (**Figure 39**). Though, despite the poor activity in the CBS the structural configuration cannot isomerise to the trans-isomer. A study reveals that some six-membered ring linkers markedly decreased the activity in CA-4 analogues bearing imidazole and pyrazine linkers (Wang *et al.*, 2002).

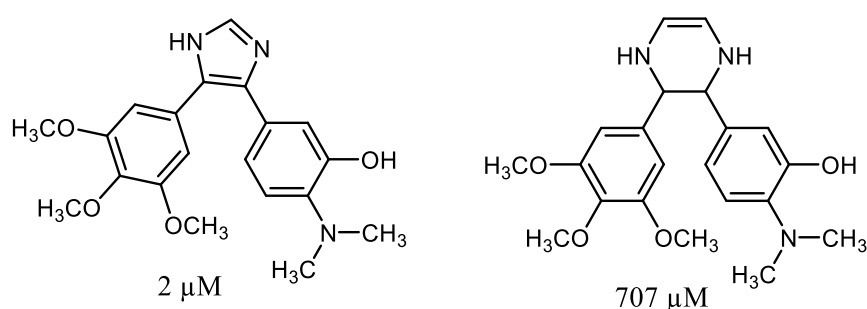


Figure 39: Imidazole and pyrazine analogue of CA-4 showing decreased activity in 5 and 6-membered ring.

Therefore, exploring and alteration of linkers with a cyclic ring system may provide an insight to new residual interaction of CBS and drug molecules. Much data is currently available that has explored the activity of CA-4 analogues on different cancer cells (Daniel, Siyaram and James, 2017; McLoughlin and O'Boyle, 2020).

Structural modification mostly focused on the linkers (**Figure 40**) bearing two, three, four, five or six membered units that can be either noncyclic or cyclic members such as heterocycles (Seddigi *et al.*, 2017). The linker is believed contribute to improved solubility, structural stability and itself may even contribute to interactions with the binding site of target (Harrold and Zavod, 2018; Chen *et al.*, 2018a).

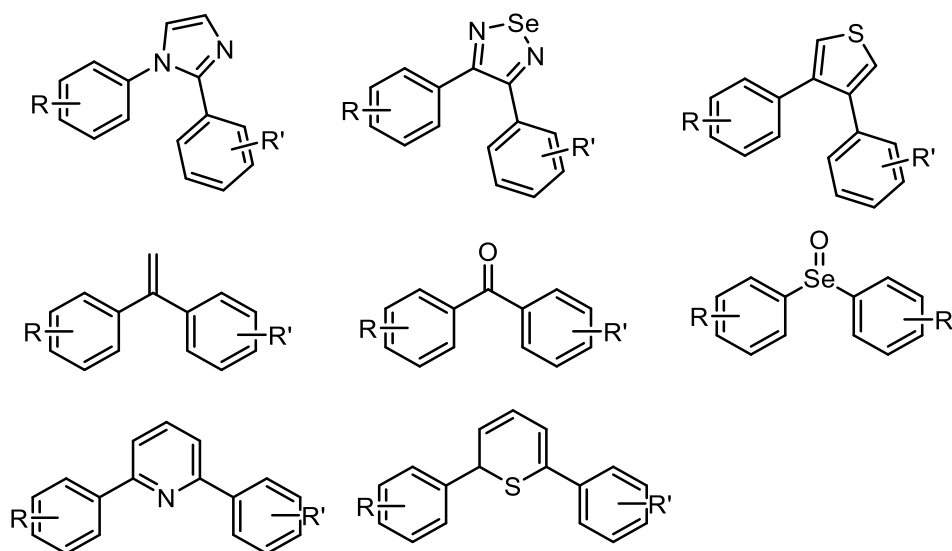


Figure 40: Different linker modification with R and R' denoting atom or functional group at different positions of the ring

1.4.3 Chalcone analogues of CA-4

Chalcones (or keto stilbenes) are naturally occurring products found in a Chinese plant *Scutellaria barbata*. It is traditionally administered as an antimalarial (Chen *et al.*, 2017), anti-inflammatory and diuretic (Rathnakar *et al.*, 2020). Chalcones have antitumour activity and have been observed to inhibit proliferation in different types of cancer cells including breast, colorectal, cervical and lung cancers (Yin *et al.*, 2004).

Methanolic extract of *Scutellaria barbata* was fractionated into different components and tested for cytotoxicity on a human leukaemia cell line (K562) using the MTT assay; and one of the fractions showed micromolar activity. Further purification of the fraction gave E-1-(4'-hydroxyphenyl)-but-1-en-3-one (**Figure 41**) as the active component of the extract (Ducki *et al.*, 1996).

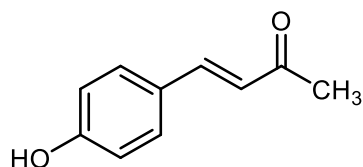


Figure 41: Structure of E-1-(4'-hydroxyphenyl)-but-1-en-3-one

Using the compound as a lead, (Ducki *et al.*, 1997) synthesised a series of enones bearing different substituents to test their inhibitory activity on the K562 leukaemia cell lines (K562). IC₅₀ values showed that analogues of with electron withdrawing groups (EWG) possessed a higher inhibitory activity (>30 fold) than the lead molecule (**Figure 41**) but lesser potency when no EWGs were present in the analogues (**Figure 42**) (Ducki *et al.*, 1997).

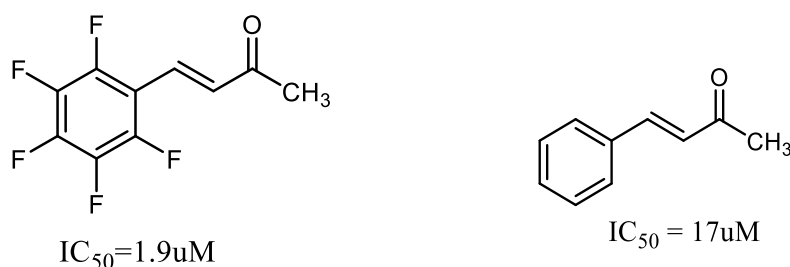


Figure 42: Chalcone analogues bearing electron withdrawing groups

These findings inspired the further investigation of chalcones where the methyl group is replaced with an aryl group to determine their effect on cancer cells. However, chalcones with aryl groups this type originally belong to family of flavonoids which are common in many plants; and their use in medicine is generally accepted (Rozmer and Perjési, 2016).

Previously, Edwards *et al.*, 1990 synthesised the 1,3-diaryl chalcone (**Figure 43**) that inhibits tubulin in HeLa cells, by interfering with the sulfhydryl group on Cys241 residue of the tubulin subunit in the colchicine binding site (Edwards, Stemerick and Sunkara, 1990; Wang *et al.*, 2016)

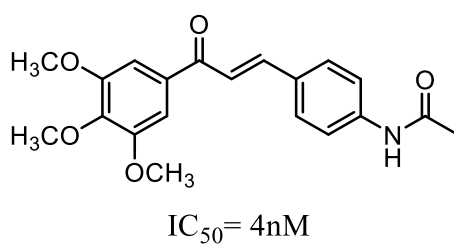


Figure 43: structure of first synthesised 1,3-diarylchalcone with tubulin inhibiting property in HeLa cells

The procedure employed by Edwards *et al.*, 1990 was adopted by (Lawrence *et al.*, 2000) to synthesise series of 1,3-daryl chalcones bearing different groups on the aryl ring; the chalcones were screened for cytotoxicity on K562 cells. Chalcone analogue (4)(E)-3-(3'-hydroxy-4''-methoxyphenyl)-2-methyl-1-(3',4',5'-trimethoxyphenyl)-prop-2-en-1-one (**Figure 44**) with the same moieties in CA-4 showed highest inhibition activity at a nanomolar with an IC_{50} of 4.3nM suggesting strong interaction with the CBS (Ducki *et al.*, 1998).

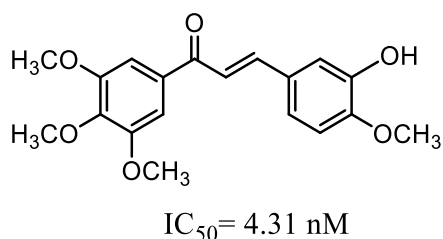


Figure 44: Modified diaryl chalcone bearing CA-4 moieties

However, insertion of a methyl group in the α -position as in (**Figure 45** left) resulted in conformational change to s-trans and a twenty-fold improvement in cytotoxicity (0.21 nM) (Ducki, 2007).

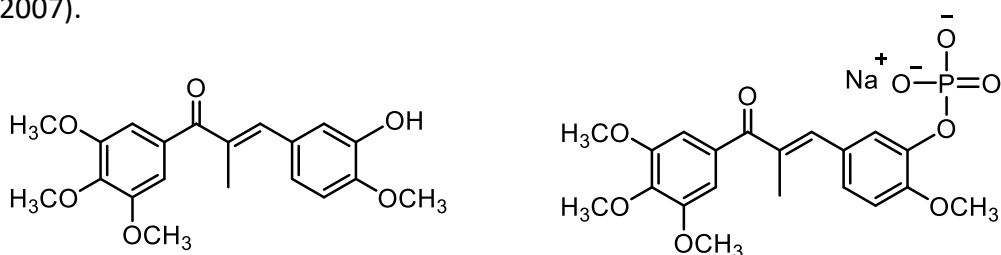


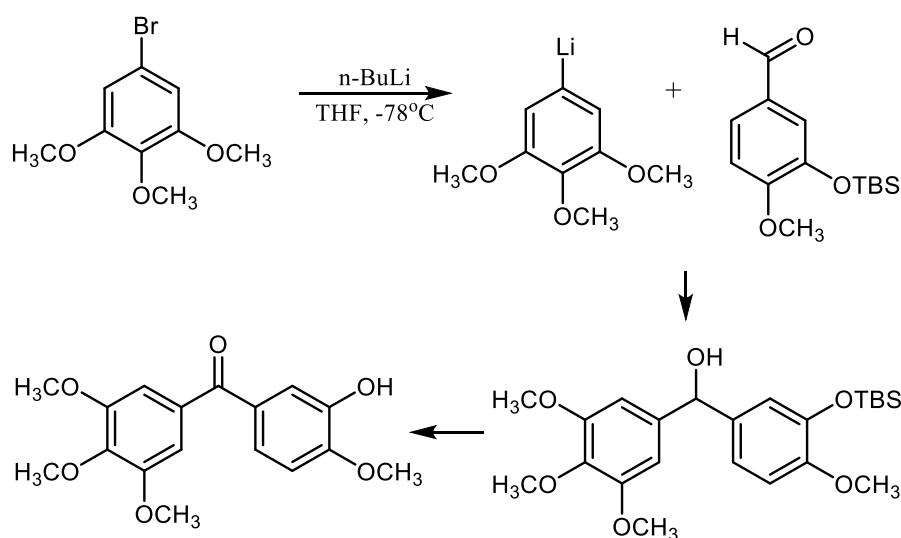
Figure 45: Diaryl-chalcones bearing methyl and phosphate moieties

A phosphate modified analogue (**Figure 45** -right) on a methyl-substituted chalcone suggested that the s-trans conformation of has better interaction with the CBS when the α -methyl is present (Pang *et al.*, 2017). Yet, despite the continued effort to modify CA-4 mimicking chalcone analogues with different moieties, it did not pass into clinical trials stage because of poor bioavailability in the plasma membrane (Fagundes *et al.*, 2017).

1.4.4 Phenstatin CA-4 analogues

Phenstatins are structurally rigid analogues of CA-4 with potent microtubule destabilising properties with cytotoxic activity recorded at a nanomolar concentration in different cancer cell lines (Chen *et al.*, 2018a). Like combretastatins, phenstatin has entered advanced clinical

trials as an antimitotic agent (Chen *et al.*, 2018a; Seddigi *et al.*, 2017). Perhaps, phenstatin analogues are metabolically stable and their potential bioavailability in the plasma membrane makes it an attractive clinical candidate for antimicrotubular drugs (Sardaru *et al.*, 2020).



Scheme 2: Synthetic steps for the synthesis of phenstatin (Pettit *et al.*, 2000)

In addition to their structural stability over combretastatin, phenstatin is easy to synthesise. They are derived from simple benzophenones which can be synthesised with commercially available reagents. The original synthesis of phenstatin is described in (Scheme 2). A lithiated aryl bromide (above) was reacted with a silyl protected benzaldehyde to give the corresponding alcohol. Mild oxidation and deprotection of the silyl group afforded the phenstatin (Pettit *et al.*, 2000). It is reported as a feasible method from which potentially active phenstatins (Zhang *et al.*, 2016) (Figure 46) are synthesised (Chen *et al.*, 2013).

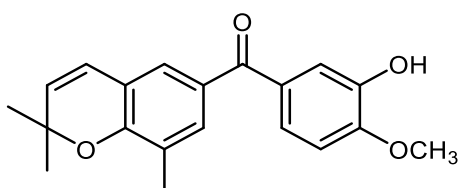


Figure 46: Structure of potentially active phenstatin

Like CA-4 and colchicine, structure activity studies on phenstatin reveals interaction of groups that determine strong activity. Methoxy groups at position 3,4,5 of ring A (Figure 47) is important for activity in CBS, likewise the methoxy group on ring B. The sp^2 carbon of the carbonyl is also essential as it overcome the problem of isomerisation. Position 3 on ring B

substituted with hydroxyl can also tolerate replacement with other groups that are electron withdrawing (**Figure 47**) (Wang *et al.*, 2018a).

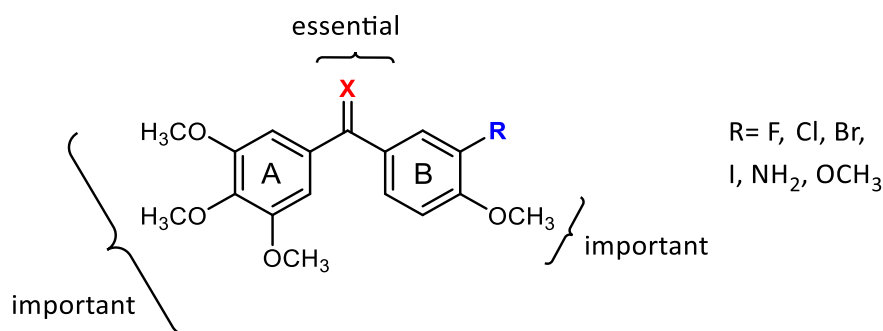


Figure 47: Active groups that contribute to activity of phenstatin with CBS

1.5 β -Diketones as inhibitors of the colchicine binding site and Wnt / β -catenin pathway

β -Diketones belong to the class of 1,3-dicarbonyl compounds with a wide application in organic and inorganic chemistry. Recently, modified derivatives of these compounds have been used in medicinal chemistry (Kljun and Turel, 2017). Also, owing to their chelating properties which enables them to form metal complexes (Shinde *et al.*, 2020); they have been used as important ligands in metal extraction and manufacture of fine materials through chemical vapour deposition (Amano *et al.*, 1993).

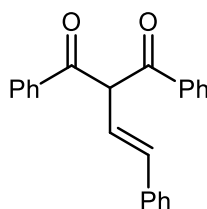


Figure 48: α -Alkenylated analogue of β -diketone used as intermediate to heterocyclic compounds

β -Diketones and their α -alkenylated analogues (**Figure 48**) have been used as medicinal intermediates for the synthesis five membered heterocyclic compounds which show a wide range of biological activities including antimicrobial (Shabalin *et al.*, 2020), antiviral, antidiabetic (Kamal *et al.*, 2015) and anticancer. For example, recently, a derivative of an important substituted β -diketone (**Figure 49**- left) was used as intermediate to synthesise aryl pyrazoles (**Figure 49**- right) showing cytotoxicity on different cancer cell lines including lung

cancer (A549) and breast cancer (MCF-7) which showed lower IC₅₀ values between 0.10 μM and 0.13 μM (Lakkakula *et al.*, 2019).

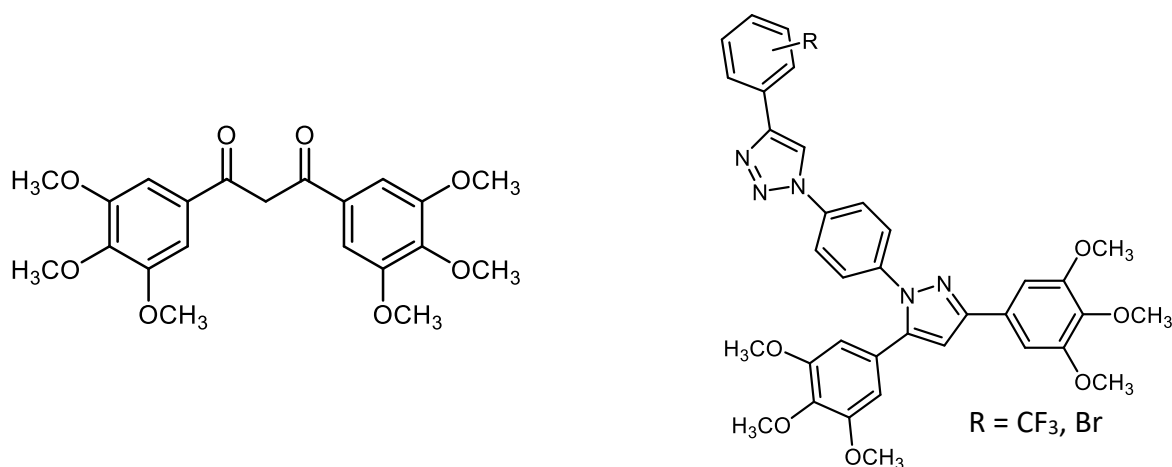


Figure 49: β-Diketone (left) used as intermediate to synthesis of substituted pyrazoles (right)

Because of their reactivity in different conditions, they also form major substrates for the biosynthesis of many compounds found in plants and animals by intramolecular cyclization in basic media; these include bioactive benzopyran derivatives such as chromones, pyrimidines and pyridines (**Figure 50**) (Reis *et al.*, 2017).

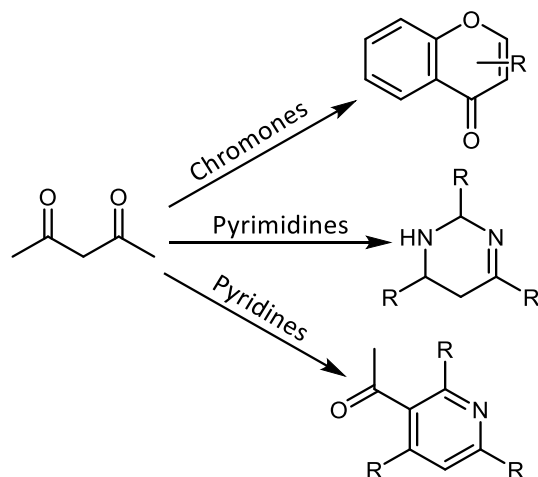


Figure 50: β-diketone as intermediate for synthesis of chromones pyrimidines and pyridines

1.5.1 Naturally occurring β-diketones as anticancer agents

Naturally occurring β-diketones are not very common in nature. However, dicarbonyls with the same functionality and structural scaffolds as the β-diketone constitute the main

structural component of the naturally occurring herbs such as the curcumins (**Figure 51**) and its derivatives (Kljun and Turel, 2017).

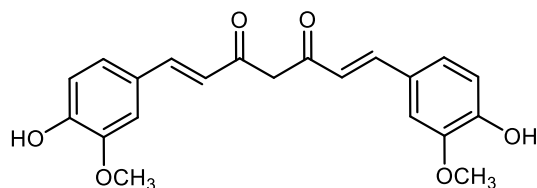


Figure 51: Structure of curcumin

Curcumin (diferuloylmethane) represents the major compound found in roots of plant *Curcuma longa*. Apart from being an antioxidant, curcumin which has a β -dicarbonyl scaffold is believed to be one of the currently known non-toxic compounds that has been clinically tested for anticancer properties (Gupta, Patchva and Aggarwal, 2013).

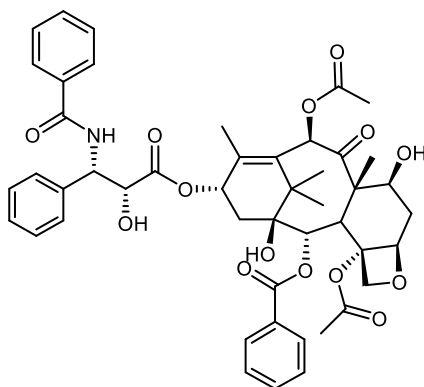


Figure 52: Structure of Taxol

Curcumin also plays an important role in preventing tumour initiations and modulating the synthesis of DNA during cell cycle by activating DNA damaging signals such as Ras and Myc (Bava *et al.*, 2005). Curcumin is used in combination with taxol (Figure 52) to enhance cell cycle arrest at G₀/G₁ and G₂/M stage (**Figure 53**) (Sa and Das, 2008).

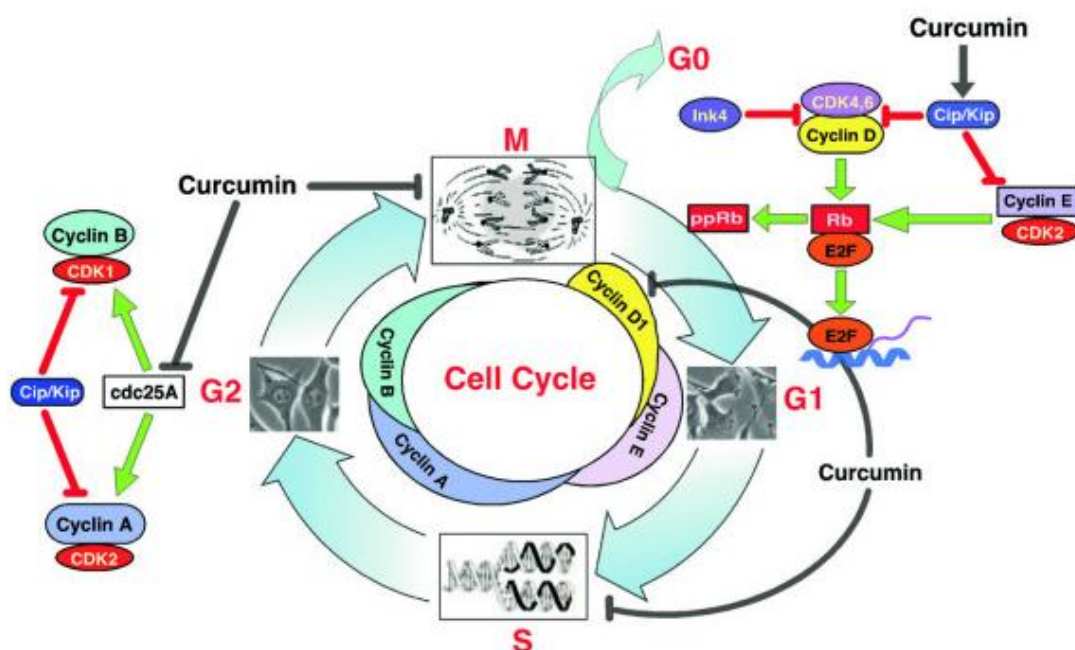


Figure 53: Curcumin activity in modulating cell different stages of cycle progression. Obtained from (Sa and Das, 2008)

Curcumin has been shown to have anticancer activity on different cell lines including pancreatic cancer cells (Sahu, Batra and Srivastava, 2009), breast cancer (Simon *et al.*, 1998; Choudhuri *et al.*, 2002), oesophageal and colorectal cancer (Ryu *et al.*, 2008). Owing to its non-toxic properties and specificity toward targeting cancer cells, it has received considerable attention and is widely studied in animal models (Dorai and Aggarwal, 2004). Based on this property, curcumin and its derivatives have recently entered clinical trials; a daily dosage as much as 4-8 g was safely administered with no harmful effects observed (Cheng *et al.*, 2001). The mechanism through which naturally occurring β -diketones inhibits cancerous cells has not been fully identified. Nevertheless, many studies show that curcumin derivatives of β -diketones can directly or indirectly interact with different proteins and transcription factors in cancer cells (Chakraborti *et al.*, 2011; Gupta *et al.*, 2006).

1.5.2 β -Diketones as inhibitors of tubulin polymerisation

In a cell viability study, it has been shown that curcumin inhibited proliferation of cervical cancer cell lines (HeLa) and breast cancer (MCF-7) cells resulting IC_{50} values of 13.8 μ M and 12.0 μ M. The antimicrotubular activity examined with immunofluorescence microscopy at curcumin concentration of 25 μ M depolymerized microtubules suggesting presence of

activity on tubulin (Gupta *et al.*, 2006). Molecular docking of curcumin with tubulin showed strong hydrogen bond interactions in the colchicine binding site (CBS) (**Figure 54**).

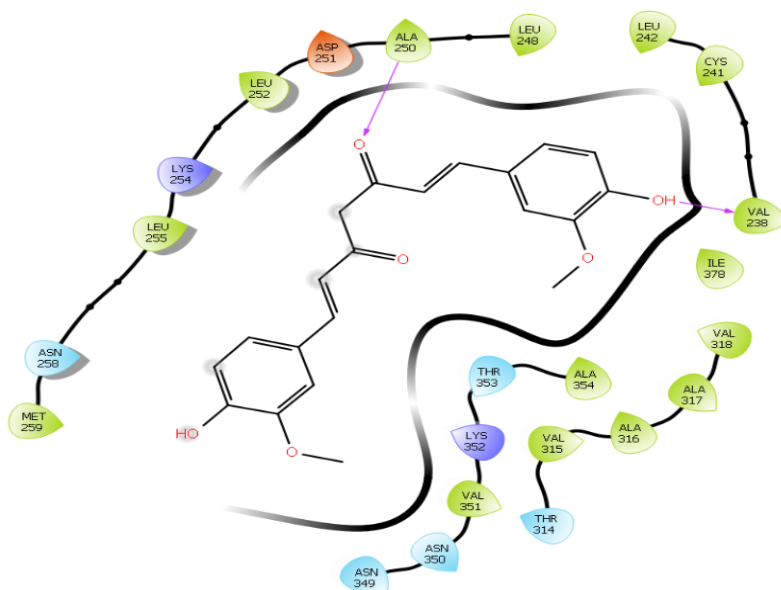


Figure 54: 2D diagram of curcumin interaction in the CBS (Docking score and -6.8 and -7.7)

Two essential interactions including other weak interactions (figure below) with the amino acid residue of the binding site receptor suggests curcumin has a role in depolymerising microtubules. The OH on ring A forms a hydrogen bond with Val238 (2.19 Å), the tautomeric enol also contributes to the formation hydrogen bond interaction with Ala250 (2.64 Å). Other weak interactions with the ligand include the residues Val318, Cys241 and Cys352 (**Figure 55**).

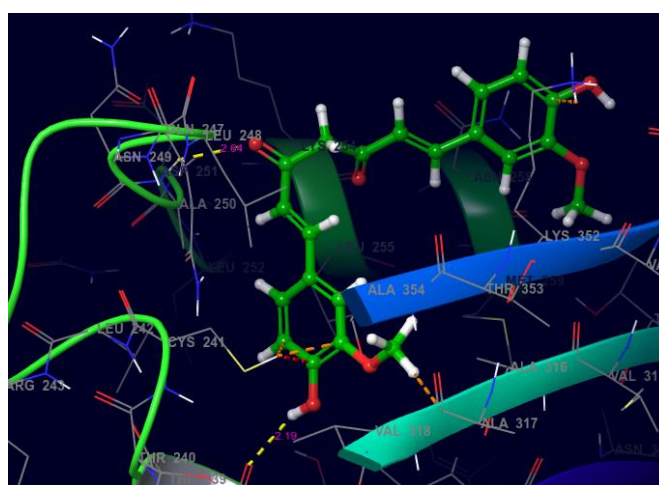


Figure 55: 3D-structure of curcumin interacting in the CBS

1.5.3 Curcumin and modulation of Wnt / β -catenin pathway leading to cancer

1.5.3.1 Wnt / β -catenin signalling pathway

Wnt / β -catenin signalling represents one of the important pathways facilitated by association of different proteins and receptors between the cellular and nuclear membrane in eukaryotic cells. As mentioned earlier, they are among the essential mediators consisting of proteins and protein kinases that regulate transcription factors for cell replication.

In the absence of Wnt activity in a normal cell, β -catenin is phosphorylated by a scaffold of cytoplasmic complex involving Axin and two other kinases, glycogen synthase kinase (GSK-3) and APC (Milad *et al.*, 2020; Cooper, 2019). This process leads to ubiquitylation and hence Wnt undergoes proteasomic degradation that keeps it from translocating into the nuclear environment (**Figure 56**).

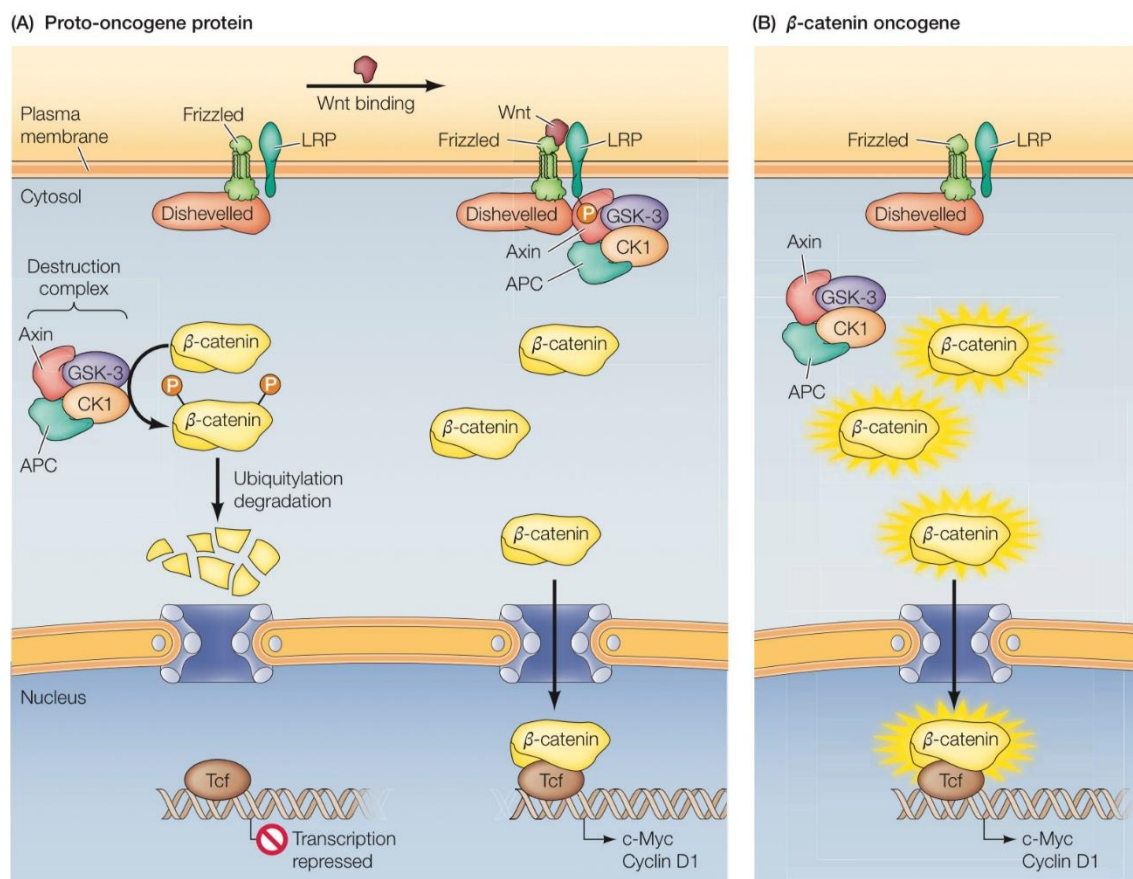
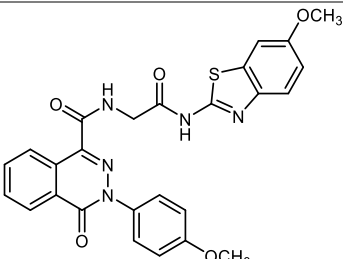
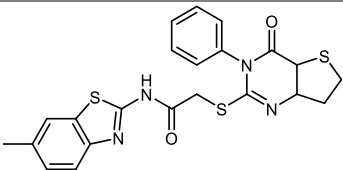
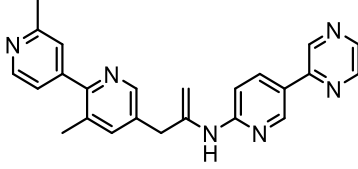
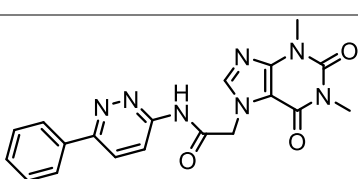


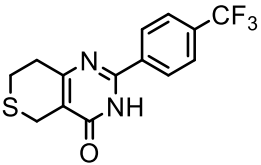
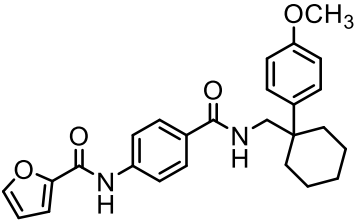
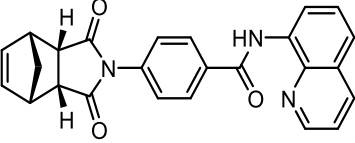
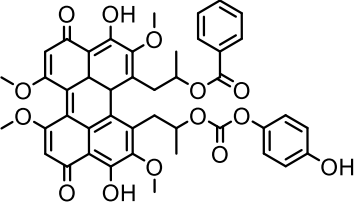
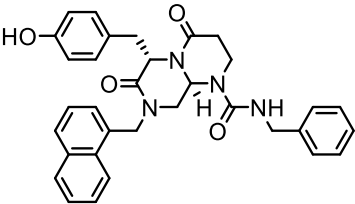
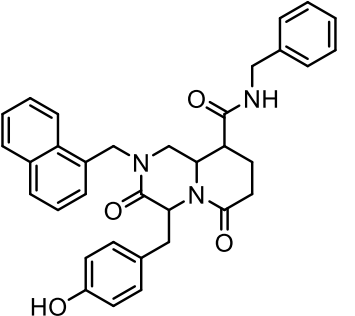
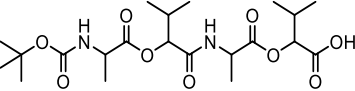
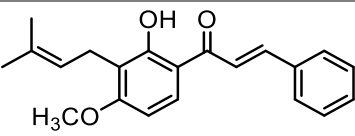
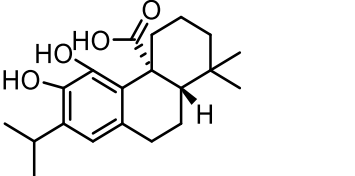
Figure 56: Inhibition and stimulation of transcription of Wnt / β -catenin signalling pathway, adapted from (Cooper, 2019).

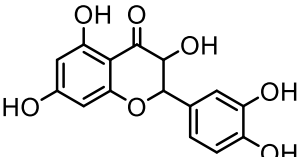
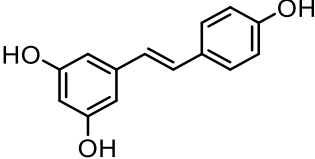
A) Normal Wnt / β -catenin pathway dimerizing Frizzled and LRP to become a proto-oncogene.
B) mutated oncogene formed through Wnt / β -catenin pathway.

On the other hand, Wnt protein bound to Frizzled and LRP membrane receptors dimerize and lead to recruitment of Dishevelled (DVL), which destabilises the scaffolded destruction complex, hence the concentration of free β -catenin in the cytoplasmic environment is increased (Liu *et al.*, 2019). When β -catenin is translocated into the nucleus, it binds with a T-cell factor (Tcf) which acts as a gene repressor and forms a complex. β -Catenin upregulates mutations associated with the absence of Wnt renders it as an oncogene with a mutated versions of either APC, cyclin D1 or c-Myc (Prasad *et al.*, 2009). Recently, most women with breast and cervical cancer and about 85 % of people with colorectal cancer have been detected to have cellular mutations in VEGF (Xu *et al.*, 2013) cyclin D1 and c-Myc related genes (Reyhaneh *et al.*, 2018; Kierszenbaum and Tres, 2016). Several small drugs and naturally occurring compounds that target Wnt / β -catenin pathway have been selected for clinical trials (**Table 2**); each has a specific or multiple target within the cascade of proteins that may be responsible for abnormal accumulation of β -catenin in the nuclear environment (Liu, Takada and Zhu, 2020).

Table 2: Wnt / β -catenin pathway targets currently in different stages of clinical trials

Compound	Structure	Target/ receptor	Corporation	Preclinical/clinical trail	Ref
Small molecule					
IWP-1		Porcupine	Tocris Bioscience	Preclinical	
IWP-2		Porcupine	Tocris Bioscience	Preclinical	
LGK-974		Porcupine	Novartis	Phase I/II: BRAF-mutant Metastatic CRC and Wnt pathway mutations Phase I: Patients with Malignancies Dependent on Wnt Ligands	
ETC159		Porcupine	D3 (Drug Discovery & Development), Biomedical Sciences Institute	Phase I: Safety and Tolerability in advanced Solid tumours	

XAV939		Tankyrase	Novartis	Preclinical
JW55		Tankyrase	Tocris Bioscience	Preclinical
IWR-1		Tankyrase	Tocris Bioscience	Preclinical
PKF-115584		TCF/ β -catenin	Novartis	Preclinical
ICG001		CBP/ β -catenin	Enzo Life Science	Preclinical
PRI-724		CBP/ β -catenin	Prism, Eisai Pharmaceuticals	Phase I/II: Myeloid leukemia, colorectal cancer Phase I: Primary biliary cirrhosis
NSC668036		DVL	Tocris Bioscience	Preclinical
Natural compounds				
Derricin		-	-	Preclinical
Carnosic acid		BCL9/ β -catenin	-	Preclinical

quercetin		-	Dana-Farber Cancer Institute; Quercegen Pharmaceuticals; NIH (USA)	Phase II/III: Thromboembolism Phase I/II: Chronic obstructive pulmonary disease
resveratrol		-	GlaxoSmithKline	Phase I: Colorectal cancer, Cancer metastases, Multiple myeloma
Monoclonal antibody (mAb)/peptide				
	mAb	Frizzled receptor	Onco Med Pharmaceuticals, Bayer	Phase I: Breast cancer, pancreatic cancer, non-small cell lung cancer, solid tumours
OMP-18R5				
	FZD8-Fc fusion protein	Wnt protein	Onco Med Pharmaceuticals, Bayer	Phase I: Liver cancer, pancreatic cancer, ovarian cancer, solid tumours
OMP-54F28				
OTSA 101	mAb	Frizzled receptor	OncoTherapy Science	Phase I: Synovial sarcoma
SAH-BCL9	Peptide	BCL9/ β -catenin	-	Preclinical

1.5.3.2 Mediation of curcumin with proteins and Wnt / β -catenin signalling pathway

Recent reports have experimentally suggested that curcumin has a mode of inhibition which directly or indirectly span across many pathways in cancer progression. It was found that curcumin regulates the required homeostatic level required for different proteins related to signal transduction pathways (Shishodia, 2013). For example, curcumin induces intrinsic and extrinsic pathways that activate apoptosis in cells by mediating with Bcl2 and p53 proteins associated with tumour suppression. Also, curcumin extrinsically mediates with death receptors on cell membrane (DR4, DR5) which elevates the concentration of different intracellular protease enzymes such as Caspases 8, -3 and -7, thus resulting in cell death (Shehzad and Lee, 2013).

Curcumin alone can mediate Wnt / β -catenin pathway and exerts multiple activity on cancer cells (**Figure 57**). One of the pathways include Wnt pathway mediated by cyclin D1 and c-Myc which involves an increase in concentration of SOD enzymes that control elevated levels of ROS thus keeping cells in a well maintained condition (Wang *et al.*, 2018c).

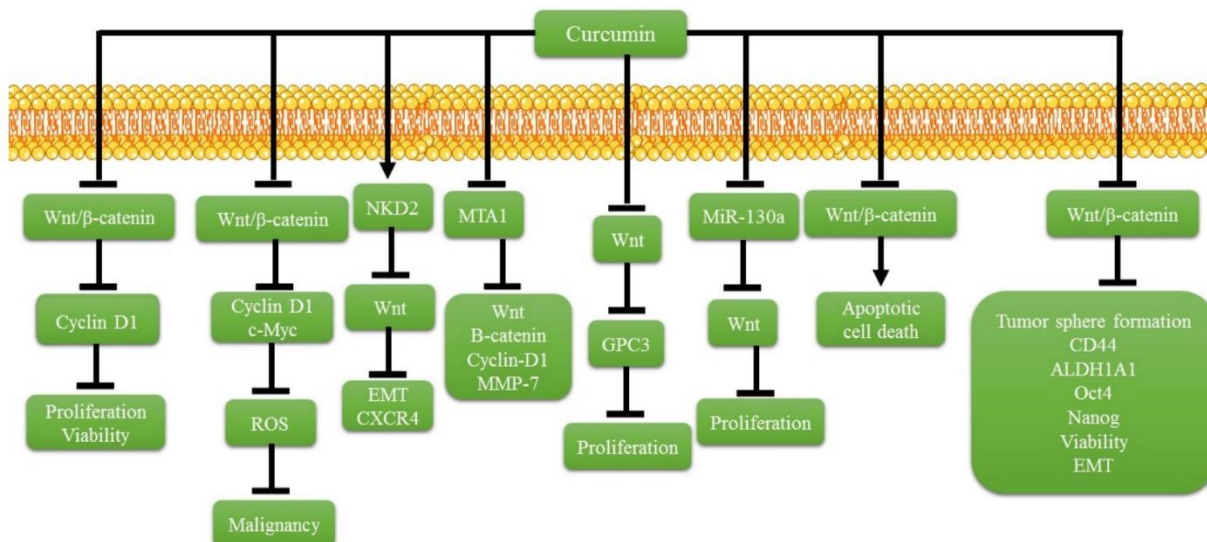


Figure 57: Different wnt / β -catenin pathways targetted by curcumin to inhibit cancer progression. Adapted from (Milad et al., 2020)

Evidence has shown that mutation in GPC3 expression is one of the factors involved in abnormal cell growth and regulation in cancer and is the genesis of most human hepatocellular carcinoma patients (Gao and Ho, 2011). As a result, curcumin also inhibits the Wnt / β -catenin pathway mediated by GPC3 and is shown to be promising in resisting abnormal proliferation due to mutated GPC3 gene in HCC cell lines (Milad *et al.*, 2020).

An insight to the molecular mechanism of curcumin with proteins members in the Wnt / β -catenin pathway reveals that two oxygen atoms in curcumin at the β position are essential for interaction with most amino acid residues, thus showing multiple activities in different pathways (Xu *et al.*, 2013). For example, a structure-based virtual screening analysis of curcumin with Dvl2 (**Figure 58**-left) in the binding pocket forming hydrogen bond interaction with the two tautomeric oxygens of the β -diketone with best scoring function (**Figure 58**).

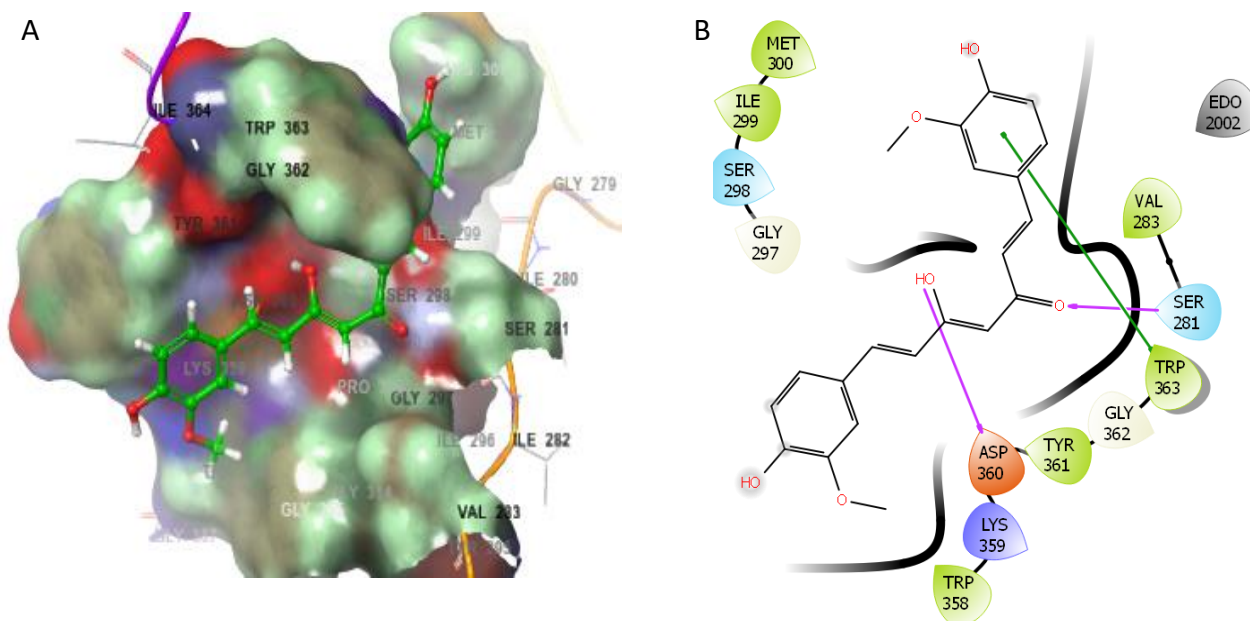


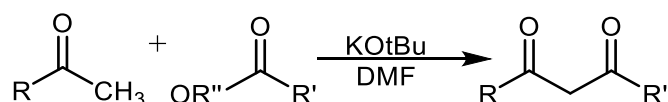
Figure 58: (Left) 3D representation of curcumin interacting with amino acid residues of Dvl2 (PDB ID: 3CBY).

The 2D representation (right) indicates the amino acid residues: Asp360, Trp363 and Ser281 that interact with curcumin . (Xu et al., 2013)

1.6 Overview on synthesis of β -diketones:

Over the past decades, large number techniques and methods for the synthesis of β -diketones and their derivatives have been reported (Alexander, 2003). The focus of these reports is mainly aimed at employing β -diketones as alternative route to isolation of active medicinal compounds. For instance, β -diketones have been widely used as precursors in synthesis of chalcones, flavonoids and heterocyclic compounds (Sambaiah *et al.*, 2017).

Claisen acylation and carbethoxylation of ketones and esters is one of the oldest existing method employed in synthesis of most of β -diketones (Swamer and Hauser, 1950). Although a strong base is used, the method gives high yield of product. The reaction usually employs sodium hydride for the deprotonation, but softer bases have also been used. Yang *et al.*, 2013, have optimized the Claisen acylation method in work by using different bases and solvents. The outcome of the work showed the reaction with sodium hydride as base with THF is the driving factor to achieving Claisen products in higher yield. Sodium hydride as a base in the Claisen reaction will remains the efficient method for synthesis in spite of the flammable nature of this base. (Yang *et al.*, 2019). Wai *et al.*, 2000 also reported a modified procedures for this method with sodium methoxide and potassium *tert*-butoxide (Wai *et al.*, 2000) The method was found to be efficient for yielding both aliphatic and aromatic β -diketones.



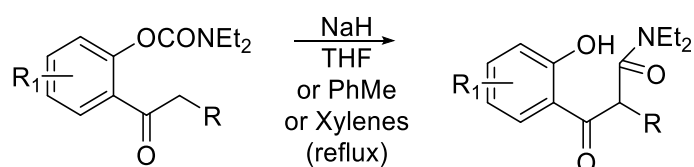
R, R', R'' = alkyl, aryl

Scheme 3: A modified Claisen condensation of ketones to a β -diketone using potassium *tert*-butoxide as a base.

An efficient way of obtaining aliphatic and aromatic β -diketones was also reported according to the same procedure as in (**Scheme 3**). Due to its flexibility and milder conditions, it has been used in synthesising several commercial diketones with sterically hindered substituted such as 2,2,6,6-tetramethyl-3,5-heptanedione (Nandurkar *et al.*, 2007).

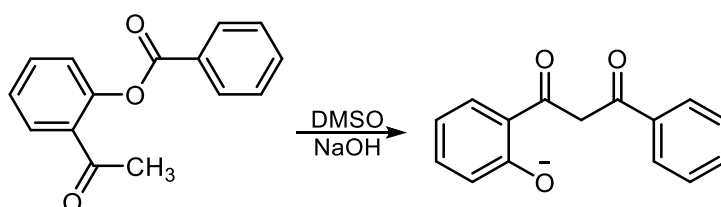
Baker-Venkataraman is also one of the most efficient methods that allows rapid synthesis of β -diketones and many classes of natural product-like compounds such as flavones and chromones (Gomes *et al.*, 2009; Kalinin *et al.*, 1998). The method employs *o*-benzoyloxyacetophenones to undergo a base-catalysed intermolecular Claisen condensation

of esters and ketones to produce β -diketones (Scheme 4). The advantage of this method is that it allows the use of different solvents of choice giving high yields of product. This method also gives reasonable yields under microwave conditions which can improve the reaction time compared to the classical methods (Ameen and Snape, 2015).



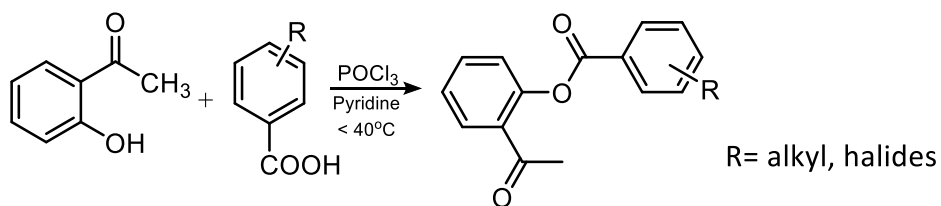
Scheme 4: Optimisable Baker-Venkataraman conversion of aromatic esters to β -diketones

A rapid method for the preparation of β -diketones like the Baker-Venkataraman rearrangement has been reported by Wallet and Gaydou (1996) using a phenyl benzoate through dibenzoylation. It is a fast and efficient method which does not require heating throughout the entire process. However, isolation of product from larger volume of reaction could be difficult with DMSO as solvent (Scheme 5).

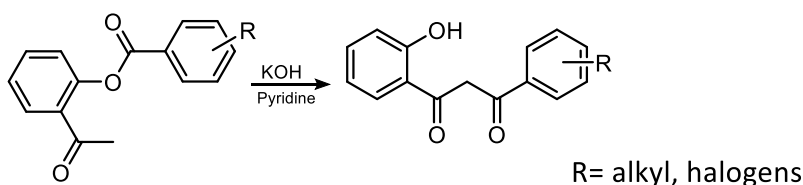


Scheme 5: Baker-Venkataraman rearrangement of phenylbenzoate to β -diketone using DMSO as solvent

Likewise, substituted β -diketones bearing halogenated substituents were synthesised by a rapid method from acetophenones and aromatic acids to give the corresponding benzoate in two steps (Scheme 6 and Scheme 7) (Sartape, Gadde and Salunkhe, 2015). Reports that employed a similar procedure showed that the method is associated with purification problems related to isolation of product from pyridine (Bansal *et al.*, 2017).

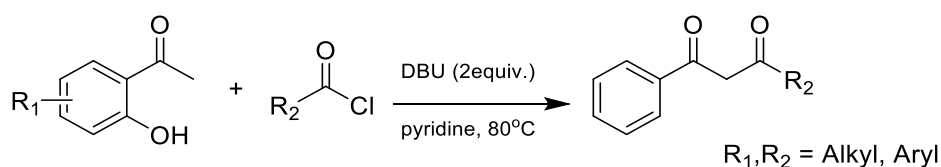


Scheme 6: Isolation of aromatic esters from aromatic acetophenone and carboxylic acid



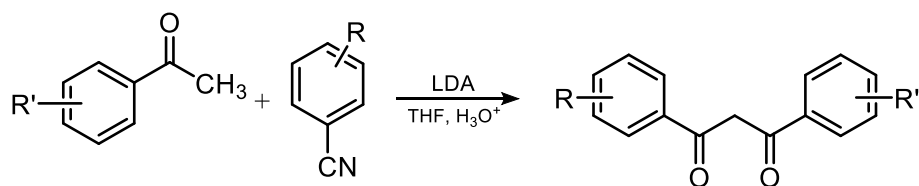
Scheme 7: Rearrangement of aromatic ester into β -diketone.

Similarly, β -diketones have been also synthesised by refluxing *o*-hydroxyacetophenone with aroyl chlorides with dry potassium carbonate. In this method different methoxy substituents containing *o*-hydroxyacetophenones were treated with potassium hydroxide or potassium carbonate. The method has been employed in preparing β -diketones under microwave conditions in the presence of 1,8-Diazabicyclo[5.4.0]undec-7-ene (DBU) as base and pyridine as solvent (Abdel Ghani *et al.*, 2008). One of the drawbacks related with this method is the difficulty of isolating the compound from the excess of pyridine., and therefore considered unreliable solvent of choice (Scheme 8).



Scheme 8: Modified Baker-Venkataraman synthesis of β -diketone bearing alkyl and aryl groups from DBU and pyridine

A more efficient method that overcomes the use of high boiling point solvents was employed by Jae *et al.*, 2005. An acetophenone and benzoyl cyanide gave β -diketones by condensation in the presence of lithium diisopropylamide (LDA) (Scheme 9). This method employs THF, and thus serves as an efficient alternative to pyridine and DMSO (Lee and Son, 2005).



Scheme 9: A modified route to preparation of β -diketone using THF as solvent

Recently, most of the papers reviewed on synthesis of β -diketones relied on procedures that avoid the use of solvents with higher boiling points. Therefore, the method used for the preparation of most β -diketones for this thesis relied on the use of THF and inorganic bases to achieve easy extraction and purification from solvents.

1.7 Aims and objectives

Despite the interest of many researchers on anticancer activity of curcumin and its excellent profile as one of the non-toxic compounds, its lack of solubility and bioavailability in the target receptor poses challenge for its clinical development. Reducing the bridge length and introducing different groups on the two aromatic rings (Figure 59) offers a rational approach in drug design (Ghinet *et al.*, 2013) and development. Introducing electron withdrawing groups (EWG) and electron donating groups (EDG) at different positions of ring A and B will provide β -diketones with the potential to offer anticancer activity.

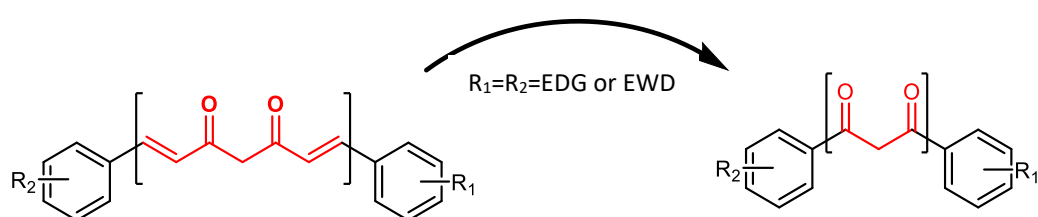


Figure 59: Replacement of the olefinic length of curcumin chain in β -diketone

Hepta-1,6-diene-3,5-dione replaced with 1,3-diphenylpropane-1,3-dione bearing different substituents of R_1 and R_2 on the dibenzoyl rings.

The aim of this thesis is to synthesise and characterise novel β -diketone analogues and investigate their anticancer activity on different cell lines. These cell lines include: lung carcinoma cell line (A549), hepatocellular carcinoma (HepG2), Rhabdomyosarcoma (A204), cancerous cervical cancer cells (HeLa) and osteosarcoma epithelial cells (U2Os). Effects of

some selected β -diketones and benzoylthioureas will be determined on three different leukaemia cell lines in order to widen the scope of their activity of different cancer cell lines. The project will also explore the molecular interactions between the active analogues and the colchicine binding site of tubulin by docking analysis. This will enable to identify amino acid residues that are essential for interaction with these compounds.

The objective of the thesis is as follows:

1. To synthesise novel analogues of β -diketones and benzoylthiourea bearing different substituents on the rings.
2. To evaluate the cytotoxicity of synthesised compounds on different cell lines by MTT assay.
3. To conduct a molecular docking analysis to identify the amino-acid residues that that bind with these molecules in the colchicine binding site of tubulin.

CHAPTER TWO

Materials and Methods

Chapter two

2.0 Materials and Methods

2.1 Synthesis and purification of 1,3-diketones

All reagents and chemicals were obtained from Fluorochem Ltd, Apollo Scientific Ltd and Thermo Fisher Scientific.

Chromatography

Thin-layer chromatography (TLC) was carried out on pre-coated silica gel (0.20 mm) with fluorescent indicator UV₂₅₄. TLC spots are observed with a handheld UV lamp (UVGL-58 LW/SW) viewed under a fluorescent analysis cabinet (Spectroline model CM-10). Flash chromatography was carried out with silica gel of high purity grade having a pore size of 60 Å, 220-440 mesh particle size, 35-75 μm particle size from Fluka.

Melting points:

Melting points are uncorrected and were recorded with Electrothermal MP apparatus and a Stuart Digital® melting point apparatus model number SMP20. A preliminary melting point for each sample was determined, and the exact melting point was recorded in triplicate.

NMR spectrometer:

Bruker AC-400 MHz and 600 MHz NMR spectrometer was used to obtain the spectra for proton (¹H), fluorine (¹⁹F), carbon (¹³C) and nitrogen (¹⁵N) NMR and related techniques such as attached proton test (APT), distortionless enhancement by polarization transfer (DEPT) and 2D (COSY, HMQC and HMBC). Deuterated chloroform (CDCl₃) was used as solvent unless stated otherwise. Chemical shift (δ) of spectra were reported in parts per million (ppm), coupling constants (*J*) were presented in (Hz); patterns of in ^δH were reported as singlets (s), doublets (d), triplets (t), quartets (q) and multiplets (m). The position of atoms in the structures are numbered e.g. (1,2...1'2'.... or 1'', 2''...); these numbers will be used to address the chemical shifts assigned for each peak. Topspin 3.6.1 and Topspin 4.1.0 software was used for analysing all NMR data.

Mass spectrometer:

High resolution mass spectra (HRMS) data were obtained from the Cambridge analytical services, department of chemistry, UK, by using methanolic solutions (50% MeOH: 50% H₂O) on a 6200 Series TOF and 6500 series Q-TOF with electron spray as ionisation method (ESI).

Infra-red (IR):

Absorption spectra for all compounds was acquired using Compact Bruker ALPHA II Platinum-ATR and ThermoScientific Nicolet iS10 connected to a terminal with OMNIC Software version 8.3 and 9.0. Data for all compounds was recorded as frequencies of absorption for all compounds in reciprocal centimetres (cm^{-1}) against transmittance (%). During collection of data, a background is run first, then the sample is run. The background (CO_2) is subtracted from sample to give the IR data.

Microwave reactor:

Microwave synthesiser Discover SP, CEM corporation (programmable temperature range: 0 - 300 °C, maximum power output: 0 - 300 W (± 30 W/min) and reaction vials of volumes 10 ml and 50 ml were used for all reactions.

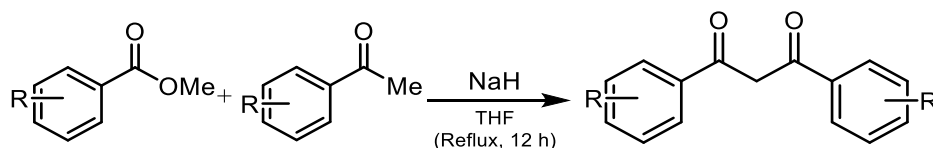
Cell viability assay (MTT):

MultiScan Ascent Thermo Fisher Scientific was used for reading 96-well plates (flat well – Lot 1020121 (SARSTEDT) between absorption range of 540 nm – 640 nm.

2.1.1 Synthesis of 1,3-diketones, benzoyl thiourea and intermediates:

General procedures

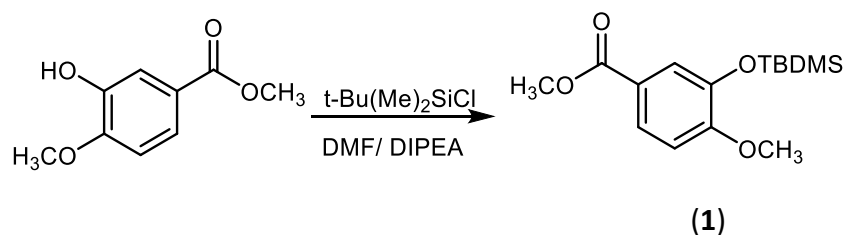
Procedure A:



Following the methods described by Dubrovina (Dubrovina *et al.*, 2003; Jin *et al.*, 2011) To a mixture of sodium hydride (60% in oil) (8.9 mmol, 3.0 eq) in THF (15 ml) under nitrogen at 0°C a ketone (3.0 mmol, 1.0 eq) in THF (15 ml) was added dropwise. After 10 minutes, ester (3.0 mmol, 1.12 eq) in THF (15 ml) was added dropwise and stirring was continued. After 30 minutes, the reaction mixture was brought to room temperature, heated under reflux for 16 hours, and monitored by TLC. After completion of the reaction was confirmed, the reaction mixture was poured into ice water (150 g) and acidified with 1.0 M hydrochloric acid (HCl). The organic layer was extracted with ethyl acetate (3 x 50 ml), washed with brine and (2 x 50 ml) and dried with magnesium sulphate (MgSO₄) and concentrated *in vacuo*. The residue was purified by column chromatography and / or recrystallised.

Procedure B:

Methyl 3-((tert-butyldimethylsilyl)oxy)-4-methoxybenzoate (**1**)



A solution of methyl-3-hydroxy-4-methoxybenzoate (0.4 g, 2.2 mmol, 1 eq) in dry DMF (35 ml) under argon was cooled to 0 °C and N,N-diisopropylethylamine (DIPEA) (0.57g , 4.4 mmol, 2 eq) was added. t-Butyldimethylsilyl chloride (TBDMS) (0.37 g, 2.7 mmol, 1.12 eq) was added over a period of 30 minutes and allowed to warm to room temperature for 1 hour. After 4 hours, the reaction mixture was poured into ice (150 g) and extracted with diethyl ether (3 x 60 ml). The combined extracts were washed with brine (2 x 60 ml), dried with MgSO₄ and the solvent removed *in vacuo*. The residue was purified by column chromatography to give a yellow oily product (Nagarathnam and Cushman, 1991). (0.37 g, 1.25 mmol, 93 %)

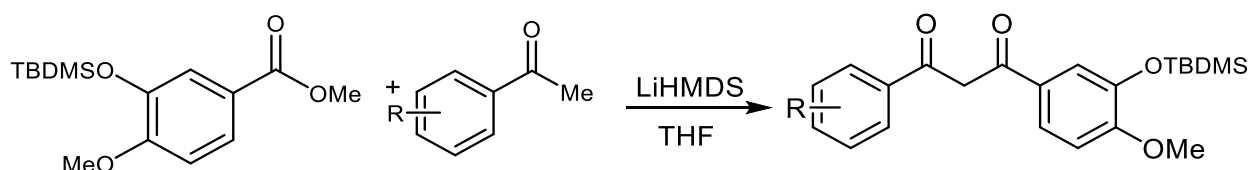
R_f: 0.27 (Hex: EtOAc 8:2)

¹H NMR (CDCl₃, 400 MHz): 0.0 (6 H, s, Si-CH₃), 0.83 (9 H, s, C(CH₃)₃), 3.69 (3 H, s, 4-OCH₃), 3.71 (3 H, s, O=C-OCH₃), 6.70 (1 H, d, J = 8.4 Hz, 5-H), 7.35 (1 H, d, J = 2.1 Hz, 2-H), 7.51 (1 H, dd, J = 8.4 Hz, 2.1 Hz, 6-H)

¹³C NMR (CDCl₃, 100 MHz): -4.65 (2 C, 1'), 18.4 (1 C, 2'), 25.7 (3 C, 3' 4',5-CH₃), 5.19 (1 C, OCH₃, 2''), 55.4 (1 C, OCH₃, 4), 110.9 (1 C, 5), 121.9 (1 C, 2), 122.7 (1 C, 3), 124.3 (1 C, 6), 144.6 (1 C, 3), 155.1 (1 C, 4), 166.8 (1 C, 1'').

IR ν_{max} : 2939, 2842, 1705 (C=O), 1584, 1506, 1546, 1435, 1284

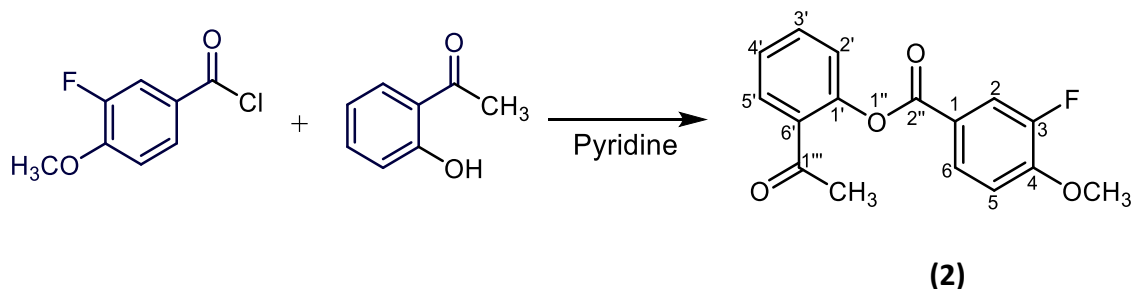
Procedure C:



A solution of lithium hexamethyldisilane in THF (1 M, 0.5 g, 2.9 mmol, 2.0 eq) (15 ml) was added dropwise to a stirred solution acetophenone (0.3 g, 1.48 mmol) in THF (15 ml) under argon atmosphere at -78 °C. After 1 hour, a solution of silyl protected ester (0.5 g, 1.48 mmol, 1.0 eq) in THF (15 ml) was added dropwise. Stirring was continued for 1 hour at -78 °C and 36 – 48 hours at room temperature and monitored with TLC. The reaction mixture was poured into ice (100 g), acidified with 1 M HCl (5 ml) and extracted with chloroform (3 x 60 ml). The combined extract was dried with MgSO₄ and concentrated *in vacuo*. The crude product was purified with column chromatography to give a diketone.

Procedure D:

A solution of acetophenone (1 g, 7.35 mmol, 1.00 eq) and 3-fluoro-4-methoxybenzoyl chloride (1.94 g, 10.28 mmol, 1.40 eq) in pyridine (10 ml) was stirred at room temperature. After 20 minutes, the reaction mixture was added to a crushed ice (100 g) containing 1 M HCl (30 ml) and stirred for 10 minutes. The precipitate was filtered and washed with cold methanol (10 ml) and cold water (10 ml). Recrystallisation from ethanol afforded the ester.



M.P: 96 - 98 °C;

δ_{H} (CDCl₃, 400 MHz): : 2.47 (3 H, s, 1'''-CH₃), 3.92 (3 H, s, 4-OCH₃), 7.02 (1 H, t, J = 8.35 Hz, 5), 7.16 (1 H, dd, J = 8.21 Hz, 1.01 Hz, 2'), 7.32 (1 H, dt, J = 7.60 Hz, 0.99 Hz, 4'), 7.54 (1 H, dt, J = 7.77 Hz, 1.65 Hz, 3'), 7.80 (1 H, dd, J = 7.76 Hz, 1.65 Hz, 6), 7.86 (1 H, dd, J = 11.65 Hz, 1.97 Hz, 2), 7.94 (1 H, d, J = 8.51 Hz, 5').

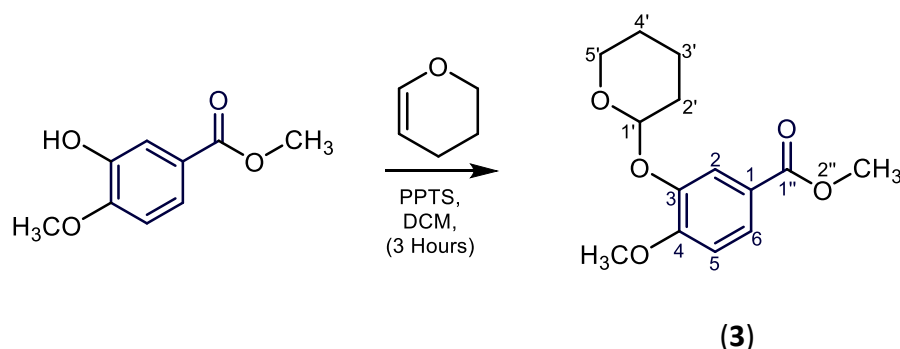
δ_{C} (CDCl₃, 100 MHz): 30.9 (1 C, 1'''-CH₃), 56.4 (1 C, 4-OCH₃), 112.7 (1 C, d, J = 2.01 Hz, 5), 118.0 (1 C, d, J = 20.3 Hz, 2), 121.9 (1 C, d, J = 6.17 Hz, 1), 123.9 (1 C, 2'), 126.2 (1 C, 4'), 127.7 (1 C, d, J = 3.36 Hz, 6), 130.3 (1 C, 3') 150.6 (1 C, 1'), 152.6 (1 C, d, J = 10.6 Hz, 4), 153.1 (1 C, d, J = 247.7, 3), 197.5 (1 C, 2''), 207.0 (1 C, 1''').

m/z HRMS (ESI) [M + H]: Calculated for C₁₆H₁₄FO₄ 289.0871, found 289.0878 ((Δ M_s=2.44 ppm)

IR ν_{max} : 2923 (C-H), 1738 (C=O).

Procedure E:

Methyl 4-methoxy-3-((tetrahydro-2H-pyran-2-yl)oxy)benzoate



Methyl-3-hydroxy-4-methoxybenzoate (2.73 g, 15.0 mmol, 1 eq) was reacted with 0.25 g pyridinium p-toluenesulfonate (0.25, 1 mmol, 0.07 eq) and 3,4-dihydro-2H-pyran (3.36 g, 40 mmol, 2.67 eq) in dichloromethane (30 ml) and stirred at room temperature overnight. After the completion of reaction was confirmed by TLC (Hexane: EtOAc 8:2), the reaction mixture was washed with 1 M NaHCO₃ solution (30 ml x 2), and brine (30 ml), dried with MgSO₄, and solvent was evaporated under reduced pressure to give a crude colourless product. Purification with column chromatography afforded a pure white product (Hexane: EtOAc 8:2). (1.21 g, 4.54 mmol, 44 %).

M.P: 96 - 98 °C; **R_f:** 0.31; (Hex:EtOAc 8:2);

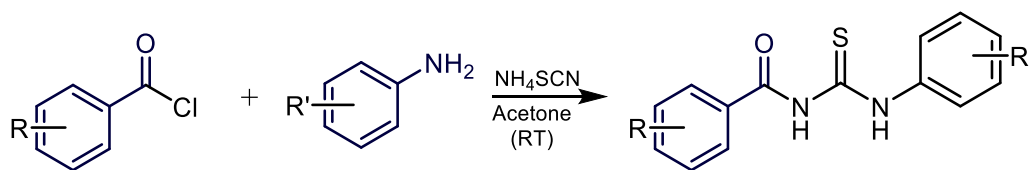
δ_H (CDCl₃, 400 MHz): 1.16 – 2.08 (6 H, m, 2', 3', 4'), 3.61 – 4.03 (2 H, m, 5'), 3.89 (3 H, s, 4-OCH₃), 3.92 (3 H, 2''-CH₃), 5.49 (1 H, t, J = 3.20 Hz, 1'), 6.93 (1 H, d, J = 8.47 Hz, 5), 7.75 (1 H, dd, J = 8.53 Hz, 2.05 Hz, 6), 7.80 (1 H, d, 2.04 Hz, 2).

δ_c (CDCl₃, 100 MHz) 18.8 (1 C, 3'), 25.2 (1 C, 4'), 30.2 (1 C, 2'), 51.9 (1 C, 2''-CH₃) 56.0 (1 C, 4-OCH₃), 62.2 (1 C, 5'), 97.5 (1 C, 1'), 111.1 (1 C, 5), 118.7 (1 C, 2), 122.7 (1 C, 1), 125.0 (1 C, 6), 145.7 (1 C, 3), 154.3 (1 C, 4), 166.8 (1 C, 1'').

m/z HRMS (ESI) [M + H]: Calculated for C₁₄H₁₈O₅ 267.1227, found 267.1207 (ΔMs=2.44 ppm)

IR **ν_{max}:** 3015 (C-H), 1715 (C=O), 1165 (C-O)

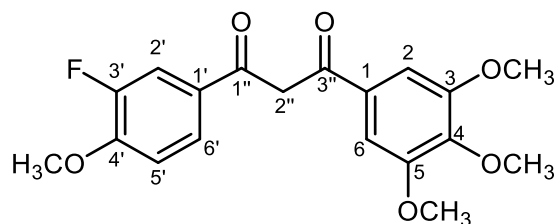
Procedure F:



A solution of acid chloride (1 mmol, 1 eq) in dry acetone (15 ml) was added dropwise to a solution of ammonium isothiocyanate (1 mmol, 1 eq) in acetone (15 ml). The mixture was stirred for 5 minutes until precipitate of isothiocyanate was formed. A solution of amine (1 mmol, 1 eq) in acetone (10 ml) was added slowly. The reaction mixture was refluxed for 30 minutes and allowed to stir at room temperature for 5 hours. The solvent was removed under reduced pressure and the product was recrystallised.

2.1.2 Synthesis of β -diketones:

1-(3-Fluoro-4-methoxyphenyl)-3-(3,4,5-trimethoxyphenyl) propane-1,3-dione (4)



(4)

Compound (4) above was synthesised from 3-fluoro-4-methoxy acetophenone (0.5 g, 2.97 mmol) and methyl-3,4,5-trimethoxybenzoate (0.85 g, 3.75 mmol) and sodium hydride as in procedure A. Following column chromatography (Hex: EtOAc 7:3) and recrystallisation from ethanol the title compound (4) was isolated as yellow crystals (0.71 g, 1.93 mmol, 65 %).

M.P: 122 – 125 °C; **Rf:** 0.28 (Hex:EtOAc 8:2);

δ_H (CDCl₃, 400 MHz): 3.96 (3 H, s, OCH₃, 4), 3.98 (6 H, s, 2 x OCH₃, 3, 5), 4.00 (3 H, s, OCH₃, 4'), 6.68 (1 H, s, 2''), 7.09 (1 H, t, $J = 8.24$ Hz, 5'), 7.23 (2 H, s, 2, 6), 7.76 (1 H, d, $J = 12.4$ Hz, 1.8 Hz, 2'), 7.81 (1 H, d, $J = 8.4$ Hz, 6'), 17.06 (1 H, s, enolic H)

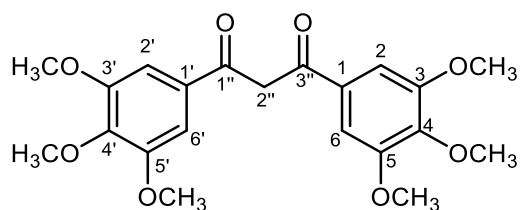
δ_C (CDCl₃, 100 MHz): 56.3 (1 C, OCH₃, 4'), 56.4 (2 C, OCH₃, 3, 5), 61.0 (1 C, OCH₃, 4), 92.2 (1 C, 2''), 104.5 (2 C, 2, 6), 112.7 (1 C, d, $J = 1.89$ Hz, 5'), 115.0 (1 C, d, $J = 20.3$ Hz, 2'), 124.1 (1 C, d, $J = 3.16$ Hz, 6'), 128.5 (1 C, d, $J = 5.94$ Hz, 1'), 130.8 (1 C, 1), 142.1 (1 C, 4), 151.4 (1 C, d, $J = 10.53$ Hz, 4'), 153.2 (2 C, 3, 5), 153.3 (1 C, d, $J = 257.85$ Hz, 3'), 183.8 (1 C, d, $J = 1.81$ Hz, 3''), 185.0 (1 C, 1'').

δ_F (400 MHz): -134.1 (1 F, dd, $J = 8.3$ Hz, 3.7 Hz, 3')

HRMS (ESI-TOF) m/z: [M+H] Calculated for C₁₉H₁₉FO₆ 363.1238; found 363.1248 ($\Delta M_s = 2.71$ ppm)

IR ν_{max} : 3366 (enolic OH), 2940 (C-H), 1632 (C=O).

1,3-Bis(3,4,5-trimethoxyphenyl) propane-1,3-dione (5)



5

This compound has been synthesised by Choshi *et al.*, 1992. 3,4,5-Trimethoxy acetophenone (0.85 g, 4.03 mmol) and methyl-3,4,5-trimethoxybenzoate (1.15 g, 5.09 mmol) and sodium hydride (0.29 g, 12.13 mmol) were reacted as in procedure A. Following column chromatography (Hex:EtOAc 7:3) and recrystallisation from ethanol compound (5) was isolated as yellow crystals (1.20 g, 2.96 mmol, 73 %).

M.P: 161 – 163 °C; lit: 154-155 °C (Choshi *et al.*, 1992); **R_f:** 0.37 (Hex:EtOAc 7:3);

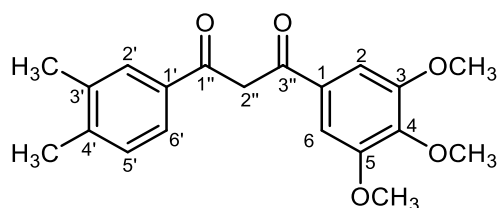
δ_H (CDCl₃, 400 MHz): 3.95 (6 H, s, 2 x OCH₃, 4, 4'), 3.97 (12 H, s, 4 x OCH₃, 3, 5, 3', 5'), 6.67 (1 H, s, 2''), 7.22 (4 H, s, 2, 6, 2', 6'), 17.06 (1 H, s, enolic H).

δ_C (CDCl₃, 100 MHz): 56.5 (4 C, OCH₃, 3, 5, 3', 5'), 61.09 (2 C, OCH₃, 4, 4'), 92.7 (1 C, 2''), 104.8 (4 C, 2, 6, 2', 6'), 130.9 (4 C, 3, 5, 3', 5'), 142.2 (2 C, 4, 4'), 153.3 (2 C, 1, 1'), 185.1 (2 C, 1'', 3'').

HRMS (ESI-TOF) m/z: [M+H] Calculated for C₂₁H₂₄O₈; 404.1471 found 404.1493. (ΔMs=3.70 ppm)

IR ν_{max}: 3108 (enolic OH), 1606 (C=O), 1553 (C=C).

1-(3,4-Dimethylphenyl)-3-(3,4,5-trimethoxyphenyl) propane-1,3-dione (6)



6

Compound (6) above was synthesised from 3,4-dimethyl acetophenone (0.5 g, 3.30 mmol) and methyl-3,4,5-trimethoxybenzoate (0.70 g, 3.11 mmol) and sodium hydride (0.24 g, 9.90 mmol) as in procedure A. Following column chromatography (Hex:EtOAc 8:2) and recrystallisation from ethanol compound (6) was isolated as yellow crystals (0.55 g, 1.60 mmol, 49 %).

M.P: 112 – 115 °C; **R_f:** 0.32 (Hex:EtOAc 8:2);

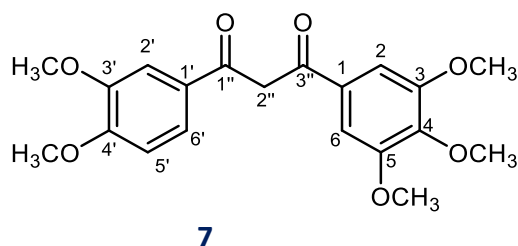
δ_H (CDCl₃, 400 MHz) : 2.36 (3 H, s, 3'CH₃), 2.37 (3 H, s, 4'-CH₃), 3.96 (3 H, s, OCH₃, 4), 3.98 (6 H, s, 2 x OCH₃ 3, 5), 6.76 (1 H, s, 2''), 7.25 (2 H, s, 2, 6), 7.27 (1 H, d, *J* = 8.2 Hz, 5'), 7.75 (1 H, dd, *J* = 8.2 Hz, 2.4 Hz, 6'), 7.78 (1 H, d, *J* = 2.4 Hz, 2'), 17.07 (1, s, enol).

δ_C (CDCl₃, 100 MHz): 19.8 (1 C, CH₃, 4'), 20.0 (1 C, CH₃, 3'), 56.4 (2 C, OCH₃, 3, 5), 61.0 (1 C, OCH₃, 4), 92.6 (1 C, 2''), 104.6 (2 C, 2, 6), 124.7 (1 C, 6'), 128.2 (1 C, 2'), 130.0 (1 C, 1), 131.2 (1C, 5'), 132.9 (1 C, 1'), 137.1 (1 C, 3'), 141.9 (1 C, 4'), 142.0 (1 C, 4), 153.2 (2 C, 3, 5), 185.0 (1 C, 3''), 185.7 (1 C, 1'').

HRMS (ESI-TOF) m/z: [M+H] Calculated for C₂₁H₂₄O₈; 343.1540 found 343.1539 (ΔM_s=0.25 ppm)

IR ν_{max}: 3114.5 (enolic OH), 1558 (C=O),

1-(3,4-Dimethoxyphenyl)-3-(3,4,5-trimethoxyphenyl) propane-1,3-dione (7)



Compound (7) above was synthesised from 3,4-dimethoxy acetophenone (0.5 g, 2.77 mmol) and methyl-3,4,5-trimethoxybenzoate (0.96 g, 4.30 mmol) and sodium hydride (0.27 g, 9.50 mmol) as in procedure A. Followed column chromatography (Hex:EtOAc 8:2) and recrystallisation from ethanol afforded compound (7) as yellow crystals (0.72 g, 1.60 mmol, 70 %).

M.P: 115 – 117 °C; **R_f**:0.25; (Hex:EtOAc 7:3);

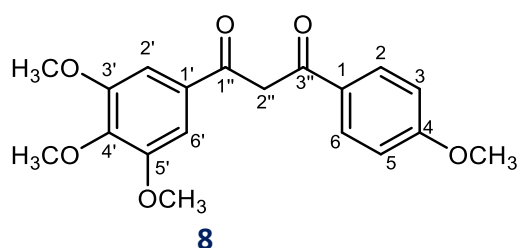
δ_H (CDCl₃, 400 MHz): 3.86 (3 H, s, OCH₃, 4), 3.88 (6 H, s, 2 x OCH₃, 3, 5), 3.89 (3 H, s, OCH₃, 3'), 3.91 (3 H, s, OCH₃, 4'), 6.64 (1 H, s, 2''), 6.88 (1 H, d, *J* = 8.41 Hz, 5'), 7.14 (2 H, s, 2, 6), 7.50 (1 H, d, *J* = 1.90 Hz, 2'), 7.55 (1 H, dd, *J* = 8.41 Hz, 1.90 Hz, 6'), 17.11 (1 H, s, enolic).

δ_C(CDCl₃, 100 MHz): 56.1 (2 C, OCH₃, 3', 4'), 56.4 (2 C, OCH₃, 3, 5), 61.0 (1 C, OCH₃, 4), 92.2 (1 C, 2''), 104.5 (2 C, 3, 5), 109.8 (1 C, 2'), 110.4 (1 C, 5'), 121.2 (1 C, 6'), 128.4 (1 C, 1'), 130.9 (1 C, 1), 141.9 (1 C, 4), 149.2 (1 C, 3'), 152.9 (1 C, 4'), 153.2 (2 C, 3, 5), 183.9 (1 C, 3''), 185.7 (1 C, 1'').

***m/z* HRMS (ESI) [M + H]:** Calculated for C₂₀H₂₂O₇; 375.1438 found 375.1441 (ΔM_s=0.73 ppm)

IR ν_{max}: 3023.1 (enol OH), 1595.9 (C=O).

1-(4-Methoxyphenyl)-3-(3,4,5-trimethoxyphenyl) propane-1,3-dione (8)



Compound (8) above was synthesised from 4-methoxy acetophenone (0.5 g, 3.33 mmol) and methyl-3,4,5-trimethoxybenzoate (0.75 g, 3.66 mmol) and sodium hydride (0.23 g, 9.90 mmol) as in procedure A. Following column chromatography (Hex:EtOAc 7:3) and recrystallisation from ethanol compound (8) was isolated as bright yellow solid (0.64 g, 1.60 mmol, 70 %).

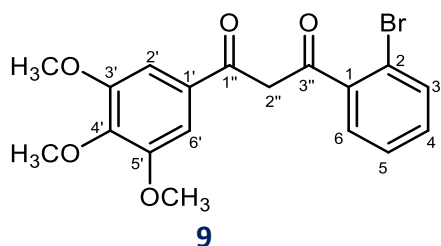
M.P: 124 – 126 °C; Lit mp 127-128 °C (Wallet and Gaydou, 1996); **R_f:** 0.32; (Hex:EtOAc 7:3);

δ_{H} (CDCl₃, 400 MHz): 3.95 (6 H, s, 4,4'-OCH₃), 3.97 (6 H, s, 3',5'-OCH₃), 6.74 (1 H, s, 2''-H), 6.94 (2 H, d, *J* = 8.40 Hz, 3,5-H), 7.55 (2 H, s, 2'6'-H), 7.61 (2 H, d, *J* = 8.40 Hz, 2,6-H), 17.15 (1 H, s, enolic).

δ_{C} (CDCl₃, 100 MHz): 56.1 (4 C, OCH₃, 3, 3', 5' 4'), 91.7 (1 C, 2''), 109.7 (2 C, 2', 6'), 110.5 (2 C, 3, 5), 121.0 (2 C, 2, 6), 128.4 (2 C, 1, 1'), 149.1 (2 C, 3', 5'), 152.7 (2 C, 4, 4'), 184.5 (1 C, 3''), 192.7 (1 C, 1'').

IR ν_{max} : 3014 (enol OH), 1593 (C=O).

1-(2-Bromophenyl)-3-(3,4,5-trimethoxyphenyl) propane-1,3-dione (9)



Compound (9) above was synthesised from 2-bromoacetophenone (0.4 g, 1.75 mmol) and methyl-3,4,5-trimethoxybenzoate (0.5 g, 2.20 mmol) and sodium hydride (0.13 g, 5.24 mmol) as in procedure A. Following column chromatography (Hex:EtOAc 7:3) and recrystallisation from ethanol compound (9) was isolated as light brown crystals (0.29 g, 1.02 mmol, 72 %).

M.P: 106 – 108 °C; **R_f**:0.41; (Hex:EtOAc 7:3);

δ_H (CDCl₃, 400 MHz): 3.92 (9 H, s, 3'4'5'-OCH₃), 6.59 (1 H, s, 2''-H), 7.20 (2 H, s, 2'6'-H), 7.34 (1 H, td, *J* = 7.8 Hz, 1.66 Hz, 5-H), 7.44 (1 H, td, *J* = 7.8 Hz, 1.66 Hz, 4-H), 7.62 (1 H, dd, 7.8 Hz, 1.60 Hz, 3-H), 7.69 (1 H, dd, *J* = 7.8 Hz, 1.59 Hz, 6-H), 16.32 (1 H, s, enolic H).

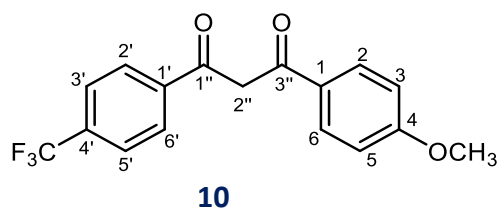
δ_C (CDCl₃, 100 MHz): 56.3 (2 C, OCH₃, 3', 5'), 61.0 (1 C, OCH₃, 4'), 98.0 (1 C, 2''), 104.7 (2 C, 2', 6'), 120.3 (1 C, 2), 127.6 (1 C, 5), 129.9 (1 C, 6), 130.2 (1 C, 1'), 131.7 (1 C, 4), 133.9 (1 C, 3), 138.2 (1 C, 1), 152.7 (1 C, 4'), 153.3 (2 C, 3', 5'), 184.8 (1 C, 3''), 186.8 (1 C, 1'').

HRMS (ESI-TOF) m/z: [M+H] Calculated for C₁₈H₁₇BrO₅; 393.0325 found 393.0329

(ΔMs=2.30 ppm)

IR ν_{max}: 3006 (enol OH), 1592 (C=O).

1-(4-Methoxyphenyl)-3-(4-(trifluoromethyl)phenyl)propane-1,3-dione (10)



Compound (10) above was synthesised from 4-methoxy acetophenone (0.5 g, 2.38 mmol) and methyl-4-trifluoromethylbenzoate (0.72 g, 2.62 mmol) and sodium hydride (0.23 g, 9.51 mmol) as in procedure A. Following column chromatography (Hex:EtOAc 8:2) and recrystallisation from ethanol compound (10) was isolated as bright yellow crystals (0.25 g, 0.78 mmol, 32 %).

M.P: 110 - 112 °C; Lit. mp 109 – 110 °C (Rao and Muthanna, 2015) **R_f:** 0.29; (Hex:EtOAc 8:2);

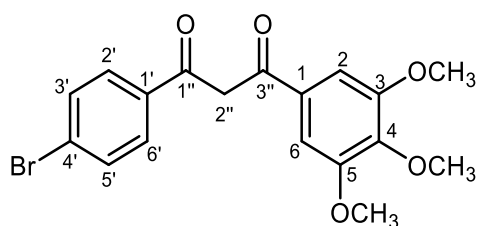
δ_H (CDCl₃, 400 MHz): 3.82 (3 H, s, OCH₃, 4), 6.73 (1 H, s, 2''), 6.93 (2 H, d, *J* = 8.4 Hz, 3, 5), 7.67 (2 H, d, *J* = 8.4 Hz, 3, '5'), 7.92 (2 H, d, *J* = 8.4, H-2,6), 7.93 (2 H, d, *J* = 8.4 Hz, 2, 6), 8.00 (2 H, d, *J* = 8.4 Hz, 2', 6'), 16.80 (1 H, s, enolic H)

δ_F (CDCl₃, 564 MHz): -62.2 (3 F, s, 4'-CF₃).

δ_C (CDCl₃, 100 MHz): 55.54 (1 C, OCH₃, 4), 93.01 (1 C, 2''), 114.01 (2 C, 3, 5), 122.37 (1 C, qt, *J* = 282.55 Hz, CF₃), 125.7 (2 C, qt, *J* = 4.74 Hz, 3' 5'), 127.3 (2 C, 2', 6'), 127.9 (1 C, 1) 129.6 (2 C, 2, 6), 133.0 (1 C, qt, *J* = 35.5 Hz, 4'), 138.8 (1 C, 1), 163.6 (1 C, 4), 181.6 (1 C, 3''), 187.2 (1 C, 1').

IR ν_{max}: 3001.5 (enol OH), 1588.2 (C=O).

1-(4-Bromophenyl)-3-(3,4,5-trimethoxyphenyl) propane-1,3-dione (11)



11

Compound (11) above was synthesised from 4-bromoacetophenone (2.00 g, 10.01 mmol) and methyl-3,4,5-trimethoxybenzoate (2.86 g, 12.86 mmol) and sodium hydride (0.72 g, 30.14 mmol) as in procedure A. Following column chromatography (Hex:EtOAc 8:2) and recrystallisation from ethanol compound (11) was isolated as brown crystals (3.1 g, 7.88 mmol, 79 %).

M.P: 147 – 149 °C; **R_f**:0.29; (Hex:EtOAc 8:2);

δ_H (CDCl₃, 400 MHz): 3.96 (3 H, s, OCH₃, 4), 3.98 (6 H, s, 2 x OCH₃, 3, 5), 6.79 (1 H, s, 2''), 7.24 (2 H, s, 2, 6), 7.64 (2 H, d, *J* = 8.6 Hz, 3', 5'), 7.88 (2 H, d, *J* = 8.6 Hz, 2', 6'), 16.92 (1 H, s, enolic H)

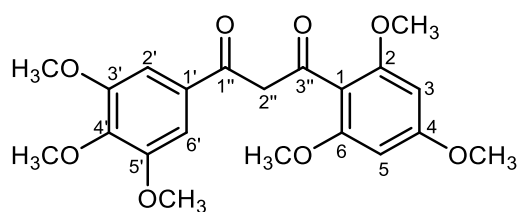
δ_C (CDCl₃, 100 MHz): 56.41 (2 C, OCH₃, 3, 5), 61.04 (1 C, OCH₃, 4), 92.77 (1 C, 2''), 104.76 (2 C, 2, 6), 127.23 (1 C, 4'), 128.58 (2 C, 2, 6), 130.78 (1 C, 1), 132.14 (2 C, Ar 3', 5'), 134.21 (1 C, 1'), 142.31 (1 C, 4), 153.28 (2 C, 3, 5), 183.26 (1 C, 3''), 186.46 (1 C, 1'').

HRMS (ESI-TOF) m/z: [M+H]⁺ : Calculated for C₁₈H₁₇BrO₅ 393.0332 found 393.0333

(ΔM_s=0.16 ppm)

IR ν_{max}: 3019 (enol OH), 1594 (C=O).

1,3-Bis(3,4,5-trimethoxyphenyl) propane-1,3-dione (12)



12

Compound (12) above was synthesised from 2,4,6-trimethoxy acetophenone (0.85 g, 4.03 mmol) and methyl-3,4,5-trimethoxybenzoate (1.15 g, 5.09 mmol) and sodium hydride (0.29 g, 12.13 mmol) as in procedure A. Following by column chromatography (Hex:EtOAc 7:3) and recrystallisation from ethanol compound (12) was isolated as yellow crystals (0.70 g, 1.73 mmol, 36.3 %).

M.P: 150 - 152 °C; **R_f:** 0.33 (Hex:EtOAc 7:3);

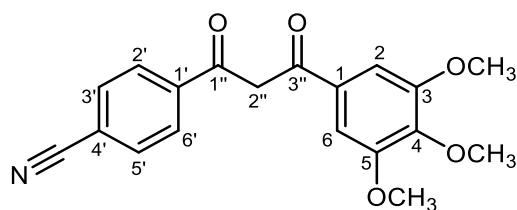
δ_H (CDCl₃, 400 MHz): 3.82 (6 H, s, 3', 5'-OCH₃), 3.86 (3 H, s, 4'-OCH₃), 3.92 (9 H, s, 2, 4, 6-OCH₃), 6.17 (2 H, s, 3, 5-H), 6.35 (1 H, s, 2''-H), 7.15 (2 H, s, 2', 6'-H), 16.35 (1 H, s, enolic H).

δ_C (CDCl₃, 100 MHz): 55.7 (1 C, 4), 56.1 (2 C, 2, 6), 56.3 (2 C, 3', 5'), 60.7 (1 C, 4'), 92.0 (2 C, 3, 5), 101.2 (1 C, 2''), 104.6 (2 C, 2, 6), 109.8 (1 C, 1), 132.9 (1 C, 1'), 143.3 (1 C, 4'), 152.8 (2 C, 3', 5'), 161.3 (2 C, 2, 6), 162.6 (1 C, 4), 172.4 (1 C, 3''), 187.9 (1 C, 1').

HRMS (ESI-TOF) m/z: [M+H] Calculated for C₂₁H₂₄O₈ 405.1544 found 405.1543 (ΔM_s=0.32 ppm)

IR ν_{max}: 2978 (enol OH), 1591 (C=O).

4-(3-oxo-3-(3,4,5-trimethoxyphenyl) propanoyl) benzonitrile (13)



13

Compound (13) above was synthesised from 3',4',5'-trimethoxyacetophenone (0.65 g, 3.11 mmol) and methyl-4-cyanobenzoate (0.5 g, 3.11 mmol) and sodium hydride (0.22 g, 9.31 mmol) as in procedure E. Completion of the reaction was confirmed by TLC (Hex:EtOAc 7:3) and recrystallisation from methanol afforded the title nitrile as orange crystals (0.90 g, 2.65 mmol, 85 %).

M.P: 215 - 217 °C; **R_f:** 0.31 (Hex:EtOAc 7:3);

δ_H (CDCl₃, 400 MHz): 3.97 (3 H, s, OCH₃, 4), 3.99 (6 H, s, 2 x OCH₃, 3,5), 6.79 (1 H, s, 2''), 7.26 (2 H, s, 2, 6), 7.82 (2 H, d, J = 8.5 Hz, 3', 5'), 8.09 (2 H, d, J = 8.5 Hz, 2', 6'), 16.78 (1 H, s, enolic)

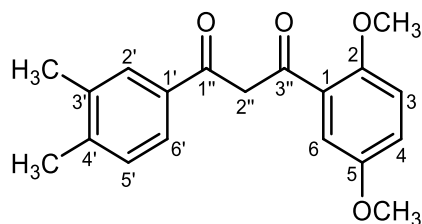
δ_C (CDCl₃, 100 MHz): 56.44 (2 C, OCH₃, 3, 5), 61.07 (1 C, OCH₃, 4), 93.74 (1 C, 2''), 104.97 (2 C, 2, 6), 115.42 (1 C, C≡N, 4'), 118.13 (1 C, 4'), 127.5 (2 C, 2', 6'), 130.6 (1 C, 1), 132.48 (2 C, 3', 5'), 139.2 (1 C, 4), 142.7 (1 C, 1'), 153.3 (2 C, 3, 5), 180.89 (1 C, 3''), 187.8 (1 C, 1'').

δ_N (CDCl₃, 60 MHz): 259.2 (1 N, 4)

HRMS (ESI-TOF) m/z: [M+H] Calculated for C₁₉H₁₇NO₅: 340.1179 found 340.1180 (ΔMs=0.53 ppm)

IR ν_{max}: 3102 (enol OH), 2221 (C≡N), 1533 (C=O).

1-(2,5-Dimethylphenyl)-3-(3,4-dimethoxyphenyl) propane-1,3-dione (14)



14

Compound **(14)** above was synthesised from 2,5-dimethoxyacetophenone (0.80 g, 4.44 mmol) and methyl-3,4-dimethylbenzoate (0.80 g, 4.88 mmol) and sodium hydride (0.46 g, 19.10 mmol) as in procedure A. Following column chromatography (Hex:EtOAc 8:2) and recrystallisation from methanol compound **(14)** was isolated as yellow flakes (0.86 g, 2.75 mmol, 62 %).

M.P: 111 – 113 °C; **R_f:** 0.31; (Hex:EtOAc 8:2);

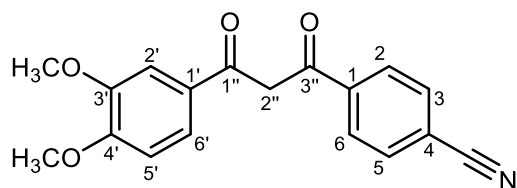
δ_H (CDCl₃, 400 MHz): 2.35 (6 H, 3',4'-CH₃), 3.85 (3 H, 5-OCH₃), 3.94 (3 H, 2-OCH₃), 6.98 (1 H, d, J = 8.82 Hz, 3), 7.06 (1 H, dd, J = 8.82 Hz, 2.96 Hz, 4), 7.18 (1 H, s, 2''), 7.26 (1 H, d, J = 8.19 Hz, 5'), 7.52 (1 H, d, J = 2.96 Hz, 6), 7.73 (1 H, dd, J = 8.19 Hz, 1.70 Hz, 6'), 7.78 (1 H, d, J = Hz, 2'), 16.93 (1 H, s, enolic H)

δ_C (CDCl₃, 100 MHz): 18.83 (1 C, 4), 20.02 (1 C, 3), 55.86 (1 C, OCH₃, 5), 56.52 (1 C, OCH₃, 2), 92.42 (1 C, 2''), 114.10 (2 C, 2', 6'), 126.04 (1 C, 6), 127.67 (1 C, 5), 128.92 (1 C, 5), 129.49 (2 C, 3', 5'), 130.70 (1 C, 2), 133.23 (1 C, 4), 135.59 (1 C, 1), 136.36 (1 C, 1'), 163.57 (1 C, 4'), 181.49 (1 C, 3''), 186.41 (1 C, 1'').

HRMS (ESI-TOF) m/z: [M+H] Calculated for C₁₉H₂₀O₄: 313.1434 found 313.1433 (ΔM_s=1.02 ppm)

IR ν_{max}: 3011 (enol OH), 1549 (C=O).

4-(3-(3,4-Dimethoxyphenyl)-3-oxopropanoyl)benzonitrile (**15**)



15

Compound (**15**) above was synthesised from 3',4'-dimethoxyacetophenone (0.5 g, 2.38 mmol) and methyl-4-cyanobenzoate (0.72 g, 2.62 mmol) and sodium hydride (0.23 g, 9.51 mmol) as in procedure E. After completion of the reaction was confirmed by TLC (Hex:EtOAc 8:2) recrystallisation from methanol afforded the title nitrile as yellow needles (0.45 g, 1.39 mmol, 61 %).

M.P: 199 - 201 °C; **R_f:** 0.34; (Hex:EtOAc 8:2);

δ_H (CDCl₃, 400 MHz): 3.97 (3 H, OCH₃, 4'), 3.98 (3 H, OCH₃, 3'), 6.81 (1 H, s, 2''), 6.95 (1 H, d, J = 8.6 Hz, 5'), 7.57 (1 H, d, J = 1.86 Hz, 2'), 7.64 (1 H, dd, J = 8.6 Hz, 1.86 Hz, 6'), 7.78 (2 H, d, J = 8.4 Hz, 2, 6), 8.06 (2 H, d, J = 8.4 Hz, 3, 5), 16.79 (1 H, s, enolic H)

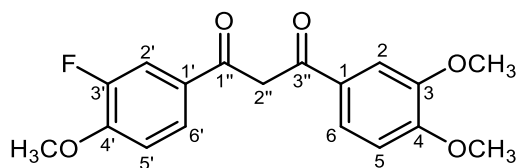
δ_c (CDCl₃, 100 MHz): 56.09 (1 C, OCH₃, 4'), 56.15 (1 C, OCH₃, 3'), 93.46 (1 C, 2''), 109.83 (1 C, 2'), 110.44 (1 C, 5'), 115.18 (1 C, 4), 118.19 (1 C, CN), 121.82 (1 C, 6'), 127.36 (2 C, 2, 6), 128.27 (1 C, 1'), 132.58 (1 C, 3, 5), 139.26 (1 C, 1), 149.26 (1 C, 3'), 153.50 (1 C, 4'), 179.59 (1 C, 3''), 188.23 (1 C, 1'').

δ_N (CDCl₃, 60 MHz): 258.9 (1 N, 4)

HRMS (ESI-TOF) m/z: [M+H] Calculated for C₁₈H₁₅NO₄ 310.1074 found 310.1078 (ΔM_s=0.11 ppm)

IR ν_{max}: 3109 (enol OH), 2219 (C≡N), 1593 (C=O).

1-(3,4-Dimethoxyphenyl)-3-(3-fluoro-4-methoxyphenyl)propane-1,3-dione (16)



16

Compound (16) above was synthesised from 3',4'-dimethoxyacetophenone (1.50 g, 8.30 mmol) and methyl-3-fluoro-4-methoxybenzoate (1.68 g, 9.12 mmol) and sodium hydride (1.00 g, 41.68 mmol) as in procedure A. Following column chromatography (Hex:EtOAc 7:3) and recrystallisation from ethanol compound (16) was isolated as brown crystals (2.53 g, 7.61 mmol, 91 %).

M.P: 137 – 139 °C; **R_f**:0.37; (Hex:EtOAc 7:3);

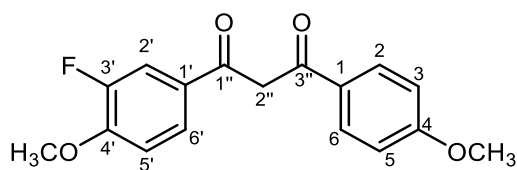
δ_H (CDCl₃, 400 MHz): 3.98 (6 H, s, 2 x OCH₃, 3, 4), 4.00 (3 H, OCH₃, 4'), 6.71 (1 H, s, 2''), 6.96 (1 H, d, *J* = 8.5 Hz, 5), 7.07 (1 H, tr, *J* = 8.45 Hz, 5'), 7.56 (1 H, d, *J* = 2.01 Hz, 2), 7.63 (1 H, dd, *J* = 8.4 Hz, 2.01 Hz, 6), 7.75 (1 H, d, *J* = 12 Hz, 2.04 Hz, 2'), 7.80 (1 H, dd, *J* = 8.4 Hz, 2.01 Hz, 6'), 16.79 (1 H, s, enolic H)

δ_C (CDCl₃, 100 MHz): 56.06 (1 C, OCH₃, 3), 56.09 (1 C, OCH₃, 4), 56.3 (1 C, OCH₃, 4'), 91.7 (1 C, 2''), 109.7 (1 C, 2), 110.5 (1 C, 5), 112.7 (1 C, d, *J* = 1.94 Hz, 5'), 114.8 (1 C, d, *J* = 19.64 Hz, 2'), 121.2 (1 C, 6), 123.9 (1 C, d, *J* = 3.10 Hz, 6'), 128.3 (1 C, 1), 128.5 (1 C, d, *J* = 5.89 Hz, 1'), 149.1 (1 C, 3), 151.2 (1 C, d, *J* = 10.78 Hz, 4'), 152.9 (1 C, 4), 153.3 (1 C, d, *J* = 246.8 Hz, 3'), 182.7 (1 C, 1'), 185.5 (1 C, 3'').

HRMS (ESI-TOF) m/z: [M+H] Calculated for C₁₈H₁₇FO₅ 333.1133 found 333.1140 (ΔM_s=2.12 ppm)

IR ν_{max}: 3094 (enol OH), 1615 (C=O).

1-(3-Fluoro-4-methoxyphenyl)-3-(4-methoxyphenyl) propane-1,3-dione (17)



17

Compound (17) above was synthesised from 4'-methoxyacetophenone (0.50 g, 2.38 mmol) and methyl-3-fluoro-4-methoxybenzoate (0.72 g, 2.62 mmol) and sodium hydride (0.23 g, 9.51 mmol) as in procedure E. After completion of the reaction was confirmed by TLC (Hex:EtOAc 8:2), recrystallisation from methanol afforded the title compound (17) as yellow crystals (0.20 g, 0.66 mmol, 24 %).

M.P: 148 – 150 °C; **R_f:** 0.3; (Hex:EtOAc 8:2);

δ_H (CDCl₃, 400 MHz): 3.91 (3H, s, 4-OCH₃), 3.99 (3H, s, 4'-OCH₃), 6.72 (1H, s, 2''-H), 7.02 (2 H, d, J = 8.8 Hz, 3, 5-H), 7.07 (1 H, t, J = 5.4 Hz, 5'-H), 7.76 (1 H, dd, J = 12.1 Hz, 2.1 Hz, 2'-H), 7.80 (1 H, d, J = 8.6 Hz, 6'-H), 7.99 (2 H, d, J = 8.7 Hz, 2, 6-H) 17.03 (1H, s, enolic H).

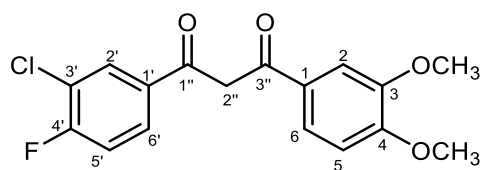
δ_C (CDCl₃, 100 MHz): 55.51 (1 C, OCH₃, 4), 56.31 (1 C, OCH₃, 4'), 91.63 (1 C, 2''), 112.68 (1 C, d, J = 1.86 Hz, 5'), 114.01 (2 C, 3, 5), 114.94 (1 C, d, J = 19.8 Hz, 2'), 123.96 (1 C, d, J = 3.3 Hz, 6') 127.88 (1 C, 1), 128.71 (1 C, d, J = 5.94 Hz, 1'), 129.19 (2 C, 2, 6), 151.18 (1 C, d, J = 10.36 Hz, 4'), 153.33 (1 C, d, J = 246.8 Hz, 3'), 163.22 (1 C, 4), 183.46 (1 C, 3''), 186.85 (1 C, 1'').

δ_F (CDCl₃, 564 MHz): -134.3 (1 F, dd, J = 8.02 Hz, 4.16 Hz, 3')

HRMS (ESI-TOF) m/z: [M+H] Calculated for C₁₇H₁₅FO₄ 303.1027 found 303.1027 (ΔMs=0.01 ppm)

IR ν_{max}: 3076 (enol OH), 1602 (C=O).

1-(3-Chloro-4-fluorophenyl)-3-(3,4-dimethoxyphenyl) propane-1,3-dione (18)



18

Compound (18) was synthesised from 3-chloro-4-fluoroacetophenone (0.40 g, 2.32 mmol) and methyl-3,4-dimethoxybenzoate (0.50 g, 2.55 mmol) and sodium hydride (0.23 g, 9.27 mmol) as in procedure E. After completion of the reaction was confirmed by TLC (Hex:EtOAc 8:2), recrystallisation from ethanol afforded the title compound (18) as a yellow powder (0.53 g, 1.57 mmol, 67 %).

M.P: 136 - 138 °C; **R_f:** 0.35; (Hex:EtOAc 8:2);

δ_H (CDCl₃, 400 MHz): 3.99 (3 H, s, 4-OCH₃), 4.01 (3 H, s, 3-OCH₃), 6.73 (1 H, s, 2''-H), 6.97 (1 H, d, J = 8.2 Hz, 5-H), 7.04 (1 H, d, J = 8.9 Hz, 5'-H), 7.57 (1 H, d, J = 2.0 Hz, 2-H), 7.65 (1 H, dd, J = 8.2 Hz, 2.0 Hz, 6-H), 7.94 (1 H, dd, J = 8.8 Hz, 2.1 Hz, 6'-H), 8.03 (1 H, d, J = 2.1 Hz, 2'-H), 17.06 (1H, s, enolic H).

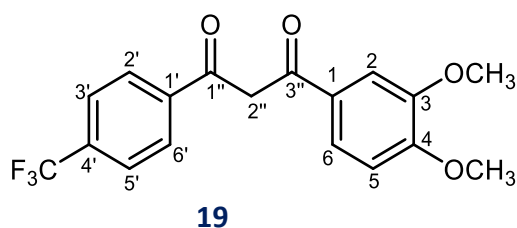
δ_c (CDCl₃, 400 MHz): 56.0 (1 C, 4-OCH₃), 56.1 (1 C, 3-OCH₃), 92.3 (1 C, 2''), 109.7 (1 C, 5), 110.5 (1 C, 1), 116.4 (1 C, d, J = 19.9 Hz, 5'), 117.7 (1 C, d, J = 18.5 Hz, 3'), 121.5 (1 C, 6), 123.7 (1 C, d, J = 3.53 Hz, 2'), 128.1 (1 C, 1), 132.6 (1 C, d, J = 2.52 Hz, 1'), 149.2 (1 C, 3), 153.2 (1 C, 4), 154.2 (1 C, d, J = 246.1 Hz, 4'), 181.3 (1 C, 1''), 186.5 (1 C, 3'').

δ_F (CDCl₃, 564 MHz): -134.3 (1 F, m)

m/z HRMS (ESI) [M + H]: Calculated for C₁₇H₁₄ClFO₄ 337.0637 found 337.0638 (ΔM_s=0.20 ppm)

IR ν_{max}: 3056 (enol OH), 1646 (C=O).

1-(3-fluoro-4-methoxyphenyl)-3-(4-methoxyphenyl) propane-1,3-dione (19)



Compound (19) was synthesised from 4-(trifluoromethyl) acetophenone (0.40 g, 2.12 mmol) and methyl-3,4-dimethoxybenzoate (0.46 g, 2.34 mmol) and sodium hydride (0.21 g, 8.50 mmol) as in procedure E. After completion of the reaction was confirmed by TLC (Hex:EtOAc 8:2), recrystallisation from ethanol afforded the title compound (19) as a white powder (0.45 g, 1.38 mmol, 65 %).

M.P: 109 - 111 °C; **R_f:** 0.31; (Hex:EtOAc 8:2);

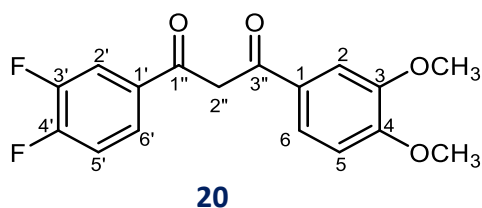
δ_H (CDCl₃, 400 MHz): 3.99 (3 H, s, OCH₃, 4), 4.01 (3 H, s, OCH₃, 3), 6.84 (1 H, s, 2''), 6.98 (1 H, d, *J* = 8.4 Hz, 5), 7.60 (1 H, d, *J* = 1.99 Hz, 2), 7.67 (1 H, dd, *J* = 8.4 Hz, 1.99 Hz, 6), 7.78 (2 H, d, *J* = 8.4 Hz, 3', 5'), 8.09 (2 H, d, *J* = 8.4 Hz, 2', 6'), 17.04 (1 H, s, enolic H)

δ_F (CDCl₃, 564 MHz): -62.8 (3 F, s, 4'-CF₃).

δ_C (CDCl₃, 100 MHz): 56.09 (1 C, OCH₃, 3), 56.12 (1 C, OCH₃, 4), 93.17 (1 C, 2''), 109.81 (1 C, 5), 110.45 (1 C, 2), 121.68 (1 C, 6'), 125.71 (2 C, q, *J* = 3.70 Hz, 3', 5'), 127.80 (1 C, q, *J* = 272.80 Hz, CF₃), 128.39 (2 C, 2' 6'), 129.28 (1 C, 1), 133.95 (1 C, q, *J* = 32.50 Hz, 4'), 138.59 (1 C, 1'), 149.2 (1 C, 3), 153.3 (1 C, 4), 179.6 (1 C, 3''), 187.8 (1 C, 1'').

IR ν_{max}: 3034 (enol OH), 1641 (C=O).

1-(3,4-Difluorophenyl)-3-(3,4-dimethoxyphenyl)propane-1,3-dione (20)



Compound (20) was synthesised from 3,4-difluoroacetophenone (0.47 g, 3.01 mmol) and methyl-3,4-dimethoxybenzoate (0.55 g, 3.31 mmol) and sodium hydride (0.28 g, 12.04 mmol) as in procedure E. After completion of the reaction was confirmed by TLC (Hex:EtOAc 8:2), recrystallisation from ethanol afforded the difluoro compound (20) as a yellow powder (0.61 g, 1.90 mmol, 58 %).

M.P: 111 - 113 °C; **R_f:** 0.29; (Hex:EtOAc 8:2);

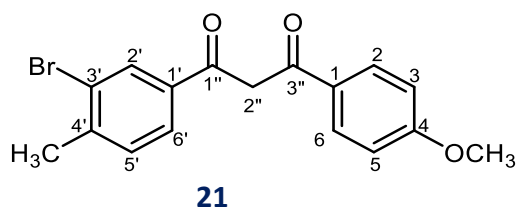
δ_H (CDCl₃, 400 MHz): 3.96 (6 H, s, 3, 4-OCH₃), 6.80 (1 H, s, 2''-H), 7.01 (1 H, d, J = 8.4 Hz, 5-H), 7.36 (1 H, dd, J = 10.0 Hz, 8.1 Hz, 5'-H), 7.57 (1 H, d, J = 1.82 Hz, 2-H), 7.69 (1 H, dd, J = 8.4 Hz, 1.82 Hz, 6-H), 7.84 (2 H, m, 2', 6'-H), 17.02 (1H, s, enolic H).

δ_C (CDCl₃, 100 MHz): 56.3 (2 C, OCH₃, 3, 4), 92.7 (1 C, 2''), 110.2 (1 C, 5), 111.1 (1 C, 2), 116.7 (1 C, d, J = 18.7 Hz, 5'), 118.0 (1 C, d, J = 18.0 Hz, 2'), 121.9 (1 C, 6), 124.2 (1 C, m, 6'), 128.2 (1 C, 1), 133.2 (1 C, m, 1'), 149.7 (1 C, 3), 152.1 (1 C, dd, J = 250.4 Hz, 12.7 Hz, 3'), 153.9 (1 C, 4), 154.5 (1 C, dd, J = 253.2 Hz, 12.5 Hz, 4'), 181.8 (1 C, 3''), 186.8 (1 C, 1'').

δ_F (CDCl₂, 564 MHz): -132.5 (1 F, m, 3'), -137.4 (1 F, m, 4').

IR ν_{max}: 3021 (enol OH), 1658 (C=O).

1-(3-Bromo-4-methylphenyl)-3-(4-methoxyphenyl) propane-1,3-dione (21)



Compound (21) was synthesised from 4-methoxyacetophenone (0.30 g, 1.98 mmol) and methyl-3-bromo-4-methylbenzoate (0.5 g, 2.18 mmol) and sodium hydride (0.15 g, 5.95 mmol) as in procedure E. After completion of the reaction was confirmed by TLC (Hex:EtOAc 8:2), recrystallisation from ethanol afforded the title bromo compound (21) as a yellow powder (0.59 g, 1.70 mmol, 78 %).

M.P: 119 - 121 °C; **R_f:** 0.28; (Hex:EtOAc 8:2);

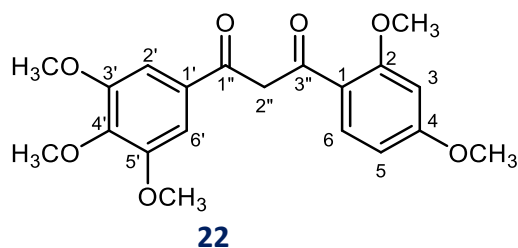
δ_H (CDCl₃, 400 MHz): 2.49 (3 H, s, 4'-CH₃), 3.91 (3 H, s, 4-OCH₃), 6.75 (1 H, s, 2''-H), 7.02 (2 H, d, J = 8.69 Hz, 3, 5-H), 7.37 (1 H, d, J = 8.01 Hz, 5'-H), 7.84 (1 H, dd, J = 8.01 Hz, 1.99 Hz, 6'-H), 8.01 (1 H, d, J = 8.77 Hz, 2, 6-H), 8.15 (1 H, d, J = 1.99 Hz, 2'-H), 16.96 (1 H, s, enolic H).

δ_C (CDCl₃, 100 MHz): 23.2 (1 C, 4'-CH₃), 55.5 (1 C, 4-OCH₃), 92.2 (1 C, 2''), 114.0 (2 C, 3, 5), 125.2 (1 C, 3'), 125.6 (1 C, 1), 127.9 (1 C, 1), 129.4 (2 C, 2, 6), 130.8 (1 C, 5'), 130.9 (1 C, 2'), 135.0 (1 C, 1'), 142.4 (1 C, 4'), 163.4 (1 C, 4), 182.7 (1 C, 3''), 185.9 (1 C, 1'').

m/z HRMS (ESI) [M + H]: Calculated for C₁₇H₁₅BrO₃ 347.0277 found 347.0277 (ΔMs=0.14 ppm)

IR ν_{max}: 3079 (enol OH), 1610 (C=O).

1-(2,4-Dimethoxyphenyl)-3-(3,4,5-trimethoxyphenyl) propane-1,3-dione (22)



Compound (22) was synthesised from 2,4-dimethoxyacetophenone (0.50 g, 2.77 mmol) and methyl-3,4,5-trimethoxybenzoate (0.79 g, 3.50 mmol) and sodium hydride (0.21 g, 8.32 mmol) as in procedure E. After completion of the reaction was confirmed by TLC (Hex:EtOAc 9:1), recrystallisation from ethanol afforded the title compound (22) as a white solid (0.75 g, 2.00 mmol, 72 %).

M.P: 137 - 139 °C; **R_f:** 0.22; (Hex:EtOAc 9:1);

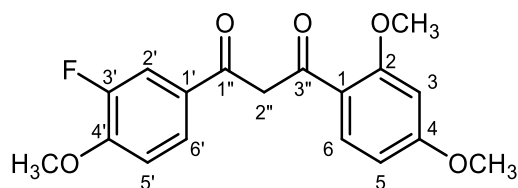
δ_H (CDCl₃, 400 MHz): 3.88 (3 H, s, 4'-OCH₃), 3.94 (3 H, s, OCH₃-4), 3.96 (9 H, s, OCH₃-2, 3', 5'), 6.54 (1 H, d, J = 2.3 Hz, 3-H), 6.64 (1 H, dd, J = 8.5 Hz, 2.3 Hz, 5-H), 7.14 (1 H, s, 2''-H), 7.24 (2 H, s, 2', 6'-H), 8.03 (1 H, d, J = 8.6 Hz, 6-H), 17.05 (1 H, s, enolic H).

δ_C (CDCl₃, 100 MHz): 55.4 (1 C, OCH₃, 4), 55.7 (1 C, OCH₃, 2), 56.2 (2 C, OCH₃, 3', 5'), 61.0 (1 C, OCH₃, 4'), 97.3 (1 C, 3), 98.8 (1 C, 2''), 104.6 (2 C, 2', 6'), 105.3 (1 C, 5), 117.3 (1 C, 1), 131.8 (1 C, 1'), 132.0 (1 C, 6), 141.6 (1 C, 4'), 153.1 (2 C, 3', 5'), 160.4 (1 C, 2), 164.1 (1 C, 4), 182.1 (1 C, 3''), 185.9 (1 C, 1'').

m/z HRMS (ESI) [M + H]: Calculated for C₂₀H₂₂O₇ 375.1438 found 375.1438 (ΔMs=0.05 ppm)

IR ν_{max}: 3181 (enol OH), 1646 (C=O).

1-(2,4-Dimethoxyphenyl)-3-(3-fluoro-4-methoxyphenyl)propane-1,3-dione (23)



23

Compound (23) was synthesised from 2,4-dimethoxyacetophenone (0.60 g, 3.33 mmol) and methyl-3-fluoro-4-methoxybenzoate (0.77 g, 4.20 mmol) and sodium hydride (0.24 g, 9.99 mmol) as in procedure E. After completion of the reaction was confirmed by TLC (Hex:EtOAc 9:1), recrystallisation from ethanol afforded the title compound (23) as a yellow powder 0.62 g, 1.69 mmol, 56 %).

M.P: 112 – 114 °C; **R_f:** 0.40; (Hex:EtOAc 8:2);

δ_H (CDCl₃, 400 MHz): 3.87 (3 H, s, 2-OCH₃), 3.95 (6 H, s, 4,4'-OCH₃), 6.51 (1 H, d, J = 2.20 Hz, 3-H), 6.60 (1 H, dd, J = 8.77 Hz, 2.20 Hz, 5-H), 7.03 (1 H, t, J = 8.50 Hz, 5'-H), 7.09 (1 H, s, 2''-H), 7.70 (1 H, dd, J = 12.2 Hz, 2.13 Hz, 2'-H), 7.75 (1 H, d, J = 8.62 Hz, 6'-H), 8.00 (1 H, d, J = 8.77 Hz, 6-H), 17.01 (1 H, s, enolic H).

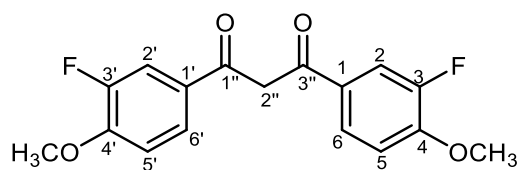
δ_C (CDCl₃, 100 MHz): 55.6 (1 C, OCH₃, 4), 55.8 (1 C, OCH₃, 2), 56.3 (1 C, OCH₃, 4), 96.9 (1 C, 2''), 98.7 (1 C, 3), 105.3 (1 C, 5), 112.6 (1 C, d, J = 2,3 Hz, 5'), 114.9 (1 C, d, J = 19.3 Hz), 117.2 (1 C, 1), 124.1 (1 C, d, J = 3.41 Hz, 6'), 129.4 (1 C, d, J = 6.82 Hz, 1'), 132.0 (1 C, 6), 151.0 (1 C, d, J = 11.3 Hz, 4'), 153.3 (1 C, d, J = 246.3 Hz), 160.4 (1 C, 2), 164.1 (1 C, 4), 182.2 (1 C, 3''), 184.5 (1 C, d, J = 1.93 Hz).

δ_F (CDCl₂, 564 MHz): -134.1 (1 F, dd, J = 8.3 Hz, 3.7 Hz, 3').

m/z HRMS (ESI) [M + H]: Calculated for C₁₈H₁₇FO₅ 333.1133 found 333.1133 (ΔM_s=0.01 ppm)

IR ν_{max}: 3176 (enol OH), 1608 (C=O).

1,3-Bis(3-fluoro-4-methoxyphenyl)propane-1,3-dione (24)



24

Compound (24) was synthesised from 3-fluoro-4-methoxyacetophenone (0.50 g, 2.97 mmol) and methyl-3-fluoro-4-methoxybenzoate (0.69 g, 3.75 mmol) and sodium hydride (0.21 g, 8.92 mmol) as in procedure E. After completion of the reaction was confirmed by TLC (Hex:EtOAc 8:2), recrystallisation from ethanol afforded the title compound (24) as a bright yellow solid (0.8 g, 2.50 mmol, 84 %).

M.P: 178 – 180 °C; **R_f:** 0.37; (Hex:EtOAc 8:2);

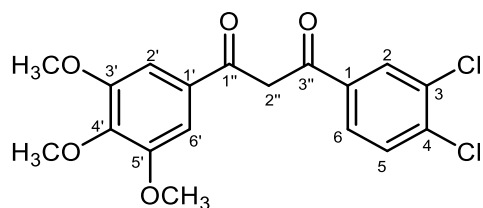
δ_H (CDCl₃, 400 MHz): 3.90 (6 H, s, 4, 4'-OCH₃), 6.58 (1 H, s, 2''-H), 6.99 (2 H, t, J = 8.44 Hz, 5, 5'-H), 7.66 (2 H, dd, J = 12.02 Hz, 2.15 Hz, 6, 6'-H), 7.71 (2 H, d, J = 8.68 Hz, 2,2'-H), 16.83 (1 H, s, enolic).

δ_C (CDCl₃, 100 MHz): 56.3 (2 C, OCH₃, 4, 4'), 91.8 (1 C, 2''), 112.7 (2 C, d, J = 2.10 Hz, 5, 5'), 115.0 (2 C, d, J = 19.60 Hz, 2, 2'), 124.1 (2 C, d, J = 3.21 Hz, 6, 6'), 128.4 (2 C, d, J = 5.93 Hz, 1, 1'), 151.4 (2 C, d, J = 10.6 Hz, 4, 4'), 153.4 (2 C, d, J = 247.4 Hz, 3, 3'), 183.7 (2 C, d, J = 2.11 Hz, 1'', 3'').

m/z HRMS (ESI) [M + H]: Calculated for C₁₇H₁₄F₂O₄ 321.0933 found 321.0934 (ΔMs=0.41 ppm)

IR ν_{max}: 3084 (enol OH), 1614 (C=O).

3-(3,4-Dichlorophenyl)-1-(3,4,5-trimethoxyphenyl)-1,3-propanedione (25)



25

Compound (25) was synthesised from 3,4-dichloroacetophenone (0.50 g, 2.64 mmol) and methyl-3,4,5-trimethoxybenzoate (0.50 g, 3.33 mmol) and sodium hydride (0.20 g, 7.93 mmol) as in procedure E. After completion of the reaction was confirmed by TLC (Hex:EtOAc 8.5:1.5), recrystallisation from ethanol afforded the title dichloro compound (25) as a yellow powder (0.32 g, 0.83 mmol, 30 %).

M.P: 146 – 148 °C; **R_f**:0.35; (Hex:EtOAc 8.5:1.5);

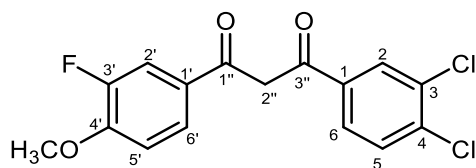
δ_H (CDCl₃, 400 MHz): 3.87 (3 H, s, 4'-OCH₃), 3.90 (6 H, s, 3',5'-OCH₃), 6.62 (1 H, s, 2''), 7.15 (2 H, s, H-2' and 6'), 7.51 (1 H, d, J = 8.6 Hz, H-5), 7.74 (1 H, dd, J = 8.6 Hz, 2.0 Hz, H-6), 7.98 (1 H, d, J = 2.0 Hz, 2-H), 16.78 (1 H, s, enolic H)

δ_C (CDCl₃, 100 MHz): 56.5 (2 C, OCH₃-3', 5'), 61.1 (1 C, OCH₃,4'), 92.9 (1 C, 2''), 104.8 (2 C, 2', 6'), 126.1 (1 C, 6), 128.9 (1 C, 2), 130.5 (1 C, 1'), 130.8 (1 C, 5), 133.3 (1 C, 1), 135.3 (1 C, 4), 136.7 (1 C, 3), 153.3 (2 C, 3', 5'), 158.3 (1 C, 4'), 181.9 (1 C, 3''), 186.6 (1 C, 1'').

m/z HRMS (ESI) [M + H]: Calculated for C₁₈H₁₆Cl₂O₅ 383.0488 found 383.0448 (ΔM_s=0.19 ppm)

IR ν_{max}: 3087 (enol OH), 1651 (C=O).

1-(3,4-Dichlorophenyl)-3-(3-fluoro-4-methoxyphenyl)-1,3-propanedione (26)



26

Compound (26) was synthesised from 3,4-dichloroacetophenone (0.60 g, 3.17 mmol) and methyl-3-fluoro-4-methoxybenzoate (0.74 g, 4.00 mmol) and sodium hydride (0.23 g, 9.52 mmol) as in procedure E. After completion of the reaction was confirmed by TLC (Hex: EtOAc 8:2), recrystallisation from ethanol afforded the dichloro compound (26) as a bright yellow solid (0.7 g, 2.05 mmol, 64 %).

M.P: 155 – 157 °C; **R_f:** 0.24; (Hex:EtOAc 8:2);

δ_H (CDCl₃, 400 MHz): 4.01 (3 H, s, 4'-OCH₃), 6.71 (1 H, s, 2''-H), 7.09 (1 H, t, J = 8.40 Hz, 5'-H), 7.60 (1 H, d, J = 8.47 Hz, 5-H), 7.78 (1 H, dd, J = 12.01 Hz, 2.26 Hz, 2'-H), 7.82 (2 H, dd, J = 8.43 Hz, 2.03 Hz, 6, 6'-H), 8.07 (1 H, d, J = 1.98 Hz, 2-H), 16.76 (1 H, s, enolic H)

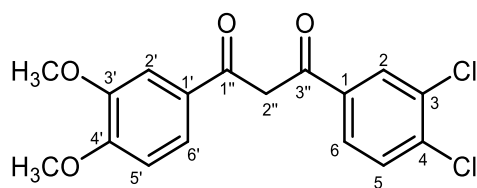
δ_C (CDCl₃, 100 MHz): 56.4 (1 C, OCH₃, 4'), 92.5 (1 C, 2''), 112.7 (1 C, d, J = 2.18 Hz, 5'), 115.2 (1 C, d, J = 20.01 Hz, 2'), 124.4 (1 C, d, J = 3.19 Hz, 6'), 125.3 (1 C, d, J = 7.51 Hz, 1'), 126.1 (1 C, 6), 129.1 (1 C, 2), 130.8 (1 C, 5), 133.3 (1 C, 1), 135.2 (1 C, 4), 136.7 (1 C, 3), 151.8 (1 C, d, 10.01 Hz, 4'), 153.4 (1 C, d, J = 247.5 Hz, 3'), 181.7 (1 C, 3''), 185.3 (1 C, d, J = 2.08 Hz, 1'').

δ_F (CDCl₃, 564 MHz): -133.8 (1 F, dd, J = 8.3 Hz, 3.9 Hz, 3')

m/z HRMS (ESI) [M + H]: Calculated for C₁₆H₁₁Cl₂FO₃ 341.0142 found 341.0142 (ΔMs=0.16 ppm)

IR ν_{max}: 3092 (enol OH), 1613 (C=O).

1-(3,4-Dichlorophenyl)-3-(3,4-dimethoxyphenyl)-1,3-propanedione (27)



27

Compound (27) was synthesised from 3,4-dichloroacetophenone (0.50 g, 2.65 mmol) and methyl-3, 4-dimethoxybenzoate (0.65 g, 3.33 mmol) and sodium hydride (0.19 g, 7.93 mmol) as in procedure E. After completion of the reaction was confirmed by TLC (Hex: EtOAc 9:1), recrystallisation from ethanol afforded the title dichloro compound (27) as a bright yellow solid (0.76 g, 2.15 mmol, 81 %).

M.P: 97 – 99 °C; **R_f:** 0.18; (Hex:EtOAc 9:1);

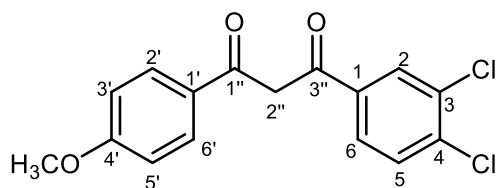
δ_H (CDCl₃, 400 MHz): 3.99 (3 H, s, 4'-OCH₃), 4.01 (3 H, s, 3'-OCH₃), 6.75 (1 H, s, 2''-H), 6.97 (1 H, d, J = 8.4, H-5'), 7.58 (1 H, d, J = 2.20 Hz, H-2'), 7.59 (1 H, d, J = 8.4 Hz, H-5), 7.66 (1 H, dd, J = 8.4 Hz, 2.2 Hz, H-6'), 7.83 (1 H, dd, J = 8.4 Hz, 2.20 Hz H-6), 8.07 (1 H, d, J = 2.1 Hz, H-2), 16.90 (1 H, s, enolic H)

δ_C (CDCl₃, 100 MHz): 56.11 (1 C, OCH₃, 4'), 56.14 (1 C, OCH₃, 3'), 92.6 (1 C, 2''), 109.8 (1 C, 2'), 110.5 (1 C, 5'), 121.6 (1 C, 6'), 126.0 (1 C, 6), 128.2 (1 C, 3), 128.9 (1 C, 2), 130.7 (1 C, 5), 133.3 (1 C, 1'), 135.3 (1 C, 1), 136.5 (1 C, 4), 149.2 (1 C, 3'), 153.4 (1 C, 4'), 180.6 (1 C, 3''), 187.1 (1 C, 1'').

m/z HRMS (ESI) [M + H]: Calculated for C₁₇H₁₄Cl₂O₄ 353.0347 found 353.0340 (ΔMs=2.00 ppm)

IR ν_{max}: 3102 (enol OH), 1591 (C=O).

1-(3,4-Dichlorophenyl)-3-(4-methoxyphenyl)-1,3-propanedione (28)



28

Compound (28) was synthesised from 3,4-dichloroacetophenone (0.70 g, 3.70 mmol) and methyl-4-methoxybenzoate (0.78 g, 4.67 mmol) and sodium hydride (0.27 g, 11.1 mmol) as in procedure E. After completion of the reaction was confirmed by TLC (Hex: EtOAc 8:2), recrystallisation from ethanol afforded the title dichloro compound (28) as a yellow product (0.24 g, 0.74 mmol, 20 %).

M.P: 124 – 126 °C; **R_f:** 0.23; (Hex:EtOAc 8:2);

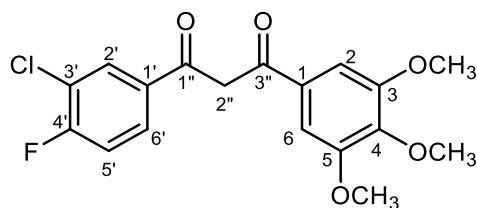
δ_H (CDCl₃, 400 MHz): 3.92 (3 H, s, 4'-OCH₃), 6.75 (1 H, s, 2''-H), 7.02 (2 H, d, J = 8.2 Hz, H-3', 5'), 7.59 (1 H, d, J = 8.45 Hz, H-5), 7.83 (1 H, dd, J = 8.45 Hz, 2.14 Hz, H-6), 8.01 (2 H, d, J = 8.3 Hz), 8.07 (1 H, d, J = 2.13 Hz), 16.90 (1 H, s, enolic H)

δ_C (CDCl₃, 100 MHz): 56.6 (1 C, 4'-OCH₃), 92.4 (1 C, 2''), 114.1 (2 C, 3', 5'), 126.0 (1 C, 6), 127.7 (1 C, 1'), 129.0 (1 C, 2'), 129.5 (2 C, 2', 6'), 130.7 (1 C, 5), 133.2 (1 C, 3), 135.5 (1 C, 1), 136.4 (1 C, 4), 163.6 (1 C, 4'), 181.5 (1 C, 3''), 186.4 (1 C, 1'').

m/z HRMS (ESI) [M + H]: Calculated for C₁₆H₁₂Cl₂O₃ 323.0236 found 323.0236 (ΔM_s=0.06 ppm)

IR ν_{max}: 3081 (enol OH), 1646 (C=O).

3-(3-Chloro-4-fluorophenyl)-1-(3,4,5-trimethoxyphenyl)-1,3-propanedione (29)



29

Compound (29) was synthesised from 3,4-dichloroacetophenone (0.40g, 2.32 mmol) and methyl-3,4,5-trimethoxybenzoate (0.66 g, 2.92 mmol) and sodium hydride (0.20 g, 6.95 mmol) as in procedure E. After completion of the reaction was confirmed by TLC (Hex:EtOAc 9:1), recrystallisation from ethanol afforded the trimethoxy compound (29) as a yellow solid (0.71 g, 1.94 mmol, 83 %).

M.P: 128 – 130 °C; **R_f:** 0.29; (Hex:EtOAc 9:1);

δ_H (CDCl₃, 400 MHz): 3.93, 3.95, 3.98 (9 H, 3s, 3 x OCH₃), 6.68 (1 H, s, olefinic H), 7.04 (1 H, d, J = 8.4 Hz, H-5''), 7.23 (2 H, s, H-2' and 6'), 7.95 (1 H, dd, J = 8.4 Hz, 2.0 Hz, H-6''), 8.03 (1 H, d, J = 2.0 Hz, H-2''), 17.04 (1 H, s, enolic H)

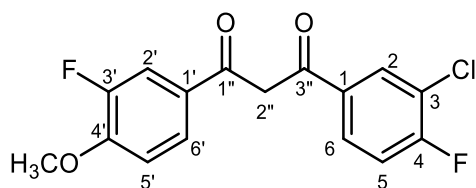
δ_C (CDCl₃, 100 MHz): 55.55 (1 C, OCH₃, 4'), 92.42 (1 C, 2), 114.10 (2 C, 2'' and 6''), 126.04 (1 C, 6'), 127.67 (1 C, 5'), 128.92 (1 C, 5'), 129.49 (2 C, 3'' and 5''), 130.70 (1 C, 2'), 133.23 (1 C, 4'), 135.59 (1 C, 1'), 136.36 (1 C, 1''), 163.57 (1 C, 4''), 181.49 (1 C, 3''), 186.41 (1 C, 1'').

δ_F (CDCl₃, 564 MHz): -108 (1 F, m, 4')

m/z HRMS (ESI) [M + H]: Calculated for C₁₈H₁₆ClFO₅ 367.0743 found 367.0743 (ΔMs=0.05 ppm)

IR ν_{max}: 3546.8 (enol OH), 1580.9 (C=O).

1-(3-Chloro-4-fluorophenyl)-3-(3-fluoro-4-methoxyphenyl) propane-1,3-dione (30)



30

Compound (30) was synthesised from 3-fluoro-4-chloroacetophenone (0.30 g, 1.72 mmol) and methyl-3-fluoro-4-methoxybenzoate (0.40 g, 1.72 mmol) and sodium hydride (0.13 g, 5.17 mmol) as in procedure E. After completion of the reaction was confirmed by TLC (Hex:EtOAc 9:1), recrystallisation from ethanol afforded the title compound (30) as a bright-yellow solid (0.47 g, 1.48 mmol, 67 %).

M.P: 157 – 159 °C; **R_f:** 0.26; (Hex:EtOAc 9:1);

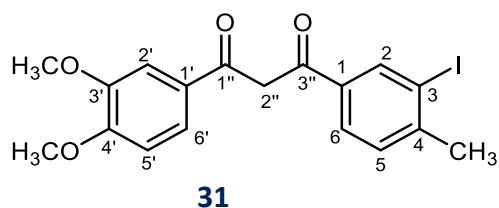
δ_H (CDCl₃, 400 MHz): 3.88 (3 H, s, 4'-OCH₃), 6.64 (1 H, s, 2''), 7.07 (2 H, m, 5, 5'), 7.73 (1 H, dd, J = 12.20 Hz, 2.13 Hz, 6'), 7.77 (1 H, d, J = 8.98 Hz, 2'), 7.87 (1 H, dd, J = 8.70 Hz, 2.25 Hz, 6), 7.99 (1 H, J = 2.25 Hz, 2), 16.90 (1 H, s, enolic H)

δ_C (CDCl₃, 100 MHz): 56.2 (1 C, 4'-OCH₃), 91.7 (1 C, 2''), 11.6 (1 C, 2), 112.7 (1 C, d, J = 1.69 Hz, 5'), 114.9 (1 C, d, J = 19.9 Hz, 2'), 122.9 (1 C, 3), 124.1 (1 C, d, J = 3.24 Hz, 6'), 127.5 (1 C, 5), 128.4 (1 C, d, J = 7.8 Hz, 1''), 128.6 (1 C, 1), 129.2 (1 C, 6), 151.4 (1 C, d, J = 10.8 Hz, 4') 153.3 (1 C, d, J = 247.7 Hz, 3'), 158.3 (1 C, 4), 183.6 (1 C, 3''), 183.7 (1 C, d, J = 2.36 Hz, 1'').

m/z HRMS (ESI) [M + H]: Calculated for C₁₆H₁₁ClF₂O₃ 325.0438 found 325.0446 (ΔMs=2.61 ppm)

IR ν_{max}: 3074.6 (enol OH), 1615.5 (C=O).

1-(3,4-Dimethoxyphenyl)-3-(3-iodo-4-methyl)-1,3-propanedione (31)



Compound (31) was synthesised from 3,4-dimethoxyacetophenone (0.49 g, 2.71 mmol) and methyl-3-iodo-4-methylbenzoate (0.56 g, 3.41 mmol) and sodium hydride (0.19 g, 8.09 mmol) as in procedure E. After completion of the reaction was confirmed by TLC (Hex:EtOAc 8:2), recrystallisation from ethanol afforded the title iodo compound (31) as a dark brown solid (0.78 g, 1.88 mmol, 54 %).

M.P: 103 – 105 °C; **R_f:** 0.27; (Hex:EtOAc 8:2);

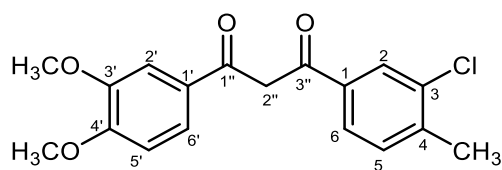
δ_H (CDCl₃, 400 MHz): 2.49 (3 H, s, 4-CH₃), 3.96 (3 H, s, 4'-OCH₃), 3.98 (3 H, s, 3'-OCH₃), 6.73 (1 H, s, 2''-H), 6.94 (1 H, d, *J* = 8.4 Hz, H-5'), 7.35 (1 H, d, *J* = 8.0 Hz, H-5), 7.57 (1 H, d, *J* = 2.0 Hz, H-2), 7.64 (1 H, dd, *J* = 8.4 Hz, 2.0 Hz, H-6'), 7.86 (1 H, dd, *J* = 8.0 Hz, 1.6 Hz, H-6), 8.40 (1 H, d, *J* = 1.6 Hz, H-2), 16.96 (1 H, s, enolic H)

δ_C (CDCl₃, 100 MHz): 28.3 (1 C, 4-CH₃), 56.1 (2 C, 3', 4'-OCH₃), 92.3 (1 C, 2''), 101.2 (1 C, 3), 109.8 (1 C, 2'), 110.4 (1 C, 5'), 109.8 (1 C, 6'), 110.4 (1 C, 6), 128.4 (1 C, 1), 129.8 (1 C, 5), 134.7 (1 C, 1'), 137.4 (1 C, 2), 146.0 (1 C, 4), 149.1 (1 C, 3'), 153.0 (1 C, 4'), 181.7 (1 C, 3''), 186.6 (1 C, 1'').

***m/z* HRMS (ESI) [M + H]:** Calculated for C₁₈H₁₇IO₄ 425.0244 found 425.0246 (ΔMs=0.40 ppm)

IR ν_{max}: 3076.2 (enol OH), 1674.4 (C=O).

1-(3-Chloro-4-methylphenyl)-3-(3,4-dimethoxyphenyl)propane-1,3-dione (32)



32

Compound (32) was synthesised from 3,4-dimethoxyacetophenone (0.50 g, 2.77 mmol) and methyl-3-chloro-4-methylbenzoate (0.57 g, 3.41 mmol) and sodium hydride (0.19 g, 8.10 mmol) as in procedure E. After completion of the reaction was confirmed by TLC (Hex:EtOAc 7:3), recrystallisation from ethanol afforded the title chloro compound (32) as a yellow solid (0.78 g, 2.34 mmol, 68 %).

M.P: 106 – 108 °C; **R_f:** 0.29; (Hex:EtOAc 7:3);

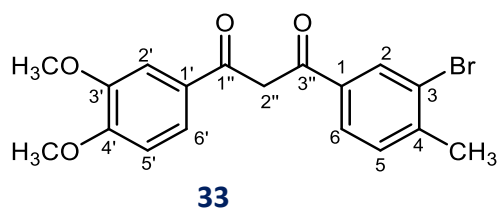
δ_H (CDCl₃, 400 MHz): 2.47 (3 H, s, CH-4), 3.99 (3 H, s, 4'-OCH₃), 4.01 (3 H, s, 3'-OCH₃), 6.76 (1 H, s, 2''-H), 6.96 (1 H, d, J = 8.4 Hz, H-5'), 7.36 (1 H, d, J = 8.23 Hz, H-5), 7.58 (1 H, d, J = 2.12 Hz, H-2), 7.65 (1 H, dd, J = 8.4 Hz, 2.11 Hz, H-6'), 7.79 (1 H, dd, J = 8.23 Hz, 2.11 Hz, H-6), 7.96 (1 H, d, J = 2.12 Hz, H-2'), 16.96 (1 H, s, enolic H)

δ_C (CDCl₃, 100 MHz): 20.3 (1 C, 4-CH₃), 56.1 (2 C, 3', 4'-OCH₃), 92.31 (1 C, 2''), 109.74 (1 C, 2'), 110.74 (1 C, 5'), 121.45 (1 C, 6'), 125.11 (1 C, 6), 127.55 (1 C, 2), 128.41 (1 C, 1'), 131.15 (1 C, 5), 134.69 (1 C, 4), 134.92 (1 C, 3), 140.62 (1 C, 1), 149.14 (1 C, 3'), 153.05 (1 C, 4'), 182.06 (1 C, 3''), 186.6 (1 C, 1'').

m/z HRMS (ESI) [M + H]: Calculated for C₁₈H₁₇ClO₄ 333.0888 found 333.0889 (ΔMs=0.20 ppm)

IR ν_{max}: 3099.7 (enol OH), 1718.3 (C=O).

1-(3-Bromo-4-methylphenyl)-3-(3,4-dimethoxyphenyl)propane-1,3-dione (33)



Compound (33) was synthesised from 3,4-dimethoxyacetophenone (0.50 g, 2.77 mmol) and methyl-3-bromo-4-methylbenzoate (0.57 g, 3.41 mmol) and sodium hydride (0.20 g, 8.12 mmol) as in procedure E. After completion of the reaction was confirmed by TLC (Hex:EtOAc 7:3), recrystallisation from ethanol afforded the title bromo compound (33) as a yellow solid (1.15 g, 3.04 mmol, 89 %).

M.P: 128 – 130 °C; **R_f:** 0.33; (Hex:EtOAc 7:3);

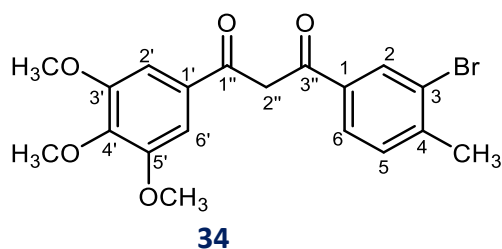
δ_H (CDCl₃, 400 MHz): 2.45 (3 H, s, 4-CH₃), 3.95 (3 H, s, 4'-OCH₃), 3.97 (3 H, s, 3'-OCH₃), 6.72 (1 H, s, 2''), 6.93 (1 H, d, J = 8.37 Hz, 5'-H), 7.32 (1 H, d, J = 8.00 Hz, 5-H), 7.54 (1 H, d, J = 2.00 Hz, 2'-H), 7.62 (1 H, dd, J = 8.37 Hz, 1.97 Hz, 6'-H), 7.80 (1 H, dd, J = 8.00 Hz, 1.65 Hz, 6-H), 8.11 (1 H, d, J = 1.65 Hz, 2-H), 16.9 (1 H, s, enolic H).

δ_C (CDCl₃, 100 MHz): 23.2 (1 C, 4-CH₃), 56.1 (2 C, 3',4'-OCH₃), 92.3 (1 C, 2''), 109.6 (1 C, 2'), 110.4 (1 C, 5'), 121.5 (1 C, 6'), 125.3 (1 C, 3), 125.8 (1 C, 6), 128.3 (1 C, 1'), 130.8 (1 C, 5), 130.9 (1 C, 2), 134.8 (1 C, 1), 142.4 (1 C, 4), 149.1 (1 C, 3'), 153.1 (1 C, 4'), 181.8 (1 C, 3''), 186.6 (1 C, 1'').

m/z HRMS (ESI) [M + H]: Calculated for C₁₈H₁₇BrO₄ 377.0383 found 377.0380 (ΔMs=0.71 ppm)

IR ν_{max}: 3079 (enol OH), 1679 (C=O).

1-(3-Bromo-4-methylphenyl)-3-(3,4,5-trimethoxyphenyl) propane-1,3-dione (34)



Compound (34) was synthesised from 3',4',5'-trimethoxyacetophenone (0.49 g, 2.72 mmol) and methyl-3-bromo-4-methylbenzoate (0.56 g, 3.41 mmol) and sodium hydride (0.20 g, 8.15 mmol) as in procedure E. After completion of the reaction was confirmed by TLC (Hex:EtOAc 8:2), recrystallisation from ethanol afforded the title bromo compound (34) as yellow crystals (0.38 g, 0.90 mmol, 28 %).

M.P: 108 – 110 °C; **R_f:** 0.29; (Hex:EtOAc 8:2);

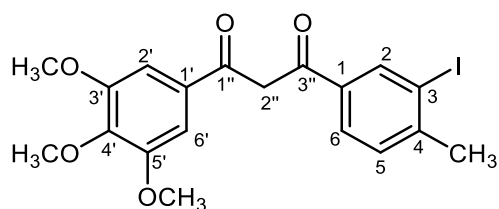
δ_H (CDCl₃, 400 MHz): 2.47 (3 H, s, 4-CH₃), 3.93 (3 H, s, 4'-OCH₃), 3.96 (6 H, s, 3', 5'-OCH₃), 6.69 (1 H, s, 2''), 7.22 (2 H, s, 2', 6'-H), 7.35 (1 H, d, *J* = 8.13 Hz, 5-H), 7.87 (1 H, dd, *J* = 8.13 Hz, 2.01 Hz, 6-H), 8.40 (1 H, d, *J* = 2.01 Hz, H-2), 16.9 (1 H, s, enolic H)

δ_C (CDCl₃, 100 MHz): 23.2 (1 C, 4-CH₃), 56.4 (2 C, 3',4'-OCH₃), 61.0 (1 C, 4'-OCH₃), 92.7 (1 C, 2''), 104.7 (2 C, 2', 6'), 125.3 (1 C, 4), 125.9 (1 C, 6), 130.8 (1 C, 1'), 131.0 (1 C, 5), 131.0 (1 C, 1'), 134.8 (1 C, 1'), 140.5 (1 C, 4'), 142.8 (1 C, 3), 153.3 (2 C, 3', 5'), 183.1 (1 C, 3''), 186.1 (1 C, 1'').

***m/z* HRMS (ESI) [M + H]:** Calculated for C₁₉H₁₉BrO₅ 407.0489 found 407.0486 (ΔMs=0.58 ppm)

IR ν_{max}: 3065.7 (enol OH), 1678.6 (C=O).

1-(3-Iodo-4-methylphenyl)-3-(3,4,5-trimethoxyphenyl)propane-1,3-dione (35)



35

Compound (35) was synthesised from 3',4',5'-trimethoxyacetophenone (0.50 g, 2.38 mmol) and methyl-3-iodo-4-methylbenzoate (0.83 g, 3.00 mmol) and sodium hydride (0.17 g, 4.14 mmol) as in procedure E. After completion of the reaction was confirmed by TLC (Hex:EtOAc 9:1), recrystallisation from ethanol afforded the title iodo compound (35) as a brown solid (0.95 g, 2.10 mmol, 88 %).

M.P: 107 – 109 °C; **R_f:** 0.25; (Hex:EtOAc 9:1);

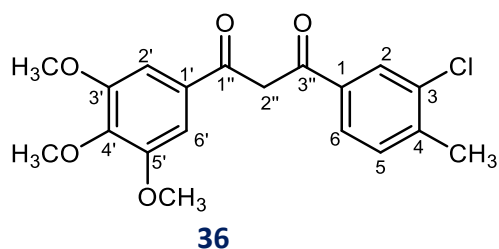
δ_H (CDCl₃, 400 MHz): 2.51 (3 H, s, 4-CH₃), 3.95 (3 H, s, 4'-OCH₃), 3.98 (6 H, s, 3',5'-OCH₃), 6.67 (1 H, s, 2''), 7.20 (2 H, s, 2',6'-H), 7.32 (1 H, d, *J* = 8.06 Hz, 5-H), 7.84 (1 H, dd, *J* = 8.06 Hz, 1.88 Hz, 6-H), 8.37 (1 H, d, *J* = 1.87 Hz, 2-H), 16.9 (1 H, s, enolic H)

δ_C (CDCl₃, 100 MHz): 28.4 (1 C, 4-CH₃), 56.4 (2 C, 3',5'-OCH₃), 61.0 (1 C, 4'-OCH₃), 92.7 (1 C, 2''), 101.2 (1 C, 3), 104.8 (2 C, 2' 6'), 126.8 (1 C, 6), 129.8 (1 C, 5), 130.8 (1 C, 1'), 134.6 (1 C, 1), 137.5 (1 C, 2), 142.2 (1 C, 3), 146.2 (1 C, 4'), 153.2 (2 C, 3', 5'), 182.9 (1 C, 3''), 186.1 (1 C, 1'').

***m/z* HRMS (ESI) [M + H]:** Calculated for C₁₉H₁₉ClO₅ 455.0350 found 455.0352 (Δ*M*_s=0.47 ppm)

IR *u*_{max}: 3099.1 (enol OH), 1676.3 (C=O).

1-(3-Chloro-4-methylphenyl)-3-(3,4,5-trimethoxyphenyl) propane-1,3-dione (36)



Compound (36) was synthesised from 3',4',5'-trimethoxyacetophenone (0.50 g, 2.38 mmol) and methyl-3-chloro-4-methylbenzoate (0.83 g, 3.00 mmol) and sodium hydride (0.17 g, 7.14 mmol) as in procedure E. After completion of the reaction was confirmed by TLC (Hex:EtOAc 7:3), recrystallisation from ethanol afforded the title chloro compound (36) as a yellow solid (0.83 g, 2.29 mmol, 76 %).

M.P: 108 – 110 °C; **R_f:** 0.42; (Hex:EtOAc 7:3);

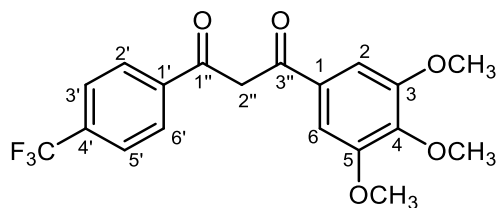
δ_H (CDCl₃, 400 MHz): 2.47 (3 H, s, 4-CH₃), 3.96 (3 H, s, 4'-OCH₃), 3.98 (6 H, s, 3', 5'-OCH₃), 6.72 (1 H, s, 2''), 7.24 (2H, s, 2', 6'-H), 7.37 (1 H, d, *J* = 7.80 Hz, 5-H), 7.80 (1 H, dd, *J* = 7.89 Hz, 1.82 Hz, 6-H), 7.96 (1H, d, *J* = 1.82 Hz, 2-H), 16.9 (1 H, s, enolic H)

δ_C (CDCl₃, 100 MHz): 20.4 (1 C, 4-CH₃), 56.4 (2 C, 3',5'-OCH₃), 61.0 (1 C, 4'-OCH₃), 92.7 (1 C, 2''), 104.7 (2 C, 2',6'), 125.2 (1 C, 5), 127.7 (1 C, 6), 130.8 (1 C, 1'), 131.2 (1 C, 2), 134.6 (1 C, 1), 134.9 (1 C, 3), 140.9 (1 C, 4'), 142.5 (1 C, 4), 153.3 (2 C, 3',5), 183.2 (1 C, 3''), 186.1 (1 C, 1'').

***m/z* HRMS (ESI) [M + H]:** Calculated for C₁₉H₁₉ClO₅ 363.0994 found 363.0994 (ΔM_s=0.05 ppm)

IR u_{max}: 3065.6 (enol OH), 1674.0 (C=O).

1-(4-(Trifluoromethyl)phenyl)-3-(3,4,5-trimethoxyphenyl)propane-1,3-dione (37)



37

Compound (37) was synthesised from 3',4',5'-trimethoxyacetophenone (0.50 g, 2.38 mmol) and methyl-4-(trifluoromethyl) benzoate (0.83 g, 3.00 mmol) and sodium hydride (0.17 g, 7.14 mmol) as in procedure E. After completion of the reaction was confirmed by TLC (Hex:EtOAc 7:3), recrystallisation from ethanol afforded the title trifluoromethyl compound (37) as a yellow solid (0.81 g, 3.29 mmol, 89 %).

M.P: 98 – 100 °C; **R_f:** 0.38; (Hex:EtOAc 7:3);

δ_H (CDCl₃, 400 MHz): 3.87 (3 H, s, 4-OCH₃), 3.89 (6 H, s, 3, 5-OCH₃), 6.70 (1 H, s, 2''), 7.16 (2 H, s, 2, 6-H), 7.69 (2 H, d, *J* = 8.19 Hz, H-3',5'), 8.01 (2 H, d, *J* = 8.19 Hz, H-2',6'), 16.7 (1 H, s, enolic H).

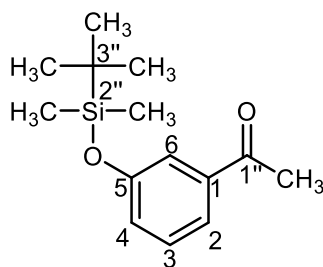
δ_C (CDCl₃, 100 MHz): 20.4 (1 C, 4-CH₃), 56.4 (2 C, 3, 5-OCH₃), 61.0 (1 C, 4-OCH₃), 93.5 (1 C, 2''), 104.9 (2 C, 2,6), 125.7 (2 C, q, *J* = 3.4 Hz, 3', 5'), 127.4 (1 C, 2', 6'), 127.8 (1 C, q, *J* = 274.4 Hz, C-F₃), 130.7 (1 C, 1), 134.1 (1 C, q, *J* = 33.5 Hz, 4'), 138.5 (1 C, 4), 142.5 (1 C, 1'), 153.3 (2 C, 3, 5), 182.0 (1 C, 3''), 187.4 (1 C, 1'').

δ_F (CDCl₃, 564 MHz): -63.2 (3 F, s, 4'-CF₃).

***m/z* HRMS (ESI) [M + H]:** Calculated for C₁₉H₁₇F₃O₅ 383.1101 found 383.1103 (ΔMs=0.66 ppm)

IR ν_{max}: 3076.6 (enol OH), 1667.3 (C=O)

1-[3-(tert-Butyldimethylsilyloxy)phenyl]ethanone (38)



(38)

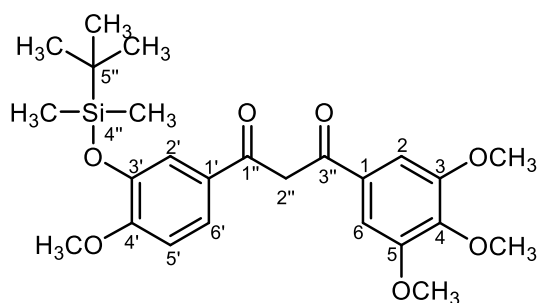
To a solution of 3-hydroxyacetophenone (1 g, 6.57 mmol) in dry DMF (15 mL) and N,N-diisopropylethylamine (0.85 g, 6.57 mmol) was added t-butyldimethylsilyl chloride (1.89 g, 7.88 mmol) according to procedure B. A crude oily product was obtained which was purified by column chromatography (Hex:EtOAc 8:2, R_f = 0.3) to give the title ketone (38) as a colourless oil. (1.21 g, 5.40 mmol, 84 %)

δ_{H} (CDCl₃, 400 MHz): 0.0 (6 H, s, 2''-CH₃), 0.78 (9 H, s, 3''-CH₃), 2.34 (3 H, s, O=C-CH₃), 6.83 (1 H, dd, J = 8.12 Hz, 2.55 Hz, 4), 7.11 (1 H, t, J = 7.44 Hz, 3), 7.20 (1 H, t, J = 2.04 Hz, 6), 7.33 (1 H, dt, J = 7.85 Hz, 0.86 Hz, 2) (Aggarwal *et al.*, 2003).

δ_{C} (CDCl₃, 100 MHz): -4.18 (2 C, 2''-CH₃), 18.2 (1 C, 3''), 25.6 (3 C, 3''), 25.6 (3 C, 3''-(CH₃)₃), 26.7 (1C, 1''-CH₃), 119.4 (1 C, 4), 121.6 (1 C, 3), 124.9 (1 C, 6), 129.5 (1 C, 2), 138.6 (1 C, 1), 155.9 (1 C, 1'').

IR ν_{max} : 1683.2 (C=O), 1550.8 (C=C)

(Z)-1-(3-((tert-Butyldimethylsilyloxy)-4-methoxyphenyl)-3-hydroxy-3-(3,4,5-trimethoxyphenyl)prop-2-en-1-one (39)



(39)

LiHMDS (1M, 0.5 g, 2.98 mmol) was added to 3,4,5-trimethoxyacetophenone (0.3 g, 1.48 mmol) in THF (15 mL) according to procedure C. After 30 minutes a solution of methyl-3-[(tert-butyldimethylsilyloxy) benzoate (0.44 g, 1.48 mmol) in THF (8 mL) was added and stirring continued for 60 minutes at -78 °C and at room temperature for 48 hours. After completion of the reaction was confirmed by TLC (Hex:EtOAc 7:3) column chromatography gave the title compound (39) as a yellow oil (0.11 g, 0.23 mmol, 5 %).

R_f: 0.29; (Hex:EtOAc 7:3);

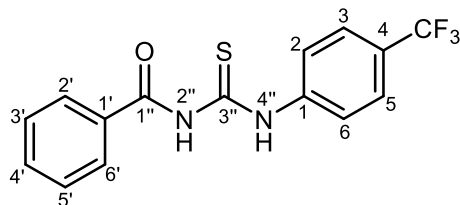
δ H(CDCl₃, 400 MHz): 0.0 (6 H, s, Si-CH₃), 0.83 (9 H, s, C-(CH₃)₃), 3.70 (3H, s, 4'-OCH₃), 3.73 (3H, s, OCH₃, 4), 3.76 (6 s, OCH₃, 3,5), 6.47 (1H, s, 2''), 6.73 (1H, d, J = 8.4 Hz, 5'), 7.0 (2 H, s, 2, 6-H), 7.31 (1H, d, J = 2.29 Hz, 2'), 7.43 (1H, dd, J = 2.29 Hz, 8.4 Hz, 6') 16.79 (1 H, s, enolic)

13 C NMR (CDCl₃, 100 MHz): -4.6 (2 C, 4''), 18.5 (1 C, 5''), 25.7 (3 C, C(CH₃)₃), 55.5 (1 C, OCH₃, 4), 56.3 (2 C, OCH₃, 3,5), 61.0 (1 C, OCH₃, 4'), 92.3 (1 C, 2''), 104.5 (2 C, 2, 6), 111.2 (1 C, 5'), 119.6 (1 C, 2''), 121.9 (1 C, 6'), 128.3 (1 C, 1'), 131.1 (1 C, 1), 141.8 (1 C, 3'), 145.1 (1 C, 4'), 153.2 (1 C, 4), 155.0 (2 C, 3, 5), 184.4 (1 C, 3''), 185.1 (1 C, 1'')

IR ν_{max} : 3021.6 (enol OH), 1649.1 (C=O)

BENZOYL THIOUREA ANALOGUES

N-((4-(trifluoromethyl)phenyl)carbamothioyl)benzamide (40)



40

Compound (40) was synthesised from benzoyl chloride (0.5 g, 3.56 mmol) and 4-methyl-trifluoroaniline (0.57 g, 3.56 mmol) and ammonium isothiocyanate (0.27 g, 3.56 mmol) as in **procedure F**. After completion of the reaction was confirmed by TLC (Hex:EtOAc 8:2), recrystallisation from methanol afforded the title amide (40) as white crystals (0.69 g, 2.13 mmol, 59 %).

M.P: 108 – 110 °C; lit. (107-108 °C) (Rauf *et al.*, 2013), **R_f**:0.38; (Hex:EtOAc 8:2);

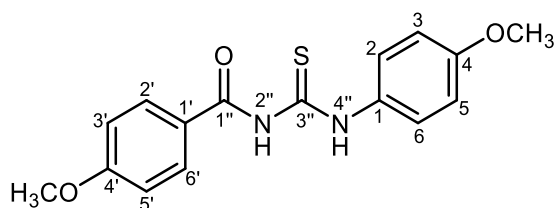
δ H(CDCl₃, 600 MHz): 7.56 – 7.60 (2 H, m, Ar-H), 7.68 – 7.72 (3 H, m, Ar-H), 7.91 – 7.96 (4 H, m, Ar-H), 9.13 (1 H, s, 2''), 12.9 (1 H, s, 4'').

13 C NMR (CDCl₃, 150 MHz): 123.7 (2 C, 2,6), 126.1 (2 C, q, J = 3.67 Hz, 3, 5), 127.1 (1 C, q, J = 270.1 Hz, 4-CF₃), 127.5 (2 C, 2', 6'), 128.9 (1 C, q, 33.7 Hz, 4), 129.3 (2 C, 3', 5'), 131.3 (1 C, 1'), 134.0 (1 C, 4'), 140.6 (1 C, 1), 167.7 (1 C, 1''), 178.4 (1 C, 3'').

19 F NMR (400 MHz): -62.4 (3 F, s, 4-CF₃).

IR ν_{max} : 3227.7 (NH), 1673.5 (C=O), 1236.2 (C=S).

4-Methoxy-N-((4-methoxyphenyl)carbamothioyl)benzamide (41)



41

Compound (41) was prepared from 4-methoxybenzoyl chloride (2.0 g, 11.7 mmol) and p-anisidine (4-methoxyaniline) (1.44 g, 11.7 mmol) and ammonium isothiocyanate (0.88 g, 11.7 mmol) as in procedure F. After completion of the reaction was confirmed by TLC (Hex:EtOAc 8:2), recrystallisation from methanol afforded the title benzamide (41) as white crystals (3.26 g, 10.3 mmol, 87 %).

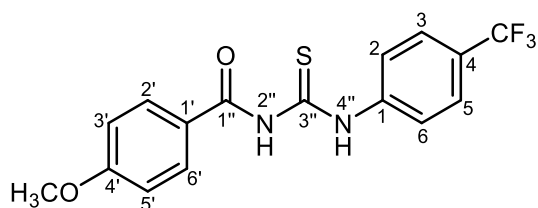
M.P: 159 - 161 °C; lit: 152 – 155 °C (Huang *et al.*, 2013) **R_f**:0.31; (Hex:EtOAc 8:2);

δ_H(CDCl₃, 400 MHz): 3.82 (3 H, s, 4'-OCH₃), 3.88 (3 H, s, 4-OCH₃), 6.94 (2 H, d, J = 8.9 Hz, 3, 5), 7.00 (2 H, d, J = 8.8 Hz, 3', 5'), 7.57 (2 H, d, J = 8.9 Hz, 2, 6), 7.86 (2 H, d, J = 8.8 Hz, 2', 6'), 9.06 (1 H, s, 1''), 12.5 (1 H, s, 3'').

δ_C (CDCl₃, 100 MHz): 55.5 (1 C, 4-OCH₃), 56.7 (1 C, 4'-OCH₃), 114.1 (2 C, 3',5'), 114.5 (2 C, 3, 5), 123.5 (1 C, 1), 128.9 (2 C, 2', 6'), 129.7 (2 C, 2, 6), 130.7 (1 C, 1'), 158.2 (1 C, 4), 164.0 (1 C, 4'), 166.4 (1 C, 1''), 178.9 (1 C, 3'')

IR ν_{max}: 3413 (NH), 16545 (C=O), 1233 (C=S).

4-Methoxy-N-((4-(trifluoromethyl)phenyl)carbamothioyl)benzamide



42

Compound (42) was prepared from 4-methoxybenzoyl chloride (0.50 g, 2.93 mmol) and 4-methyl-trifluoroaniline (0.47 g, 2.93 mmol) and ammonium isothiocyanate (0.22 g, 2.93 mmol) as in [procedure F](#). The completion of the reaction was confirmed by TLC (Hex : EtOAc 7:3), recrystallisation from methanol afforded the title benzamide as yellow crystals (0.71 g, 2.00 mmol, 68 %).

M.P: 144 - 148 °C, lit. 154 – 156 °C (Qiao *et al.*, 2017); **R_f**:0.25; (Hex : EtOAc 7:3);

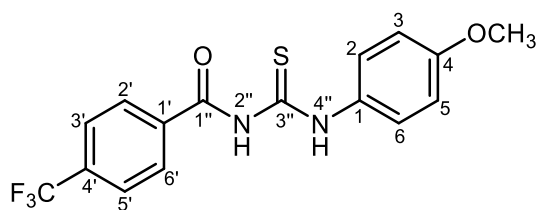
δ_H(CDCl₃, 400 MHz): 3.90 (3 H, 4'-OCH₃), 7.03 (2 H, d, J = 8.86 Hz, 3' 5'), 7.68 (2 H, d, J = 8.60 Hz, 2, 6), 7.88 (2 H, d, J = 8.86 Hz, 2', 6'), 7.93 (2 H, d, J = 8.60 Hz, 3, 5), 9.06 (1 H, s, 2''), 12.9 (1 H, s, 4'').

δ_C (CDCl₃, 100 MHz): 55.7 (1 C, 4'-OCH₃), 114.6 (2 C, 3', 5'), 123.1 (1 C, 1'), 123.7 (2 C, q, J = 2, 6), 126.1 (2 C, q, J = 3.53 Hz, 3, 5), 127.9 (1 C, q, J = 268.8 Hz, CF₃), 128.8 (1 C, q, 32.8 Hz, 4), 129.8 (2 C, 2', 6'), 140.8 (1 C, 1), 164.3 (1 C, 4'), 166.5 (1 C, 1''), 178.6 (1 C, 3'').

δ_F (CDCl₃, 564 MHz): -62.3 (3 F, s, 4-CF₃)

IR ν_{max}: 3184 (NH), 1678 (C=O), 1212(C=S)

N-((4-methoxyphenyl)carbamothioyl)-4-(trifluoromethyl)benzamide (43)



43

Compound (43) was prepared from 4-(trifluoromethyl) benzoyl chloride (0.50 g, 2.40 mmol) and p-anisidine (4-methoxyaniline) (0.30 g, 2.40 mmol) and ammonium isothiocyanate (0.18 g, 2.40 mmol) as in [procedure F](#). The completion of the reaction was confirmed by TLC (Hex: EtOAc 6:4), recrystallisation from methanol afforded the title benzamide (43) as yellow crystals (0.80 g, 2.24 mmol, 94 %).

M.P: 132 – 134 °C; Rf:0.37; (Hex: EtOAc 6:4).

δ_{H} (CDCl₃, 600 MHz): 3.86 (3 H, s, 4-OCH₃), 6.99 (2 H, d, J = 8.70 Hz, 3, 5), 7.60 (2 H, d, J = 8.70 Hz, 2, 6), 7.85 (2 H, d, J = 8.24 Hz, 3', 5'), 8.04 (2 H, J = 8.24 Hz, 2' 6'), 9.08 (1 H, s, 2''), 12.3 (1 H, s, 4'').

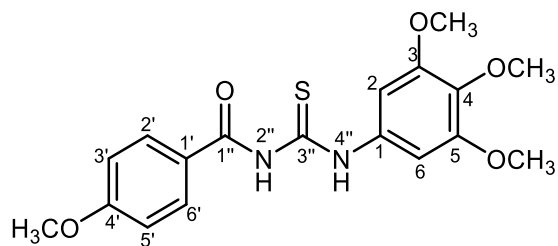
δ_{C} (CDCl₃, 150 MHz): 55.2 (1 C, 4-OCH₃), 114.1 (2 C, 3, 5), 126.3 (2 C, 2, 6), 127.3 (2 C, q, J = 3.41 Hz, 3', 5'), 127.9.1 (1 C, q, J = 266.3 Hz, CF₃), 128.7 (1 C, q, J = 1.23 Hz, 2, 6), 131.2 (1 C, 1), 132.4 (1 C, q, J = 31.6 Hz, 4'), 136.7 (1 C, 1'), 156.6 (1 C, 4), 167.3 (1 C, 1''), 177.4 (1 C, 3'').

δ_{F} (CDCl₃, 564 MHz): -62.3 (3 F, s, 4-CF₃)

m/z HRMS (ESI) [M + H]: Calculated for C₁₆H₁₃F₃N₂O₂S 355.0723 found 355.0721 ($\Delta M_s=0.47$ ppm)

IR ν_{max} : 3083 (NH), 1622 (C=O), 1243 (C=S)

4-Methoxy-N-((3,4,5-trimethoxyphenyl)carbamothioyl)benzamide (44)



44

Compound (44) was prepared from 4-methoxybenzoyl chloride (1.00 g, 4.34 mmol) and 3,4,5-trimethoxyaniline (0.47 g, 4.34 mmol) and ammonium isothiocyanate (0.33 g, 4.34 mmol) as in [procedure F](#). The completion of the reaction was confirmed by TLC (Hex: EtOAc 8:2), recrystallisation from methanol afforded the title benzamide (44) as yellow crystals (0.98 g, 2.60 mmol, 60 %).

M.P: °C; **R_f**:0.29; (Hex: EtOAc 8:2);

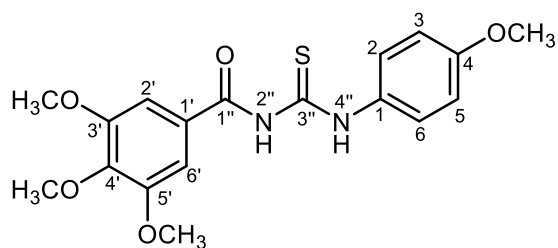
δ_H(CDCl₃, 400 MHz): 3.88 (3 H, s, 4'-OCH₃), 3.89 (6 H, s, 3, 5-OCH₃), 3.92 (3 H, s, 4'-OCH₃), 7.03 (2 H, d, J = 8.88 Hz, 3, 5), 7.09 (2 H, s, 2, 6), 7.89 (2 H, d, J = 8.88 Hz, 2, 6), 9.02 (1 H, s, 2''), 12.7 (1 H, s, 4'').

δ_C (CDCl₃, 100 MHz): 55.7 (1 C, 4-OCH₃), 56.2 (2 C, 3, 5-OCH₃), 60.9 (1 C, 4-OCH₃), 101.2 (2 C, 2, 6), 114.5 (2 C, 3', 5'), 123.4 (1 C, 1'), 129.7 (2 C, 2', 6'), 133.4 (1 C, 4), 136.4 (1 C, 1), 153.2 (2 C, 3, 5), 164.2 (1 C, 4'), 166.4 (1 C, 1''), 177.8 (1 C, 3'').

m/z HRMS (ESI) [M + H]: Calculated for C₁₈H₂₀N₂O₅S 377.1166 found 377.1164 (ΔM_s=0.42 ppm)

IR ν_{max}: 3132 (NH), 1656 (C=O), 1219 (C=S)

3,4,5-Trimethoxy-N-((4-methoxyphenyl)carbamothioyl)benzamide (45)



45

Compound (45) was prepared from 3,4,5-trimethoxybenzoyl chloride (1.20 g, 5.20 mmol) and 4-methoxyaniline (0.64 g, 5.20 mmol) and ammonium isothiocyanate (0.39 g, 5.20 mmol) as in [procedure F](#). The completion of the reaction was confirmed by TLC (Hex: EtOAc 7:3), recrystallisation from methanol afforded the title benzamide (45) as white needle (1.06 g, 2.82 mmol, 54 %).

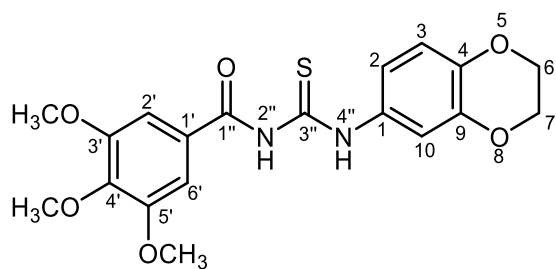
M.P: 165 - 168 °C; lit (Saeed *et al.*, 2010); **R_f**:0.33; (Hex: EtOAc 7:3);

δ_H(CDCl₃, 400 MHz): 3.84 (3 H, s, 4-OCH₃), 3.95 (3 H, 4'-OCH₃), 3.96 (6 H, s, 3', 5'-OCH₃), 6.97 (2 H, d, J = 8.58 Hz, 3, 5), 7.10 (2 H, s, 2', 6'), 7.60 (2 H, d, J = 8.58 Hz, 2, 6), 9.08 (1 H, s, 2''), 12.4 (1 H, s, 4'').

δ_c (CDCl₃, 100 MHz): 55.5 (1 C, 4-OCH₃), 56.5 (2 C, 3', 5'- OCH₃), 61.1 (1 C, 4'- OCH₃), 104.9 (2 C, 2', 6'), 114.1 (2 C, 3, 5), 125.8 (2 C, 2, 6), 126.6 (1 C, 1'), 130.5 (1 C, 1), 142.9 (1 C, 4'), 153.6 (2 C, 3', 5'), 158.43 (1 C, 4), 166.7 (1 C, 1''), 178.6 (1 C, 3'').

IR ν_{max}: 3234 (NH), 1665 (C=O), 1214 (C=S)

N-((2,3-Dihydrobenzo[b][1,4]dioxin-6-yl)carbamothioyl)-3,4,5-trimethoxybenzamide (46)



(46)

Compound (46) was prepared from 3,4,5-trimethoxybenzoyl chloride (0.50 g, 2.18 mmol) and 2,3-dihydro-1,4-benzodioxin-6-amine (1.20 g, 2.18 mmol) and ammonium isothiocyanate (0.17 g, 2.17 mmol) as in **procedure F**. The completion of the reaction was confirmed by TLC (Hex: EtOAc 8:2), recrystallisation from methanol afforded the title benzamide (46) as white crystals (0.59 g, 1.46 mmol, 67 %).

M.P: 184 - 186 °C; **R_f**:0.21; (Hex: EtOAc 8:2);

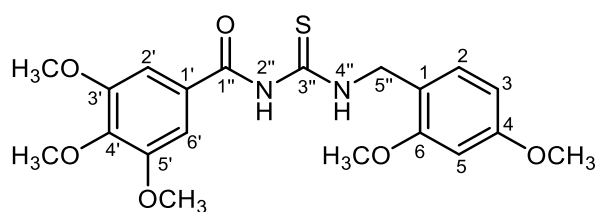
δ_H(CDCl₃, 400 MHz): 3.95 (3 H, s, 4'-OCH₃), 3.96 (6 H, s, 3', 5'-OCH₃), 4.30 (4 H, s, 6, 7), 6.93 (1 H, d, J = 8.63 Hz, 3), 7.08 (1 H, dd, J = 8.63 Hz, 2.45 Hz, 2), 7.10 (2 H, s, 2', 6'), 7.35 (1 H, d, J = 2.45 Hz, 10), 9.05 (1 H, s, 1''), 12.43 (1 H, s, 4'').

δ_C (CDCl₃, 100 MHz): 56.5 (2 C, 3', 5'-OCH₃), 61.1 (1 C, 4'-OCH₃), 64.3 (2 C, 6, 7), 104.9 (2 C, 3', 5'), 113.7 (1 C, 10), 117.3 (1 C, 2), 117.7 (1 C, 3), 126.6 (1 C, 1'), 131.0 (1 C, 1), 142.4 (1 C, 9), 142.9 (1 C, 4'), 143.4 (1 C, 4), 153.6 (1 C, 2, 3', 5'), 166.6 (1 C, 1''), 178.4 (1 C, 3'').

m/z HRMS (ESI) [M + H]: Calculated for C₁₉H₂₀N₂O₆S 405.1115 found 405.1113 (ΔM_s=0.48 ppm)

IR ν_{max}: 3221 (NH), 1628 (C=O), 1198 (C=S)

N-((2,4-Dimethoxybenzyl)carbamothioyl)-3,4,5-trimethoxybenzamide (47)



(47)

Compound (47) was prepared from 3,4,5-trimethoxybenzoyl chloride (0.50 g, 2.17 mmol) and 2,4-benzylamine (1.20 g, 2.17 mmol) and ammonium isothiocyanate (0.16 g, 2.17 mmol) as in [procedure F](#). The completion of the reaction was confirmed by TLC (Hex: EtOAc 8:2), recrystallisation from methanol afforded the title benzamide (47) as orange crystals (0.45 g, 1.07 mmol, 49 %).

M.P: 154 - 156 °C; **R_f**:0.28; (Hex: EtOAc 8:2);

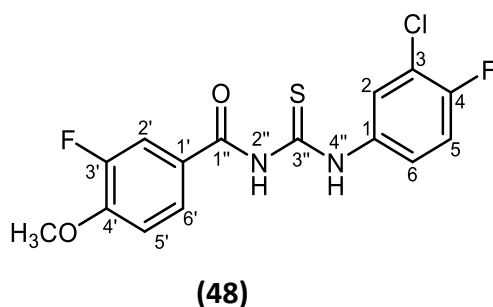
δ_H(CDCl₃, 400 MHz): 3.82 (3 H, s, 4'-OCH₃), 3.91 (3 H, s, 4-OCH₃), 3.92 (3 H, s, 5-OCH₃), 3.93 (6 H, s, 3', 5'-OCH₃), 4.87 (2 H, d, J = 5.26 Hz, 5''), 6.50 (1 H, dd, J = 8.38 Hz, 2.20 Hz, 3), 6.51 (1 H, d, J = 2.21 Hz, 5), 7.02 (2 H, s, 2', 6'), 7.34 (1 H, d, J = 8.20 Hz, 2), 8.92 (1 H, s, 2''), 11.03 (1 H, s, 4'').

δ_C (CDCl₃, 100 MHz): 45.5 (1 C, 5''), 55.4 (1 C, 6-OCH₃), 55.5 (1 C, 4-OCH₃), 56.5 (2 C, 3', 5'-OCH₃), 61.0 (1 C, 4'-OCH₃), 98.7 (1 C, 5), 103.9 (1 C, 3), 104.8 (2 C, 2', 6'), 116.8 (1 C, 1), 127.1 (1 C, 1'), 131.0 (1 C, 2), 142.5 (1 C, 4'), 153.5 (2 C, 3', 5'), 158.7 (1 C, 4), 161.0 (1 C, 6), 166.2 (1 C, 3''), 178.9 (1 C, 3'').

m/z HRMS (ESI) [M + H]: (not found)

IR ν_{max}: 3221 (NH), 1628 (C=O), 1198 (C=S)

N-((3-Chloro-4-fluorophenyl)carbamothioyl)-3-fluoro-4-methoxybenzamide (48)



Compound (48) was prepared from 3-fluoro-4-methoxybenzoyl chloride (1.00 g, 5.30 mmol) and 3-chloro-4-fluoroaniline (2.66 g, 5.33 mmol) and ammonium isothiocyanate (0.40 g, 5.33 mmol) as in [procedure F](#). The completion of the reaction was confirmed by TLC (Hex: EtOAc 7:3), recrystallisation from methanol afforded the title benzamide (48) as orange crystals (1.55 g, 4.34 mmol, 81 %).

M.P: 205 – 207 °C; **R_f**:0.21; (Hex: EtOAc 7:3);

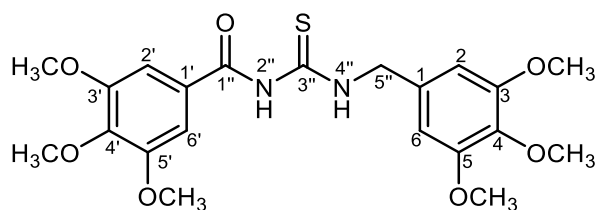
δ_H(DMSO-600 MHz): 3.95 (3 H, s, 4'-OCH₃), 7.34 (1 H, t, J = 8.56 Hz, 5'), 7.49 (1 H, t, J = 9.03 Hz, 5), 7.61 (1 H, m, 6), 7.93 (2 H, m, 2, 6'), 8.00 (1 H, dd, J = 8.55 Hz, 2.23 Hz, 2), 11.6 (1 H, s, 2''), 12.5 (1 H, s, 4'').

δ_C (DMSO-150 MHz): 56.3 (1 C, 4'-OCH₃), 113.2 (1 C, d, J = 1.54 Hz, 5'), 116.3 (1 C, d, J = 20.4 Hz, 2'), 116.8 (1 C, d, J = 22.0 Hz, 5), 119.0 (1 C, d, J = 19.0 Hz, 3), 123.9 (1 C, d, J = 5.86 Hz, 1'), 125.8 (1 C, d, J = 8.65 Hz, 6), 126.5 (1 C, d, J = 3.34 Hz, 2), 126.8 (1 C, 6'), 135.2 (1 C, d, J=3.38 Hz, 1), 151.3 (1 C, d, J = 9.81 Hz, 4'), 151.7 (1 C, d, J = 247.8 Hz, 3'), 156.3 (1 C, d, J = 246.1 Hz, 4), 166.2 (1 C, 1''), 179.8 (1 C, 3'').

m/z HRMS (ESI) [M + H]: Calculated for C₁₅H₁₁ClF₂N₂O₂S 357.0271 found 357.0270 (ΔM_s=0.11 ppm)

IR ν_{max}: 3206 (NH), 1673(C=O), 1216 (C=S)

3,4,5-Trimethoxy-N-((3,4,5-trimethoxybenzyl)carbamothioyl)benzamide (50)



(50)

Compound (50) was prepared from 3,4,5-trimethoxybenzoyl chloride (0.24 g, 1.01 mmol) and 3,4,5-trimethoxybenzylamine (0.20 g, 1.01 mmol) and ammonium isothiocyanate (0.08 g, 1.01 mmol) as in [procedure F](#). The completion of the reaction was confirmed by TLC (Hex: EtOAc 7:3), recrystallisation from methanol afforded the title benzamide (50) as orange crystals (0.22 g, 0.49 mmol, 48 %).

M.P: 159 – 161 °C; R_f : 0.25; (Hex: EtOAc 7:3);

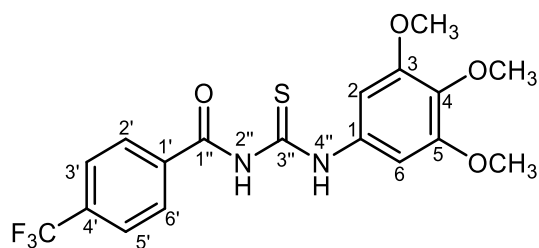
δ_H (CDCl₃, 400 MHz): 3.78 (3 H, s, 4-OCH₃), 3.81 (6 H, s, 3, 5-OCH₃), 3.85 (9 H, s, 3', 4', 5'-OCH₃), 4.77 (2 H, d, $J = 5.09$ Hz, 5''), 6.56 (2 H, s, 2, 6), 6.93 (2 H, s, 2', 6'), 8.97 (1 H, s, 2''), 10.92 (1 H, s, 4'').

δ_C (CDCl₃, 100 MHz): 45.8 (1 C, 5''), 56.1 (2 C, 3, 5-OCH₃), 56.3 (2 C, 3', 5'-OCH₃), 60.7 (1 C, 4'-OCH₃), 60.8 (1 C, 4-OCH₃), 104.9 (2 C, 2, 6), 105.1 (2 C, 2', 6'), 129.8 (1 C, 1'), 135.3 (1 C, 1), 136.2 (1 C, 4), 141.7 (1 C, 4'), 152.3 (2 C, 3', 5'), 153.8 (2 C, 3, 5), 165.9 (1 C, 1''), 178.1 (1 C, 3'').

m/z HRMS (ESI) [M + H]: Calculated for C₂₁H₂₆N₂O₇S 451.1533 found 451.1511 ($\Delta M_s = 4.95$ ppm)

IR ν_{max} : 3233 (NH), 1665 (C=O), 1208 (C=S)

3,4,5-Trimethoxy-N-((4-(trifluoromethyl)phenyl)carbamothioyl)benzamide (52)



52

Compound (BTU-13) was prepared from 4-(trifluoromethyl)benzoyl chloride (0.60 g, 2.88 mmol) and 3,4,5-trimethoxyaniline (0.51 g, 2.88 mmol) and ammonium isothiocyanate (0.22 g, 2.88 mmol) as in **procedure F**. The completion of the reaction was confirmed by TLC (Hex: EtOAc 7:3), recrystallisation from methanol afforded the title benzamide (52) as orange crystals (1.15 g, 2.76 mmol, 96 %).

M.P: 188 – 190 °C; **R_f:**0.26; (Hex: EtOAc 7:3);

δ_H (CDCl₃, 600 MHz): 3.87 (3 H, s, 4-OCH₃), 3.89 (6 H, s, 3, 5-OCH₃), 7.08 (2 H, s, 2, 6), 7.85 (2 H, d, J = 8.57 Hz, 3', 5'), 8.05 (2 H, d, J = 8.57 Hz, 2', 6'), 9.17 (1 H, s, 2''), 12.50 (1 H, s, 4'').

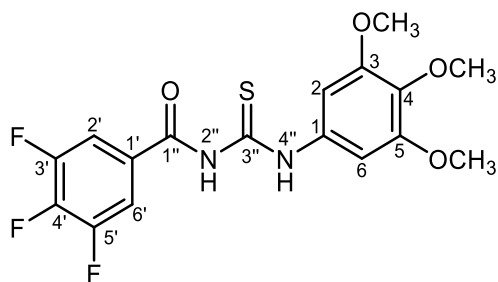
δ_C (CDCl₃, 150 MHz): 56.2 (2 C, 3, 5-OCH₃), 60.9 (1 C, 4-OCH₃), 101.6 (2 C, 2, 6), 126.5 (2 C, q, J = 3.70 Hz, 3', 5'), 127.4 (2 C, 2', 6'), 127.6 (1 C, q, J = 270.9 Hz, CF₃), 132.9 (1 C, 4), 134.1 (1 C, q, J = 33.1 Hz, 4'), 135.2 (1 C, 1), 138.2 (1 C, 1'), 153.2 (2 C, 3, 5), 163.8 (1 C, 3''), 177.0 (1 C, 1'')

δ_F (CDCl₃, 564 MHz): -63.6 (3 F, s, 4'-CF₃)

m/z HRMS (ESI) [M + H]: Calculated for C₁₈H₁₇F₃N₂O₄S 415.0934 found 415.0939 (ΔM_s=1.21)

IR ν_{max}: 3140 (NH), 1679 (C=O), 1225 (C=S)

3,4,5-Trifluoro-N-((3,4,5-trimethoxyphenyl)carbamothioyl)benzamide (53)



53

Compound (53) was prepared from 3,4,5-trimethoxybenzoyl chloride (0.50 g, 2.57 mmol) and 3,4,5-trimethoxyaniline (0.47 g, 2.57 mmol) and ammonium isothiocyanate (0.22 g, 2.88 mmol) as in [procedure F](#). The completion of the reaction was confirmed by TLC (Hex: EtOAc 7:3), recrystallisation from methanol afforded the title benzamide (53) as orange crystals (0.98 g, 2.45 mmol, 96 %).

M.P: 189 – 191 °C; **R_f**:0.26; (Hex : EtOAc 7:3);

δ_H(CDCl₃, 400 MHz): 3.79 (3 H, s, OCH₃, 4'), 3.81 (6 H, s, OCH₃, 3',5'), 6.96 (2 H, s, 2',6'), 7.53 (2 H, t, J = 6.72 Hz, 2,6), 9.02 (1 H, s, 2''), 12.27 (1 H, s, 4').

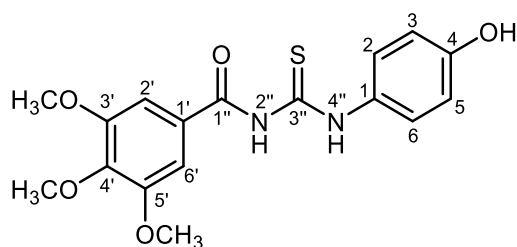
δ_C (CDCl₃, 100 MHz): 56.3 (2 C, OCH₃, 3' 5'), 60.9 (1 C, OCH₃, 4'), 92.42 (1 C, 2), 101.3 (2 C, 2',6'), 112.7 (2 C, dd, J = 16.5 Hz, 6.4 Hz, 2,6), 127.4 (1 C, m, 1), 133.0 (1 C, 1'), 136.7 (1 C, 4'), 143.4 (1 C, dt, J = 263.3 Hz, 15.3 Hz), 152.8 (1 C, ddd, J = 254.41 Hz, 10.5 Hz, 3.6 Hz, 3, 5), 153.2 (2 C, 3', 5'), 163.9 (1 C, 1''), 176.9 (1 C, 3'')

δ_F (CDCl₃, 564 MHz): -154.3 (1 F, s, 4'), -133.2 (2 F, s, 3', 5')

m/z HRMS (ESI) [M + H]: Calculated for C₁₇H₁₅F₃N₂O₄S 401.0777 found 401.0776 (ΔM_s=0.35)

IR ν_{max}: 3137.7 (NH), 1678.7 (C=O), 1225.4 (C=S)

N-((4-Hydroxyphenyl)carbamothioyl)-3,4,5-trimethoxybenzamide (54)



54

Compound (54) was prepared from 3,4,5-trimethoxybenzoyl chloride (1.00 g, 4.35 mmol) and 4-aminophenol (0.47 g, 4.35 mmol) and ammonium isothiocyanate (0.33 g, 4.35 mmol) as in **procedure F**. The completion of the reaction was confirmed by TLC (Hex: EtOAc 8:2), recrystallisation from methanol afforded the title phenol (54) as grey crystals (1.24 g, 3.42 mmol, 79 %).

M.P: 180 – 182 °C; **R_f**:0.31; (Hex: EtOAc 8:2);

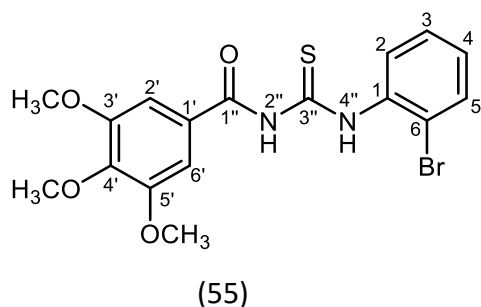
δ_H(CDCl₃, 400 MHz): 3.87 (9 H, s, OCH₃), 5.68 (1 H, OH, 4), 6.82 (2 H, d, J = 8.4 Hz, 3, 5), 7.03 (2 H, s, 2', 6'), 7.43 (2 H, d, J = 8.4 Hz, 2',6'), 9.10 (1 H, s, 2''), 12.35 (1 H, s, 4'').

δ_C (CDCl₃, 100 MHz): 56.5 (2 C, 3',5'-OCH₃), 61.6 (1 C, 4'-OCH₃), 105.5 (2 C, 2',6'), 115.7 (2 C, 3,5), 126.1 (2 C, 2, 6), 126.6 (1 C, 1'), 130.4 (1 C, 1), 142.9 (1 C, 4'), 154.7 (1 C, 4), 155.5 (2 C, 3',5'), 166.6 (1 C, 1''), 178.8 (1 C, 3'').

m/z HRMS (ESI) [M + H]: Calculated for C₁₇H₁₈N₂O₅S 363.1009 found 363.1010 (ΔM_s=0.31)

IR ν_{max}: 3213.3 (NH), 1606.1 (C=O), 1241.6 (C=S)

N-((2-Bromophenyl)carbamothioyl)-3,4,5-trimethoxybenzamide (55)



Compound (55) was prepared from 3,4,5-trimethoxybenzoyl chloride (1.20 g, 5.20 mmol) and 4-bromoaniline (0.90 g, 5.20 mmol) and ammonium isothiocyanate (0.39 g, 5.20 mmol) as in **procedure F**. The completion of the reaction was confirmed by TLC (Hex: EtOAc 8:2), recrystallisation from DMF/methanol (1:9) afforded the title bromo compound (55) as brown crystals (1.45 g, 3.41 mmol, 65 %).

M.P: 154 – 156 °C; **R_f:**0.28; (Hex: EtOAc 8:2);

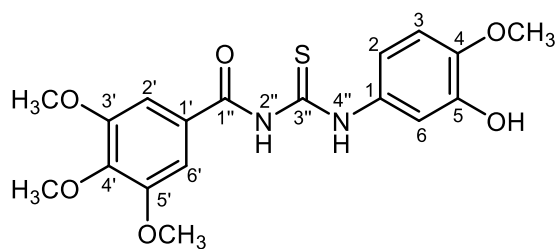
δ_H(CDCl₃, 400 MHz): 3.97 (9 H, s, 3', 4', 5'-OCH₃), 7.14 (2 H, s, 2', 6'), 7.22 (1 H, dt, J = 7.65 Hz, 1.33 Hz, 4), 7.44 (1 H, dt, J = 7.65 Hz, 1.11 Hz, 3), 7.70 (1 H, dd, J = 8.04 Hz, 1.33 Hz, 5), 8.29 (1 H, dd, J = 7.65 Hz, 1.11 Hz, 2), 9.14 (1 H, s, 2''), 12.63 (1 H, s, 4'')

δ_C (CDCl₃, 100 MHz): 56.6 (2 C, 3', 5'-OCH₃), 61.1 (1 C, 4'-OCH₃), 105.1 (2 C, 2' 6'), 118.64 (1 C, 6), 126.4 (1 C, 1'), 127.2 (1 C, 2), 127.6 (1 C, 4), 128.3 (1 C, 3), 133.0 (1 C, 5), 136.4 (1 C, 1), 143.0 (1 C, 4'), 153.6 (2 C, 3', 5'), 166.4 (1 C, 1''), 179.0 (1 C, 3'').

m/z HRMS (ESI) [M + H]: Calculated for C₁₇H₁₇BrN₂O₄S 425.0165 found 425.0166 (ΔMs=0.10)

IR ν_{max}: 3294 (NH), 1667 (C=O), 1238 (C=S)

N-((3-Hydroxy-4-methoxyphenyl) carbamothioyl)-3,4,5-trimethoxybenzamide (56)



56

Compound (56) was prepared from 3,4,5-trimethoxybenzoyl chloride (2.00 g, 8.67 mmol) and 5-amino-2-methoxyphenol (1.21 g, 8.67 mmol) and ammonium isothiocyanate (0.65 g, 8.67 mmol) as in [procedure F](#). The completion of the reaction was confirmed by TLC (Hex: EtOAc 8:2), recrystallisation from methanol afforded the title phenol (56) as white crystals (3.20 g, 8.15 mmol, 94 %).

M.P: 174 – 176 °C; **R_f**:0.33; (Hex: EtOAc 8:2);

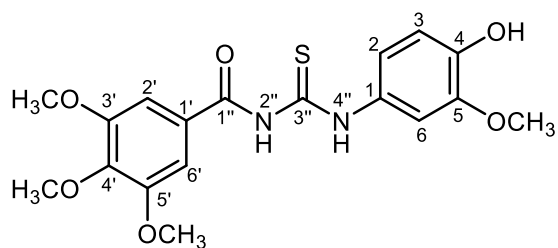
δ_H(CDCl₃, 400 MHz): 3.93 (3 H, s, 4'-OCH₃), 3.95 (3 H, s, 4-OCH₃), 3.96 (6 H, s, 3', 5'-OCH₃), 5.79 (1 H, s, OH, 5), 6.91 (1 H, d, J = 8.61 Hz, 3), 7.09 (2 H, s, 2', 6'), 7.19 (1 H, dd, J = 8.61 Hz, 2.51 Hz, 2), 7.29 (1 H, d, J = 2.51 Hz, 6), 9.09 (1 H, s, 2''), 12.43 (1 H, s, 4'')

δ_C (CDCl₃, 100 MHz): 56.1 (1 C, 4-OCH₃), 56.5 (2 C, 3', 5'-OCH₃), 61.1 (1 C, 4'-OCH₃), 104.92 (2 C, 2', 6'), 110.5 (1 C, 6), 111.4 (1 C, 3), 116.2 (1 C, 2), 126.7 (1 C, 1), 131.16 (1 C, 1''), 142.9 (1 C, 4'), 145.5 (1 C, 5), 145.8 (2 C, 3', 5'), 153.5 (2 C, 3', 5'), 166.7 (1 C, 1''), 178.5 [1 C, 3'').

m/z HRMS (ESI) [M + H]: Calculated for C₁₈H₂₀N₂O₆S 393.1115 found 393.1114 (ΔM_s=0.41)

IR ν_{max}: 3123 (NH), 1608 (C=O), 1212 (C=S)

N-(H-hydroxy-4-methoxyphenyl)carbamothioyl)-3,4,5-trimethoxybenzamide (57)



(57)

Compound (57) was prepared from 3,4,5-trimethoxybenzoyl chloride (0.50 g, 2.17 mmol) and 4-amino-2-methoxyphenol (0.30 g, 2.17 mmol) and ammonium isothiocyanate (0.16 g, 2.17 mmol) as in [procedure F](#). The completion of the reaction was confirmed by TLC (Hex: EtOAc 6:4), recrystallisation from methanol afforded the title phenol (57) as brown crystals (0.77 g, 1.96 mmol, 90 %).

M.P: 164 – 166 °C; Rf:0.37; (Hex: EtOAc 6:4);

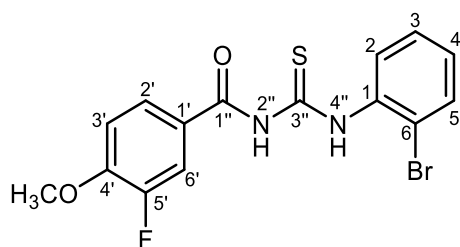
δ_{H} (CDCl₃, 400 MHz): 3.95 (3 H, s, 4-OCH₃), 3.96 (3 H, s, 4'-OCH₃), 3.97 (6 H, s, 3, 5-OCH₃), 5.73 (1 H, s, 4-OH), 6.97 (1 H, d, J = 7.67 Hz, 3), 7.06 (1 H, dd, J = 7.67 Hz, 2.26 Hz, 2), 7.11 (2 H, s, 2', 6'), 7.50 (1 H, d, J = 2.26 Hz, 5), 9.06 (1 H, s, 2''), 12.6 (1 H, s, 4'').

δ_{C} (CDCl₃, 100 MHz): 56.1 (1 C, 5-OCH₃), 56.5 (2 C, 3', 5'-OCH₃), 61.1 (1 C, 4'-OCH₃), 104.9 (2 C, 2', 6'), 107.7 (1 C, 6), 114.4 (1 C, 3) 117.2 (1 C, 2), 126.6 (1 C, 1), 130.1 (1 C, 1), 144.5 (1 C, 4), 146.2 (1 C, 5), 153.6 (2 C, 3' 5'), 166.7 (1 C, 1''), 178.1 (1 C, 3'').

m/z HRMS (ESI) [M + H]: Calculated for C₁₈H₂₀N₂O₆S 393.1115 found 393.1114 ($\Delta M_s=0.27$)

IR ν_{max} : 3178.3 (NH), 1658 (C=O), 1213 (C=S)

N-((2-Bromophenyl)carbamothioyl)-3-fluoro-4-methoxybenzamide (58)



(58)

Compound (58) was prepared from 3-fluoro-4-methoxybenzoyl chloride (0.70 g, 3.71 mmol) and 2-bromoaniline (0.64 g, 3.71 mmol) and ammonium isothiocyanate (0.28 g, 3.71 mmol) as in **procedure F**. The completion of the reaction was confirmed by TLC (Hex: EtOAc 7:3), recrystallisation from methanol afforded the title bromo compound (58) as a white powder (0.33 g, 0.86 mmol, 23 %).

M.P: 196 – 198 °C; **R_f**:0.35; (Hex: EtOAc 7:3);

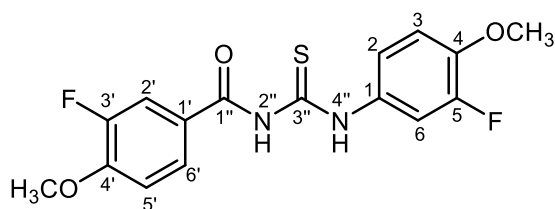
δ_H(CDCl₃, 400 MHz): 4.02 (3 H, s, 4'-OCH₃), 7.12 (1 H, t, J = 8.15 Hz, 3'), 7.22 (1 H, t, J = 7.61 Hz, 4), 7.44 (1 H, t, J = 8.05 Hz, 3), 7.75 (3 H, m, 2,5, 2'), 8.27 (1 H, d, J = 8.25 Hz, 6'), 9.07 (1 H, s, 2''), 12.58 (1 H, s, 4'')

δ_C (CDCl₃, 100 MHz): 56.5 (1 C, 4'OCH₃), 113.0 (1 C, d, J = 2.22 Hz, 3'), 116.1 (1 C, d, J = 20.5 Hz, 6'), 118.7 (1 C, 6), 123.9 (1 C, J = 5.96 Hz, 1'), 124.4 (1 C, d, J = 2.47 Hz), 127.1 (1 C, 2), 127.6 (1 C, 4), 128.3 (1 C, 3), 133.0 (1 C, 5), 136.4 (1 C, 1), 151.3 (1 C, d, J = 10.3 Hz, 4'), 151.8 (1 C, d, J = 245.4 Hz, 5'), 166.7 (1 C, d, J = 1.98 Hz, 1''), 180.4 (1 C, 3'').

m/z HRMS (ESI) [M + H]: Calculated for C₁₅H₁₂BrFN₂O₂S 382.9860 found 382.9862 (ΔM_s=0.53)

IR ν_{max}: 3100.4 (NH), 1613.8 (C=O), 1202.7 (C=S)

3-Fluoro-N-((3-fluoro-4-methoxyphenyl)carbamothioyl)-4-methoxybenzamide (59)



59

Compound (59) was prepared from 3-fluoro-4-methoxybenzoyl chloride (1.20 g, 6.36 mmol) and 3-fluoro-4-methoxyaniline (0.90 g, 6.36 mmol) and ammonium isothiocyanate (0.48 g, 6.36 mmol) as in procedure F. The completion of the reaction was confirmed by TLC (Hex: EtOAc 8:2), recrystallisation from methanol afforded the title benzamide (59) as white crystals (1.10 g, 3.12 mmol, 49 %).

M.P: 114 °C; **R_f**:0.27; (Hex: EtOAc 8:2);

δ_H(CDCl₃, 400 MHz): 3.85 (3 H, s, 4-OCH₃), 3.92 (3 H, s, 4'-OCH₃), 7.00 (1 H, t, J = 8.91 Hz, 3), 7.08 (1 H, t, J = 8.51 Hz, 5'), 7.32 (1 H, d, J = 8.76 Hz, 2), 7.68 (3 H, m, 2', 6', 6), 9.04 (1 H, s, 2''), 12.46 (1 H, s, 4'').

δ_C (CDCl₃, 100 MHz): 56.4 (1 C, 4'-OCH₃), 56.5 (1 C, 4-OCH₃), 113.1 (3 C, dd, J = 20.5 Hz, 2.53 Hz, 3, 6, 5'), 116.0 (1 C, d, J = 20.3 Hz, 2'), 120.2 (1 C, d, J = 3.54 Hz, 2), 124.3 (1 C, d, J = 3.54 Hz, 6'), 123.9 (1 C, d, J = 6.65 Hz, 1), 130.6 (1 C, d, J = 9.25 Hz, 1'), 146.5 (1 C, d, J = 10.7 Hz, 4), 152.6 (1 C, d, J = 10.9 Hz, 4'), 152.9 (1 C, d, J = 246.6 Hz, 3'), 153.5 (1 C, d, J = 250.0 Hz, 5'), 165.4 (1 C, d, J = 1.90 Hz, 1''), 178.5 (1 C, 3'').

m/z HRMS (ESI) [M + H]: Calculated for C₁₆H₁₄F₂N₂O₃S 353.0766 found 353.0766 (ΔM_s=0.01)

IR ν_{max}: 2098 (NH), 1621 (C=O), 1220 (C=S)

2.2 Biological activity of β -diketones

Materials and methods

2.2.1 Cell lines profiles and culture tips:

A549

The lung carcinoma cell line, A549 was obtained from the University of Salford cell bank located at Cockcroft building. It was isolated for the first time in 1973 during an attempt to establish a guideline for morphological continuity from 200 human tumours. Its specimens were collected from different hospitals and medical centres including University of Colorado Medical Centre and University of Minnesota medical school (Giard *et al.*, 1973). The key feature of the cell line can be characterised by their ability to synthesise and accumulate lipid products in the cytoplasm by the cytidine diphosphocholine pathway. Subculturing of the cell line can be maintained under physiological condition of commercially available medium of RPMI at 37 °C / 5 % CO₂ (Cooper, 2012).

HepG2

HepG2 cell line was also obtained from the University of Salford cell bank. It was originally isolated from a liver tissue of a hepatocellular carcinoma patient in a 15-year-old Caucasian male (Qiu *et al.*, 2015). They are mainly characterised as adherent epithelial cells that form a single layer during replication and growth, each having 55 pair of chromosomes. One of their key features also include the secretion of plasma proteins such as albumins and fibrinogen (ECACC, 2017). They are physiologically stable condition for *in vitro* studies in RPMI at 37 °C / 5 % CO₂ and normally takes 5 to 6 days to attain confluency when seeded at 1:4.

A-204

Also obtained from the University of Salford cell bank. A-204 is a solid tumour epithelial cell line of Human muscle Rhabdomyosarcoma tissue was isolated by D. J. Giard (Giard *et al.*, 1973). It originates from the abnormal tissues of skeletal muscles in children and dominates about 5 – 6% of neoplasia cases in paediatric patients (Pappo, 1995) and there is expected 90 % chances of survival for up to 5 years in patients with low risk conditions (Dawson *et al.*, 2020). The main feature of this A 204 cell lines is associated with the loss of heterozygosity in

the region of chromosome at 11p15.5 and abnormal regulation of PAX3 and PAX7 transcription factors that are associated with different types of disorders such as Beckwith-Wiedemann syndrome (Scholl *et al.*, 2000; Scrable *et al.*, 1987). As in many cell lines, A-204 can be cultured for *in vitro* studies in RPMI at 37 °C / 5 % CO₂.

HeLa

HeLa is a cancerous cervical tissue cell originated from Henrietta Lacks, a patient at John Hopkins Hospital; and ever since, contributed to a data of over 60,000 publications of biological research. One of the important roles contributed by HeLa is in the development of polio vaccine and its correlation between the papilloma virus and cervical cancer. The cell line has also contributed to the mechanistic basis of telomerase in controlling chromosome degradation (Landry *et al.*, 2013). They have a characteristic of rapid division that doubles the amount within a period of 24 hours. HeLa cells are cultured *in vitro* in DMEM media supplemented with serum and incubated at 37 °C and 5 % CO₂. This cell line was also collected from the University of Salford cell bank.

U2OS

U2OS is a human bone osteosarcoma epithelial cells, cultivated from the tissue of a fifteen-year-old girl with differentiated sarcoma of the tibia. The cancer is found in 3 – 5 % children and is linked with various syndromes such as bloom syndrome and Diamond Blackfan anemia (Liu, 2018). Like most cell lines, U2OS are cultured RPMI with serum and incubated at 37 °C and 5 % CO₂.

CCRF-CEM

CCRF is obtained from C.E.M, a 2-year-old patient diagnosed with an acute lymphosarcoma by lymph node biopsy at C.C.R.F. For the experiments in this thesis, the cells were obtained from University of Salford cell bank. It grows on suspension in different growth medium including RPMI and EME with 2mM glutamine and 20% foetal bovine serum (FBS). Like most of the cell lines tested, CCRF-CEM are cultures for invitro studies in RPMI-1640 at 37⁰C / 5% and CO₂.

K562

K562 cell lines are lymphoblasts that were isolated from a 53-year-old female patient diagnosed with chronic myelogenous leukaemia (CML) in blast crisis. The cells are characterised as non-adherent with fully rounded shapes (Anderson, Nilsson and Gahmberg, 1979). K562-cells are maintained for invitro studies in a RPMI-1640 media at 37 °C / 5% and CO₂.

MOLT-4

This cell line was isolated from a 19-year-old patient in relapse, suffering with acute lymphoblastic leukaemia. The cell line is characterised with a hypertetraploid number of chromosomes (Josh *et al.*, 1988). It is also classified as a suspension cell and can be maintained for invitro studies in RPMI-1640 medium at 37 °C with 95%, 5% air and CO₂ respectively.

2.2.2 Cell conditioning maintenance

Cell medium

Cell media (RPMI-1640) without L-Glutamine catalogue number 12-167F, ordered from BioWhittaker Lonza was used for cell growth and maintenance of all cell lines in the bioassays. It was prepared by enriching 440 ml of the media with supplements that contains 10 % foetal bovine serum (FBS), 1 % L-glutamine and 1 % penicillin /streptomycin (BioWhittaker catalogue number DE 17-602E). The prepared media is always stored at 4 °C to a maximum of 3 weeks.

Cell thawing and subculturing

Prior to the thawing of cells in the cryovial, the culture media (RPMI) was warmed in a 37 °C water bath for a period of about 30 minutes. A T-75 flask was prepared in the sterile hood with the appropriate volume of media (10 – 30 ml for T-75 flask). The frozen cells contained the cryovial was removed from the cryogene and gently warmed in a water bath to defreeze at least within 2 minutes. Vial was quickly decontaminated with 70 % ethanol and moved into the sterile hood. The cell content in vial was transferred into 10 ml sterile centrifuge tube containing 9 ml of media and centrifuged for 5 minutes at 1500 rpm. The media and DMSO content were carefully discarded without disturbing the coagulated cell at the bottom and media (2 ml) was added to suspend the cells. The content was transferred to the previously prepared T-75 flask and thoroughly mixed by gently tilting the flask sideways. The flask was

kept in incubator at 37 °C / 5 % CO₂ and regularly checked for confluency and changing of media. The procedure was applied for thawing of all cell lines used in the bioactivity tests.

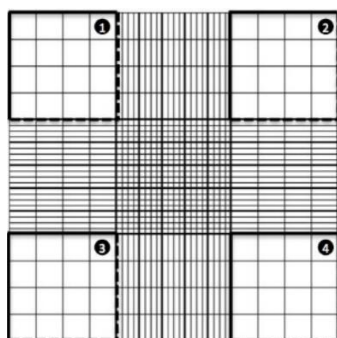
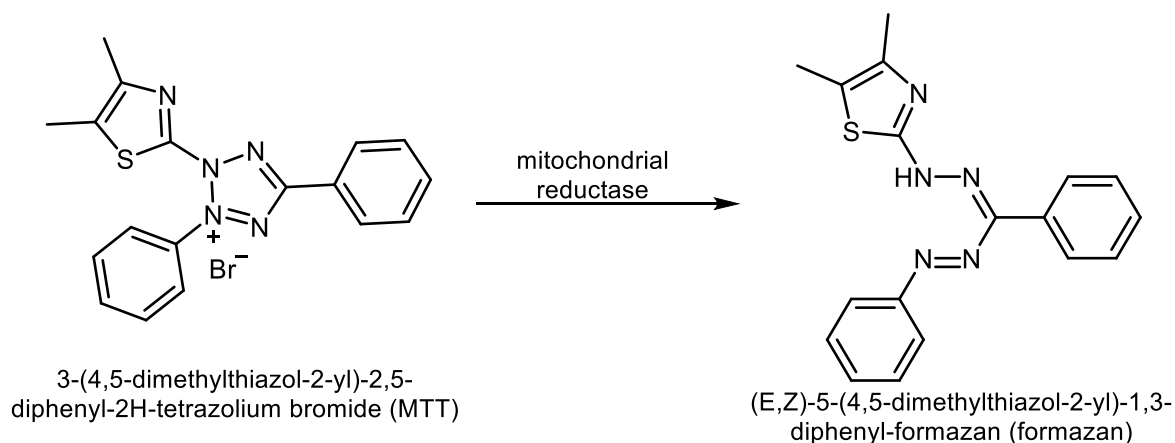


Figure 60: Haemocytometer reading plate. Obtained from Invitrogen Cell culture basics Handbook.

The cells were counted by Haemocytometer method. 10 µl of trypan blue was added to a 10 µl of cell suspension and mixed gently. 10 µl of the mixture was carefully transferred to the of the thin plate on the haemocytometer (Figure 60). Only the cells in the 4 sets of 16 corner squares are counted, cells that touch the margin of the dotted lines are excluded from the count. The average cell count was then calculated, multiplied by the dilution factor, and multiplied by 10⁴ to represent number of cells per millilitres.

2.2.3 Cell viability

MTT is an assay that is used to measure the viability of cells based on their metabolic activity. The main aspect relies on the chemical reduction and ring opening of tetrazolium salt (3-(4,5-dimethylthiazol-2-yl)-2,5-diphenyltetrazolium bromide or MTT) which is converted to formazan. During the reduction process there is a resulting colour change from a yellow MTT to purple which its intensity depends the metabolic activity of nicotinamide adenine dinucleotide phosphate (NADPH)-dependent enzymes in the mitochondria of living cells that catalyse the reduction process. This idea can be used to determine the cytotoxicity of drugs on cells, because only healthy cells are capable of metabolic reduction which result in colour change. The intensity of the purple colour is proportional to the viability of cells that reduce the MTT salt to formazan (Bahuguna *et al.*, 2017; Rai *et al.*, 2018).



Scheme 10: Reduction and ring opening of MTT to formazan

The reduced formazan salt is dissolved in DMSO which can be easily quantified by measuring the absorbance between at the range between 500 and 600 nm (Bahuguna *et al.*, 2017). Viability of the cells can be measured based on the absorbance values of formazan concentration.

The MTT stock solution (Thiazolyl Blue tetrazolium bromide, 98%, L11939.06 Alfa Aesar, Thermo Fisher Scientific) was prepared by dissolving 500 mg solid MTT in 10 ml phosphate buffer solution. The solution is stirred with a magnetic stirrer for 15 minutes in the dark because the MTT sensitivity to light. The stock solution was kept in a glass vial and stored at a temperature below 6 °C. A solution of 5 mg / ml was prepared from the stock prepared for all the experiments carried out during the assay.

Cell viability MTT assay for the five cell lines (A549, HepG2, A-204, HeLa and U2OS) was carried out in a 96-well plate by seeding cells with a density of 5×10^3 in each well according to cell culture procedure mentioned in section 2.2.1 and 2.2.2. Prior to seeding on 96-well plates, all cell lines attained a confluence of 70 – 80 %. After cell seeding and incubation for 24 hours at 37 °C in a CO₂ incubator, cells were treated with drugs of 6 different concentrations 6.25 μM, 12.5 μM, 25.0 μM, 50.0 μM, 100.0 μM and 200.0 μM. Concentrations for each drug used for testing was prepared by serial dilution from a 5 mM stock solution of drug in DMSO. The cells treated with drug were incubated for 120 hours.

After the incubation period, 50 μl MTT solution was added to each well and incubated for additional 4 hours. The liquid mixture was carefully aspirated without disturbing the purple layer of reduced formazan. Following the aspiration, 200 μl of DMSO was added to each well

and the plate was placed on the Ascent plate reader for thorough shaking and measurement of absorption values. The actual absorbance was obtained by subtracting the background intensity values (690nm) from the main intensity (540nm). These values were normalised by taking the ratio of actual absorbance values to the absorbance value of positive control and multiplied by 100%.

$$\text{Normalised value} = \frac{\text{Absorbance value}}{\text{positive control}} \times 100\%$$

The formula was applied on an excel worksheet to determine the normalised value. The normalised values were transferred to the software to produce the calibration curve (Log of concentration against %viability) along with the computed IC₅₀ values for each compound (Swinney, 2011). The experiment is repeated three times in triplicates and then averaged to obtain the final values for analysis. GraphPad Prism 6 and OriginPro 2019 was used for graphing and generation of graphical charts and IC₅₀ values.

2.2.4 Ligand Docking Studies

The procedure for ligand docking and analysis was carried out according to the procedure reported by Khan *et al.* (2019). The three-dimensional structure of tubulin (PDB ID: 1 SA0) was downloaded from in a PDB format from the protein data bank. The structures were prepared for docking using UCSF Chimera Version 1.14 (build 42094) and Protein preparation wizard of Maestro Schrödinger suite (Version 12.5). The receptor grid was generated based on colchicine area in the tubulin receptor site using the Glide tool. The Van der Waals radius was set to a scaling factor of 1.0 and partial charge cut off with 0.25 C. The 3D conformation of ligands was drawn using a ChemDraw software and the file was saved in .mol file format. The ligand structures (β -diketones) were prepared using the LigPrep tool accompanied with the Maestro Schrödinger suite. Empirical pKa (Epik 2.2) was used to determine the bioavailability profile and within a pH 7.0 +/- 2.0 to obtain the required ligand output. Glide extra precision (XP) parameters was carefully selected for the ligand docking to obtain the best docking score between ligand and receptor.

CHAPTER THREE

Results and Discussions

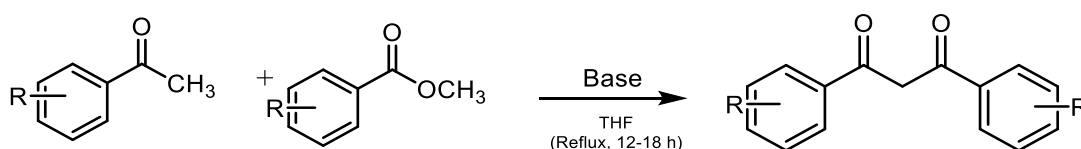
Chapter three

3.0 Results and discussion

3.1 Synthesis and characterisation of β -diketones:

Different methods have been employed in synthesising β -diketones. Among these methods, Claisen condensation is considered the oldest one and has been known since 1887. It is a frequently used reaction for obtaining diketones by condensation between a ketone and esters in the presence of a suitable base in order to promote the reaction forward (Shokova, Kim and Kovalev, 2015). It is one of the most popular methods of synthesis for compounds that involve C-C formation (Kljun and Turel, 2017).

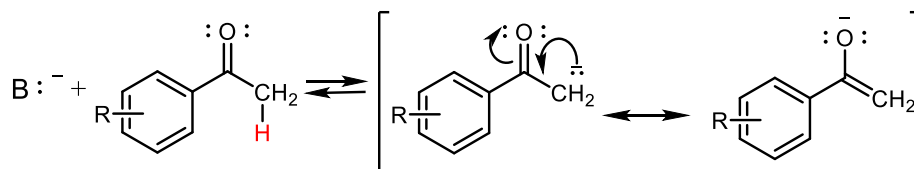
The method of synthesis for β -diketone compounds bearing three methoxy groups on the A ring was carried out as in **Scheme 11** below:



Scheme 11: Claisen condensation of ketone and ester to form β -diketone

The reactions were carried out under basic conditions (with base serving as catalyst.) The first stage of the reaction was to form the enolate ion from the ketone with sodium hydride as base (according to the procedure adapted from (Jin *et al.*, 2011)).

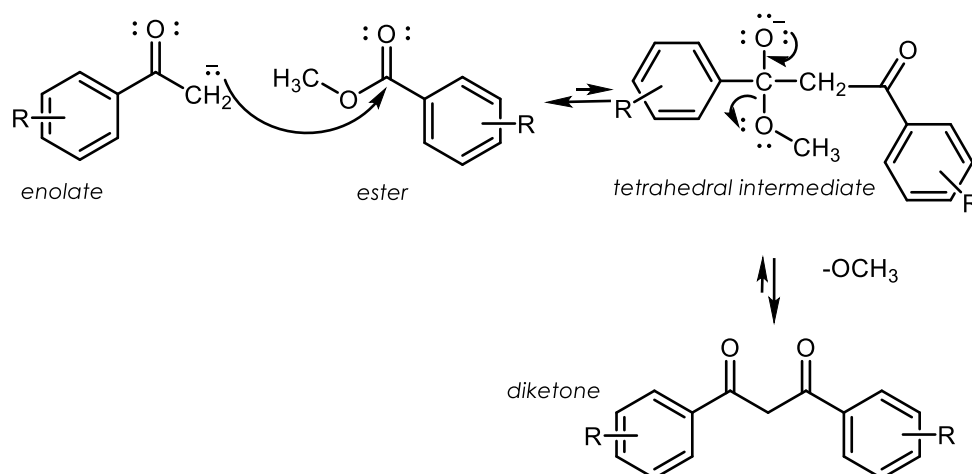
Sodium hydride served as a nucleophile in the reaction and attempt to carry the reaction as to adding the ester or the ketone first, the reaction gave the same product because the nucleophilic centre in both starting materials is the carbonyl group. The mechanism is highlighted in the **Scheme 12** below:



Scheme 12: Resonance stabilised formation of enolate ion

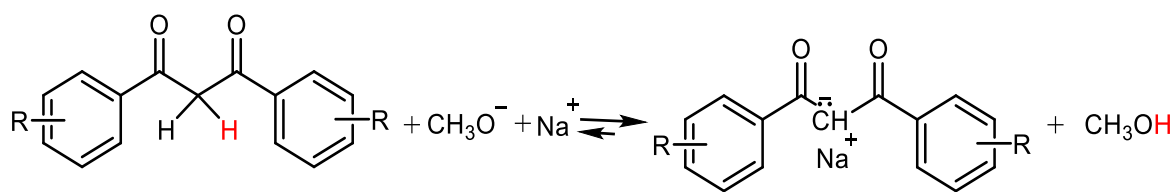
From the scheme above (**Scheme 12**), the nucleophilic base attacks the acidic hydrogen on the α carbon centre of a ketone which ionises to give a resonance stabilised enolate ion.

Following the generation of enolate ion, formation of the diketone is a two-step process; firstly, carbon centre of the ester is attacked by the enolate ion which is accompanied by the formation of a reversible tetrahedral intermediate and loss of a leaving group as shown in **Scheme 13**.



Scheme 13: Mechanism of formation of β -diketone

The equilibrium of the reactions in the formation of diketone generally favoured to the side of the reactants as most β -keto esters have lesser stability than corresponding esters from which they are obtained. In aqueous medium, the proton at the alpha position of diketone is acidic ($pK_a \approx 9$) with the methoxy anion removing the proton to form a conjugate basic product:

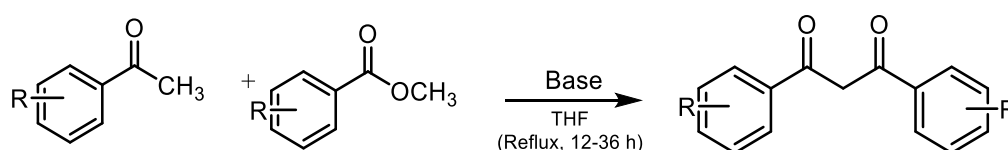


Scheme 14: Equilibrium of β -diketone in the basic medium

From **Scheme 14**, the reaction favours the formation of the species on the right as the methoxide anion removes the acidic proton in diketone to form an alcohol (methanol has a pK_a value of 15.5). To isolate the product from the ionic state, an equivalent of amount 1 molar HCl is added to neutralise the base and precipitate the un-ionised diketone.

3.1.1 Optimisation of reaction parameters (temperature and base equivalents):

As mentioned in the experimental part, one of the procedures employed for the synthesis of the β -diketones was adapted from (Jin *et al.*, 2011). To optimise the yield of compounds, the effect of varying reflux period, bases and catalyst equivalent in the reactions was considered. Four compounds (**4**, **5**, **6** and **7**) were selected, and different conditions were considered with respect to time and type of base. Table 3 summarises the outcome of the reaction time and yield when base and temperature were altered.



Scheme 15: Synthesis of β -diketones

Table 3: Yields of optimisation of β -diketones with different reaction conditions.

	Compound	Base	Equivalent	Refluxing time	Solvent	% Yield
1	4	NaH / NaOMe	3.0 mmol	12 hrs	THF	\approx 46
	5					\approx 35
	6					\approx 32
	7					\approx 51
2	4	NaH	3.5 mmol	36 hrs		\approx 65
	5					\approx 73
	6					\approx 49
	7					\approx 70

* All reactions were carried out under inert conditions (Argon atmosphere).

Owing to the high yields of products, subsequent β -diketones bearing 3-methoxy groups on the A or B ring were produced using the optimised procedure (Table 3). As it can be seen from Table 3 (*above*), the reaction conditions in the second group having higher equivalents of base and prolonged reaction time of 36 hours and gave higher yields compared to the first group with reaction time of 12 hours and lower equivalent of bases.

Compounds **13** and **15** bearing a nitrile group ($C\equiv N$) on one of the aromatic rings were efficiently prepared at room temperature. The procedure for obtaining these two β -diketones required the same molar equivalent of starting materials and base. The product

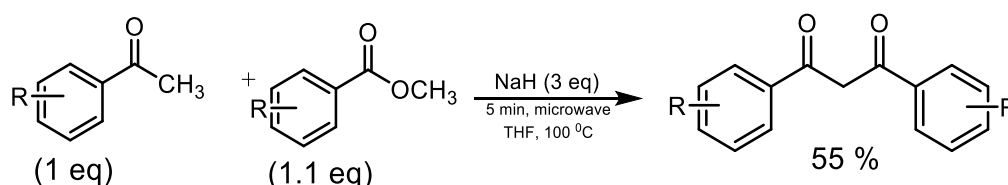
was directly recrystallised without column purification, and the final product yields were above 70 %.

3.1.2 Effect of reaction time on irradiation under microwave

Microwave assisted reactions are considered a widely used technique in green chemistry. One of the important features of performing reactions in microwave is because of its efficient heat transfer. It also enables reactions to take place at a higher temperature than a solvent's boiling point. Commonly known reactions such as Diels-Alder, Huisgen Cu-catalysed cycloaddition, condensation and Claisen rearrangement can be successfully achieved much faster using a microwave reactor compared to conventional methods and in higher yields (Ondruschka, Bonrath and Stuerger, 2013).

Owing to this advantage, a microwave assisted condensation strategy for synthesising β -diketones with optimal microwave reaction conditions was explored, to see if this could greatly enhance reaction time and yield compared to conventional methods.

Elucidating important factors such as the reaction solvent and finding a suitable relaxation time is essential for carrying a microwave assisted reaction, especially when there is no literature available to describe a method for particular compound (Wiles *et al.*, 2002).



Scheme 16: Microwave assisted synthesis of β -diketones:

Therefore, different reactions parameters have been tested according to (Table 4 below) to find a suitable reaction condition using a microwave reactor. However, the reacting equivalents were assumed to have no impact on the reaction and therefore, the same equivalents as in the conventional method were employed.

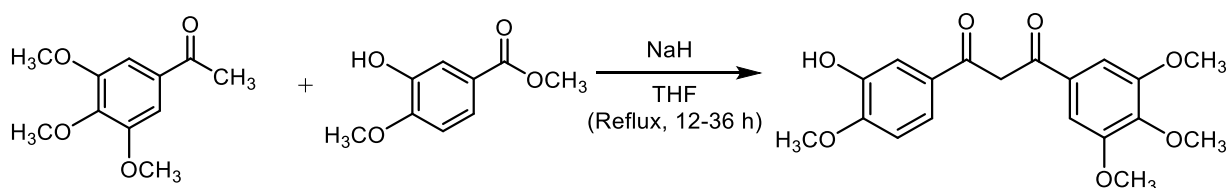
Table 4: Attempted microwave assisted synthesis of β -diketone:

Temperature ($^{\circ}\text{C}$)	Time (minutes)	Volume of THF (cm^{-3})	% yield
100	5	15	55%
100	20		(>40 %) Unknown impurities
65	60		(>40) Starting materials present
60	30		(>40) Starting materials present
50	20		(>40) Starting materials present

Compound **12** was isolated by optimising the temperature and reaction time according to **Table 4** (above). Keeping the temperature at 100°C and microwave reaction time for 5 minutes brought the reaction to completion with no starting materials present. Although, the purification was difficult because of unwanted products formed during the reaction before isolating the final compound.

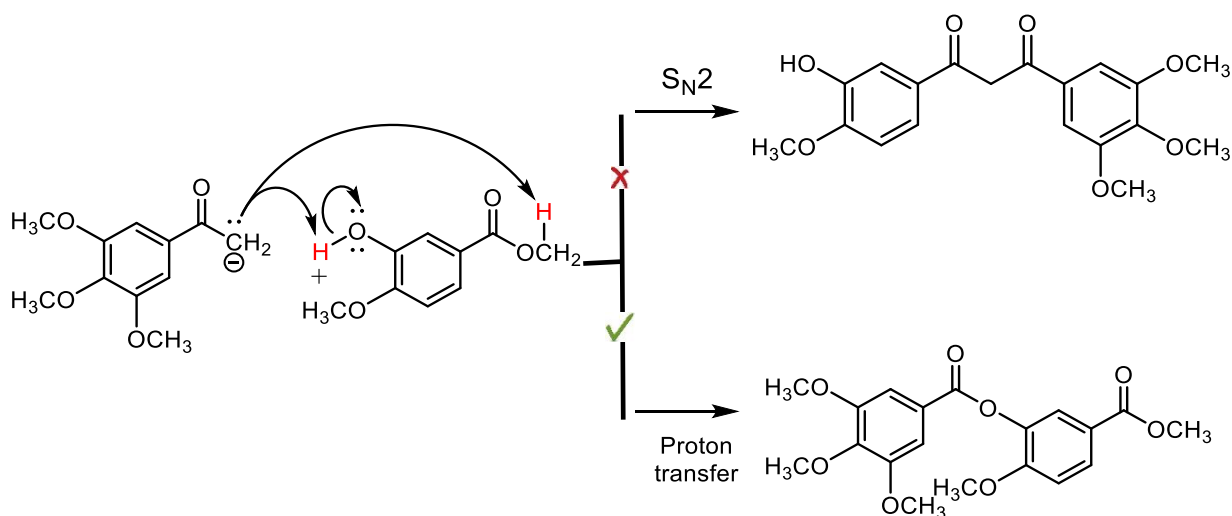
3.1.3 Attempted synthesis of β -diketones mimicking combretastatin-A4

One of the targets of this thesis is to synthesise a β -diketone that mimics combretastatin CA-4 (**Scheme 17**). CA-4 was used as drug control in the cell viability experiments (**Table 7**). Many reports have shown that CA-4 is highly toxic to several cancer cells and effectively inhibits the polymerisation of microtubules. This urged the attempt to develop of a synthetic route to obtain β -diketones bearing similar substituents as CA-4. The first attempt to make a β -diketone mimicking combretastatin-A4 was carried out according to the method in procedure A. However, the compound was not formed, since the ^1H NMR characteristic enolic proton signal between 15 ppm to 17 ppm was not present, which is not consistent with β -diketones.



Scheme 17: Proposed synthesis of CA-4 analogue of β -diketone

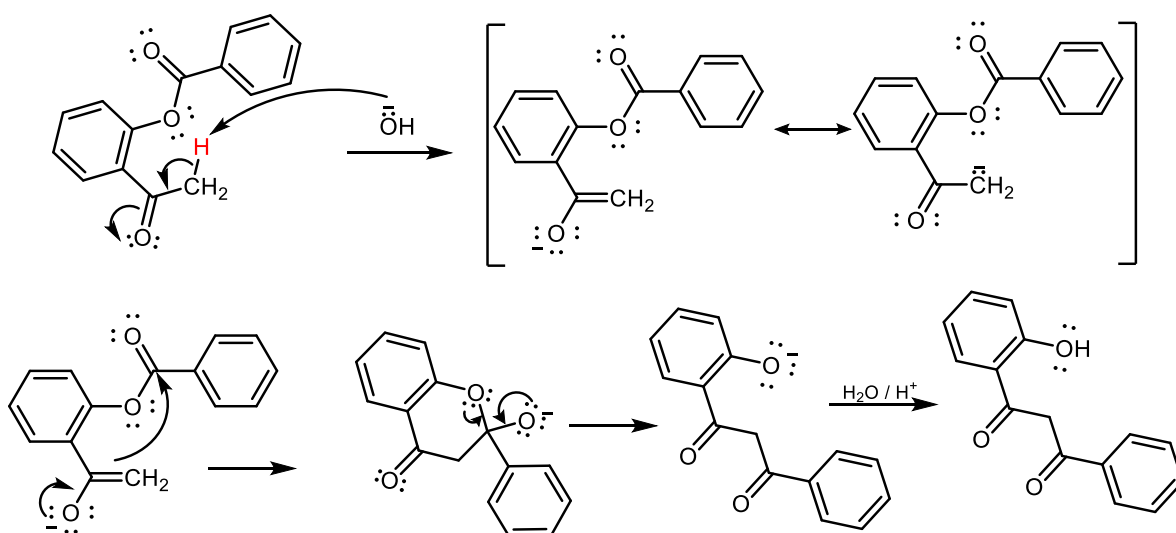
The NMR data according to reaction in (**Scheme 17**) indicate the formation of a high amount of an aromatic ester product; suggesting that the ketone reacted with the hydroxyl ester at the meta position (**Scheme 18**):



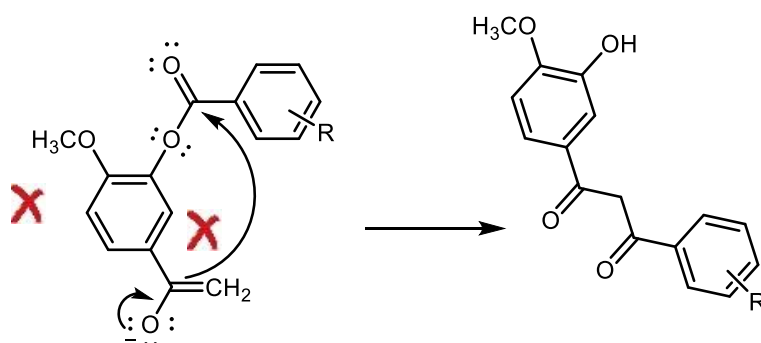
Scheme 18: Product during the first attempted synthesis of CA4- analogue of β -diketone

The reaction is competitive between S_N2 and proton transfer. The methylene anion simultaneously acts as nucleophile and a base, thus deprotonating the OH group and displaces the acidic proton on the ester group. And because the rate of proton transfer is faster than the rate of substitution nucleophilic reaction, the reaction formed the aromatic ester (**Scheme 18**) instead of the expected β -diketone.

Further attempt to employ Baker-Venkataraman rearrangement (Kalinin *et al.*, 1998) was suggested, although, the strategy did not work, as the rearrangement requires the presence of ester group to be at the ortho position to the ketone group (**Scheme 19**). The difficulty in obtaining the β -diketone analogue of combretastatin-A4 by the Baker-Venkataraman rearrangement is hypothetically attributed to the ester group being located meta to the ketone group, instead of in the ortho position, and this could make it difficult to undergo rearrangement and cyclisation (**Scheme 20**).



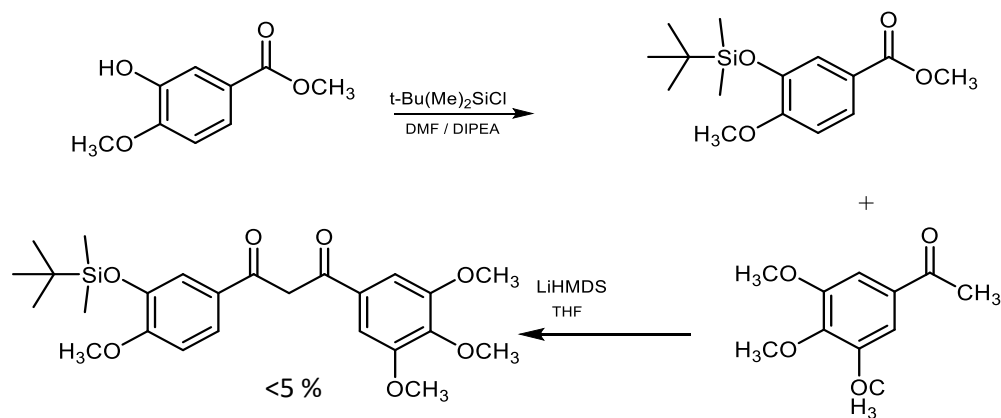
Scheme 19: Ester group at ortho-position is essential for baker-Venkatraman rearrangement



Scheme 20: Formation of product fails when ester group is at meta-position from ketone (R = OCH₃ at position 3, 4, and 5)

Protection with a silyl group:

A different strategy was attempted by introducing to overcome the synthetic trap, that is to introduce a protecting group on the hydroxyl group. The ester in the reaction was protected with a silyl group followed by condensation with LiHMDS (**Scheme 21**) (Nagarathnam and Cushman, 1991).

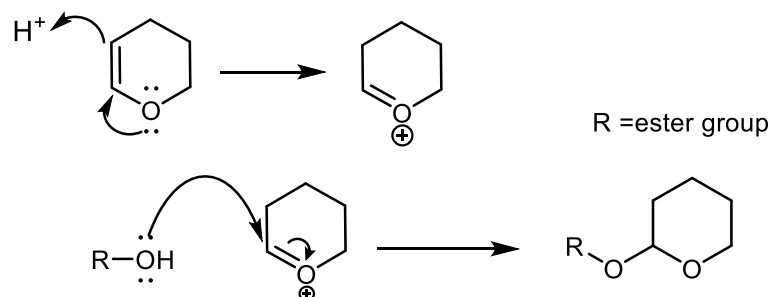


Scheme 21: Formation of silyl-protected β -diketone

The protected β -diketone according to (**Scheme 21**) was obtained in low yield despite increasing the reaction time from 24 to 68 hours, with >90 % of starting materials present. The use of strong base as sodium hydride (NaH) was used instead but the yield did not improve any further. Attempts to deprotect the silyl group in the compound was not carried as the amount would be difficult to isolate the expected β -diketone CA-4 analogue.

Protection with 3,4-dihydro-2H-pyran:

Following the earlier discussion on the attempted synthesis of a β -diketone CA-4 analogue, it was possible that the protection of the phenol with a silyl group was not yielding the required product due to the bulk and steric nature of silyl group. Instead, a less bulky protecting group such as 2,4-dihydropyran (**Scheme 22**) was suggested. This groups is expected to be more stable under basic reaction conditions (Wuts, 2014). The protection takes place under acidic conditions. Following the activation of dihydropyran, the electrophilic addition of the hydroxylated ester is converted into a pyran protected ester.

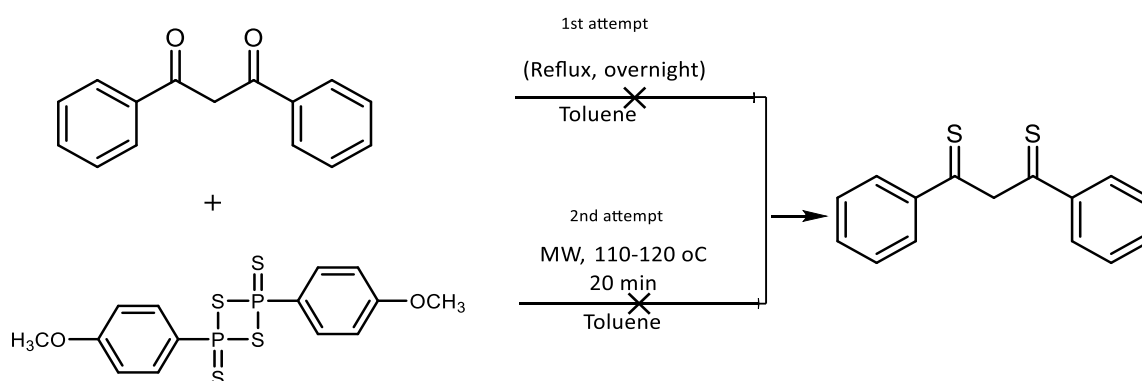


Scheme 22: Mechanism of pyran protected ester

The protected ester was used in the next step to form the β -diketone according to modified procedure A (mentioned in section 2.1.1). The expected diketone did not form either, instead NMR confirms only the presence of a deprotected ester and the starting ketone.

3.1.4 Attempted thionation of β -diketones

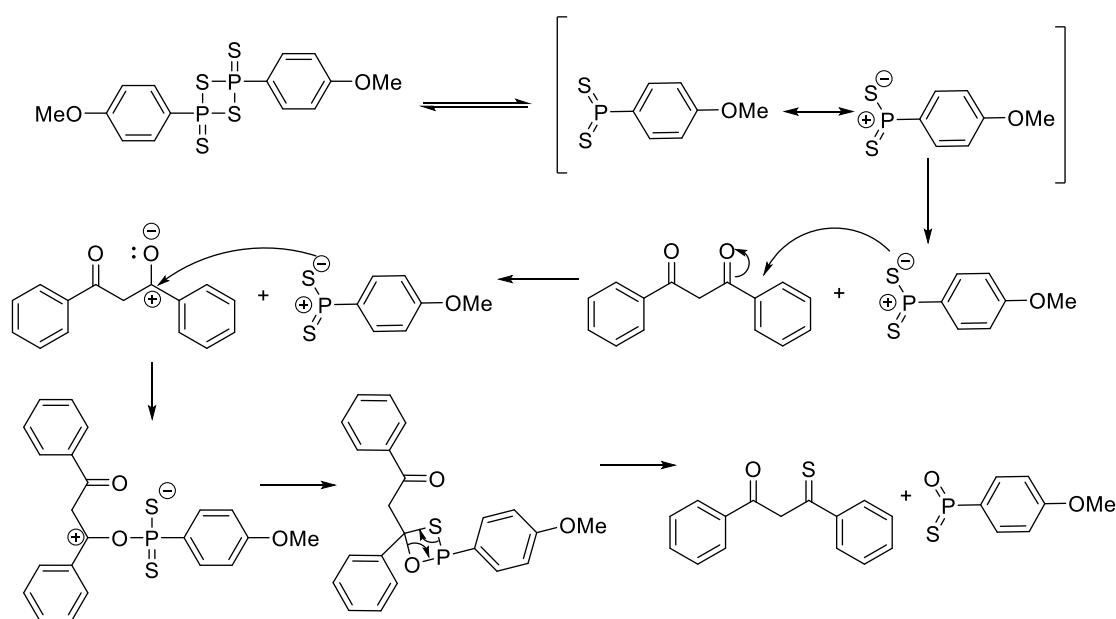
As part of the plan of the research to investigate anticancer activity of β -diketones, thionation of a non-substituted β -diketone have been attempted as a model to see if different series of substituted thionated analogues of dithiones can be formed. The first attempt at thionation of β -diketone was carried out under laboratory conditions according to the method of Almelah et al., 2016. The procedure according to this method consisted of molar amounts of both diketone and a Lawesson's reagent (2,4-bis(p-methoxyphenyl)-1,3-dithiaphosphetane-2,4-disulfide, LR) in toluene with heating under reflux overnight (Almelah *et al.*, 2016). After solvent evaporation, an orange coloured crude product was obtained which did not show the presence of expected product (**Scheme 23**) on the TLC. The reaction was unsuccessful despite changing different conditions such as prolonging reflux time, carrying out the reaction at room temperature and doubling the equivalents of the LR. The second attempt was carried out under microwave conditions with an equivalent amount of reagents subjected for 20 minutes at temperature of 115 °C.



Scheme 23: Proposed thionation of β -diketones

Different fractions of the components was collected by column chromatography and characterised by NMR which showed characteristics of different aromatic fragments that were not consistent with the expected product. Some of them could possibly be stable

methoxyphenyl intermediates that are energetically more favourable to form than the desired product. The scheme proposed for the thionation by LR (**Scheme 24**) is typically employed for single carbonyl containing compounds and is a widely accepted reaction mechanism and is supported by DFT calculations (Legnani *et al.*, 2016). So far, there is no evidence in the literature apart from Almelah *et al.*, 2016 on thionation of β -diketone by LR or any thionating agent. However, lack of success in thionating β -diketones could be related to steric hindrance involved with the coupled of stable adducts during the reaction process.



Scheme 24: Proposed mechanism for the thionation of β -diketones with Lawesson's reagent, (Polshettiwar and Kaushik, 2006)

3.1.5 Position of the enolic protons on the proton NMR:

The enol proton peak on the β -diketone is of great significance in confirming the formation of the compound. According to (Zawadiak and Mrzyczek, 2013), it represents one of the unique peaks that appears in β -diketones including the ones that have been recorded in this thesis. The chemical shift of both the enolic and acidic protons of β -diketones, according as postulated by du Plessis, depends on two factors: the substituent electronegativity of the group neighbouring either of the adjacent carbonyl groups and their resonance stability (du Plessis, Vosloo and Swarts, 1998). The peaks of the enolic protons normally have a chemical shift between 15.05-17.20 ppm (

Table 5) whereas the acidic proton between the two β -carbonyls appear at 6.20 – 7.10 ppm.

Table 5: ¹H-NMR Chemical shifts of enolic protons in prepared β-diketones

	Compound	Enolic protons (ppm)	Olefinic protons (ppm)
1.	DBM (dibenzoylmethane)	16.93	6.89
2.	4	16.91	6.68
3.	5	17.03	6.67
4.	6	17.09	6.76
5.	7	17.11	6.64
6.	8	17.15	6.74
7.	9	16.25	6.59
8.	10	16.90	6.73
9.	11	16.91	6.79
10.	12	16.35	6.35
11.	13	16.35	6.79
12.	14	16.93	7.18
13.	15	16.79	6.81
14.	16	16.79	6.71
15.	17	17.03	6.72
16.	18	17.06	6.73
17.	19	17.04	6.84
18.	20	17.02	6.80
19.	21	16.96	6.75
20.	22	17.05	7.14
21.	23	17.01	7.09
22.	24	16.93	6.58
23.	25	16.78	6.62
24.	26	16.76	6.71
25.	27	16.90	6.75
26.	28	16.90	6.75
27.	29	17.04	6.68
28.	30	16.90	6.64
29.	31	16.96	6.73
30.	32	16.96	6.76
31.	33	16.90	6.72
32.	34	16.90	6.69
33.	35	16.90	6.67
34.	36	16.90	6.92
35.	37	16.70	6.70

3.1.4 NMR couplings of fluorinated β -diketones:

The inclusion of fluorine in drug molecules offers a very important role in improving bioactivity of essential drug molecules. Due to its polarity, size, and steric properties, a single fluorine substituted in a molecule can contribute to a large changes to the physical and chemical properties of a molecule (Dolbier, 2009). One of its medicinal features is its ability to contribute to enhanced metabolic stability; especially in lipophilic drugs which are prone for oxidation by p450 in the liver (Shah and Westwell, 2007). As a result, most of the compounds prepared in this thesis have been prepared by considering the importance of fluorine related to the properties mentioned above. However, worthy to mention also, is the characteristic couplings of fluorine substituents in some of the prepared β -diketones and benzoyl thiourea.

The chemical shift scale for most reported ^{19}F values typically appear between maxima and minima values from -500 ppm to 600 ppm (Reich, 2005). The position of the shifts, like the ^1H and ^{13}C chemical shifts depends on the chemical environment where the fluorine atom is present. For most fluoroaromatics with fluorine directly attached to the benzene ring, their shifts are found between -200 ppm and -95 ppm. For aromatic methyl fluorides such as $-\text{CF}_3$, the shift goes further downfield from -70 ppm – 0 ppm; with slight variations depending on the solvents used to dissolve a sample. Fluorine can couple with neighbouring protons and their characteristic large coupling constants can be used to identify the couplings between the ^1H - ^{19}F . Furthermore, unlike hydrogen, oxygen, and chlorine, when the proton decoupler is switched off, the signals appear as singlets on ^{13}C the spectrum, the ^{13}C - ^{19}F can be observed even with the proton decoupler is disabled. Although, as in the proton couplings, the $n + 1$ rule suitably applies in determining the characteristic couplings of ^{13}C peaks. Most of the fluorinated β -diketones prepared in this thesis are categorised as fluorine atoms directly substituted on the ring; or a trifluoromethyl (CF_3) group (**Figure 61**).

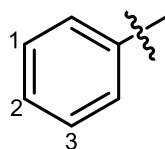


Figure 61: Substitution of fluorine or trifluoromethyl at position numbered 1, 2 or 3

Chemical shifts of fluorine on ^{13}F NMR

The chemical shift fluorine in **4** and **17** and similar β -diketones for instance appear at -134.2 ppm which is an indication that the fluorine atom directly substituted to the ring. The same chemical shift applies for the benzoyl thiourea series. Chemical shift of some fluoro-substituted compounds is highlighted in **Table 6** (below):

Table 6: Chemical shifts of some fluoro-substituted β -diketones

	Compounds	Chemical shift (ppm)
1.	4	-134.17
2.	17	-134.31
3.	18	-109.23
4.	23	-134.62
5.	26	-133.81
6.	29	-108.78

From the table **Table 6** (above), **18** and **29** have chemical shifts downfield due to the presence of chlorine, an electron withdrawing group neighbouring the fluorine atom.

^{13}C Chemical shifts and ^{19}F - ^{13}C couplings:

Fluorine couplings of ^{19}F splits carbons that are up to four bonds apart. The couplings of the carbons in aromatic rings normally varies depending on the distance of the carbon from the fluorine atom. The coupling constants vary from 245.3 Hz to 3.3 Hz depending on the bond proximity (Dolbier, 2009).

However, these couplings of carbon substituted to the fluorine (ipso carbon) may vary slightly depending on the substituents attached to the ring. Likewise, coupling constants for the carbon of trifluoromethyl group ($-\text{CF}_3$) as it can be split into a quartet (1:3:3:1), and because of the amplified electronegative effect of the three directly bonded fluorine (**Figure 62**), the coupling constants may extend up to 271 Hz (Pretsch, Buhlmann and Badertscher, 2009).

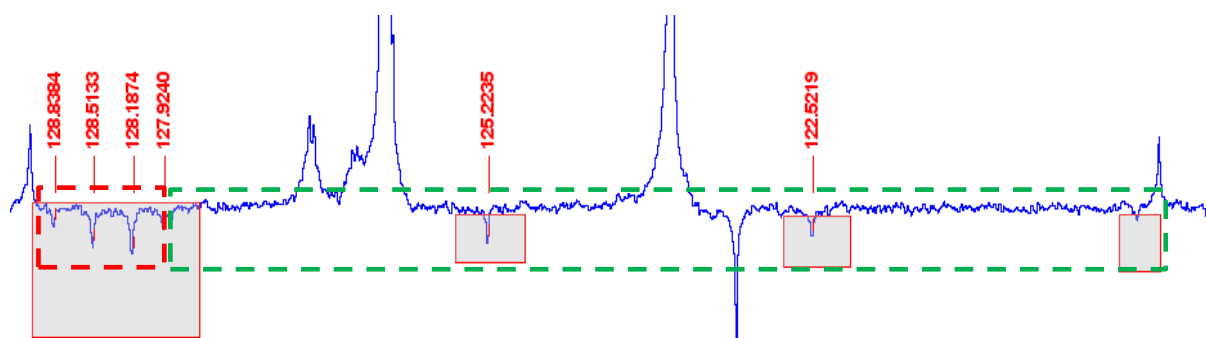


Figure 62: Coupling of carbon in the trifluoromethyl group (CF_3) and aromatic ipso carbon. Weak signals in the red dotted box (highlighted grey) represent 3 identical fluorine atoms coupling with an aromatic ipso carbon (31-33 Hz) neighbouring a $-\text{CF}_3$. The grey highlighted signals represent coupling of the 3 fluorine atoms bonded directly to the carbon (271-272 Hz).

From (**Figure 62**) couplings of quaternary carbon that are completely substituted with fluorine appeared as weak signals, and due to the slow relaxation time splits the peaks into many peaks that disappear in the noise or overlap on larger signals that can be difficult to detect. However, altering some parameters such as increasing the concentration of the sample, number of scans and frequency of hardware, the signals can be improved to more easily detected signals.

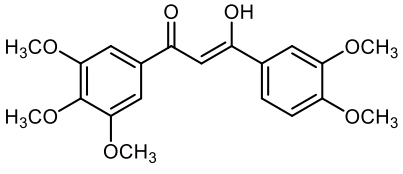
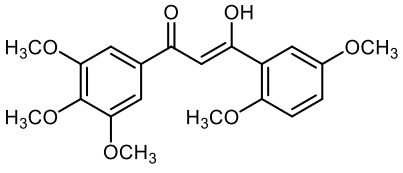
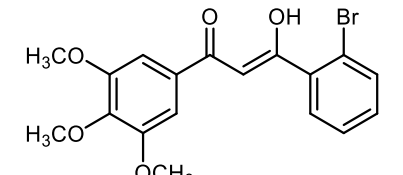
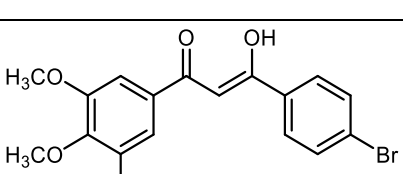
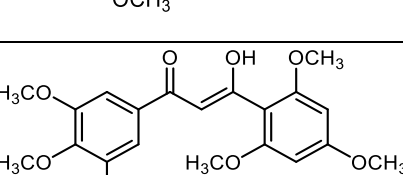
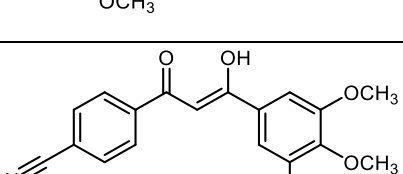
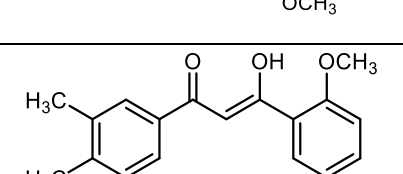
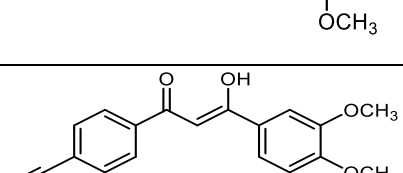
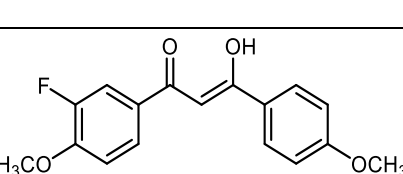
3.2 Discussion of biological activity of β -diketones

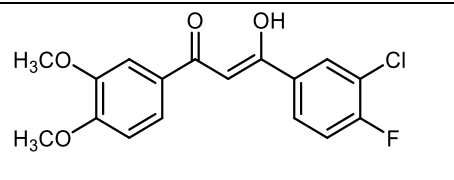
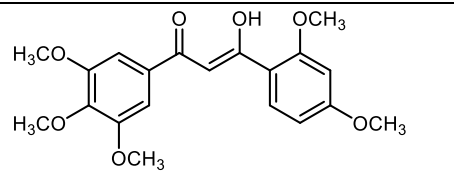
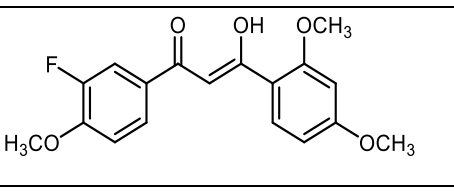
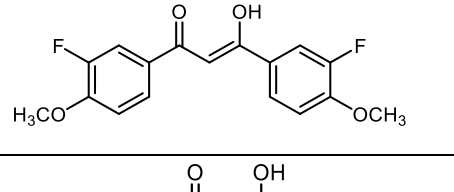
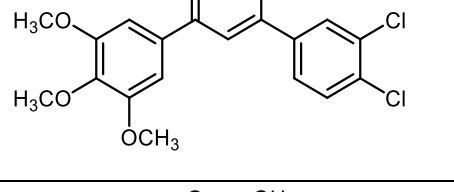
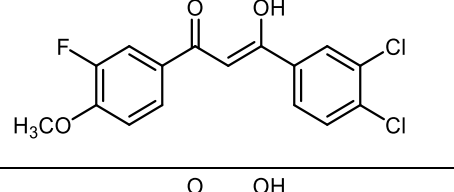
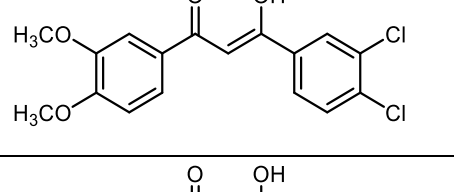
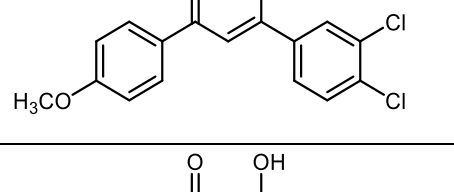
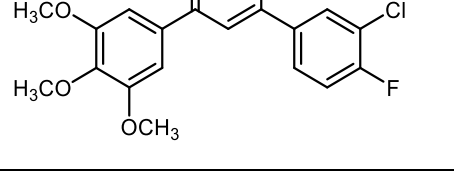
3.2.1 Effects of β -diketones on cancer cells

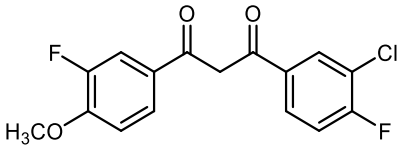
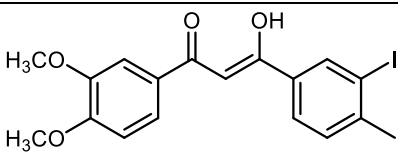
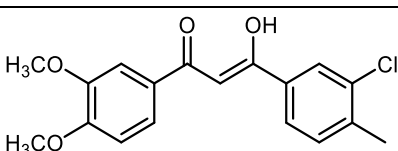
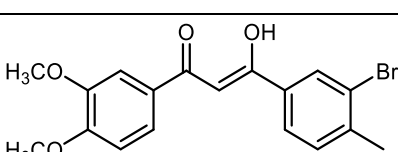
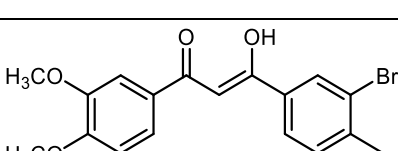
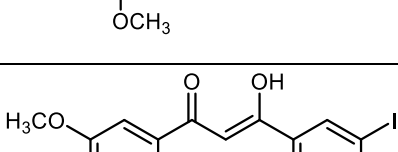
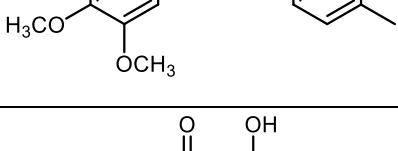
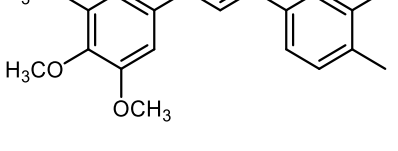
30 β -diketones were tested on different cancer cell lines. All the compounds in the entry have shown IC_{50} values greater than combretastatin CA-4 which was used as a control for the test. Results of tested compounds were presented below in (Table 7) and (Table 8) along with their cell viability graphs and bar chart of compounds tested for each cell line. Most of the compounds have shown inhibitory activity with IC_{50} ranging between 3 μ M to 125 μ M. Combretastatin-A4 (CA-4) is a compound with strong antiproliferative activity on different cell lines and was used as a positive reference in the assay. IC_{50} for some compounds were not detected and are represented with an asterisk in the table.

Table 7: IC_{50} values of synthesised benzoyl thiourea (BTU) series determined by MTT assay after 120 hours of drug exposure. The experiments were carried out in triplicates

Compound ID	STRUCTURE	IC_{50} (μ M)				
		A204	A549	HeLa	HepG2	U2OS
CA-4		0.053±0.45	0.048±3.03	0.045±1.53	5.90±2.01	0.008±0.06
4		14.32±6.80	10.80±5.09	28.27±13.63	49.53±24.03	32.82±15.80
5		13.40±6.15	29.72±9.26	57.01±24.04	108.10±11.85	10.80±4.89
6		4.89±1.91	72.10±24.14	19.80±7.80	41.88±15.39	12.39±3.30

7		6.65±3.44	35.69±30.32	45.22±31.41	44.94±18.32	43.18±15.76
8		8.42±3.51	42.92±10.82	64.67±29.26	57.35±24.64	4.83±1.29
9		7.37±3.76	83.92±28.04	18.26±5.08	17.76±23.50	3.38±2.23
11		4.62±1.65	88.13±37.07	24.3±19.53	35.51±15.43	33.76±17.20
12		6.47±4.99	45.53±39.86	113.40±40.66	112.60±31.21	20.27±9.54
13		*	*	*	*	*
14		20.68±15.72	44.94±18.32	43.81±25.60	35.51±3.40	7.57±2.29
15		*	*	38.61±27.74	*	7.81±1.23
17		6.33±2.61	34.08±16.35	66.54±69.41	47.17±20.01	21.03±7.12

18		18.73±11.62	62.35±30.36	82.96±37.61	120.50±30.22	44.47±18.34
22		23.82±17.75	25.56±20.47	38.93±25.03	116.80±3.75	34.47±19.95
23		8.61±5.01	44.32±38.63	33.35±22.39	86.81±29.80	42.97±15.25
24		5.99±3.54	27.5±10.59	84.69±22.36	37.85±18.08	27.06±6.89
25		5.37±3.73	17.26±16.35	*	115.50±12.39	23.72±16.54
26		4.81±1.80	35.85±10.35	33.00±16.33	*	6.49±2.39
27		7.36±4.50	58.05±27.71	82.41±20.09	79.22±39.61	29.46±25.60
28		9.79±3.16	117.00±2.30	54.32±13.20	61.16±27.24	55.82±28.14
29		6.98±5.03	32.68±14.95	*	44.25±14.85	30.23±10.60

30		3.87±2.56	92.07±13.64	31.58±19.05	85.20±15.35	29.39±13.11
31		3.61±2.02	18.28±9.15	64.98±29.54	*	7.76±3.33
32		3.63±2.44	99.15±21.45	19.60±5.96	*	8.54±3.39
33		7.56±3.43	44.94±13.36	55.06±12.17	68.02±28.75	22.51±9.01
34		3.78±1.23	52.74±11.84	60.76±10.64	50.57±16.36	23.77±9.38
35		9.56±14.29	37.18±18.81	33.51±8.82	57.01±14.96	22.32±7.40
36		7.25±4.75	73.79±27.37	48.45±15.70	*	44.18±11.25
37		9.28±5.77	71.86±26.13	111.30±21.78	50.19±10.66	77.77±11.67

Results recorded represent mean of three experiments

Asterisks denotes compounds whose IC₅₀ have not been determined.

Chart A: β -diketone series treated on different cancer cells:

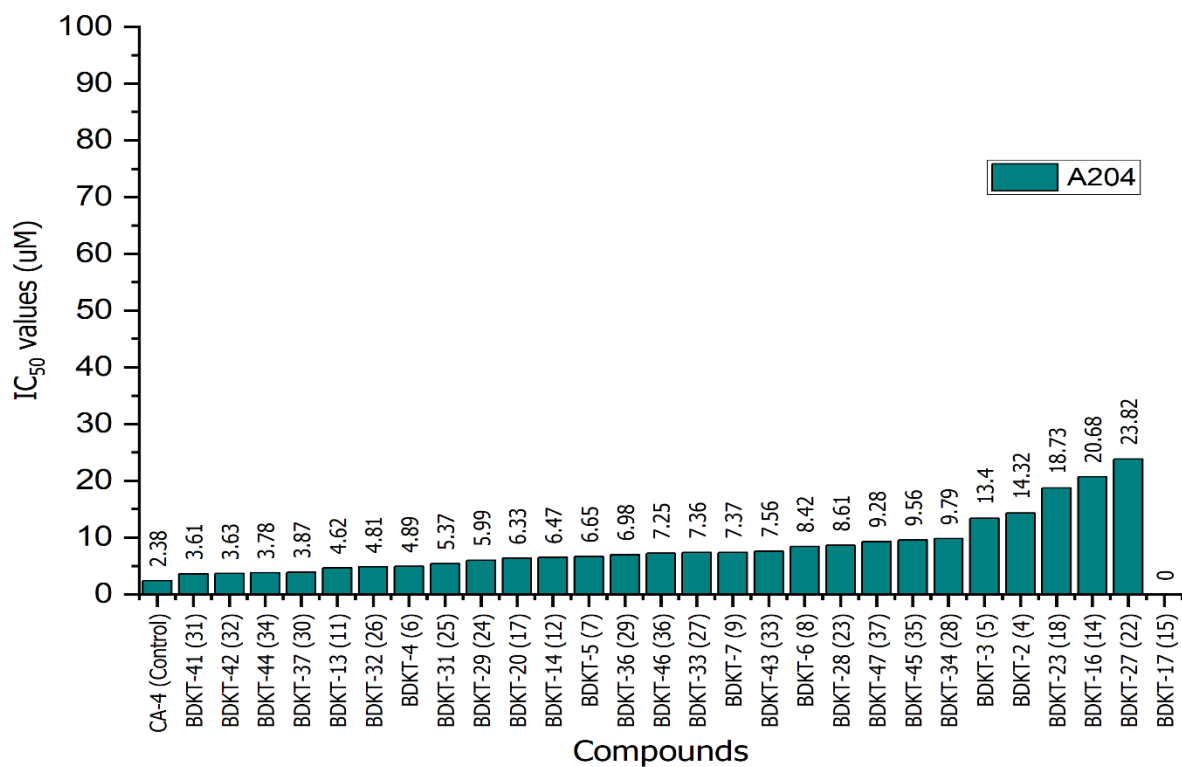


Figure 63: IC_{50} of β -diketones tested on A204 cell line. 0 indicate compounds with undetermined activity.

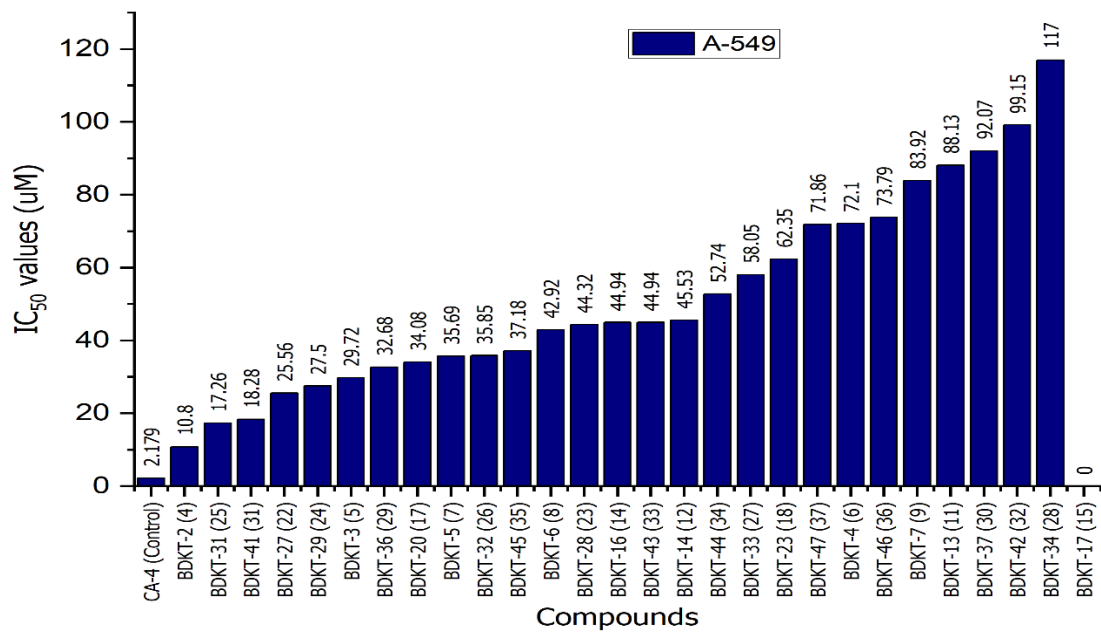


Figure 64: IC₅₀ of β-diketones tested on A549 cell lines. 0 indicate compounds with undetermined activity.

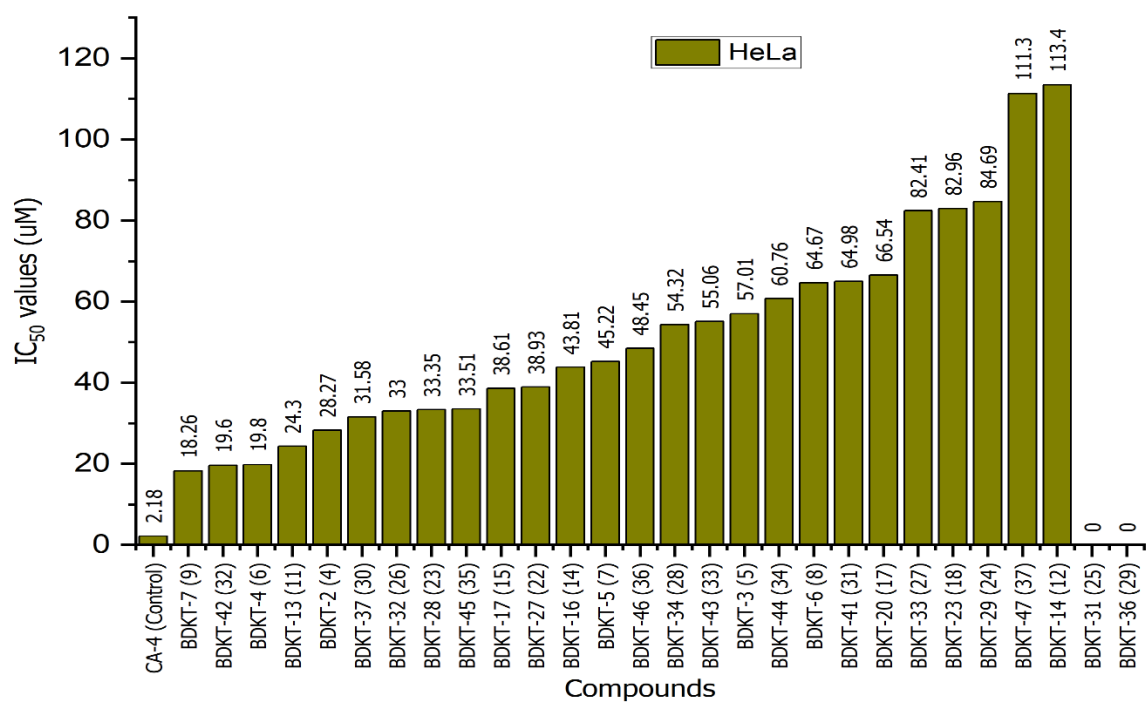


Figure 65: IC₅₀ of β-diketones tested on HeLa cell line. 0 indicate compounds with undetermined activity.

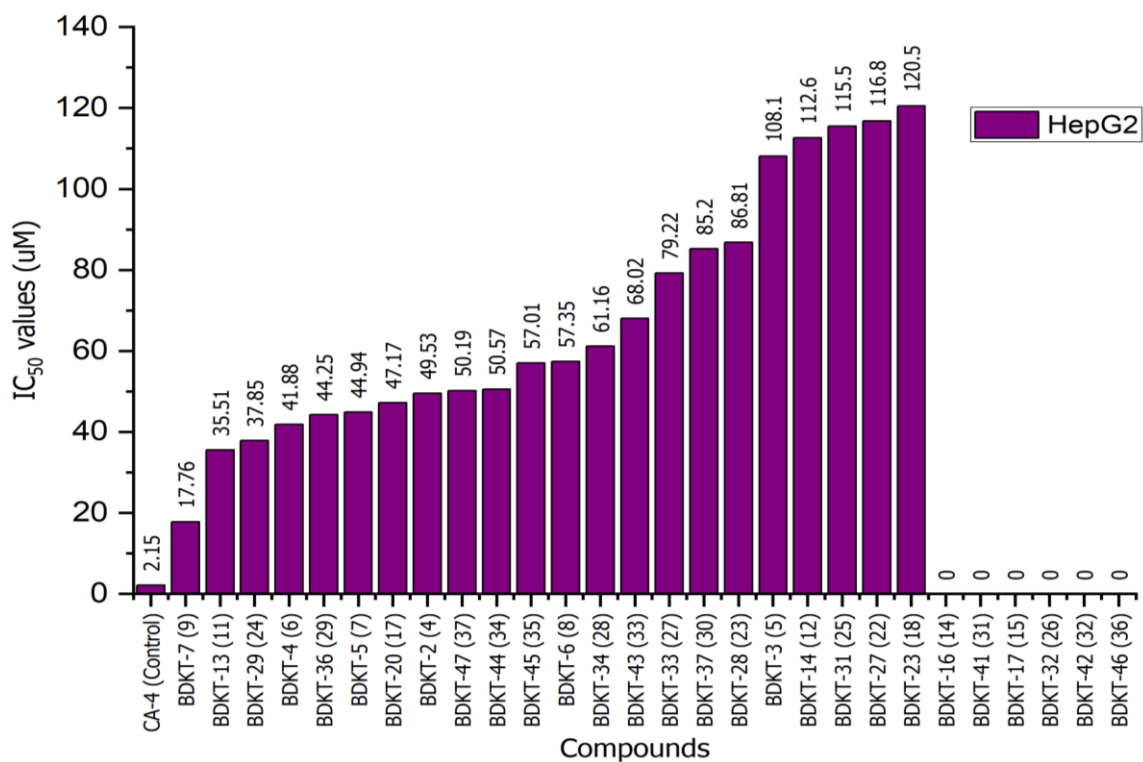


Figure 66: IC₅₀ of β -diketones tested on HepG2 cell line. 0 indicate compounds with undetermined activity.

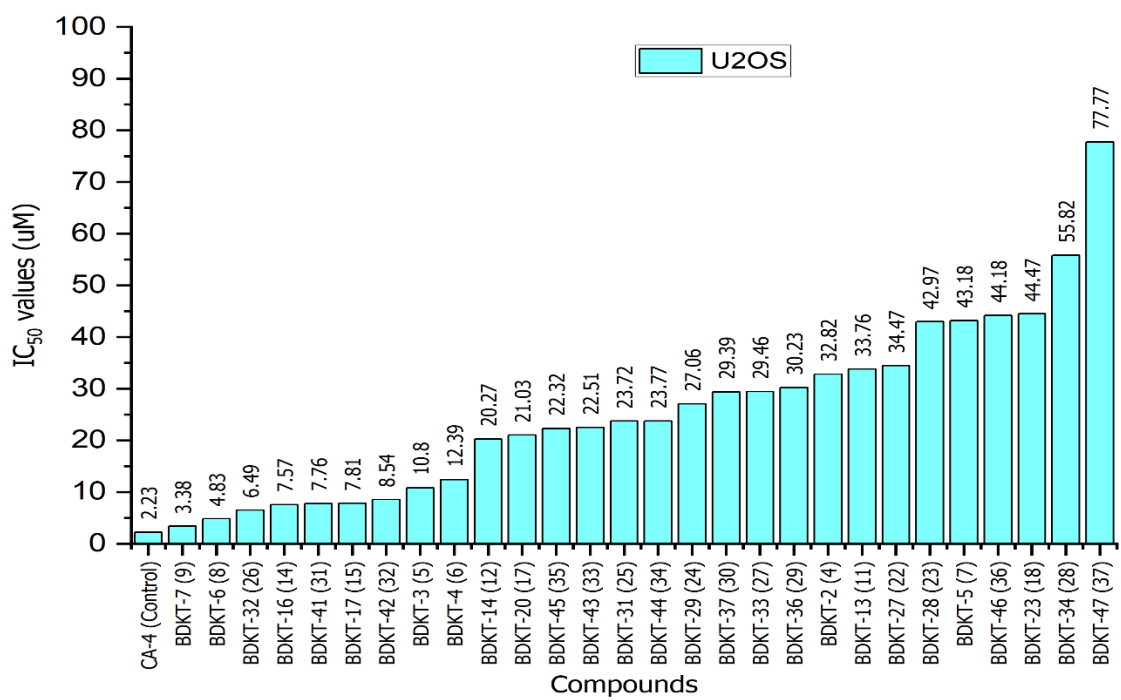
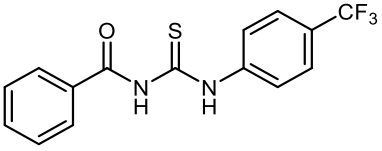
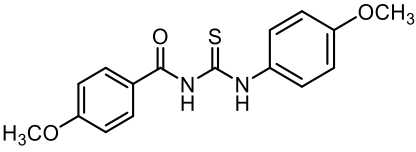
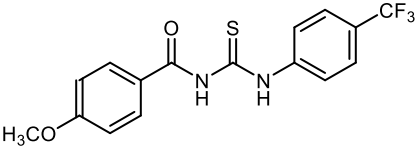
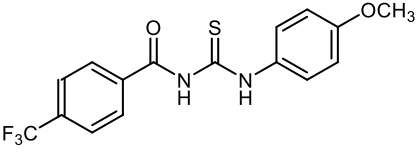
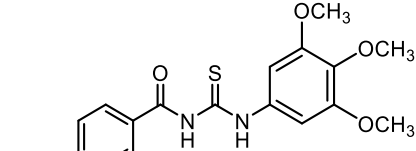
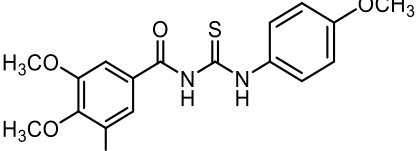
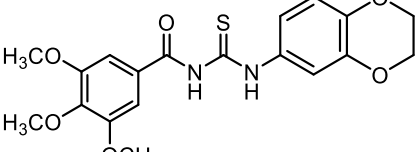
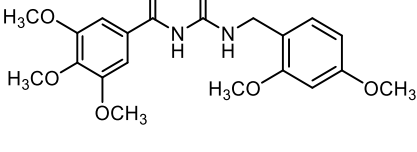
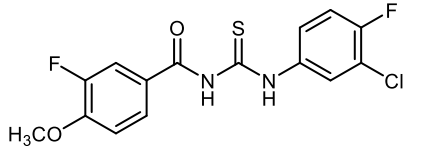
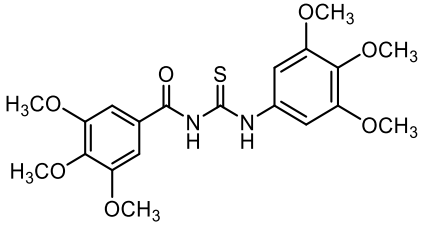
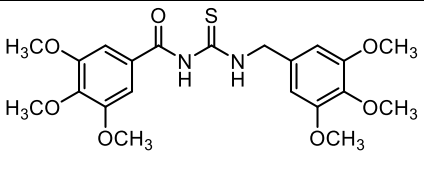
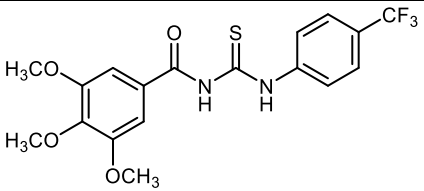
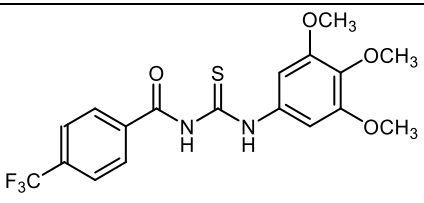
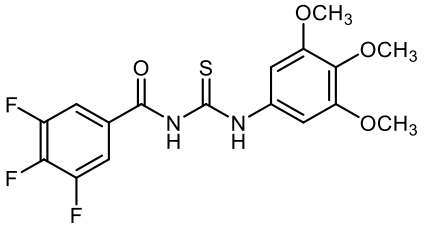
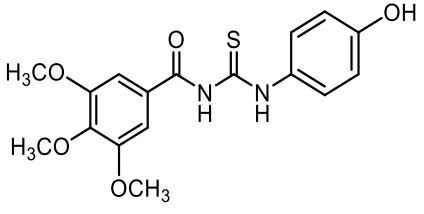
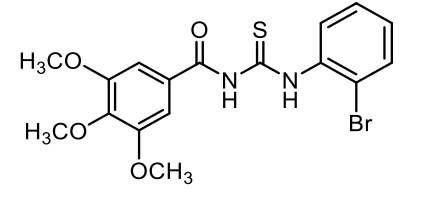


Figure 67: IC₅₀ of β-diketones tested on U2OS cell line.

Table 8: IC₅₀ values of synthesised benzoyl thiourea (BTU) series determined by MTT assay after 120 hours of drug exposure. The experiments were carried out in triplicates.

Compound ID	STRUCTURE	IC ₅₀ (μM)				
		A204	A549	HeLa	HepG2	U2OS
40		6.59±1.61	26.46±11.99	9.63±5.81	33.39±23.88	23.92±8.99
41		5.53±1.82	11.60±2.48	20.86±11.90	6.53±2.44	10.75±5.29
42		*	*	*	*	*
43		6.56±2.28	16.84±3.56	8.73±2.37	7.26±1.55	8.22±3.25
44		4.32±1.43	10.90±4.03	9.76±22.72	81.73±31.12	28.88±14.23
45		5.77±3.85	10.64±4.70	5.06±4.72	117.70±27.90	18.56±13.63
46		5.49±4.04	5.51±2.73	8.06±13.60	*	6.17±3.62
47		5.6±2.72	6.75±2.99	6.53±4.76	115.60±31.23	11.56±12.21

48		3.76±1.44	5.99±0.99	4.89±5.03	27.34±14.11	15.47±6.08
49		4.86±2.76	7.41±3.42	8.04±4.27	89.38±23.35	22.93±15.96
50		9.36±3.54	19.86±14.15	25.49±8.83	18.37±9.19	39.24±14.25
51		5.06±1.53	26.24±15.45	73.98±23.41	141.30±35.25	11.18±5.48
52		5.73±4.78	35.02±23.82	3.64±28.29	112.80±18.14	47.70±11.02
53		3.97±1.43	20.02±11.72	6.28±5.29	55.09±15.47	40.15±15.34
54		4.58±2.09	28.12±7.62	*	24.29±14.97	8.70±3.15
55		4.32±1.43	10.90±4.03	9.76±22.72	81.73±31.12	28.88±14.23

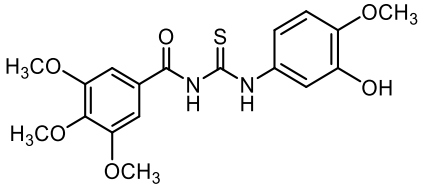
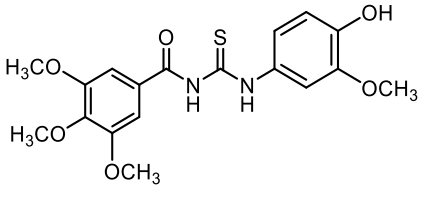
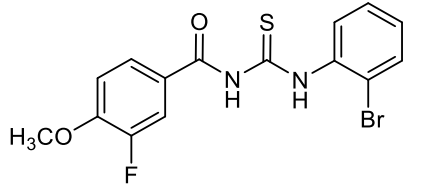
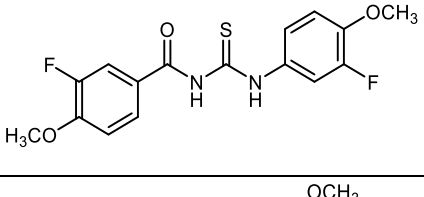
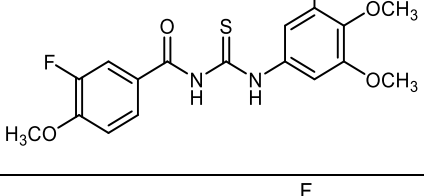
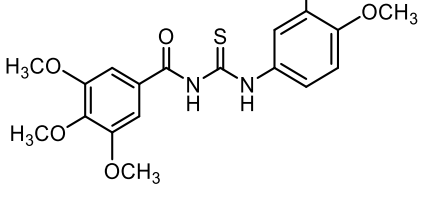
56		3.65±1.38	15.35±8.15	18.56±13.56	71.93±21.23	14.03±3.69
57		5.48±15.40	7.39±3.69	4.37±4.70	48.53±20.05	52.21±18.60
58		*	*	*	*	*
59		5.52±2.14	11.06±12.33	4.44±2.22	12.61±7.24	18.44±13.44
60		3.76±0.95	6.83±1.85	3.17±9.11	21.06±16.34	10.55±4.03
61		3.75±2.83	9.14±2.00	12.67±12.86	113.20±27.75	16.20±9.95

Chart B: Benzoyl thiourea (BTU) series treated on different cancer cells:

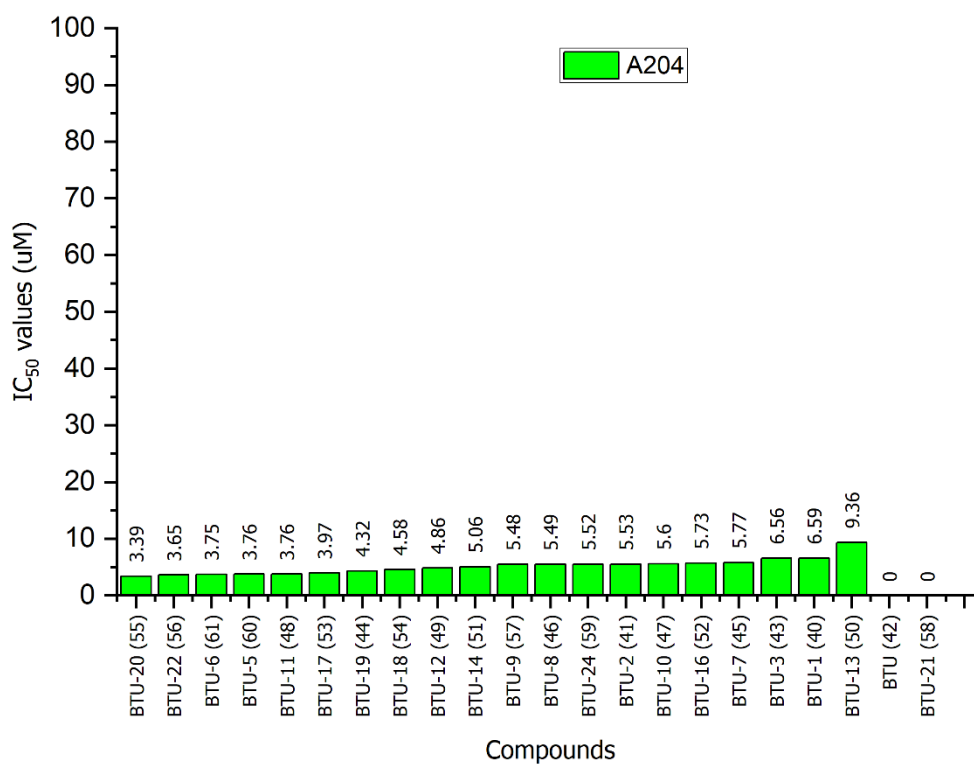


Figure 68: IC₅₀ of benzoyl thiourea tested on **A204** cell line. 0 indicate compounds with undetermined activity.

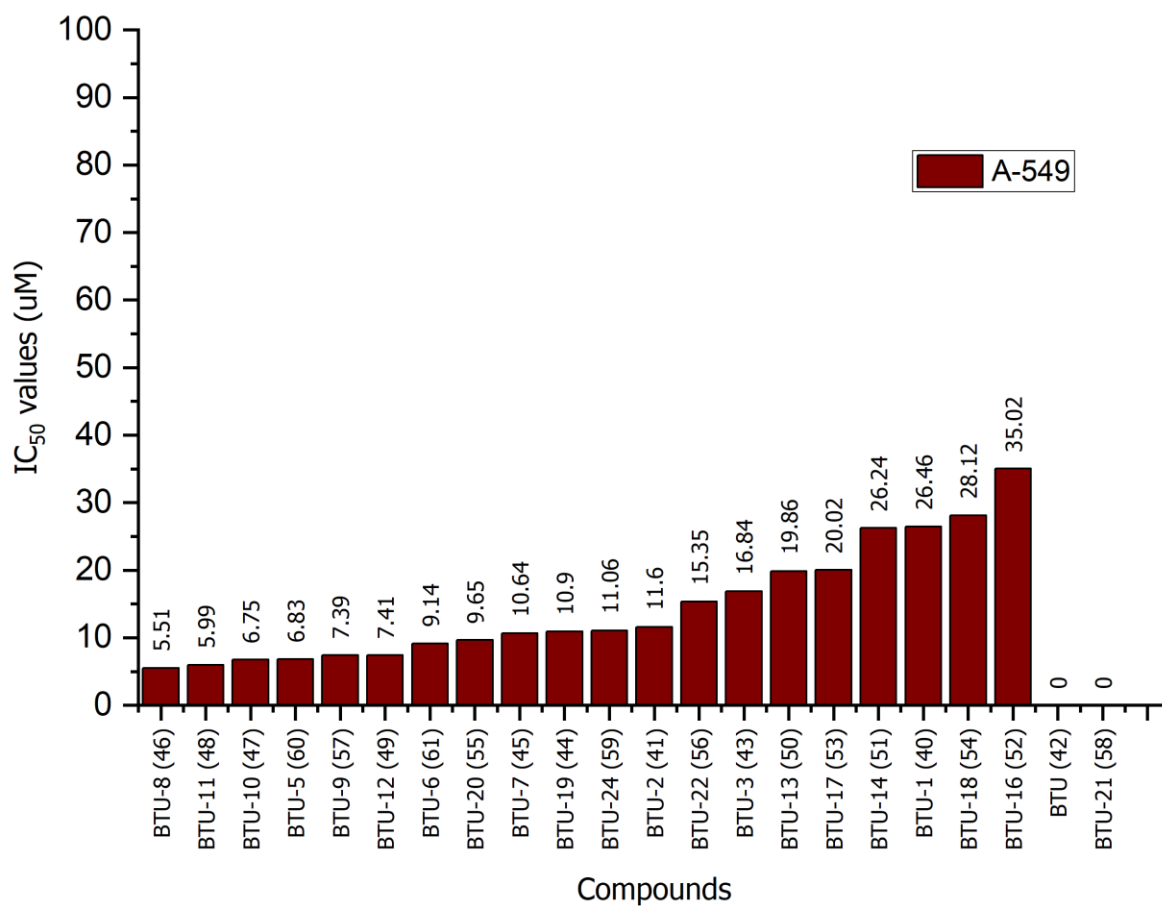


Figure 69: IC₅₀ of benzoyl thiourea tested on **A549** cell line. 0 indicate compounds with undetermined activity.

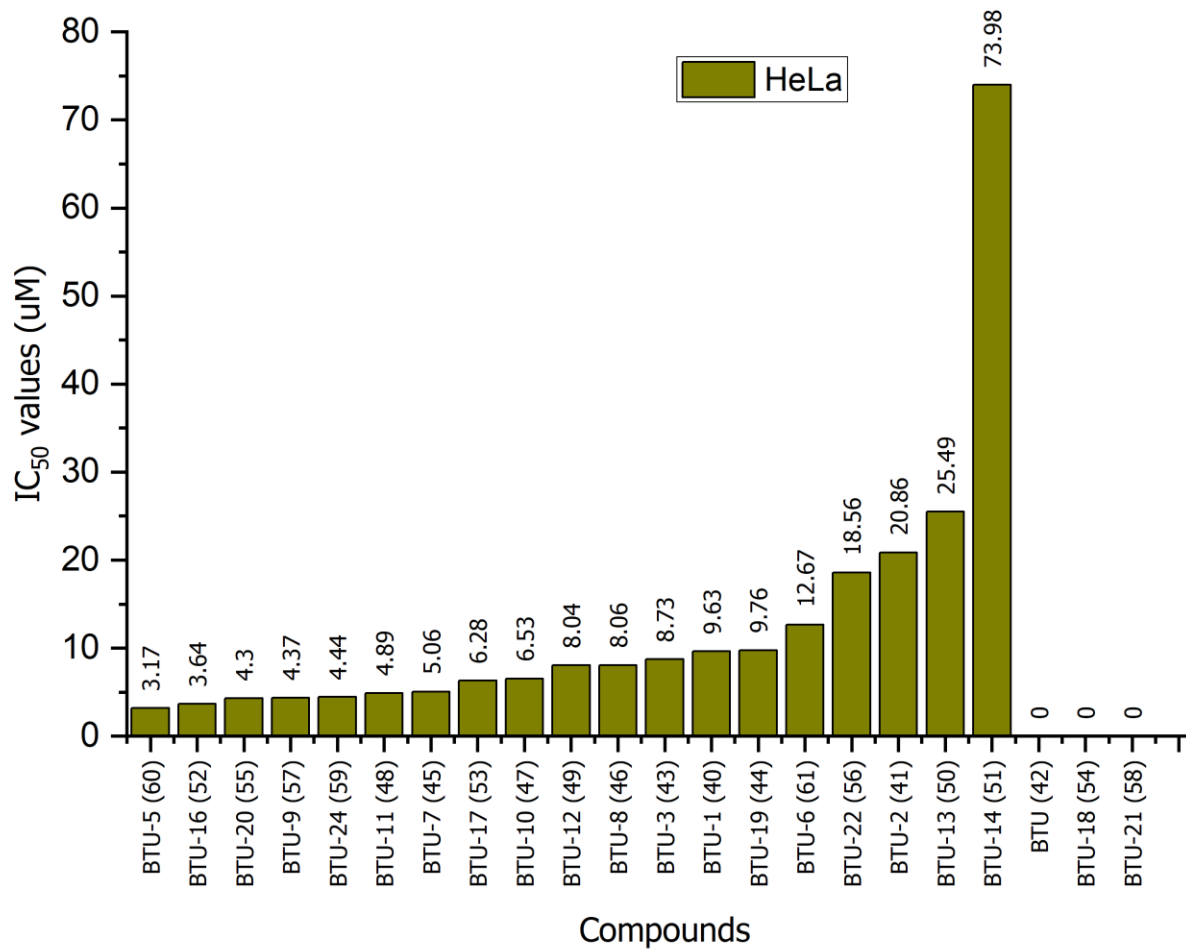


Figure 70: IC₅₀ of benzoyl thiourea tested on **HeLa** cell line. 0 indicate compounds with undetermined activity.

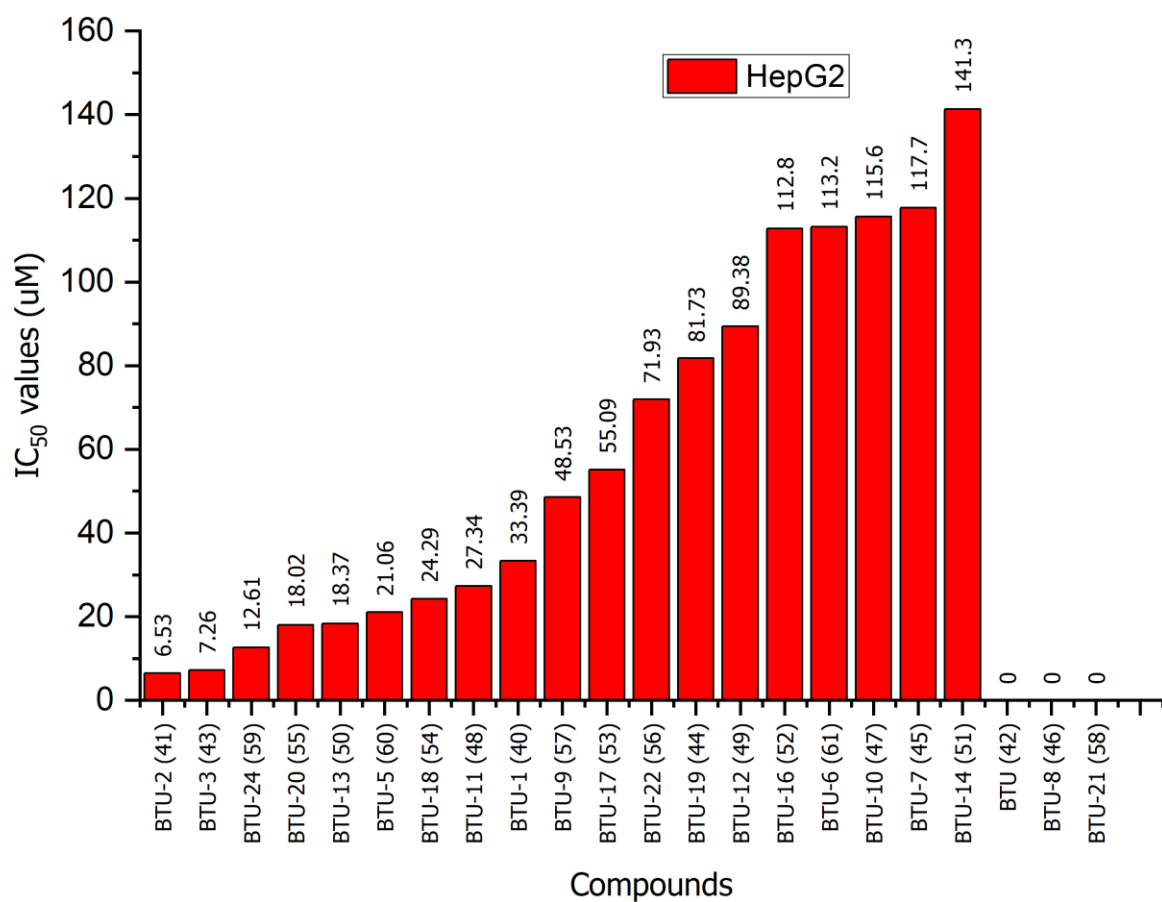


Figure 71: IC₅₀ of benzoyl thiourea tested on **HepG2** cell line. 0 indicate compounds with undetermined activity.

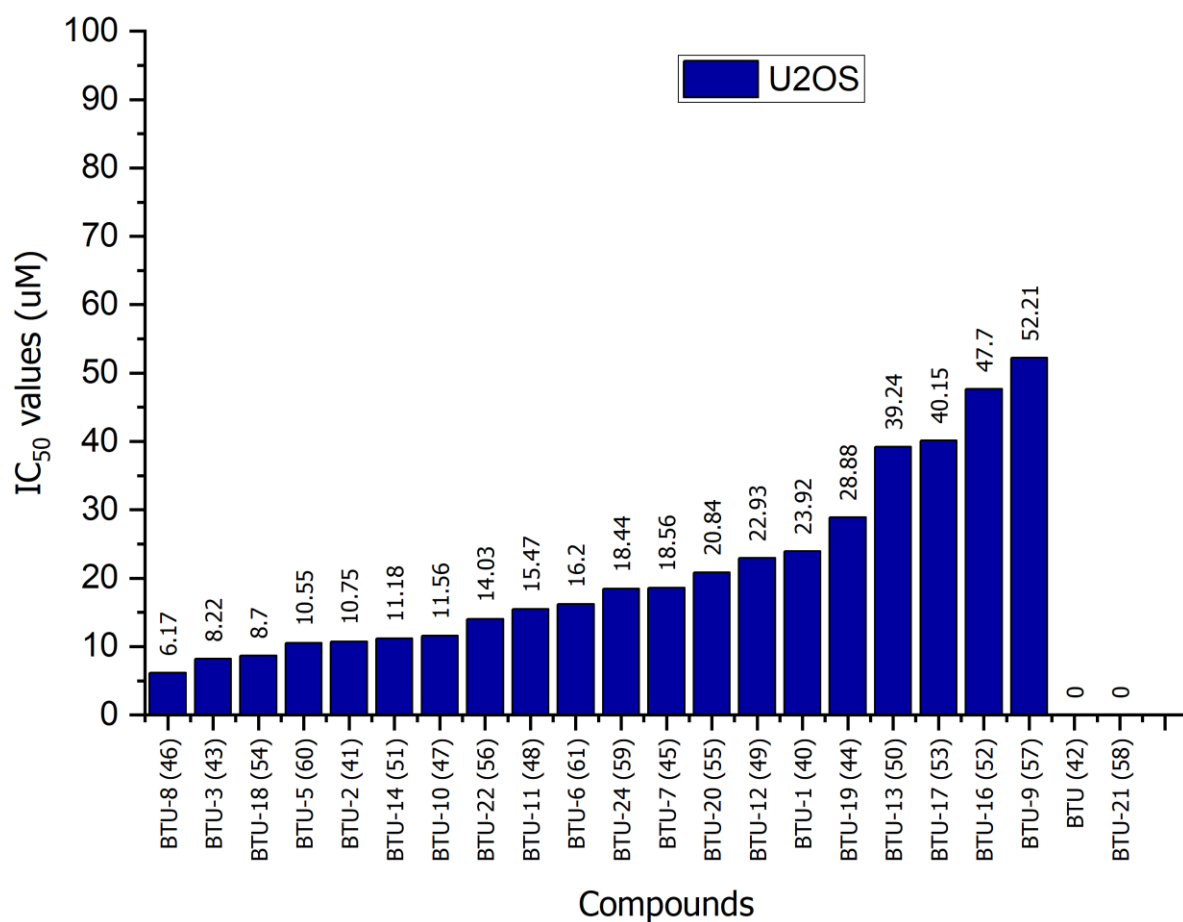


Figure 72: IC₅₀ of benzoyl thiourea tested on **U2OS** cell line. 0 indicate compounds with undetermined activity.

β -diketones and benzoyl thioureas showed significant activity on A204 cells:

A204 tested with series of prepared compounds have shown an impressive cytotoxicity compared to the other cell lines tested. Both BDKT and BTU series of compounds have shown an inhibiting activity ranging from 3.3 – 23.8 μ M. However, the BTU series appear to be more active than BDKT series. Three among the BDKT compounds **30**, **31**, **32** and **34** showed an IC_{50} vales of 3.61 μ M, 3.63 μ M, 3.78 μ M and 3.87 μ M respectively, table 7 and (Figure 73). The presence of halogen groups as substituents has greatly contributed to their better activity.

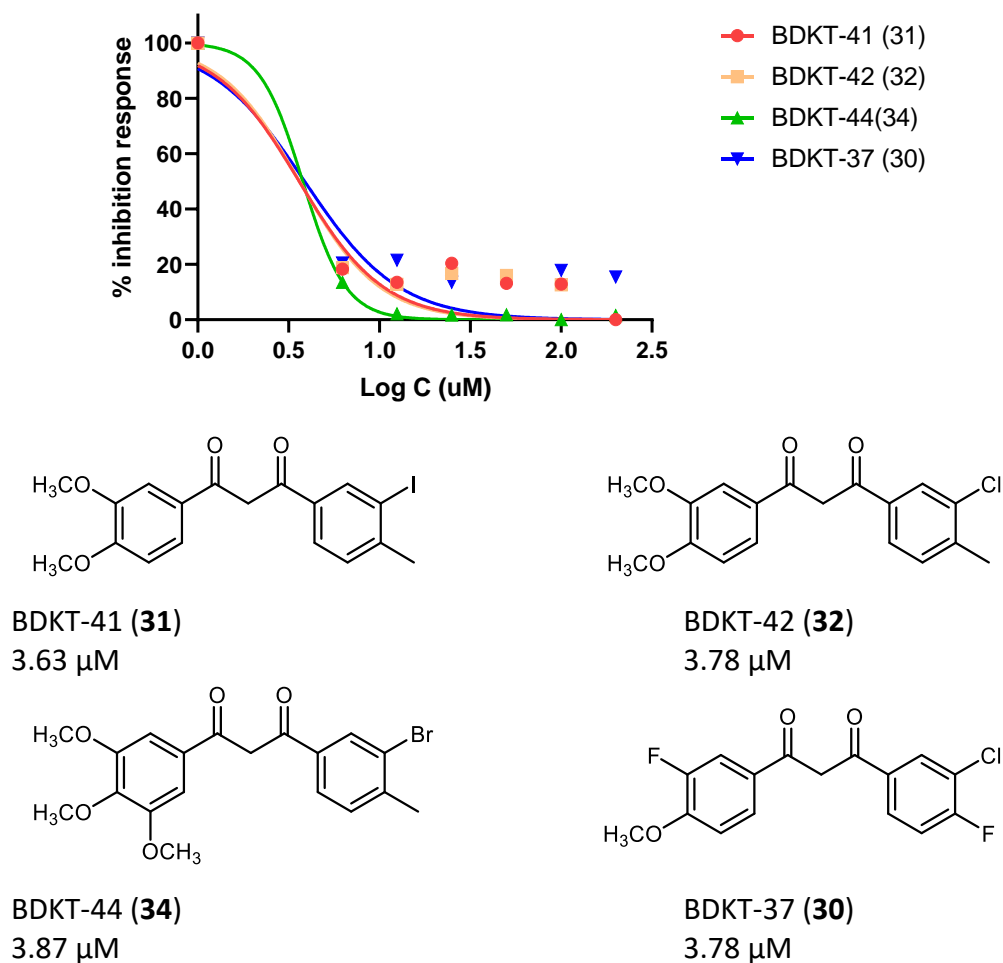


Figure 73: Sensitivity of the most active BDKT analogues on A204 cells

Compound **22** has shown the highest IC_{50} value among the BDKT series bearing methoxy groups only. It is expected that absence of halogen groups in the rings is contributing to its reduced activity. Although, the insertion of a methoxy group (OCH_3) at position 2 of ring B is attributed to the reduced activity, and the same applies to **18** bearing the same group at ortho position (**Figure 74**). However, the presence of OCH_3 at position 3, 4 and 5 on ring B of

compound **5** has slightly improved the activity. Whereas restricting the OCH₃ group of aromatic positions to only 3 and 4 of ring B as in **7** even led to better activity (**Figure 74**).

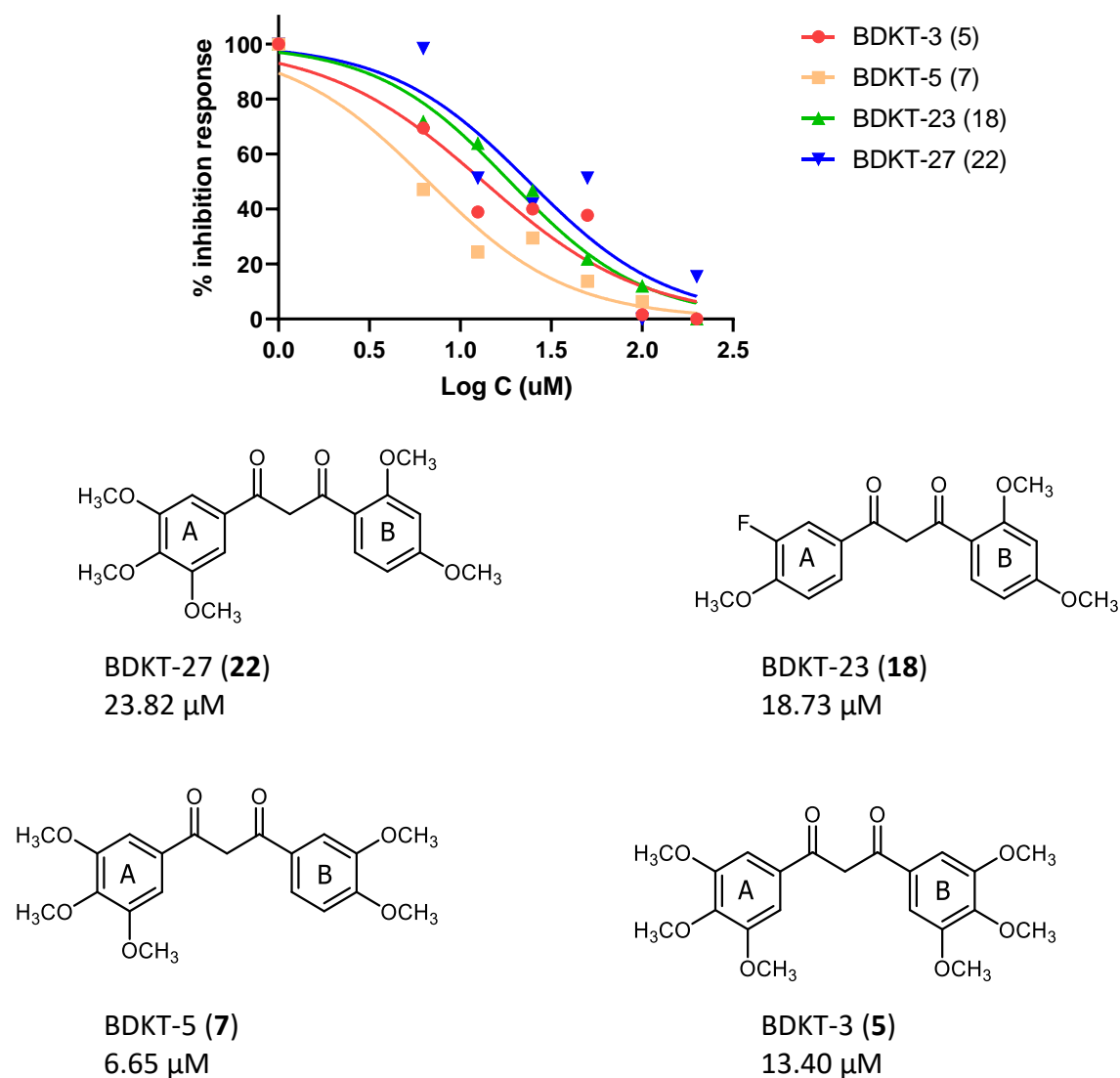


Figure 74: improvement of β-diketone activity on A204 by changing the positions of methoxy groups on the aromatic ring

The BTU analogues tested on A204 cells showed IC₅₀ range between 3.39 to 9.36 µM. Six among the 22 of these compounds (**55**, **56**, **61**, **60**, **48** and **53**) have IC₅₀ values below 4 µM. Except **48**, the interesting trend among these compounds is the presence of a hydroxyl group (OH) or a halogen group along with bulk of -OCH₃ groups present on the second aromatic ring at positions 3, 4, and 5 (**Figure 75**). **55** has higher activity on A204 (IC₅₀ = 3.39 µM). It is expected that the electron density of bromine atom at the ortho position contributes to its greater activity. Likewise, the electronegative hydroxyl group at the *meta* position of **56** also

contributed to activity (3.65 μM). Changing the position to para position as in **57** slightly reduced the activity ($\text{IC}_{50} = 5.48 \mu\text{M}$). Modification of 60 and 61 by flipping the substituents on the ring did not improve the activity of the compounds (**Figure 75**).

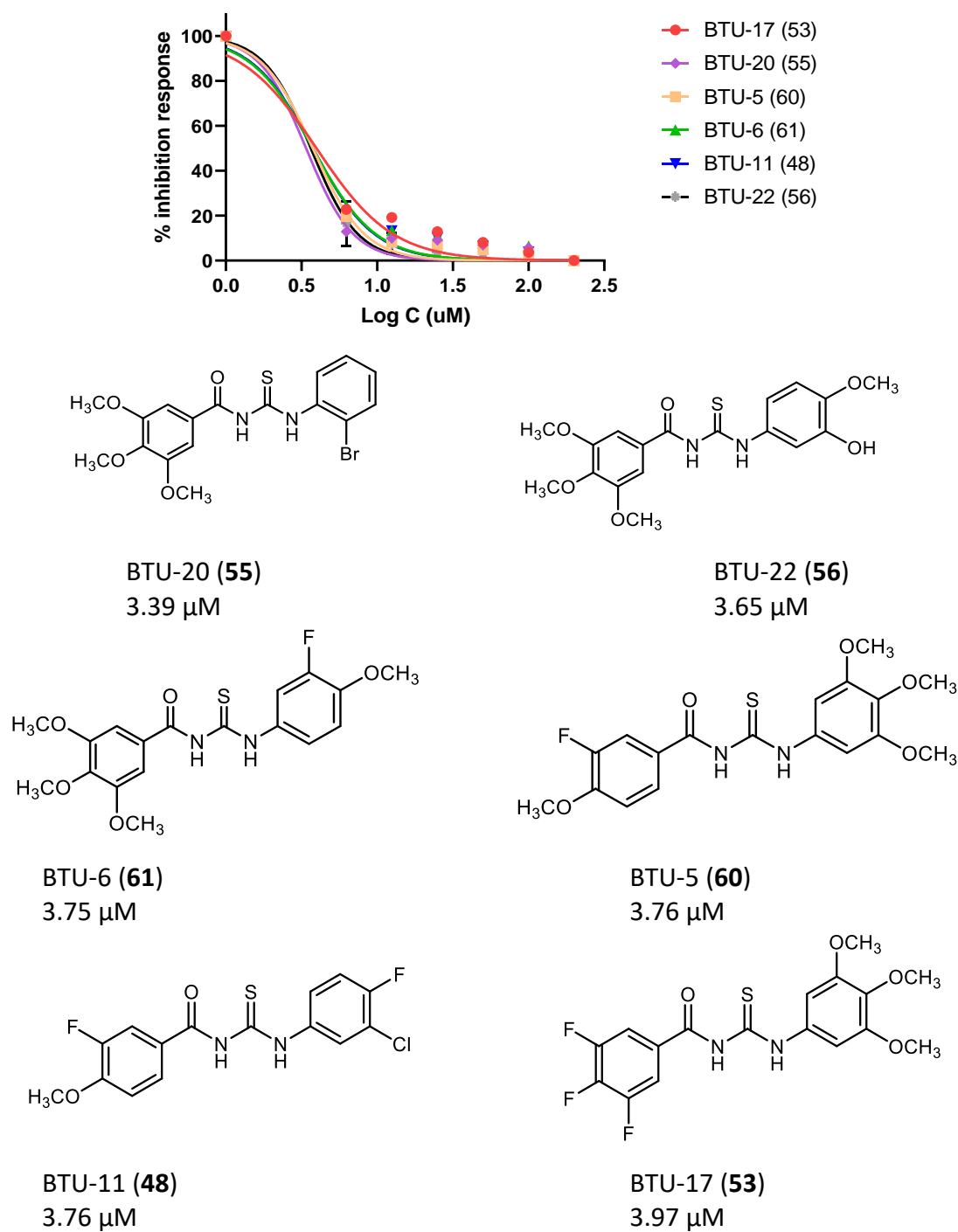
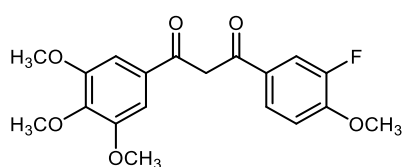
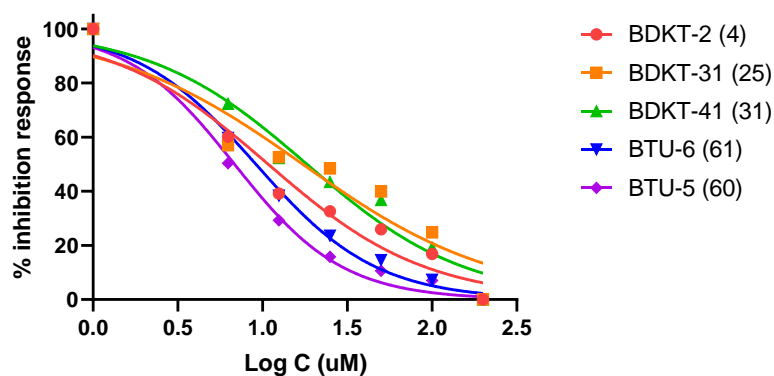


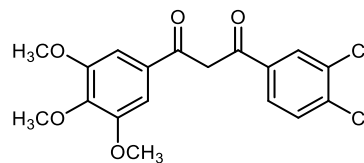
Figure 75: BTU analogues with activity of A204 showing IC_{50} values below $4 \mu\text{M}$

Inhibitory effect of β -diketones and benzoyl thiourea on A549 cells

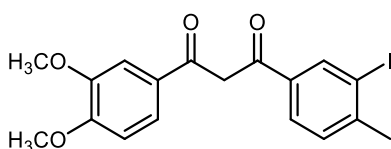
From the results in table (Table 7) and Figure 63, the inhibitory activity of tested compounds ranged from lower IC_{50} values of 10.8 μ M to 117.0 μ M for the β -diketones and 5.51 μ M to 35.02 μ M for the benzoyl thiourea series (Table 8). Compounds 4 and 25 and 31 (Figure 76) have presented an IC_{50} values 10.8 μ M, 17.26 μ M and 18.28 respectively, which is relatively nearer to the IC_{50} value of a β -diketone analogue, curcumin that was reported by Wu *et al.*, 2015 . Compound 60 and 61 bearing the same substituents on the rings as 4 has shown inhibitory activity of 9.14 μ M. It was expected that the presence of halogen atoms and the presence of 3 methoxy groups at positions 3,4 and 5 in the aromatic ring is contributing to their activity.



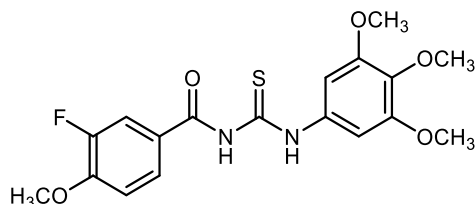
BDKT-2 (4)
 IC_{50} = 10.80 μ M



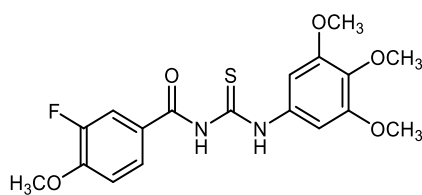
BDKT-31 (25)
 IC_{50} = 17.26 μ M



BDKT-41 (31)
 IC_{50} = 18.28 μ M



BTU-6 (61)
 IC_{50} = 9.14 μ M

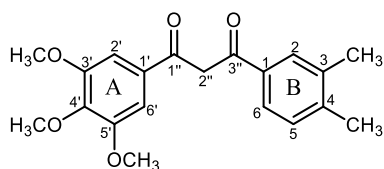
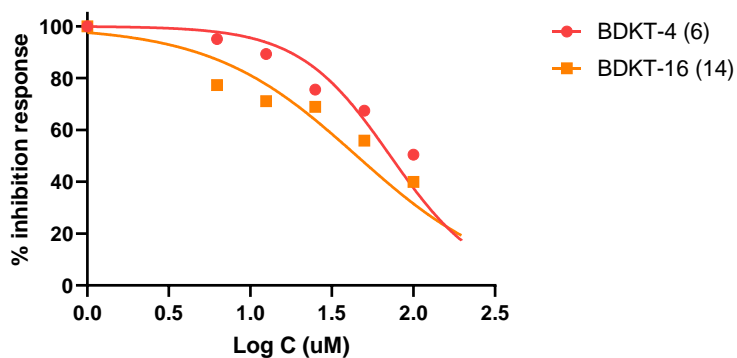


BTU-5

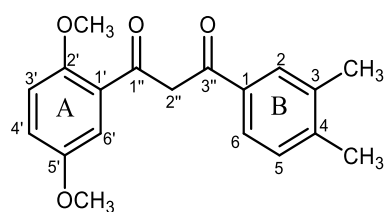
$IC_{50} = 6.83 \mu M$

Figure 76: Inhibitory effect of the most active compounds tested on A549 cells

It was expected that the presence of the methyl group in the structure contributes to better solubility in cell media than the non-substituted diketone, dibenzoylmethanes. This is due to the presence of many polar groups present in most of the synthesised compounds and is likely anticipated to contribute to its solubility in the media. A modification was attempted on both ring A and B of the β -diketone scaffold to see if the number of methoxy groups in ring A with different halogen groups on B will slightly enhance the activity of the compound. Introducing a methyl group to ring B at the 3 and 4 positions in compound **6** decreased the activity on cells (**Figure 77**), thus showing an IC_{50} value of $72.1 \mu M$. Changing the positions of methoxy groups on ring A bearing 2 methoxy groups at position 3', 5' positions and a methyl group on ring B at position 3 and 4 in **14** increased the activity slightly, giving an IC_{50} value of $44.94 \mu M$.



6 ($IC_{50} = 72.10 \mu M$)



14 ($IC_{50} = 44.94 \mu M$)

Figure 77: Trend in activity of compound by modification of ring substituents

31 bearing an iodo group (**Figure 78**) showed an activity better than **32** and **33** substituted with chlorine and bromine, respectively, which could be due to the difference in the electron densities of the corresponding atoms. No significant increase in activity was observed by introducing an additional methoxy group at 5', as in **34**, **35**, **36**. However, their IC₅₀ is maintained within 20-30 μM range. Increasing the number electronegative substituents in the molecules by adding chlorine and fluorine in **26** did not lead to significant activity. Furthermore, to explore role of the ring substituents and observe whether the 1,3-diketone bridge replacement will contribute to change in the cytotoxicity on the A549 cell lines, a series of benzoyl thioureas were synthesised for the purpose of comparison. Most of the substituents in the ring bear the same atoms as in the β-diketone series listed earlier (**Table 7**).

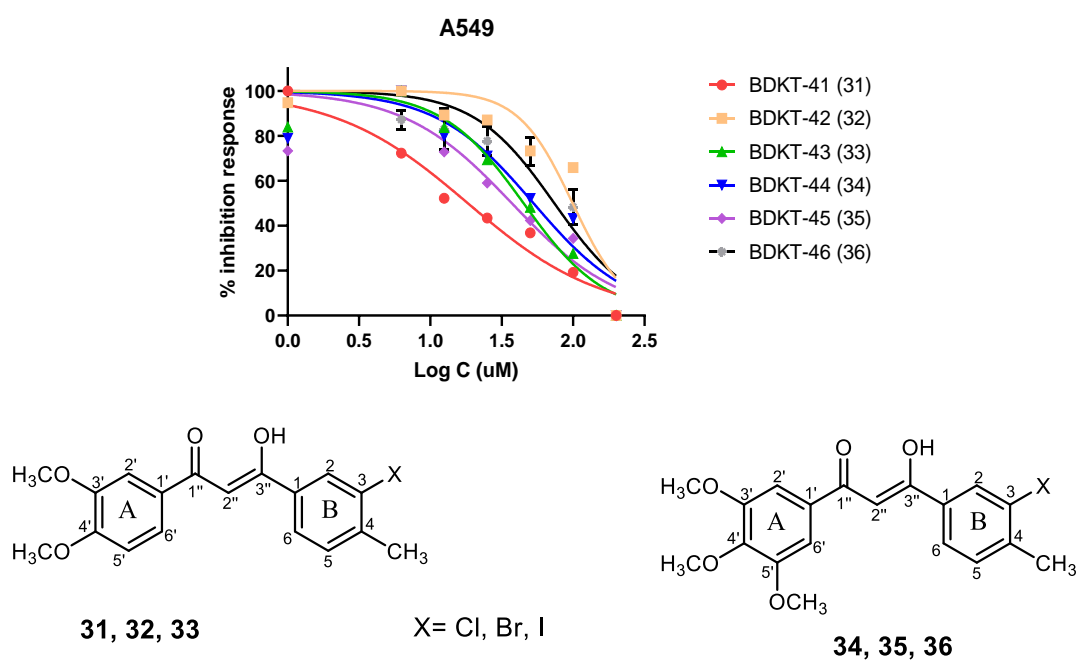


Figure 78: Sensitivity of 31, 32 and 33 bearing halogen groups on A549 cells

From table (**Table 7**) and table (**Table 8**) of the IC₅₀ results, a simple comparison of activity between the compounds with similar substituents from each series have been selected. The IC₅₀ gave smaller values signifying increase in activity of the benzoyl thiourea (**40-59**) tested on A549 cells than the compounds **4-37**. For instance, from **60** and **61** among the benzoylthiourea series have shown a slight improvement in activity than **4** bearing the same substituent (**Figure 79**).

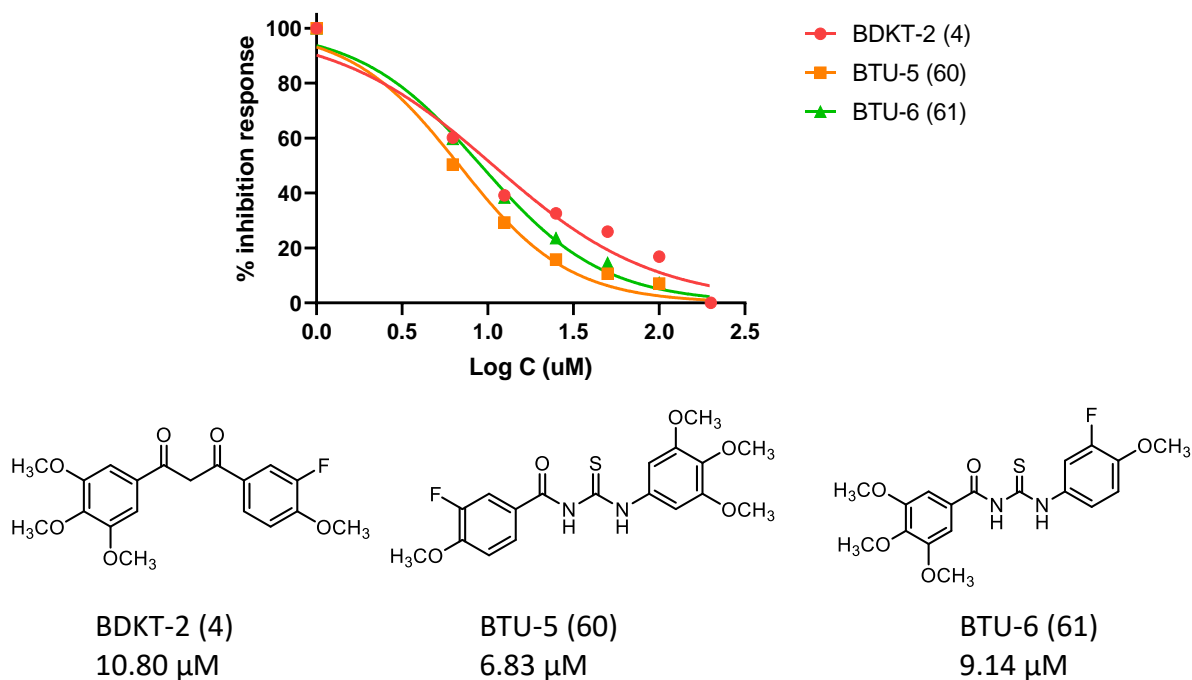
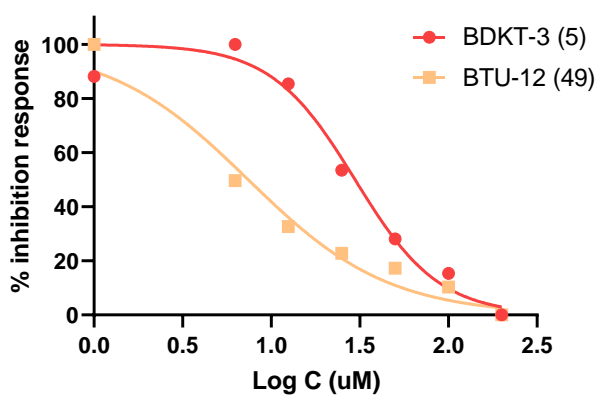
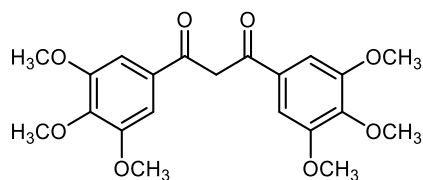


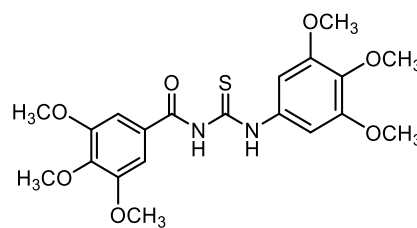
Figure 79: Slight improvement in the activity of β -diketone and benzoyl thiourea series bearing the same substituents in their rings tested on A549 cells

β -diketones bearing a bromo substitution at ortho and para positions in compounds **9** and **11** increased the activity further above $50 \mu\text{M}$ (Figure 64). Its corresponding analogue, **55** among the BTU series showed a good activity with IC_{50} value of $9.65 \mu\text{M}$. Whereas activity of **5** according to literature (Lakkakula *et al.*, 2019) that corresponded with data below displayed low activity ($35.69 \mu\text{M}$) than **49** ($7.41 \mu\text{M}$), suggesting that introducing a benzoylthiourea bridge contributed to improved antiproliferative activity of A549 cells than its corresponding 1,3-diketone bridge (Figure 80).





BDKT-3 (5)
35.69 μM



BTU-12 (49)
7.41 μM

Figure 80: Analogue BTU-12 (49) bearing methoxy substituents have better activity on A549 ($\text{IC}_{50} = 7.41 \mu\text{M}$) than BDKT-3 (5) ($\text{IC}_{50} = 35.69 \mu\text{M}$) with the same substituent.

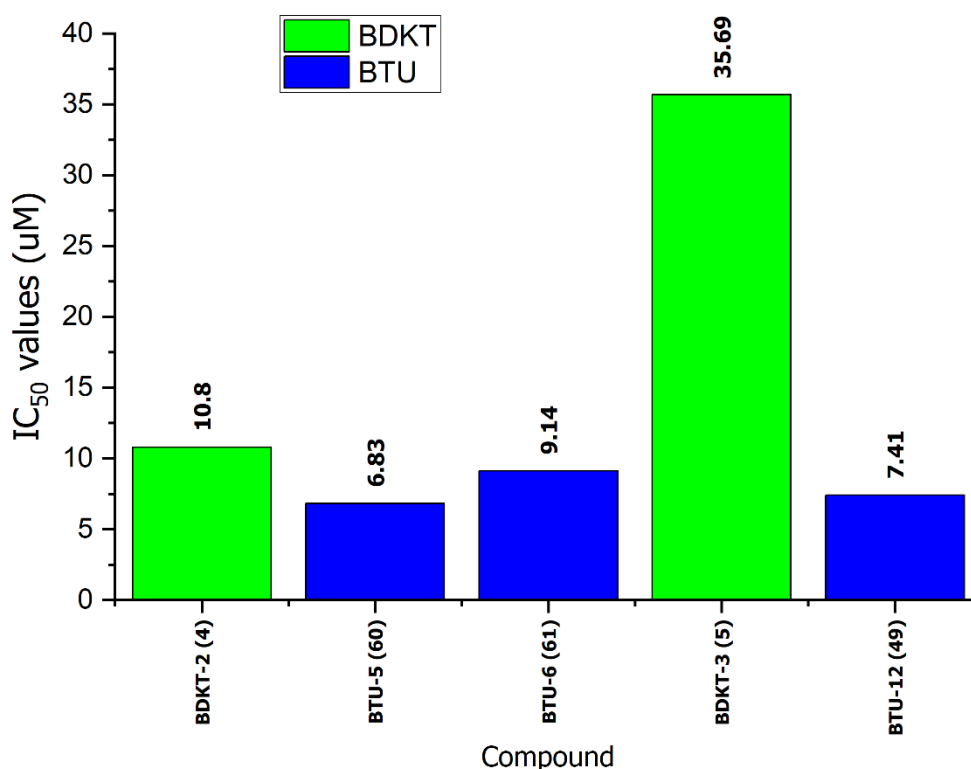
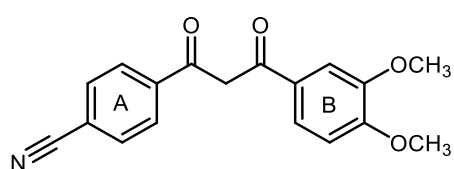
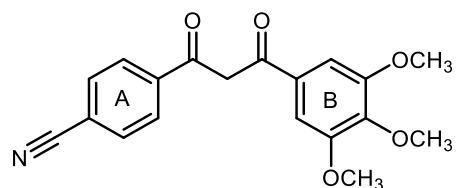


Figure 81: Comparison between structure activity of BTU and BDKT series bearing the same ring substituents

Continued attempt to investigate the activity of β -diketone across all cell lines, a nitrile group was chosen as a substituent on ring A of the β -diketone. The anticipation was that electron withdrawing effect of the nitrile would increase the activity further than the halogenated groups. Two analogues bearing a nitrile group on A ring with different number of methoxy groups on ring B was prepared (**Figure 82**).



15



13

Figure 82: Activity of β -diketones bearing nitrile group

Unexpectedly, A549 cells treated with **15** did not show any activity (**Figure 64**). However, one of the suspected reasons could be due to lack of solubility in the cell media, because precipitates that resembles compound was observed during the third round of the cell treatment. Although an IC_{50} greater than $50\ \mu\text{M}$ was recorded when the drug was tested on HeLa cells. As a result, there is no absolute certainty about its activity on the remaining cell lines tested. **13** was not treated on cells due to time factor considerations and because of the observed outcome related with lack of solubility of **15** in cell media and further experiment and analysis would be required to ascertain this hypothesis.

Sensitivity of HeLa, HepG2 and U2OS treated with BDKT and BTU series

HeLa and HepG2 treated with BDKT have shown higher IC_{50} values. However, **9** has the least IC_{50} of $17.76\ \mu\text{M}$ and $18.26\ \mu\text{M}$ for HepG2 and HeLa respectively (**Figure 83**). It is obvious from the results that these compounds are not significantly sensitive on both cell lines. Furthermore, **14**, **31**, **15**, **26**, **32** and **36** are not active on HepG2, whereas **25** and **29** are not active on HeLa giving higher IC_{50} values (**Figure 65** and **Figure 66**).

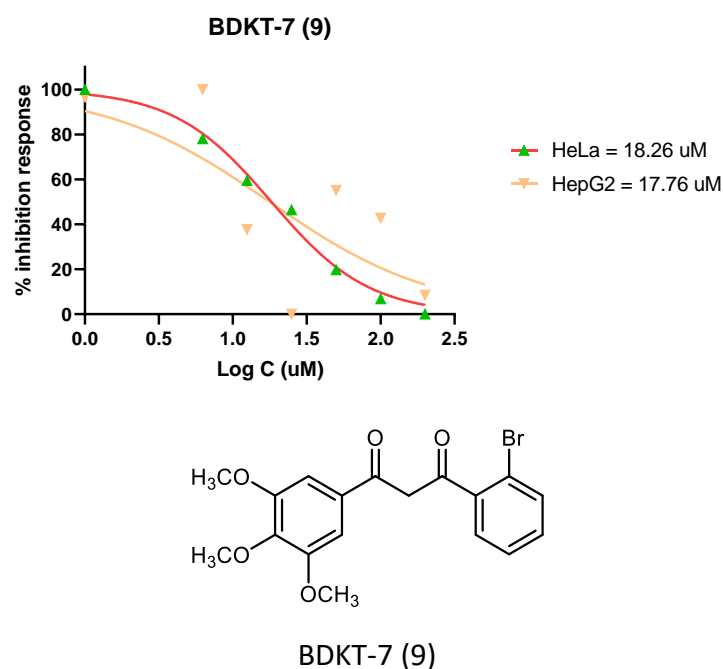
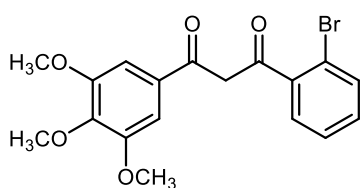
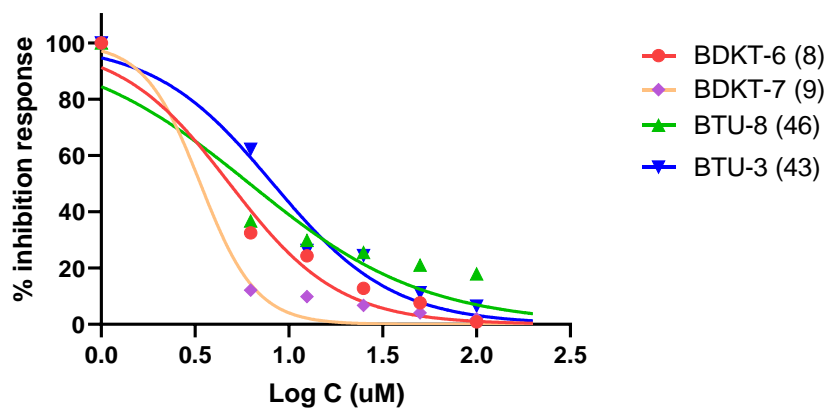


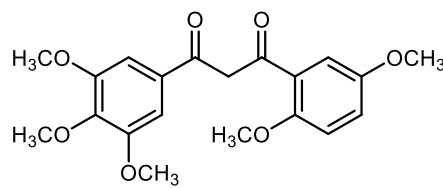
Figure 83: HeLa and HepG2 treated with BDKT-7 (9) showing the least value among the BDKT series

The sensitivity of BTU series is by far better than the BDKT series after treatment on HeLa cells. **60** and **52** are more active, giving an IC₅₀ of 3.17 μM and 3.64 μM. Except **51** (IC₅₀ = 73.98 μM), the remaining compounds in the BTU series have a significant IC₅₀ values ranging from 3 to 26 μM (**Figure 70**). Excluding **41** and **43**, HepG2 cells treated with most of the BTU analogues did not show a significant trend (**Figure 71**).

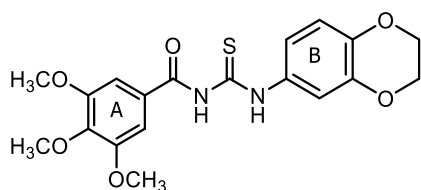
From the comparison between the activity of osteosarcoma cells (U2OS) treated with BDKT and BTU, **9** and **8** appeared to have lowest IC₅₀ values 3.38 μM and 4.83 μM respectively. Whereas compounds **46** and **43** of the BTU series showed an IC₅₀ of 6.17 μM and 8.22 μM (**Figure 84**).



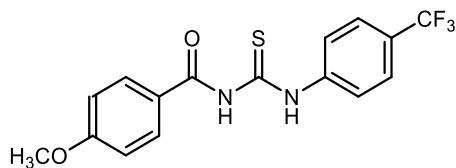
BDKT-7 (9)
3.38 μ M



BDKT-6 (8)
4.83 μ M



BTU-8 (46)
6.17 μ M



BTU-3 (43)
8.22 μ M

Figure 84: Chart showing the lowest IC₅₀ values of U2OS cells treated with 9, 8, 46 and 43

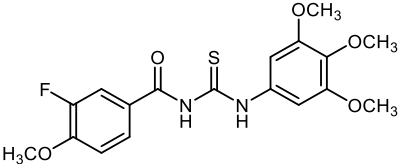
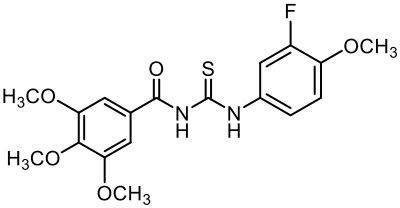
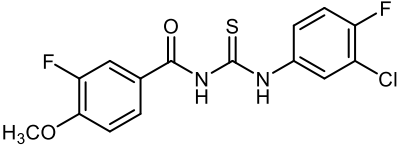
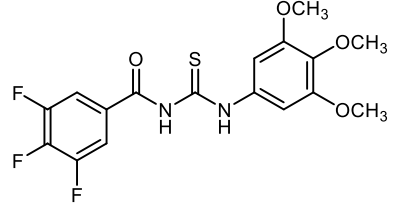
As in the case of A549 cells treated with 46, the bulk of dioxane ring attached to ring B expected to have contributed to the activity of the compound U2OS cells (Figure 84). Except for 46, 43 and 54 that have shown some activity <10 μ M among the BTU, the remaining compounds in the series treated on U2OS fall within IC₅₀ values ranging from 10 μ M to 53 μ M (Figure 72).

3.2.2 Assessment of some substituted β -diketones and benzoyl thiourea on leukaemia cells

As mentioned previously, one of the goals of this thesis is to investigate the effect of compounds bearing electron withdrawing groups such as 15 and 16 on some leukaemia cell lines. Both analogues of the diketones and benzoyl thioureas were chosen and treated on chronic myeloid leukaemia (K562) and acute lymphoblastic leukaemia (CCRF-CEM and MOLT-4) cell lines. Similar procedure as mentioned in section 2.2.3 was carried out for the assay except that the plates were incubated for 72 hours (3 days) after treating them with the compounds. The results of the assay have been recorded in (Table 9).

Table 9: Cytotoxicity some selected β -diketone and benzoyl thiourea analogues tested against multiple leukaemia cell lines

Compound	Structures	IC ₅₀ (μ M)		
		CCRF-CEM	K562	MOLT-4
DBM Dibenzolymethane		17.81	59.43	41.57
4		29.72	107.89	69.01
13		33.84	37.52	113.47
15		34.53	31.29	89.26
16		17.45	129.86	72.53
24		69.74	36.04	111.02
29		36.97	73.73	72.13
40		73.51	n.d.	107.84

60		84.53	n.d.	128.10
61		63.37	28.49	74.57
48		125.13	40.29	26.13
53		57.80	70.90	101.42

*Results recorded represent mean of three experiments

*ND denotes IC₅₀s that have not been determined.

The data obtained (Table 9) for the results of the cytotoxicity showed high IC₅₀ values with most of them above 20 μM across the three leukaemia cell lines: CCRF-CEM, K562 and MOLT-4. Nevertheless, during the cells treatment, it was hypothesised that the parent β-diketone (DBM) be included for testing. This was considered to see if a significant difference in activity could be noticed in the substituted compounds than the parent diketone. Unexpectedly, the results of the showed that the parent β-diketone is more cytotoxic than the prepared compounds. **DBM** and **16** showed a relative IC₅₀ value of about 17 μM on CCRF-CEM, an activity of 2 – 6 times fold across the selected compounds chosen for the test (Figure 85). **DBM** was not expected to show activity whereas the substituted series were expected to be active.

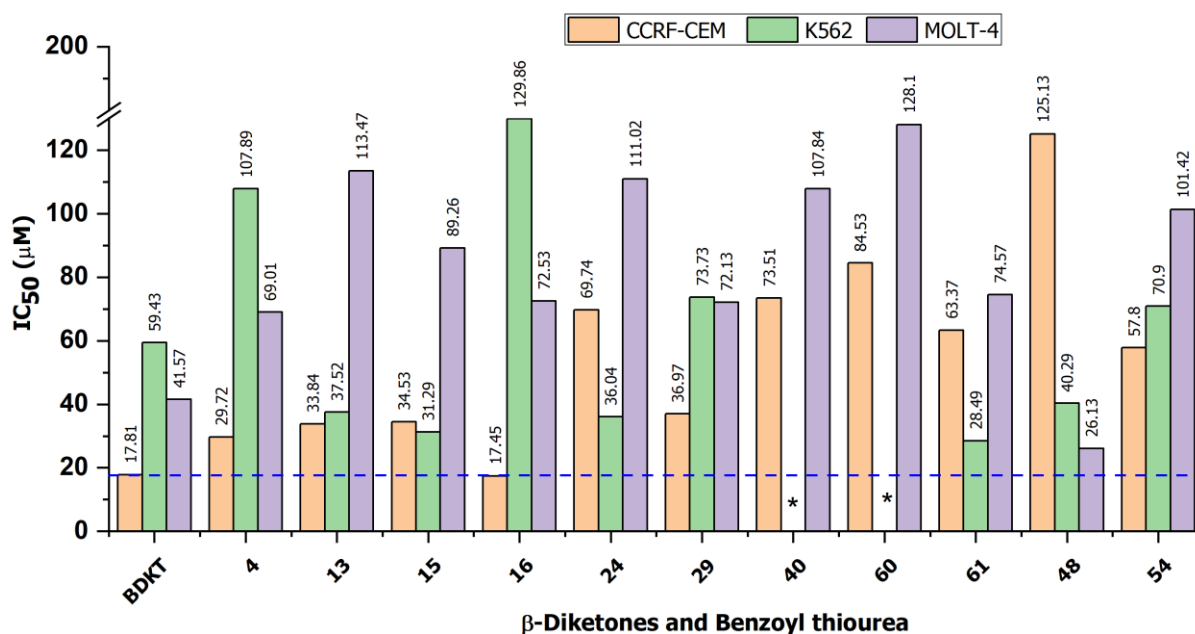


Figure 85: IC₅₀ of β-diketones and benzoyl thiourea treated with acute lymphoblastic leukaemia (CCRF-CEM and MOLT-4) and chronic myeloid leukaemia (K562) cell lines.

Asterisks (*) indicate compounds with no activity.

Likewise, most of the compounds tested on MOLT-4 cells have shown sensitivities closer to the same compounds tested on CCFR-CEM (**Figure 85**). Although, there is a slight decrease in activity as compared to CCFR-CEM, except that **48** showed cytotoxicity of about 4-times fold than the remaining compounds. **13**, **15**, **44** and **48** showed a significant decrease in proliferation of K562 than the remaining compounds. It is expected that the nitrile group in **13** and **15** is contributing to the activity of the compound on the K562 cells. Despite the presence of electronegative groups on **40** and **61**, no activity was detected for K562 cells.

CHAPTER FOUR

Molecular docking of β -diketone in the colchicine binding site

Chapter four

4.0 Molecular docking of β -diketone in the colchicine binding site

4.1 Protein preparation:

The three-dimensional structure of tubulin (PDB ID: 1 SA0) was downloaded from in a PDB format from the protein data bank. The structures were prepared for docking using UCSF Chimera Version 1.14 (build 42094) and Protein preparation wizard of Maestro Schrödinger suite (Version 12.5). Assignment of bond orders and additions of hydrogen atoms to the heavy atoms was carried out; water molecules were also deleted from the atoms, unwanted metal ions, ligands repeated domains were also removed from the structure. And finally, the structure was pre-processed, minimised, and optimised using default force field parameters available on the software known as Optimised Potentials for Liquid Simulations force field (OPLS_2005)

4.1.1 Generation of Grid in the receptor site:

The receptor grid was generated based on colchicine area in the tubulin receptor site using the Glide tool. The Van der Waals radius was set to a scaling factor of 1.0 and partial charge cut off with 0.25 C. When the ligand in the receptor site (Colchicine in this case) is clicked, the grid box appears, and the dimensions was set to 16 Å x 15 Å x 10 Å to accommodate the receptor area of the ligand. The remaining parameters are left at their default values and OPLS_2005 was chosen to generate receptor grid file.

4.2 Ligand preparation:

The 3D conformation of ligands was drawn using a ChemDraw software and the file was saved in .mol file format. The ligand structures (β -diketones) were prepared using the LigPrep tool accompanied with the Maestro Schrödinger suite. Empirical pKa (Epik 2.2) was used to determine the bioavailability profile and within a pH 7.0 +/- 2.0. The minimization parameter was again carried out using OPLS_2005 force field with maximum capacity to generate up to 32 stereoisomers depending on number of chiral centres in ligands included for optimization. Ligand output files was saved in a Maestro file format for compatibility.

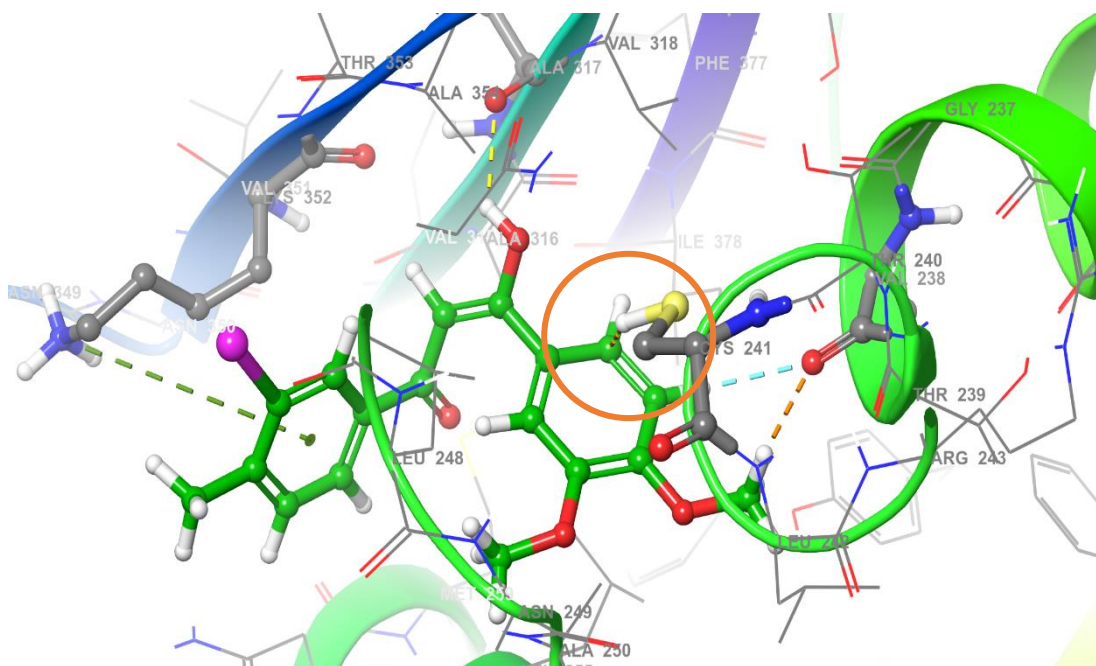
4.3 Glide Extra precision (XP) ligand docking:

Glide extra precision (XP) ligand docking was selected for the docking parameters. The parameter allows the determination of binding affinity with a higher accuracy (Friesner *et al.*, 2006). Prior to submission for docking analysis, the Van der Waals scaling factor and partial charge cut off was set to 0.80 and 0.15 C, respectively.

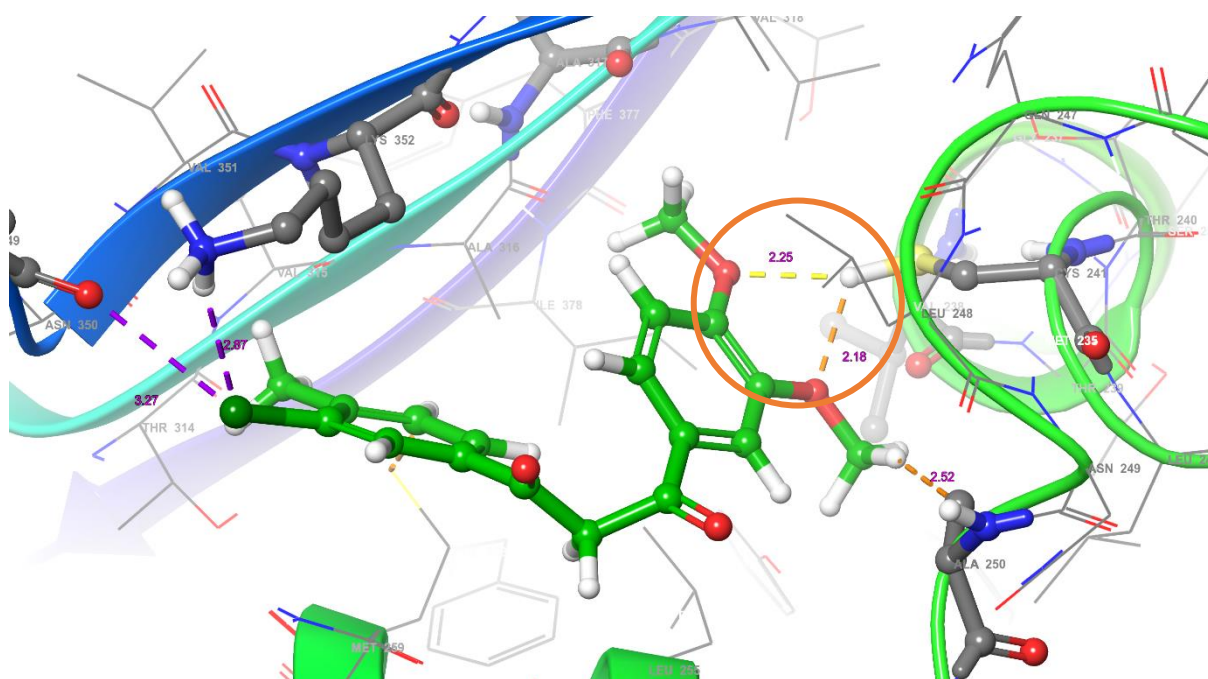
4.3.1 Discussion of docking result

To investigate the mode of action of β -diketones and identify the amino acid residue that bind with the drug, a molecular docking analysis was performed using Glide program. The colchicine binding site in tubulin was chosen for the docking because it is the common site of interaction for most anti-microtubule drugs (Figure 87).

(a) BDKT-41 (31)



(b) BDKT-42 (**32**)



(c) BDKT-44 (**34**)

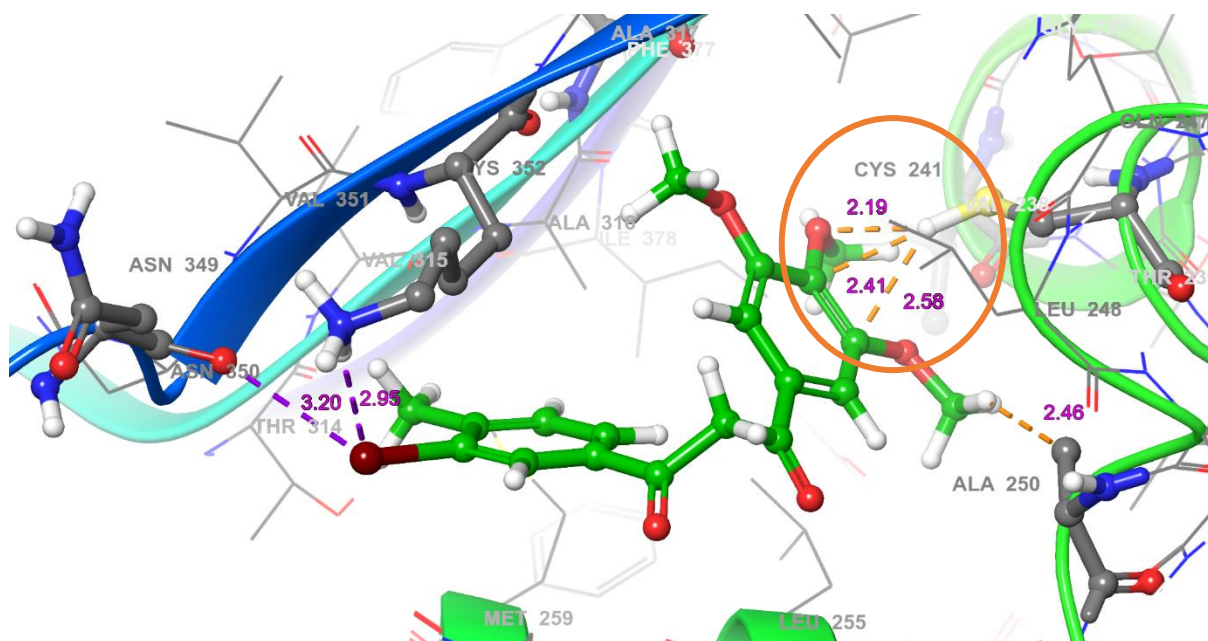


Figure 86: 3D view of BDKT-41 (**31**), BDKT-42 (**32**) and BDKT-44(**34**) docking in the binding site of tubulin (PDB ID: 1SA0). Interactions shown with coloured broken lines. The orange circles points to the essential amino acid residue cys241 that binds with the ligand molecules. This interaction is present in many active antimicrotubular agents reported from literature.

Table 10: Different types of interactions exhibited by BDKT-41 (31) and BDKT-42 (32)

Residue	Distance (Å)	Type of interaction
BDKT-41 (31):		
- Cys241	2.57	Aromatic hydrogen bonding
- Lys352	5.97	π -cation
- Ala317	2.13	Hydrogen bonding
- Val238	2.52	Aromatic hydrogen bonding
- Val235	2.35	Hydrogen bonding
BDKT-42 (32):		
- Cys241	2.25	Hydrogen bonding
- Cys241	2.18	Hydrogen bonding
- Lys352	2.87	Halogen (Cl)
- Asn349	3.27	Halogen (Cl)
- Ala250	2.52	Alkyl
BDKT-44 (34)		
- Cys241	2.19	Hydrogen bonding
- Cys241	2.41	Aromatic hydrogen bonding
- Cys241	2.58	Aromatic hydrogen bonding
- Ala250	2.46	Alkyl (hydrophobic interaction)
- Lys352	2.95	Halogen (Br)
- Asn349	3.20	Halogen (Br)

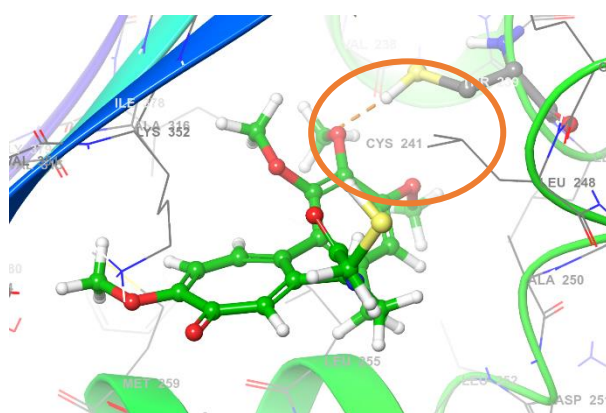


Figure 87: Refined tubulin crystal structure (PDB:1sa0) showing colchicine binding site on chain B. The encircled region is an interaction with Cys241, an essential interaction in most anti-microtubular drugs.

As mentioned before, the crystal structure of tubulin protein, 1SA0 was obtained from the Brookhaven Protein Data Bank (<http://www.rcsb.org/pdb>). All the BDKT series were docked into the binding site of the tubulin crystal structure. The first three active molecules on A204 cell line were analysed and their mode of interaction was presented in Table **10** and Figure **87**.

The snapshots of the docking presented in Figure **87** shows the three molecules have interactions with the amino acid residue in the colchicine binding site. As shown from the three figures for BDKT-41 (**31**), BDKT-42 (**32**) and BDKT-44 (**34**), the molecules adopted a similar conformation to that of colchicine. The trimethoxy moieties in the molecules formed hydrogen bonding Ala317 and Cys241 (within relatively shorter bond distances). Val238 formed a hydrophobic interaction with the aromatic hydrogens of the ligand. The aromatic ring BDKT-41 (**31**) goes further to form a π -cation interaction with Lys352 (Figure **87a**) which is also expected contribute to its activity. BDKT-42 (**32**) formed a hydrophobic interaction with Ala250 and two halogen interactions with Asn349 and Lys352. Likewise, with the bromine present on BDKT-44 (**32**), it forms two interactions with the residues Lys352 and Asn349. This suggests that the mode of interaction of molecules bearing halogen groups are essential for activity the colchicine binding site of tubulin. Although, colchicine competitive binding assay will be necessary for future studies to ascertain the activity of these compounds.

CHAPTER FIVE

Conclusion and future perspective

Chapter Five

Conclusions and future prospect

Cancer, as defined by the World Health Organization (WHO): is the abnormal and uncontrolled growth and spread of cells. The most considered method for treating cancer during the middle of the 20th century was surgery and radiotherapy (Agostinis *et al.*, 2011). Towards the middle of 20th century, chemotherapy emerged as the most suitable alternative for treatment of cancer. As a result, research in cancer chemotherapy has become important in the past decades. Ever since, many compounds with anticancer activity have been identified and their mode of action has also been explored. For instance, naturally occurring compounds such as colchicine and combretastatins have been known to inhibit cancer replication through binding to tubulin, which disrupts the function of microtubules (Ducki *et al.*, 2009; Ducki *et al.*, 1998). Several modifications and identification of new compounds that target tubulin have become the interest of many researchers. Curcumin, a naturally occurring β -diketone with wide range of anticancer activities has also been shown to interact with microtubules. A study has shown that derivatives of these compounds bearing a β -diketone group bind to tubulin at 32 Å away from the colchicine binding site (Soumyananda, 2011).

This thesis deals with synthesis and characterization of some novel 1,3- β -diketones as anticancer agents. The synthesised compounds have been substituted with different groups to improve their physical and chemical properties which should result in improved bioactivity. Attempts have also been made to introduce substitution of different groups, some which are present in the aromatic rings of combretastatin CA-4, (e.g: the 3,4,5-trimethoxy groups). The thesis also explored the synthesis of some benzoyl thiourea (BTU) analogues bearing oxygen and sulphur atoms in their bridge. In order to compare their activities, some of the BTU series bear the same ring substituents with β -diketones. Unfortunately, synthesis of β -diketones that contain exact substituents of CA-4 on the aromatic rings was not successful and is considered for future research.

Chapter three discussed the cytotoxicity of synthesized β -diketones. The compounds have been tested on eight different cell lines: A549, U2OS, HepG2, A204, HeLa and human myeloid leukaemia cells: K-562, MOLT-4 and CCRF-CEM. Results of the tests showed that the prepared compounds are more active on A204 cell lines, with IC₅₀ values ranging from 3.61 μ M to 23.82 μ M. β -Diketones **31** and **32** and **34** and **30** have shown the best activity with IC_{50s} 3.61 μ M,

3.63 μM and 3.78 μM and 3.87 respectively. β -Diketones **4**, **25**, **31** have shown moderate IC_{50} values lesser than 20 μM , which is relative to IC_{50} values reported from literature for curcumins (Wu et al., 2015). However, comparison between the activity of β -diketones and benzoyl thiourea bearing the same substituents show that benzoyl thioureas have better activity than β -diketones (Table **7** and Table **8**). β -Diketones substituted with a nitrile group (**15**) showed poor solubility and their IC_{50} was not determined in some cell lines. **9** showed moderate activity in HeLa cells and HepG2, with IC_{50} values 18.26 μM and 17.76 μM respectively (Figure **83**). U2OS treated with **9**, **8**, **46** and **43** showed significant IC_{50} s 3.38 μM , 4.83 μM , 6.17 μM and 8.22 μM respectively (Figure **84**).

A general and significant trend observed from the outcome of the results in this research is the sensitivity of most of the compounds on A204 (Rhabdomyosarcoma cell lines) compared to other cell lines tested. Table **7** and Table **8** shown that both the series of compounds (BDKT and BTU) are sensitive on A204 and have lower IC_{50} values. Previous literature has already revealed that clinically administered treatment for rhabdomyosarcoma patients is the combination of the three clinically approved drugs: vincristine, dactinomycin and cyclophosphamide. Although the main challenge with this combination are the resultant side-effects associated with patients, such as neurotoxicity, hair loss and cause of death in some patients. Ever since, need for less toxic drugs have become a necessity.

β -diketones and related compounds are known for their anticancer property and because of their wide importance, most of their analogues have been used in spices (e.g. curcumin) and for herbal medication (Fukai and Nomura, 1994). Because of the sensitivity of the compounds tested on A204 cells, further investigation would be needed to understand the genetic and phenotypic differences that led to their sensitivity than the other cell lines. Because dibenzoylmethane (DBM) analogue of β -diketone affected the expression of cell cycle regulatory genes in colon cancer cells (COLO 205) and (HT-29) (Jin-Liern Hong, 2007), real time PCR and Western Blotting techniques would be considered for future research to identify the mechanism of these compounds on A204 cells, and the proteins involved in the process.

Molecular docking analysis was presented in chapter four. Molecular docking is an *in-silico* structure-based technique that is more often used in drug discovery. It enables the understanding of how chemical compounds interact with their biological targets, more especially proteins. It also gives a detailed information about the different types of bonding

interactions between ligand and its biological target, including the atoms contributing to the interaction (Singh, 2020). All the synthesized molecules were docked into the colchicine binding site in tubulin. As summarized in (Table 10), the binding site of the three active compounds that are sensitive on A204 cell lines were chosen for analysis. The analysis shows that β -diketones interact Cys241 residue. It is an essential amino acid residue that colchicine (Figure 87) and related antimicrotubular drugs form different interactions with (Hu *et al.*, 2019; Shuai *et al.*, 2020). 31 is found to be more active due to the presence of π -cation interaction from the aromatic ring with Lys352 (Figure 86 a). The general trend derived from docking results shows that activity 31, 32 and 34 is due to the presence of halogen groups that interact with most of the residues in the tubulin binding site (Table 10).

Future research is also required to better understand the molecular mechanisms of β -diketone analogues. As mentioned previously, analogues of these compounds such as curcumin, inhibit cancer cells through different pathways by inducing G2/M cell cycle arrest (Hu *et al.*, 2017) and modulation of wnt/ β -catenin pathways (Reyhaneh *et al.*, 2018). Understanding these pathways would be an important for modifying β -diketone scaffolds that can lead to molecules capable of treating cancers. Cell cycle analysis and tubulin polymerization assay will be considered an essential work for future research. This will enable to ascertain if these compounds have a microtubule inhibition property.

Antimalarial activity of β -diketones will also be considered for future research. A more recent review on medicinal properties of β -diketones (Gonzalo and Alcántara, 2021) have shown that some of these compounds have shown antimalarial activity against chloroquine-resistant *Plasmodium-falciparum* (Dalal *et al.*, 2020). The report has explored β -diketones that have similarities with scaffolds as the ones recorded in this thesis.

References

References

- Abdel Ghani, S. B., Weaver, L., Zidan, Z. H., Ali, H. M., Keevil, C. W. and Brown, R. C. D. (2008) 'Microwave-assisted synthesis and antimicrobial activities of flavonoid derivatives', *Bioorganic & Medicinal Chemistry Letters*, 18(2), pp. 518-522.
- Abraham, J. and Staffurth, J. (2020) 'Hormonal therapy for cancer', *Medicine*, 48(2), pp. 103-107.
- Adams, J. (2004) 'The proteasome: a suitable antineoplastic target', *Nature Reviews Cancer*, 4(5), pp. 349-360.
- Aggarwal, R., Birkbeck, A. A., Giles, R. G. F., Green, I. R., Gruchlik, Y. and Oosthuizen, F. J. (2003) 'Regioselectivity in the Syntheses of Enantiopure 2-Benzopyrans through Intramolecular Cyclization of Tethered Lactaldehydes. Conformations of the Products', *Australian Journal of Chemistry*, 56(5), pp. 489-498.
- Agostinis, P., Berg, K., Cengel, K. A., Foster, T. H., Girotti, A. W., Gollnick, S. O., Hahn, S. M., Hamblin, M. R., Juzeniene, A., Kessel, D., Korbelik, M., Moan, J., Mroz, P., Nowis, D., Piette, J., Wilson, B. C. and Golab, J. (2011) 'Photodynamic therapy of cancer: an update', *CA: a cancer journal for clinicians*, 61(4), pp. 250-281.
- Alexander, V. K. i. (2003) 'Recent Advances in the Synthesis of 1,3-Diketones', *Current Organic Chemistry*, 7(16), pp. 1691-1711.
- Almelah, E., Smith, D. P. T., McGown, A., Aziz, A., Potgieter, H. J. and Ragazzon, P. (2016) 'Dibenzoyl-methane Derivatives as a Potential and Exciting New Therapy for the Treatment of Childhood Bone Cancer', *Anticancer Research*, 36(11), pp. 6043.
- Amano, R., Shiokawa, Y., Sato, N. and Suzuki, Y. (1993) 'Chemical vapor deposition using lanthanide β -diketone chelates with difluorodichloromethane', *Journal of Radioanalytical and Nuclear Chemistry*, 172(1), pp. 81-86.
- Ameen, D. and Snape, T. J. (2015) 'Mechanism and Application of Baker–Venkataraman O \rightarrow C Acyl Migration Reactions', *Synthesis*, 47(02), pp. 141-158.
- Anderson, L. C., Nilsson, K. and Gahmberg, C. G. (1979) 'K62- A human erythroleukemic cell line', *Int. J. Cancer*, 23, pp. 5.
- Angel, M. M. and Consuelo, B. (2009) 'The Rational Design of Anticancer Platinum Complexes: The Importance of the Structure-Activity Relationship', *Current Medicinal Chemistry*, 16(18), pp. 2235-2260.
- Arruebo, M., Vilaboa, N., Sáez-Gutierrez, B., Lambea, J., Tres, A., Valladares, M. and González-Fernández, A. (2011) 'Assessment of the evolution of cancer treatment therapies', *Cancers*, 3(3), pp. 3279-3330.
- Avendano, C. and Menendez, J. C. (2015) *Medicinal Chemistry of Anticancer*. 2nd edn.: Elsevier.
- Avendaño, C. and Menéndez, J. C. (2015a) 'Chapter 2 - Antimetabolites That Interfere with Nucleic Acid Biosynthesis', in Avendaño, C. and Menéndez, J.C. (eds.) *Medicinal Chemistry of Anticancer Drugs (Second Edition)*. Boston: Elsevier, pp. 23-79.

- Avendaño, C. and Menéndez, J. C. (2015b) 'Chapter 5 - DNA Alkylating Agents', in Avendaño, C. and Menéndez, J.C. (eds.) *Medicinal Chemistry of Anticancer Drugs (Second Edition)*. Boston: Elsevier, pp. 197-241.
- Bahuguna, A., Khan, I., Bajpai, V. K. and Kang, S. C. (2017) 'MTT assay to evaluate the cytotoxic potential of a drug', *Bangladesh J Pharmacol*, 12, pp. 5.
- Bajaj, S., Kumar, M. S., Peters, G. and Mayur, Y. (2020) 'Targeting telomerase for its advent in cancer therapeutics', *Medicinal Research Reviews*, n/a(n/a), pp. 1-49.
- Bansal, M., Kaur, K., Tomar, J. and Kaur, L. (2017) 'Synthesis of Flavones', *Biomedical Journal of Scientific and Technological Research*, 1(6).
- Barbier, P., Zejneli, O., Martinho, M., Lasorsa, A., Belle, V., Smet-Nocca, C., Tsvetkov, P. O., Devred, F. and Landrieu, I. (2019) 'Role of Tau as a Microtubule-Associated Protein: Structural and Functional Aspects', *Frontiers in Aging Neuroscience*, 11(204).
- Baudrin, L. G., Deleuze, J.-F. and How-Kit, A. (2018) 'Molecular and Computational Methods for the Detection of Microsatellite Instability in Cancer', *Frontiers in Oncology*, 8(621).
- Bava, S. V., Puliappadamba, V. T., Ayswaria Deepti, A. N., Karunagaran, D. and Anto, R. J. (2005) 'Sensitization of Taxol-induced Apoptosis by Curcumin Involves down-regulation of Nuclear Factor- B and the Serine/Threonine Kinase Akt and Is Independent of Tubulin Polymerization', *Journal of Biological Chemistry*, 280(8), pp. 6301–6308.
- Bielenberg, D. R. and Zetter, B. R. (2015) 'The Contribution of Angiogenesis to the Process of Metastasis', *Cancer journal (Sudbury, Mass.)*, 21(4), pp. 267-273.
- Blackburn, E. H. (2005) 'Telomerase and Cancer', *Molecular Cancer Research*, 3(9), pp. 477.
- Bonelli, P., Tuccillo, F. M., Borrelli, A., Schiattarella, A. and Buonaguro, F. M. (2014) 'CDK/CCN and CDKI Alterations for Cancer Prognosis and Therapeutic Predictivity', *BioMed Research International*, 2014, pp. 361020.
- Bonneau, S. and Vever-Bizet, C. (2008) 'Tetrapyrrole photosensitisers, determinants of subcellular localisation and mechanisms of photodynamic processes in therapeutic approaches', *Expert Opinion on Therapeutic Patents*, 18(9), pp. 1011-1025.
- Brown, T. A. (2016) *Gene Cloning and DNA Analysis: An Introduction*. 7 edn.: Wiley-Blackwell, p. 286-288.
- Browning, R. J., Reardon, P. J. T., Parhizkar, M., Pedley, R. B., Edirisinghe, M., Knowles, J. C. and Stride, E. (2017) 'Drug Delivery Strategies for Platinum-Based Chemotherapy', *Acs Nano*, 11(9), pp. 8560-8578.
- Burger, A. M., Dai, F., Schultes, C. M., Reszka, A. P., Moore, M. J., Double, J. A. and Neidle, S. (2005) 'The G-Quadruplex-Interactive Molecule BRACO-19 Inhibits Tumor Growth, Consistent with Telomere Targeting and Interference with Telomerase Function', *Cancer Research*, 65(4), pp. 1489-1496.
- Burney, I. (2011) 'Cancer Chemotherapy and Biotherapy: Principles and Practice', *Sultan Qaboos University Medical Journal*, 11(3), pp. 424-425.

- Busse, D., Yakes, F. M., Lenferink, A. E. G. and Arteaga, C. L. (2001) 'Tyrosine kinase inhibitors: Rationale, mechanisms of action, and implications for drug resistance', *Seminars in Oncology*, 28, pp. 47-55.
- Castano, A. P., Mroz, P. and Hamblin, M. R. (2006) 'Photodynamic therapy and anti-tumour immunity', *Nature reviews. Cancer*, 6(7), pp. 535-545.
- Chabner, B. and Longo, D. L. (2019) *Cancer chemotherapy, immunotherapy and biotherapy : principles and practice*. 6th edn. Philadelphia: Wolters Kluwer, p. 1004.
- Chagas, C. M. and Alisaraie, L. (2019) 'Metabolites of Vinca Alkaloid Vinblastine: Tubulin Binding and Activation of Nausea-Associated Receptors', *ACS Omega*, 4(6), pp. 9784-9799.
- Chakraborti, S., Das, L., Kapoor, N., Das, A., Dwivedi, V., Poddar, A., Chakraborti, G., Janik, M., Basu, G., Panda, D., Chakrabarti, P., Surolia, A. and Bhattacharyya, B. (2011) 'Curcumin Recognizes a Unique Binding Site of Tubulin', *Journal of Medicinal Chemistry*, 54(18), pp. 6183-6196.
- Chen, C.-C., Kao, C.-P., Chiu, M.-M. and Wang, S.-H. (2017) 'The anti-cancer effects and mechanisms of Scutellaria barbata D. Don on CL1-5 lung cancer cells', *Oncotarget*, 8(65), pp. 109340-109357.
- Chen, J., Brown, D. P., Wang, Y.-J. and Chen, Z.-S. (2013) 'New phenstatin–fatty acid conjugates: Synthesis and evaluation', *Bioorganic & Medicinal Chemistry Letters*, 23(18), pp. 5119-5122.
- Chen, X., Wang, S. M., Kumar, G. B., Bare, G. A. L., Leng, J., Bukhari, S. N. A. and Qin, H. L. (2018a) 'Recent Developments on Phenstatins as Potent Antimitotic Agents', *Curr Med Chem*, 25(20), pp. 2329-2352.
- Chen, Y. M., Jia, Y. P., Song, W. G. and Zhang, L. (2018b) 'Therapeutic Potential of Nitrogen Mustard Based Hybrid Molecules', *Frontiers in Pharmacology*, 9, pp. 12.
- Cheng, A. L., Hsu, C. H., Lin, J. K., Hsu, M. M., Ho, Y. F., Shen, T. S., Ko, J. Y., Lin, J. T., Lin, B. R., Ming-Shiang, W., Yu, H. S., Jee, S. H., Chen, G. S., Chen, T. M., Chen, C. A., Lai, M. K., Pu, Y. S., Pan, M. H., Wang, Y. J., Tsai, C. C. and Hsieh, C. Y. (2001) 'Phase I clinical trial of curcumin, a chemopreventive agent, in patients with high-risk or pre-malignant lesions', *Anticancer Res*, 21(4b), pp. 2895-900.
- Choshi, T., Horimoto, S., Wang, C. Y., Nagase, H., Ichikawa, M., Sugino, E. and Hibino, S. (1992) 'Synthesis of dibenzoylmethane derivatives and inhibition of mutagenicity in Salmonella typhimurium', *Chem Pharm Bull (Tokyo)*, 40(4), pp. 1047-9.
- Choudhuri, T., Pal, S., Agwarwal, M. L., Das, T. and Sa, G. (2002) 'Curcumin induces apoptosis in human breast cancer cells through p53-dependent Bax induction', *FEBS Letters*, 512(1-3), pp. 334-340.
- Cleaves, H. J. (2011) 'Watson–Crick Pairing', in Gargaud, M., Amils, R., Quintanilla, J.C., Cleaves, H.J., Irvine, W.M., Pinti, D.L. and Viso, M. (eds.) *Encyclopedia of Astrobiology*. Berlin, Heidelberg: Springer Berlin Heidelberg, pp. 1775-1776.
- Cooper, G. (2019) *The Cell: A Molecular Approach*. 8 edn. New York: Sinauer Associates.

Cooper, J., Public Health England (2012) *A549 (ECACC catalogue no. 86012804)*. United Kingdom.

Coulup, S. K. and Georg, G. I. (2019) 'Revisiting microtubule targeting agents: α -Tubulin and the pironetin binding site as unexplored targets for cancer therapeutics', *Bioorganic & Medicinal Chemistry Letters*, 29(15), pp. 1865-1873.

Crawford, L. J., Walker, B. and Irvine, A. E. (2011) 'Proteasome inhibitors in cancer therapy', *Journal of cell communication and signaling*, 5(2), pp. 101-110.

Dalal, A., Kumar, P., Khanna, R., Kumar, D., Paliwal, D. and Kamboj, R. C. (2020) 'Hydroxyenone Derivatives: *In vitro* Anti-malarial and Docking Studies against *P. falciparum*', *Infectious Disorders - Drug Targets*, 20, pp. 7.

Daniel, T., Siyaram, P. and James, M. (2017) 'Review of Cytotoxic CA4 Analogues that Do Not Target Microtubules: Implications for CA4 Development', *Mini-Reviews in Medicinal Chemistry*, 17(16), pp. 1507-1514.

Dawson, L. E., D'Agostino, L., Hakim, A. A., Lackman, R. D., Brown, S. A., Sensenig, R. B., Antonello, Z. A. and Kuzin, I. I. (2020) 'Induction of Myogenic Differentiation Improves Chemosensitivity of Chemoresistant Cells in Soft-Tissue Sarcoma Cell Lines', *Sarcoma*, 2020, pp. 8647981.

De Luca, A., Parker, L. J., Ang, W. H., Rodolfo, C., Gabbarini, V., Hancock, N. C., Palone, F., Mazzetti, A. P., Menin, L., Morton, C. J., Parker, M. W., Lo Bello, M. and Dyson, P. J. (2019) 'A structure-based mechanism of cisplatin resistance mediated by glutathione transferase P1-1', *Proceedings of the National Academy of Sciences*, 116(28), pp. 13943.

Disis, M. L. (2014) 'Mechanism of Action of Immunotherapy', *Seminars in Oncology*, 41, pp. S3-S13.

Dolbier, W. R. (2009) *Guide to Fluorine NMR for Organic Chemists*. New Jersey: John Wiley & Sons.

Dong, H. and Markovic, S. (2018) *The Basics of Cancer Immunotherapy*. 1 edn. Switzerland: Springer International Publishing.

Dorai, T. and Aggarwal, B. B. (2004) 'Role of chemopreventive agents in cancer therapy', *Cancer Letters*, 215(2), pp. 129-140.

du Plessis, W., C., Vosloo, T., G. and Swarts, J., C. (1998) ' β -Diketones containing a ferrocenyl group: synthesis, structural aspects, pKa1 values, group electronegativities and complexation with rhodium(I)', *Journal of the Chemical Society, Dalton Transactions*, (15), pp. 2507-2514.

Dubrovina, N. V., Tararov, V. I., Monsees, A., Kadyrov, R., Fischer, C. and Börner, A. (2003) 'Economic preparation of 1,3-diphenyl-1,3-bis(diphenylphosphino)propane: a versatile chiral diphosphine ligand for enantioselective hydrogenations', *Tetrahedron: Asymmetry*, 14(18), pp. 2739-2745.

Ducki, S. (2007) 'The development of chalcones as promising anticancer agents', *IDrugs : the investigational drugs journal*, 10 1, pp. 42-6.

Ducki, S., Forrest, R., Hadfield, J. A., Kendall, A., Lawrence, N. J., McGown, A. T. and Rennison, D. (1998) 'Potent antimitotic and cell growth inhibitory properties of substituted chalcones', *Bioorganic & Medicinal Chemistry Letters*, 8(9), pp. 1051-1056.

Ducki, S., Hadfield, J. A., Hepworth, L. A., Lawrence, N. J., Liu, C.-Y. and McGown, A. T. (1997) 'Synthesis and cell growth inhibitory properties of substituted (E)-1-phenylbut-1-en-3-ones', *Bioorganic & Medicinal Chemistry Letters*, 7(24), pp. 3091-3094.

Ducki, S., Hadfield, J. A., Lawrence, N. J., Liu, C.-Y., McGown, A. T. and Zhang, X. (1996) 'Isolation of E-1-(4'-Hydroxyphenyl)-but-1-en-2-one from *Scutellaria barbata*', *Planta Medica*, 62(2), pp. 185-186.

Ducki, S., Rennison, D., Woo, M., Kendall, A., Chabert, J. F. D., McGown, A. T. and Lawrence, N. J. (2009) 'Combretastatin-like chalcones as inhibitors of microtubule polymerization. Part 1: Synthesis and biological evaluation of antivasular activity', *Bioorganic & Medicinal Chemistry*, 17(22), pp. 7698-7710.

ECACC, England, P.H. (2017) *Hep-G2 142BR (ECACC 90011806)*. England.

Edwards, M. L., Stemerick, D. M. and Sunkara, P. S. (1990) 'Chalcones: a new class of antimitotic agents', *Journal of Medicinal Chemistry*, 33(7), pp. 1948-1954.

Esfahani, K., Roudaia, L., Buhlaiga, N., Del Rincon, S. V., Papneja, N. and Miller, W. H., Jr. (2020) 'A review of cancer immunotherapy: from the past, to the present, to the future', *Current oncology (Toronto, Ont.)*, 27(Suppl 2), pp. S87-S97.

Fagundes, G. E., Damiani, A. P., Borges, G. D., Teixeira, K. O., Jesus, M. M., Daumann, F., Ramlov, F., Carvalho, T., Leffa, D. D., Rohr, P. and Moraes De Andrade, V. (2017) 'Effect of green juice and their bioactive compounds on genotoxicity induced by alkylating agents in mice', *J Toxicol Environ Health A*, 80(13-15), pp. 756-766.

Fidler, I. J. (2003) 'The pathogenesis of cancer metastasis: the 'seed and soil' hypothesis revisited', *Nature Reviews Cancer*, 3(6), pp. 453-458.

Findeisen, P., Mühlhausen, S., Dempewolf, S., Hertzog, J., Zietlow, A., Carlomagno, T. and Kollmar, M. (2014) 'Six Subgroups and Extensive Recent Duplications Characterize the Evolution of the Eukaryotic Tubulin Protein Family', *Genome Biology and Evolution*, 6(9), pp. 2274-2288.

Folkman, J. (1971) 'Tumor Angiogenesis: Therapeutic Implications', *New England Journal of Medicine*, 285(21), pp. 1182-1186.

Forli, S. (2014) 'Epothilones: From discovery to clinical trials', *Current topics in medicinal chemistry*, 14(20), pp. 2312-2321.

Friesner, R. A., Murphy, R. B., Repasky, M. P., Frye, L. L., Greenwood, J. R., Halgren, T. A., Sanschagrín, P. C. and Mainz, D. T. (2006) 'Extra Precision Glide: Docking and Scoring Incorporating a Model of Hydrophobic Enclosure for Protein-Ligand Complexes', *Journal of Medicinal Chemistry*, 49(21), pp. 6177-6196.

Fusi, C., Materazzi, S., Benemei, S., Coppi, E., Trevisan, G., Marone, I. M., Minocci, D., De Logu, F., Tuccinardi, T., Di Tommaso, M. R., Susini, T., Moneti, G., Pieraccini, G., Geppetti, P. and

Nassini, R. (2014) 'Steroidal and non-steroidal third-generation aromatase inhibitors induce pain-like symptoms via TRPA1', *Nature Communications*, 5(1), pp. 5736.

Gao, W. and Ho, M. (2011) 'The role of glypican-3 in regulating Wnt in hepatocellular carcinomas', *Cancer reports*, 1(1), pp. 14-19.

Ghinet, A., Tourteau, A., Rigo, B., Stocker, V., Leman, M., Farce, A., Dubois, J. and Gautret, P. (2013) 'Synthesis and biological evaluation of fluoro analogues of antimetabolic phenstatin', *Bioorganic & Medicinal Chemistry*, 21(11), pp. 2932-2940.

Giard, D. J., Aaronson, S. A., Todaro, G. J., Arnstein, P., Kersey, J. H., Dosik, H. and Parks, W. P. (1973) 'In Vitro Cultivation of Human Tumors: Establishment of Cell Lines Derived From a Series of Solid Tumors²', *JNCI: Journal of the National Cancer Institute*, 51(5), pp. 1417-1423.

Gilkes, D. M. and Semenza, G. L. (2013) 'Role of hypoxia-inducible factors in breast cancer metastasis', *Future oncology (London, England)*, 9(11), pp. 1623-1636.

Giovanni, A. and David, P. F. (2005) 'Protease Inhibitors in the Clinic', *Medicinal Chemistry*, 1(1), pp. 71-104.

Golonko, A., Lewandowska, H., Świśłocka, R., Jasińska, U. T., Priebe, W. and Lewandowski, W. (2019) 'Curcumin as tyrosine kinase inhibitor in cancer treatment', *European Journal of Medicinal Chemistry*, 181, pp. 111512.

Gomes, A., Neuwirth, O., Freitas, M., Couto, D., Ribeiro, D., Figueiredo, A. G. P. R., Silva, A. M. S., Seixas, R. S. G. R., Pinto, D. C. G. A., Tomé, A. C., Cavaleiro, J. A. S., Fernandes, E. and Lima, J. L. F. C. (2009) 'Synthesis and antioxidant properties of new chromone derivatives', *Bioorganic & Medicinal Chemistry*, 17(20), pp. 7218-7226.

Gomtsyan, A. (2012) 'Heterocycles in drugs and drug discovery', *Chemistry of Heterocyclic Compounds*, 48(1), pp. 7-10.

Gonzalo, G. d. and Alcántara, A. R. (2021) 'Recent Developments in the Synthesis of β -Diketones', *Pharmaceuticals*, 14(10), pp. 26.

Goustin, A. S., Leof, E. B., Shipley, G. D. and Moses, H. L. (1986) 'Growth Factors and Cancer', *Cancer Research*, 46(3), pp. 1015-1029.

Gupta, A. K., Tulsyan, S., Bharadwaj, M. and Mehrotra, R. (2019) 'Systematic Review on Cytotoxic and Anticancer Potential of N-Substituted Isatins as Novel Class of Compounds Useful in Multidrug-Resistant Cancer Therapy: In Silico and In Vitro Analysis', *Topics in Current Chemistry*, 377(3), pp. 15.

Gupta, K. K., Bharne, S. S., Rathinasamy, K., Naik, N. R. and Panda, D. (2006) 'Dietary antioxidant curcumin inhibits microtubule assembly through tubulin binding', *The FEBS Journal*, 273(23), pp. 5320-5332.

Gupta, M. L., Jr., Bode, C. J., Georg, G. I. and Himes, R. H. (2003) 'Understanding tubulin-Taxol interactions: mutations that impart Taxol binding to yeast tubulin', *Proc Natl Acad Sci U S A*, 100(11), pp. 6394-7.

Gupta, S. and Bhattacharyya, B. (2003) 'Antimicrotubular drugs binding to vinca domain of tubulin', *Molecular and Cellular Biochemistry*, 253(1), pp. 41-47.

- Gupta, S. C., Patchva, S. and Aggarwal, B. B. (2013) 'Therapeutic roles of curcumin: lessons learned from clinical trials', *The AAPS Journal*, 15(1), pp. 195-218.
- Hadfield, J. A., Gaukroger, K., Hirst, N., Weston, A. P., Lawrence, N. J. and McGown, A. T. (2005) 'Synthesis and evaluation of double bond substituted combretastatins', *European Journal of Medicinal Chemistry*, 40(6), pp. 529-541.
- Harley, C. B., Futcher, A. B. and Greider, C. W. (1990) 'Telomeres shorten during ageing of human fibroblasts', *Nature*, 345(6274), pp. 458-460.
- Harrold, M. W. and Zavod, R. M. (2018) *Basic Concepts in Medicinal Chemistry*. Canada: ASHP.
- He, J., Zhang, M., Tang, L., Liu, J., Zhong, J., Wang, W., Xu, J.-P., Wang, H.-T., Li, X.-F. and Zhou, Z.-Z. (2020) 'Synthesis, Biological Evaluation, and Molecular Docking of Arylpyridines as Antiproliferative Agent Targeting Tubulin', *ACS Medicinal Chemistry Letters*, 11(8), pp. 1611-1619.
- Hejmo, T., Student, S., Poterała-Hejmo, A., Leśniak, A. and Bułdak, R. (2020) 'Anti-androgen hormonal therapy for cancer and other diseases', *European Journal of Pharmacology*, 866, pp. 172783.
- Hoffmeyer, K., Raggioli, A., Rudloff, S., Anton, R., Hierholzer, A., Del Valle, I., Hein, K., Vogt, R. and Kemler, R. (2012) 'Wnt/ β -Catenin Signaling Regulates Telomerase in Stem Cells and Cancer Cells', *Science*, 336(6088), pp. 1549-1554.
- Hong, R.-L., Spohn, W. H. and Hung, M.-C. (1999) 'Curcumin inhibits tyrosine kinase activity of p185neu and also depletes p185neu', *Clinical Cancer Research*, 5(7), pp. 1884.
- Hsu, H. L., Liao, P. L., Cheng, Y. W., Huang, S. H., Wu, C. H., Li, C. H. and Kang, J. J. (2019) 'Chloramphenicol Induces Autophagy and Inhibits the Hypoxia Inducible Factor-1 Alpha Pathway in Non-Small Cell Lung Cancer Cells', *International Journal of Molecular Sciences*, 20(1), pp. 16.
- Hu, A., Huang, J.-J., Zhang, J.-F., Dai, W.-J., Li, R.-L., Lu, Z.-Y., Duan, J.-L., Li, J.-P., Chen, X.-P., Fan, J.-P., Xu, W.-H. and Zheng, H.-L. (2017) 'Curcumin induces G2/M cell cycle arrest and apoptosis of head and neck squamous cell carcinoma in vitro and in vivo through ATM/Chk2/p53-dependent pathway', *Oncotarget*, 8(31), pp. 50747-50760.
- Hu, S., Sun, W., Wang, Y. and Yan, H. (2019) 'Design, synthesis and anticancer activities of halogenated Phenstatin analogs as microtubule destabilizing agent', *Medicinal Chemistry Research*, 28(4), pp. 465-472.
- Hu, X., Li, L., Zhang, Q., Wang, Q., Feng, Z., Xu, Y., Xia, Y. and Yu, L. (2020) 'Design, synthesis and biological evaluation of a novel tubulin inhibitor SKLB0565 targeting the colchicine binding site', *Bioorganic Chemistry*, 97, pp. 103695.
- Huang, L., Liu, M., Man, S., Ma, D., Feng, D., Sun, Z., Guan, Q., Zuo, D., Wu, Y., Zhang, W. and Bao, K. (2020) 'Design, synthesis and bio-evaluation of novel 2-aryl-4-(3,4,5-trimethoxybenzoyl)-5-substituted-1,2,3-triazoles as the tubulin polymerization inhibitors', *European Journal of Medicinal Chemistry*, 186, pp. 111846.

Huang, Y.-D., Dong, X.-L., Zhang, L.-L., Chai, W. and Chang, J.-Y. (2013) 'Structure–property correlation of benzoyl thiourea derivatives as organogelators', *Journal of Molecular Structure*, 1031, pp. 43-48.

Huang, Y. and Li, L. (2013) 'DNA crosslinking damage and cancer - a tale of friend and foe', *Translational cancer research*, 2(3), pp. 144-154.

Huzil, J. T., Ludueña, R. F. and Tuszynski, J. (2006) 'Comparative modelling of human β tubulin isotypes and implications for drug binding', *Nanotechnology*, 17(4), pp. S90-S100.

Ibrahim, T. S., Hawwas, M. M., Malebari, A. M., Taher, E. S., Omar, A. M., Neamatallah, T., Abdel-Samii, Z. K., Safo, M. K. and Elshaier, Y. A. M. M. (2021) 'Discovery of novel quinoline-based analogues of combretastatin A-4 as tubulin polymerisation inhibitors with apoptosis inducing activity and potent anticancer effect', *Journal of Enzyme Inhibition and Medicinal Chemistry*, 36(1), pp. 802-818.

Ionov, Y., Peinado, M. A., Malkhosyan, S., Shibata, D. and Perucho, M. (1993) 'Ubiquitous somatic mutations in simple repeated sequences reveal a new mechanism for colonic carcinogenesis', *Nature*, 363(6429), pp. 558-561.

Janke, C. and Chloë Bulinski, J. (2011) 'Post-translational regulation of the microtubule cytoskeleton: mechanisms and functions', *Nature Reviews Molecular Cell Biology*, 12(12), pp. 773-786.

Jin, H., Zhang, W., Wang, D., Chu, Z., Shen, Z., Zou, D., Fan, X. and Zhou, Q. (2011) 'Dendron-Jacketed Electrophosphorescent Copolymers: Improved Efficiency and Tunable Emission Color by Partial Energy Transfer', *Macromolecules*, 44(24), pp. 9556-9564.

Josh, G., R, G.-S., CW, W., BJ, S. and JH, K. (1988) 'Immunophenotypic and cytogenetic analysis of Molt-3 and Molt-4: human T-lymphoid cell lines with rearrangement of chromosomes', *Blood*, 72(5), pp. 5.

Kalinin, A. V., da Silva, A. J. M., Lopes, C. C., Lopes, R. S. C. and Snieckus, V. (1998) 'Directed ortho metalation - cross coupling links. Carbamoyl rendition of the baker-venkataraman rearrangement. Regiospecific route to substituted 4-hydroxycoumarins', *Tetrahedron Letters*, 39(28), pp. 4995-4998.

Kamal, A., Shaik, A. B., Polepalli, S., Kumar, G. B., Reddy, V. S., Mahesh, R., Garimella, S. and Jain, N. (2015) 'Synthesis of arylpyrazole linked benzimidazole conjugates as potential microtubule disruptors', *Bioorganic & Medicinal Chemistry*, 23(5), pp. 1082-1095.

Karmakar, S., Poetsch, I., Kowol, C. R., Heffeter, P. and Gibson, D. (2019) 'Synthesis and Cytotoxicity of Water-Soluble Dual- and Triple-Action Satraplatin Derivatives: Replacement of Equatorial Chlorides of Satraplatin by Acetates', *Inorganic Chemistry*, 58(24), pp. 16676-16688.

Kaur, R., Kaur, G., Gill, R. K., Soni, R. and Bariwal, J. (2014) 'Recent developments in tubulin polymerization inhibitors: An overview', *European Journal of Medicinal Chemistry*, 87, pp. 89-124.

Kesikli, S. A. and Guler, N. (2015) 'Chemotherapeutic Agents in Cancer Treatment and Tryptophan Metabolism', in Engin, A. and Engin, A.B. (eds.) *Tryptophan Metabolism:*

Implications for Biological Processes, Health and Disease. Cham: Springer International Publishing, pp. 291-333.

Khan, M. F., Verma, G., Akhtar, W., Shaquiquzzaman, M., Akhter, M., Rizvi, M. A. and Alam, M. M. (2019) 'Pharmacopore modeling, 3D-QSAR, docking study and ADME prediction of acyl 1,3,4-thiadiazole amides and sulfonamides as antitubulin agents', *Arabian Journal of Chemistry*, 12, pp. 19.

Kierszenbaum, A. L. and Tres, L. L. (2016) *Histology and Cell Biology*. 4 edn. Philadelphia: Elsevier, p. 114-118.

Kljun, J. and Turel, I. (2017) ' β -Diketones as Scaffolds for Anticancer Drug Design – From Organic Building Blocks to Natural Products and Metallodrug Components', *European Journal of Inorganic Chemistry*, 2017(12), pp. 1655-1666.

Korubo, K. I., Madu, A. J., Okoye, H. C. and Nwogoh, B. (2017) 'Bortezomib Prescription Pattern for the Treatment of Multiple Myeloma by Hematologists in Nigeria', *Journal of Global Oncology*, (4), pp. 1-7.

Kumbhar, B. V., Bhandare, V. V., Panda, D. and Kunwar, A. (2020) 'Delineating the interaction of combretastatin A-4 with $\alpha\beta$ tubulin isotypes present in drug resistant human lung carcinoma using a molecular modeling approach', *Journal of Biomolecular Structure and Dynamics*, 38(2), pp. 426-438.

Labazi, M. and Phillips, A. C. (2003) 'Oncogenes as regulators of apoptosis', *Essays Biochem*, 39, pp. 89-104.

Lai, H.-W., Chien, S.-Y., Kuo, S.-J., Tseng, L.-M., Lin, H.-Y., Chi, C.-W. and Chen, D.-R. (2012) 'The Potential Utility of Curcumin in the Treatment of HER-2-Overexpressed Breast Cancer: An In Vitro and In Vivo Comparison Study with Herceptin', *Evidence-Based Complementary and Alternative Medicine*, 2012, pp. 486568.

Lakkakula, R., Roy, A., Mukkanti, K. and Sridhar, G. (2019) 'Synthesis and Anticancer Activity of 1,2,3-Triazole Fused N-Arylpyrazole Derivatives', *Russian Journal of General Chemistry*, 89(4), pp. 831-835.

Landry, J. J., Pyl, P. T., Rausch, T., Zichner, T., Tekkedil, M. M., Stütz, A. M., Jauch, A., Aiyar, R. S., Pau, G., Delhomme, N., Gagneur, J., Korbelt, J. O., Huber, W. and Steinmetz, L. M. (2013) 'The genomic and transcriptomic landscape of a HeLa cell line', *G3 (Bethesda)*, 3(8), pp. 1213-24.

Lawrence, N., McGown, A. T., Ducki, S. and Hadfield, J. (2000) 'The interaction of chalcones with tubulin', *Anti-cancer Drug Design*, 15(2), pp. 135-141.

Lee, C. S., Bishop, E. S., Zhang, R., Yu, X., Farina, E. M., Yan, S., Zhao, C., Zheng, Z., Shu, Y., Wu, X., Lei, J., Li, Y., Zhang, W., Yang, C., Wu, K., Wu, Y., Ho, S., Athiviraham, A., Lee, M. J., Wolf, J. M., Reid, R. R. and He, T.-C. (2017) 'Adenovirus-Mediated Gene Delivery: Potential Applications for Gene and Cell-Based Therapies in the New Era of Personalized Medicine', *Genes & diseases*, 4(2), pp. 43-63.

Lee, J. I. and Son, H.-S. (2005) 'A Novel Synthesis of Flavones from 2-Methoxybenzoic Acids', *Bulletin of the Korean Chemical Society*, 26(9), pp. 1461-1463.

Lee, S. and Lee, J.-S. (2019) 'Cellular senescence: a promising strategy for cancer therapy', *BMB reports*, 52(1), pp. 35-41.

Legault, J., Gaulin, J.-F., Mounetou, E., Bolduc, S., Lacroix, J., Poyet, P. and C.-Gaudreault, R. (2000) 'Microtubule Disruption Induced in Vivo by Alkylation of β -Tubulin by 1-Aryl-3-(2-Chloroethyl)Ureas, a Novel Class of Soft Alkylating Agents', *Cancer Research*, 60(4), pp. 985-992.

Legnani, L., Toma, L., Caramella, P., Chiacchio, M. A., Giofrè, S., Delso, I., Tejero, T. and Merino, P. (2016) 'Computational Mechanistic Study of Thionation of Carbonyl Compounds with Lawesson's Reagent', *The Journal of Organic Chemistry*, 81(17), pp. 7733-7740.

Li, B. and Qu, G. (2019) 'Inhibition of the hypoxia-induced factor-1 and vascular endothelial growth factor expression through ginsenoside Rg3 in human gastric cancer cells', *Journal of Cancer Research and Therapeutics*, 15(7), pp. 1642-1646.

Li, W., Sun, H., Xu, S., Zhu, Z. and Xu, J. (2017) 'Tubulin inhibitors targeting the colchicine binding site: a perspective of privileged structures', *Future Medicinal Chemistry*, 9(15), pp. 1765-1794.

Liu, C., Takada, K. and Zhu, D. (2020) 'Targeting Wnt/ β -Catenin Pathway for Drug Therapy', *Medicine in Drug Discovery*, 8, pp. 100066.

Liu, D. (2018) *Tumours and Cancers Skin-soft tissue-bone-urogenitals*. CRC Press, Taylor & Francis Group.

Liu, D., Chen, L., Zhao, H., Vaziri, N. D., Ma, S.-C. and Zhao, Y.-Y. (2019) 'Small molecules from natural products targeting the Wnt/ β -catenin pathway as a therapeutic strategy', *Biomedicine & Pharmacotherapy*, 117, pp. 108990.

Logan, J. K., Wickramaratne Senarath Yapa, S., Harinstein, L., Saluja, B., Muñoz, M., Sahajwalla, C., Neuner, R. and Seymour, S. (2020) 'Drug Interaction Between Febuxostat and Thiopurine Antimetabolites: A Review of the FDA Adverse Event Reporting System and Medical Literature', *Pharmacotherapy: The Journal of Human Pharmacology and Drug Therapy*, 40(2), pp. 125-132.

Löwe, J., Li, H., Downing, K. H. and Nogales, E. (2001) 'Refined structure of $\alpha\beta$ -tubulin at 3.5 Å resolution', *Journal of Molecular Biology*, 313(5), pp. 1045-1057.

Lu, X. (2012) '9 - p53: A Target and a Biomarker of Cancer Therapy?', in Liu, X.-Y., Pestka, S. and Shi, Y.-F. (eds.) *Recent Advances in Cancer Research and Therapy*. Oxford: Elsevier, pp. 197-213.

Lu, Y., Chen, J., Xiao, M., Li, W. and Miller, D. D. (2012) 'An overview of tubulin inhibitors that interact with the colchicine binding site', *Pharmaceutical research*, 29(11), pp. 2943-2971.

Ludueno, R. F. and Roach, M. C. (1991) 'Tubulin sulfhydryl groups as probes and targets for antimitotic and antimicrotubule agents', *Pharmacology & Therapeutics*, 49(1), pp. 133-152.

Lv, Z., Chu, Y. and Wang, Y. (2015) 'HIV protease inhibitors: a review of molecular selectivity and toxicity', *HIV/AIDS (Auckland, N.Z.)*, 7, pp. 95-104.

- Manning, G., Plowman, G. D., Hunter, T. and Sudarsanam, S. (2002) 'Evolution of protein kinase signaling from yeast to man', *Trends Biochem Sci*, 27(10), pp. 514-20.
- Marinello, J., Delcuratolo, M. and Capranico, G. (2018) 'Anthracyclines as Topoisomerase II Poisons: From Early Studies to New Perspectives', *International journal of molecular sciences*, 19(11), pp. 3480.
- McKinnell, R. G., Parchment, R. E., Perantoni, A. O., Pierce, G. B. and Damjanov, I. (2006) *The Biological Basis of Cancer*. 2 edn. Cambridge: Cambridge University Press.
- McLoughlin, E. and O'Boyle, N. M. (2020) 'Colchicine-Binding Site Inhibitors from Chemistry to Clinic: A Review', *Pharmaceuticals*, 13(1), pp. 43.
- Mehrgou, A. and Akouchekian, M. (2016) 'The importance of BRCA1 and BRCA2 genes mutations in breast cancer development', *Medical journal of the Islamic Republic of Iran*, 30, pp. 369-369.
- Metibemu, D. S., Akinloye, O. A., Akamo, A. J., Ojo, D. A., Okeowo, O. T. and Omotuyi, I. O. (2019) 'Exploring receptor tyrosine kinases-inhibitors in Cancer treatments', *Egyptian Journal of Medical Human Genetics*, 20(1), pp. 35.
- Milad, A., Zahra, A., Reza, M., Habib, Y., Maria-Corina, S., Hossein, M. O. and Amirhossein, S. (2020) 'Curcumin Therapeutic Modulation of the Wnt Signaling Pathway', *Current Pharmaceutical Biotechnology*, 21(11), pp. 1006-1015.
- Mirzaei, S., Eisvand, F., Hadizadeh, F., Mosaffa, F., Ghasemi, A. and Ghodsi, R. (2020) 'Design, synthesis and biological evaluation of novel 5,6,7-trimethoxy-N-aryl-2-styrylquinolin-4-amines as potential anticancer agents and tubulin polymerization inhibitors', *Bioorganic Chemistry*, 98, pp. 103711.
- Muggia, F. M., Bonetti, A., Hoeschele, J. D., Rozenzweig, M. and Howell, S. B. (2015) 'Platinum Antitumor Complexes: 50 Years Since Barnett Rosenberg's Discovery', *Journal of Clinical Oncology*, 33(35), pp. 4219-4226.
- Müller, C. E. (2009) 'Prodrug Approaches for Enhancing the Bioavailability of Drugs with Low Solubility', *Chemistry & Biodiversity*, 6(11), pp. 2071-2083.
- Nagarathnam, D. and Cushman, M. (1991) 'A practical synthesis of flavones from methyl salicylate', *Tetrahedron*, 47(28), pp. 5071-5076.
- Nainwal, L. M., Alam, M. M., Shaquiquzzaman, M., Marella, A. and Kamal, A. (2019) 'Combretastatin-based compounds with therapeutic characteristics: a patent review', *Expert Opinion on Therapeutic Patents*, 29(9), pp. 703-731.
- Nandurkar, N. S., Bhanushali, M. J., Patil, D. S. and Bhanage, B. M. (2007) 'Synthesis of Sterically Hindered 1,3-Diketones', *Synthetic Communications*, 37(23), pp. 4111-4115.
- Negrini, S., Gorgoulis, V. G. and Halazonetis, T. D. (2010) 'Genomic instability — an evolving hallmark of cancer', *Nature Reviews Molecular Cell Biology*, 11(3), pp. 220-228.
- NIH (2020) *Cancer Classification* SEER Training: National Cancer Institute. Available at: <https://training.seer.cancer.gov/disease/categories/classification.html> (Accessed: 9 July 2020).

- Niu, M.-M., Qin, J.-Y., Tian, C.-P., Yan, X.-F., Dong, F.-G., Cheng, Z.-Q., Fida, G., Yang, M., Chen, H.-Y. and Gu, Y.-Q. (2014) 'Tubulin inhibitors: pharmacophore modeling, virtual screening and molecular docking', *Acta pharmacologica Sinica*, 35(7), pp. 967-979.
- Ondruschka, B., Bonrath, W. and Stuerge, D. (2013) *Properties and Use of Microreactors. Development and design of laboratory and pilot scale reactors for microwave-assisted chemistry* 2 edn. Berlin: Wiley-VCH Verlag GmbH.
- Oronsky, B. T., Reid, T., Knox, S. J. and Scicinski, J. J. (2012) 'The scarlet letter of alkylation: a mini review of selective alkylating agents', *Translational oncology*, 5(4), pp. 226-229.
- Pang, Y., Yan, J., An, B., Huang, L. and Li, X. (2017) 'The synthesis and evaluation of new butadiene derivatives as tubulin polymerization inhibitors', *Bioorganic & Medicinal Chemistry*, 25(12), pp. 3059-3067.
- Papoutsoglou, P. and Moustakas, A. (2020) 'Long non-coding RNAs and TGF-beta signaling in cancer', *Cancer Sci*, pp. 10.
- Pappo, A. S. (1995) 'Rhabdomyosarcoma and other soft tissue sarcomas of childhood', *Current Opinion in Oncology*, 7(4).
- Perkins, N. D. (2012) 'The diverse and complex roles of NF- κ B subunits in cancer', *Nature Reviews Cancer*, 12(2), pp. 121-132.
- Pettit, G. R., Grealish, M. P., Herald, D. L., Boyd, M. R., Hamel, E. and Pettit, R. K. (2000) 'Antineoplastic Agents. 443. Synthesis of the Cancer Cell Growth Inhibitor Hydroxyphenstatin and Its Sodium Diphosphate Prodrug', *Journal of Medicinal Chemistry*, 43(14), pp. 2731-2737.
- Polshettiwar, V. and Kaushik, M. P. (2006) 'Recent advances in thionating reagents for the synthesis of organosulfur compounds', *Journal of Sulfur Chemistry*, 27(4), pp. 353-386.
- Prasad, C. P., Rath, G., Mathur, S., Bhatnagar, D. and Ralhan, R. (2009) 'Potent growth suppressive activity of curcumin in human breast cancer cells: Modulation of Wnt/beta-catenin signaling', *Chem Biol Interact*, 181(2), pp. 263-71.
- Prasad, R., Pal, D. and Mohammad, W. (2020) 'Therapeutic Targets in Telomerase and Telomere Biology of Cancers', *Indian J Clin Biochem*, 35(2), pp. 135-146.
- Pretsch, E., Buhlmann, P. and Badertscher, M. (2009) *Structure Determination of Organic Compounds Tables of Spectral Data*. 4th edn. Berlin: Springer.
- Pucci, C., Martinelli, C. and Ciofani, G. (2019) 'Innovative approaches for cancer treatment: current perspectives and new challenges', *Ecancermedicalscience*, 13, pp. 961-961.
- Qiao, L., Huang, J., Hu, W., Zhang, Y., Guo, J., Cao, W., Miao, K., Qin, B. and Song, J. (2017) 'Synthesis, characterization, and in vitro evaluation and in silico molecular docking of thiourea derivatives incorporating 4-(trifluoromethyl)phenyl moiety', *Journal of Molecular Structure*, 1139, pp. 149-159.
- Qiu, G.-H., Xie, X., Xu, F., Shi, X., Wang, Y. and Deng, L. (2015) 'Distinctive pharmacological differences between liver cancer cell lines HepG2 and Hep3B', *Cytotechnology*, 67(1), pp. 1-12.

- Rai, Y., Pathak, R., Kumari, N., Sah, D. K., Pandey, S., Kalra, N., Soni, R., Dwarakanath, B. S. and Bhatt, A. N. (2018) 'Mitochondrial biogenesis and metabolic hyperactivation limits the application of MTT assay in the estimation of radiation induced growth inhibition', *Scientific Reports*, 8(1), pp. 1531.
- Rakashanda, S. and Amin, S. (2013) 'Proteases as Targets in Anticancer Therapy Using Their Inhibitors', *Journal of Life Sciences*, 5(2), pp. 133-138.
- Rao, H. S. P. and Muthanna, N. (2015) 'Variations in the Blaise Reaction: Conceptually New Synthesis of 3-Amino Enones and 1,3-Diketones', *European Journal of Organic Chemistry*, 2015(7), pp. 1525-1532.
- Rathnakar, B., Kumar, G. S., Mahammad, S. P., Gattu, S., Kalyani, S., Nimma, R. and Satyanarayana, M. (2020) 'Design, synthesis, and evaluation of novel combretastatin A-4 based chalcone derivatives as anticancer agents', *Journal of Heterocyclic Chemistry*, n/a(n/a).
- Rauf, M. K., Talib, A., Badshah, A., Zaib, S., Shoaib, K., Shahid, M., Flörke, U., Imtiaz ud, D. and Iqbal, J. (2013) 'Solution-phase microwave assisted parallel synthesis of N,N'-disubstituted thioureas derived from benzoic acid: Biological evaluation and molecular docking studies', *European Journal of Medicinal Chemistry*, 70, pp. 487-496.
- Ravelli, R. B. G., Gigant, B., Curmi, P. A., Jourdain, I., Lachkar, S., Sobel, A. and Knossow, M. (2004) 'Insight into tubulin regulation from a complex with colchicine and a stathmin-like domain', *Nature*, 428(6979), pp. 198-202.
- Raymond, E., Faivre, S., Chaney, S., Woynarowski, J. and Cvitkovic, E. (2002) 'Cellular and molecular pharmacology of oxaliplatin', *Mol Cancer Ther*, 1(3), pp. 227-35.
- Reich, H. J. (2005) 'Introducing JCE ChemInfo: Organic', *Journal of Chemical Education*, 82(3), pp. 495.
- Reis, J., Gaspar, A., Milhazes, N. and Borges, F. (2017) 'Chromone as a Privileged Scaffold in Drug Discovery: Recent Advances', *Journal of Medicinal Chemistry*, 60(19), pp. 7941-7957.
- Reyhaneh, M.-M., Seyed Mahdi, H., Soodabeh, S., Amir, A. and Majid, K. (2018) 'Curcumin Effects on the Wnt Signaling Pathway in Colorectal Cancer Stem Cells', *Basic & Clinical Cancer Research*, 10(2).
- Rozmer, Z. and Perjési, P. (2016) 'Naturally occurring chalcones and their biological activities', *Phytochemistry Reviews*, 15(1), pp. 87-120.
- Ruden, M. and Puri, N. (2013) 'Novel anticancer therapeutics targeting telomerase', *Cancer Treatment Reviews*, 39(5), pp. 444-456.
- Ryu, M. J., Cho, M., Song, J. Y., Yun, Y. S., Choi, I. W., Kim, D. E., Park, B. S. and Oh, S. (2008) 'Natural derivatives of curcumin attenuate the Wnt/beta-catenin pathway through down-regulation of the transcriptional coactivator p300', *Biochem Biophys Res Commun*, 377(4), pp. 1304-8.
- Sa, G. and Das, T. (2008) 'Anti cancer effects of curcumin: cycle of life and death', *Cell division*, 3, pp. 14-14.

- Saeed, A., Khera, R. A., Abbas, N., Latif, M., Sajid, I. and Florke, U. (2010) 'Synthesis, characterization, crystal structures, and antibacterial activity of some new 1-(3,4,5-trimethoxybenzoyl)-3-aryl thioureas', *Turkish Journal of Chemistry*, 34, pp. 335 – 345.
- Sahu, R. P., Batra, S. and Srivastava, S. K. (2009) 'Activation of ATM/Chk1 by curcumin causes cell cycle arrest and apoptosis in human pancreatic cancer cells', *British Journal of Cancer*, 100(9), pp. 1425-1433.
- Sambaiah, M., Raghavulu, K., Shiva Kumar, K., Yennam, S. and Behera, M. (2017) 'Synthesis of novel fused chromone–pyrimidine hybrids and 2,4,5-trisubstituted pyrimidine derivatives via ANRORC rearrangement', *New Journal of Chemistry*, 41(18), pp. 10020-10026.
- Sánchez-Martínez, C., Gelbert, L. M., Lallena, M. J. and de Dios, A. (2015) 'Cyclin dependent kinase (CDK) inhibitors as anticancer drugs', *Bioorganic & Medicinal Chemistry Letters*, 25(17), pp. 3420-3435.
- Sardaru, M.-C., Craciun, A. M., Al Matarneh, C.-M., Sandu, I. A., Amarandi, R. M., Popovici, L., Ciobanu, C. I., Peptanariu, D., Pinteala, M., Mangalagiu, I. I. and Danac, R. (2020) 'Cytotoxic substituted indolizines as new colchicine site tubulin polymerisation inhibitors', *Journal of Enzyme Inhibition and Medicinal Chemistry*, 35(1), pp. 1581-1595.
- Sarkar, A. (2017) 'Novel platinum compounds and nanoparticles as anticancer agents', *Pharmaceutical Patent Analyst*, 7(1), pp. 33-46.
- Sartape, A. S., Gadde, R. P. and Salunkhe, S. T. (2015) 'Efficient Synthesis of Flavones Derivatives from Aromatic Acids', *International Journal of Chemical and Pharmaceutical Analysis*, 2(2), pp. 84-87.
- Scholl, F. A., Betts, D. R., Niggli, F. K. and Schäfer, B. W. (2000) 'Molecular features of a human rhabdomyosarcoma cell line with spontaneous metastatic progression', *British Journal of Cancer*, 82(6), pp. 1239-1245.
- Schwarzerová, K., Bellinvia, E., Martinek, J., Sikorová, L., Dostál, V., Libusová, L., Bokvaj, P., Fischer, L., Schmit, A. C. and Nick, P. (2019) 'Tubulin is actively exported from the nucleus through the Exportin1/CRM1 pathway', *Scientific Reports*, 9(1), pp. 5725.
- Scrable, H. J., Witte, D. P., Lampkin, B. C. and Cavenee, W. K. (1987) 'Chromosomal localization of the human rhabdomyosarcoma locus by mitotic recombination mapping', *Nature*, 329(6140), pp. 645-7.
- Seddigi, Z. S., Malik, M. S., Saraswati, A. P., Ahmed, S. A., Babalghith, A. O., Lamfon, H. A. and Kamal, A. (2017) 'Recent advances in combretastatin based derivatives and prodrugs as antimitotic agents', *MedChemComm*, 8(8), pp. 1592-1603.
- Shabalin, D. A., Ivanova, E. V., Ushakov, I. A., Schmidt, E. Y. and Trofimov, B. A. (2020) 'Retrosynthetic Analysis of α -Alkenyl- β -Diketones: Regio- and Stereoselective Two-Step Synthesis of Highly Arylated Representatives from Acetylenes, Ketones, and Acyl Chlorides', *The Journal of Organic Chemistry*, 85(13), pp. 8429-8436.
- Shah, P. and Westwell, A. D. (2007) 'The role of fluorine in medicinal chemistry', *Journal of Enzyme Inhibition and Medicinal Chemistry*, 22(5), pp. 527-540.

- Shay, J. W., Zou, Y., Hiyama, E. and Wright, W. E. (2001) 'Telomerase and cancer', *Human Molecular Genetics*, 10(7), pp. 677-685.
- Shehzad, A. and Lee, Y. S. (2013) 'Molecular mechanisms of curcumin action: Signal transduction', *BioFactors*, 39(1), pp. 27-36.
- Shinde, M. P., B.Toche, R., B.Aware, P. and Chvan, S. M. (2020) 'Synthesis and Characterization and of transition metal (II) Complexes of 1-(3, 5-bis(trifluoromethyl) phenyl -4-4-4-trifluorobutane-1,3-dione', *SSRG International Journal of Applied Chemistry*, 7(1), pp. 69-76.
- Shishodia, S. (2013) 'Molecular mechanisms of curcumin action: Gene expression', *BioFactors*, 39(1), pp. 37-55.
- Shokova, E. A., Kim, J. K. and Kovalev, V. V. (2015) '1,3-Diketones. Synthesis and properties', *Russian Journal of Organic Chemistry*, 51(6), pp. 755-830.
- Shuai, W., Li, X., Li, W., Xu, F., Lu, L., Yao, H., Yang, L., Zhu, H., Xu, S., Zhu, Z. and Xu, J. (2020) 'Design, synthesis and anticancer properties of isocombretapyridines as potent colchicine binding site inhibitors', *European Journal of Medicinal Chemistry*, 197, pp. 112308.
- Si, M. and Lang, J. (2018) 'The roles of metallothioneins in carcinogenesis', *Journal of Hematology & Oncology*, 11(1), pp. 107.
- Simon, A., Allais, D. P., Duroux, J. L., Basly, J. P., Durand-Fontanier, S. and Delage, C. (1998) 'Inhibitory effect of curcuminoids on MCF-7 cell proliferation and structure–activity relationships', *Cancer Letters*, 129(1), pp. 111-116.
- Simpkins, F., Garcia-Soto, A. and Slingerland, J. (2013) 'New insights on the role of hormonal therapy in ovarian cancer', *Steroids*, 78(6), pp. 530-537.
- Singh, D. B. (ed.) (2020) *Computer-Aided Drug Design*. Singapore: Springer.
- Sontag, C. A., Staley, J. T. and Erickson, H. P. (2005) 'In vitro assembly and GTP hydrolysis by bacterial tubulins BtubA and BtubB', *The Journal of cell biology*, 169(2), pp. 233-238.
- Steinmetz, M. O. and Prota, A. E. (2018) 'Microtubule-Targeting Agents: Strategies To Hijack the Cytoskeleton', *Trends in Cell Biology*, 28(10), pp. 776-792.
- Stephens, F. O. and Aigner, K. R. (2009) *Basics of Oncology*. Dordrecht Heidelberg, London and New York: Springer.
- Swamer, F. W. and Hauser, C. R. (1950) 'Claisen Acylations and Carbethoxylations of Ketones and Esters by Means of Sodium Hydride', *Journal of the American Chemical Society*, 72(3), pp. 1352-1356.
- Swanson, T. A., Kim, S. I. and Glucksman, M. J. (2013) *BRS Biochemistry, Molecular Biology, and Genetics*. 5 edn. Philadelphia: Lippincott Williams and Wilkins, p. 323-333.
- Swinney, D. C. (2011) 'Chapter 18 - Molecular Mechanism of Action (MMoA) in Drug Discovery', in Macor, J.E. (ed.) *Annual Reports in Medicinal Chemistry*: Academic Press, pp. 301-317.

Tanaka, K. and Hirota, T. (2016) 'Chromosomal instability: A common feature and a therapeutic target of cancer', *Biochimica et Biophysica Acta (BBA) - Reviews on Cancer*, 1866(1), pp. 64-75.

Tassinari, D., Cherubini, C., Tamburini, E., Drudi, F., Papi, M., Fantini, M., Lazzari-Agli, L. and Sartori, S. (2017) 'Antimetabolites in the treatment of advanced pleural mesothelioma: a network meta-analysis of randomized clinical trials', *J Chemother*, 29(6), pp. 365-371.

Torin Huzil, J., Winter, P., Johnson, L., Weis, A. L., Bakos, T., Banerjee, A., Luduena, R. F., Damaraju, S. and Tuszynski, J. A. (2010) 'Computational Design and Biological Testing of Highly Cytotoxic Colchicine Ring A Modifications', *Chemical Biology & Drug Design*, 75(6), pp. 541-550.

Trezza, A., Cicaloni, V., Pettini, F. and Spiga, O. (2020) 'Chapter 2 - Potential roles of protease inhibitors in anticancer therapy', in Gupta, S.P. (ed.) *Cancer-Leading Proteases*: Academic Press, pp. 13-49.

Trialists, E. B. C. (2015) 'Aromatase inhibitors versus tamoxifen in early breast cancer: patient-level meta-analysis of the randomised trials', *The Lancet*, 386(10001), pp. 1341-1352.

Tron, G. C., Pirali, T., Sorba, G., Pagliai, F., Busacca, S. and Genazzani, A. A. (2006) 'Medicinal Chemistry of Combretastatin A4: Present and Future Directions', *Journal of Medicinal Chemistry*, 49(11), pp. 3033-3044.

Tsihlias, J., Kapusta, L. and Slingerland, J. (1999) 'The prognostic significance of altered cyclin-dependent kinase inhibitors in human cancer', *Annu Rev Med*, 50, pp. 401-23.

Vargas-Rondón, N., Villegas, V. E. and Rondón-Lagos, M. (2017) 'The Role of Chromosomal Instability in Cancer and Therapeutic Responses', *Cancers*, 10(1), pp. 4.

Vogelstein, B. and Kinzler, K. W. (2004) 'Cancer genes and the pathways they control', *Nature Medicine*, 10(8), pp. 789-799.

Wagener, C., Stocking, C. and Muller, O. (2017) *Cancer Signaling*. Germany: Wiley, p. 136-138.

Wai, J. S., Egbertson, M. S., Payne, L. S., Fisher, T. E., Embrey, M. W., Tran, L. O., Melamed, J. Y., Langford, H. M., Guare, J. P., Zhuang, L., Grey, V. E., Vacca, J. P., Holloway, M. K., Naylor-Olsen, A. M., Hazuda, D. J., Felock, P. J., Wolfe, A. L., Stillmock, K. A., Schleif, W. A., Gabryelski, L. J. and Young, S. D. (2000) '4-Aryl-2,4-dioxobutanoic Acid Inhibitors of HIV-1 Integrase and Viral Replication in Cells', *Journal of Medicinal Chemistry*, 43(26), pp. 4923-4926.

Waldman, A. D., Fritz, J. M. and Lenardo, M. J. (2020) 'A guide to cancer immunotherapy: from T cell basic science to clinical practice', *Nature Reviews Immunology*.

Wallet, J.-C. and Gaydou, E. M. (1996) 'A Practical Synthesis of Dibenzoylmethanes', *Synthetic Communications*, 26(22), pp. 4097-4103.

Wang, L., Woods, K. W., Li, Q., Barr, K. J., McCroskey, R. W., Hannick, S. M., Gherke, L., Credo, R. B., Hui, Y.-H., Marsh, K., Warner, R., Lee, J. Y., Zielinski-Mozng, N., Frost, D., Rosenberg, S. H. and Sham, H. L. (2002) 'Potent, Orally Active Heterocycle-Based Combretastatin A-4 Analogues: Synthesis, Structure-Activity Relationship, Pharmacokinetics, and In Vivo Antitumor Activity Evaluation', *Journal of Medicinal Chemistry*, 45(8), pp. 1697-1711.

- Wang, M., Qin, H. L., Leng, J., Amedduzafar, Amjad, M. W., Raja, M. A. G., Hussain, M. A. and Bukhari, S. N. A. (2018a) 'Synthesis and biological evaluation of new tetramethylpyrazine-based chalcone derivatives as potential anti-Alzheimer agents', *Chem Biol Drug Des*, 92(5), pp. 1859-1866.
- Wang, Q., Li, G., Liu, Z., Tan, X., Ding, Z., Ma, J., Li, L., Li, D., Han, J. and Wang, B. (2018b) 'Naphthalimide Platinum(IV) Compounds as Antitumor Agents with Dual DNA Damage Mechanism to Overcome Cisplatin Resistance', *European Journal of Inorganic Chemistry*, 2018(40), pp. 4442-4451.
- Wang, Y., Branicky, R., Noë, A. and Hekimi, S. (2018c) 'Superoxide dismutases: Dual roles in controlling ROS damage and regulating ROS signaling', *The Journal of cell biology*, 217(6), pp. 1915-1928.
- Wang, Y., Zhang, H., Gigant, B., Yu, Y., Wu, Y., Chen, X., Lai, Q., Yang, Z., Chen, Q. and Yang, J. (2016) 'Structures of a diverse set of colchicine binding site inhibitors in complex with tubulin provide a rationale for drug discovery', *The FEBS Journal*, 283(1), pp. 102-111.
- Warda, E. T., Shehata, I. A., El-Ashmawy, M. B. and El-Gohary, N. S. (2020) 'New series of isoxazole derivatives targeting EGFR-TK: Synthesis, molecular modeling and antitumor evaluation', *Bioorganic & Medicinal Chemistry*, 28(21), pp. 27.
- Weaver, B. A. A. and Cleveland, D. W. (2006) 'Does aneuploidy cause cancer?', *Current Opinion in Cell Biology*, 18(6), pp. 658-667.
- Wheate, N. J., Walker, S., Craig, G. E. and Oun, R. (2010) 'The status of platinum anticancer drugs in the clinic and in clinical trials', *Dalton Transactions*, 39(35), pp. 8113-8127.
- Wiles, C., Watts, P., Haswell, S. J. and Pombo-Villar, E. (2002) 'The regioselective preparation of 1,3-diketones within a micro reactor', *Chemical Communications*, (10), pp. 1034-1035.
- Wilson, B. C. 'Photonic and non-photonic based nanoparticles in cancer imaging and therapeutics'. *Photon-based Nanoscience and Nanobiotechnology*, Dordrecht, 2006//: Springer Netherlands, 121-157.
- Wu, J., Cai, Z., Wei, X., Chen, M., Ying, S., Shi, L., Xu, R.-A., He, F., Liang, G. and Zhang, X. (2015) 'Anti-Lung Cancer Activity of the Curcumin Analog JZ534 In Vitro', *BioMed Research International*, 2015, pp. 504-529.
- Wuts, P. G. W. (2014) *Greene's Protective Groups in Organic Synthesis*. Fifth edn. New Jersey: John Wiley & Sons.
- Xu, M. X., Zhao, L., Deng, C., Yang, L., Wang, Y., Guo, T., Li, L., Lin, J. and Zhang, L. (2013) 'Curcumin suppresses proliferation and induces apoptosis of human hepatocellular carcinoma cells via the wnt signaling pathway', *Int J Oncol*, 43(6), pp. 1951-1959.
- Yang, Q., Sheng, M., Henkelis, J. J., Tu, S., Wiensch, E., Zhang, H., Zhang, Y., Tucker, C. and Ejeh, D. E. (2019) 'Explosion Hazards of Sodium Hydride in Dimethyl Sulfoxide, N,N-Dimethylformamide, and N,N-Dimethylacetamide', *Organic Process Research & Development*, 23(10), pp. 2210-2217.

- Yin, X., Zhou, J., Jie, C., Xing, D. and Zhang, Y. (2004) 'Anticancer activity and mechanism of *Scutellaria barbata* extract on human lung cancer cell line A549', *Life Sciences*, 75(18), pp. 2233-2244.
- Yingge, W., Yongfang, Y., Hai-Liang, Z. and Yongtao, D. (2020) 'Butterfly Structure: A Privileged Scaffold Targeting Tubulin-Colchicine Binding Site', *Current Topics in Medicinal Chemistry*, 20(17), pp. 1505-1508.
- Yu, C., Wang, Z., Sun, Z., Zhang, L., Zhang, W., Xu, Y. and Zhang, J.-J. (2020) 'Platinum-Based Combination Therapy: Molecular Rationale, Current Clinical Uses, and Future Perspectives', *Journal of Medicinal Chemistry*.
- Zawadiak, J. and Mrzyczek, M. (2013) 'Correlation of substituted aromatic β -diketones' characteristic protons chemical shifts with Hammett substituent constants', *Magnetic Resonance in Chemistry*, 51(11), pp. 689-694.
- Zhang, S., An, B., Yan, J., Huang, L. and Li, X. (2016) 'The synthesis and evaluation of new benzophenone derivatives as tubulin polymerization inhibitors', *RSC Advances*, 6(91), pp. 88453-88462.
- Zheng, S., Zhong, Q., Mottamal, M., Zhang, Q., Zhang, C., Lemelle, E., McFerrin, H. and Wang, G. (2014) 'Design, synthesis, and biological evaluation of novel pyridine-bridged analogues of combretastatin-A4 as anticancer agents', *Journal of medicinal chemistry*, 57(8), pp. 3369-3381.
- Zhong, Z., Yu, J., Virshup, D. M. and Madan, B. (2020) 'Wnts and the hallmarks of cancer', *Cancer and Metastasis Reviews*.
- Zhou, J., Kang, Y., Chen, L., Wang, H., Liu, J., Zeng, S. and Yu, L. (2020) 'The Drug-Resistance Mechanisms of Five Platinum-Based Antitumor Agents', *Frontiers in pharmacology*, 11, pp. 343-343.

Appendix

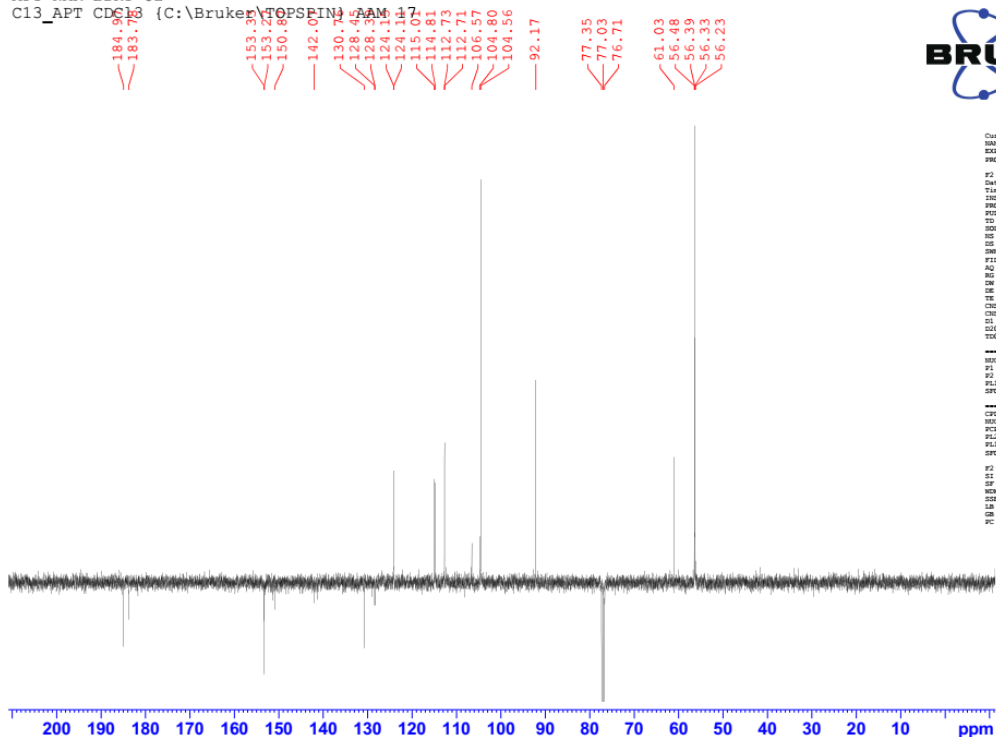
Spectral data of compounds

Appendix

Chemical Spectra of compounds

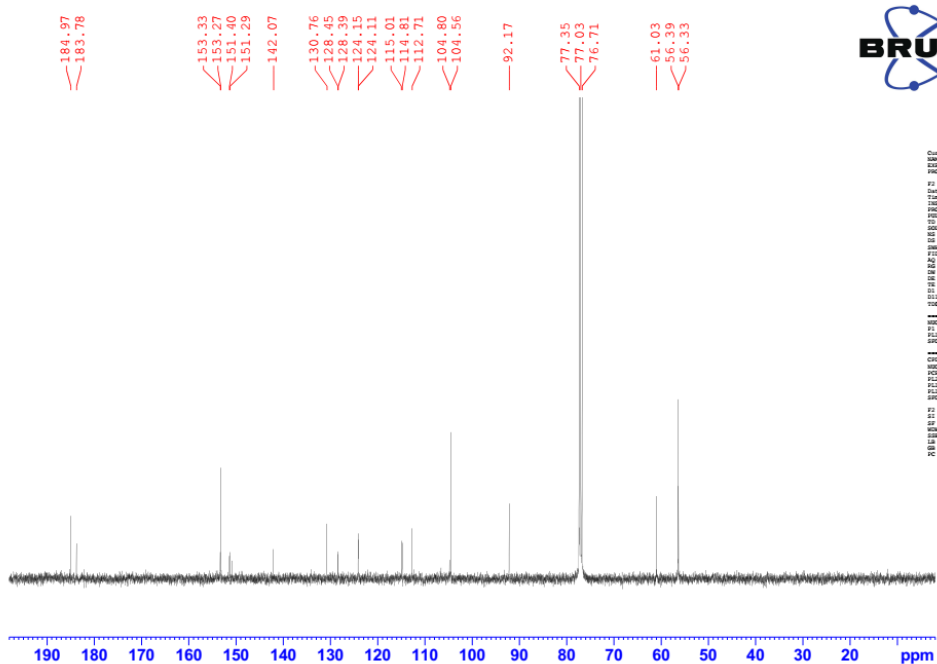
BDKT-02

APT NMR BDKT-02
C13_APT CDC113 {C:\Bruker\TOPSPIN\AAM 17



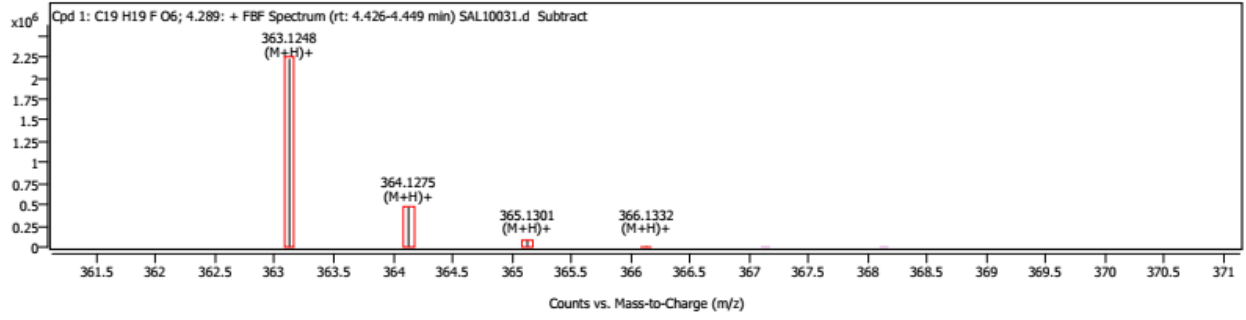
```
Current Data Parameters
NAME      Nov14-2009-100
EXPNO    14
PROCNO   1
F2 - Acquisition Parameters
Date_    20091125
Time     20.30
INSTRUM  spect
PROBHD   5 mm BBO BB-1H
PULPROG  zgpg30
TD        65536
SOLVENT  CDCl3
NS        4
DS        23980.814 Hz
FIDRES   0.345918 Hz
AQ        1.3645226 sec
RG        14384
CW        20.850 usec
DE        6.50 usec
TE        298.2 K
CQ1CH1   145.000000
CQ1CH11  1.0000000
CQ1CH12  2.0000000
CQ1CH13  0.00684653 sec
TOD      1
===== CHANNEL f1 =====
NUC1      13C
P1        1.00
PL1       0.00 usec
SFO1      100.628378 MHz
===== CHANNEL f2 =====
CPDPRG2   waltz16
NUC2      1H
P2        18.00
PL2       0.00 usec
SFO2      400.1316005 MHz
F2 - Processing parameters
SI        32768
SF        100.6127690 MHz
WDW        EM
SSB        0
LB        1.00 Hz
GB        0
PC        1.40
```

13C NMR BDKT-02
c13org CDC13 {C:\Bruker\TOPSPIN\ AAM 17



```
Current Data Parameters
NAME      Nov14-2009-100
EXPNO    11
PROCNO   1
F2 - Acquisition Parameters
Date_    20091125
Time     18.04
INSTRUM  spect
PROBHD   5 mm BBO BB-1H
PULPROG  zgpg30
TD        65536
SOLVENT  CDCl3
NS        4
DS        23980.814 Hz
FIDRES   0.345918 Hz
AQ        1.3645226 sec
RG        14384
CW        20.850 usec
DE        6.50 usec
TE        298.2 K
CQ1CH1   145.000000
CQ1CH11  1.0000000
CQ1CH12  2.0000000
CQ1CH13  0.00684653 sec
TOD      1
===== CHANNEL f1 =====
NUC1      13C
P1        1.00
PL1       0.00 usec
SFO1      100.628378 MHz
===== CHANNEL f2 =====
CPDPRG2   waltz16
NUC2      1H
P2        18.00
PL2       0.00 usec
SFO2      400.1316005 MHz
F2 - Processing parameters
SI        32768
SF        100.6127690 MHz
WDW        EM
SSB        0
LB        1.00 Hz
GB        0
PC        2.00
```

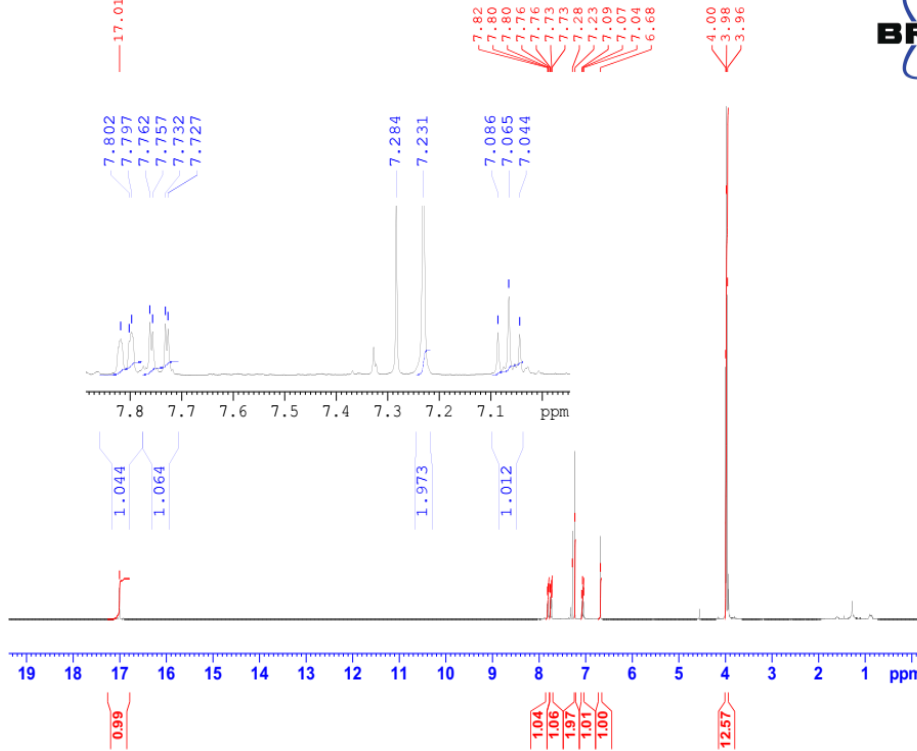
Compound Spectra



Spectrum Peaks

m/z	m/z (Calc)	Diff (ppm)	Abund	Height %	Height % (Calc)	Ion Species	Z
363.1248	363.1238	2.71	2228268	100.00	100.00	(M+H) ⁺	1
364.1275	364.1272	0.67	480023	21.54	21.01	(M+H) ⁺	1
365.1301	365.1297	1.20	78940	3.54	3.33	(M+H) ⁺	1
366.1332	366.1323	2.25	9328	0.42	0.39	(M+H) ⁺	1

¹H NMR BDKT-UZ
 PROTON64 CDCl₃ {C:\Bruker\TOPSPIN} AAM 17



```

Current Data Parameters
NAME Nov4*1000-400
EXPNO 10
PROCNO 1
P2 = Acquisition Parameters
Date_ 20201125
Time 15.26
INSTRUM spect
PROBHD 5 mm BBO BB-1H
PULPROG zgpg30
TD 65536
SOLVENT cdcl3
NS 64
DS 4
SWH 8802.817 Hz
FIDRES 0.156383 Hz
AQ 3.197271 sec
RG 322.5
SN 56.800 sec
TE 6.30 sec
TC 296.2 K
TI 2.5999990 sec
TDO 1
===== CHANNEL f1 =====
NUC1 1H
P1 10.00 sec
PL1 -1.00 dB
SFO1 400.1333626 MHz
P2 = Processing parameters
SI 32768
SF 400.1330000 MHz
WDW EM
SSB 0
LB 0.30 Hz
GB 0
PC 1.00
    
```

BB H1 Coupled F19 NMR of B-diketone [BDKT-2 (4)] in CDCl3

-134.19
-134.18
-134.18
-134.20

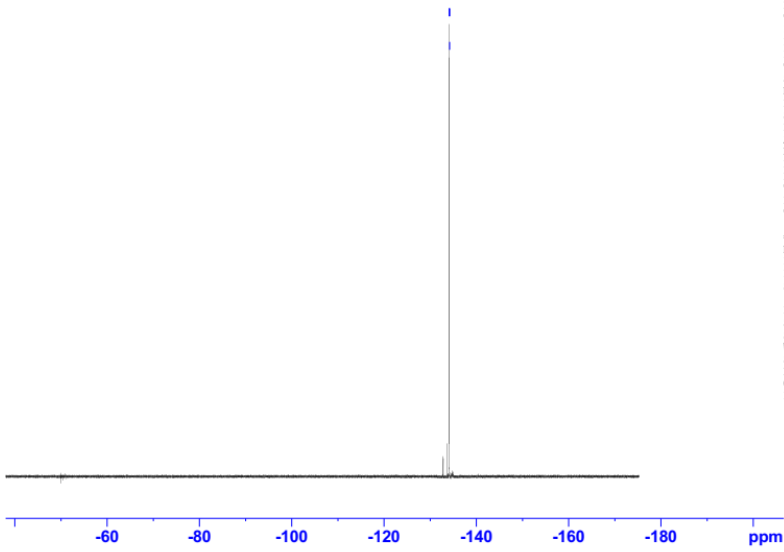


Current Data Parameters
NAME Feb11-2019-AAM
EXPNO 11
PROCNO 1

F2 - Acquisition Parameters
Date_ 20190211
Time 9.01
INSTRUM spect
PROBHD 5 mm BBO BB-1H
PULPROG zg
TD 131072
SOLVENT CDCl3
NS 128
DS 2
SWH 94339.625 Hz
FIDRES 0.719754 Hz
AQ 0.6946816 sec
RG 35.9
DW 5.300 usec
DE 7.57 usec
TE 296.2 K
D1 4.28999996 sec
TDO 1

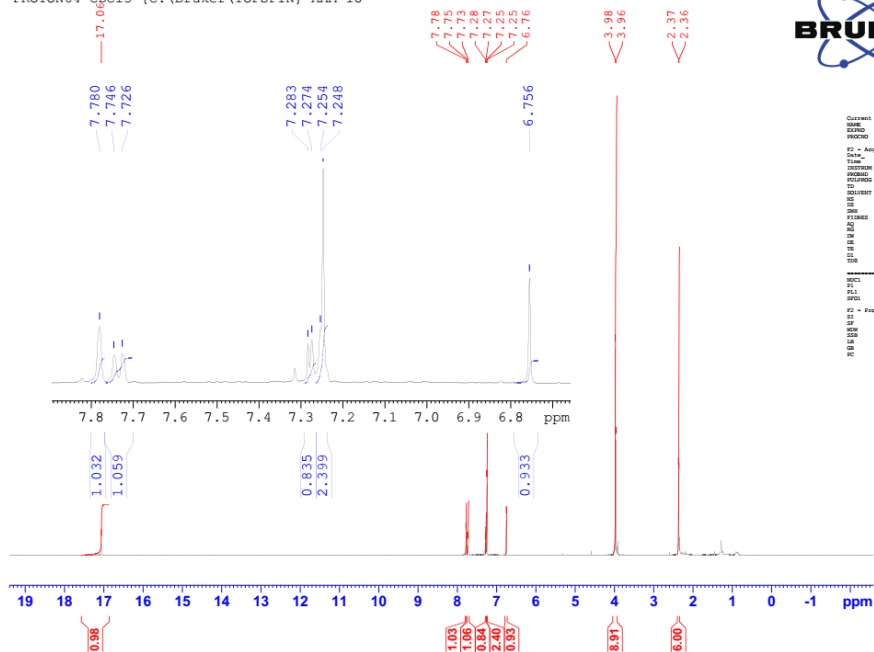
===== CHANNEL f1 =====
NUC1 19F
P1 9.50 usec
PL1 0 dB
SFO1 376.4795411 MHz

F2 - Processing parameters
SI 262144
SF 376.4983660 MHz
WDW EM
SSB 0
LB 0.20 Hz
GB 0
PC 1.00



BDKT-04

1H NMR BDKT-04
 PROTON64 CDCl3 {C:\Bruker\TOPSPIN} AAM 18



```

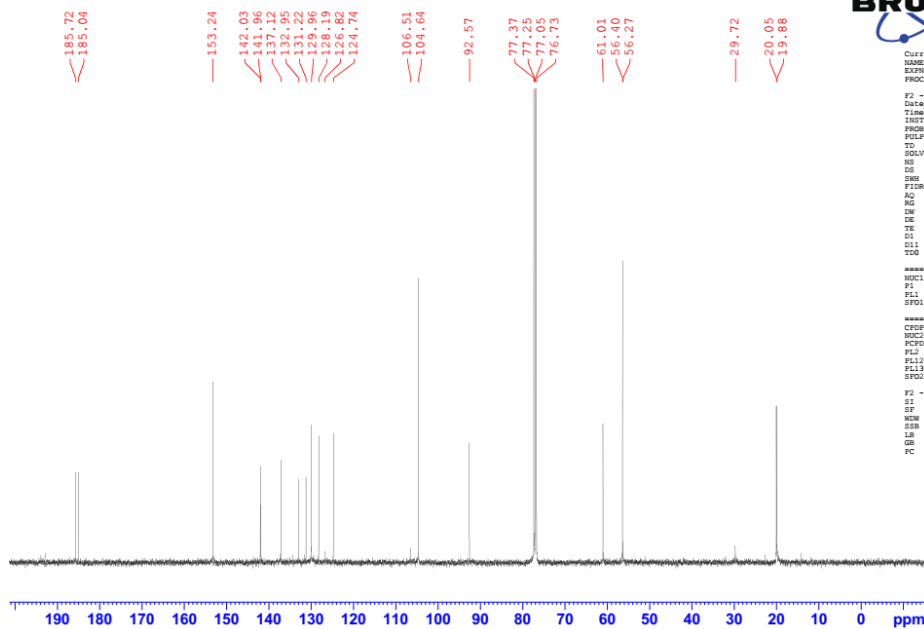
Current Data Parameters
NAME      Nov24-2020-AAM
EXPNO    1
PROCNO   1

F2 - Acquisition Parameters
Date_    20201125
Time     11:38
INSTRUM  spect
PROBHD   5 mm BBO BB-1H
PULPROG  zgpg30
TD        65536
SOLVENT  CDCl3
NS        64
DS        4
SWH       8802.817 Hz
FIDRES   0.16288 Hz
AQ        3.197721 sec
RG        320
WDW       EM
SSB       0
LB        30.00 Hz
GB        0
PC        2.5899990 sec
TD0       1

===== CHANNEL f1 =====
NUC1      1H
P1         19.00 usec
PL1       0.000000 dB
SFO1      400.146000 MHz

F2 - Processing parameters
SI         32768
SF         400.146000 MHz
WDW        EM
SSB        0
LB         1.00 Hz
GB         0
PC         2.00
  
```

13C NMR BDKT-04
 cl3org CDCl3 {C:\Bruker\TOPSPIN} AAM 18



```

Current Data Parameters
NAME      Nov24-2020-AAM
EXPNO    1
PROCNO   1

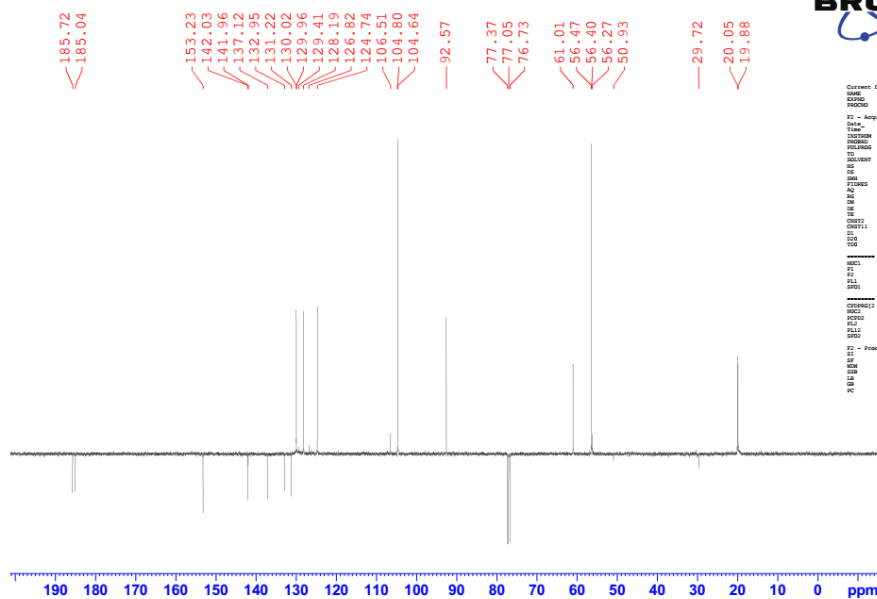
F2 - Acquisition Parameters
Date_    20201125
Time     21:35
INSTRUM  spect
PROBHD   5 mm BBO BB-1H
PULPROG  zgpg30
TD        65536
SOLVENT  CDCl3
NS        1024
DS        4
SWH       23980.814 Hz
FIDRES   0.345018 Hz
AQ        1.3664256 sec
RG        18390.4
WDW       EM
SSB       0
LB        20.850 usec
GB        0
PC        296.2 Hz
SFO1      2.00000000 sec
SFO2      0.03000000 sec
TD0       1

===== CHANNEL f1 =====
NUC1      13C
P1         9.00 usec
PL1       0.000000 dB
SFO1      100.628259 MHz

===== CHANNEL f2 =====
CPDPRG2  waltz16
NUC2      1H
PCPD2     80.00 usec
PL2       -2.00 dB
PL12      15.98 dB
PL13      19.58 dB
SFO2      400.1316005 MHz

F2 - Processing parameters
SI         32768
SF         100.628259 MHz
WDW        EM
SSB        0
LB         1.00 Hz
GB         0
PC         2.00
  
```

APT NMR BDKT-04
 C13_APT CDC13 {C:\Bruker\TOPSPIN} AAM 18



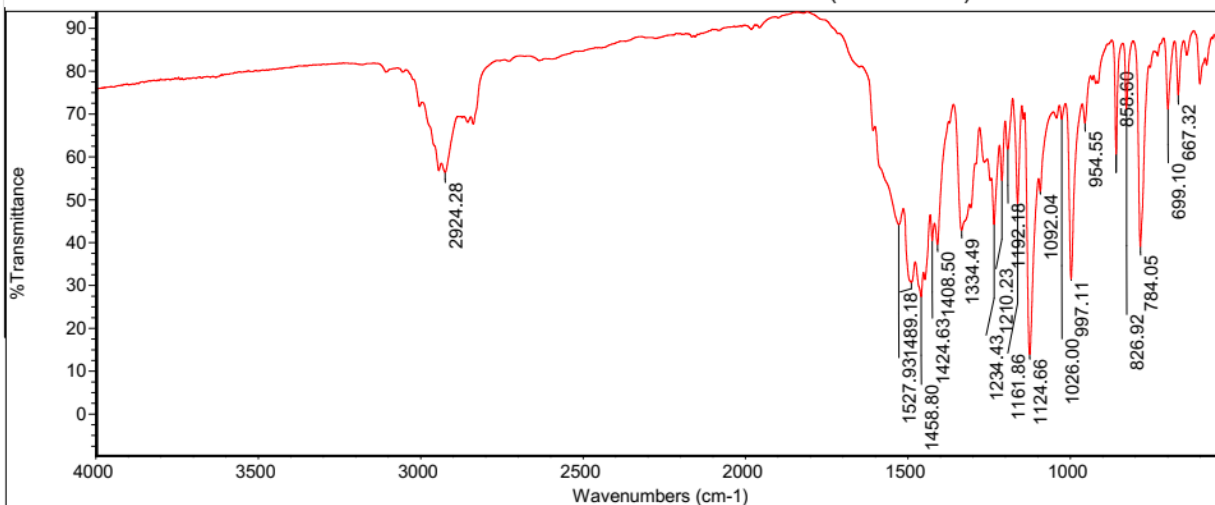
```

Current Data Parameters
NAME: 1850130
PROCNO: 1
F2 - Acquisition Parameters
Date_: 20211215
Time: 18:00:24
INSTRUM: spect
PROBHD: 5 mm BBO
PULPROG: zgpg30
TD: 65536
AQ: 0.0213
RG: 327.1
SI: 3271
SF: 125.760 MHz
FIDRES: 0.000188 Hz
AQRES: 1.165328 Hz
SFO: 125.760 MHz
NUC1: 13C
NUC2: 13C
PCPDW: 20.850 usec
DE: 5.20 usec
TE: 298.2 K
===== CHANNEL f1 =====
NUC1: 13C
P1: 12.00 usec
PL1: 0.00 dB
PL12: 0.00 dB
PL13: 100.00 dB
===== CHANNEL f2 =====
NAME: 1H
NUC1: 1H
P1: 12.00 usec
PL1: 0.00 dB
PL12: 19.00 dB
PL13: 400.131000 MHz
F2 - Processing parameters
SI: 3271
SF: 100.617900 MHz
WDW: EM
SSB: 0
GB: 0
PC: 1.00 Hz
RB: 1.40
  
```

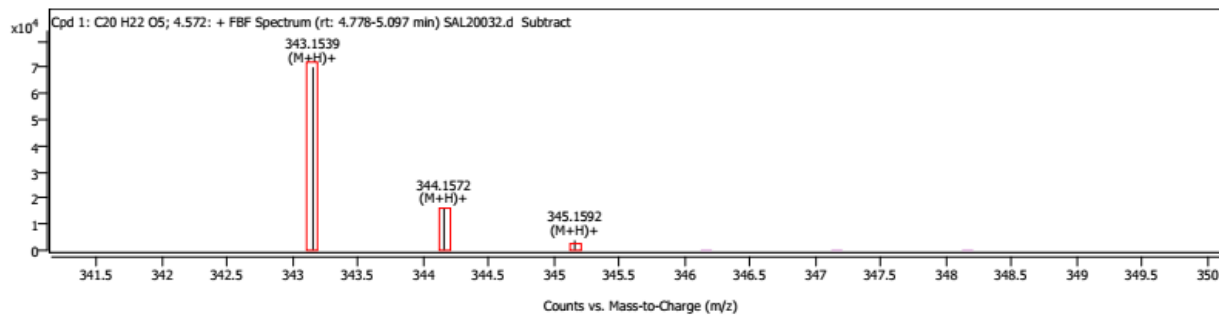
ThermoFisher
 SCIENTIFIC

Wed Dec 15 18:00:24 2021

BDKT-04:Wed Jan 20 10:20:43 2021 (GMT+00:00)



Compound Spectra

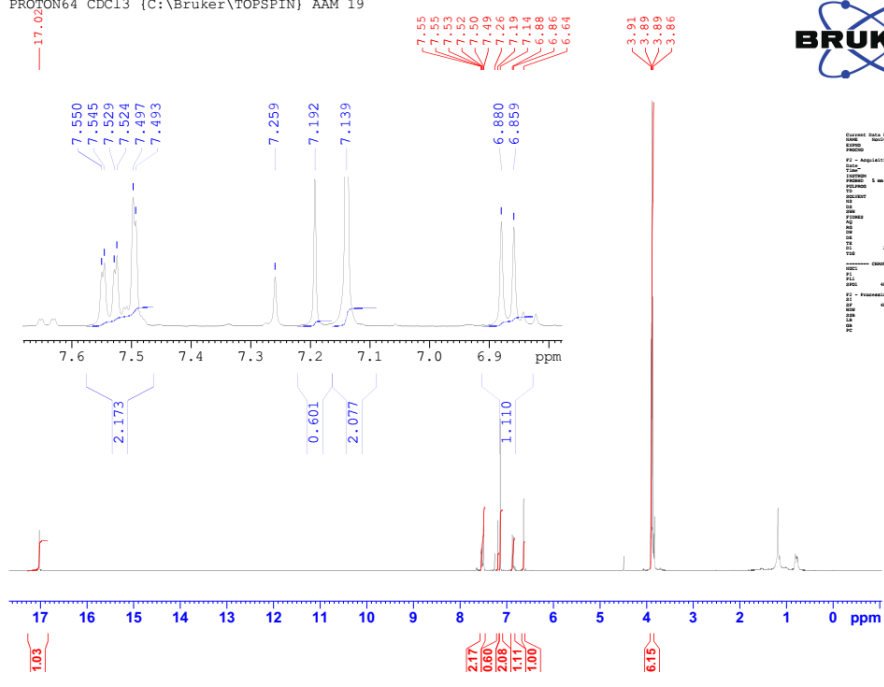


Spectrum Peaks

m/z	m/z (Calc)	Diff (ppm)	Abund	Height %	Height % (Calc)	Ion Species	Z
343.1539	343.1540	-0.25	69947	100.00	100.00	(M+H)+	1
344.1572	344.1574	-0.71	16045	22.94	22.09	(M+H)+	1
345.1592	345.1600	-2.28	3790	5.42	3.35	(M+H)+	1

BDKT-05

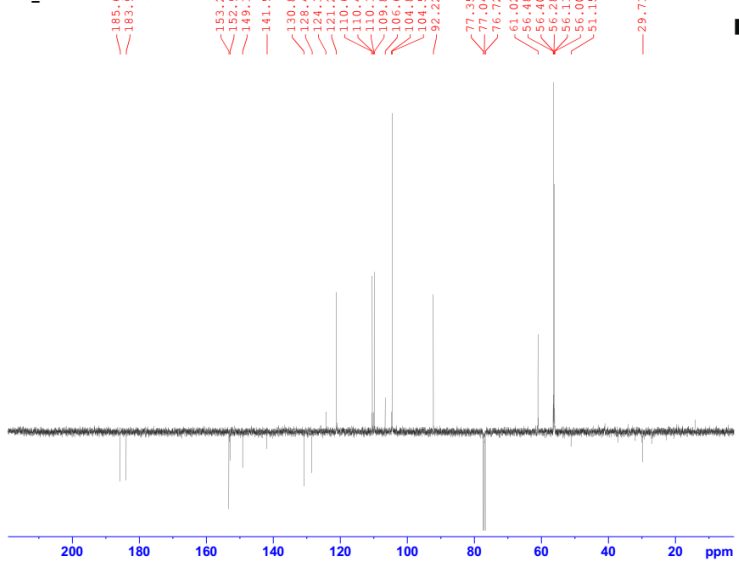
1H NMR BDKT-05
 PROTON64 CDCl3 (C:\Bruker\TOPSPIN) AAM 19



```

Current Data Parameters
NAME: PROTON64
PROCNO: 19
F2 - Acquisition Parameters
Date_   : 201212
Time    : 15:51
INSTRUM : spect
PROBHD  : 5 mm BBO SPC1
PULPROG : smpt
TD      : 65536
SOLVENT : CDCl3
NS      : 4
DS      : 4
SWH     : 23186.814 Hz
F2RES   : 0.360318 Hz
AQ      : 1.3644156 sec
RG      : 328
DE      : 2.000000
TE      : 300.2 K
CH2F2   : 145.000000
CH2F11  : 1.000000000 sec
DQ      : 0.000000000 sec
DD      : 0.000000000 sec
DD2     : 0.000000000 sec
DD3     : 0.000000000 sec
----- CHANNEL f1 -----
NUC1    : 13C
P1      : 18.000000 sec
PL1     : 0.00 dB
PC1     : 0.00 dB
SFO1    : 100.6213709 MHz
----- CHANNEL f2 -----
CPDPRG2 : waltz16
NUC2     : 1H
P2       : 9.000000 sec
PL2      : -2.00 dB
PC2      : 0.00 dB
SFO2     : 400.1314000 MHz
F2 - Processing parameters
SI      : 32768
SF       : 400.1314000 MHz
WDW      : EM
SSB      : 0
LB        : 3.00 Hz
GB        : 0
PC        : 2.00
  
```

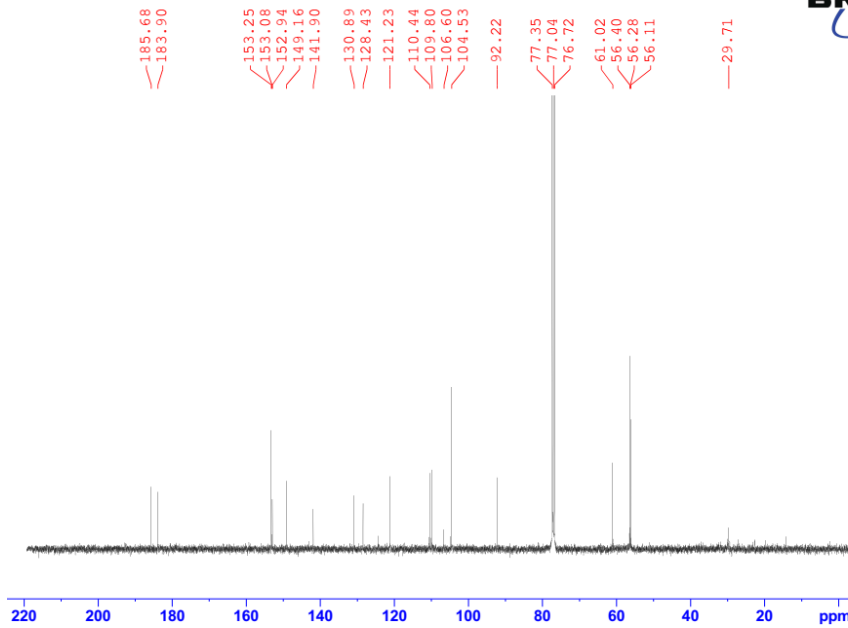
APT NMR BDKT-05
 C13_APT CDCl3 (C:\Bruker\TOPSPIN) AAM 19



```

Current Data Parameters
NAME: C13_APT
PROCNO: 19
F2 - Acquisition Parameters
Date_   : 201212
Time    : 15:51
INSTRUM : spect
PROBHD  : 5 mm BBO SPC1
PULPROG : smpt
TD      : 65536
SOLVENT : CDCl3
NS      : 4
DS      : 4
SWH     : 23186.814 Hz
F2RES   : 0.360318 Hz
AQ      : 1.3644156 sec
RG      : 328
DE      : 2.000000
TE      : 300.2 K
CH2F2   : 145.000000
CH2F11  : 1.000000000 sec
DQ      : 0.000000000 sec
DD      : 0.000000000 sec
DD2     : 0.000000000 sec
DD3     : 0.000000000 sec
----- CHANNEL f1 -----
NUC1    : 13C
P1      : 18.000000 sec
PL1     : 0.00 dB
PC1     : 0.00 dB
SFO1    : 100.6213709 MHz
----- CHANNEL f2 -----
CPDPRG2 : waltz16
NUC2     : 1H
P2       : 9.000000 sec
PL2      : -2.00 dB
PC2      : 0.00 dB
SFO2     : 400.1314000 MHz
F2 - Processing parameters
SI      : 32768
SF       : 400.1314000 MHz
WDW      : EM
SSB      : 0
LB        : 3.00 Hz
GB        : 0
PC        : 2.00
  
```


13C NMR BDKT-05
 c13org CDCl3 (C:\Bruker\TOPSPIN) AAM 19



```

Current Data Parameters
NAME      Nov14-2020-AAM
EXPNO    31
PROCNO   1

F2 - Acquisition Parameters
Date_    20201126
Time_    1.87
INSTRUM  spect
PROBHD   5 mm BBO
PULPROG  zgpg30
TD        65536
SOLVENT  CDCl3
NS        1024
DS        4
SFR       23880.814 Hz
AQ         0.365918 Hz
RG         1.3664256 sec
RG1        18380.4
RG2        1.3664256 sec
RG3        18380.4
RG4        1.3664256 sec
RG5        18380.4
RG6        1.3664256 sec
RG7        18380.4
RG8        1.3664256 sec
RG9        18380.4
RG10       1.3664256 sec
RG11       18380.4
RG12       1.3664256 sec
RG13       18380.4
RG14       1.3664256 sec
RG15       18380.4
RG16       1.3664256 sec
RG17       18380.4
RG18       1.3664256 sec
RG19       18380.4
RG20       1.3664256 sec
RG21       18380.4
RG22       1.3664256 sec
RG23       18380.4
RG24       1.3664256 sec
RG25       18380.4
RG26       1.3664256 sec
RG27       18380.4
RG28       1.3664256 sec
RG29       18380.4
RG30       1.3664256 sec
RG31       18380.4
RG32       1.3664256 sec
RG33       18380.4
RG34       1.3664256 sec
RG35       18380.4
RG36       1.3664256 sec
RG37       18380.4
RG38       1.3664256 sec
RG39       18380.4
RG40       1.3664256 sec
RG41       18380.4
RG42       1.3664256 sec
RG43       18380.4
RG44       1.3664256 sec
RG45       18380.4
RG46       1.3664256 sec
RG47       18380.4
RG48       1.3664256 sec
RG49       18380.4
RG50       1.3664256 sec
RG51       18380.4
RG52       1.3664256 sec
RG53       18380.4
RG54       1.3664256 sec
RG55       18380.4
RG56       1.3664256 sec
RG57       18380.4
RG58       1.3664256 sec
RG59       18380.4
RG60       1.3664256 sec
RG61       18380.4
RG62       1.3664256 sec
RG63       18380.4
RG64       1.3664256 sec
RG65       18380.4
RG66       1.3664256 sec
RG67       18380.4
RG68       1.3664256 sec
RG69       18380.4
RG70       1.3664256 sec
RG71       18380.4
RG72       1.3664256 sec
RG73       18380.4
RG74       1.3664256 sec
RG75       18380.4
RG76       1.3664256 sec
RG77       18380.4
RG78       1.3664256 sec
RG79       18380.4
RG80       1.3664256 sec
RG81       18380.4
RG82       1.3664256 sec
RG83       18380.4
RG84       1.3664256 sec
RG85       18380.4
RG86       1.3664256 sec
RG87       18380.4
RG88       1.3664256 sec
RG89       18380.4
RG90       1.3664256 sec
RG91       18380.4
RG92       1.3664256 sec
RG93       18380.4
RG94       1.3664256 sec
RG95       18380.4
RG96       1.3664256 sec
RG97       18380.4
RG98       1.3664256 sec
RG99       18380.4
RG100      1.3664256 sec

===== CHANNEL f1 =====
NUC1      13C
P1        9.00 usec
PC1       6.60 dB
SFO1      100.623218 MHz

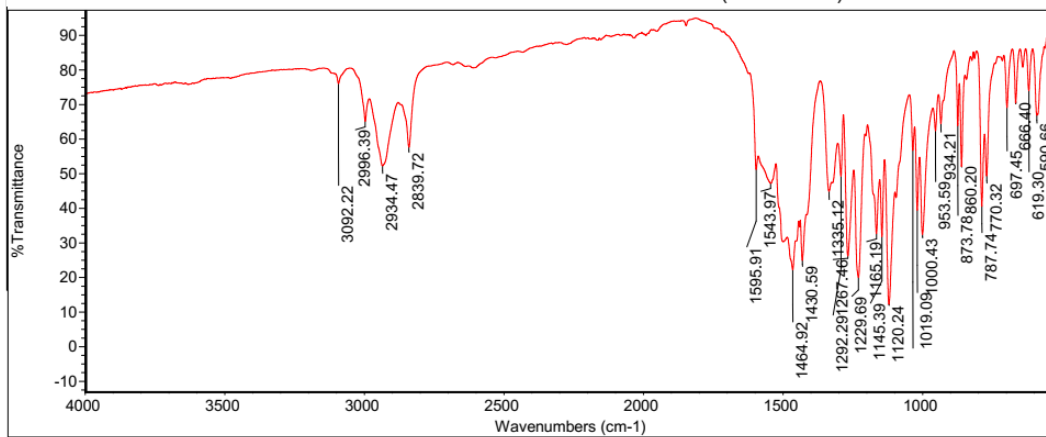
===== CHANNEL f2 =====
CPDPRG2   waltz16
NUC2      1H
PCPD2     80.00 usec
PFL2      2.00 dB
PFL12     15.98 dB
PFL13     15.50 dB
SFO2      400.1316005 MHz

F2 - Processing parameters
SI        32768
SF        100.6127630 MHz
RG        0
SSB       0
GB        1.00 Hz
PC        2.00
  
```

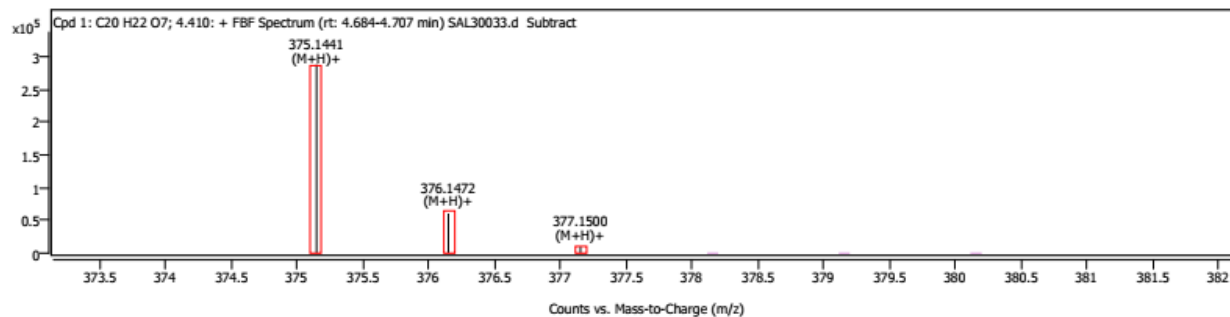
ThermoFisher
 SCIENTIFIC

Wed Dec 15 18:02:51 2021

BDKT-05: Wed Jan 20 10:23:54 2021 (GMT+00:00)



Compound Spectra

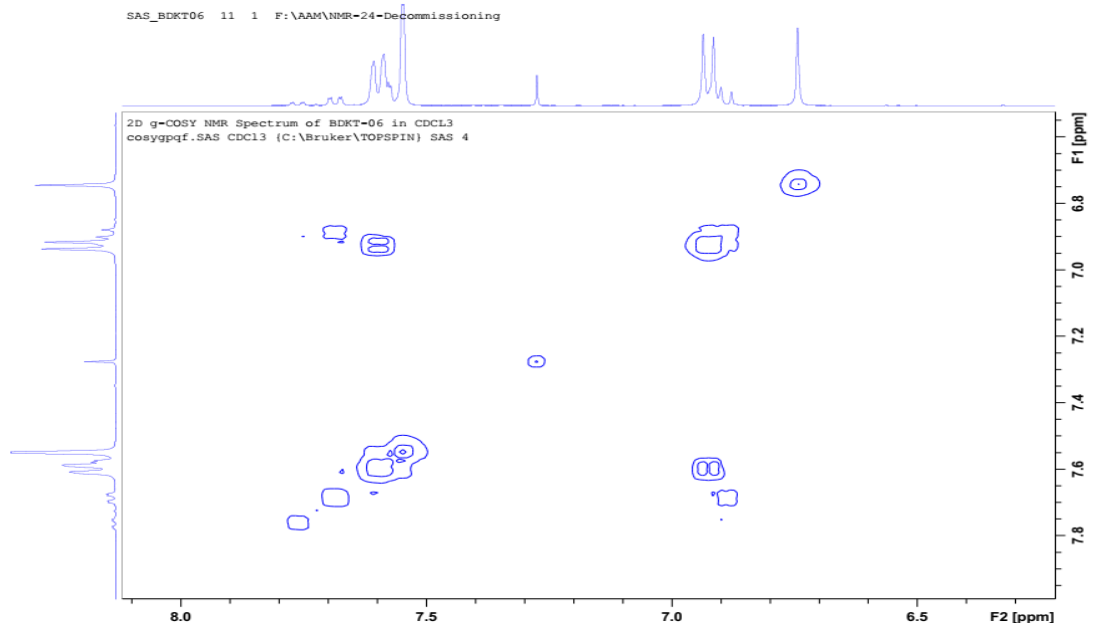
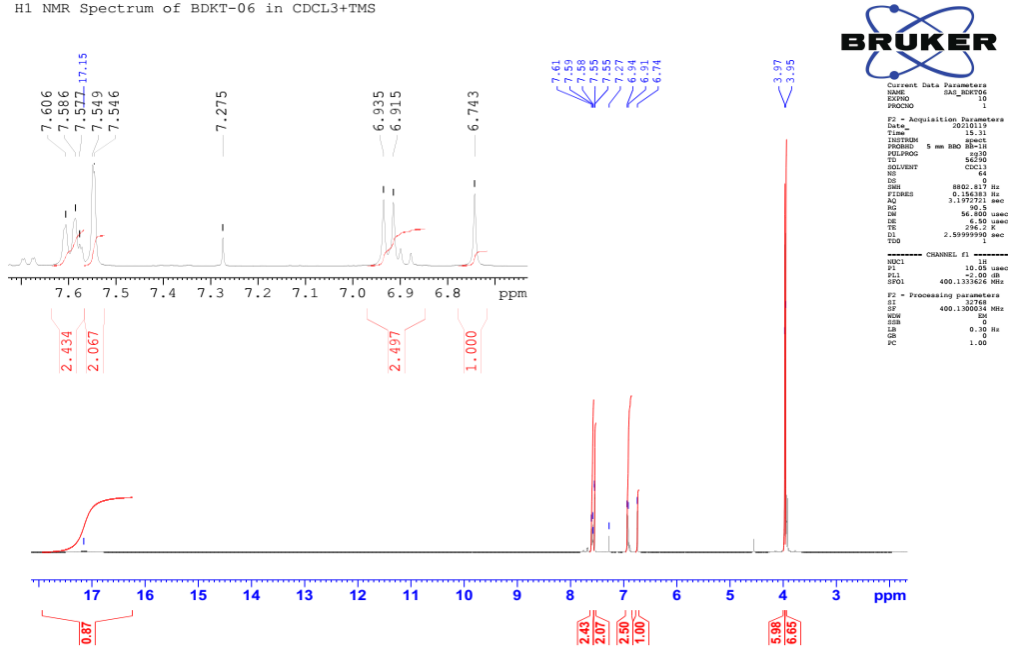


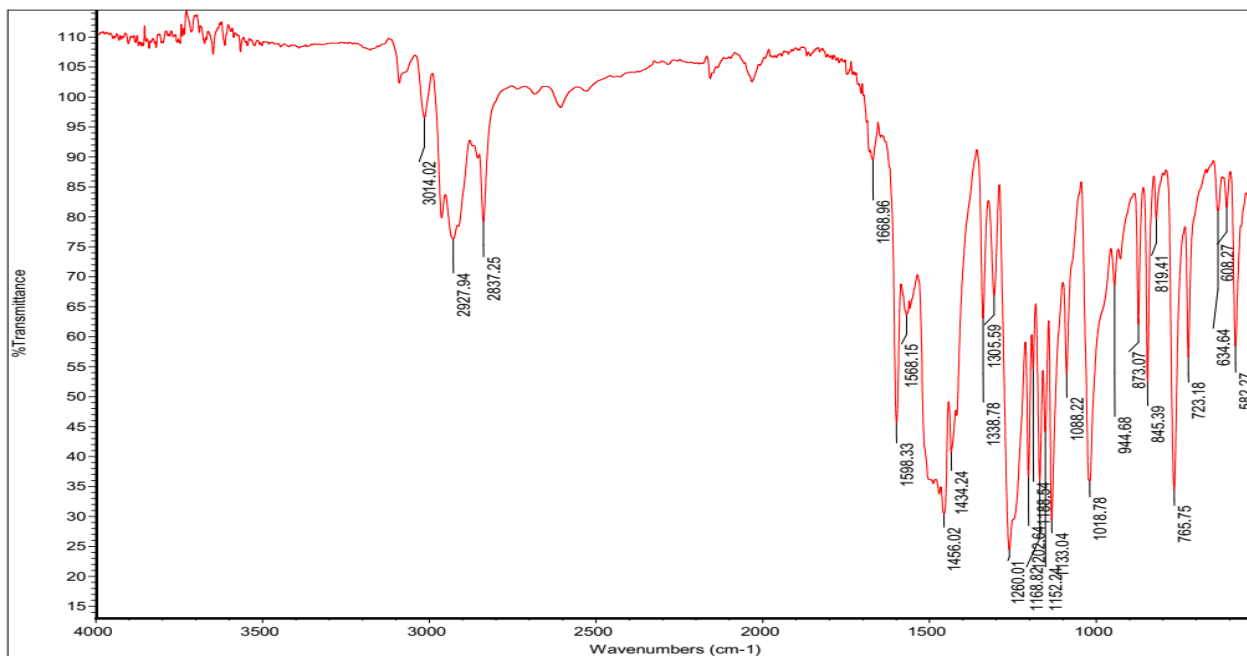
Spectrum Peaks

m/z	m/z (Calc)	Diff (ppm)	Abund	Height %	Height % (Calc)	Ion Species	Z
375.1441	375.1438	0.73	288236	100.00	100.00	(M+H)+	1
376.1472	376.1472	-0.02	60317	20.93	22.16	(M+H)+	1
377.1500	377.1497	0.92	10141	3.52	3.78	(M+H)+	1

BDKT-06

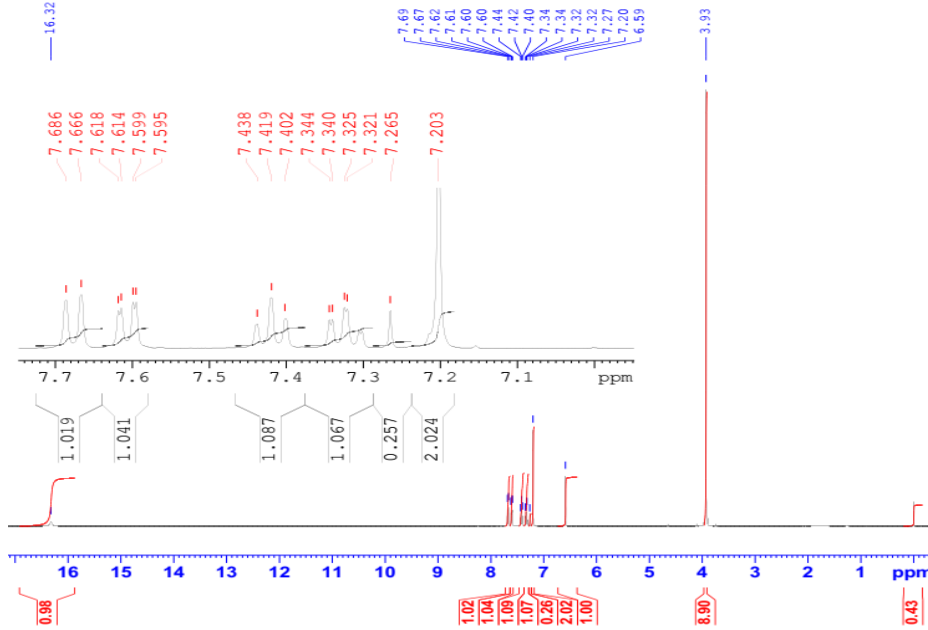
H1 NMR Spectrum of BDKT-06 in CDCL3+TMS





BDKT-7

H1 NMR Spectrum of BDKT-07 in CDCl₃+TMS
 PROTON64 CDCl₃ (C:\Bruker\TOPSPIN) SAS 3



Current Data Parameters
 NAME SAS_BDKT07
 EXPNO 10
 PROCNO 1

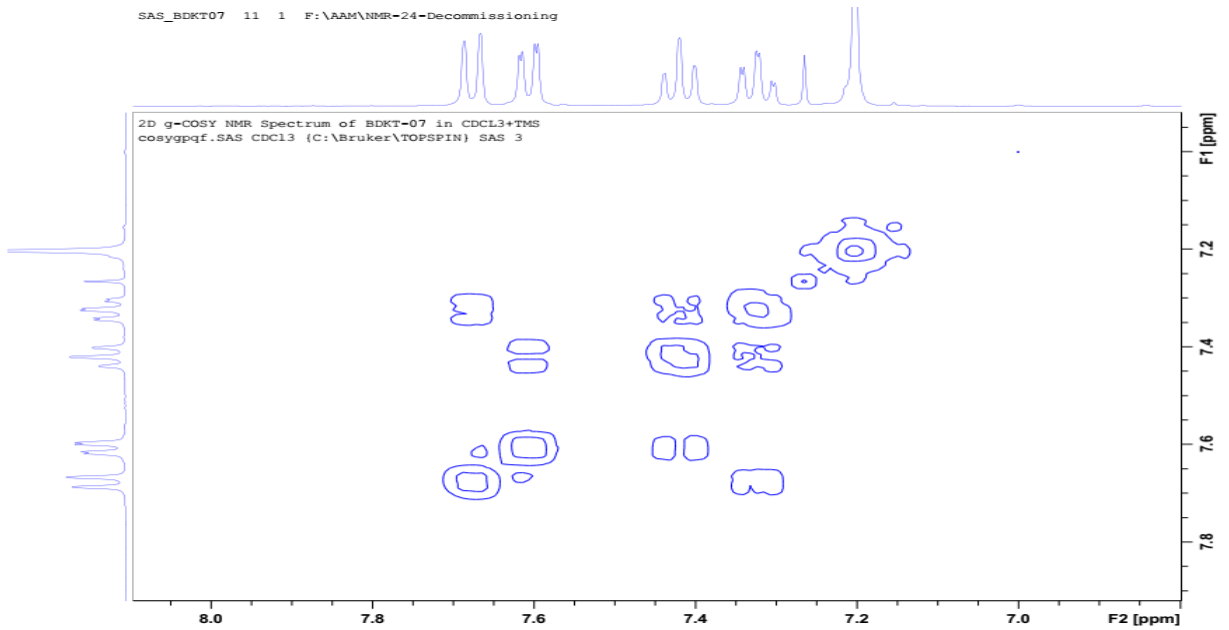
F2 - Acquisition Parameters
 Date_ 20210121
 Time 13.24
 INSTRUM spect
 PROBHD 5 mm BBO BB-1H
 PULPROG zg30
 TD 56290
 SOLVENT CDCl3
 NS 64
 DS 0
 SWH 8802.817 Hz
 FIDRES 0.156383 Hz
 AQ 3.1972721 sec
 RG 128
 DW 56.800 usec
 DE 6.50 usec
 TE 296.2 K
 D1 2.59999990 sec
 TDO 1

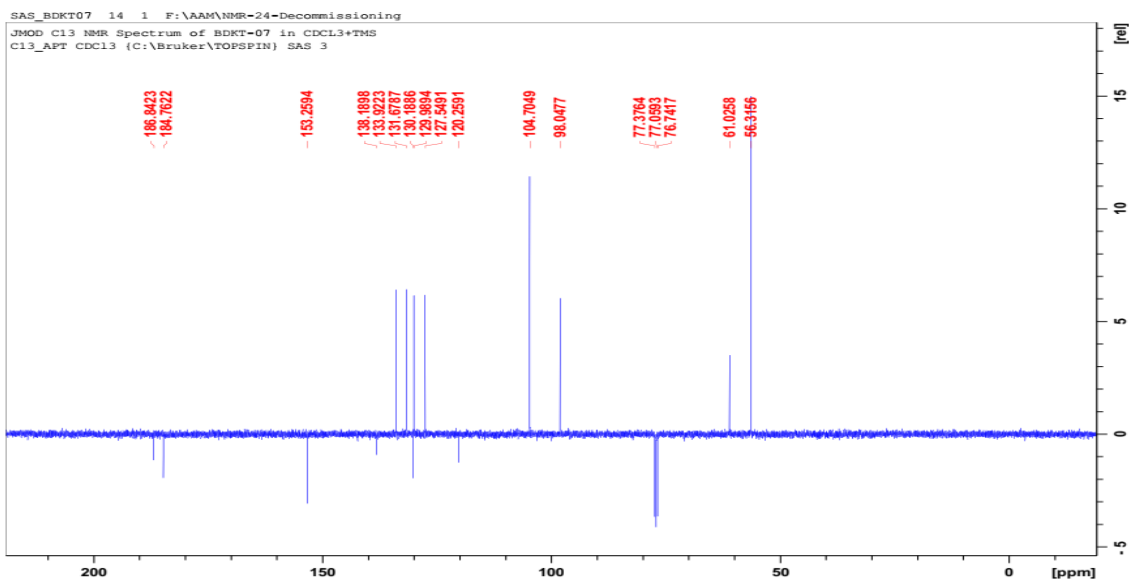
===== CHANNEL f1 =====
 NUC1 1H
 P1 10.05 usec
 PL1 -2.00 dB
 SFO1 400.1333626 MHz

F2 - Processing parameters
 SI 32768
 SF 400.1300072 MHz
 WDW EM
 SSB 0
 LB 0.30 Hz
 GB 0
 PC 10.00

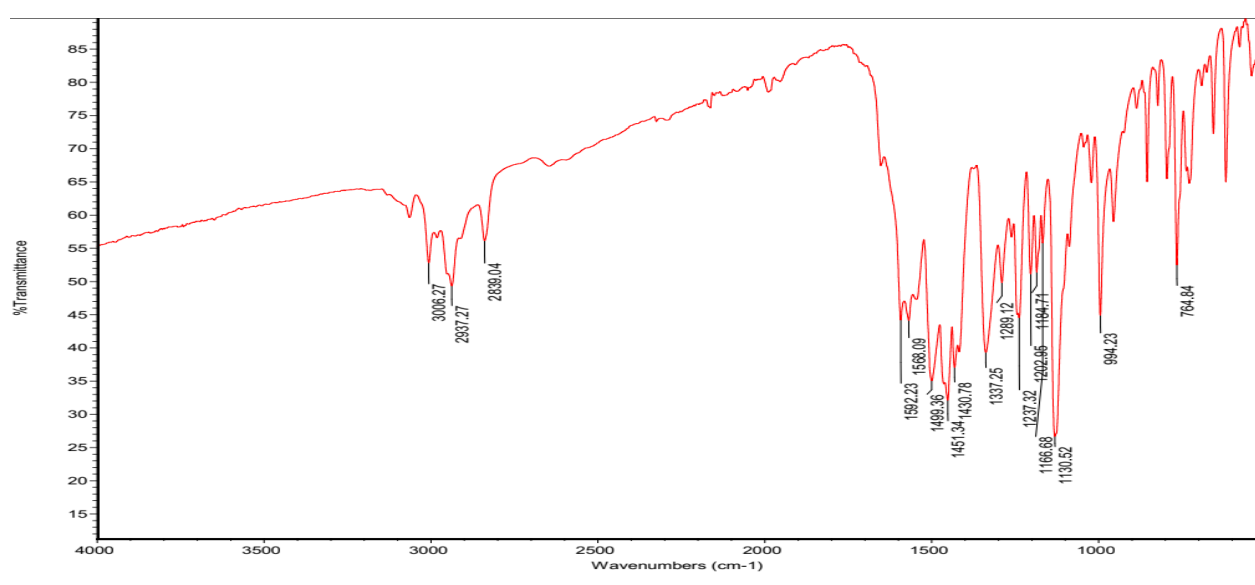
SAS_BDKT07 11 1 F:\AAM\NMR-24-Decommissioning

2D g-COSY NMR Spectrum of BDKT-07 in CDCl₃+TMS
 cosygpf.SAS CDCl₃ (C:\Bruker\TOPSPIN) SAS 3





IR



Single Mass Analysis

Tolerance = 1000.0 PPM / DBE: min = -1.5, max = 50.0

Element prediction: Off

Number of isotope peaks used for i-FIT = 3

Monoisotopic Mass, Even Electron Ions

9 formula(e) evaluated with 1 results within limits (up to 5 closest results for each mass)

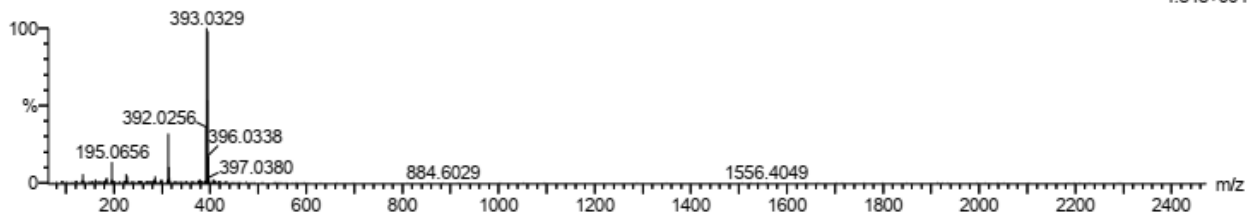
Elements Used:

C: 0-18 H: 0-18 O: 1-5 Br: 0-1

AB300321 SAL 4

AB300321 SAL 4 1117 (2.401) Cm (1066:1130)

1: TOF MS ASAP+
4.54e+004

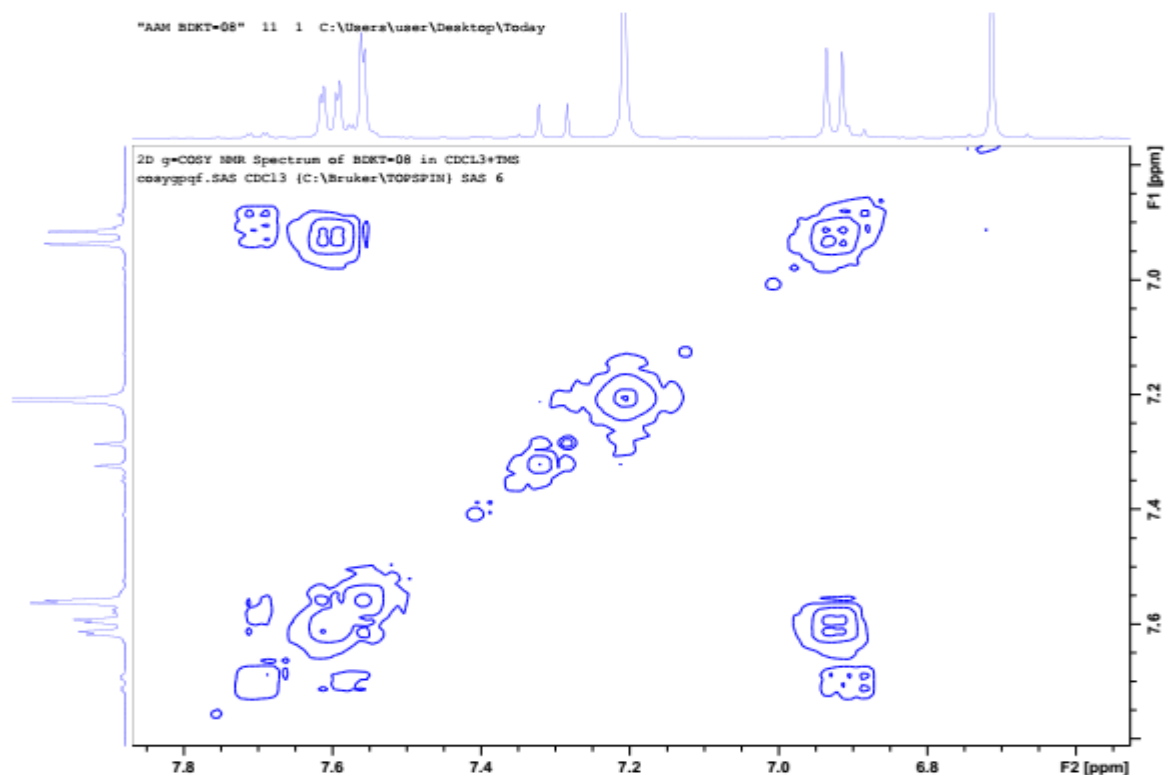
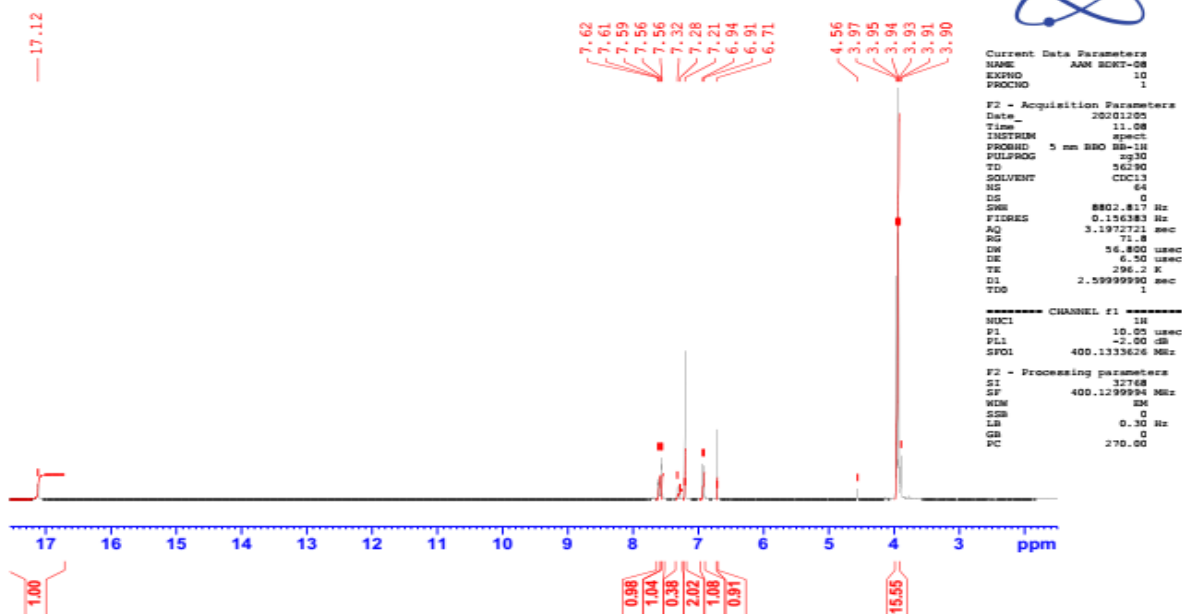


Minimum: -1.5
Maximum: 5.0 1000.0 50.0

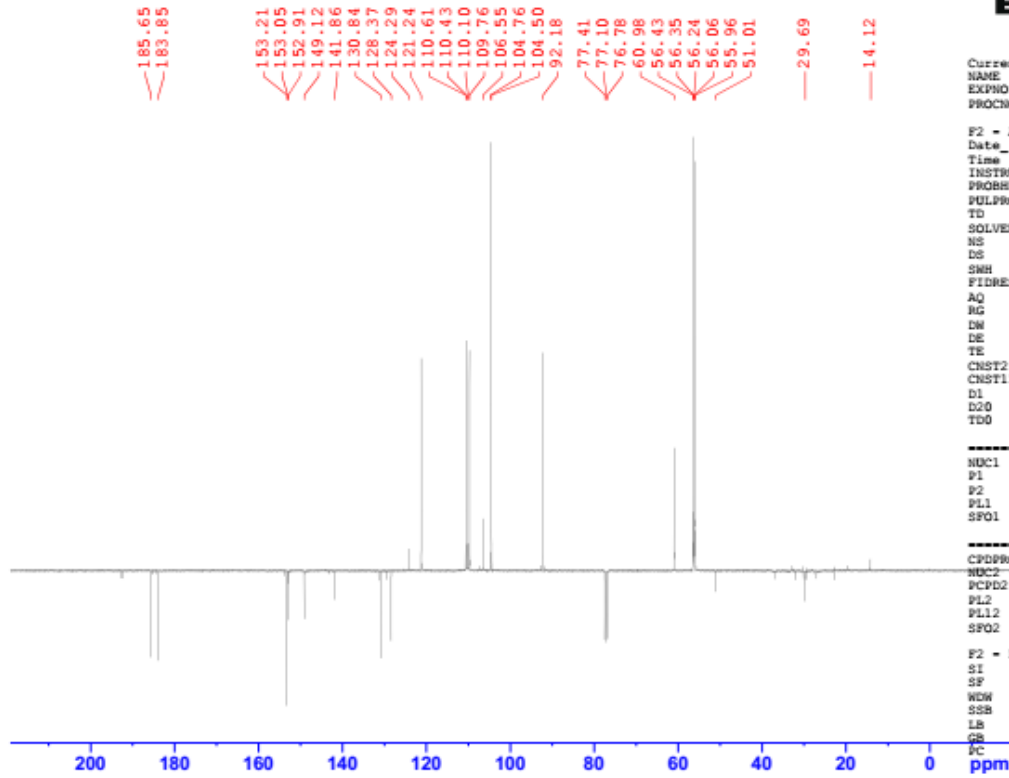
Mass	Calc. Mass	mDa	PPM	DBE	i-FIT	Norm	Conf(%)	Formula
393.0329	393.0338	-0.9	-2.3	9.5	253.7	n/a	n/a	C18 H18 O5 Br

BDKT-08

H1 NMR Spectrum of BDKT-08 in CDCL3+TMS
 PROTON64 CDC13 {C:\Bruker\TOPSPIN} SAS 6

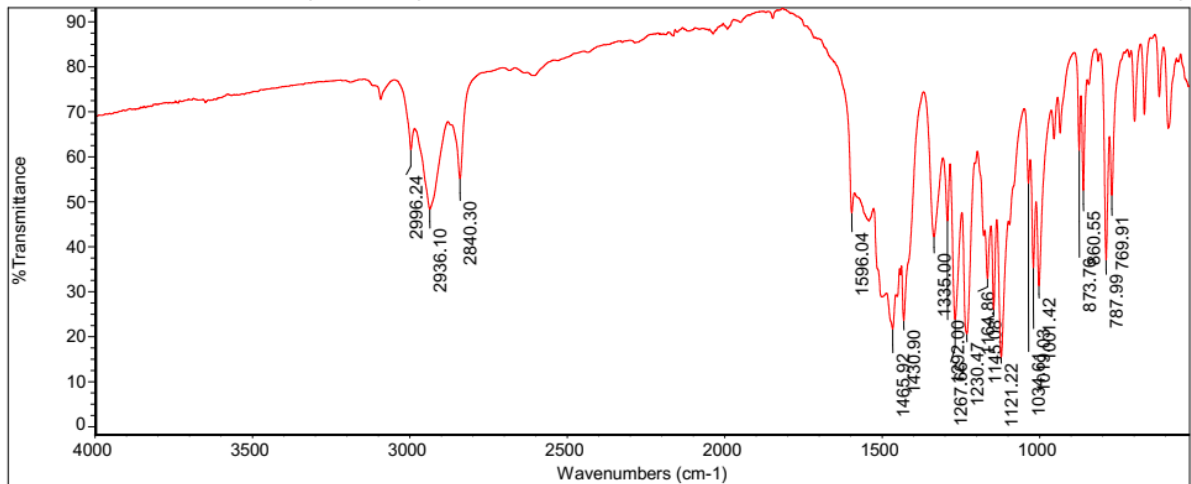


JMOD C13 NMR Spectrum of BDKT-08 in CDCL3+TMS
 C13_APT CDC13 {C:\Bruker\TOPSPIN} SAS 6



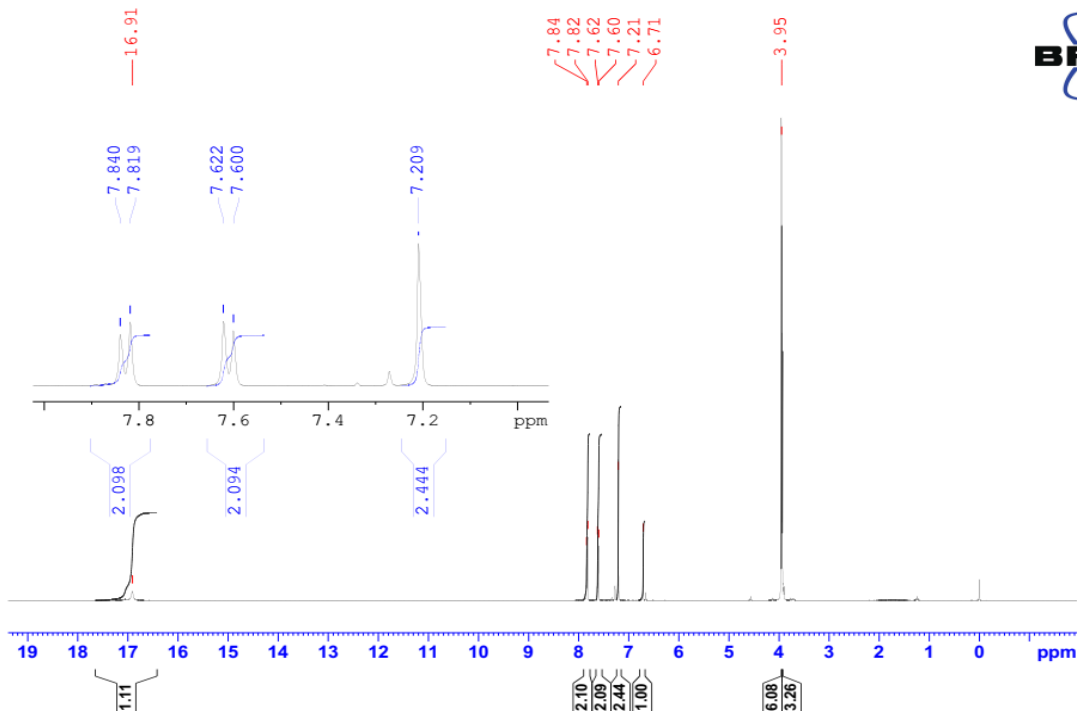
Title: Thu Jan 21 12:17:31 2021 (GMT+00:00):BDKT-08

Thu Jan 20 09:55:17 2022 (C



BDKT-13

H1 NMR Spectrum of BDKT-13 in CDCL3+TMS



```

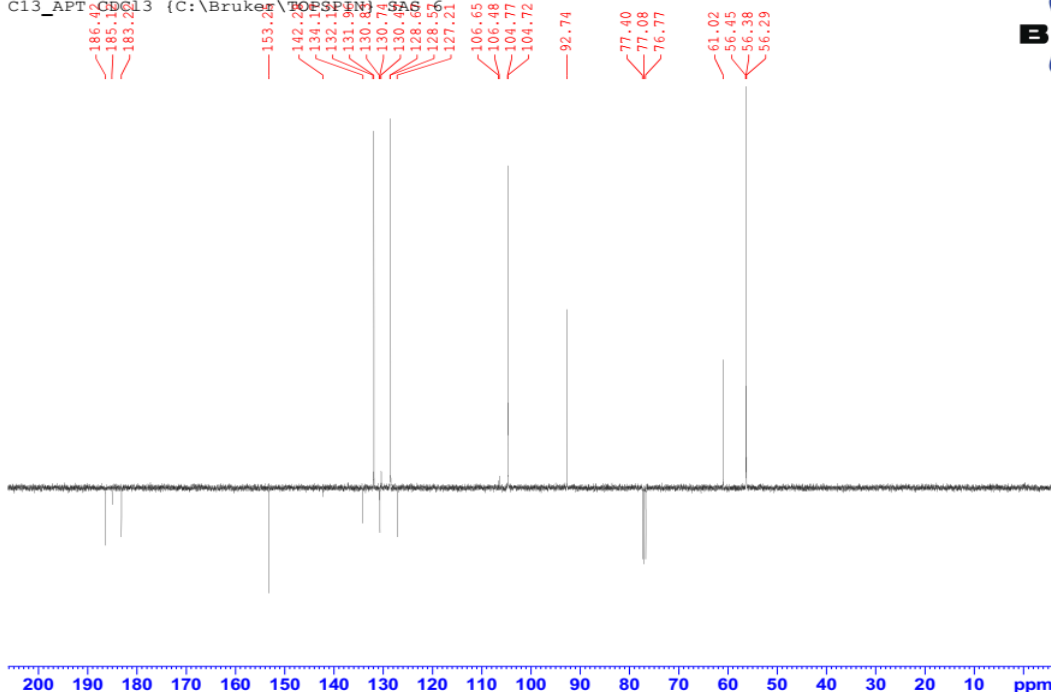
Current Data Parameters
NAME      SAS_BDKT13
EXPNO     20
PROCNO    1

F2 - Acquisition Parameters
Date_     20210123
Time      10.53
INSTRUM   spect
PROBHD    5 mm BBO BB-1H
PULPROG   zg30
TD         66290
SOLVENT   CDCL3
NS         64
DS         4
SWH        8802.81 Hz
FIDRES    0.156383 Hz
AQ         3.197271 sec
RG         71.8
SW         56.800 usec
DE         6.50 usec
TE         298.2 K
D1         2.59999990 sec
TD0        1

----- CHANNEL f1 -----
NUC1       1H
P1         10.00 usec
PL1        -2.00 dB
SFO1       400.1333626 MHz

F2 - Processing parameters
SI         65516
SF         400.1300051 MHz
WDW        EM
SSB        0
LB         0.30 Hz
GB         0
PC         1.00
    
```

JMOD C13 NMR Spectrum of BDKT-13 in CDCL3
 C13_APT CDCL3 {C:\Bruker\TOPSPIN\SAS 6



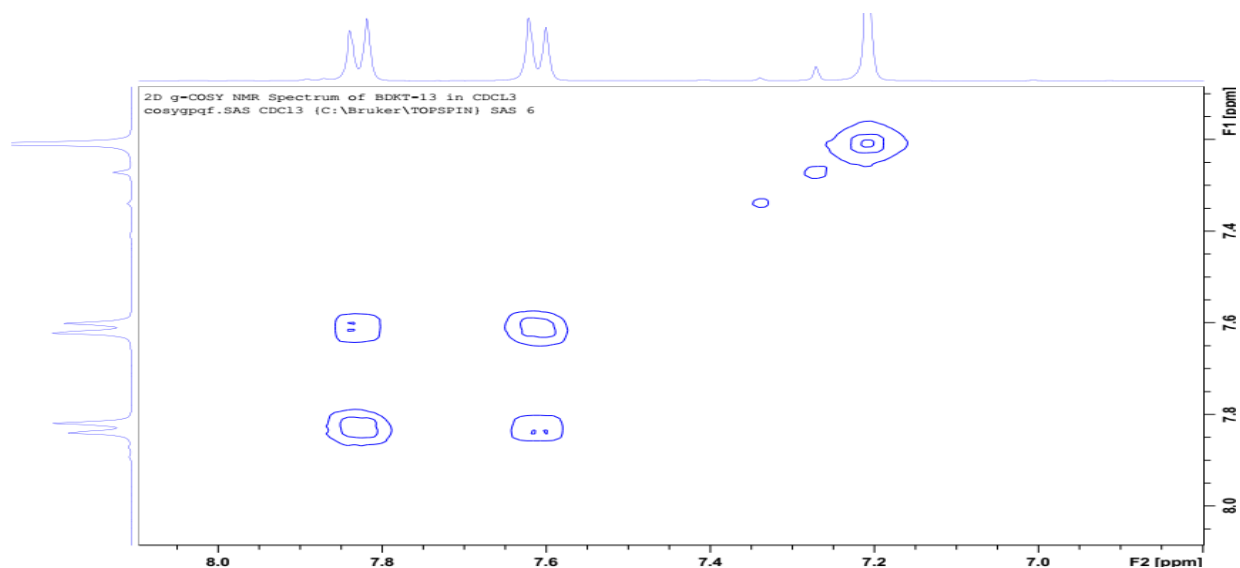
```

Current Data Parameters
NAME      SAS_BDKT13
EXPNO     23
PROCNO    1

F2 - Acquisition Parameters
Date_     20210125
Time      16.33
INSTRUM   spect
PROBHD    5 mm BBO BB-1H
PULPROG   jmod
TD         65516
SOLVENT   CDCL3
NS         1024
DS         4
SWH        23980.814 Hz
FIDRES    0.363918 Hz
AQ         1.364236 sec
RG         14384
SW         20.800 usec
DE         6.50 usec
TE         298.2 K
CHST2     145.0000000
NUC1       13C
P1         9.00 usec
PL1        -18.00 dB
SFO1       100.6228298 MHz

----- CHANNEL f2 -----
CPDPRG2   waltz16
NUC2       1H
PCPD2     80.00 usec
PL2       -2.00 dB
PL12      15.98 dB
SFO2       400.1314005 MHz

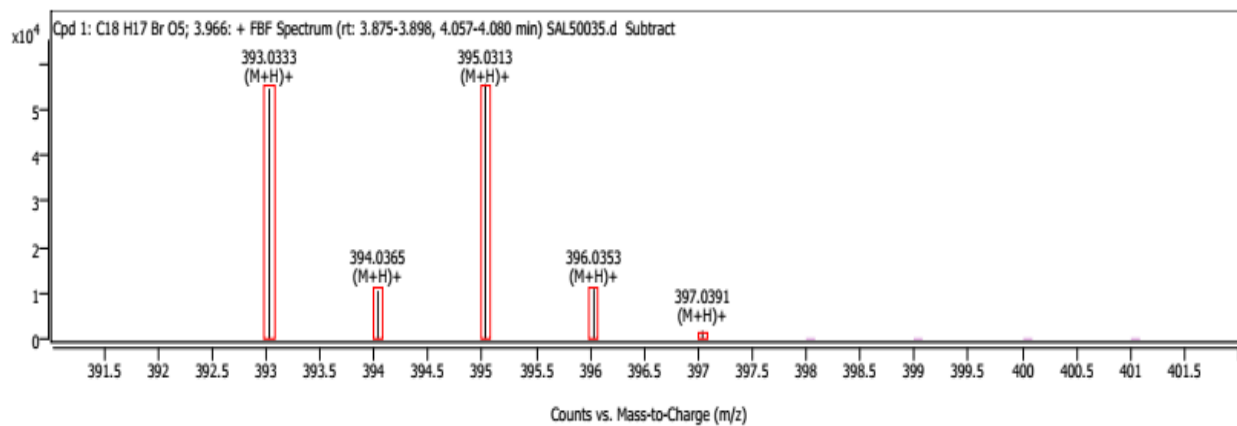
F2 - Processing parameters
SI         65516
SF         100.6127775 MHz
WDW        EM
SSB        0
LB         1.00 Hz
GB         0
PC         1.20
    
```



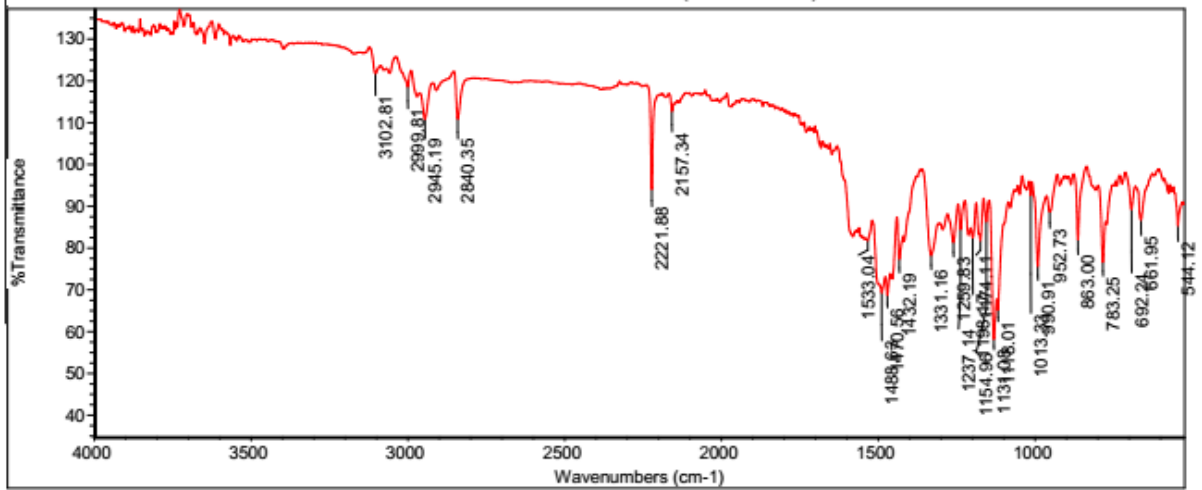
Spectrum Peaks

m/z	Z	Abund	Diff (ppm)	Height %	Height % (Calc)	Ion Species	Formula
393.0333	1	54484	0.16	98.15	99.83	(M+H) ⁺	C ₁₈ H ₁₇ BrO ₅
394.0365	1	10468	-0.20	18.86	19.83	(M+H) ⁺	C ₁₈ H ₁₇ BrO ₅
395.0313	1	55511	-0.22	100.00	100.00	(M+H) ⁺	C ₁₈ H ₁₇ BrO ₅
396.0353	1	10922	1.49	19.68	19.61	(M+H) ⁺	C ₁₈ H ₁₇ BrO ₅
397.0391	1	1772	4.92	3.19	2.84	(M+H) ⁺	C ₁₈ H ₁₇ BrO ₅

Compound Spectra



Fri Jan 22 12:00:34 2021 (GMT+00:00):BDKT-15



N15IG.SAS CDC13 {C:\Bruker\TOPSPIN} SAS 6

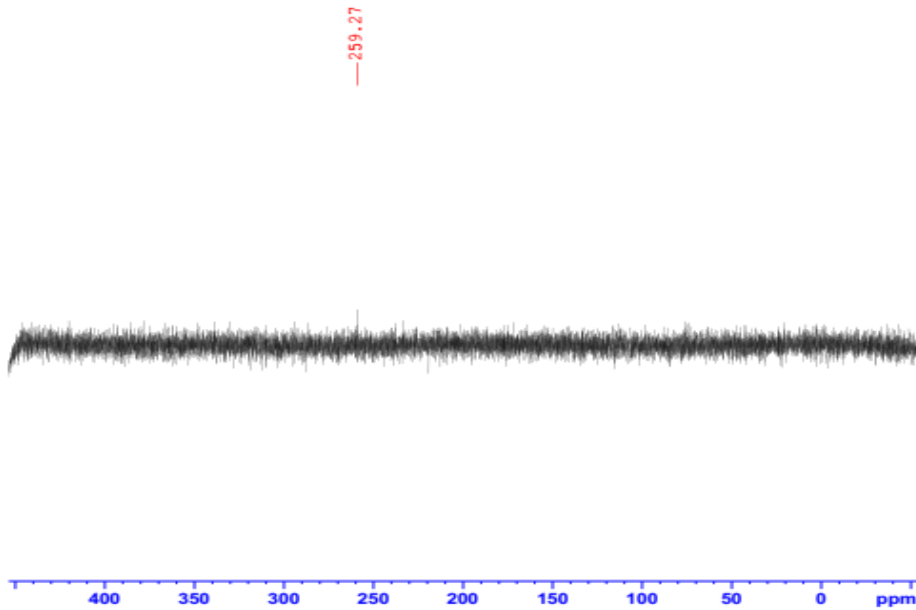


```

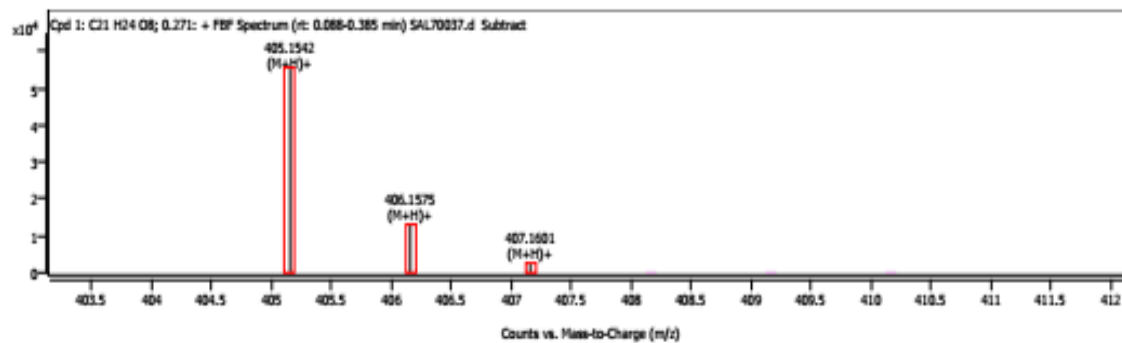
Current Data Parameters
NAME          BDKT-15
EXPNO        31
PROCNO       1

F2 - Acquisition Parameters
Date_        20210515
Time         15.31 h
INSTRUM      spect
PROBHD       2114607_0886 (
PULPROG      zgpg
TD           32768
SOLVENT      CDCl3
NS           9296
DS           4
SFR          30864.197 Hz
FIDRES       1.883801 Hz
AQ           0.5308416 sec
EC           64
DM           16.200 usec
DE           6.50 usec
TE           298.0 K
D1           10.00000000 sec
D11          0.03000000 sec
TD0          1
SFO1         60.8268606 MHz
NUC1         15N
P1           18.00 usec
PLW1         138.9799571 W
SFO2         600.1724007 MHz
NUC2         1H
CPDPRG2      waltz16
PCPD2       70.00 usec
PLW2         24.58099937 W
PLW12        0.50164998 W

F2 - Processing parameters
SI           16384
SF           60.8146980 MHz
WDW          EM
SSB          0
LB           0.25 Hz
GB           0
PC           1.00
    
```



Compound Spectra

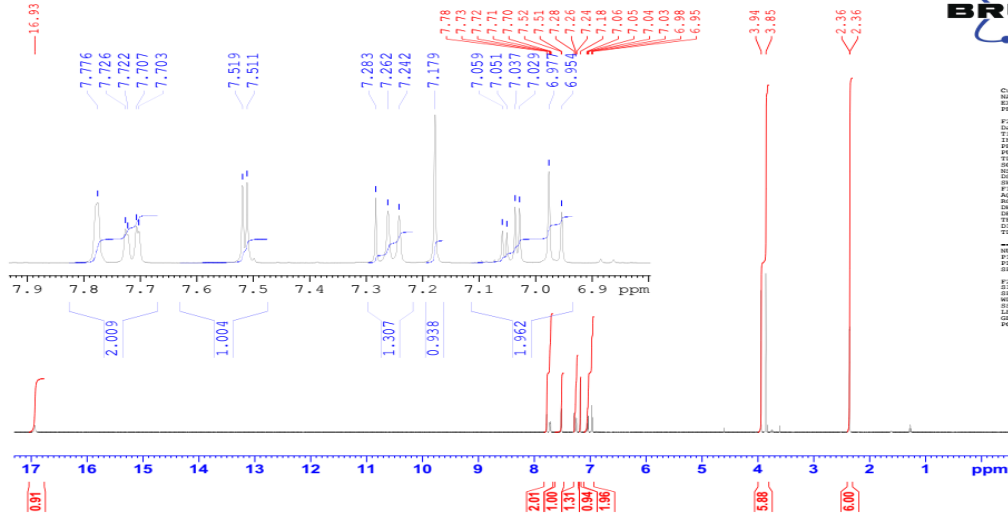


Spectrum Peaks

m/z	m/z (Calc)	Diff (ppm)	Abund	Height %	Height % (Calc)	Ion Species	Z
405.1542	405.1544	-0.53	55280	100.00	100.00	(M+H)+	1
406.1575	406.1578	-0.61	12949	23.42	23.31	(M+H)+	1
407.1601	407.1602	-0.16	2371	4.29	4.24	(M+H)+	1

BDKT-16

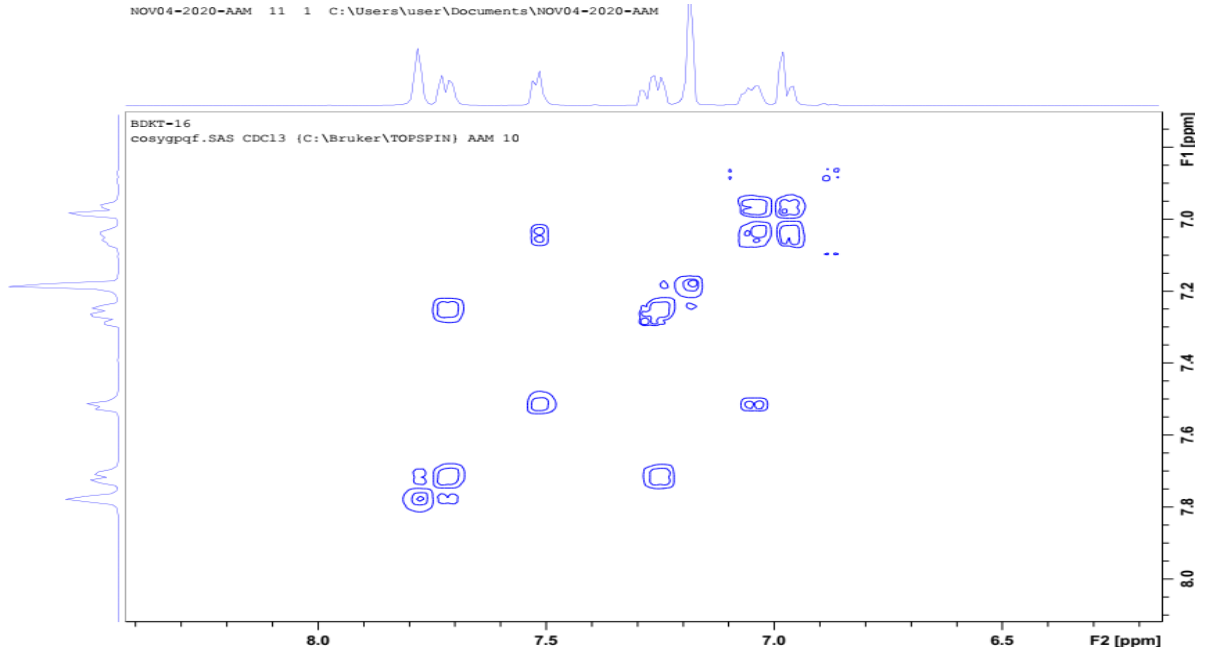
BDKT-16
 PROTON64 CDC13 (C:\Bruker\TOPSPIN) AAM 10



```

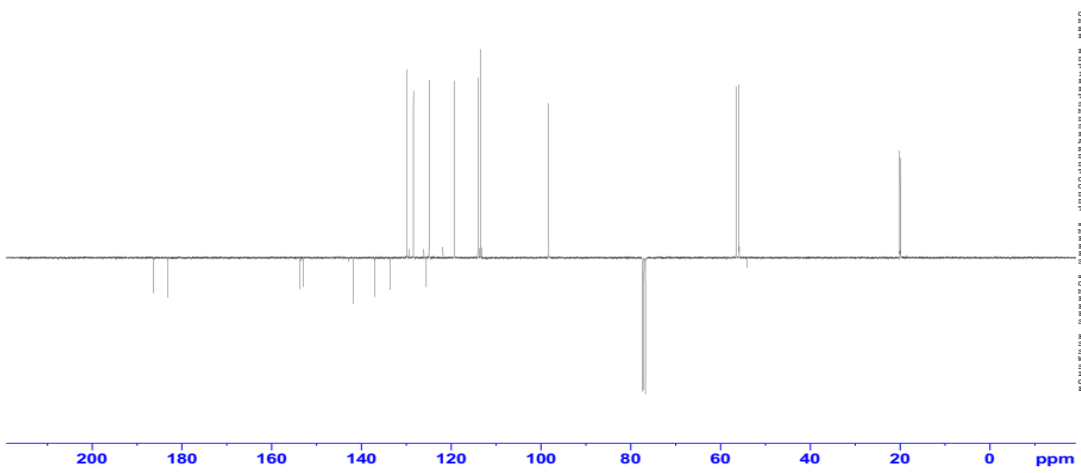
Current Data Parameters
NAME      NOV04-2020-AAM
EXPNO    10
PROCNO   1
-----
F2 - Acquisition Parameters
Date_    2021105
Time     14.54
INSTRUM  spect
PROBHD   5 mm BBO
PULPROG  zgpg30
TD       65536
SOLVENT  CDCl3
DS       4
SWH      8802.617 Hz
FIDRES   0.184333 Hz
AQ       3.197721 sec
RG       328.11
SI       36.400
DE       2.50
TE       300.2 K
DQ       2.59999792 sec
-----
CHANNEL f1
NUC1     13C
P1       15.00 usec
PL1     0.00 dB
SFO     400.133204 MHz
-----
F2 - Processing parameters
SI       36.400
SF       400.1300000 MHz
WDW      EM
SSB      0
LB       0.30 Hz
GB       0.0
PC       1.00
    
```

NOV04-2020-AAM 11 1 C:\Users\user\Documents\NOV04-2020-AAM



APT-NMR BDKT-16 in CDCl3
 C13_APT CDCl3 {C:\Bruker\TOPSPIN} AAM 10

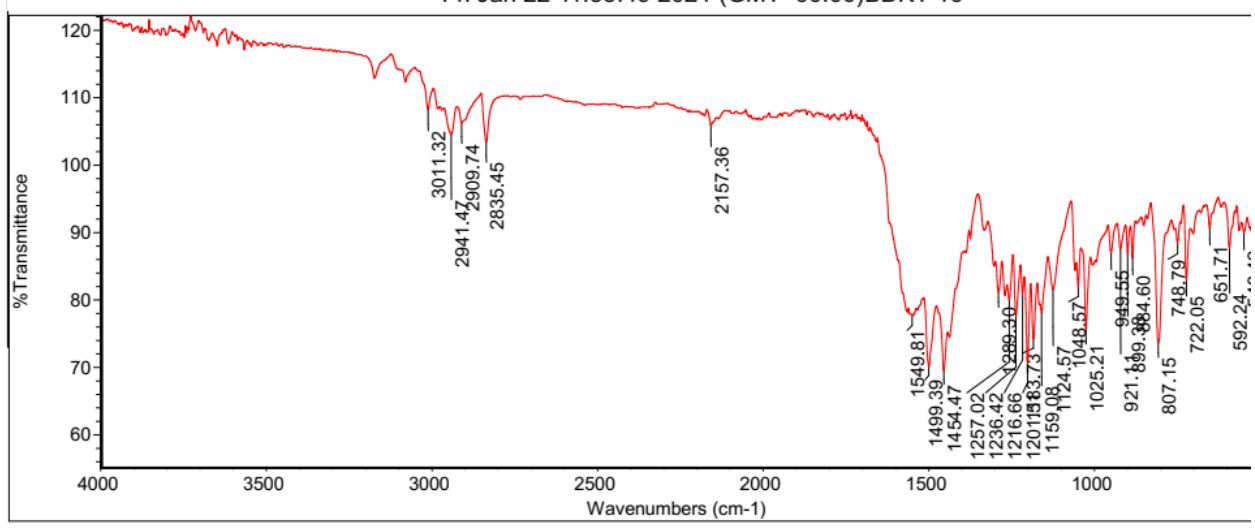
186.34
 183.15
 153.63
 153.58
 152.89
 142.96
 141.79
 136.97
 133.57
 129.88
 129.33
 128.41
 126.07
 125.52
 124.91
 121.81
 119.25
 114.04
 113.75
 113.41
 113.16
 98.26
 77.36
 77.04
 76.72
 56.52
 55.86
 55.78
 54.15
 20.08
 20.03
 19.90
 19.84



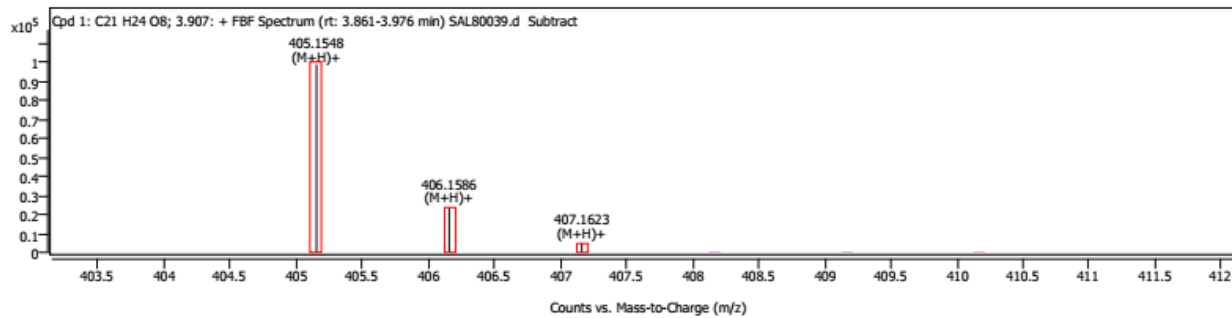
ThermoFisher
 SCIENTIFIC

Tue Dec 14 18:22:51 2021 (

Fri Jan 22 11:55:49 2021 (GMT+00:00)BDKT-16



Compound Spectra

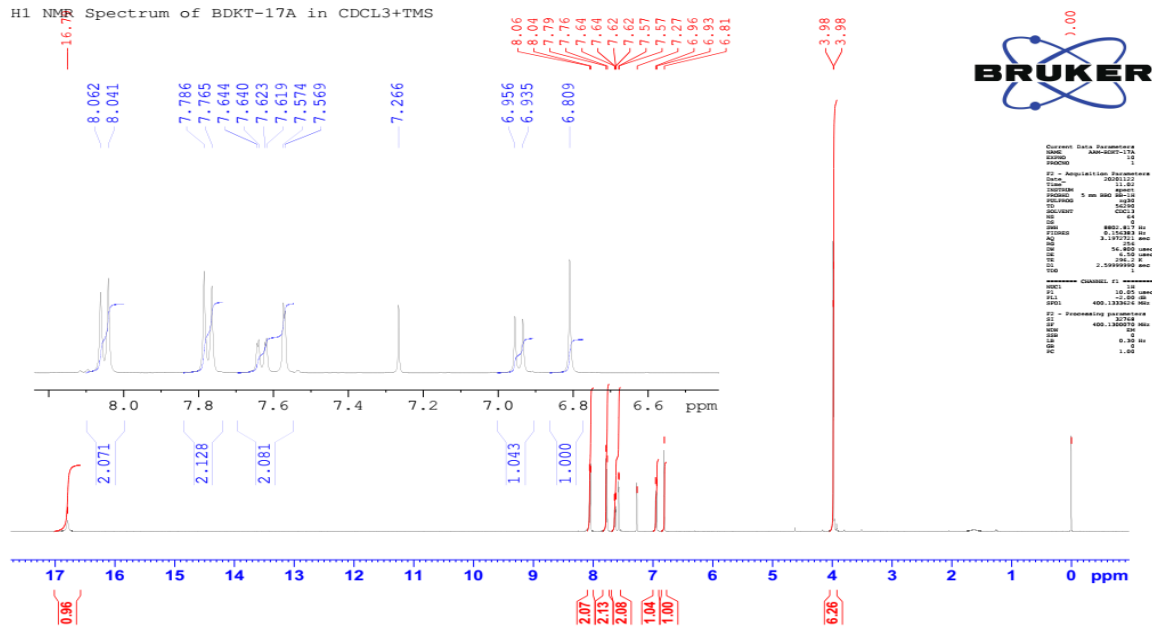


Spectrum Peaks

m/z	m/z (Calc)	Diff (ppm)	Abund	Height %	Height % (Calc)	Ion Species	Z
405.1548	405.1544	1.02	98874	100.00	100.00	(M+H)+	1
406.1586	406.1578	1.98	23462	23.73	23.31	(M+H)+	1
407.1623	407.1602	5.17	4960	5.02	4.24	(M+H)+	1

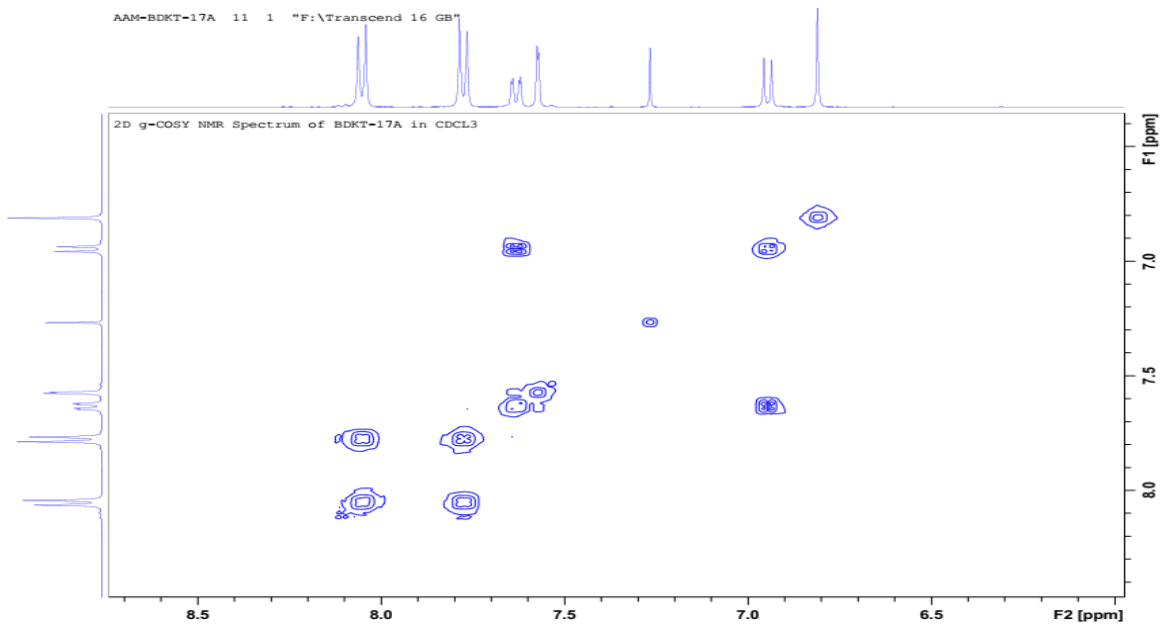
BDKT-17

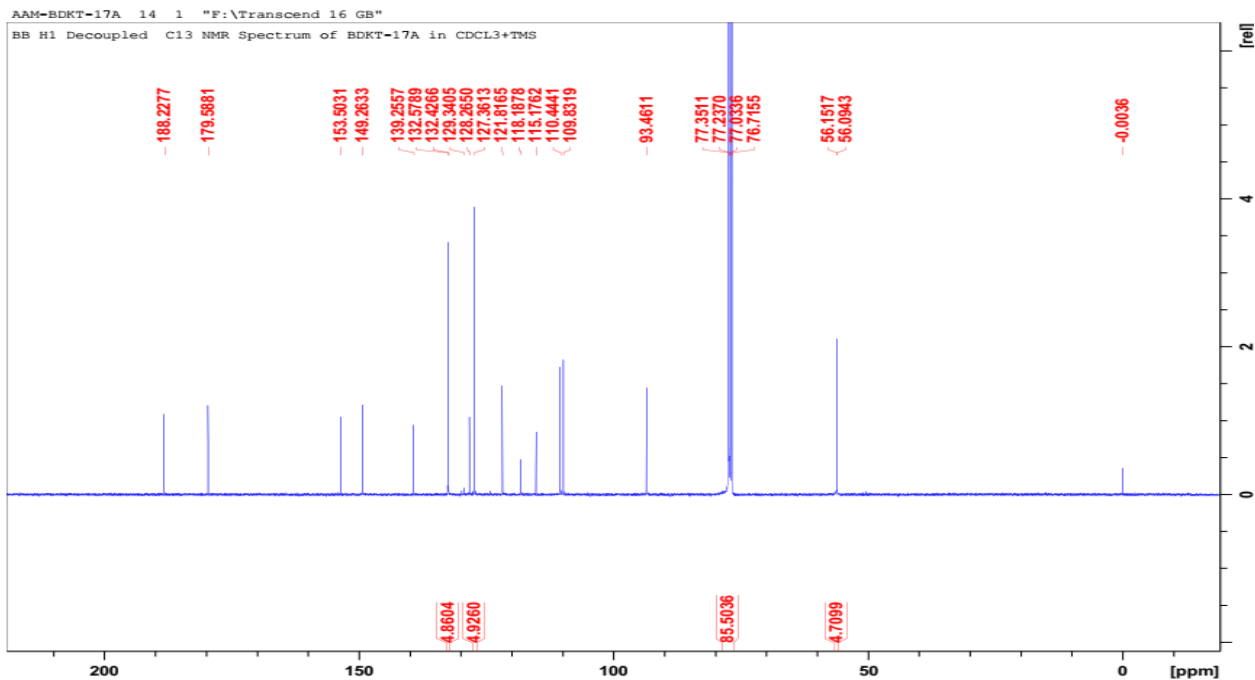
H1 NMR Spectrum of BDKT-17A in CDCL₃+TMS



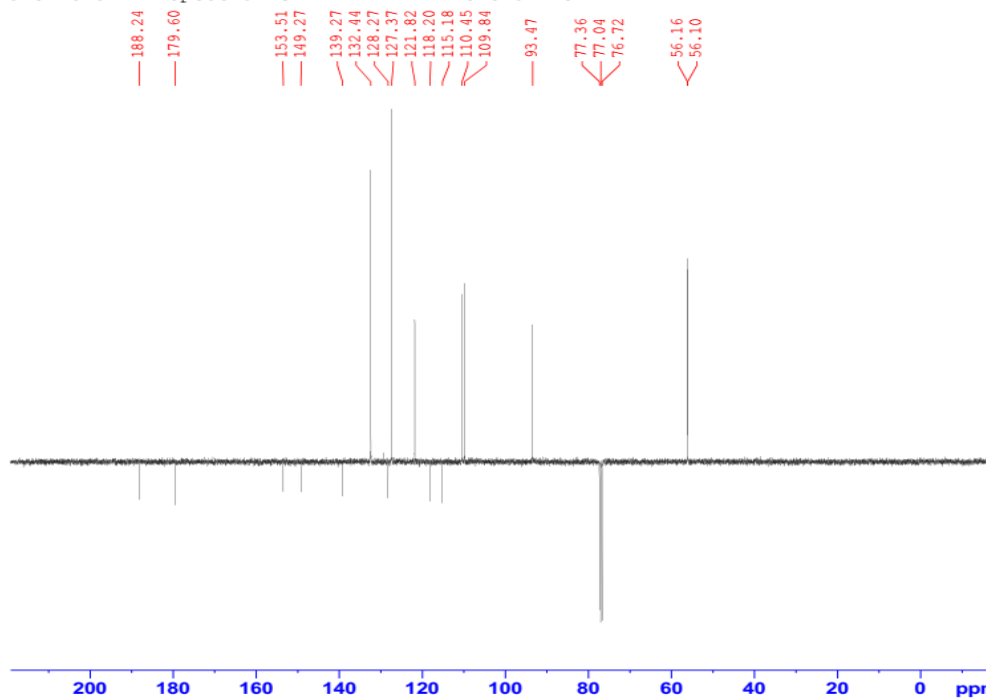
BRUKER

Current Data Parameters
 NAME: AAM-BDKT-17A
 EXPNO: 1
 PROCNO: 1
 F2 - Acquisition Parameters
 CHAN: 0001121
 DATE_: 11
 TIME: 11:01
 INSTRUM: spect
 PULPROG: zgpg30
 SFO: 500.136299 MHz
 AQ: 0.10000000
 SOLVENT: CDCl3
 NS: 640
 DS: 4
 SWH: 10.639 MHz
 FIDRES: 0.147694 Hz
 AQRES: 0.147694 Hz
 ALG: 3.147694 Hz
 RG: 640
 DWDW: 0.10000000
 SSB: 0
 BPC: 0
 SFO2: 7.54809992 MHz
 ===== CHANNEL f1 =====
 NAME: f1
 CHAN: 0001121
 DATE_: 11
 TIME: 11:01
 INSTRUM: spect
 PULPROG: zgpg30
 SFO: 500.136299 MHz
 AQ: 0.10000000
 SOLVENT: CDCl3
 NS: 640
 DS: 4
 SWH: 10.639 MHz
 FIDRES: 0.147694 Hz
 AQRES: 0.147694 Hz
 ALG: 3.147694 Hz
 RG: 640
 DWDW: 0.10000000
 SSB: 0
 BPC: 0
 SFO2: 7.54809992 MHz





JMOD C13 NMR Spectrum of BDKT-17A in CDCL3+TMS



Current Data Parameters
 NAME AAM-BDKT-17A
 EXFNO 13
 PROCNO 1

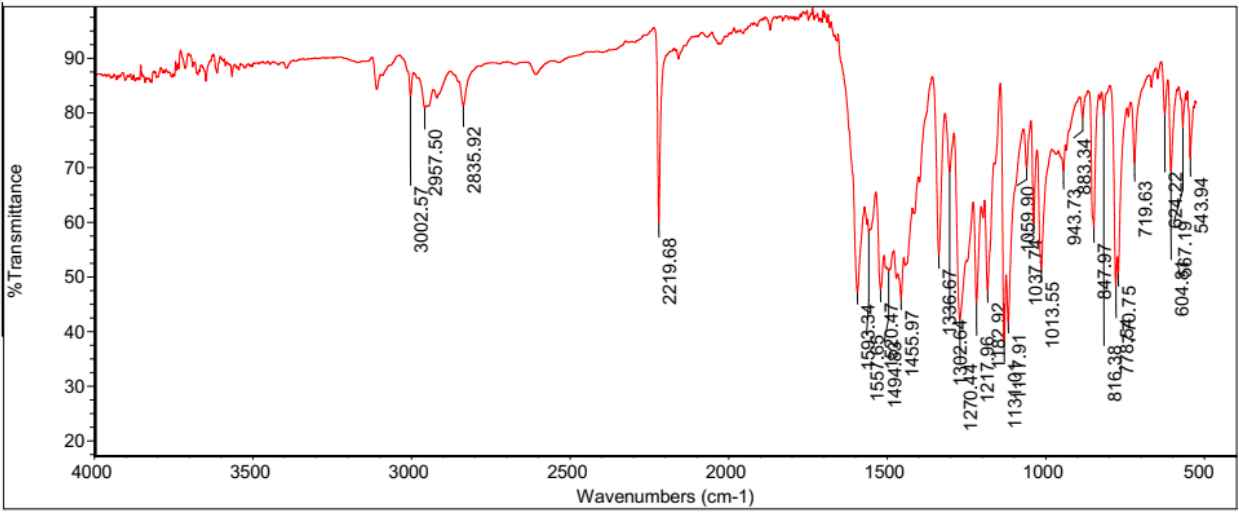
F2 - Acquisition Parameters
 Date 20201122
 Time 12.32
 INSTRUM spect
 PROBHD 5 mm BBO BB-1H
 PULPROG jmod
 TD 65536
 SOLVENT CDCL3
 NS 824
 DS 4
 SWH 23980.814 Hz
 FIDRES 0.365918 Hz
 AQ 1.3664256 sec
 RG 16384
 DW 20.850 usec
 DE 6.50 usec
 TE 296.2 K
 CNST2 145.000000
 CNST11 1.000000
 D1 2.0000000 sec
 D20 0.00689655 sec
 TDO 1

===== CHANNEL f1 =====
 NUC1 13C
 P1 9.00 usec
 P2 18.00 usec
 PL1 6.60 dB
 SFO1 100.6228298 MHz

===== CHANNEL f2 =====
 CPDPRG2 waltz16
 NUC2 1H
 PCPD2 80.00 usec
 PL2 -2.00 dB
 PL12 15.98 dB
 SFO2 400.1316005 MHz

F2 - Processing parameters
 SI 32768
 SF 100.6127690 MHz
 WDW EM
 SSB 0
 LB 1.00 Hz
 GB 0
 PC 4.00

Fri Jan 22 12:05:23 2021 (GMT+00:00):BDKT-17



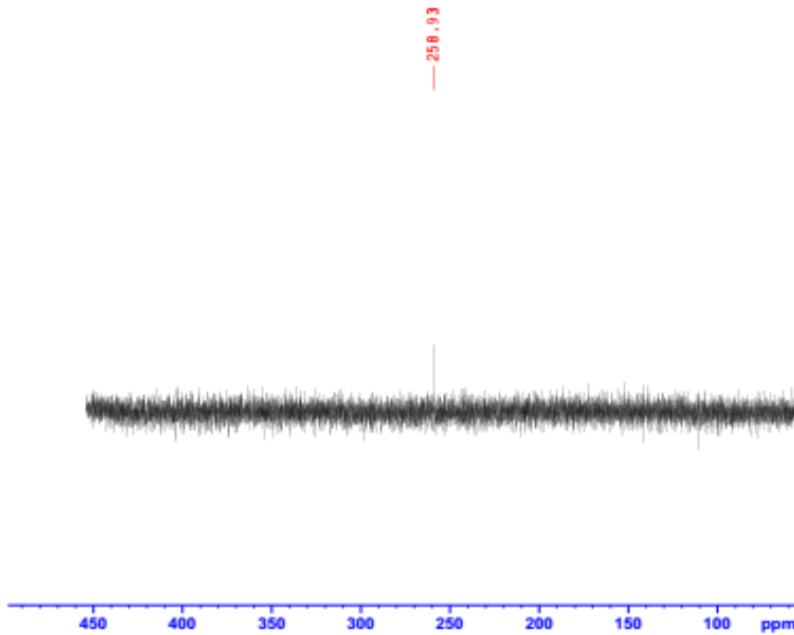
Inv Gated N15 NMR Spectrum of BDKT-17 in CDCl3
N15IG.SAS CDCl3 [C:\Bruker\TOPSPIN] SAS 7



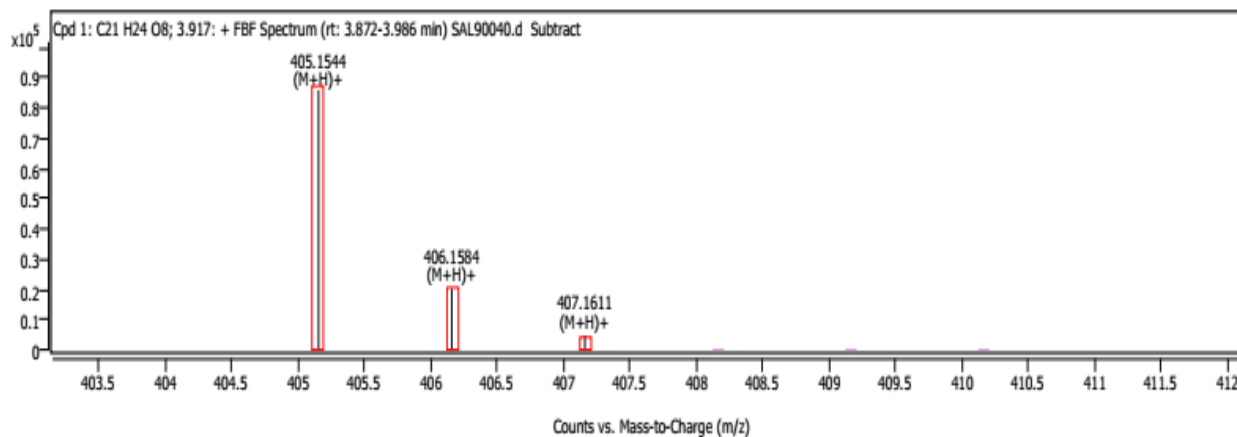
Current Data Parameters
NAME BDKT-17
EXPNO 31
PROCNO 1

F2 - Acquisition Parameters
Date_ 20210517
Time_ 19.17 h
INSTRUM spect
PROBHD 2114607 5mm E
PULPROG zgpg
TD 32768
SOLVENT CDCl3
NS 17468
DS 4
SWH 30964.197 Hz
FIDRES 1.883851 Hz
AQ 0.5308416 sec
RG 64
SW 14.250 usec
DE 6.50 usec
TE 298.0 K
DQ 10.0000000 sec
DD1 0.03000000 sec
TSD 1
SFO1 60.8248006 MHz
NUC1 15N
P2 18.50 usec
PLM1 138.07996573 W
SFO2 600.1724027 MHz
NUC2 1H
PCPD2 waltz16
PLM2 24.58099937 W
PLM12 0.50164998 W

F2 - Processing parameters
SI 16384
SF 60.8248006 MHz
WDW EM
SSB 0
LB 0.25 Hz
GB 0
PC 1.00



Compound Spectra

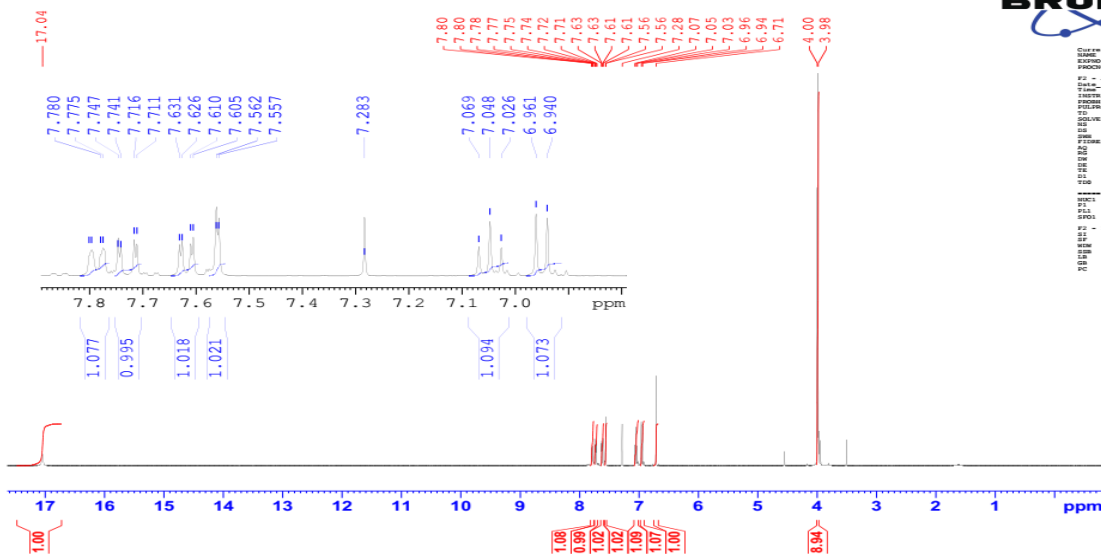


Spectrum Peaks

m/z	m/z (Calc)	Diff (ppm)	Abund	Height %	Height % (Calc)	Ion Species	Z
405.1544	405.1544	0.11	85936	100.00	100.00	(M+H)+	1
406.1584	406.1578	1.61	20202	23.51	23.31	(M+H)+	1
407.1611	407.1602	2.24	4703	5.47	4.24	(M+H)+	1

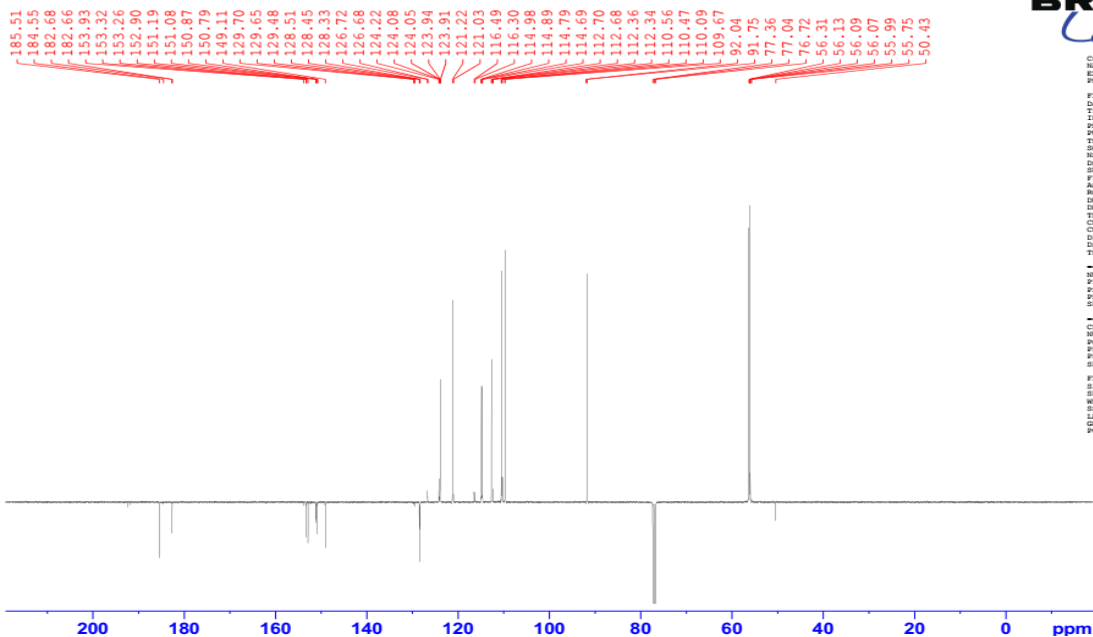
BDKT-19

¹H NMR BDKT-19
 PROTON64 CDCl3 (C:\Bruker\TOPSPIN) AAM 25

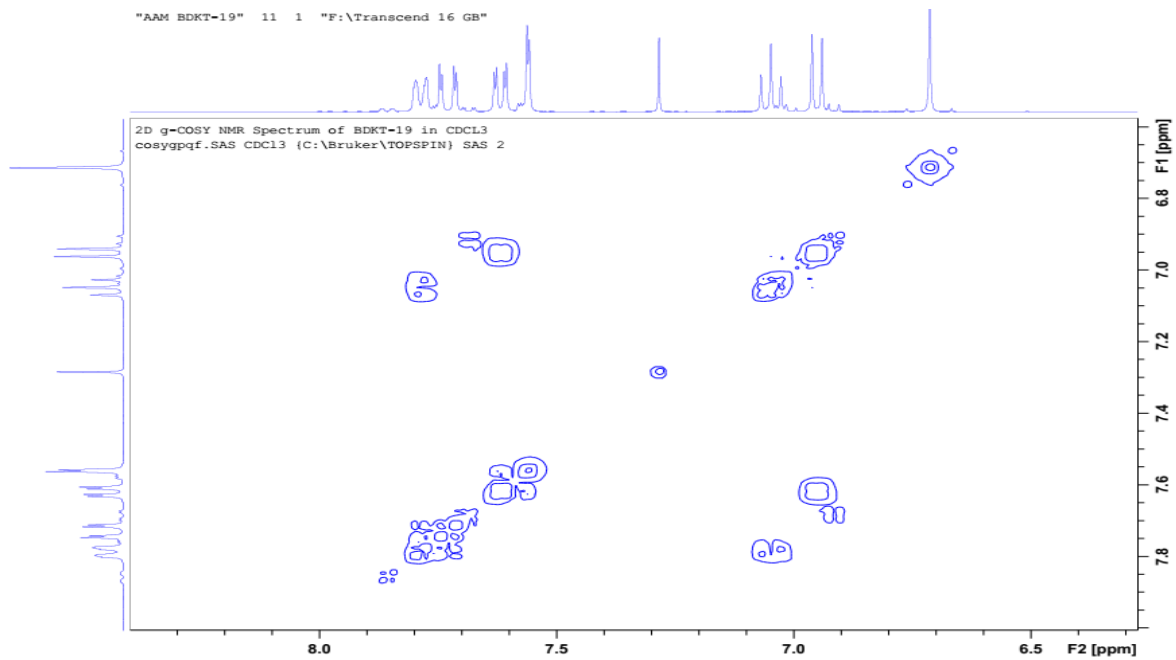


```
Current Data Parameters
NAME      20201129-184-400_8_11-09_1
EXPNO    10
PROCNO   10
F2 - Acquisition Parameters
Date_    20201129
Time     08:38
INSTRUM  spect
PROBHD   5 mm BBO BB1-1H
PULPROG  zgpg30
TD        65536
SOLVENT  CDCl3
NS        4
DS        4
SWH       23980.814 Hz
FIDRES   0.165918 Hz
AQ        1.3664256 sec
RG        14384
DE        20.850 usec
TE        296.2 K
CHFTF2   145.000000
D1        2.00000000 sec
D10       0.00696555 sec
TD0       5
===== CHANNEL f1 =====
NUC1      13C
P1         9.00 usec
P2         14.00 usec
PC1       2.60 dB
SFO1     100.6264208 MHz
===== CHANNEL f2 =====
CPOPRG12  waltz16
NUC2       1H
PCPD2     80.00 usec
PFL1      15.00 dB
PFL2      15.00 dB
SFO2     400.1314005 MHz
F2 - Processing parameters
SI         32768
SF        100.6127490 MHz
WDW        EM
SSB        0
LB         1.00 Hz
GB         0
PC         1.40
```

2D g-HMOC NMR Spectrum of BDKT-19 in CDCl3
 C13_APT CDCl3 (C:\Bruker\TOPSPIN) SAS 2



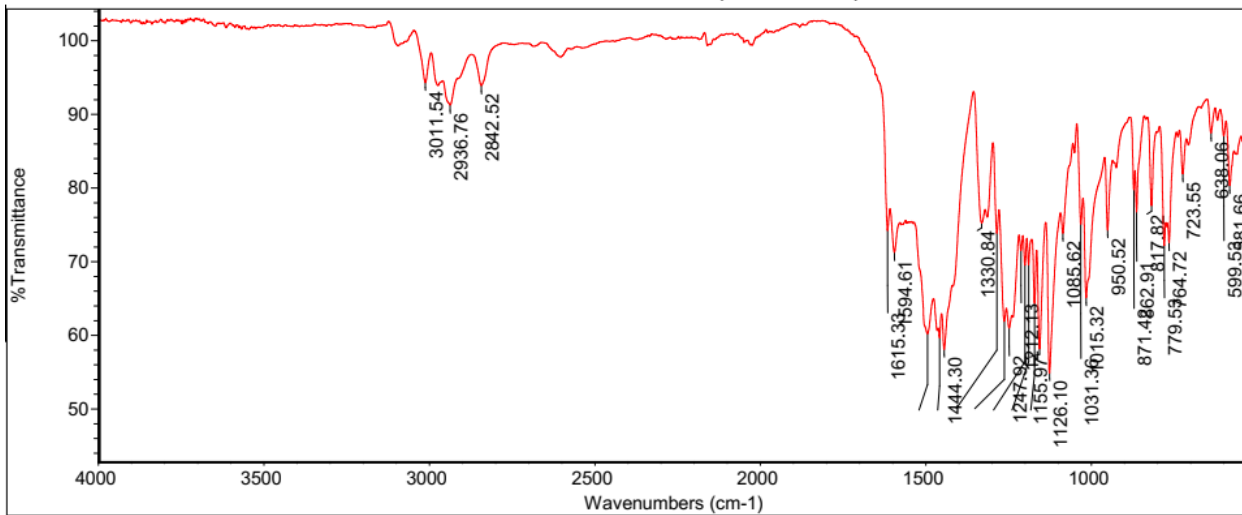
```
Current Data Parameters
NAME      AAM BDKT-19
EXPNO    13
PROCNO   13
F2 - Acquisition Parameters
Date_    20201129
Time     08:38
INSTRUM  spect
PROBHD   5 mm BBO BB1-1H
PULPROG  zgpg30
TD        65536
SOLVENT  CDCl3
NS        4
DS        4
SWH       23980.814 Hz
FIDRES   0.165918 Hz
AQ        1.3664256 sec
RG        14384
DE        20.850 usec
TE        296.2 K
CHFTF2   145.000000
D1        2.00000000 sec
D10       0.00696555 sec
TD0       5
===== CHANNEL f1 =====
NUC1      13C
P1         9.00 usec
P2         14.00 usec
PC1       2.60 dB
SFO1     100.6264208 MHz
===== CHANNEL f2 =====
CPOPRG12  waltz16
NUC2       1H
PCPD2     80.00 usec
PFL1      15.00 dB
PFL2      15.00 dB
SFO2     400.1314005 MHz
F2 - Processing parameters
SI         32768
SF        100.6127490 MHz
WDW        EM
SSB        0
LB         1.00 Hz
GB         0
PC         1.40
```



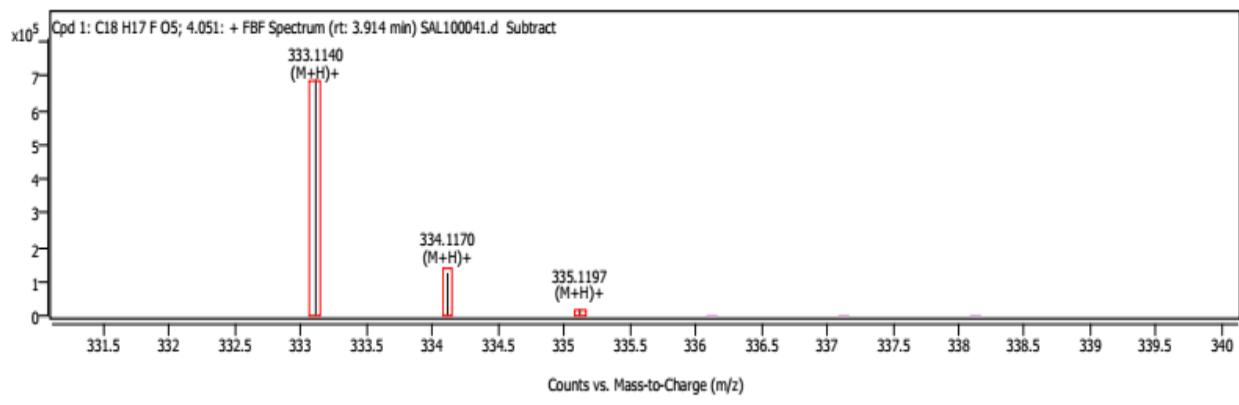
ThermoFisher
 SCIENTIFIC

Wed Dec 15 19:55:56 2021

Fri Jan 22 11:51:07 2021 (GMT+00:00):BDKT-19



Compound Spectra

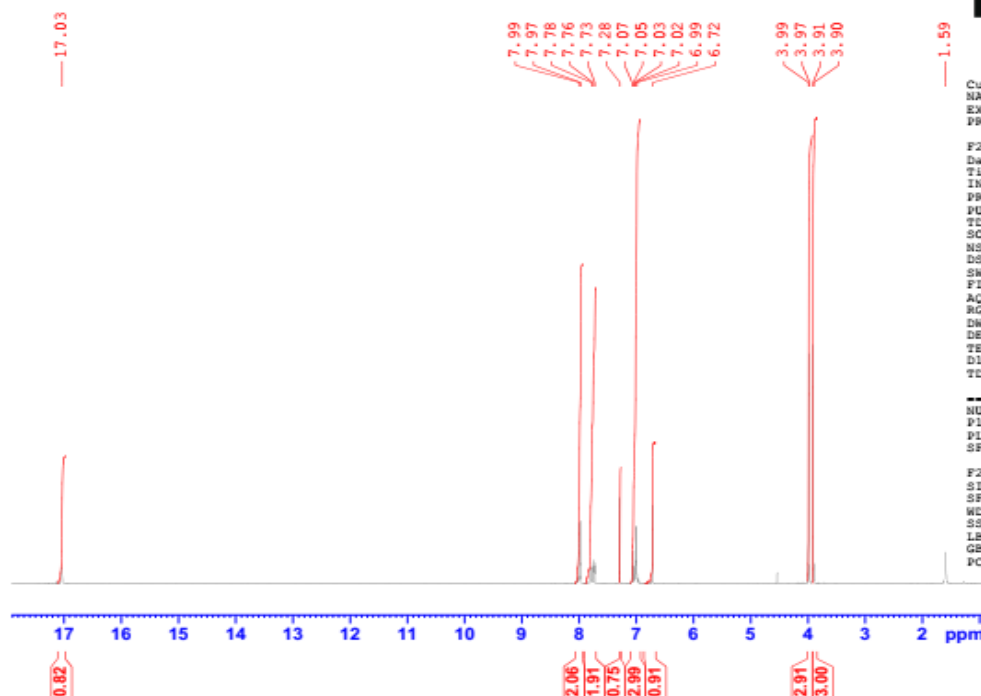


Spectrum Peaks

m/z	m/z (Calc)	Diff (ppm)	Abund	Height %	Height % (Calc)	Ion Species	Z
333.1140	333.1133	2.12	690123	100.00	100.00	(M+H)+	1
334.1170	334.1167	1.00	124999	18.11	19.87	(M+H)+	1
335.1197	335.1192	1.60	19477	2.82	2.90	(M+H)+	1

BDKT-20

1H-NMR BDKT-20 in CDC13
 PROTON64 CDC13 {C:\Bruker\TOPSPIN} AAM 25



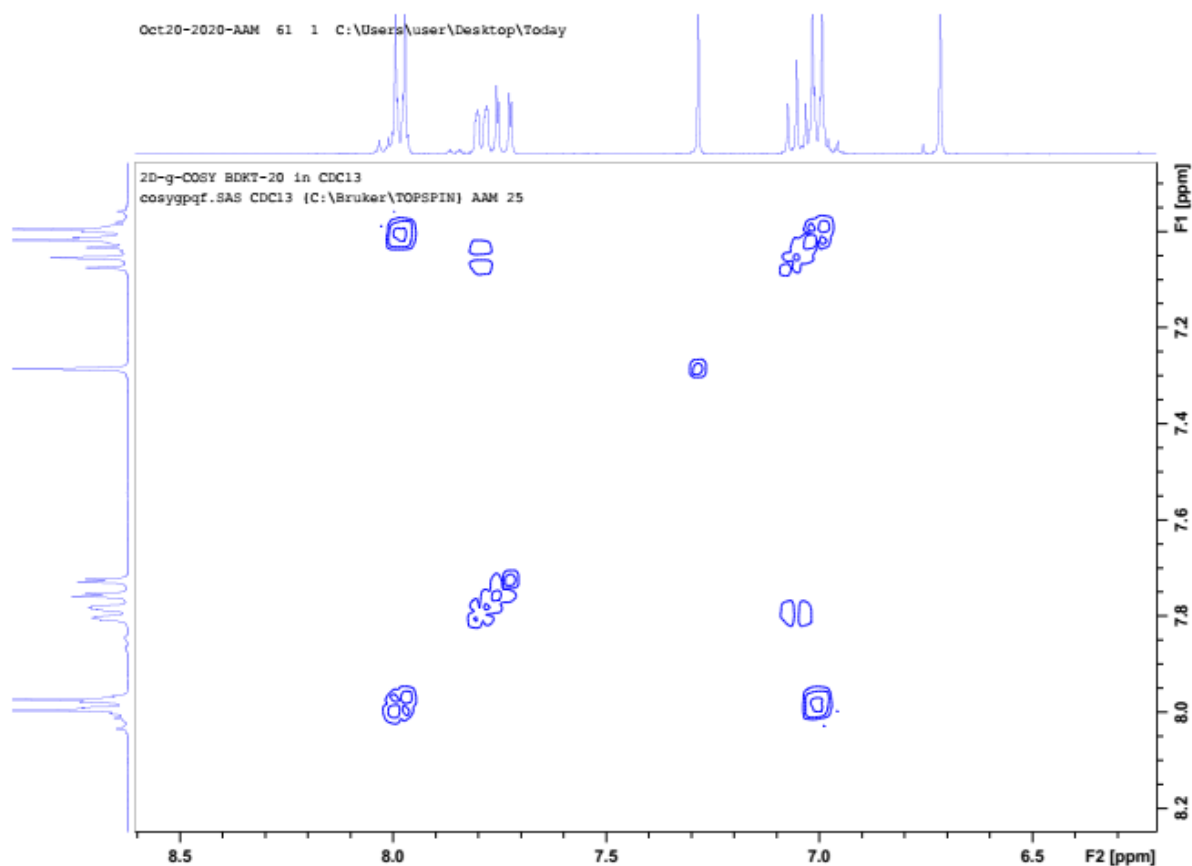
```

Current Data Parameters
NAME      Oct20-2020-AAM
EXPNO     60
PROCNO    1

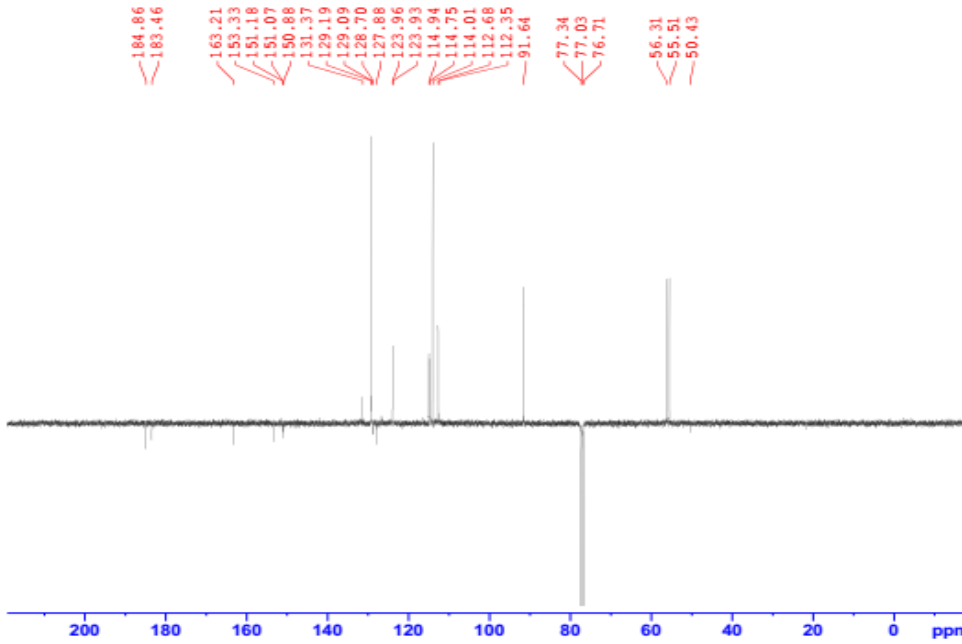
F2 - Acquisition Parameters
Date_     20201020
Time      16.53
INSTRUM   spect
PROBHD    5 mm BBO BB-1H
PULPROG   zg30
TD         56290
SOLVENT   CDC13
NS         64
DS         0
SWH        8802.817 Hz
FIDRES     0.156383 Hz
AQ         3.1972721 sec
RG         456.1
DM         56.800 usec
DE         6.50 usec
TE         296.2 K
D1         2.59999990 sec
TDD        1

----- CHANNEL f1 -----
NUC1       1H
P1         10.05 usec
PL1        -2.00 dB
SFO1       400.1333626 MHz

F2 - Processing parameters
SI         32768
SF         400.1300000 MHz
WDW        EM
SSB        0
LB         0.30 Hz
GB         0
PC         200.00
    
```



13C-APT BDKT-20 in CDCl3
 C13_APT CDC13 {C:\Bruker\TOPSPIN} AAM 25



Current Data Parameters
 NAME Oct20-2020-AAM
 EXPNO 64
 PROCNO 1

F2 - Acquisition Parameters
 Date_ 20201024
 Time_ 5.51
 INSTRUM spect
 PROBHD 5 mm BBO BB-1H
 PULPROG gmed
 TD 65536
 SOLVENT CDC13
 NS 6144
 DS 4
 SWH 23980.814 Hz
 FIDRES 0.365918 Hz
 AQ 1.3664256 sec
 RG 16384
 DW 20.850 usec
 DE 6.50 usec
 TE 296.2 K
 CHST2 145.0000000
 CHST1 1.0000000
 D1 2.0000000 sec
 D20 0.00689655 sec
 TD0 1

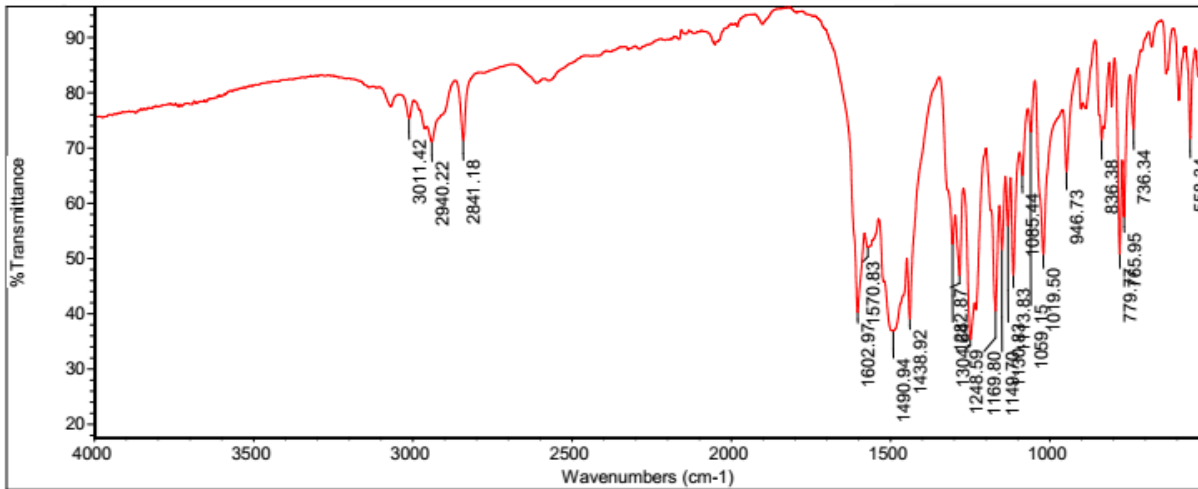
CHANNEL f1
 NUC1 13C
 P1 9.00 usec
 P2 18.00 usec
 PL1 6.60 dB
 SFO1 100.6228298 MHz

CHANNEL f2
 CPDPRG2 waltz16
 NUC2 1H
 PCPD2 80.00 usec
 PL2 -2.00 dB
 PL12 15.98 dB
 SFO2 400.1316005 MHz

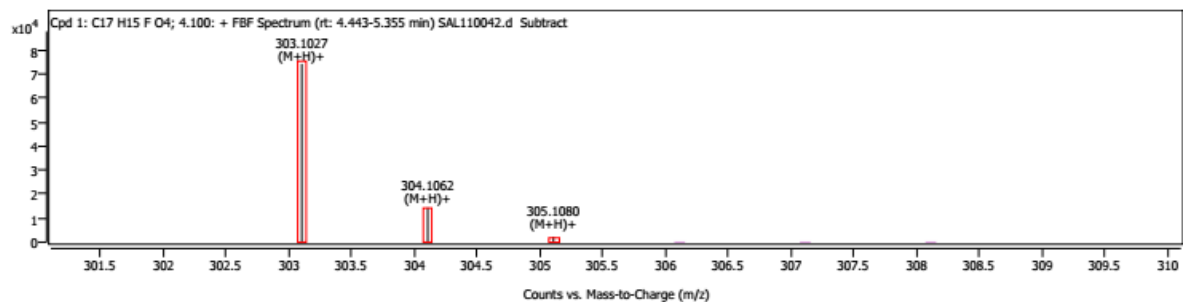
F2 - Processing parameters
 SI 32768
 SF 100.6127690 MHz
 NS 64
 SSB 0
 LB 1.00 Hz
 GB 0
 PC 1.40

Title: Thu Jan 21 12:25:21 2021 (GMT+00:00)BDKT-20

Thu Jan 20 09:27:11 2022 (C



Compound Spectra

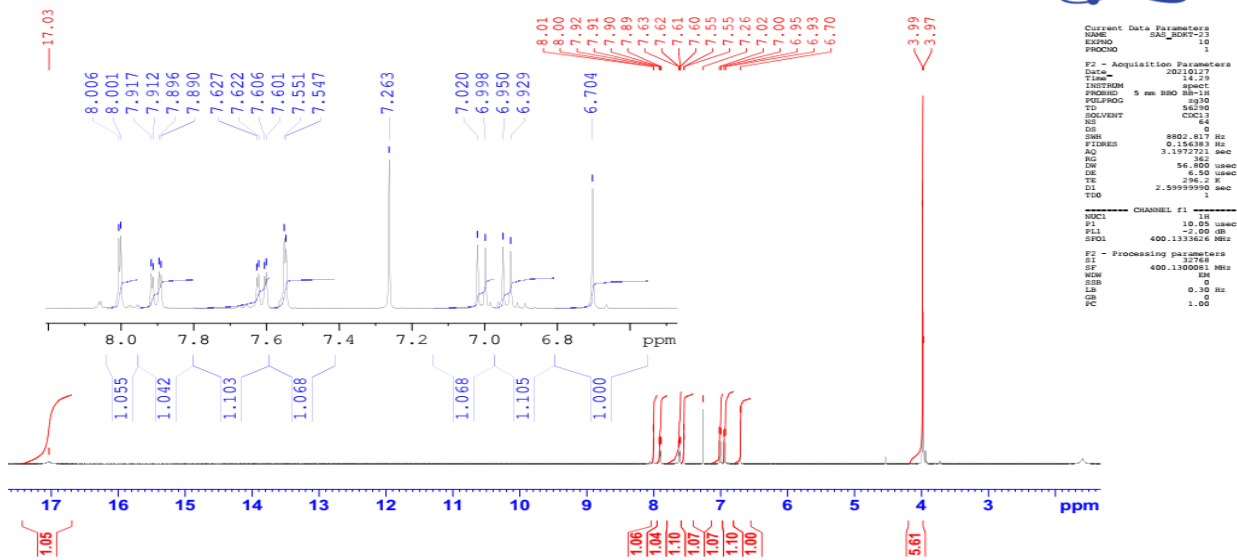


Spectrum Peaks

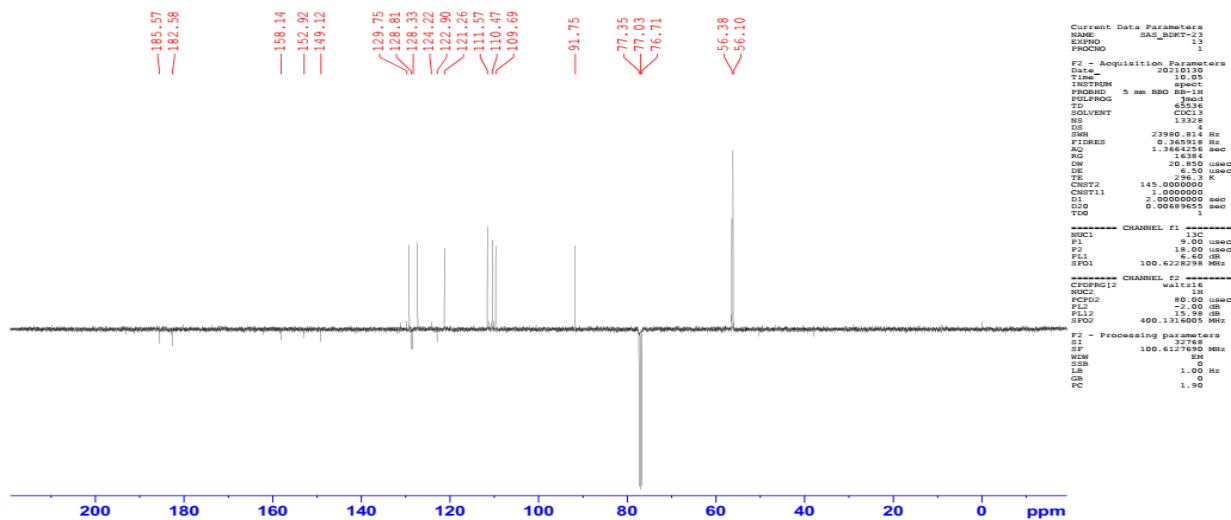
m/z	m/z (Calc)	Diff (ppm)	Abund	Height %	Height % (Calc)	Ion Species	Z
303.1027	303.1027	-0.01	74268	100.00	100.00	(M++)+	1
304.1062	304.1061	0.35	14362	19.34	18.72	(M++)+	1
305.1080	305.1087	-2.06	2232	3.01	2.48	(M++)+	1

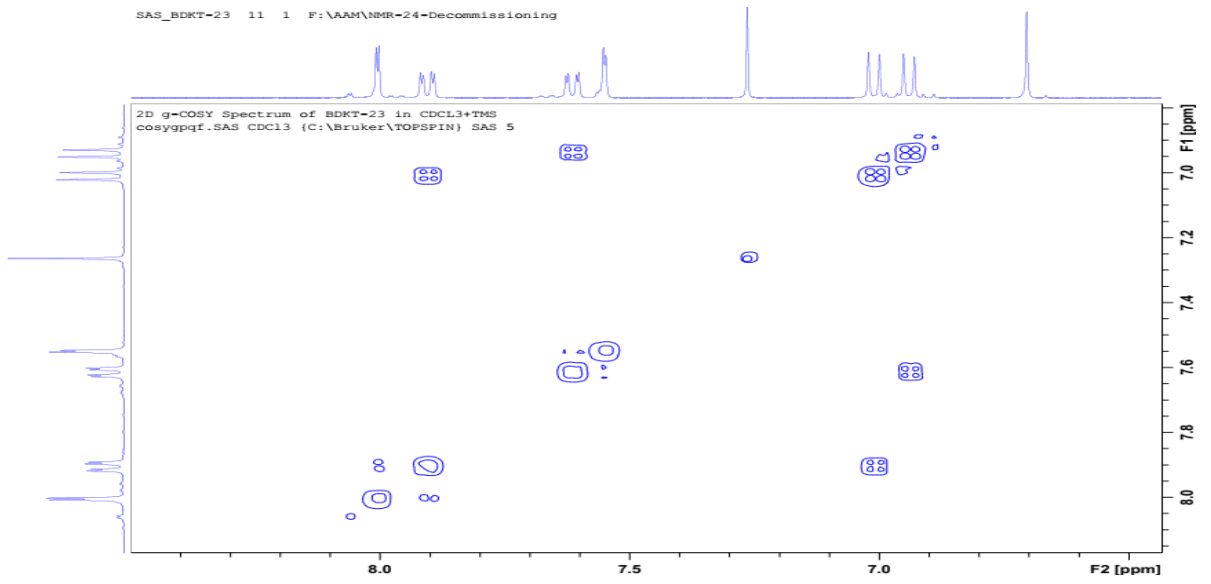
BDKT-23

H1 NMR Spectrum of BDKT-23 in CDCL3+TMS
 PROTON64 CDC13 {C:\Bruker\TOPSPIN} SAS 5



2D g-HMOC Spectrum of BDKT-23 in CDCL3+TMS
 C13_APT CDC13 {C:\Bruker\TOPSPIN} SAS 5

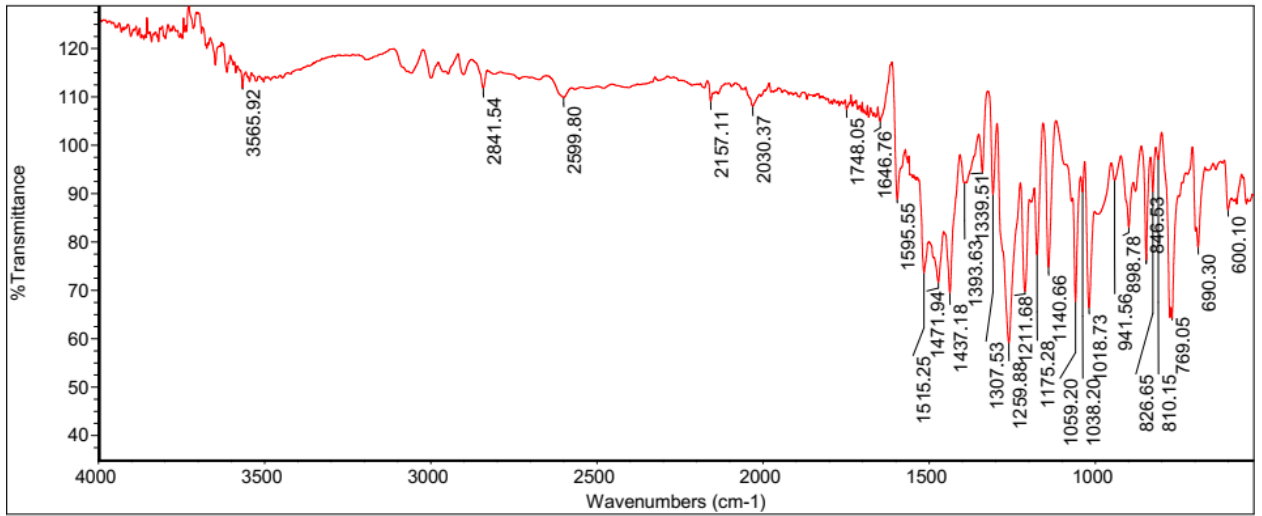




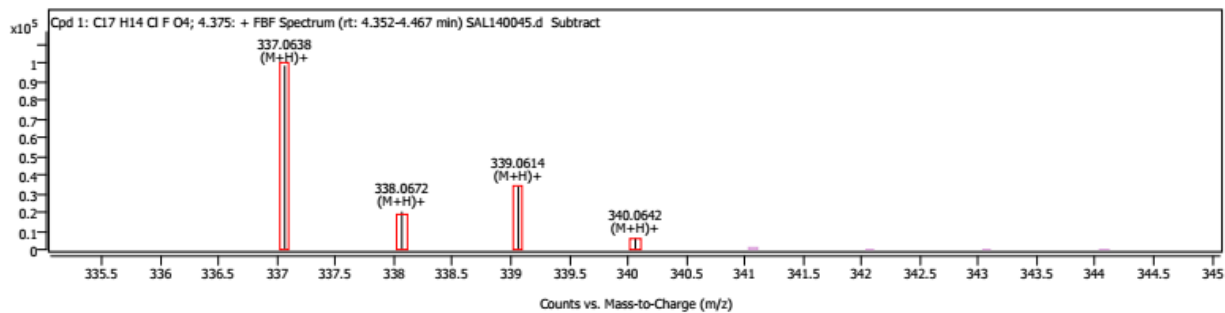
ThermoFisher
 SCIENTIFIC

Mon Dec 13 08:29:42 2021

BDKT-23



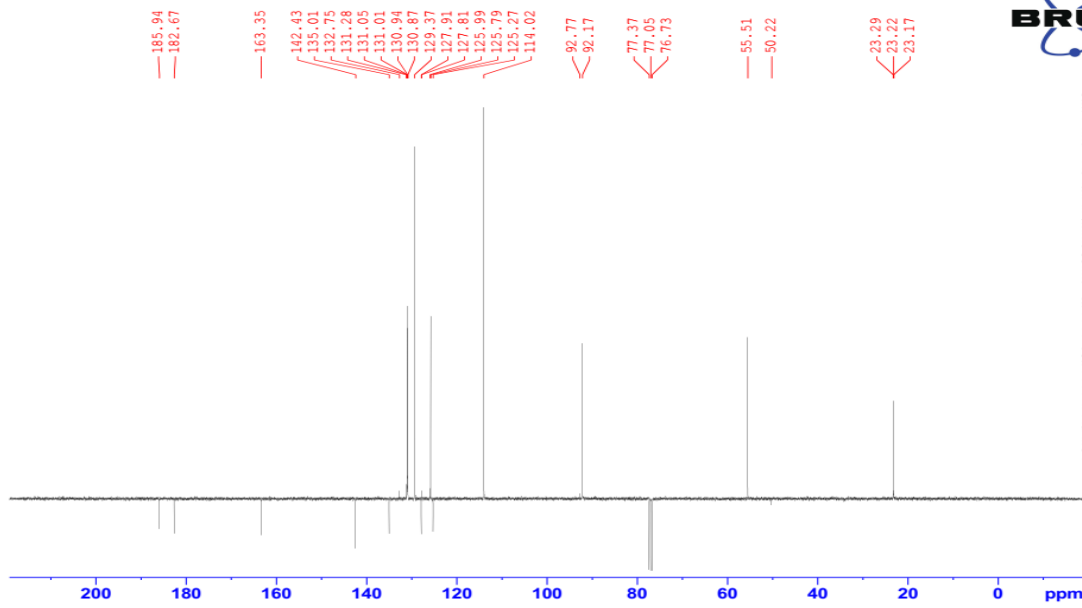
Compound Spectra



Spectrum Peaks

m/z	m/z (Calc)	Diff (ppm)	Abund	Height %	Height % (Calc)	Ion Species	Z
337.0638	337.0637	0.20	98682	100.00	100.00	(M+H)+	1
338.0672	338.0671	0.08	20428	20.70	18.71	(M+H)+	1
339.0614	339.0614	-0.22	33889	34.34	34.47	(M+H)+	1
340.0642	340.0645	-1.00	6053	6.13	6.23	(M+H)+	1

APT NMR BDKT-26 FULL SCAN
 C13_APT CDCl3 {C:\Bruker\TOPSPIN} AAM 8



```

Current Data Parameters
NAME      Cwd01-0020-26M
EXPNO    12
PROCNO   1

F2 - Acquisition Parameters
Date_    20210121
Time     18.25
INSTRUM  spect
PROBHD   5 mm BBO BB-1H
PULPROG  zgpg30
TD        65536
SOLVENT  CDCl3
NS        1024
DS        4
SWH       23982.814 Hz
FIDRES    0.365918 Hz
AQ        1.368256 sec
RG         64384
SI         20.550
SF         125.760 MHz
DE         8.50 usec
TE         296.2 K
CSTRT2    145.0000000
CH111     1.0000000
D1         2.0000000 sec
D2         0.0000000 sec
D3         0.0000000 sec
T00       1

----- CHANNEL f1 -----
NUC1       13C
P2         9.50 usec
PR         18.00 usec
PL1        6.40 dB
SFO1       100.6228298 MHz

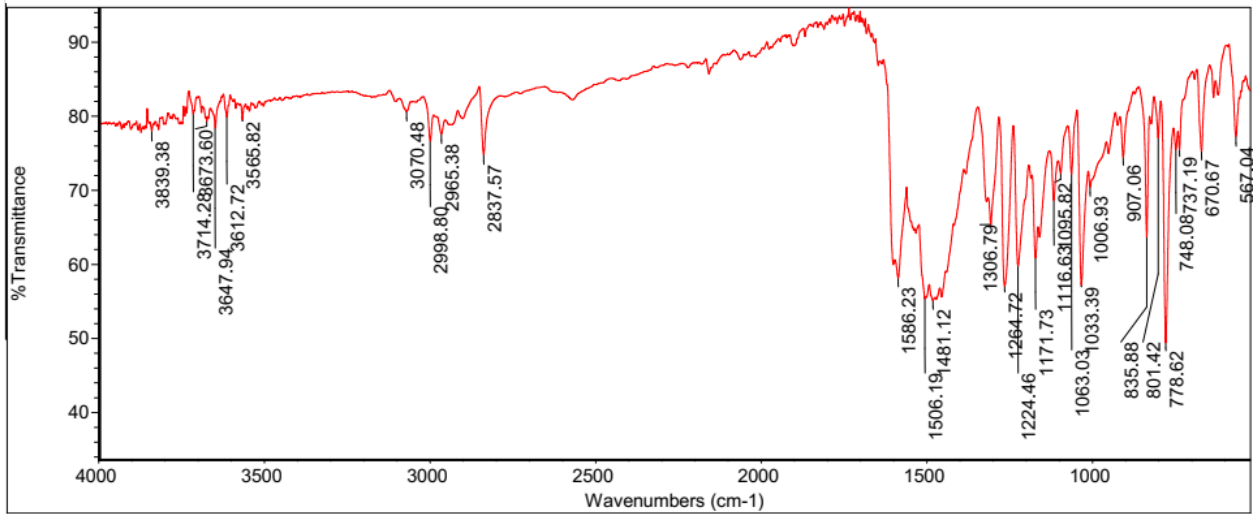
----- CHANNEL f2 -----
PCPRG2     zgpg30
NUC2       13C
P2         80.00 usec
PR         7.50 dB
PL1        19.00 dB
SFO2       400.1314000 MHz

F2 - Processing parameters
SI         32768
SF         100.6176300 MHz
WDW        EM
SSB        0
RB         1.50 Hz
GB         0
EB         0
PC         1.40
  
```

ThermoFisher
 SCIENTIFIC

Tue Dec 14 18:05:47 2021 (

Fri Jan 22 12:10:14 2021 (GMT+00:00):BDKT-26

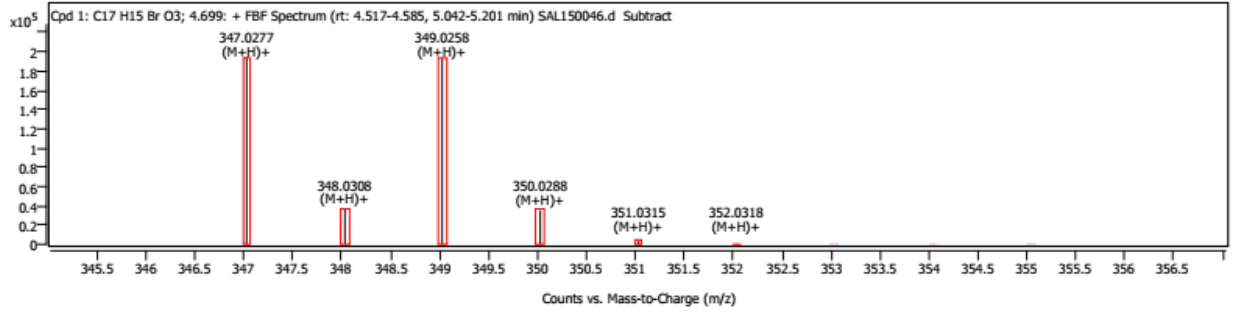


No search results for the selected spectrum!

Spectrum Peaks

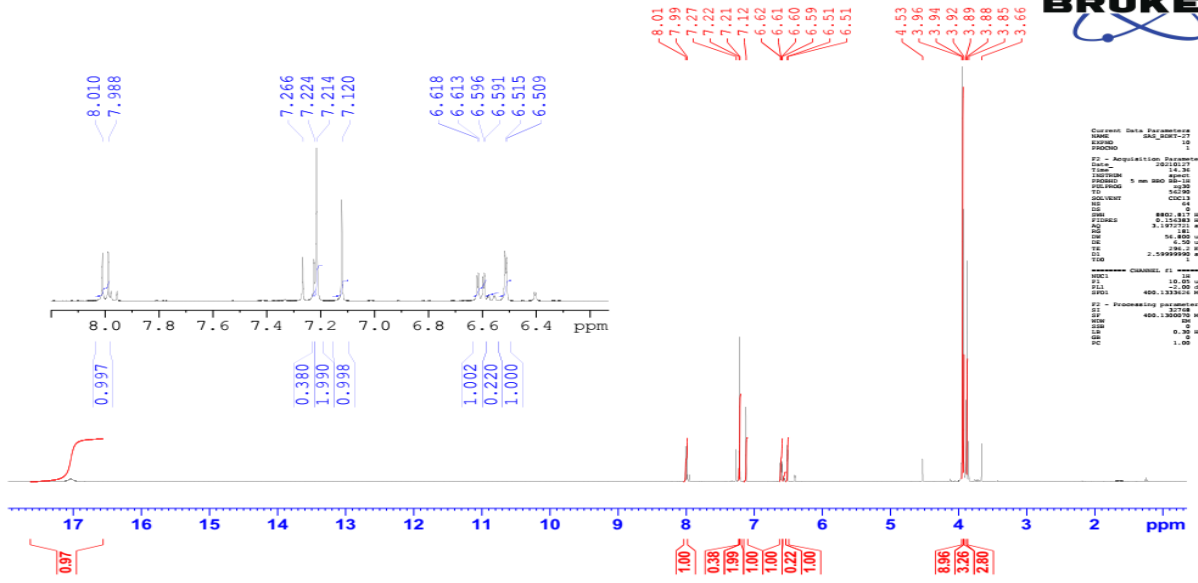
m/z	Z	Abund	Diff (ppm)	Height %	Height % (Calc)	Ion Species	Formula
347.0277	1	194601	-0.14	100.00	100.00	(M+H) ⁺	C17H15BrO3
348.0308	1	36431	-0.95	18.72	18.69	(M+H) ⁺	C17H15BrO3
349.0258	1	193324	-0.33	99.34	99.54	(M+H) ⁺	C17H15BrO3
350.0288	1	35195	-0.89	18.09	18.38	(M+H) ⁺	C17H15BrO3
351.0315	1	3882	-1.02	1.99	2.22	(M+H) ⁺	C17H15BrO3
352.0318	1	498	-7.49	0.26	0.20	(M+H) ⁺	C17H15BrO3

Compound Spectra



BDKT-27

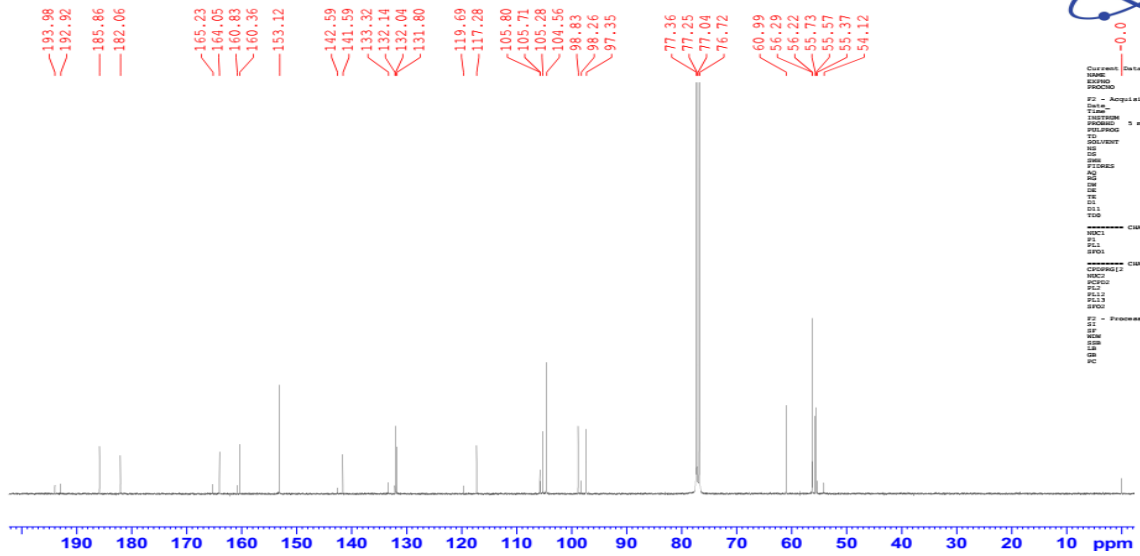
H1 NMR Spectrum of BDKT-27 in CDCL3+TMS
 PROTON64 CDC13 {C:\Bruker\TOPSPIN} SAS 6



```

Current Data Parameters
NAME      SAS_BDKT-27
EXPNO    1
PROCNO   1
F2 - Acquisition Parameters
Date_    20101130
Time     11:42
INSTRUM  spect
PROBHD   5 mm BBO BB-1H
PULPROG  zgpg30
SOLVENT  CDCl3
NS       1280
DS       4
SWH       23940.81 Hz
FIDRES   0.360174 Hz
AQ       1.1654174 sec
RG       1839.4
SQ       20.870
WDW       EM
SS       4.00
LB       1.00 Hz
GB       0.0000000
PC       2.0000000
===== CHANNEL f1 =====
NUC1      13C
P1        12.00
PL1       0.00 dB
SFO1     100.6272998 MHz
===== CHANNEL f2 =====
CPDPRG2  waltz16
NUC2      1H
P2        12.00
PL2       0.00 dB
PL12     19.20 dB
SFO2     400.1326000 MHz
F2 - Processing parameters
SI        32768
SF        400.1326000 MHz
WDW       EM
SS       4.00
LB       1.00 Hz
GB       0.0000000
PC       2.00
    
```

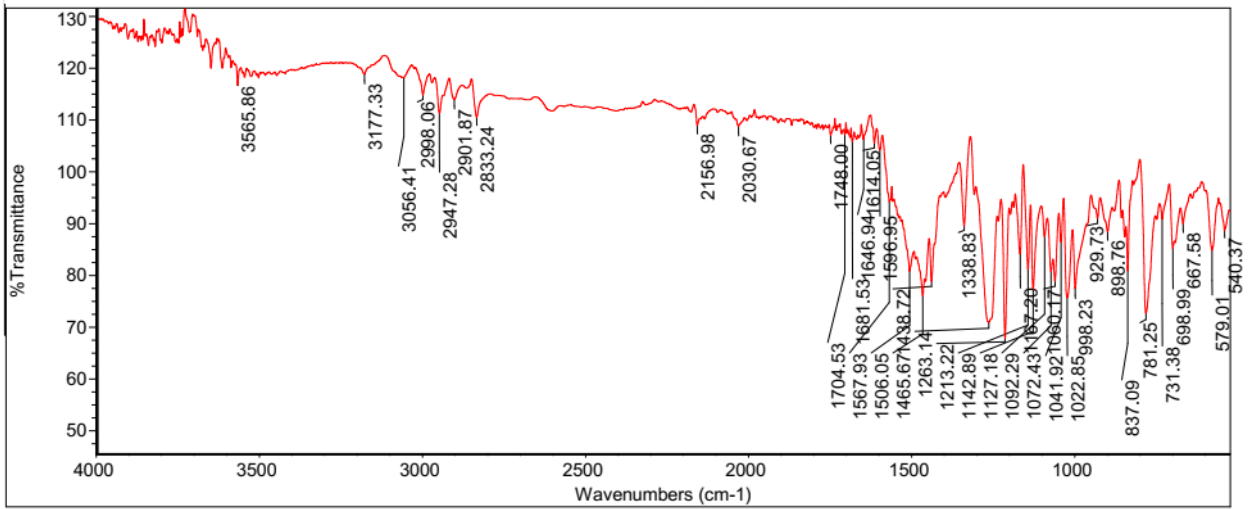
2D g-HMOC NMR Spectrum of BDKT-27 in CDCL3+TMS
 c13org CDC13 {C:\Bruker\TOPSPIN} SAS 6



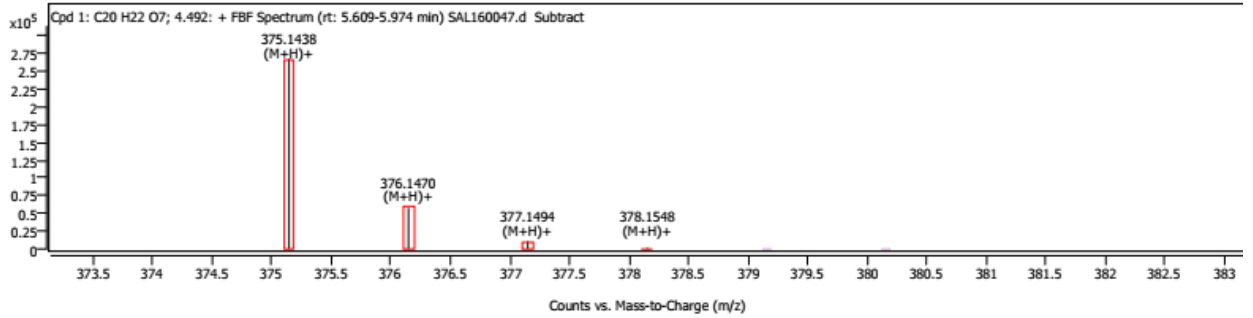
```

Current Data Parameters
NAME      SAS_BDKT-27
EXPNO    1
PROCNO   1
F2 - Acquisition Parameters
Date_    20101130
Time     11:42
INSTRUM  spect
PROBHD   5 mm BBO BB-1H
PULPROG  zgpg30
SOLVENT  CDCl3
NS       1280
DS       4
SWH       23940.81 Hz
FIDRES   0.360174 Hz
AQ       1.1654174 sec
RG       1839.4
SQ       20.870
WDW       EM
SS       4.00
LB       1.00 Hz
GB       0.0000000
PC       2.0000000
===== CHANNEL f1 =====
NUC1      13C
P1        12.00
PL1       0.00 dB
SFO1     100.6272998 MHz
===== CHANNEL f2 =====
CPDPRG2  waltz16
NUC2      1H
P2        12.00
PL2       0.00 dB
PL12     19.20 dB
SFO2     400.1326000 MHz
F2 - Processing parameters
SI        32768
SF        400.1326000 MHz
WDW       EM
SS       4.00
LB       1.00 Hz
GB       0.0000000
PC       2.00
    
```

Fri Jan 22 12:39:30 2021 (GMT+00:00):BDKT-27



Compound Spectra

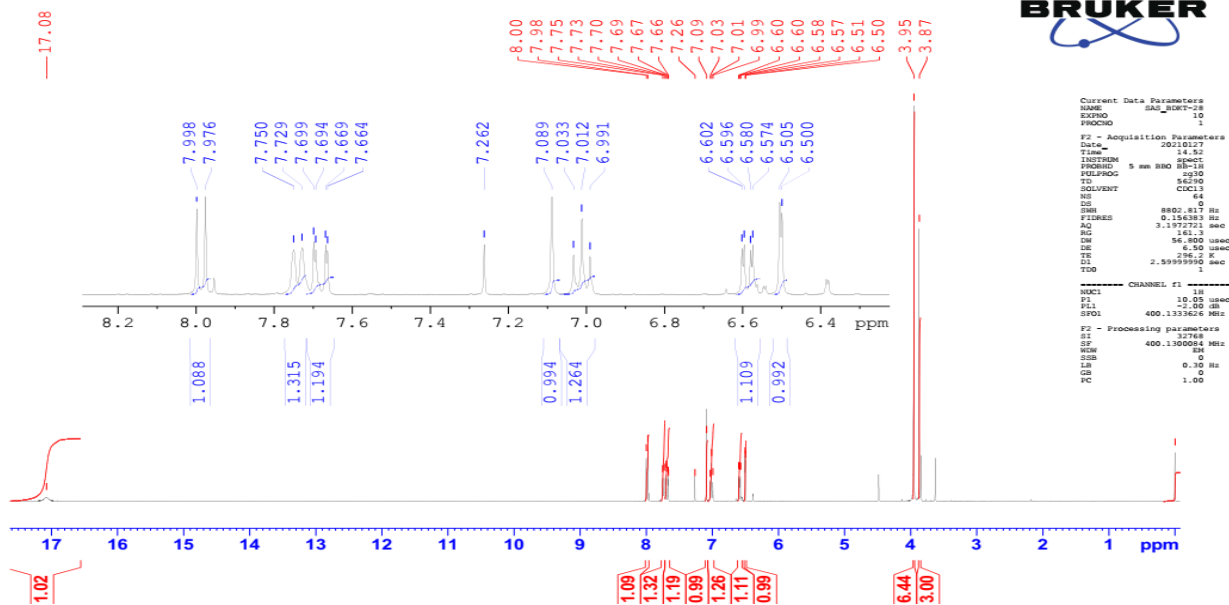


Spectrum Peaks

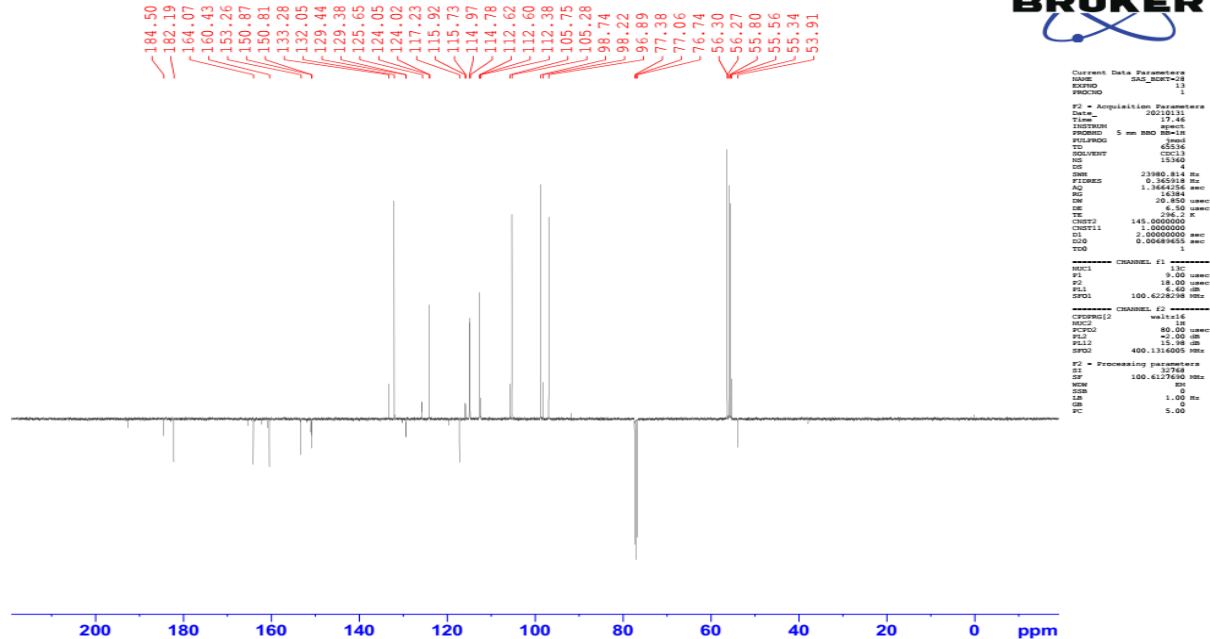
m/z	m/z (Calc)	Diff (ppm)	Abund	Height %	Height % (Calc)	Ion Species	Z
375.1438	375.1438	-0.05	267430	100.00	100.00	(M+H)+	1
376.1470	376.1472	-0.56	57670	21.56	22.16	(M+H)+	1
377.1494	377.1497	-0.81	10597	3.96	3.78	(M+H)+	1
378.1548	378.1523	6.46	1368	0.51	0.47	(M+H)+	1

BDKT-28

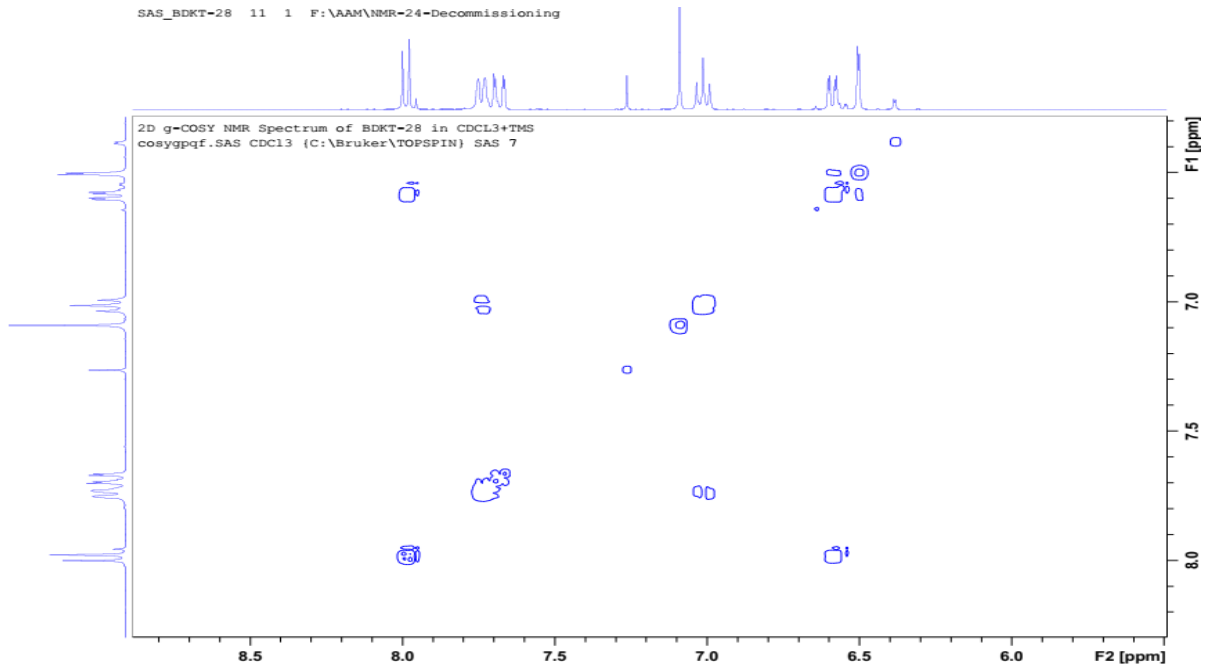
H1 NMR Spectrum of BDKT-28 in CDCL3+TMS
 PROTON64 CDC13 {C:\Bruker\TOPSPIN} SAS 7



JMOD C13 NMR Spectrum of BDKT-28 in CDCL3+TMS
 C13_APT CDC13 {C:\Bruker\TOPSPIN} SAS 7



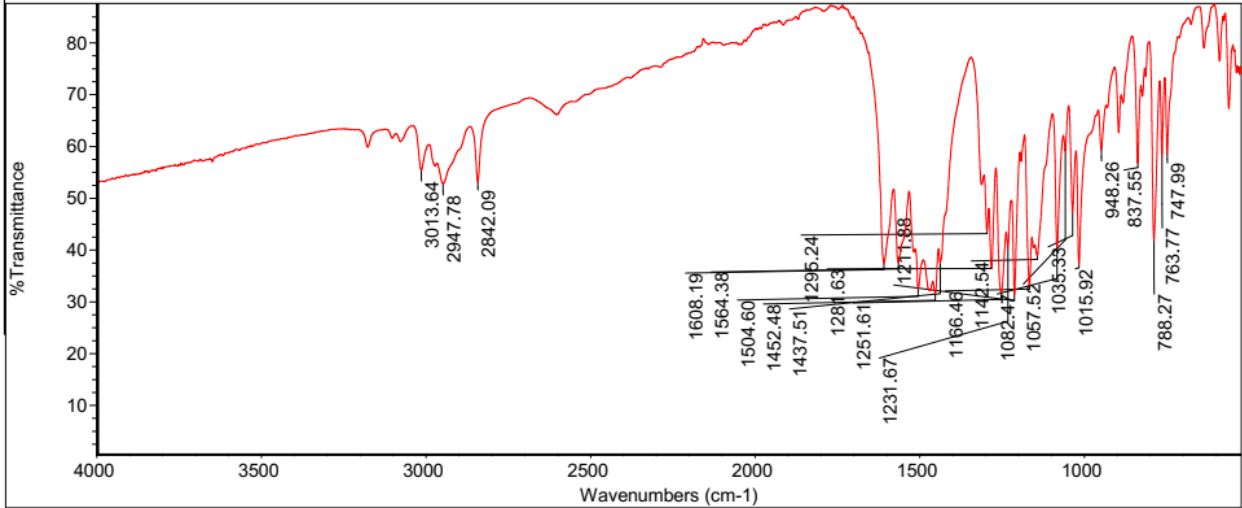
SAS_BDKT-28 11 1 F:\AAM\NMR-24-Decommissioning



ThermoFisher
SCIENTIFIC

Mon Dec 13 17:24:06 2021 (

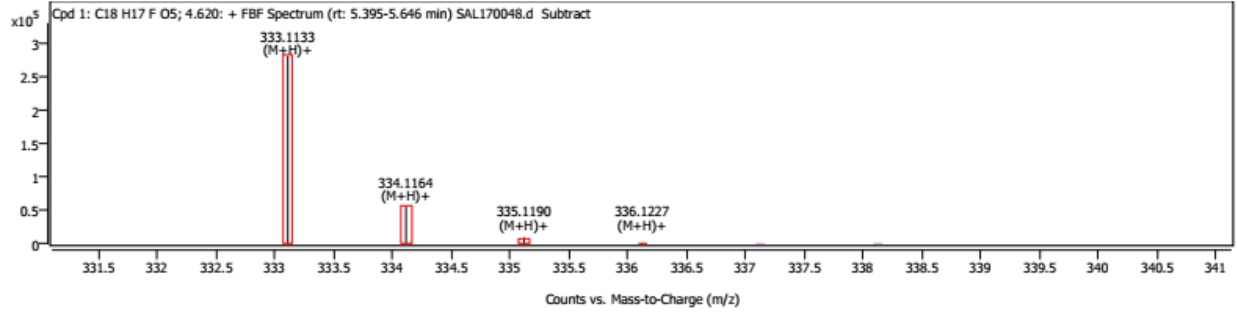
Thu Jan 21 12:29:23 2021 (GMT+00:00):BDKT-28



Spectrum Peaks

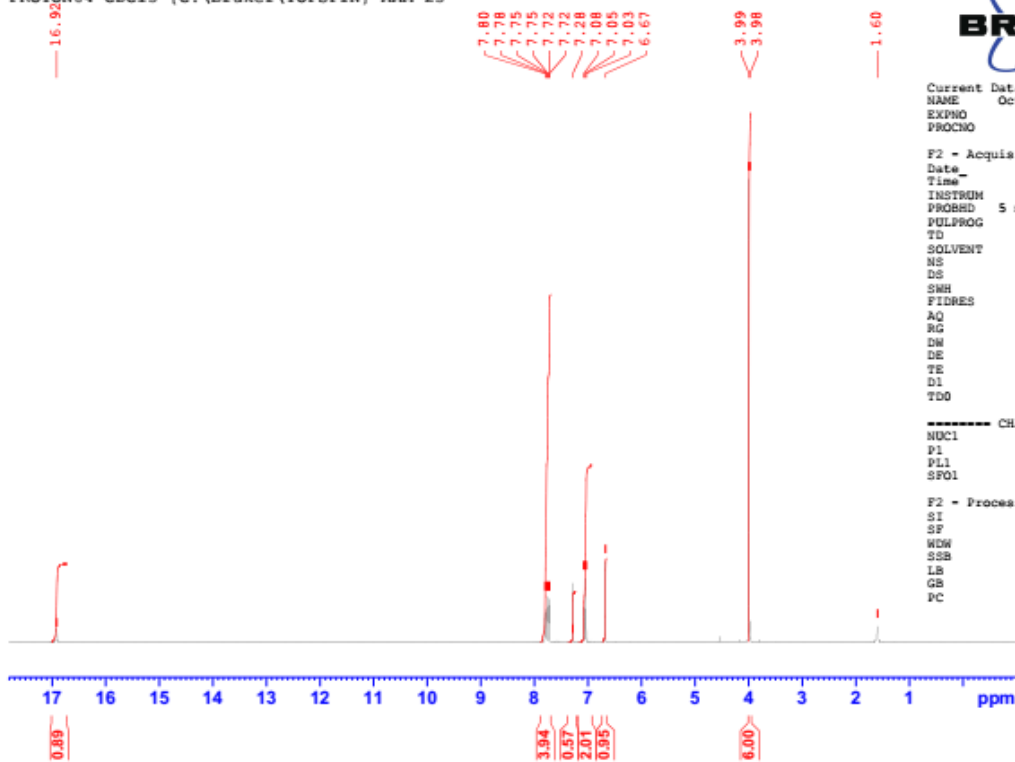
m/z	Z	Abund	Diff (ppm)	Height %	Height % (Calc)	Ion Species	Formula
333.1133	1	281075	-0.01	100.00	100.00	(M+H) ⁺	C18H17FO5
334.1164	1	55402	-0.83	19.71	19.87	(M+H) ⁺	C18H17FO5
335.1190	1	9166	-0.62	3.26	2.90	(M+H) ⁺	C18H17FO5
336.1227	1	916	2.52	0.33	0.31	(M+H) ⁺	C18H17FO5

Compound Spectra



BDKT-29

1H-NMR BDKT-29 in CDCl3 (Corrected)
 PROTON64 CDCl3 {C:\Bruker\TOPSPIN} AAM 23

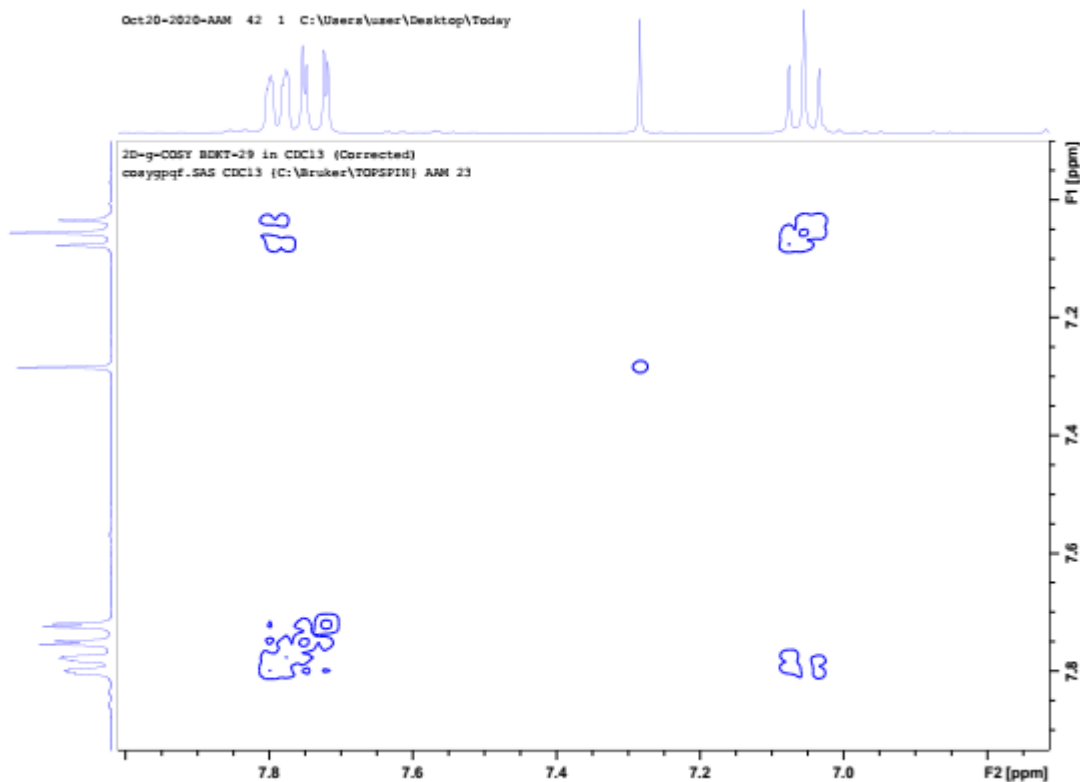


Current Data Parameters
 NAME Oct20-2020-AAM
 EXPNO 41
 PROCNO 1

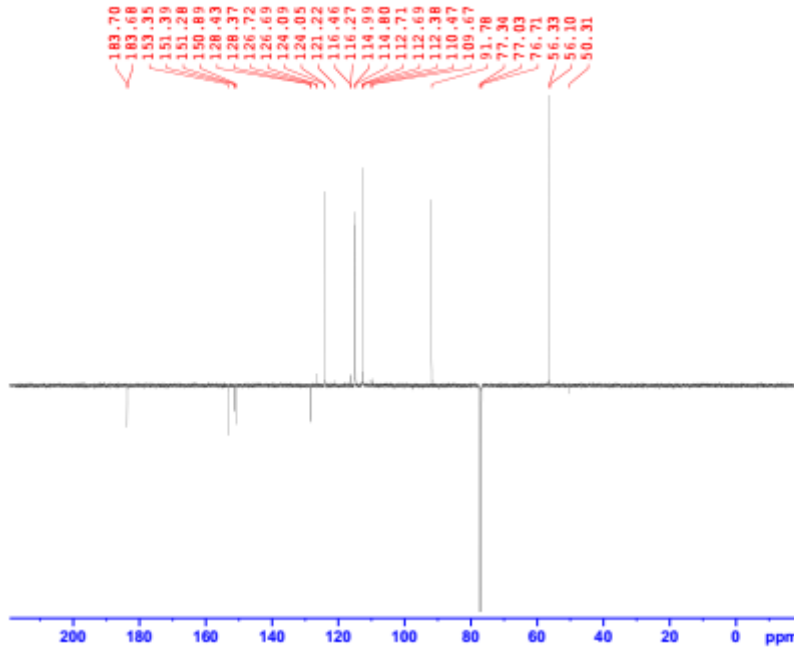
F2 - Acquisition Parameters
 Date_ 20201020
 Time_ 17.41
 INSTRUM spect
 PROBHD 5 mm BBO BB-1H
 PULPROG zg30
 TD 56290
 SOLVENT CDCl3
 NS 64
 DS 0
 SMH 8802.817 Hz
 FIDRES 0.156383 Hz
 AQ 3.1972721 sec
 RG 362
 DM 56.800 usec
 DE 6.50 usec
 TE 296.2 K
 D1 2.59999990 sec
 TDO 1

CHANNEL f1
 NUC1 1H
 P1 10.05 usec
 PL1 -2.00 dB
 SFO1 400.1333626 MHz

F2 - Processing parameters
 SI 32768
 SF 400.1300000 MHz
 WDW EM
 SSB 0
 LB 0.30 Hz
 GB 0
 PC 200.00



13C-JMOD BDKT-29 in CDCl3 (Corrected)
 C13_APT CDCl3 (C:\Bruker\TOPSPIN) AAM 23



Current Data Parameters
 NAME Oct10-2020-AAM
 EXPNO 45
 PROCNO 1

F2 - Acquisition Parameters
 Date_ 20101022
 Time 23.59
 INSTRUM spect
 PROBRD 5 mm BBO BB-1H
 PULPROG zgpg30
 TD 65536
 SOLVENT CDCl3
 NS 7168
 DS 4
 SWH 23980.814 Hz
 FIDRES 0.365918 Hz
 AQ 1.3664256 sec
 RG 16384
 DW 20.850 usec
 DE 6.50 usec
 TE 296.2 K
 CAGP2 145.000000
 CAGP1 1.000000
 D3 2.8000000 sec
 D30 0.00489655 sec
 T30 1

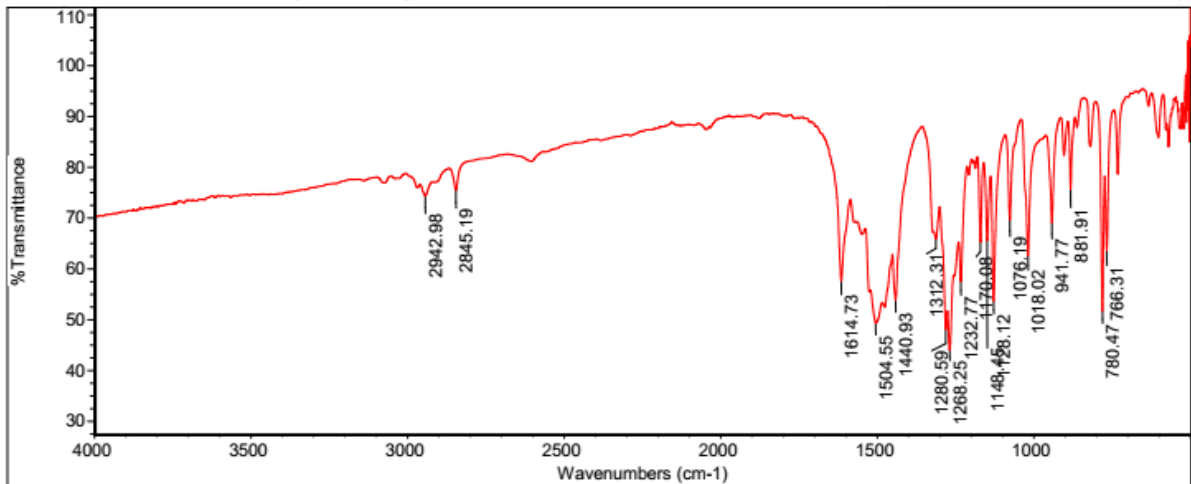
===== CHANNEL f1 =====
 NUC1 13C
 P1 6.00 usec
 P2 18.00 usec
 PL1 6.00 dB
 SFO1 100.628298 MHz

===== CHANNEL f2 =====
 CPDPRG2 waltz16
 NUC2 1H
 PCPD 80.00 usec
 PL2 -2.00 dB
 PL12 15.98 dB
 SFO2 400.131405 MHz

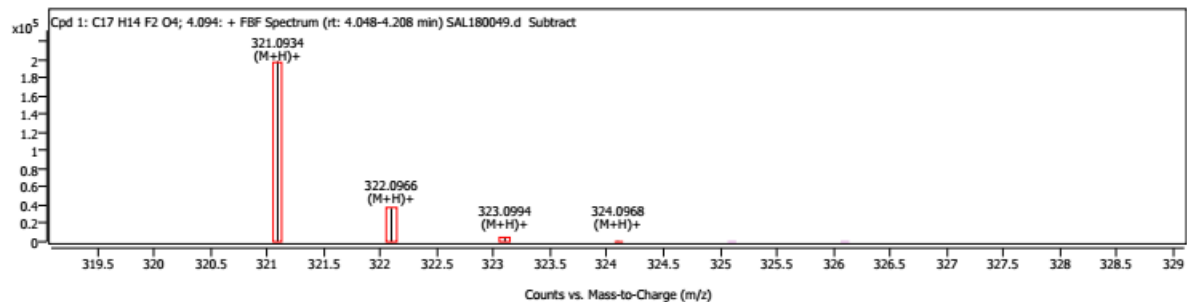
F2 - Processing parameters
 SI 32768
 SF 100.6177680 MHz
 MW 8K
 SSB 0
 LB 1.00 Hz
 GB 0
 PC 1.40

Title: Fri Jan 22 13:25:00 2021 (GMT+00:00): BDKT-29

Thu Jan 20 09:07:11 2022 (G



Compound Spectra

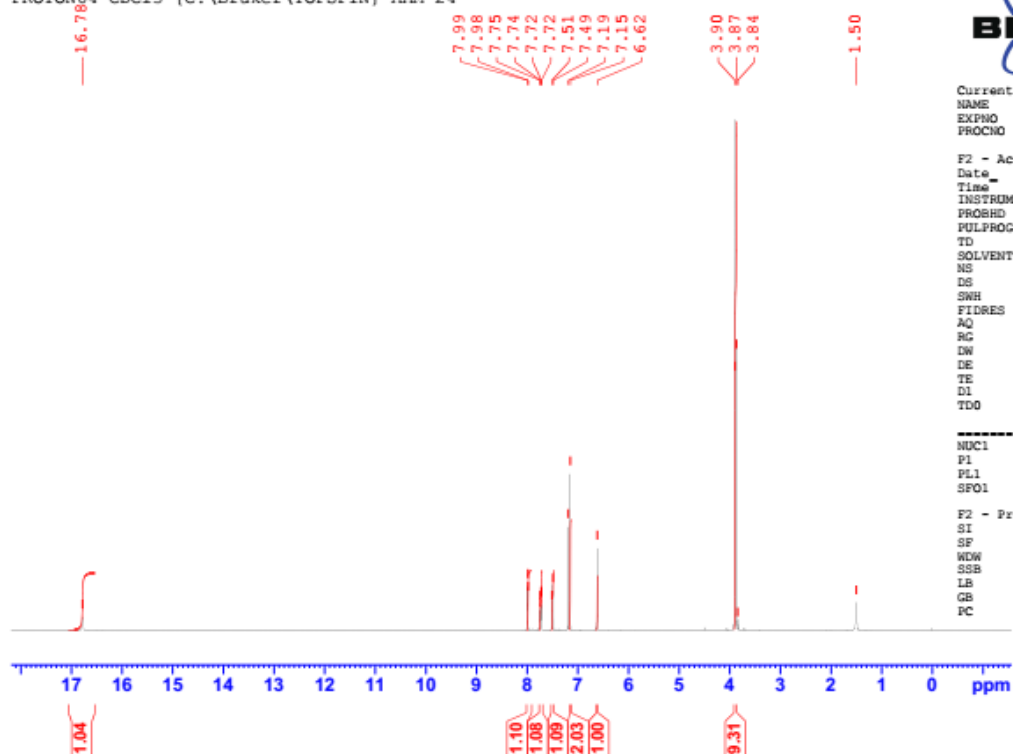


Spectrum Peaks

m/z	m/z (Calc)	Diff (ppm)	Abund	Height %	Height % (Calc)	Ion Species	Z
321.0934	321.0933	0.41	197899	100.00	100.00	(M+H) ⁺	1
322.0966	322.0967	-0.14	36694	18.54	18.71	(M+H) ⁺	1
323.0994	323.0992	0.43	5000	2.53	2.47	(M+H) ⁺	1
324.0968	324.1019	-15.65	766	0.39	0.24	(M+H) ⁺	1

BDKT-31

1H-NMR BDKT-31 in CDCl3
PROTON64 CDCl3 (C:\Bruker\TOPSPIN) AAM 24

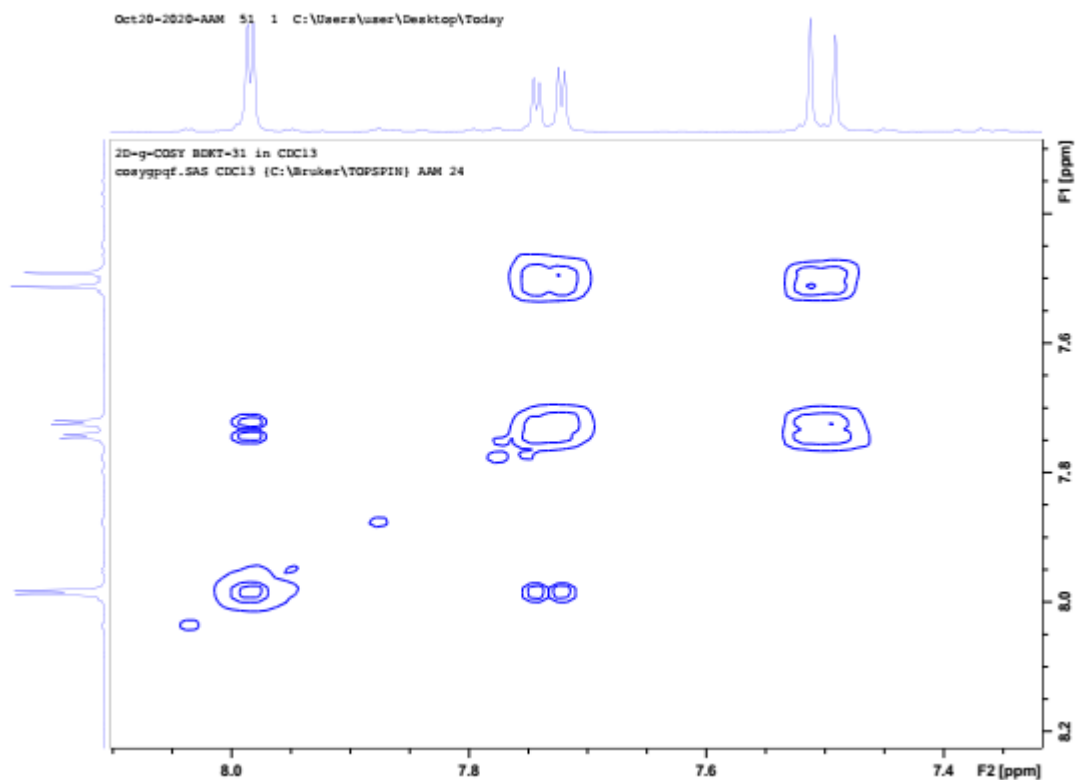


Current Data Parameters
NAME Oct20-2020-AAM
EXPNO 50
PROCNO 1

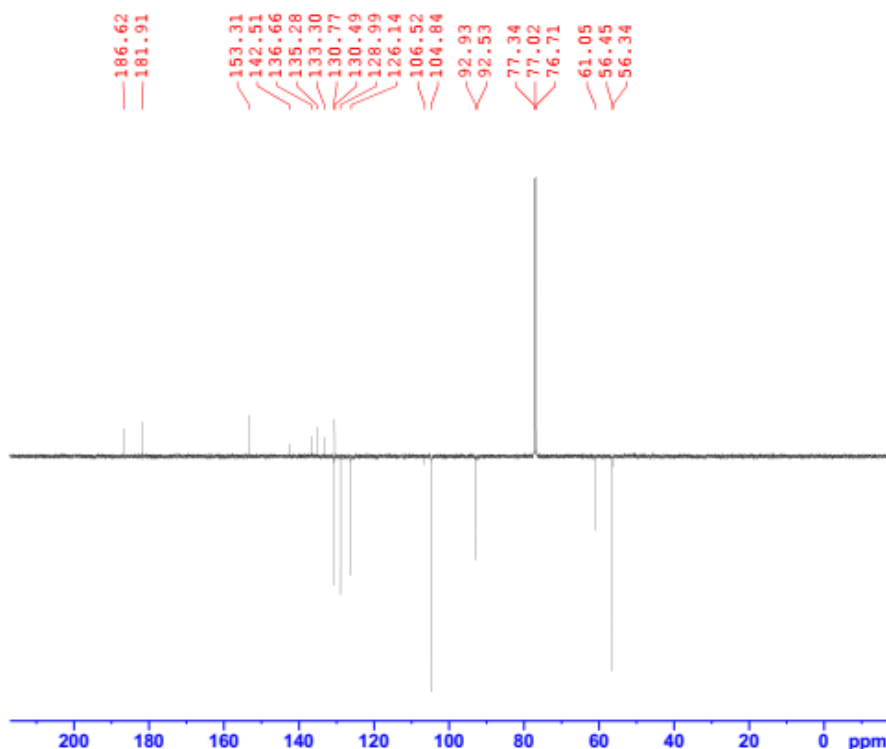
F2 - Acquisition Parameters
Date_ 20201020
Time 16.41
INSTRUM spect
PROBHD 5 mm BBO BB-1H
PULPROG zg30
TD 56290
SOLVENT CDCl3
NS 64
DS 0
SWH 8802.817 Hz
FIDRES 0.156383 Hz
AQ 3.1972721 sec
RG 456.1
DW 56.800 usec
DE 6.50 usec
TE 296.2 K
DL 2.59999990 sec
TDO 1

CHANNEL f1
NUC1 1H
P1 10.05 usec
PL1 -2.00 dB
SFO1 400.1333626 MHz

F2 - Processing parameters
SI 32768
SF 400.1300369 MHz
WDW EM
SSB 0
LB 0.30 Hz
GB 0
PC 100.00



13C-JMOD BDKT-31 in CDCl3
 C13_APT CDCl3 {C:\Bruker\TOPSPIN} AAM 24



Current Data Parameters
 NAME Oct20-2020-AAM
 EXPNO 54
 PROCNO 1

F2 - Acquisition Parameters
 Date_ 20201023
 Time 6.53
 INSTRUM spect
 PROBRD 5 mm BBO BB-1H
 PULPROG jmod
 TD 65536
 SOLVENT CDCl3
 NS 7168
 DS 4
 SWH 23980.814 Hz
 FIDRES 0.365918 Hz
 AQ 1.3664256 sec
 RG 16384
 DM 20.850 usec
 DE 6.50 usec
 TE 296.2 K
 CHST2 145.0000000
 CHST1 1.0000000
 D1 2.00000000 sec
 D20 0.00689655 sec
 TD0 1

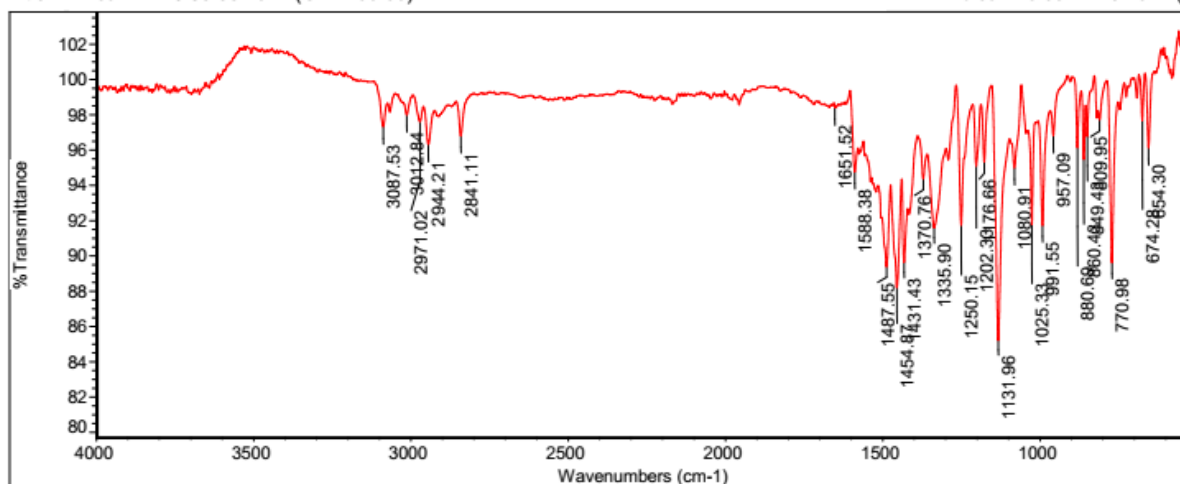
CHANNEL f1
 NUC1 13C
 P1 9.00 usec
 P2 18.00 usec
 PL1 6.60 dB
 SP01 100.6228298 MHz

CHANNEL f2
 CPDPRG2 waltz16
 NUC2 1H
 PCPD2 80.00 usec
 PL2 -2.00 dB
 PL12 15.98 dB
 SP02 400.1316005 MHz

F2 - Processing parameters
 SI 32768
 SF 100.6127690 MHz
 WDW EM
 SSB 0
 LB 1.00 Hz
 GB 0
 PC 1.40

Title: Fri Jan 22 13:35:58 2021 (GMT+00:00)

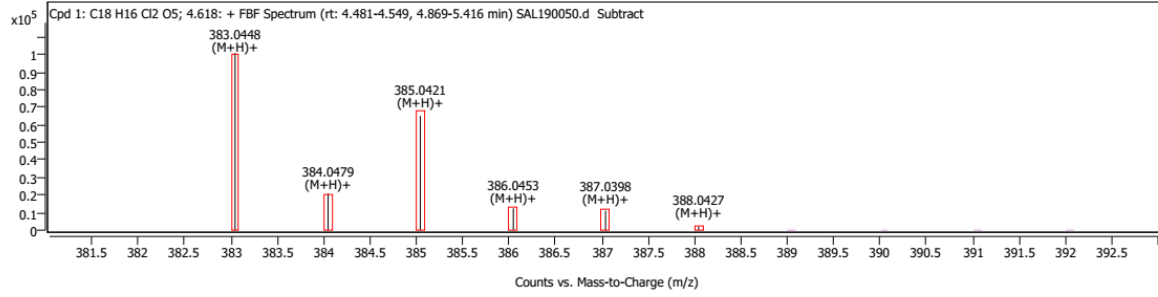
Thu Jan 20 09:17:15 2022 (C)



Spectrum Peaks

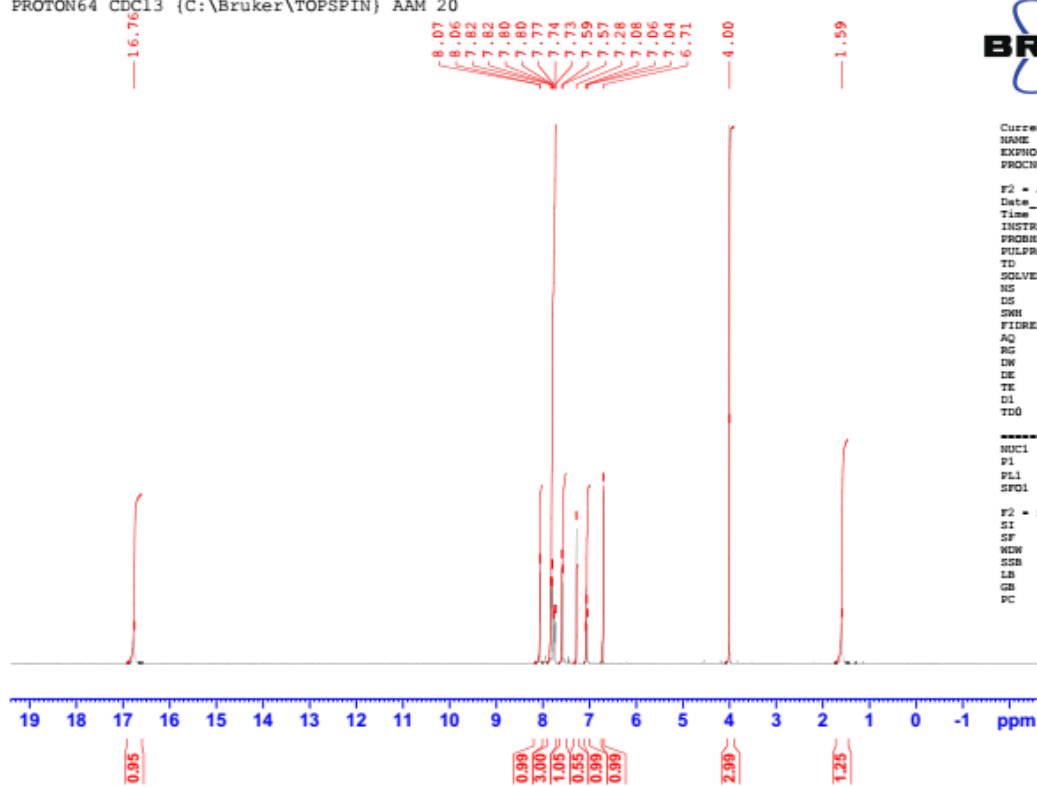
m/z	Z	Abund	Diff (ppm)	Height %	Height % (Calc)	Ion Species	Formula
383.0448	1	100771	0.19	100.00	100.00	(M+H)+	C18H16Cl2O5
384.0479	1	20917	-0.73	20.76	19.85	(M+H)+	C18H16Cl2O5
385.0421	1	65058	-0.31	64.56	66.88	(M+H)+	C18H16Cl2O5
386.0453	1	12440	-0.21	12.35	13.02	(M+H)+	C18H16Cl2O5
387.0398	1	11033	-1.19	10.95	12.12	(M+H)+	C18H16Cl2O5
388.0427	1	1984	-0.79	1.97	2.24	(M+H)+	C18H16Cl2O5

Compound Spectra



BDKT-32

¹H-NMR BDKT-32 in CDCl₃
 PROTON64 CDC13 (C:\Bruker\TOPSPIN) AAM 20

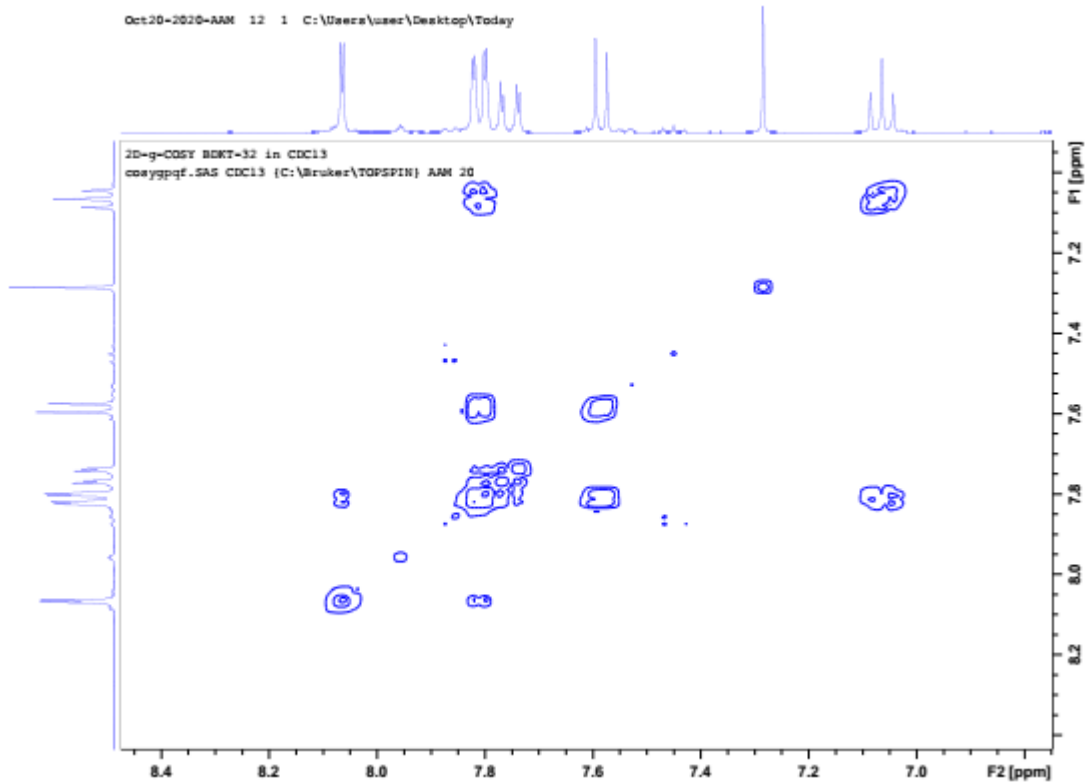


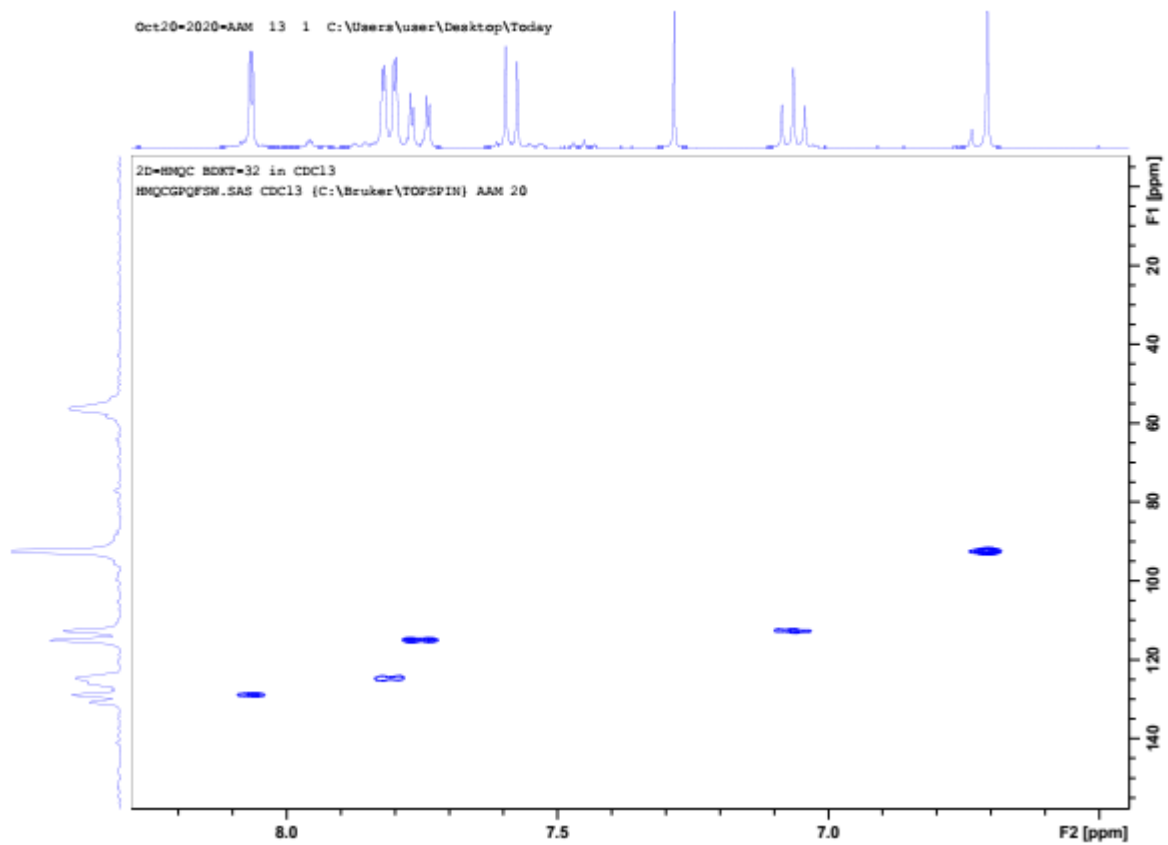
Current Data Parameters
 NAME Oct20-2020-AAM
 EXPNO 10
 PROCNO 1

F2 - Acquisition Parameters
 Date_ 20201020
 Time 15.54
 INSTRUM spect
 PROBHD 5 mm BBO BB-1H
 PULPROG zg30
 TD 56290
 TD0
 SOLVENT CDCl3
 NS 64
 DS 0
 SWH 8802.817 Hz
 FIDRES 0.156383 Hz
 AQ 3.1972721 sec
 RG 362
 DW 56.800 usec
 DE 6.50 usec
 TE 296.2 K
 D1 2.59999990 sec
 TD0 1

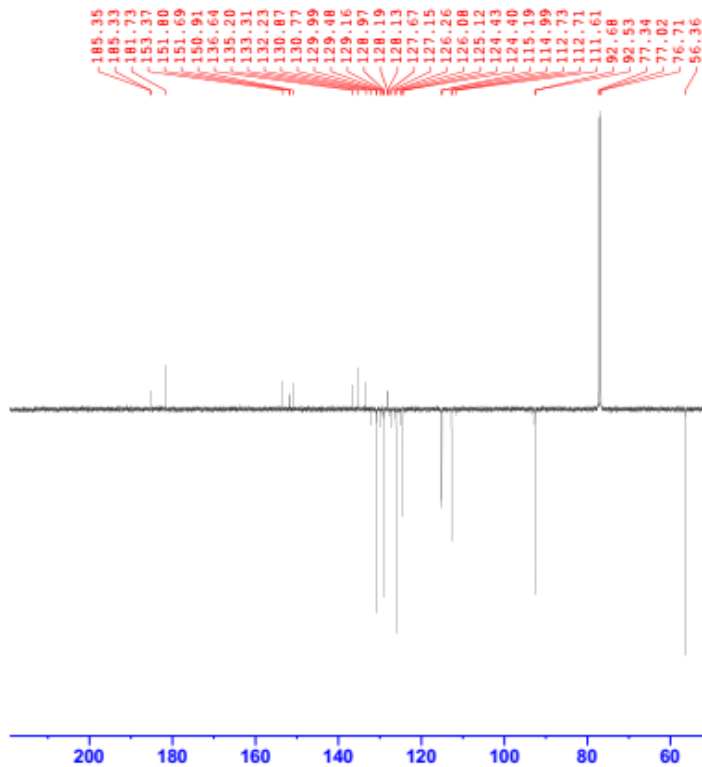
===== CHANNEL f1 =====
 NUC1 1H
 P1 10.05 usec
 PL1 -2.00 dB
 SFO1 400.133626 MHz

F2 - Processing parameters
 SI 32768
 SF 400.1300000 MHz
 WDW EM
 SSB 0
 LB 0.30 Hz
 GB 0
 PC 180.00





13C-APT BDKT-32 in CDCl3
 C13_APT CDC13 (C:\Bruker\TOPSPIN) AAM 20



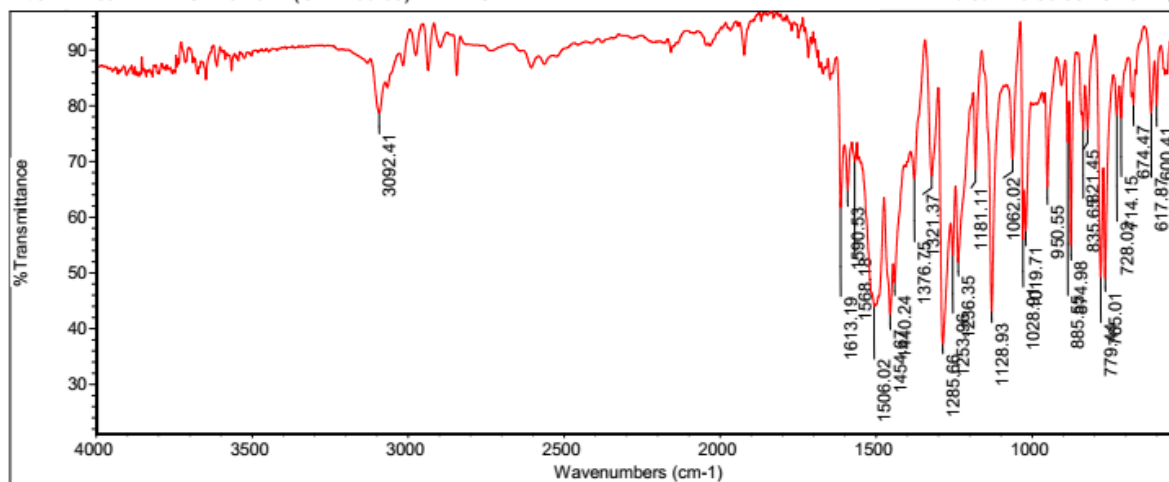
CU
 NA
 EXPNO 15
 PROCNO 1

F2 - Acquisition Parameters
 Date_ 20201021
 Time 3.20
 INSTRUM spect
 PROBHD 5 mm BBO BB-1H
 PULPROG jmod
 TD 65536
 SOLVENT cdcl3
 NS 7168
 DS 4
 SMH 23980.814 Hz
 FIDRES 0.365918 Hz
 AQ 1.3664256 sec
 RG 16384
 DM 20.850 usec
 DE 6.50 usec
 TE 296.2 K
 CNST2 145.0000000
 CNST11 1.0000000
 D1 2.0000000 sec
 D20 0.00689655 sec
 TDO 1

----- CHANNEL f1 -----
 NUC1 13C
 P1 9.00 usec
 P2 18.00 usec
 PL1 6.60 dB
 SFO1 100.6228298 MHz

----- CHANNEL f2 -----
 CPDPRG[2] waltz16
 NUC2 1H
 PCPD2 80.00 usec
 PL2 -2.00 dB
 PL12 15.98 dB
 SFO2 400.1316005 MHz

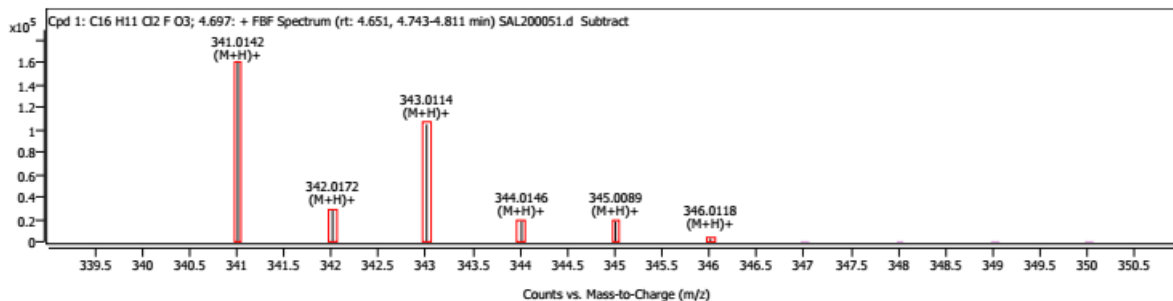
F2 - Processing parameters
 SI 32768
 SF 100.6127690 MHz
 NQW EN
 SSB 0
 LB 1.00 Hz
 GB 0
 PC 1.40



Spectrum Peaks

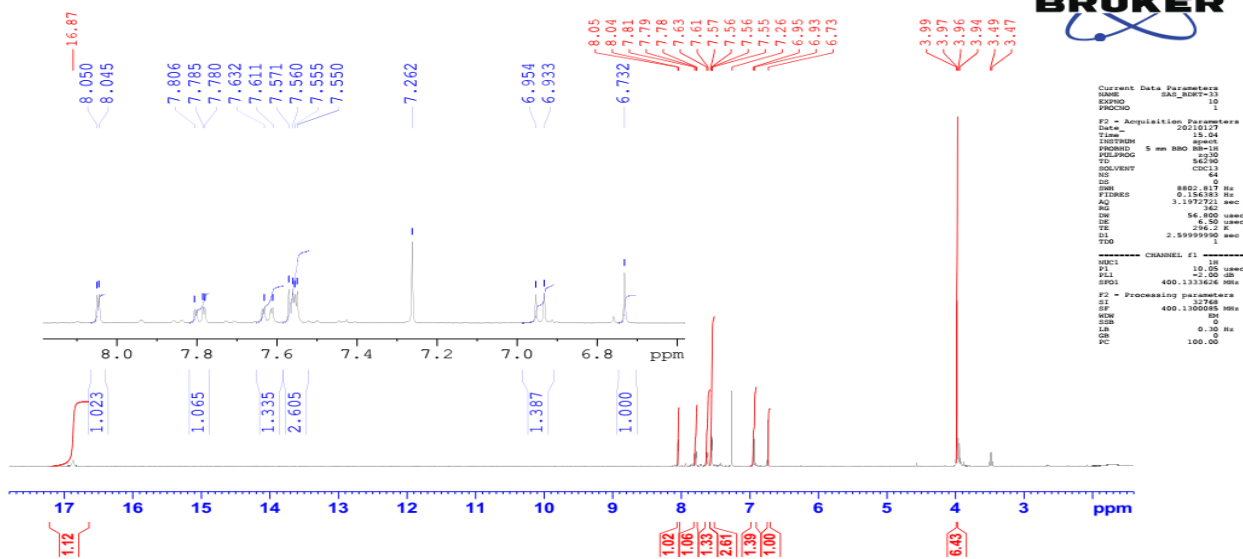
m/z	Z	Abund	Diff (ppm)	Height %	Height % (Calc)	Ion Species	Formula
341.0142	1	161795	-0.16	100.00	100.00	(M+H) ⁺	C ₁₆ H ₁₁ O ₂ F ₃
342.0172	1	29024	-1.01	17.94	17.56	(M+H) ⁺	C ₁₆ H ₁₁ O ₂ F ₃
343.0114	1	105004	-0.44	64.90	66.06	(M+H) ⁺	C ₁₆ H ₁₁ O ₂ F ₃
344.0146	1	18707	-0.45	11.56	11.42	(M+H) ⁺	C ₁₆ H ₁₁ O ₂ F ₃
345.0089	1	18346	-1.33	11.34	11.57	(M+H) ⁺	C ₁₆ H ₁₁ O ₂ F ₃
346.0118	1	2990	-1.27	1.85	1.91	(M+H) ⁺	C ₁₆ H ₁₁ O ₂ F ₃

Compound Spectra



BDKT-33

H1 NMR Spectrum of BDKT-33 in CDCL3+TMS
 PROTON64 CDC13 {C:\Bruker\TOPSPIN} SAS 8



```

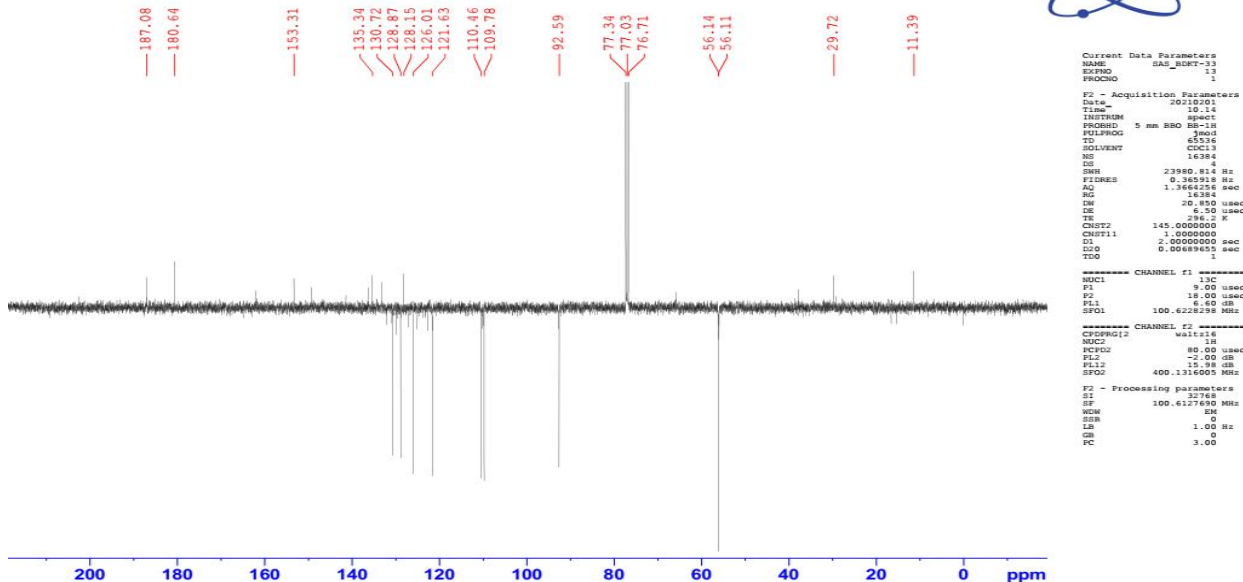
Current Data Parameters
NAME      SAS_BDKT-33
EXPNO    13
PROCNO   1

F2 - Acquisition Parameters
Date_    20121013
Time     10.14
INSTRUM  spect
PROBHD   5 mm BBO BB-1H
PULPROG  zgpg30
TD        65536
SOLVENT  CDCl3
NS        16384
DS        4
SWH       23980.814 Hz
FIDRES   0.383218 Hz
AQ        1.3664258 sec
RG        16384
DE        20.850 usec
TE        296.2 K
CNSF2    145.000000
CNSF11   1.000000
DI        2.0000000 sec
TD0       0.00689655 sec
TSD

===== CHANNEL f1 =====
NUC1      1H
P1         9.00 usec
PL1        0.00 dB
SFO1      400.132626 MHz

F2 - Processing parameters
SI         32768
SF         400.132626 MHz
WDW        EM
SSB        0
LB         1.00 Hz
GB         0
PC         3.00
    
```

JMOD C13 NMR Spectrum of BDKT-33 in CDCL3+TMS
 C13_APT CDC13 {C:\Bruker\TOPSPIN} SAS 8



```

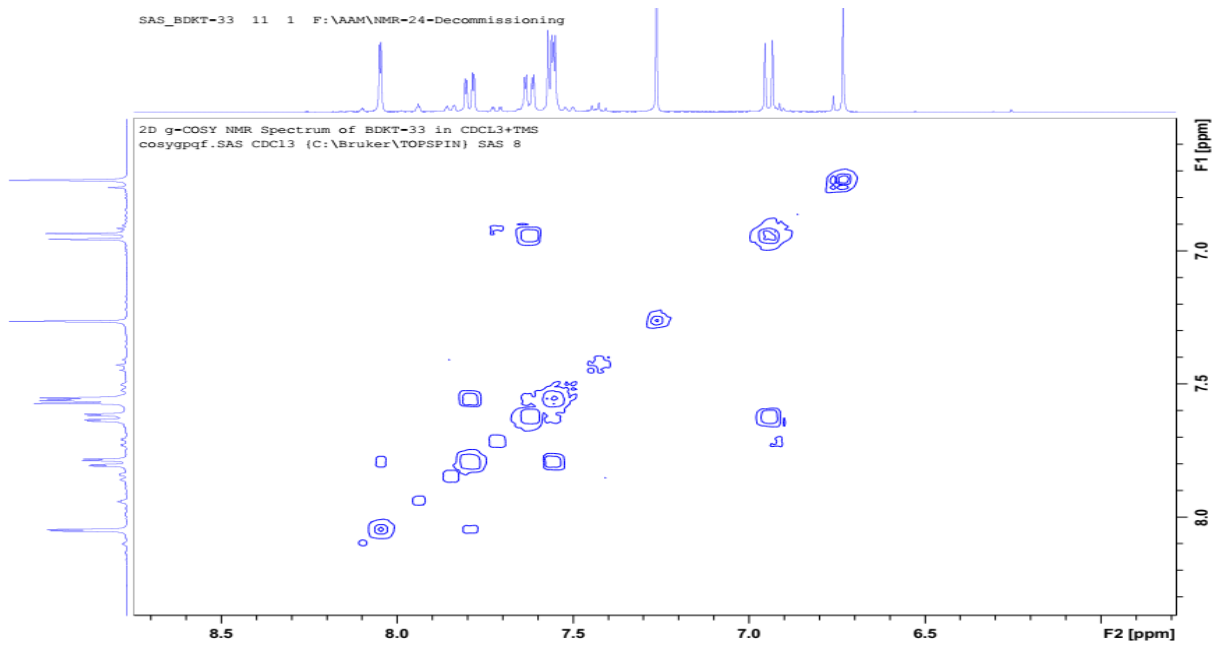
Current Data Parameters
NAME      SAS_BDKT-33
EXPNO    13
PROCNO   1

F2 - Acquisition Parameters
Date_    20121013
Time     10.14
INSTRUM  spect
PROBHD   5 mm BBO BB-1H
PULPROG  zgpg30
TD        65536
SOLVENT  CDCl3
NS        16384
DS        4
SWH       23980.814 Hz
FIDRES   0.383218 Hz
AQ        1.3664258 sec
RG        16384
DE        20.850 usec
TE        296.2 K
CNSF2    145.000000
CNSF11   1.000000
DI        2.0000000 sec
TD0       0.00689655 sec
TSD

===== CHANNEL f1 =====
NUC1      13C
P1         9.00 usec
PL1        0.00 dB
SFO1      100.622299 MHz

===== CHANNEL f2 =====
CPCPRG12 wait14
NUC2      1H
PCF02    80.00 usec
PL2       -2.00 dB
PL12      15.98 dB
SFO2      400.1316001 MHz

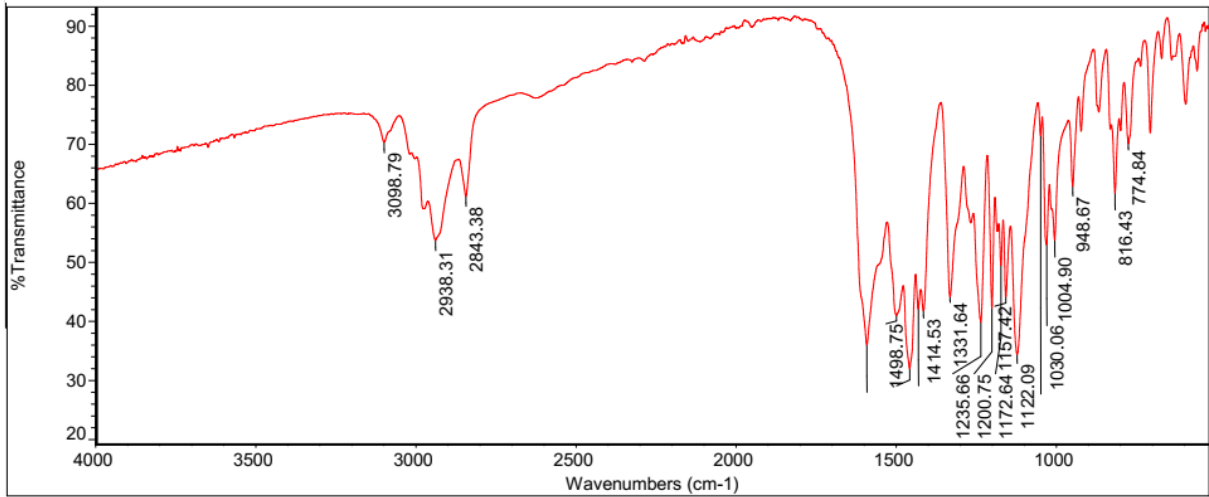
F2 - Processing parameters
SI         32768
SF         100.617600 MHz
WDW        EM
SSB        0
LB         1.00 Hz
GB         0
PC         3.00
    
```

ThermoFisher
SCIENTIFIC

Mon Dec 13 18:09:09 2021 (

Thu Jan 21 12:41:45 2021 (GMT+00:00): BDKT-33



Monoisotopic Mass, Even Electron Ions

11 formula(e) evaluated with 1 results within limits (up to 5 closest results for each mass)

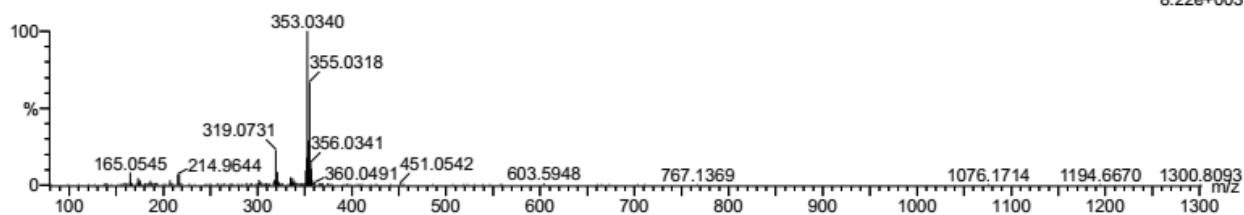
Elements Used:

C: 0-17 H: 0-15 O: 1-4 Cl: 0-2

AB300321 SAL 21

AB300321 SAL 21 1205 (2.608)

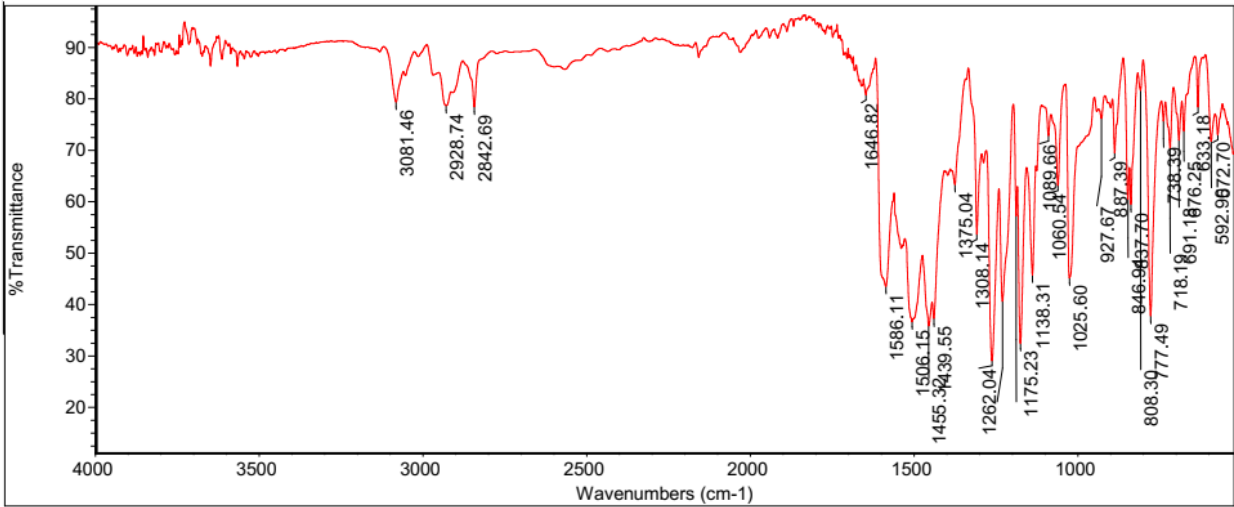
1: TOF MS ASAP+
8.22e+003



Minimum: -1.5
Maximum: 5.0 1000.0 50.0

Mass	Calc. Mass	mDa	PPM	DBE	i-FIT	Norm	Conf (%)	Formula
353.0340	353.0347	-0.7	-2.0	9.5	49.0	n/a	n/a	C17 H15 O4 Cl2

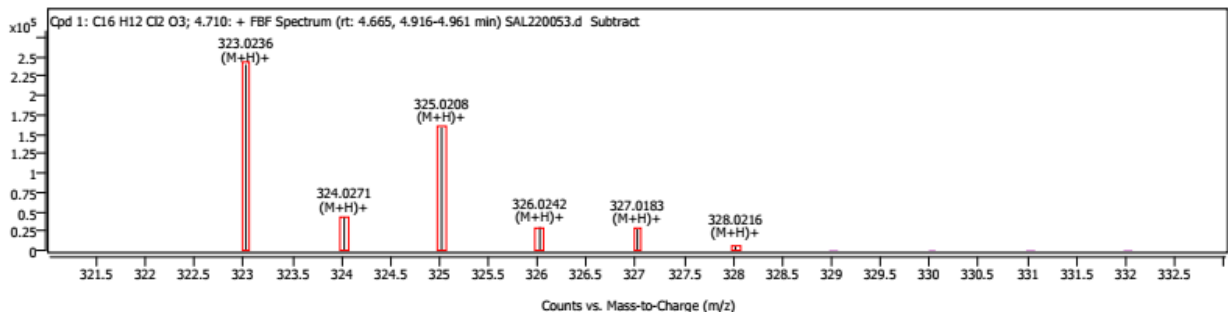
Fri Jan 22 12:43:37 2021 (GMT+00:00):BDKT-34



Spectrum Peaks

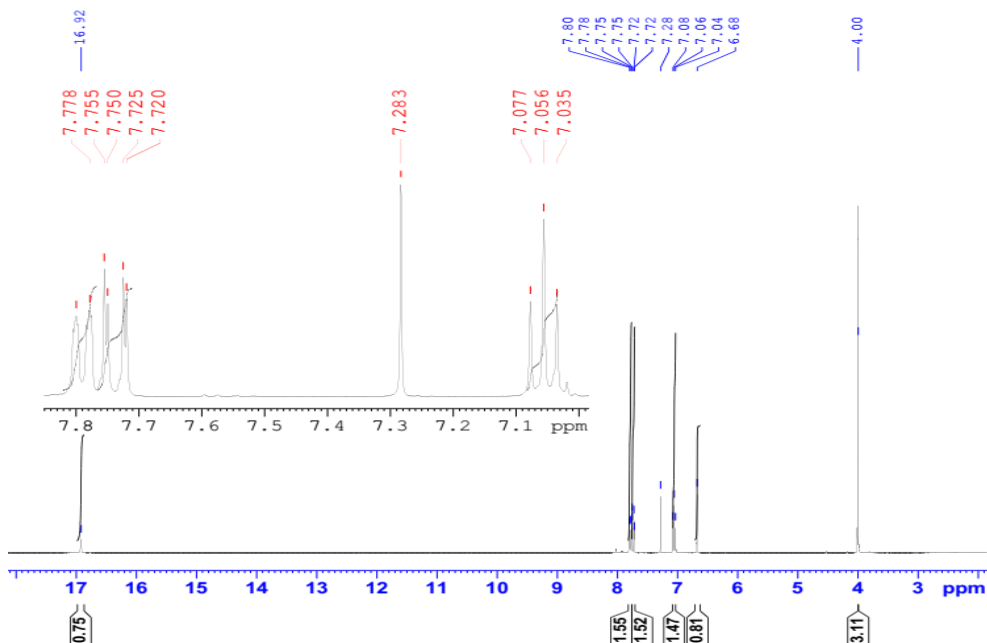
m/z	Z	Abund	Diff (ppm)	Height %	Height % (Calc)	Ion Species	Formula
323.0236	1	240402	0.06	100.00	100.00	(M+H)+	C16H12Cl2O3
324.0271	1	43222	0.23	17.98	17.57	(M+H)+	C16H12Cl2O3
325.0208	1	158847	-0.58	66.08	66.06	(M+H)+	C16H12Cl2O3
326.0242	1	30152	0.15	12.54	11.43	(M+H)+	C16H12Cl2O3
327.0183	1	27452	-1.45	11.42	11.57	(M+H)+	C16H12Cl2O3
328.0216	1	4994	-0.06	2.08	1.92	(M+H)+	C16H12Cl2O3

Compound Spectra



BDKT-35

1H-NMR-BDKT-35 in CDCl3
 PROTON64 CDC13 (C:\Bruker\TOPSPIN) AAM 19



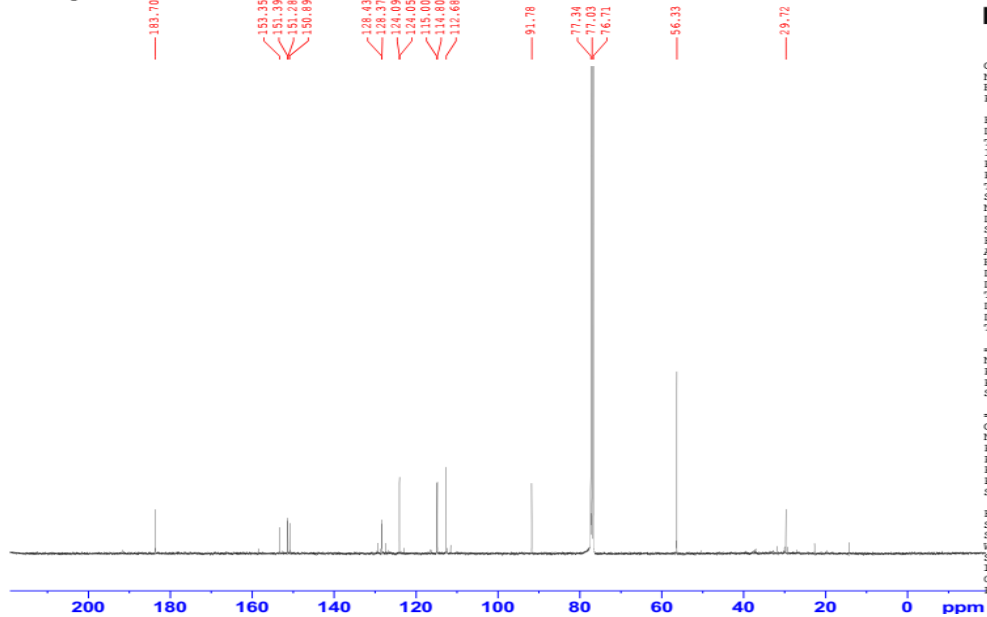
Current Data Parameters
 NAME Jan22-2020-AAM
 EXPNO 10
 PROCNO 1

F2 - Acquisition Parameters
 Date_ 20200122
 Time 13.52
 INSTRUM spect
 PROBHD 5 mm BBO BB-1H
 PULPROG zg30
 TD 56290
 SOLVENT CDC13
 NS 64
 DS 0
 SWH 8802.817 Hz
 FIDRES 0.156383 Hz
 AQ 3.1972721 sec
 RG 322.5
 DW 56.800 usec
 DE 6.50 usec
 TE 296.2 K
 D1 2.59999990 sec
 TDO 1

===== CHANNEL f1 =====
 NUC1 1H
 P1 10.05 usec
 PL1 -2.00 dB
 SFO1 400.1333626 MHz

F2 - Processing parameters
 SI 32768
 SF 400.1300000 MHz
 EM
 SSB 0
 LB 0.30 Hz
 GB 0
 PC 110.00

BB H1 Decoupled C13 NMR-BDKT-35 in CDCl3
 c13org CDC13 (C:\Bruker\TOPSPIN) AAM 19



Current Data Parameters
 NAME Jan22-2020-AAM
 EXPNO 13
 PROCNO 1

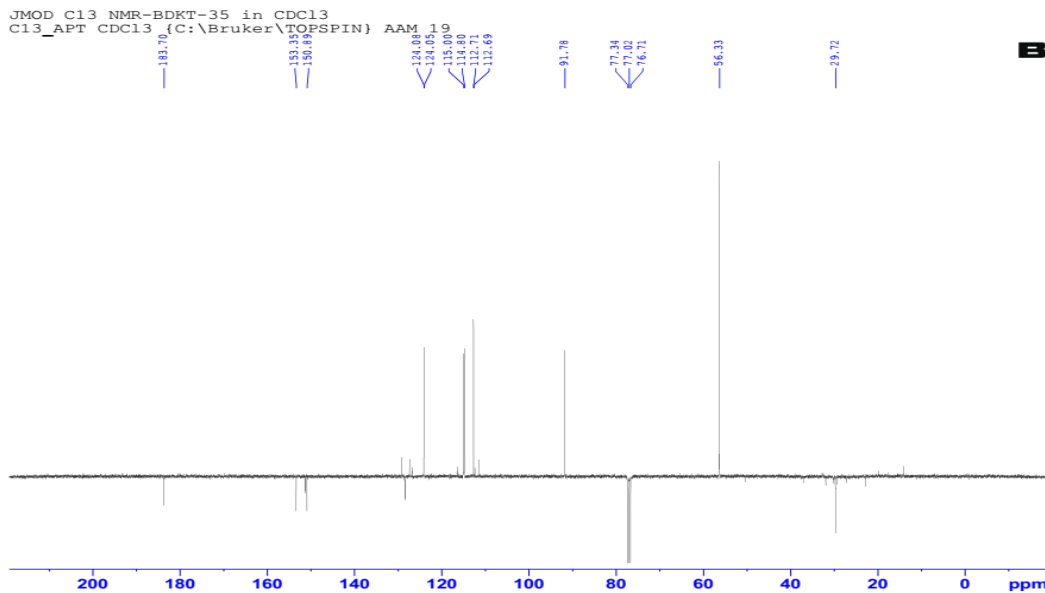
F2 - Acquisition Parameters
 Date_ 20200124
 Time 4.48
 INSTRUM spect
 PROBHD 5 mm BBO BB-1H
 PULPROG zgpg30
 TD 65536
 SOLVENT CDC13
 NS 12288
 DS 4
 SWH 23980.814 Hz
 FIDRES 0.365918 Hz
 AQ 1.3664256 sec
 RG 18390.4
 DW 20.850 usec
 DE 6.50 usec
 TE 296.2 K
 D1 2.00000000 sec
 D11 0.03000000 sec
 TDO 1

===== CHANNEL f1 =====
 NUC1 13C
 P1 9.00 usec
 PL1 6.60 dB
 SFO1 100.6228298 MHz

===== CHANNEL f2 =====
 CPDPRG[2] waltz16
 NUC2 1H
 PCPD2 80.00 usec
 PL2 -2.00 dB
 PLI2 15.98 dB
 PLI3 19.50 dB
 SFO2 400.1316005 MHz

F2 - Processing parameters
 SI 32768
 SF 100.6127690 MHz
 EM
 SSB 0
 LB 1.04 Hz
 GB 0
 PC 10.00

JMOD C13 NMR-BDKT-35 in CDCl3
 C13_APT CDCl3 (C:\Bruker\TOPSPIN) AAM



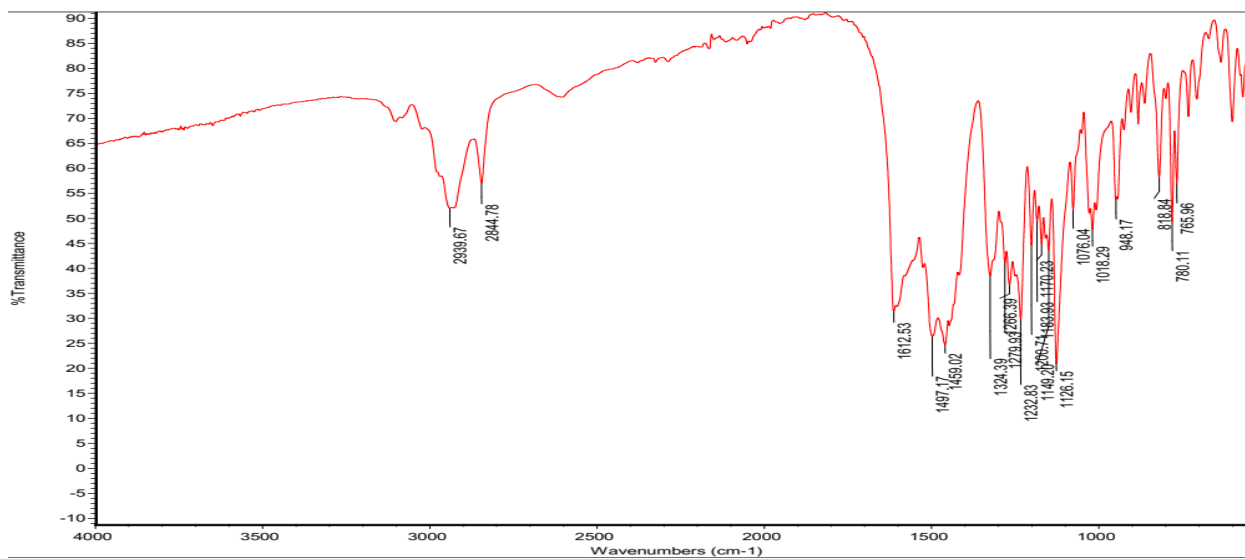
Current Data Parameters
 NAME Jan2-2020-AAM
 EXPR0 14
 PROCNO 1

F2 - Acquisition Parameters
 Date_ 20200124
 Time 22:56
 INSTRUM spect
 PROBR0 5 mm BBO BB-1H
 PULPROG jmod
 TD 65536
 SOLVENT CDCl3
 NS 6144
 DS 4
 SRR 23980.814 Hz
 FIDRES 0.365918 Hz
 AQ 1.3654256 sec
 RG 6384
 DW 20.850 usec
 DE 6.50 usec
 TE 294.4 K
 CNST2 145.0000000
 CNST11 1.0000000
 D10 2.00000000 sec
 D10 0.00688955 sec
 TDD 1

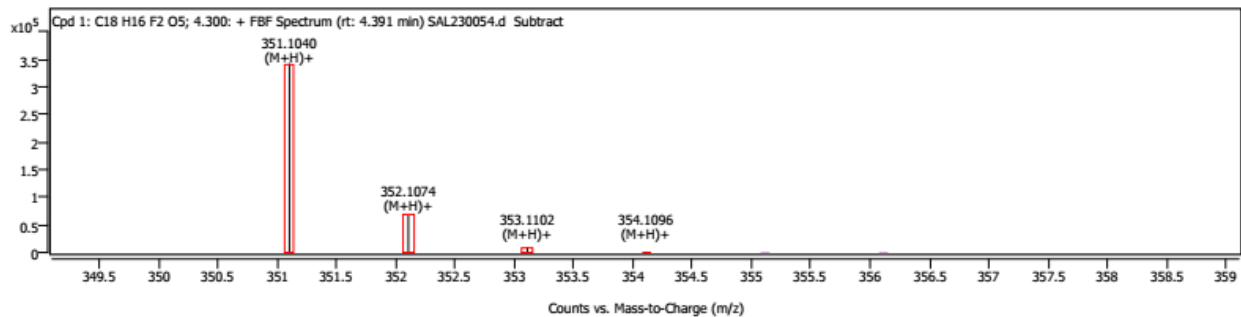
----- CHANNEL f1 -----
 NU1 13C
 P1 9.00 usec
 F2 100.628198 MHz
 PL1 6.60 dB
 SFO1 100.628198 MHz

----- CHANNEL f2 -----
 CPDPRG2 waltz16
 NU2 1H
 PCPD2 80.00 usec
 PL2 -2.00 dB
 PL12 15.08 dB
 SFO2 400.1316005 MHz

F2 - Processing parameters
 SF 32768 MHz
 SFO 100.617790 MHz
 RBW 0 Hz
 SBW 0 Hz
 LB 1.00 Hz
 FC 9.00



Compound Spectra

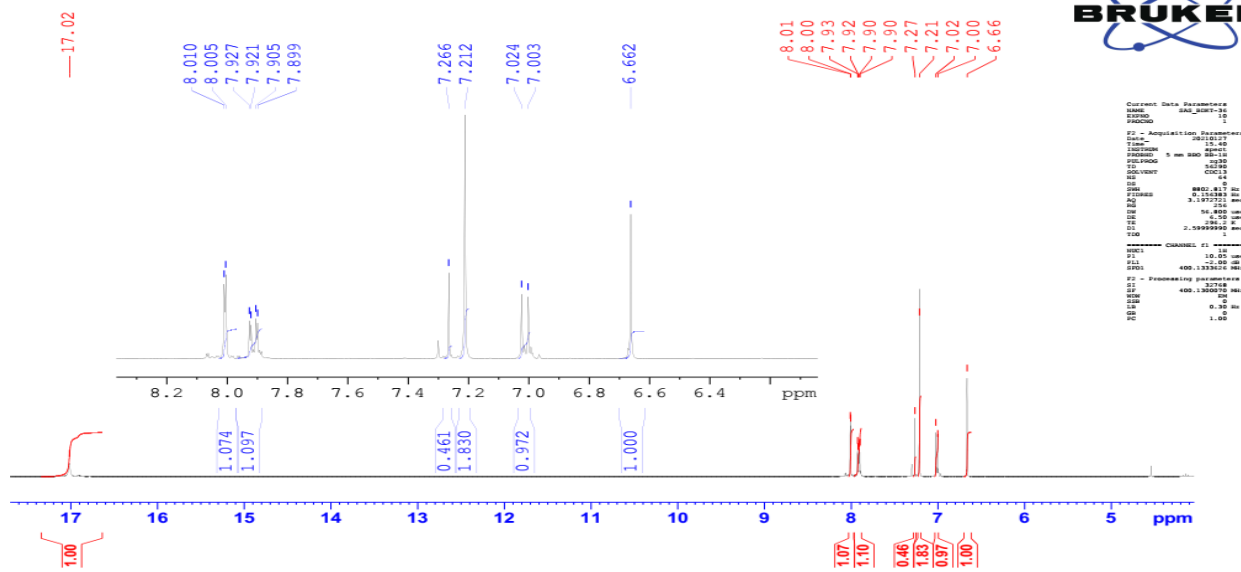


Spectrum Peaks

m/z	m/z (Calc)	Diff (ppm)	Abund	Height %	Height % (Calc)	Ion Species	Z
351.1040	351.1039	0.46	342592	100.00	100.00	(M+H)+	1
352.1074	352.1072	0.52	66999	19.56	19.85	(M+H)+	1
353.1102	353.1097	1.22	9543	2.79	2.89	(M+H)+	1
354.1096	354.1124	-7.96	1418	0.41	0.31	(M+H)+	1

BDKT-36

H1 NMR Spectrum of BDKT-36 in CDCl3+TMS
 PROTON64 CDC13 {C:\Bruker\TOPSPIN} SAS 11



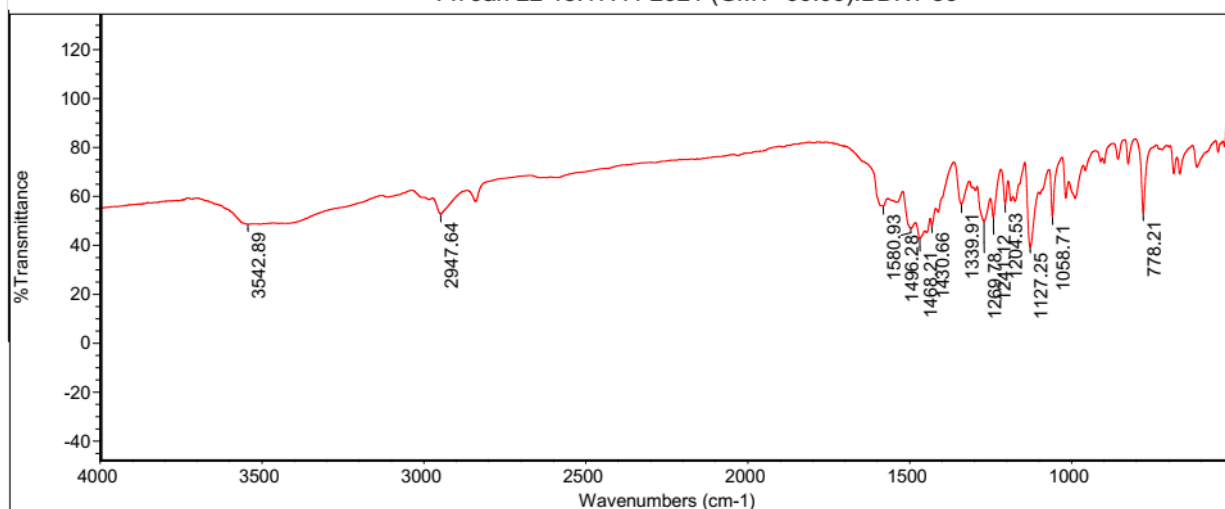
```

Current Data Parameters
NAME:   BDKT-36
PROCNO: 1
F2 - Acquisition Parameters
Date_   210217
Time    09:15:40
INSTRUM spect
PROBHD  5 mm BBO BB-1H
PULPROG zgpg30
TD       65536
SOLVENT CDCl3
NS       4096
DS       4
AQ       0.16181 sec
RG       3197721
FIDRES  0.400000
AQRES   0.500000
DE       2.5000000000000000
T1       2.5000000000000000
T1RHO   0.0000000000000000
===== CHANNEL f1 =====
NUC1     13C
P1       12.0000000000000000
PL1     -1.9000000000000000
SFO1    101.6253750000000000 MHz
F2 - Processing parameters
SI       32768
SF       101.6253750000000000 MHz
WDW      EM
SSB      0
GB       0.0000000000000000
PC       1.0000000000000000
    
```

ThermoFisher
 SCIENTIFIC

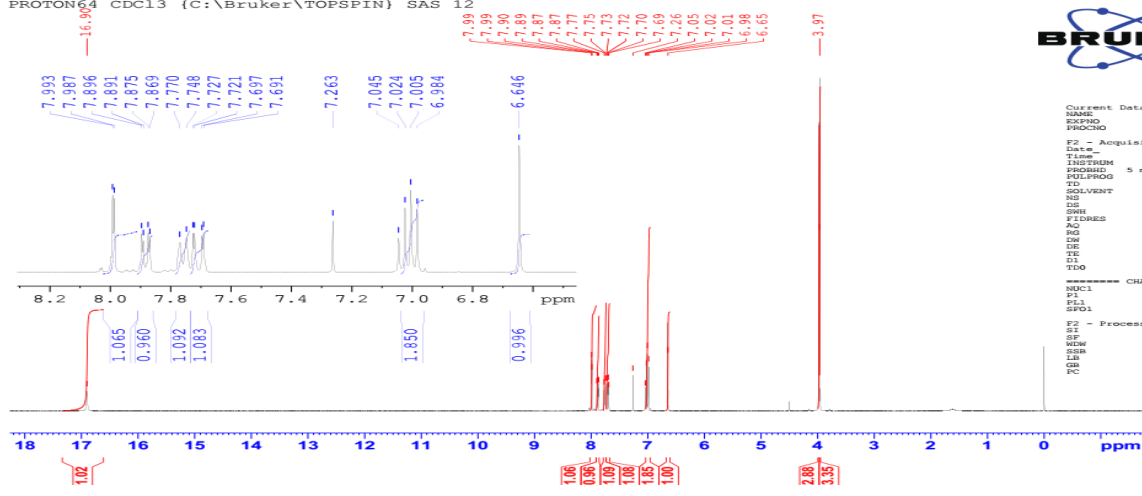
Mon Dec 13 18:44:28 2021 (

Fri Jan 22 13:17:41 2021 (GMT+00:00):BDKT-36



BDKT-37

H1 NMR Spectrum of BDKT-37 in CDCL3+TMS
 PROTON64 CDCL3 (C:\Bruker\TOPSPIN) SAS 12



```

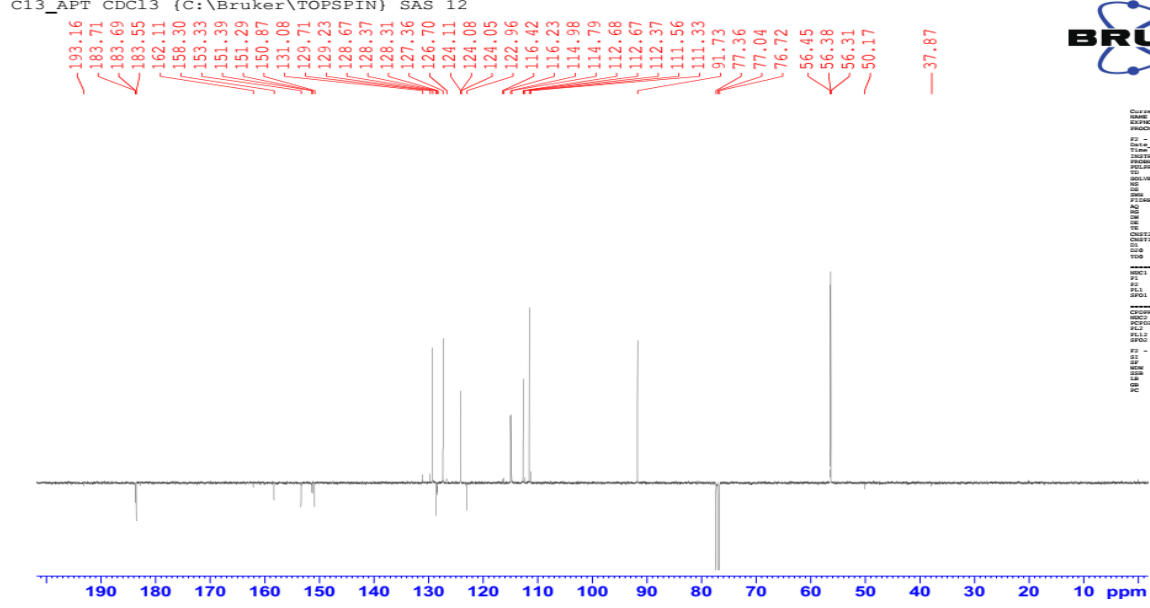
Current Data Parameters
NAME      SAS_BDKT-37
EXPNO    1
PROCNO   1

F2 - Acquisition Parameters
Date_    20210127
Time     19.52
INSTRUM  spect
PROBHD   5 mm BBO BB-1H
PULPROG  zg30
TD        65536
SOLVENT  CDCl3
NS        64
DS        0
SWH       8802.817 Hz
FIDRES    0.15538 Hz
AQ        3.1972721 sec
RG        327.68
DE        56.800 usec
TE        29.2 K
D1        2.59999990 sec
TD0       1

===== CHANNEL f1 =====
NUC1      1H
P1        10.05 usec
PL1       -2.00 dB
SFO1      400.1333626 MHz

F2 - Processing parameters
SI        32768
SF        400.1300081 MHz
WDW       EM
SSB       0
LB        0.30 Hz
GB        0
PC        1.00
    
```

2D g-HMOC NMR Spectrum of BDKT-37 in CDCL3+TMS
 C13_APT CDCL3 (C:\Bruker\TOPSPIN) SAS 12



```

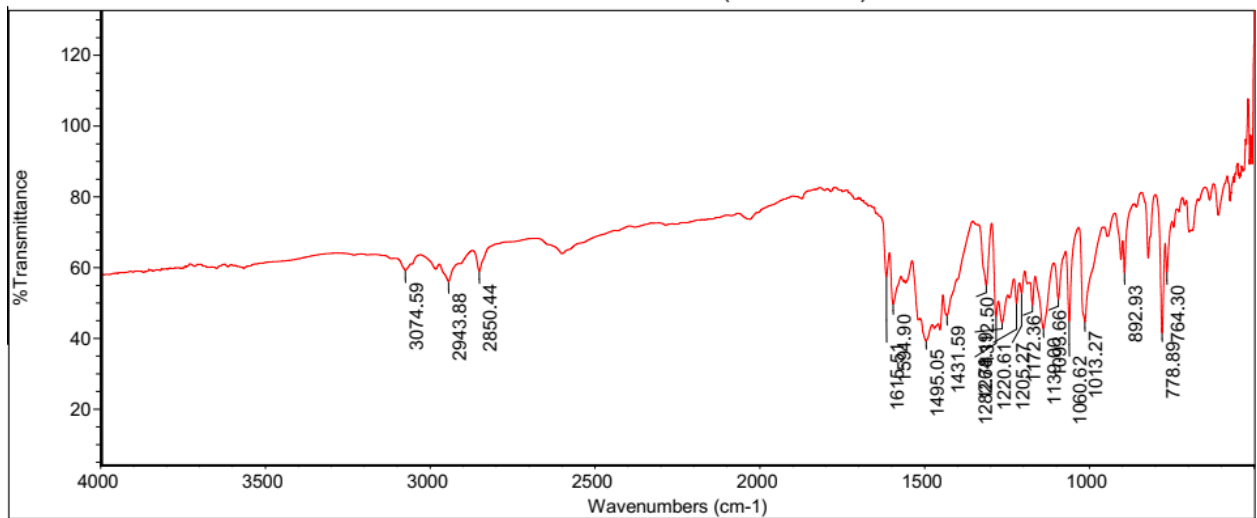
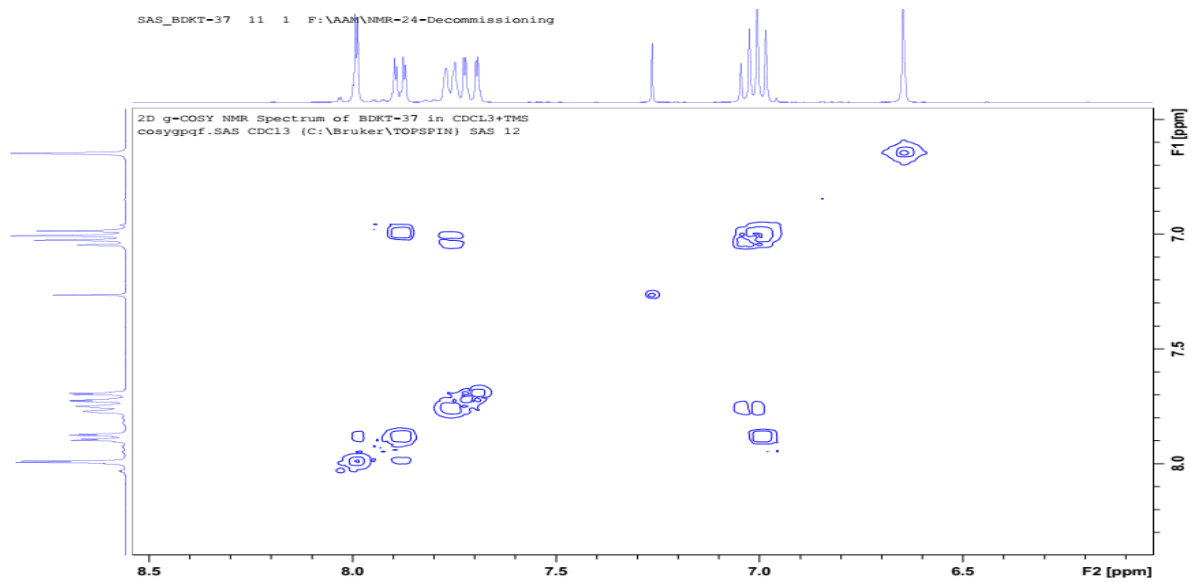
Current Data Parameters
NAME      SAS_BDKT-37
EXPNO    1
PROCNO   1

F2 - Acquisition Parameters
Date_    20210127
Time     19.52
INSTRUM  spect
PROBHD   5 mm BBO BB-1H
PULPROG  zg30
TD        65536
SOLVENT  CDCl3
NS        64
DS        0
SWH       7388.87 Hz
FIDRES    0.300514 Hz
AQ        1.305126 sec
RG        251
DE        20.800 usec
TE        29.2 K
D1        2.59999990 sec
D11       0.000000 sec
D12       0.000000 sec
D13       0.000000 sec
D14       0.000000 sec
D15       0.000000 sec
D16       0.000000 sec
D17       0.000000 sec
D18       0.000000 sec
D19       0.000000 sec
D20       0.000000 sec
D21       0.000000 sec
D22       0.000000 sec
D23       0.000000 sec
D24       0.000000 sec
D25       0.000000 sec
D26       0.000000 sec
D27       0.000000 sec
D28       0.000000 sec
D29       0.000000 sec
D30       0.000000 sec
D31       0.000000 sec
D32       0.000000 sec
D33       0.000000 sec
D34       0.000000 sec
D35       0.000000 sec
D36       0.000000 sec
D37       0.000000 sec
D38       0.000000 sec
D39       0.000000 sec
D40       0.000000 sec
D41       0.000000 sec
D42       0.000000 sec
D43       0.000000 sec
D44       0.000000 sec
D45       0.000000 sec
D46       0.000000 sec
D47       0.000000 sec
D48       0.000000 sec
D49       0.000000 sec
D50       0.000000 sec
D51       0.000000 sec
D52       0.000000 sec
D53       0.000000 sec
D54       0.000000 sec
D55       0.000000 sec
D56       0.000000 sec
D57       0.000000 sec
D58       0.000000 sec
D59       0.000000 sec
D60       0.000000 sec
D61       0.000000 sec
D62       0.000000 sec
D63       0.000000 sec
D64       0.000000 sec
D65       0.000000 sec
D66       0.000000 sec
D67       0.000000 sec
D68       0.000000 sec
D69       0.000000 sec
D70       0.000000 sec
D71       0.000000 sec
D72       0.000000 sec
D73       0.000000 sec
D74       0.000000 sec
D75       0.000000 sec
D76       0.000000 sec
D77       0.000000 sec
D78       0.000000 sec
D79       0.000000 sec
D80       0.000000 sec
D81       0.000000 sec
D82       0.000000 sec
D83       0.000000 sec
D84       0.000000 sec
D85       0.000000 sec
D86       0.000000 sec
D87       0.000000 sec
D88       0.000000 sec
D89       0.000000 sec
D90       0.000000 sec
D91       0.000000 sec
D92       0.000000 sec
D93       0.000000 sec
D94       0.000000 sec
D95       0.000000 sec
D96       0.000000 sec
D97       0.000000 sec
D98       0.000000 sec
D99       0.000000 sec
D100      0.000000 sec

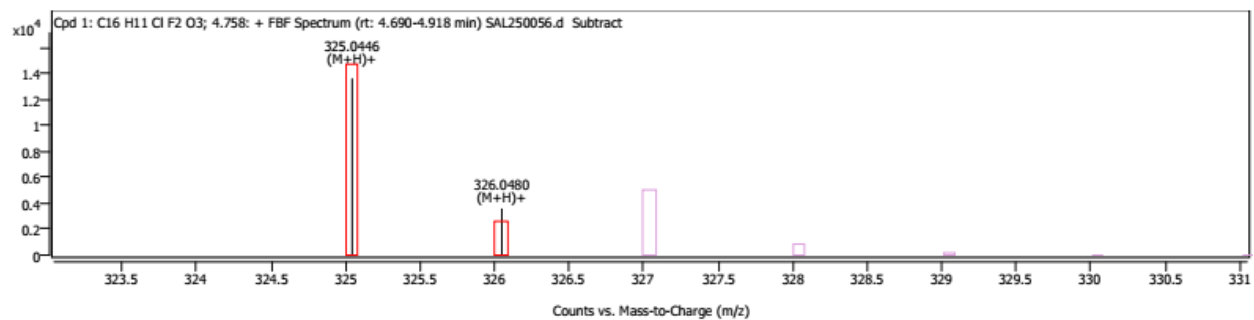
===== CHANNEL f1 =====
NUC1      13C
P1        18.00 usec
PL1       0.00 dB
SFO1      100.628359 MHz

===== CHANNEL f2 =====
CPDPRG2  waltz16
NUC2      1H
P2        8.00 usec
PL2       0.00 dB
PL12      70.00 dB
SFO2      400.1333626 MHz

F2 - Processing parameters
SI        32768
SF        100.6177030 MHz
WDW       EM
SSB       0
LB        1.00 Hz
GB        0
PC        1.40
    
```



Compound Spectra

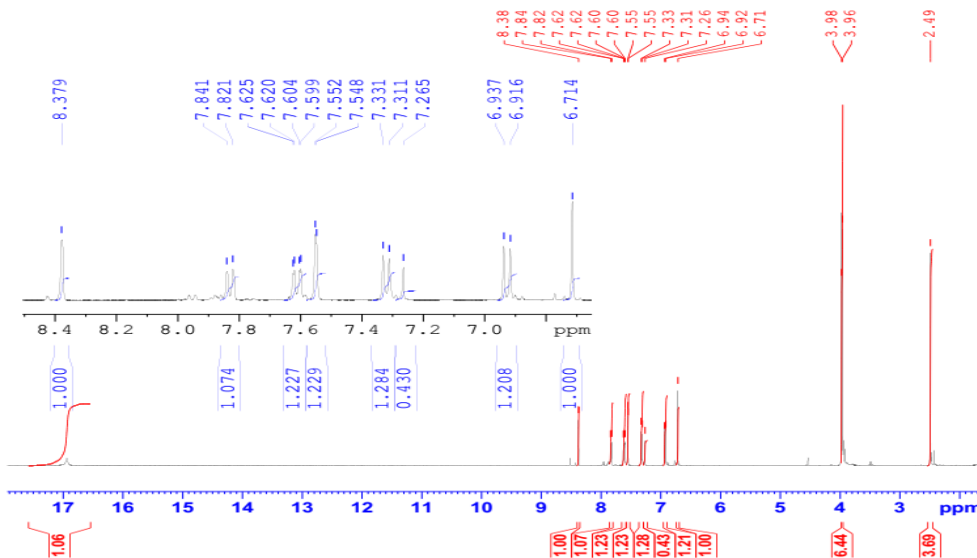


Spectrum Peaks

m/z	m/z (Calc)	Diff (ppm)	Abund	Height %	Height % (Calc)	Ion Species	Z
325.0446	325.0438	2.61	13606	100.00	100.00	(M+H) ⁺	1
326.0480	326.0471	2.77	3595	26.42	17.56	(M+H) ⁺	1

BDKT-41

H1 NMR Spectrum of BDKT-41 in CDCL3+TMS
 PROTON64 CDCL3 {C:\Bruker\TOPSPIN} SAS 8



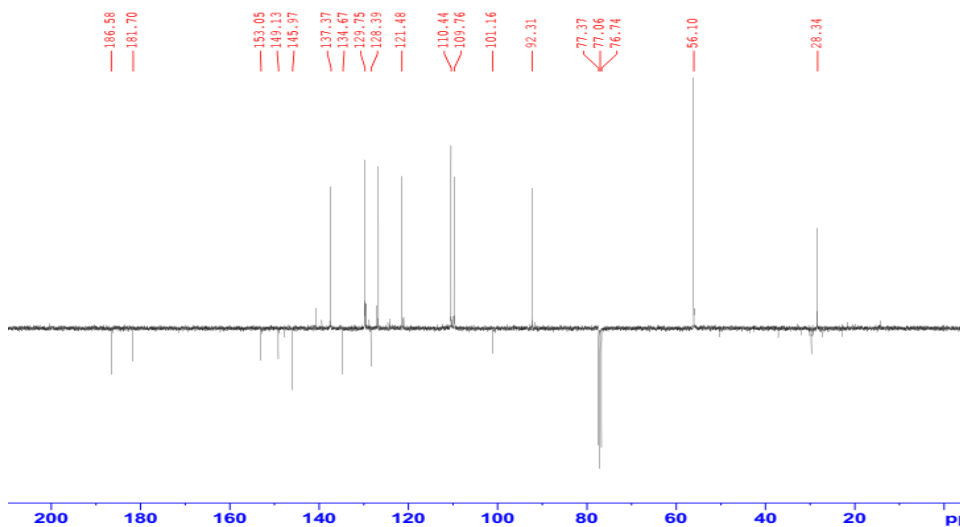
```
Current Data Parameters
NAME      SAS_BDKT41
EXPNO    10
PROCNO   1

F2 - Acquisition Parameters
Date_    20210123
Time     11.33
INSTRUM  spect
PROBHD   5 mm BBO BB-1H
PULPROG  zg30
TD        56290
SOLVENT  CDCL3
NS        64
DS        0
SWH       8802.817 Hz
FIDRES   0.156383 Hz
AQ        3.1972721 sec
RG        90.5
DW        56.800 usec
DE        6.50 usec
TE        296.2 K
D1        2.59999990 sec
TDO       1

===== CHANNEL f1 =====
NUC1      1H
P1        10.05 usec
PL1       -2.00 dB
SFO1      400.1333626 MHz

F2 - Processing parameters
SI        0
SF        400.1300073 MHz
WDW       no
SSB       0
LB        0 Hz
GB        0
PC        1.00
```

2D g-HMOC NMR Spectrum of BDKT-41 in CDCL3
 C13_APT CDCL3 {C:\Bruker\TOPSPIN} SAS 8



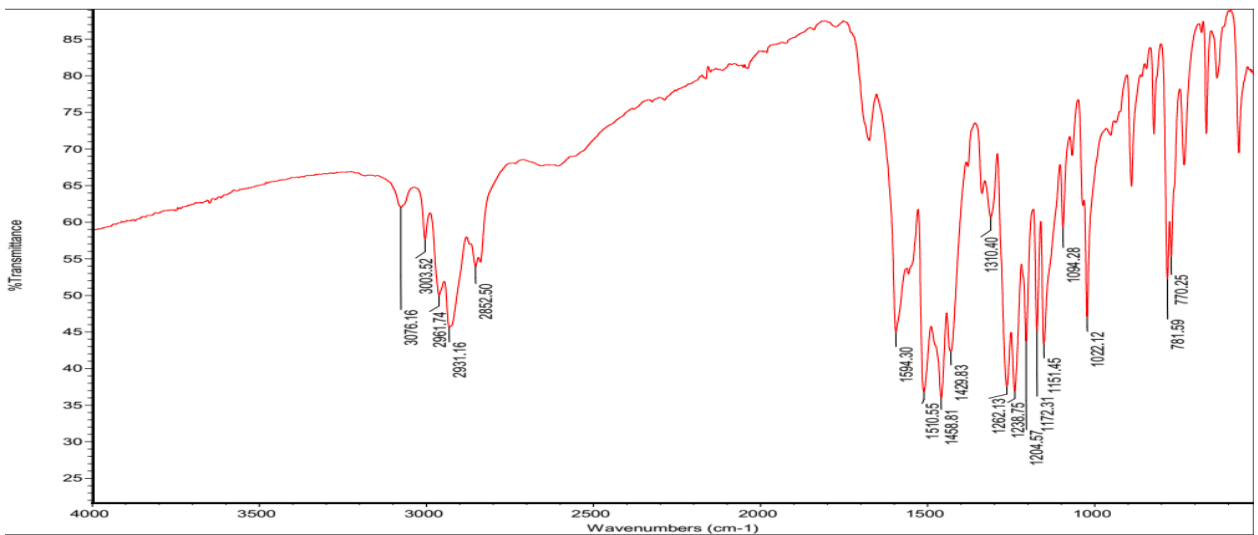
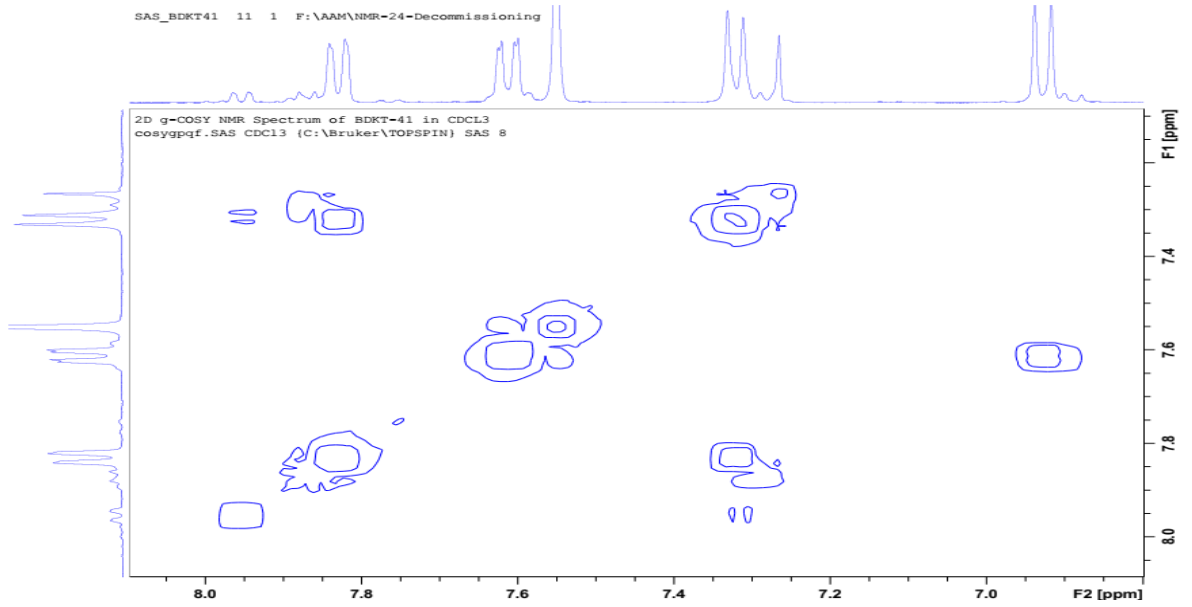
```
Current Data Parameters
NAME      SAS_BDKT41
EXPNO    13
PROCNO   1

F2 - Acquisition Parameters
Date_    20210127
Time     9.49
INSTRUM  spect
PROBHD   5 mm BBO BB-1H
PULPROG  jmod
TD        65336
SOLVENT  CDCL3
NS        5120
DS        4
SWH       23980.814 Hz
FIDRES   0.365918 Hz
AQ        1.3664256 sec
RG        16384
DW        20.850 usec
DE        6.50 usec
TE        296.2 K
CNST2    145.0000000
CNST11   1.0000000
D1        2.00000000 sec
D2        0.00689655 sec
TDO       1

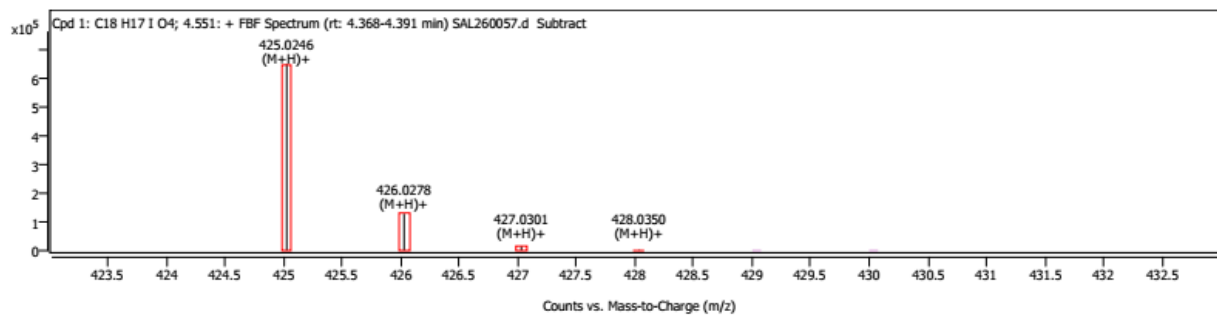
===== CHANNEL f1 =====
NUC1      13C
P1        9.00 usec
P2        18.00 usec
PL1       -2.00 dB
PL2       -2.00 dB
SFO1      100.6228298 MHz

===== CHANNEL f2 =====
CPDPRG[2] waltz16
NUC2      1H
PCPD2    80.00 usec
PL2       -2.00 dB
PL12     15.98 dB
SFO2     400.1316005 MHz

F2 - Processing parameters
SI        32768
SF        100.6127690 MHz
WDW       EM
SSB       0
LB        1.00 Hz
GB        0
PC        1.40
```



Compound Spectra

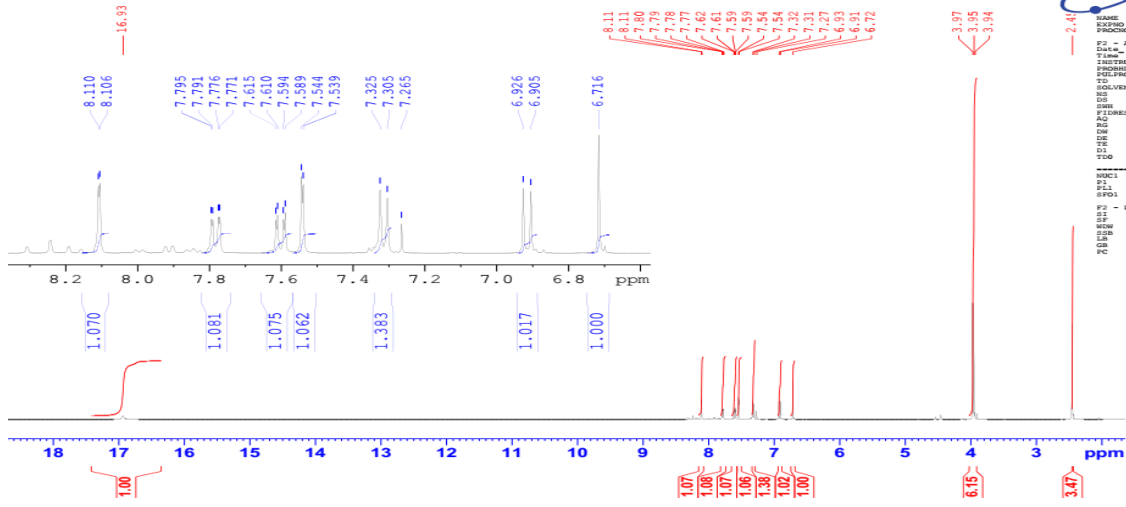


Spectrum Peaks

m/z	m/z (Calc)	Diff (ppm)	Abund	Height %	Height % (Calc)	Ion Species	Z
425.0246	425.0244	0.40	651719	100.00	100.00	(M+H)+	1
426.0278	426.0278	0.04	128655	19.74	19.83	(M+H)+	1
427.0301	427.0304	-0.72	15660	2.40	2.68	(M+H)+	1
428.0350	428.0331	4.56	1763	0.27	0.27	(M+H)+	1

BDKT-43

H1 NMR Spectrum of BDKT-43 in CDCL3+TMS
 PROTON64 CDC13 {C:\Bruker\TOPSPIN} SAS 5



```

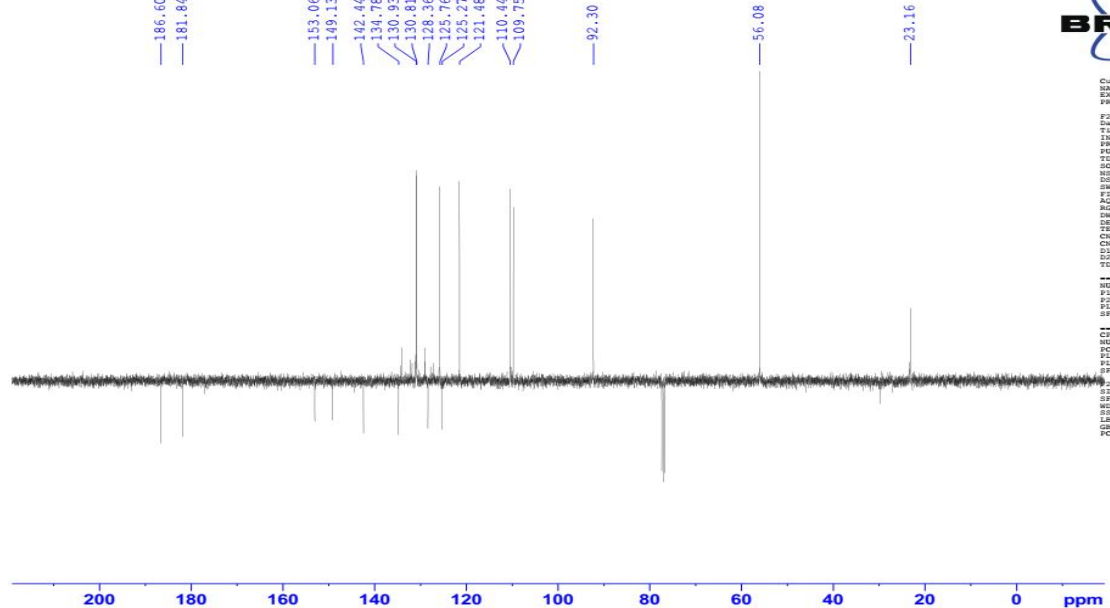
NAME          SAS_BDKT43
PROCNO        1
Date_         20210122
Time_         13:31
INSTRUM       spect
PROBHD        5 mm BBO BB-1H
PULPROG       jmod
TD            65536
SOLVENT       CDCl3
NS            44
DS            4
SWH           8900.814 Hz
FIDRES        0.156483 Hz
AQ            3.197271 sec
RG            16384
WDW           EM
SSB           0
LB            71.0 Hz
GB            0
PC            1.00 usec
TE            300.2 K
DE            2.000000 sec
DI            1
TD0           1
  
```

```

----- CHANNEL f1 -----
NUC1          13C
P1            10.00 usec
PL1           0.00 dB
SFO1          400.1334548 MHz

F2 - Processing parameters
SI            13C
SF            400.1300072 MHz
WDW           EM
SSB           0
LB            0.30 Hz
GB            0
PC            1.00
  
```

JMOD C13 NMR Spectrum of BDKT-43 in CDCL3



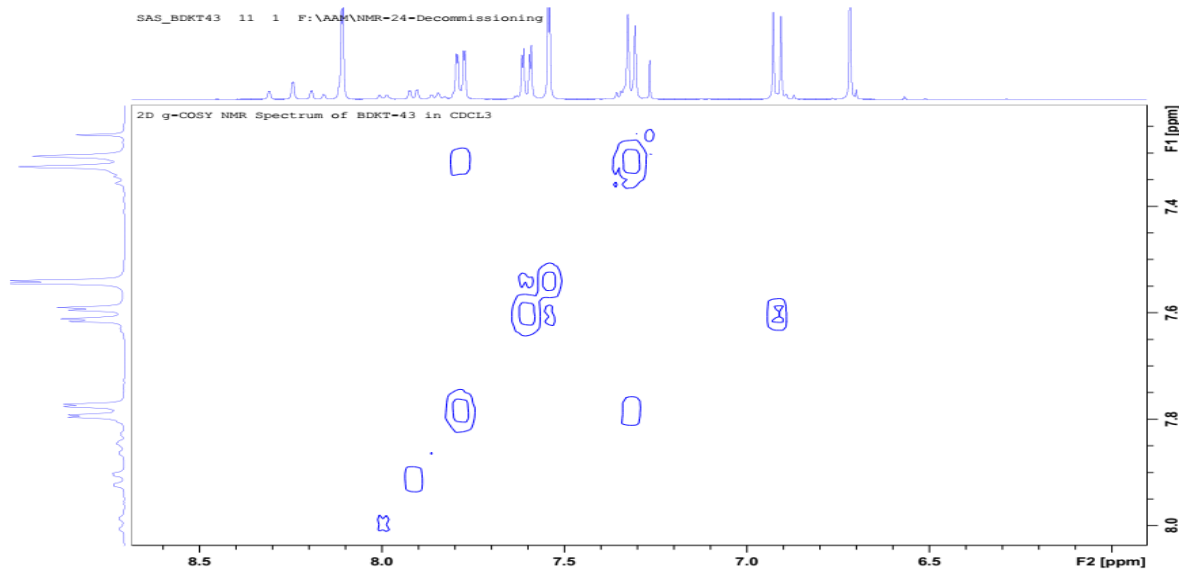
```

Current Data Parameters
NAME          SAS_BDKT43
EXPNO        13
PROCNO        1
Date_         20210122
Time_         13:31
INSTRUM       spect
PROBHD        5 mm BBO BB-1H
PULPROG       jmod
TD            65536
SOLVENT       CDCl3
NS            472
DS            4
SWH           23980.814 Hz
FIDRES        0.260518 Hz
AQ            1.3664256 sec
RG            16384
WDW           EM
SSB           0
LB            71.0 Hz
GB            0
PC            1.00 usec
TE            300.2 K
DE            2.000000 sec
DI            1
TD0           1
  
```

```

----- CHANNEL f1 -----
NUC1          13C
P1            10.00 usec
PL1           0.00 dB
SFO1          100.6228298 MHz

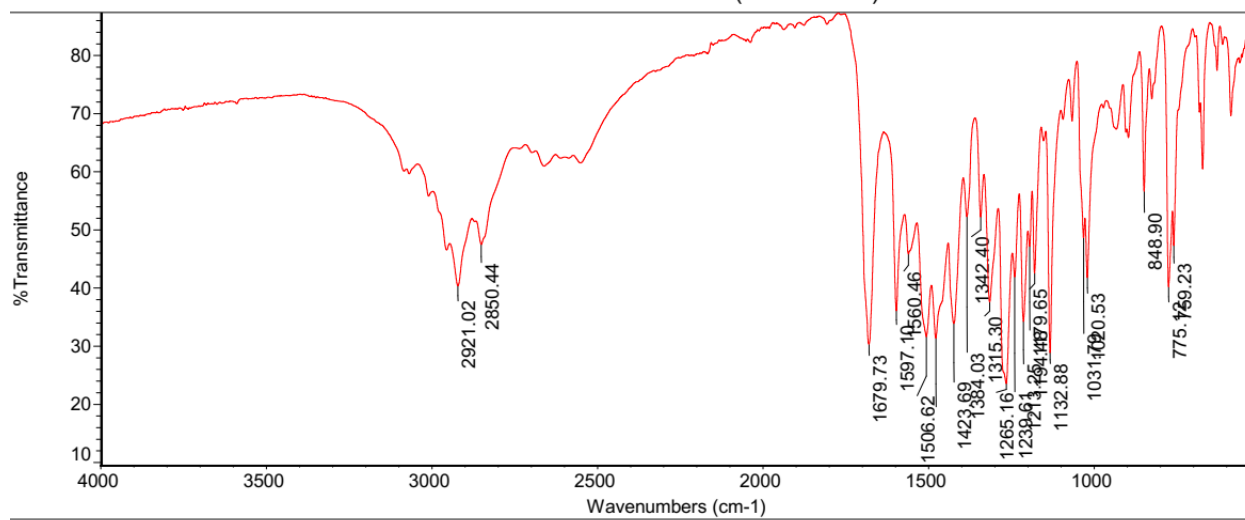
----- CHANNEL f2 -----
NAME          SAS_BDKT43
EXPNO        13
PROCNO        1
Date_         20210122
Time_         13:31
INSTRUM       spect
PROBHD        5 mm BBO BB-1H
PULPROG       jmod
TD            65536
SOLVENT       CDCl3
NS            472
DS            4
SWH           23980.814 Hz
FIDRES        0.260518 Hz
AQ            1.3664256 sec
RG            16384
WDW           EM
SSB           0
LB            71.0 Hz
GB            0
PC            1.00 usec
TE            300.2 K
DE            2.000000 sec
DI            1
TD0           1
  
```



ThermoFisher
SCIENTIFIC

Sun Dec 12 18:00:52 2021 (

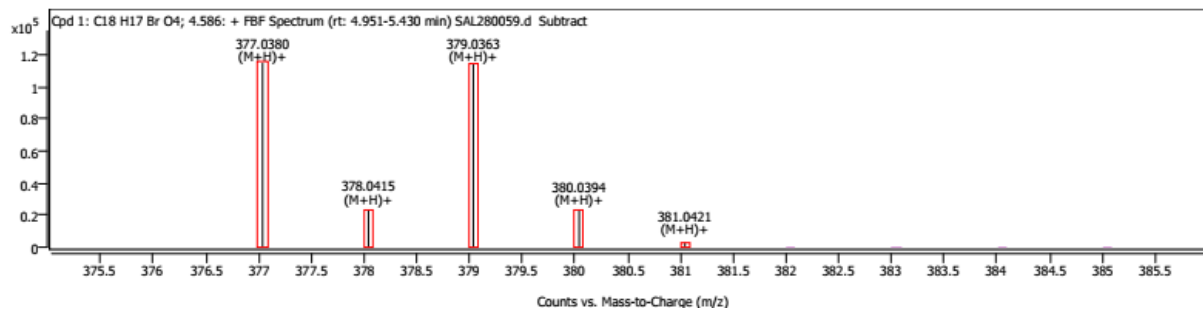
Thu Jan 21 12:07:12 2021 (GMT+00:00):BDKT-43



Spectrum Peaks

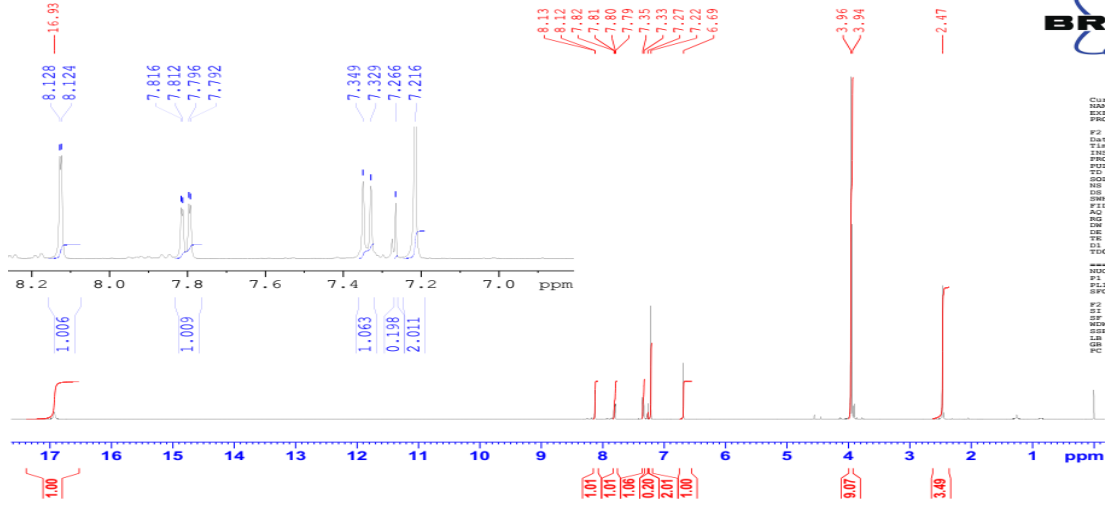
m/z	Z	Abund	Diff (ppm)	Height %	Height % (Calc)	Ion Species	Formula
377.0380	1	114795	-0.71	100.00	100.00	(M+H) ⁺	C18H17BrO4
378.0415	1	23444	-0.55	20.42	19.83	(M+H) ⁺	C18H17BrO4
379.0363	1	113853	-0.46	99.18	99.96	(M+H) ⁺	C18H17BrO4
380.0394	1	23235	-0.90	20.24	19.56	(M+H) ⁺	C18H17BrO4
381.0421	1	2948	-0.63	2.57	2.63	(M+H) ⁺	C18H17BrO4

Compound Spectra



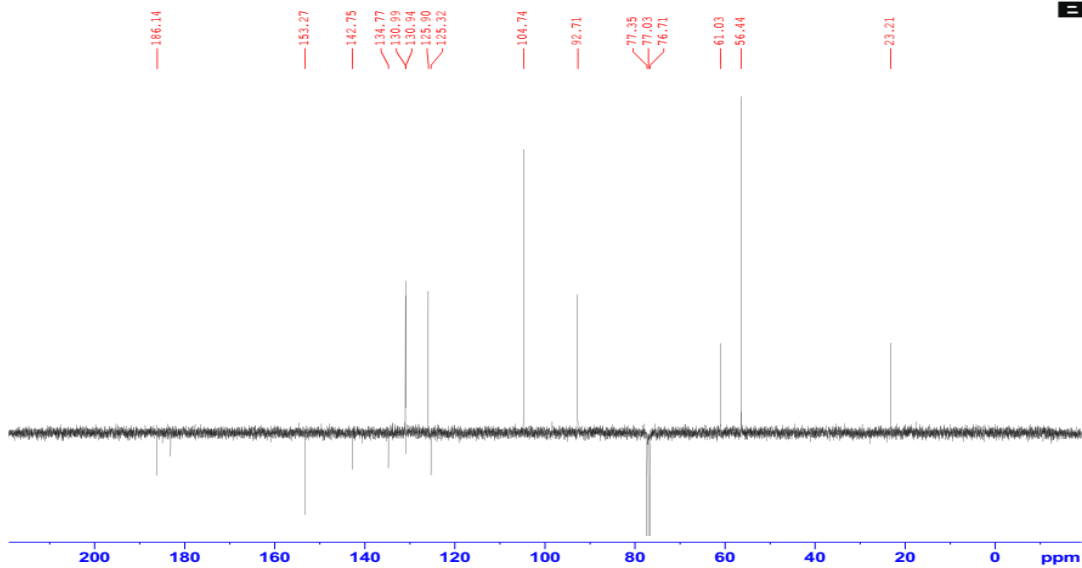
BDKT-44

H1 NMR Spectrum of BDKT- 44 in CDCL3+TMS
 PROTON64 CDC13 (C:\Bruker\TOPSPIN) SAS 9

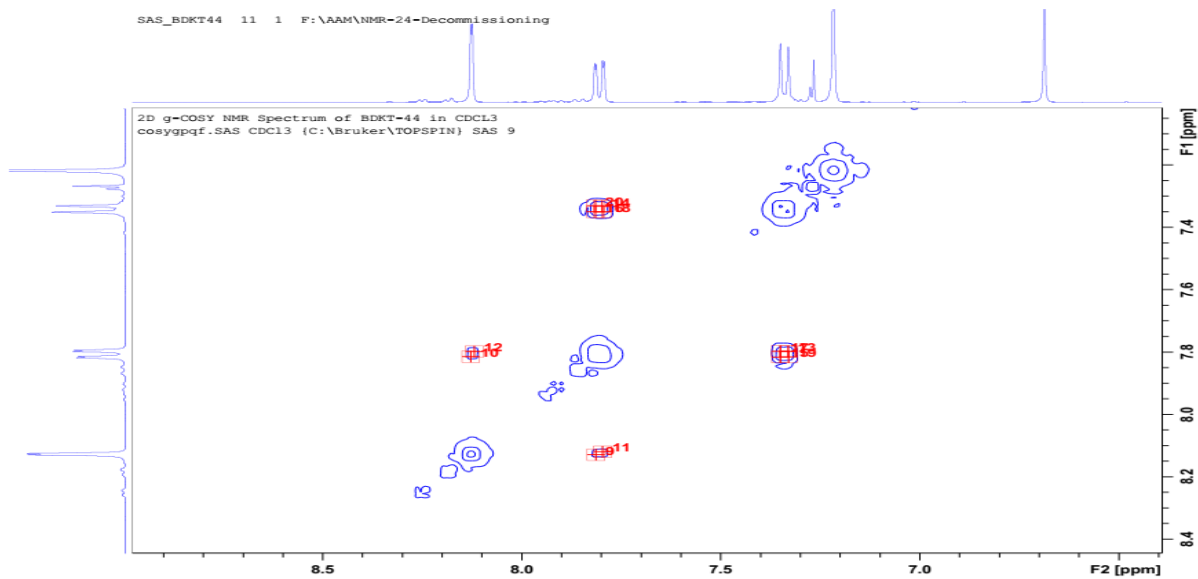


```
Current Data Parameters
NAME      SAS_MW744
EXPNO    10
PROCNO   1
F2 - Acquisition Parameters
Date_    20210123
Time     02:13
INSTRUM spect
PROBHD   5 mm BBO BB-1H
PULPROG zgpg30
SOLVENT  CDCl3
NS       64
DS       4
SWH      8602.817 Hz
FIDRES   0.156383 Hz
AQ       2.137721 sec
RG       56.800 usec
WE       6.50 usec
TE       296.2 K
DQ       2.589890 sec
TDO      1
===== CHANNEL f1 =====
NUC1      1H
P1        12.00 usec
PL1       0.00 dB
SFO1      400.13836 MHz
F2 - Processing parameters
SI        32768
SF        400.130070 MHz
WDW       EM
SSB       0
LB        0.30 Hz
GB        0
PC        1.00
```

JMOD C13 NMR Spectrum of BDKT- 44 in CDCL3
 C13_APT CDC13 (C:\Bruker\TOPSPIN) SAS 9



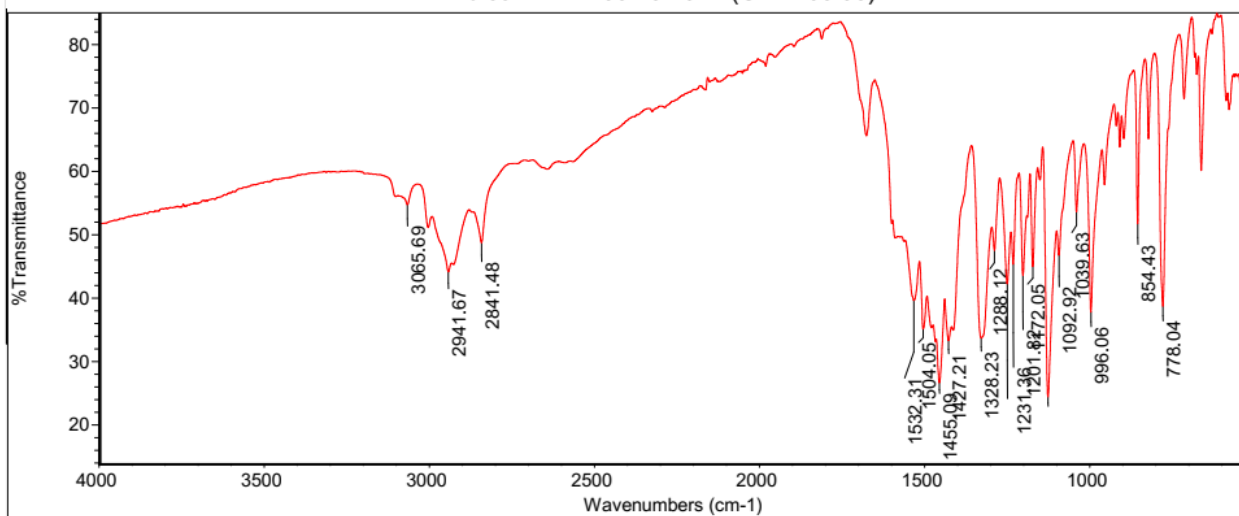
```
Current Data Parameters
NAME      SAS_MW744
EXPNO    13
PROCNO   1
F2 - Acquisition Parameters
Date_    20210123
Time     17:27
INSTRUM spect
PROBHD   5 mm BBO BB-1H
PULPROG zgpg30
SOLVENT  CDCl3
NS       64
DS       4
SWH      23980.814 Hz
FIDRES   0.248918 Hz
AQ       1.368138 sec
RG       14384
WE       6.50 usec
TE       296.2 K
DQ       2.589890 sec
TDO      1
===== CHANNEL f1 =====
NUC1      13C
P1        18.00 usec
PL1       0.00 dB
SFO1      100.6228258 MHz
===== CHANNEL f2 =====
NAME(f2)  w11k14
NUC2      1H
P2        12.00 usec
PL2       0.00 dB
SFO2      400.1316005 MHz
F2 - Processing parameters
SI        32768
SF        100.6127670 MHz
WDW       EM
SSB       0
LB        1.00 Hz
GB        0
PC        3.00
```



ThermoFisher
 SCIENTIFIC

Sun Dec 12 18:15:57 2021 (

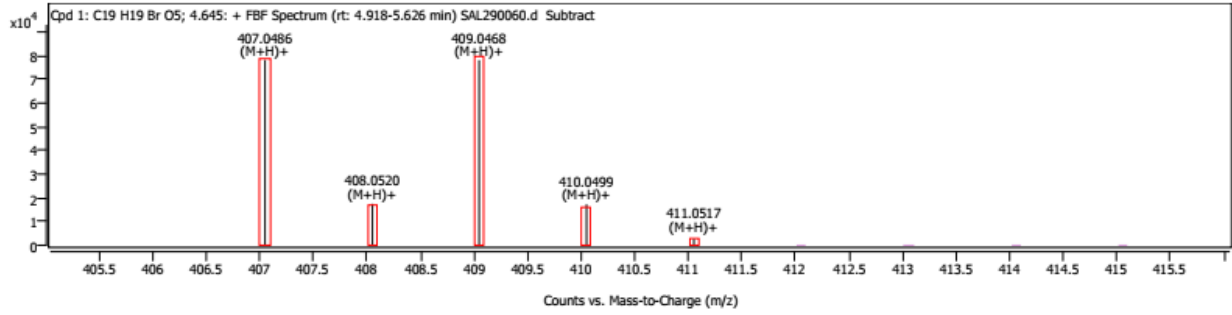
Thu Jan 21 12:00:40 2021 (GMT+00:00):BDKT-44



Spectrum Peaks

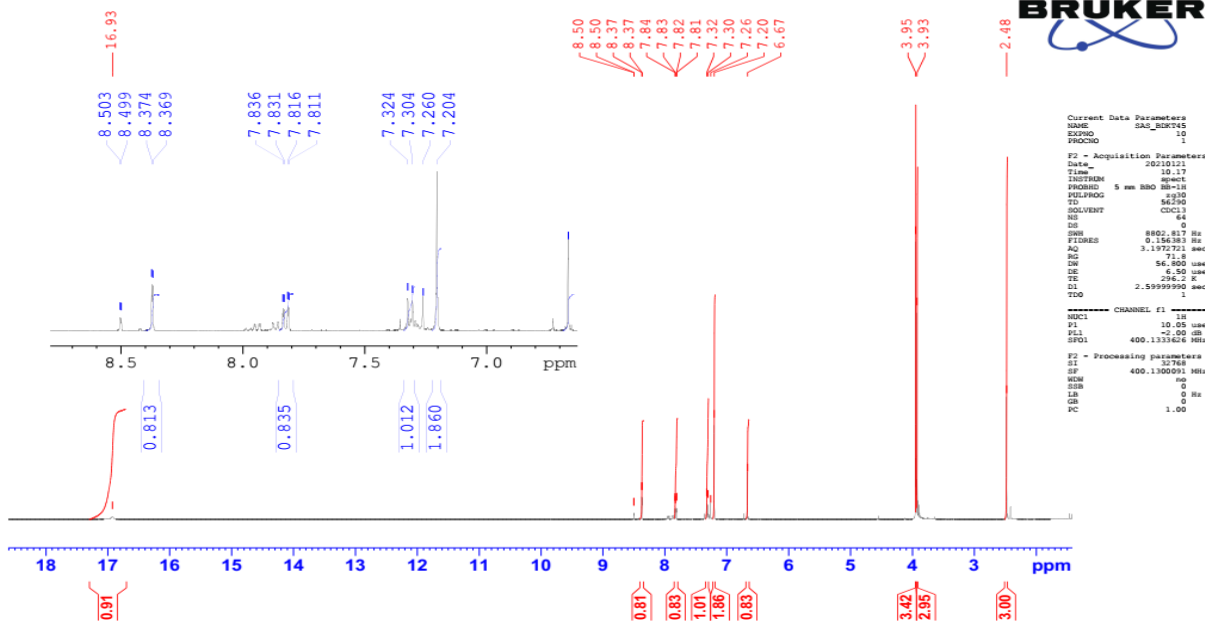
m/z	Z	Abund	Diff (ppm)	Height %	Height % (Calc)	Ion Species	Formula
407.0486	1	78130	-0.58	100.00	99.61	(M+H) ⁺	C ₁₉ H ₁₉ BrO ₅
408.0520	1	17422	-0.69	22.30	20.89	(M+H) ⁺	C ₁₉ H ₁₉ BrO ₅
409.0468	1	77993	-0.69	99.83	100.00	(M+H) ⁺	C ₁₉ H ₁₉ BrO ₅
410.0499	1	17177	-0.98	21.99	20.66	(M+H) ⁺	C ₁₉ H ₁₉ BrO ₅
411.0517	1	2663	-2.72	3.41	3.05	(M+H) ⁺	C ₁₉ H ₁₉ BrO ₅

Compound Spectra

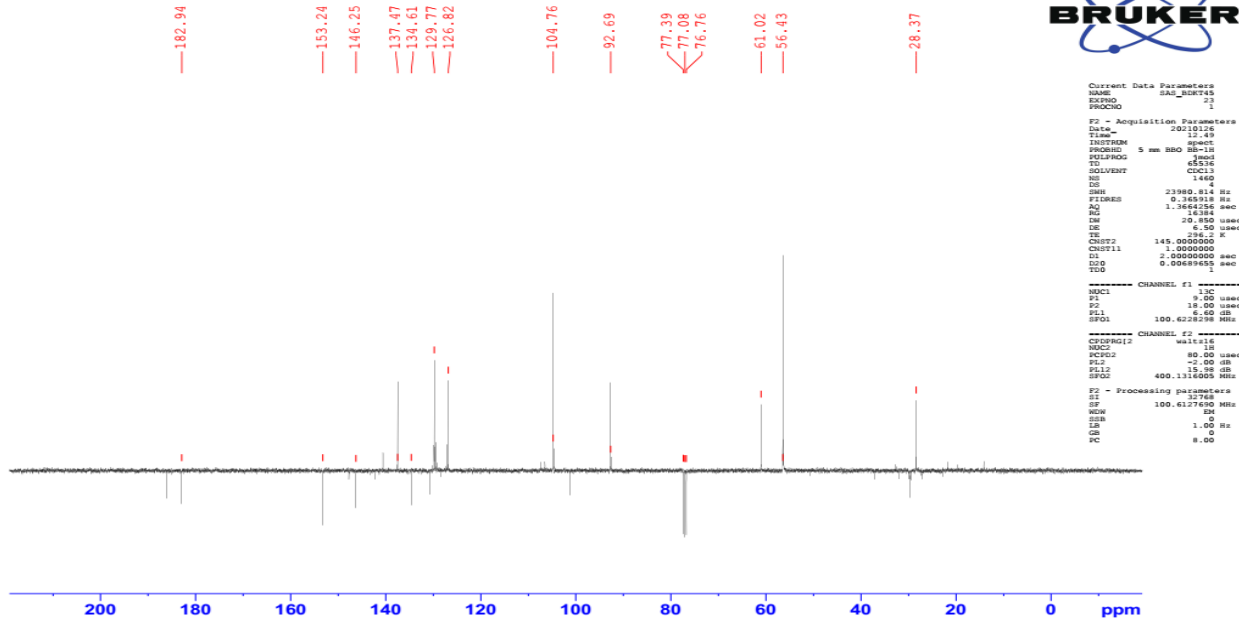


BDKT-45

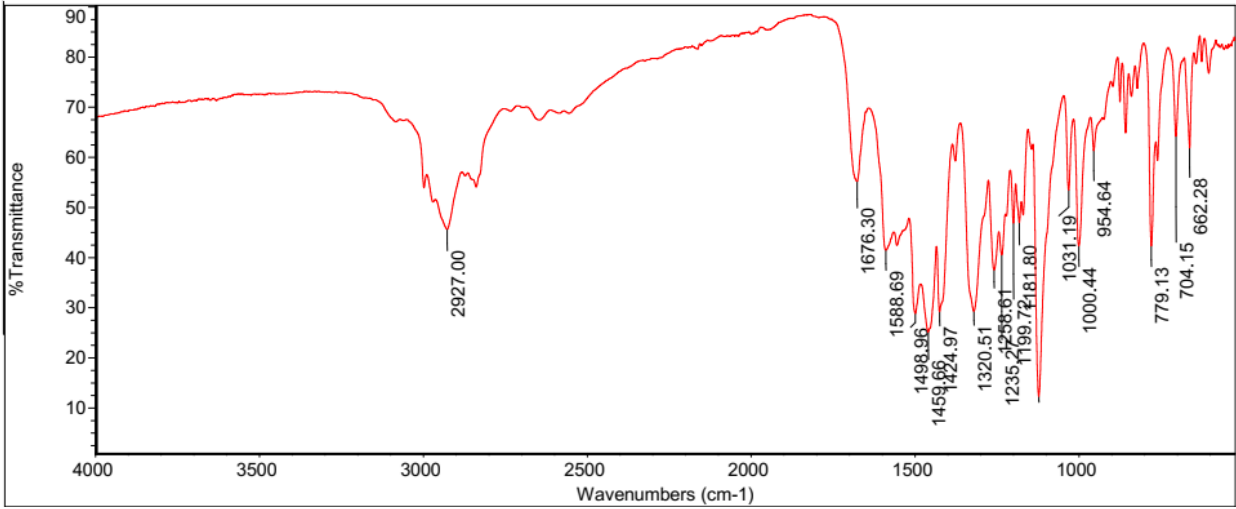
H1 NMR Spectrum of BDKT-45 in CDCl3+TMS
 PROTON64 CDCl3 (C:\Bruker\TOPSPIN) SAS 5



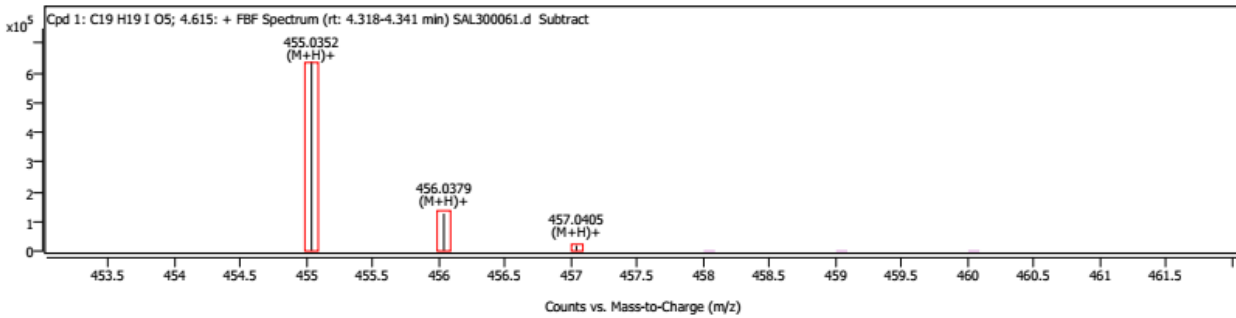
BB H1 Decoupled C13 NMR Spectrum of BDKT-45 in CDCl3
 C13_APT CDCl3 (C:\Bruker\TOPSPIN) SAS 2



Thu Jan 21 11:57:09 2021 (GMT+00:00):BDKT-45



Compound Spectra

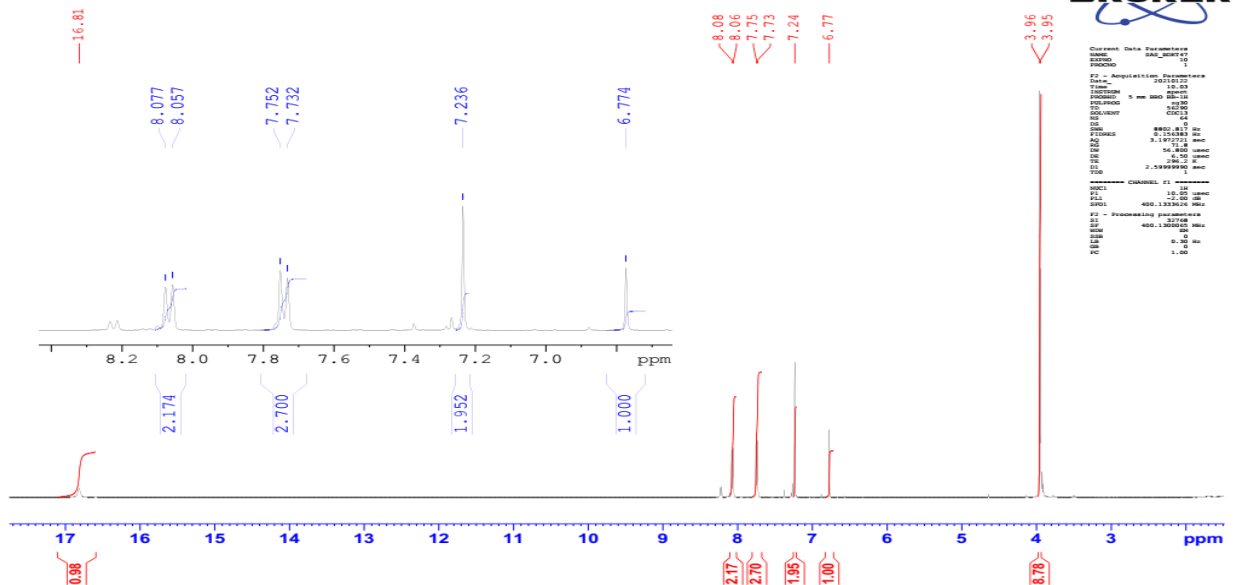


Spectrum Peaks

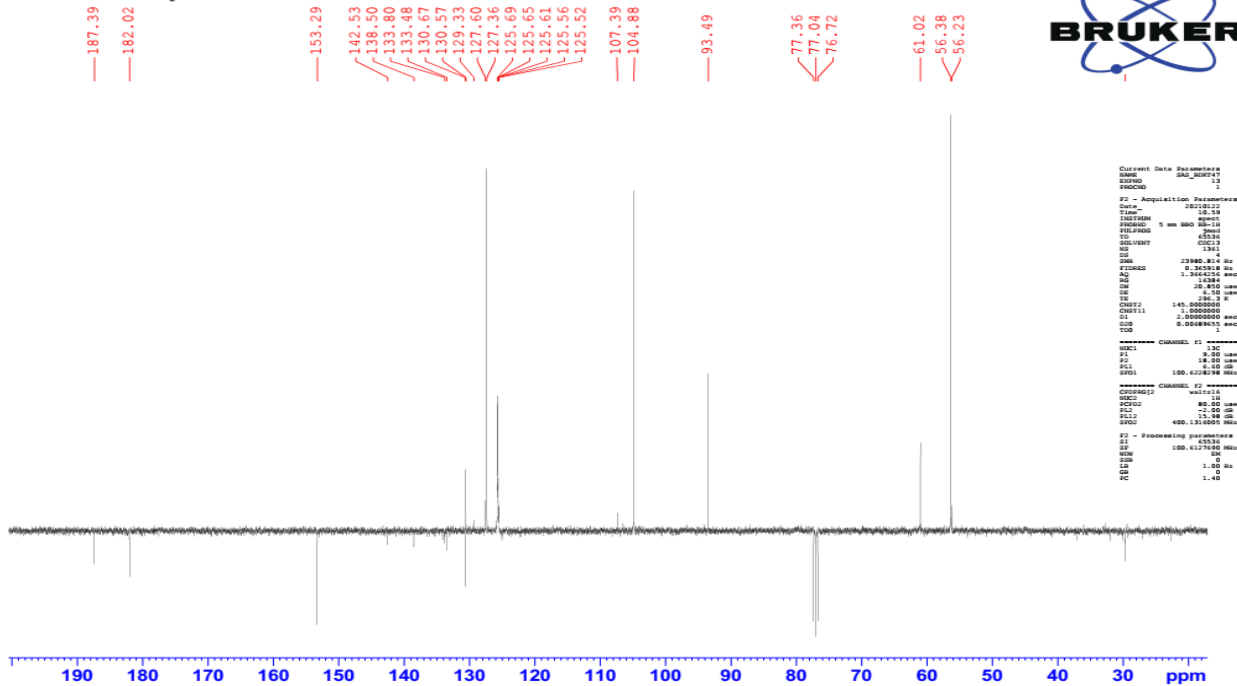
m/z	m/z (Calc)	Diff (ppm)	Abund	Height %	Height % (Calc)	Ion Species	Z
455.0352	455.0350	0.47	637986	100.00	100.00	(M+H)+	1
456.0379	456.0384	-1.03	125960	19.74	20.97	(M+H)+	1
457.0405	457.0409	-1.06	18489	2.90	3.12	(M+H)+	1

BDKT-47

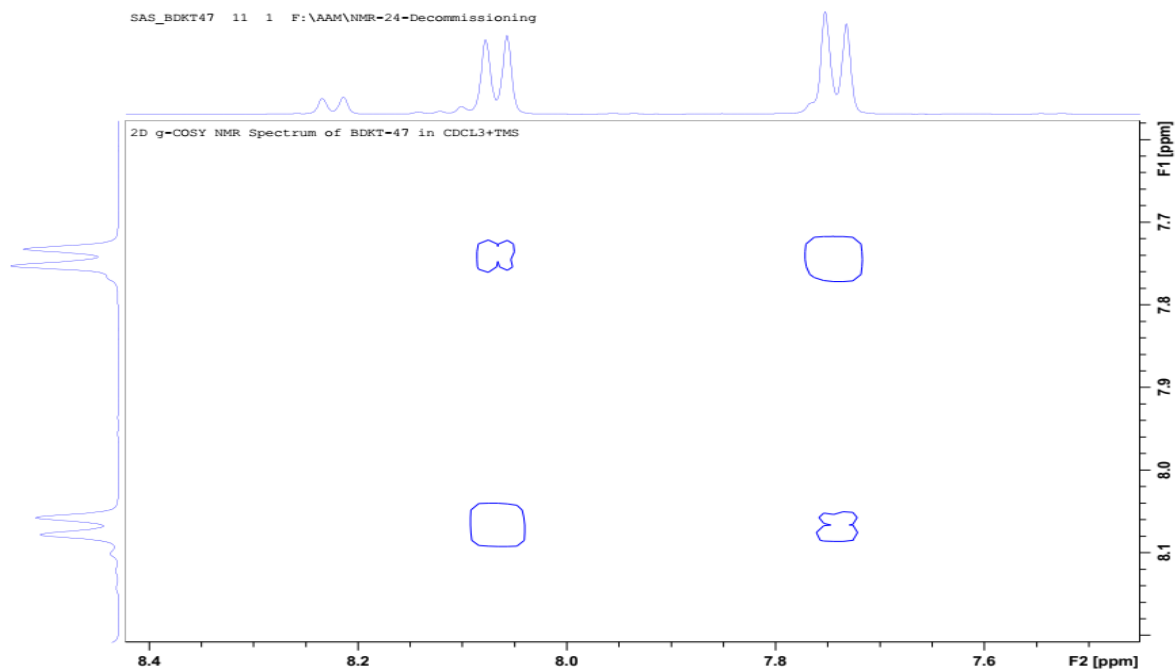
H1 NMR Spectrum of BDKT-47 in CDCL3+TMS



JMOD C13 NMR Spectrum of BDKT-47 in CDCL3+TMS



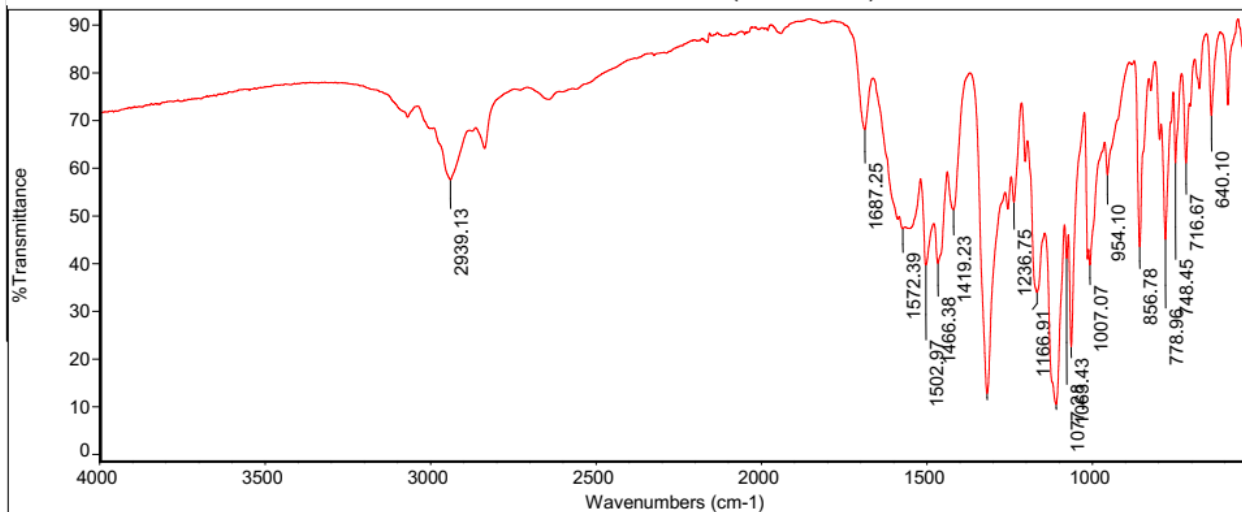
SAS_BDKT47 11 1 F:\AAM\NMR-24-Decommissioning



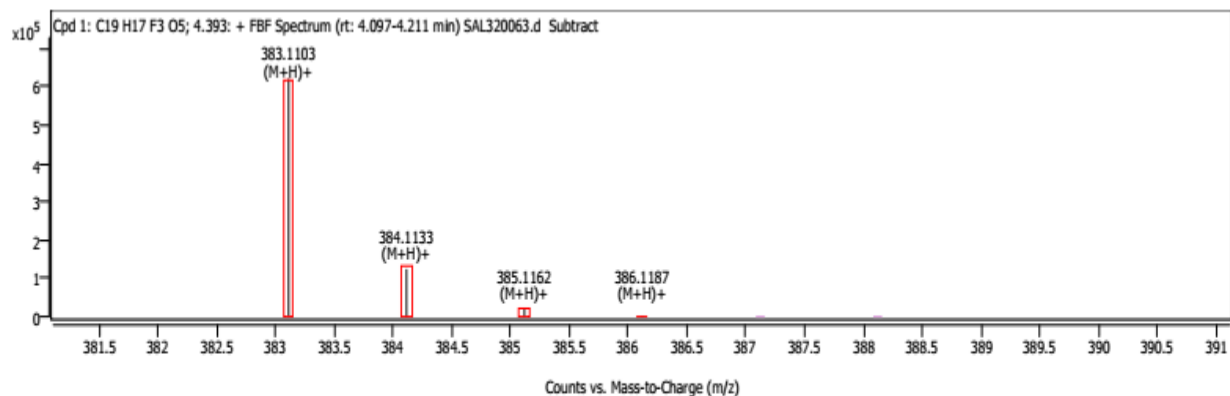
ThermoFisher
SCIENTIFIC

Mon Dec 13 07:53:55 2021 (

Thu Jan 21 11:48:02 2021 (GMT+00:00):BDKT-47



Compound Spectra

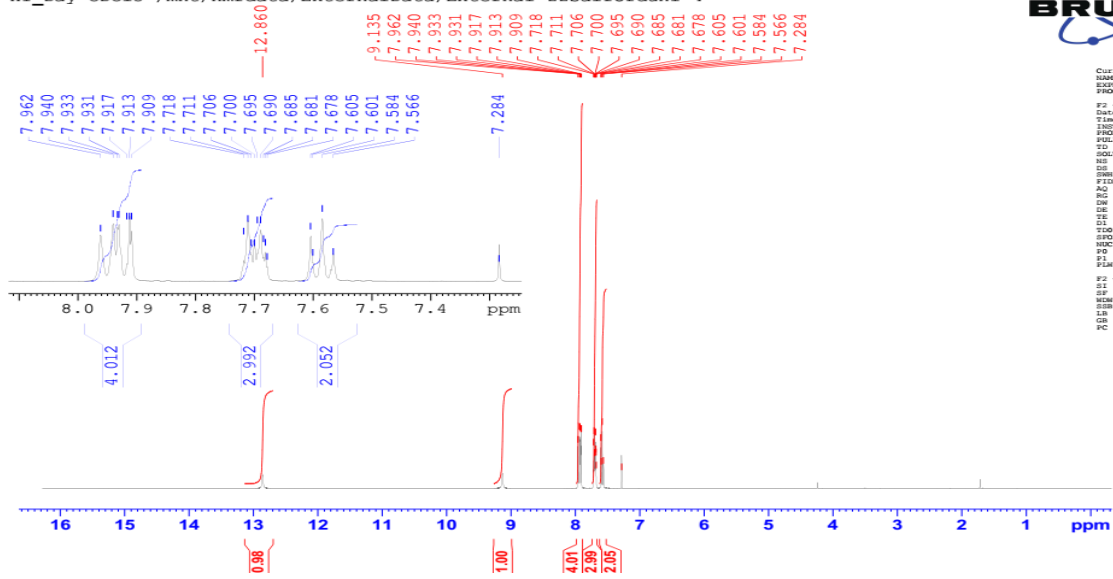


Spectrum Peaks

m/z	m/z (Calc)	Diff (ppm)	Abund	Height %	Height % (Calc)	Ion Species	Z
383.1103	383.1101	0.66	621400	100.00	100.00	(M+H) ⁺	1
384.1133	384.1135	-0.34	124394	20.02	20.95	(M+H) ⁺	1
385.1162	385.1160	0.45	18913	3.04	3.11	(M+H) ⁺	1
386.1187	386.1187	-0.09	2076	0.33	0.35	(M+H) ⁺	1

BTU-01

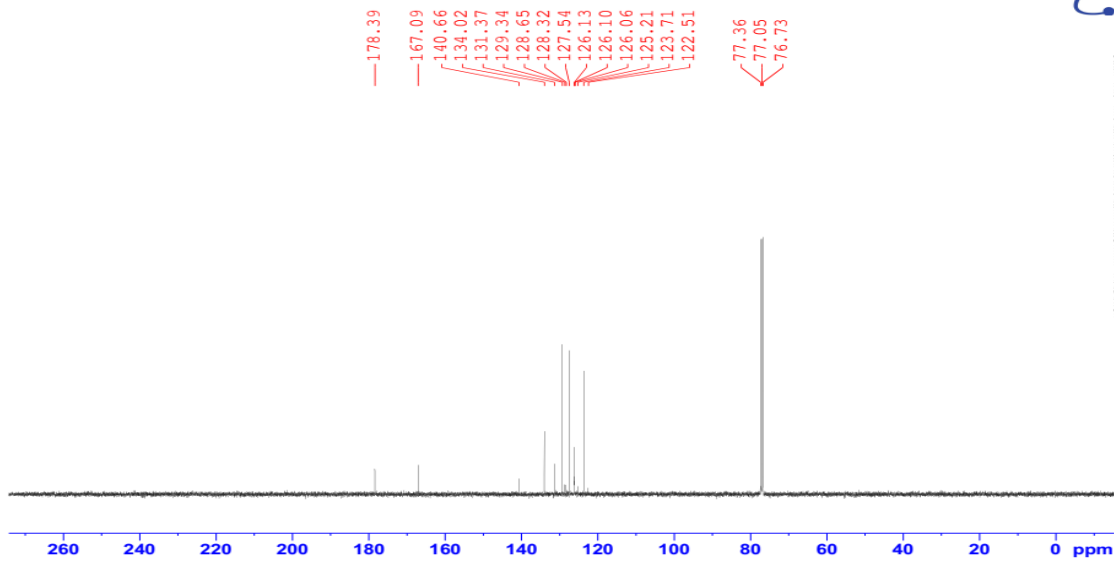
Ref BTU-01-AAM
 Group External
 H1_Day CDC13 /mnt/nmrdata/ExternalData/External zzsalforduni 4



```

Current Data Parameters
NAME      BTU-01
EXPNO    10
PROCNO   1
-----
F2 - Acquisition Parameters
Date_    2012010
Time     17:30 h
INSTRUM  spect
PROBHD   Z130030_0009.f
PULPROG  zgpg30
SOLVENT  CDCl3
NS       4
DS       2
SFORES  8223.665 Hz
FIDRES  0.250967 Hz
AQ       3.584855 sec
RG       128
DE       60.800 usec
TE       30.00 usec
TD       65536
TE1      1.00000000 sec
YD0      400.0724004 MHz
SFO1     318
NUC1     13
P1       4.00 usec
PC       1.00
FID1     7.40000010 usec
-----
F2 - Processing parameters
SI       400.0700000 MHz
SF       400.0700000 MHz
WDW      EM
SSB      0.30 Hz
LB       1.00
GB       0
PC       1.00
    
```

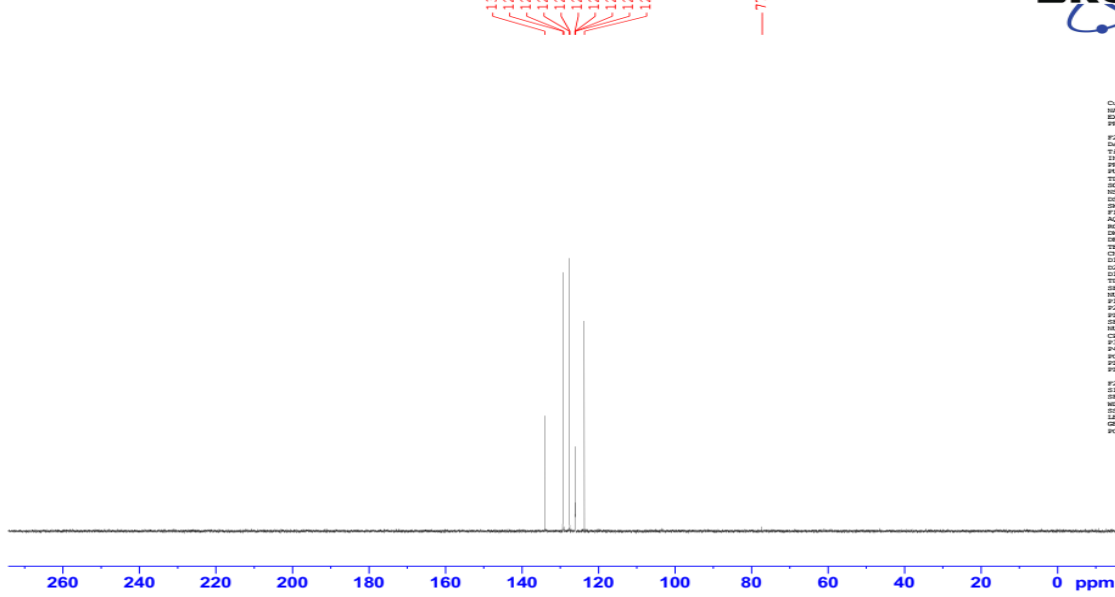
Ref BTU-01-AAM
 Group External
 C13_CPD_Day CDC13 /mnt/nmrdata/ExternalData/External zzsalforduni 4



```

Current Data Parameters
NAME      BTU-01
EXPNO    11
PROCNO   1
-----
F2 - Acquisition Parameters
Date_    2012010
Time     19:12 h
INSTRUM  spect
PROBHD   Z130030_0009.f
PULPROG  zgpg30
SOLVENT  CDCl3
NS       4
DS       2
SFORES  32051.281 Hz
FIDRES  0.478217 Hz
AQ       1.028114 sec
RG       128
DE       61.18 usec
TE       30.00 usec
TD       65536
TE1      1.00000000 sec
YD0      100.6263612 MHz
SFO1     318
NUC1     13
P1       1.30 usec
PC       1.00
FID1     32.05000000 usec
SFO2     400.0724004 MHz
SFO3     101.6261260 MHz
CPDPRG2  waltz16
NUC2     13
SFO4     100.6263612 MHz
FID2     2.13000000 usec
SFO5     125.7613600 MHz
-----
F2 - Processing parameters
SI       100.6263612 MHz
SF       100.6263612 MHz
WDW      EM
SSB      0.30 Hz
LB       1.00 Hz
GB       0
PC       1.00
    
```

Ref BTU-01-AAM
 Group External
 C13_DEPT135_Day CDC13 /mnt/nmrdata/ExternalData/External/zzsalforduni 4



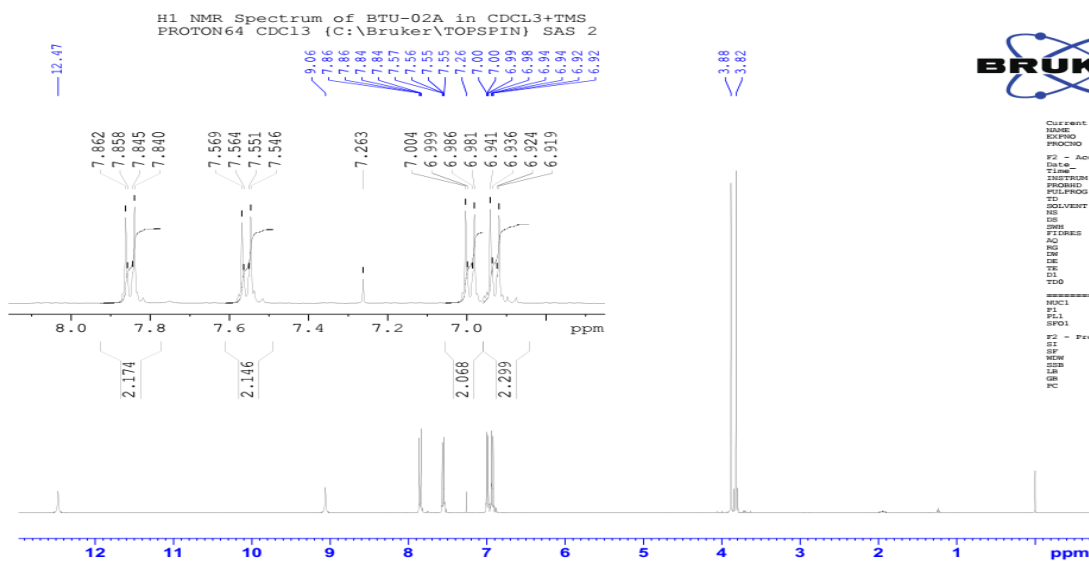
```

Current Data Parameters
NAME      BTU01
EXPNO    01
PROCNO   1

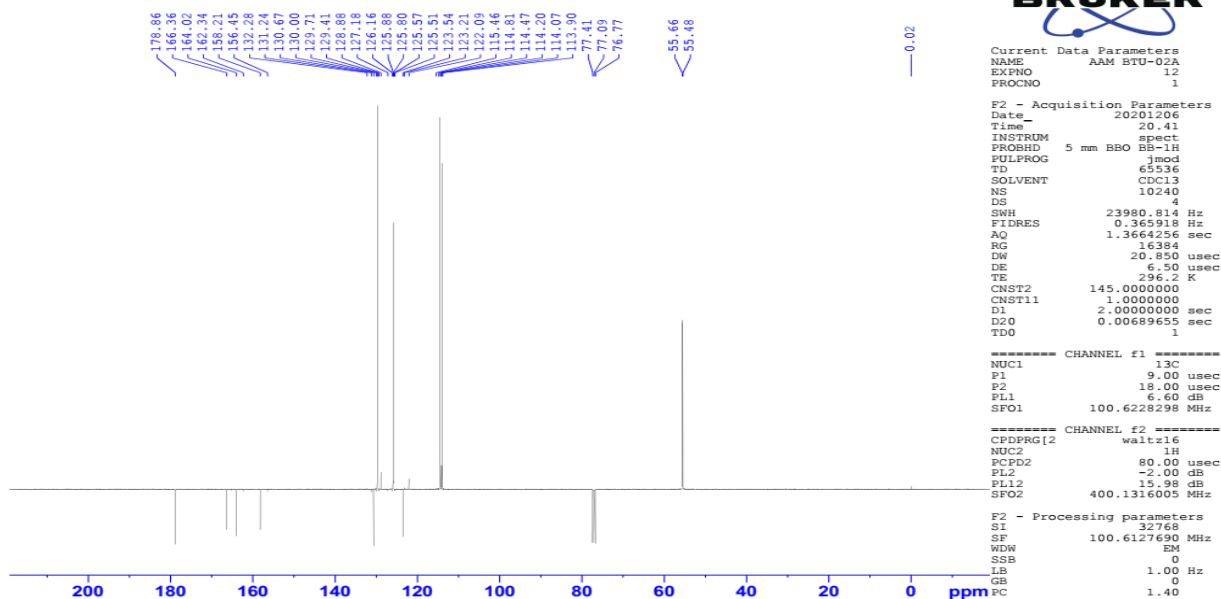
F2 - Acquisition Parameters
Date_    20110110
Time     17.40 h
INSTRUM  spect
PROBHD   13BOBO1
PULPROG  zgpg30
TD       65536
SOLVENT  CDCl3
NS       64
DS       4
SWH      32001.881 Hz
FIDRES   0.978277 Hz
AQ       1.0272516 sec
RG       60.6
DE       15.6000
WE       40.95 usec
TE       300.2 K
CHUFF2   148.0000000
CU       2.000000000
CO       0.00144318 sec
D1       0.000020000 sec
TD0      1
SFO1     100.6092502 MHz
NUC1      13C
P1       10.00 usec
PC       20.00 usec
PL1      33.00000000 W
SFO2     400.0716003 MHz
NUC2      1H
PCP2     18.00 usec
PL2      24.00 usec
PCPC2    90.00 usec
PLM1     7.40000010 W
PLM2     0.13598000 W

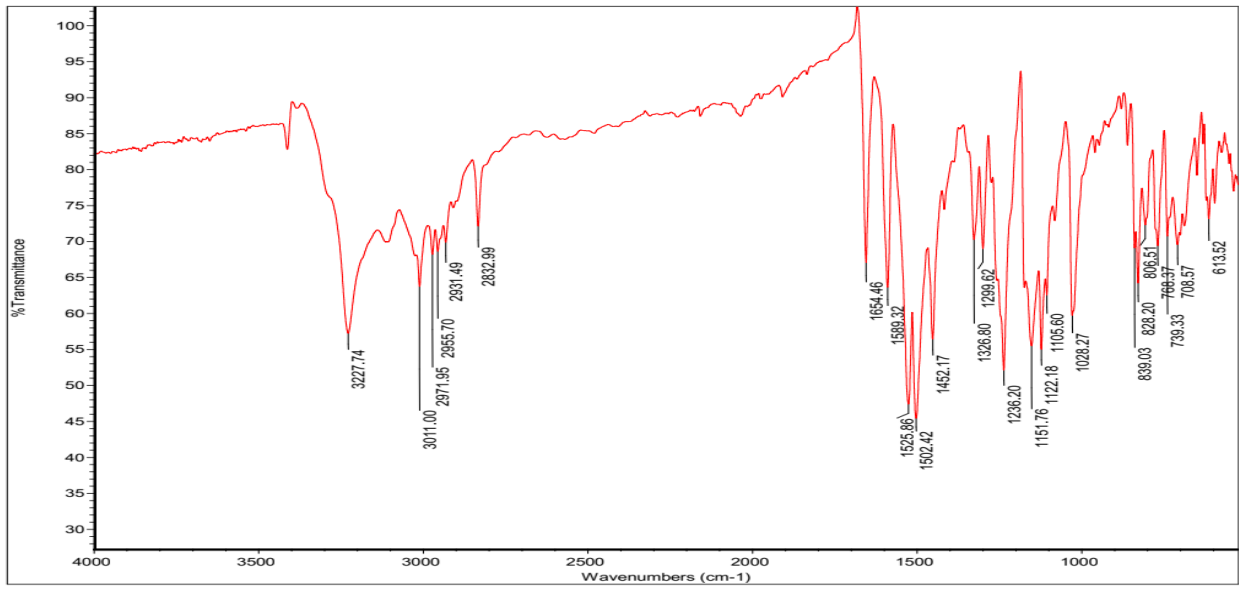
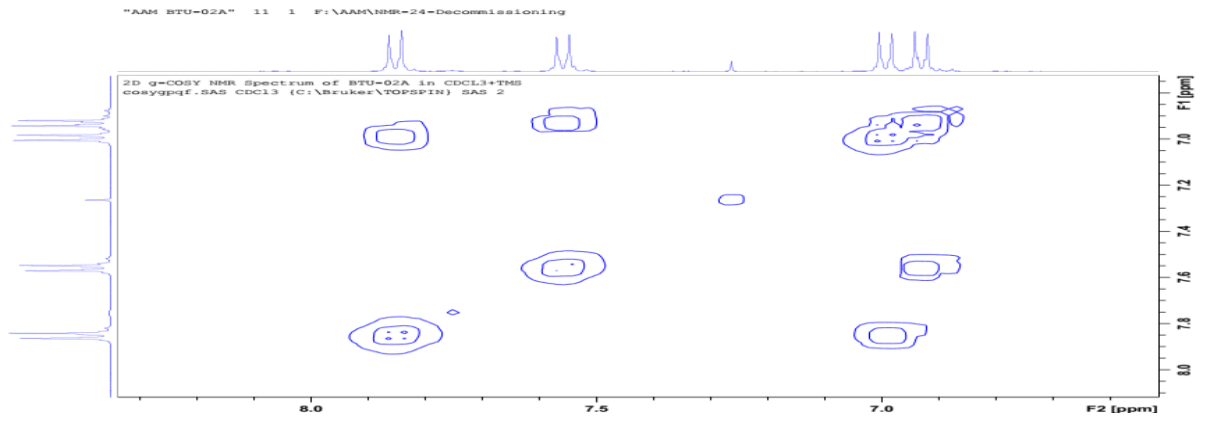
F2 - Processing parameters
SI       65536
SF       100.577415 MHz
WDW      EM
SSB      0
LB       1.00 Hz
GB       0
PC       1.40
  
```

BTU-02



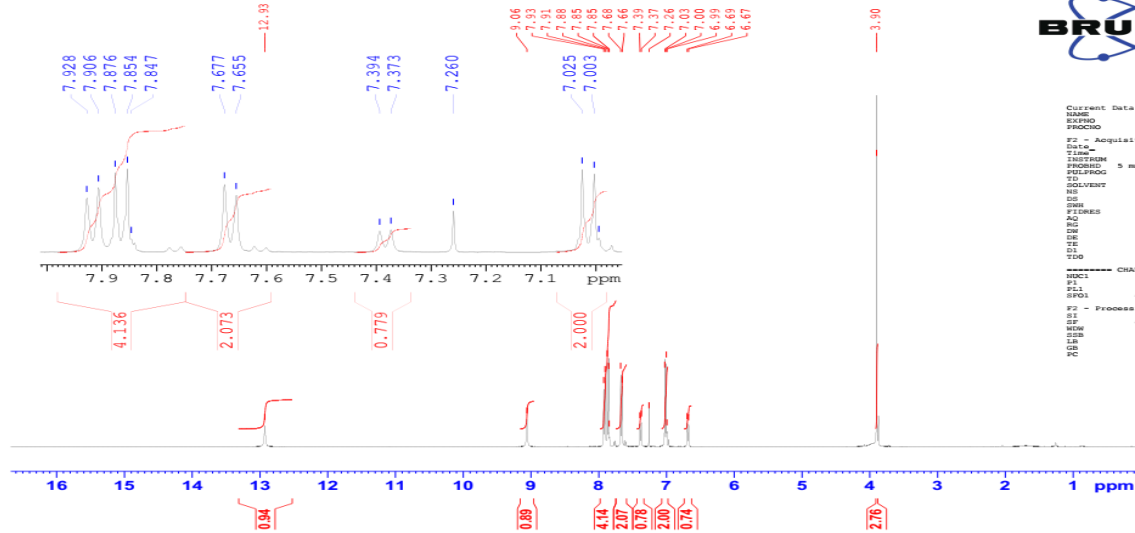
JMOD C13 NMR Spectrum of BTU-02A in CDCL3+TMS
C13_APT CDCL3 {C:\Bruker\TOPSPIN} SAS 2





BTU-03

H1 NMR Spectrum of BTU-03 in CDCL3+TMS
 PROTON64 CDCl3 (C:\Bruker\TOPSPIN) SAS 4



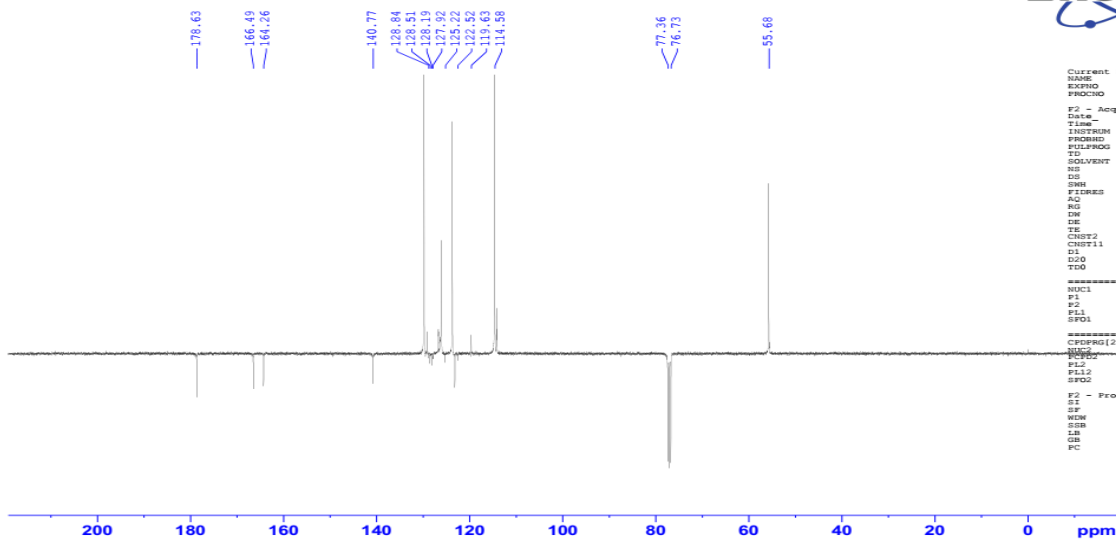
```
Current Data Parameters
NAME      AM BTU-03
EXPNO    1
PROCNO   1

F2 - Acquisition Parameters
Date_    2001209
Time     15.43
INSTRUM  spect
PROBHD   5 mm BBO BB-14
PULPROG  zgpg30
SOLVENT  CDCl3
NS       64
DS       4
SWH      8802.817 Hz
F2RES    0.135381 Hz
AQ       3.117773 sec
RG       254
DM       1.5688 usec
DE       6.90 usec
TE       298.2 K
TDO     2.59999999 sec

===== CHANNEL f1 =====
NUC1      1H
P1        10.00 usec
PL1       -2.00 dB
SFO1     400.1316005 MHz

F2 - Processing parameters
SI        32768
SF        400.130005 MHz
WDW       EM
SSB       0
LB        0.30 Hz
GB        0
PC        1.00
```

JMOD C13 NMR Spectrum of BTU-03 in CDCL3+TMS
 C13_APT CDCl3 (C:\Bruker\TOPSPIN) SAS 4



```
Current Data Parameters
NAME      AM BTU-03
EXPNO    12
PROCNO   1

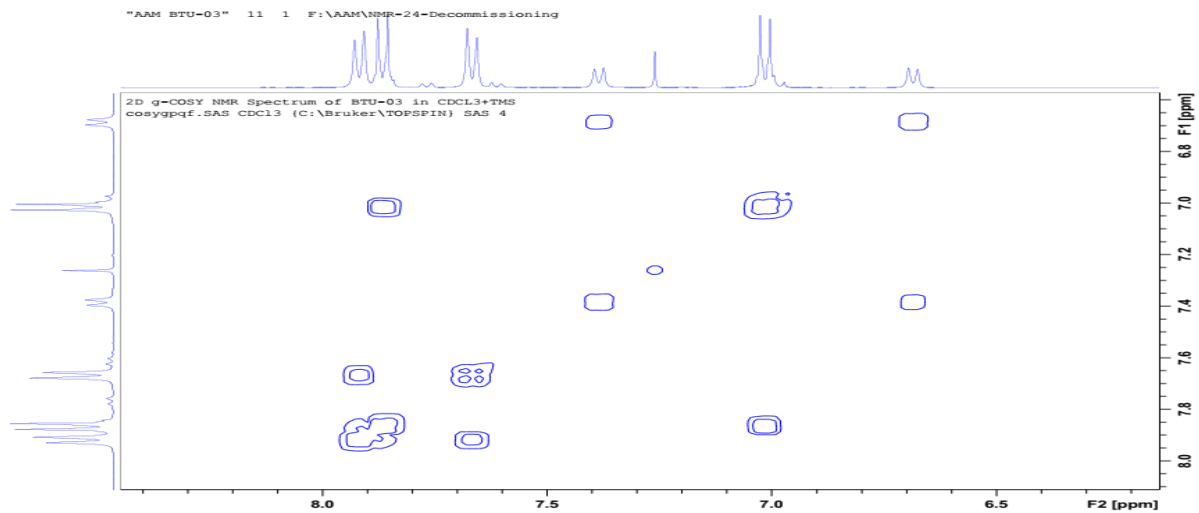
F2 - Acquisition Parameters
Date_    2001209
Time     6.43
INSTRUM  spect
PROBHD   5 mm BBO BB-1H
PULPROG  zgpg30
SOLVENT  CDCl3
NS       14336
DS       4
SWH      23980.814 Hz
F2RES    0.365918 Hz
AQ       1.3664256 sec
RG       14384
DM       20.850 usec
DE       6.50 usec
TE       298.2 K
NUC1     13C
NUC2     145.0000000
D1       2.0000000 sec
D2       0.00689055 sec
TDO     1

===== CHANNEL f1 =====
NUC1      13C
P1        9.00 usec
PL1       0.00 dB
SFO1     100.6217690 MHz

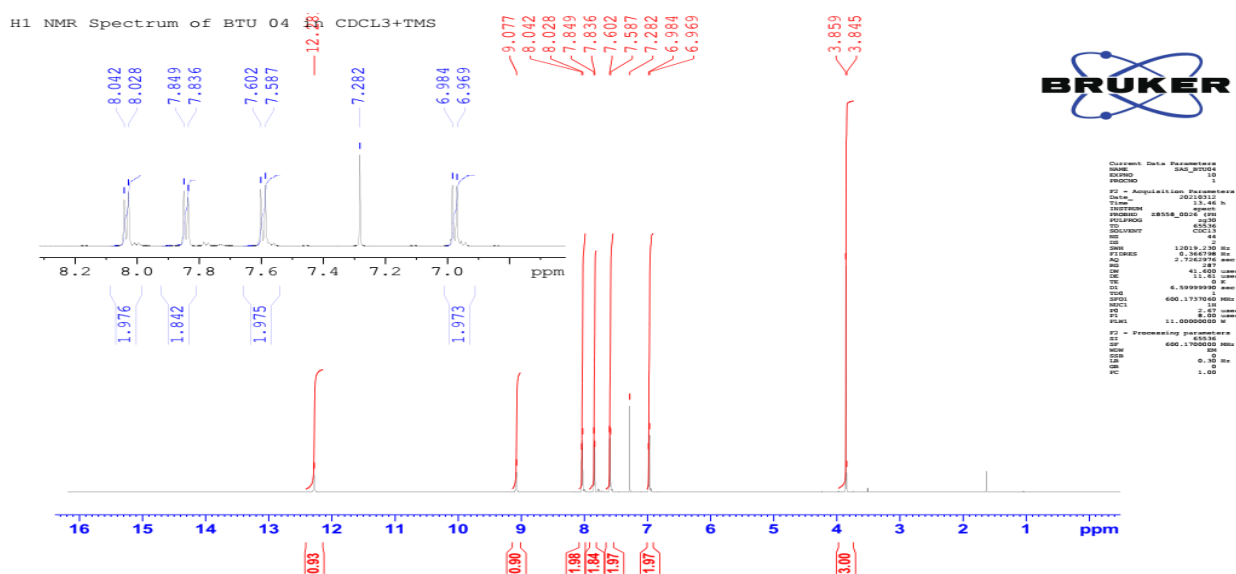
===== CHANNEL f2 =====
CPDPRG2  waltz16
NUC1     13C
NUC2     1H
P12      80.00 usec
PL12     -2.00 dB
PL13     15.98 dB
SFO2     400.1316005 MHz

F2 - Processing parameters
SI        32768
SF        100.6127690 MHz
WDW       EM
SSB       0
LB        1.00 Hz
GB        0
PC        1.40
```

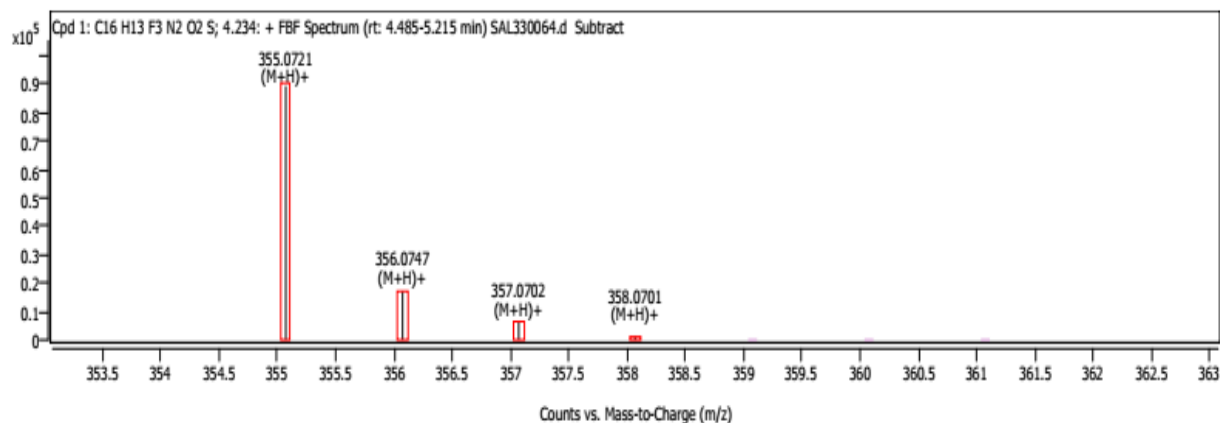
"AAM BTU-03" 11 1 F:\AAM\NMR-24-Decommissioning



BTU-04



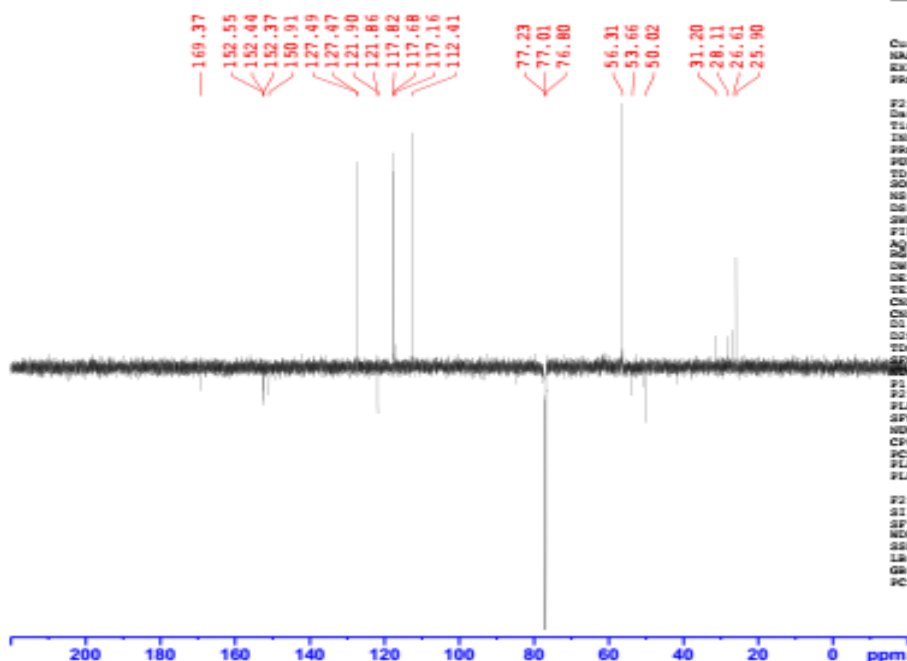
Compound Spectra



Spectrum Peaks

m/z	m/z (Calc)	Diff (ppm)	Abund	Height %	Height % (Calc)	Ion Species	Z
355.0721	355.0723	-0.47	89285	100.00	100.00	(M+H)+	1
356.0747	356.0752	-1.48	17138	19.19	19.06	(M+H)+	1
357.0702	357.0712	-2.75	6216	6.96	6.60	(M+H)+	1
358.0701	358.0728	-7.59	1053	1.18	0.99	(M+H)+	1

JMOD C13 NMR Spectrum of BTU-05 in CDCL3
 C13_APT CDC13 [C:\Bruker\TOPSPIN] SAS 17

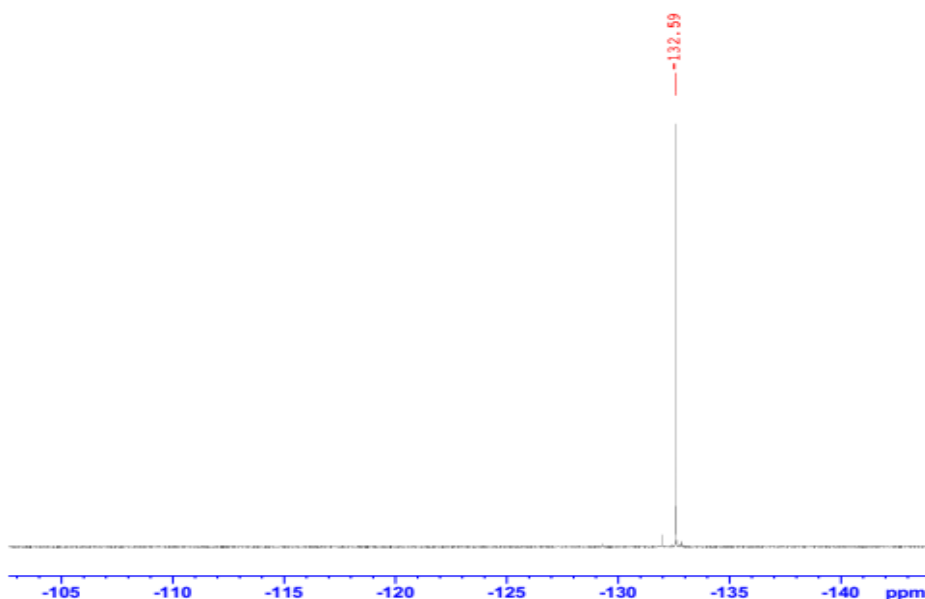


Current Data Parameters
 NAME SAS_BTU05
 EXPNO 13
 PROCNO 1

F2 - Acquisition Parameters
 Date_ 20210428
 Time_ 7.50 h
 INSTRUM spect
 PROBHD 2114607_0886 ()
 PULPROG - jmod
 TD 65536
 SOLVENT CDC13
 NS 10240
 DS 4
 SWH 36231.883 Hz
 FIDRES 1.105709 Hz
 AQ 0.9043068 sec
 RG 2050
 DM 13.800 usec
 DE 6.50 usec
 TE 297.6 K
 CHGT2 145.000000
 CHGT1 1.000000
 CC 2.0000000 sec
 CCO 0.0000000 sec
 TDO 1
 SFO1 150.9279578 MHz
 NUC1 13C
 P1 12.00 usec
 P2 24.00 usec
 PLW1 82.95099640 W
 SFO2 600.1724007 MHz
 WDC2 1H
 CPOPRG[2] waltz65
 PCPD2 70.00 usec
 PLW2 24.58099937 W
 PLW12 0.50164998 W

F2 - Processing parameters
 SI 32768
 SF 150.9128665 MHz
 WDW EM
 SSB 0
 LB 1.00 Hz
 GB 0
 PC 1.40

H1 Decoupled F19 NMR Spectrum of BTU-05 in CDCL3

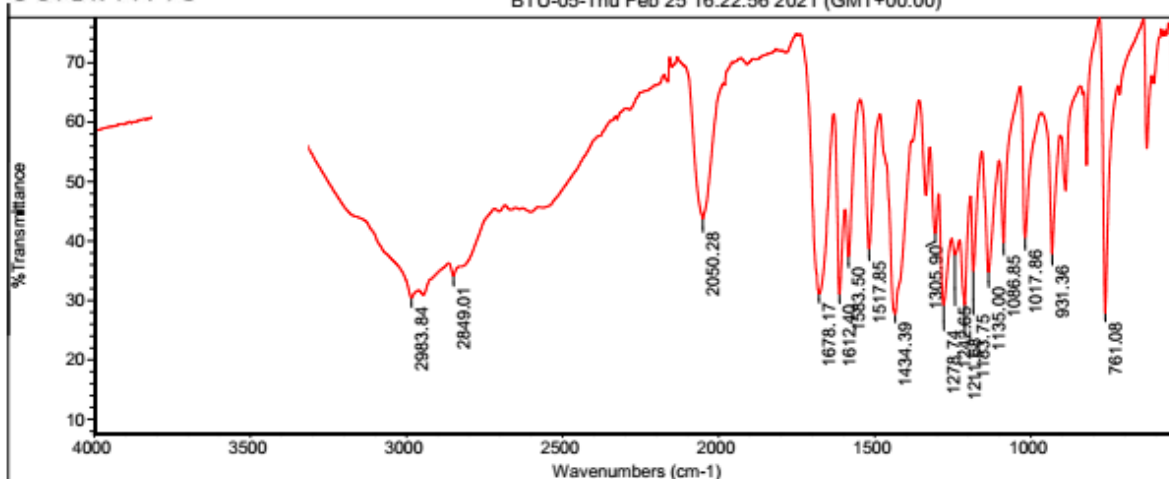


Current Data Parameters
 NAME SAS_BTU-05
 EXPNO 70
 PROCNO 1

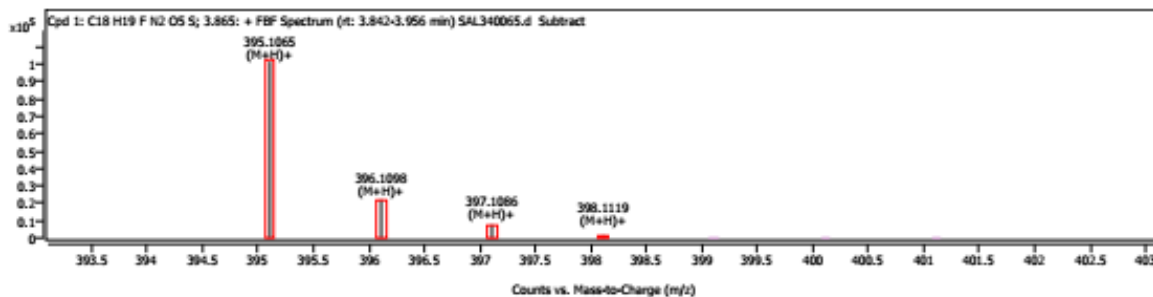
F2 - Acquisition Parameters
 Date_ 20210504
 Time_ 10.00 h
 INSTRUM spect
 PROBHD 2114607_0886 ()
 PULPROG zgpg30
 TD 134144
 SOLVENT CDC13
 NS 64
 DS 0
 SWH 277777.781 Hz
 FIDRES 4.141487 Hz
 AQ 0.2414592 sec
 RG 724
 DM 1.800 usec
 DE 6.50 usec
 TE 298.0 K
 D1 10.0000000 sec
 D11 0.03000000 sec
 D12 0.00002000 sec
 TDO 1
 SFO1 564.6890129 MHz
 NUC1 19F
 P1 12.00 usec
 PLW1 43.70700073 W
 SFO2 600.1748014 MHz
 WDC2 1H
 CPOPRG[2] waltz64
 PCPD2 70.00 usec
 PLW2 24.58099937 W
 PLW12 0.50164998 W

F2 - Processing parameters
 SI 131072
 SF 564.7240258 MHz
 WDW EM
 SSB 2
 LB 0.50 Hz
 GB 0
 PC 200.00

BTU-05-Thu Feb 25 16:22:56 2021 (GMT+00:00)



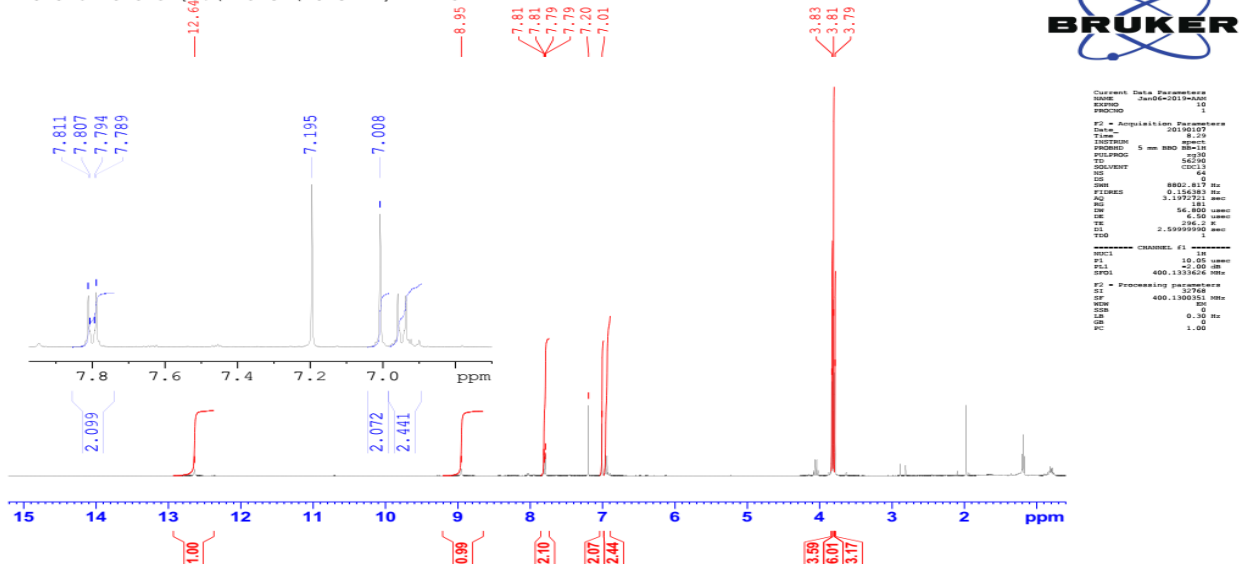
Compound Spectra



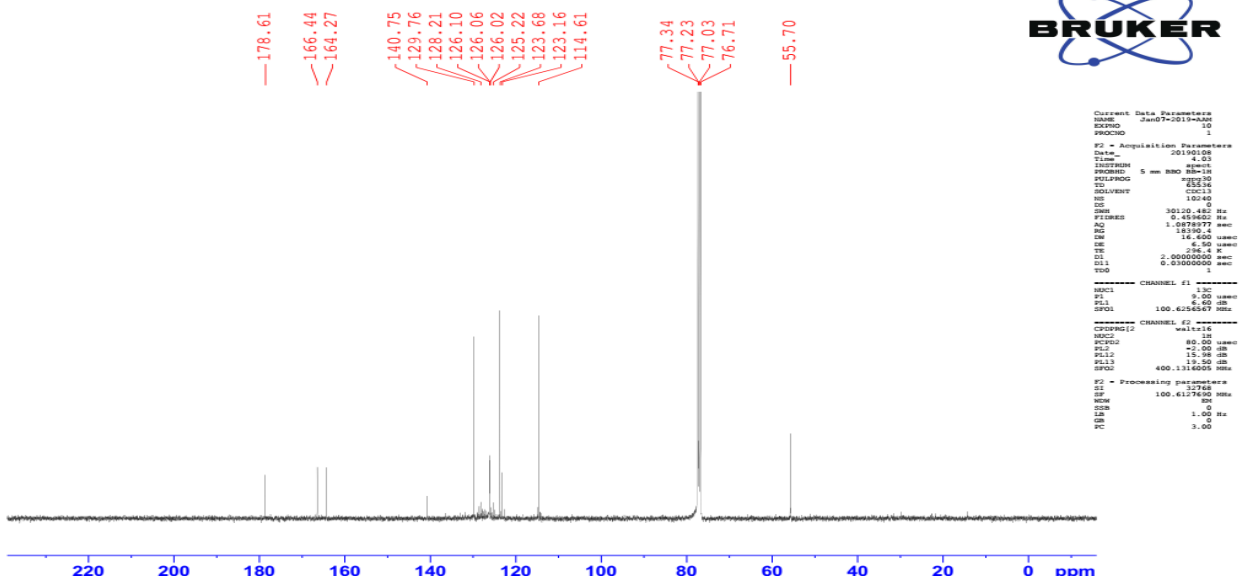
Spectrum Peaks						
m/z	m/z (Calc)	Diff (ppm)	Abund	Height %	Height % (Calc)	Ion Species
395.1065	395.1071	-1.58	101393	100.00	100.00	(M+H)+
396.1098	396.1102	-0.90	22100	21.80	21.41	(M+H)+
397.1086	397.1070	3.96	7681	7.58	7.68	(M+H)+
398.1119	398.1086	8.26	1581	1.56	1.28	(M+H)+

BTU-07

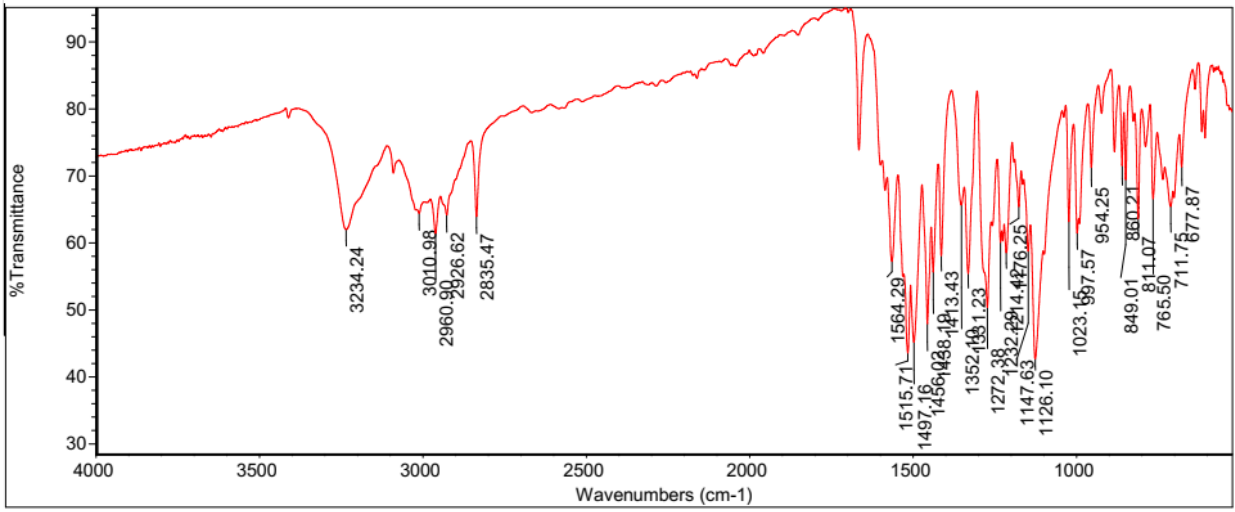
H1 NMR Thiourea (4-methoxybenzoyl chloride + 3,4,5-trimethoxyphenyl amine) in CDCl3
 PROTON64 CDCl3 {C:\Bruker\TOPSPIN} AAM 54



C13 NMR Thiourea BTU-07 in CDCl3 (1)
 C13_WIDE CDCl3 {C:\Bruker\TOPSPIN} AAM 58

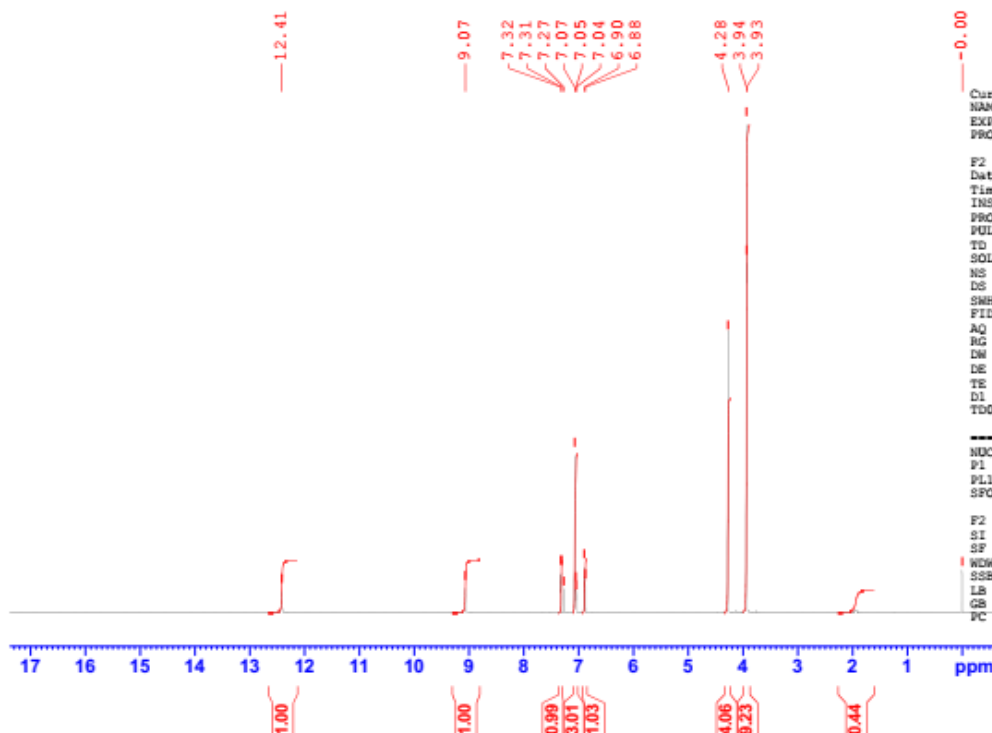


BTU-07-Thu Feb 25 17:03:51 2021 (GMT+00:00)



BTU-08

H1 NMR Spectrum of BTU-08 in CDCL3+TMS
PROTON64 CDCL3 (C:\Bruker\TOPSPIN) SAS 5

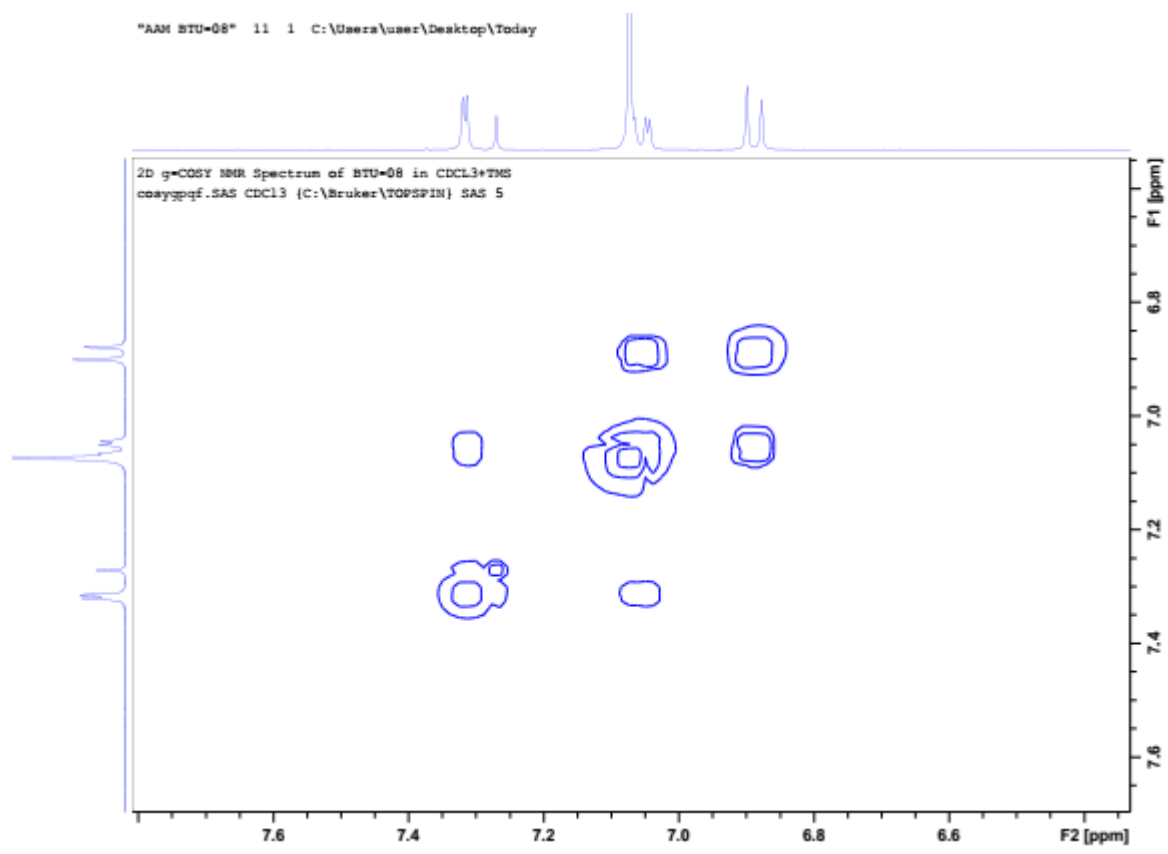


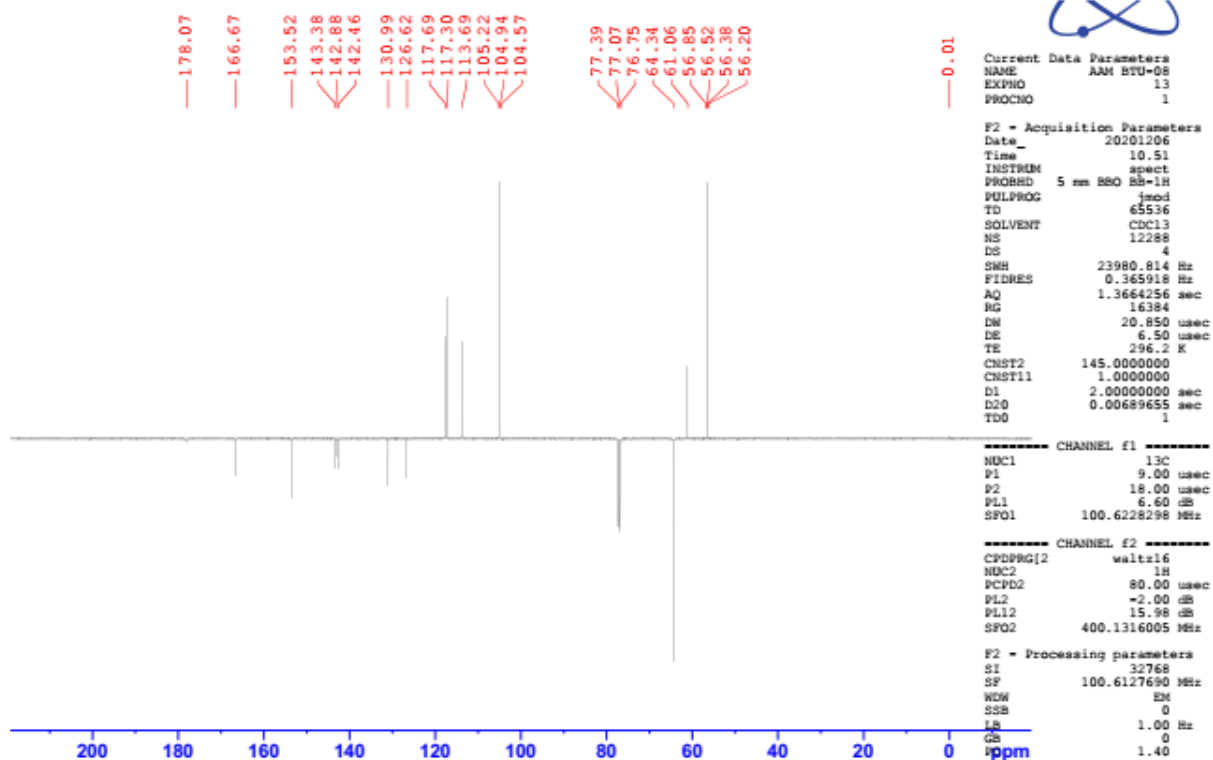
Current Data Parameters
NAME AAM BTU-08
EXPNO 10
PROCNO 1

F2 - Acquisition Parameters
Date_ 2021205
Time 11.02
INSTRUM spect
PROBHD 5 mm BBO BB-1H
PULPROG zg30
TD 56290
SOLVENT CDCL3
NS 64
DS 0
SWH 8802.817 Hz
FIDRES 0.156383 Hz
AQ 3.1972721 sec
RG 181
DW 56.800 usec
DE 6.50 usec
TE 296.2 K
DL 2.59999990 sec
TDO 1

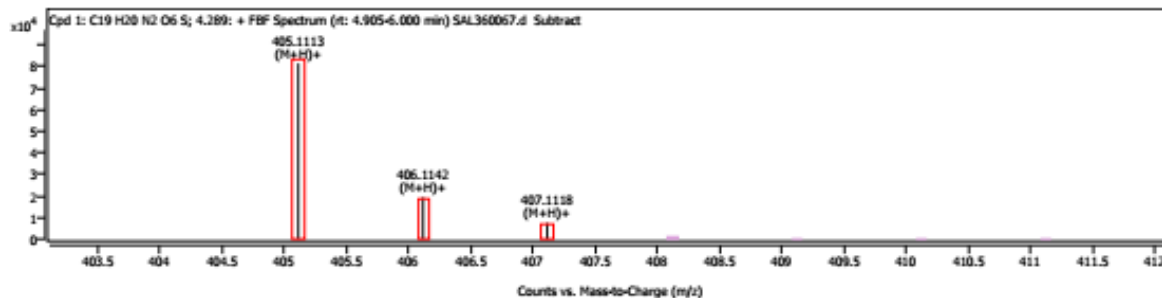
----- CHANNEL f1 -----
NUC1 1H
P1 10.05 usec
PL1 -2.00 db
SFO1 400.1333626 MHz

F2 - Processing parameters
SI 32768
SF 400.1300054 MHz
WDW no
SSB 0
LB 0 Hz
GB 0
PC 150.00



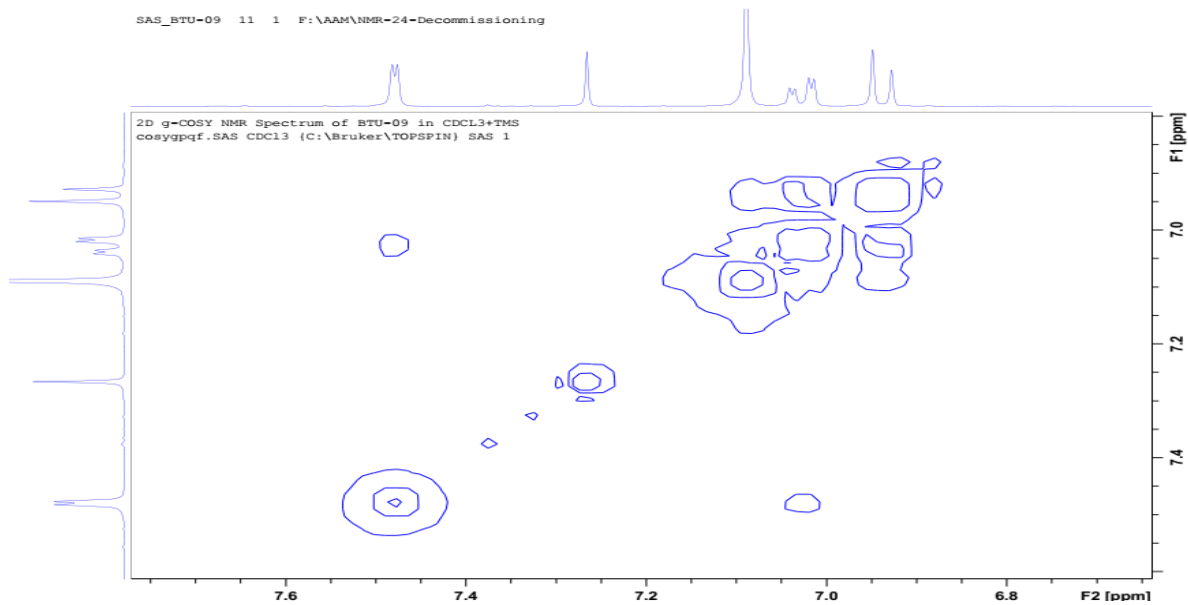


Compound Spectra



Spectrum Peaks							
m/z	m/z (Calc)	Diff (ppm)	Abund	Height %	Height % (Calc)	Ion Species	Z
405.1113	405.1115	-0.47	81522	100.00	100.00	(M+H)+	1
406.1142	406.1145	-0.81	19345	23.73	22.54	(M+H)+	1
407.1118	407.1116	0.37	7442	9.13	8.13	(M+H)+	1

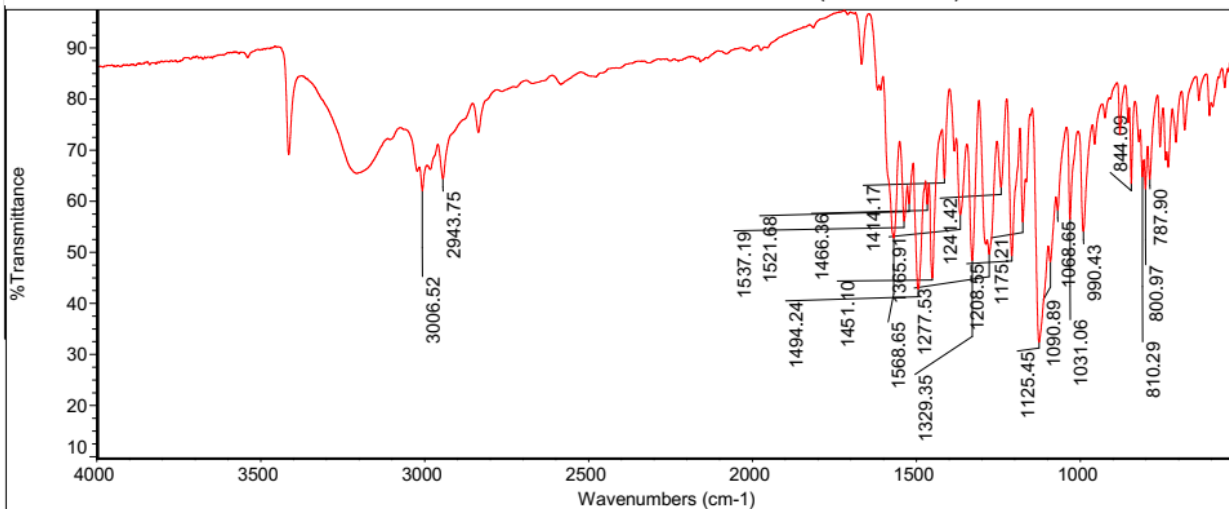
SAS_BTU-09 11 1 F:\AAM\NMR-24-Decommissioning



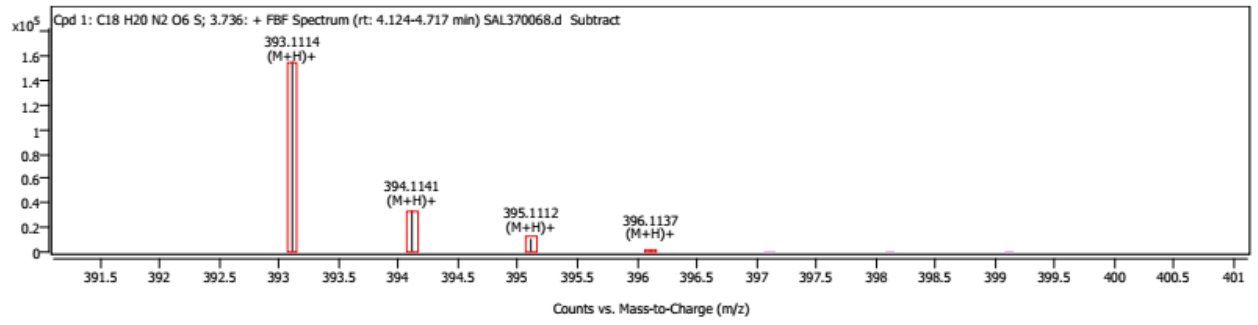
ThermoFisher
SCIENTIFIC

Mon Dec 13 19:16:33 2021 (

BTU-09-Thu Feb 25 16:36:53 2021 (GMT+00:00)



Compound Spectra

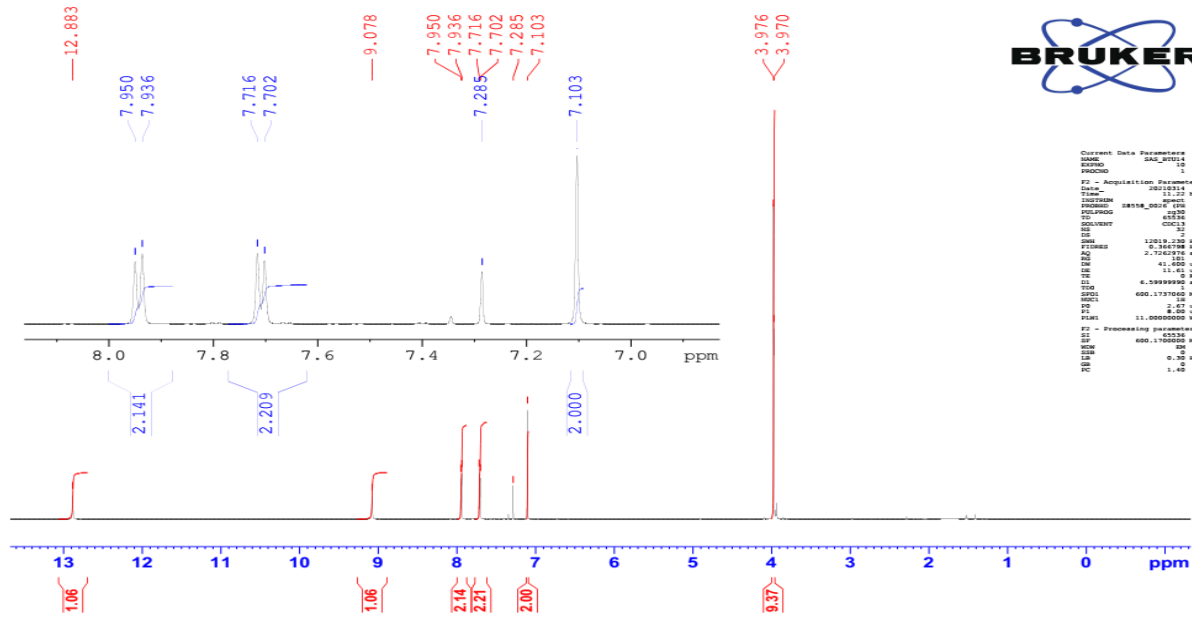


Spectrum Peaks

m/z	m/z (Calc)	Diff (ppm)	Abund	Height %	Height % (Calc)	Ion Species	Z
393.1114	393.1115	-0.27	155989	100.00	100.00	(M+H) ⁺	1
394.1141	394.1145	-1.01	34079	21.85	21.46	(M+H) ⁺	1
395.1112	395.1114	-0.70	10858	6.96	7.90	(M+H) ⁺	1
396.1137	396.1132	1.41	1994	1.28	1.33	(M+H) ⁺	1

BTU-14

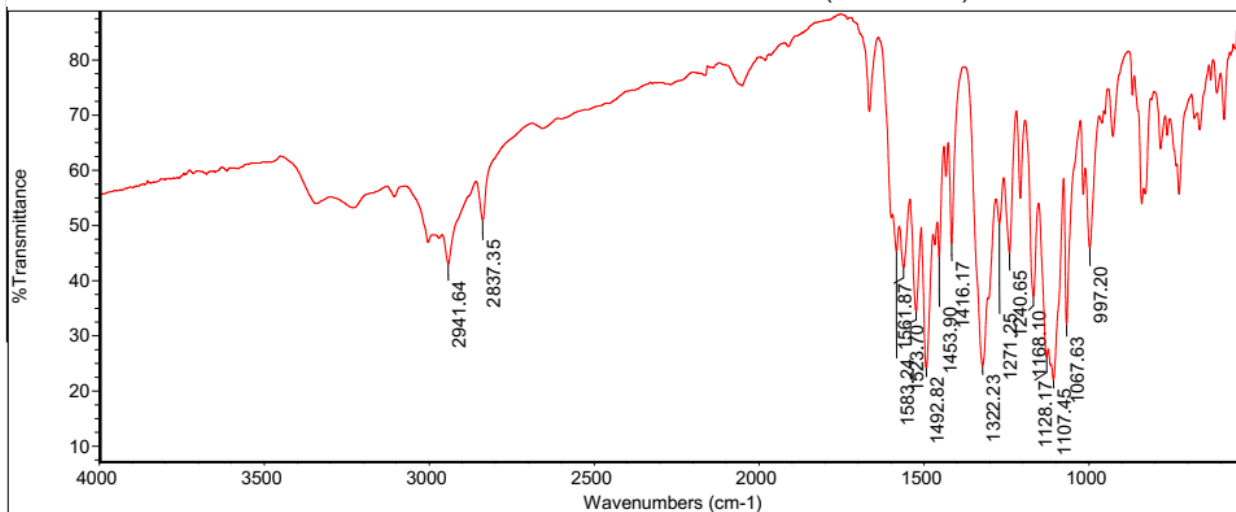
H1 NMR Spectrum of BTU 14 in CDCL3+TMS



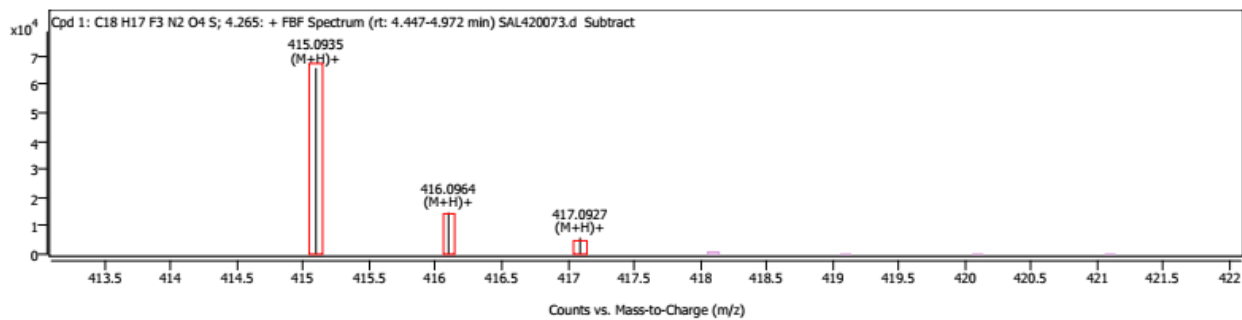
ThermoFisher
SCIENTIFIC

Thu Dec 16 18:25:37 2021 (

BTU-14-Thu Feb 25 16:33:18 2021 (GMT+00:00)



Compound Spectra

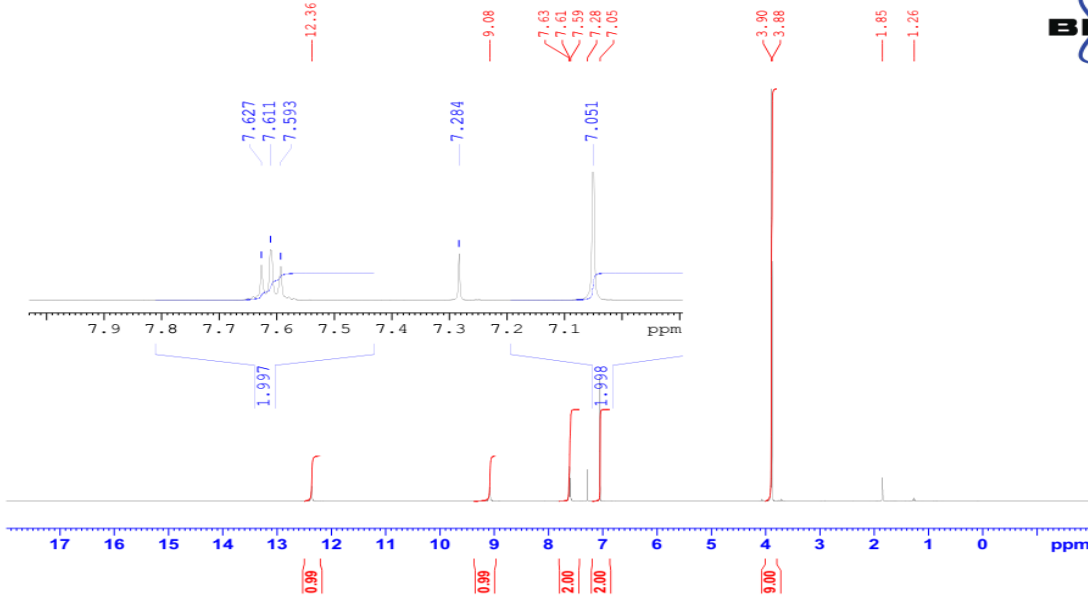


Spectrum Peaks

m/z	m/z (Calc)	Diff (ppm)	Abund	Height %	Height % (Calc)	Ion Species	Z
415.0935	415.0934	0.31	65922	100.00	100.00	(M+H)+	1
416.0964	416.0964	-0.08	14760	22.39	21.35	(M+H)+	1
417.0927	417.0931	-1.05	5829	8.84	7.47	(M+H)+	1

BTU-16

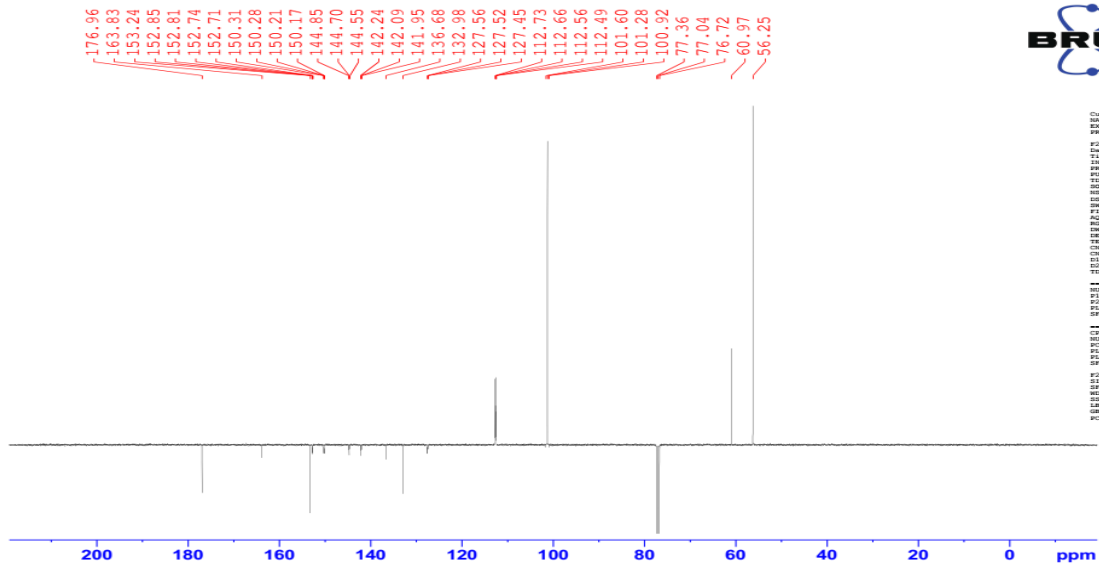
¹H NMR BTU-16 in CDCl₃
 PROTON64 CDC13 {C:\Bruker\TOPSPIN} AAM 15



```

Current Data Parameters
NAME: Aug8-2019-AAM
EXPNO: 10
PROCNO: 1
F2 - Acquisition Parameters
Date_: 20190828
Time: 14.54
INSTRUM: spect
PROBHD: 5 mm BBO
PULPROG: zgpg30
TD: 65536
SOLVENT: CDCl3
NS: 64
DS: 4
SWH: 8862.617 Hz
FIDRES: 0.152381 Hz
AQ: 3.137271 sec
RG: 256
AQ: 56.860 usec
TE: 296.2 K
DE: 2.5399990 usec
TDO: 1
===== CHANNEL f1 =====
NUC1: 13C
P1: 10.00 usec
PL1: 0.00 dB
SFO1: 400.1318200 MHz
===== CHANNEL f2 =====
CPDPRG2: waltz16
NUC2: 1H
P2: 12.00 usec
PL2: 0.00 dB
SFO2: 400.1316005 MHz
===== Processing parameters =====
SI: 32768
SF: 400.1300000 MHz
WDW: EM
SSB: 0
GB: 0.00 Hz
PC: 128.00
  
```

APT NMR BTU-16 in CDCl₃
 C13_APT CDC13 {C:\Bruker\TOPSPIN} AAM 15

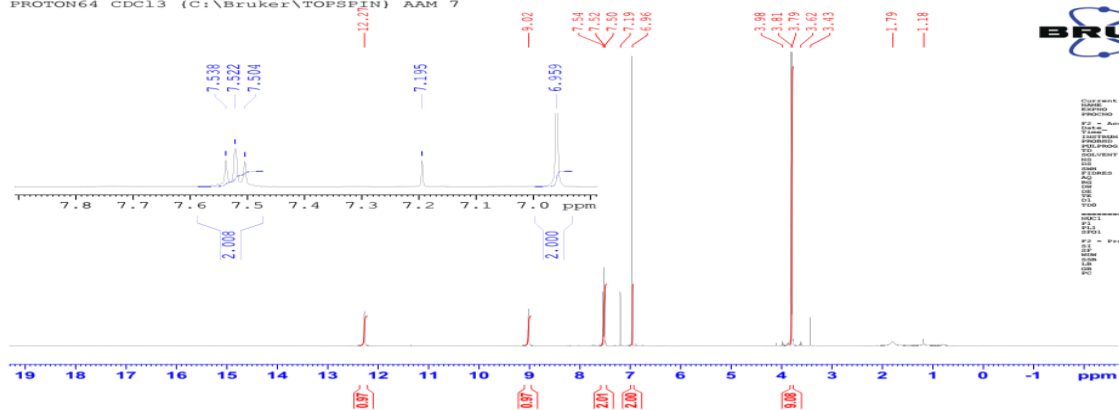


```

Current Data Parameters
NAME: Aug8-2019-AAM
EXPNO: 11
PROCNO: 1
F2 - Acquisition Parameters
Date_: 20190829
Time: 21.57
INSTRUM: spect
PROBHD: 5 mm BBO
PULPROG: zgpg30
TD: 65536
SOLVENT: CDCl3
NS: 64
DS: 4
SWH: 20982.814 Hz
FIDRES: 0.163558 Hz
AQ: 1.164238 sec
RG: 1536
AQ: 32.450 usec
TE: 296.2 K
DE: 2.5399990 usec
TDO: 1
===== CHANNEL f1 =====
NUC1: 13C
P1: 10.00 usec
PL1: 0.00 dB
SFO1: 100.6262300 MHz
===== CHANNEL f2 =====
CPDPRG2: waltz16
NUC2: 1H
P2: 12.00 usec
PL2: 0.00 dB
SFO2: 400.1316005 MHz
===== Processing parameters =====
SI: 32768
SF: 100.6174000 MHz
WDW: EM
SSB: 0
GB: 0.00 Hz
PC: 1.40
  
```


BTU-17

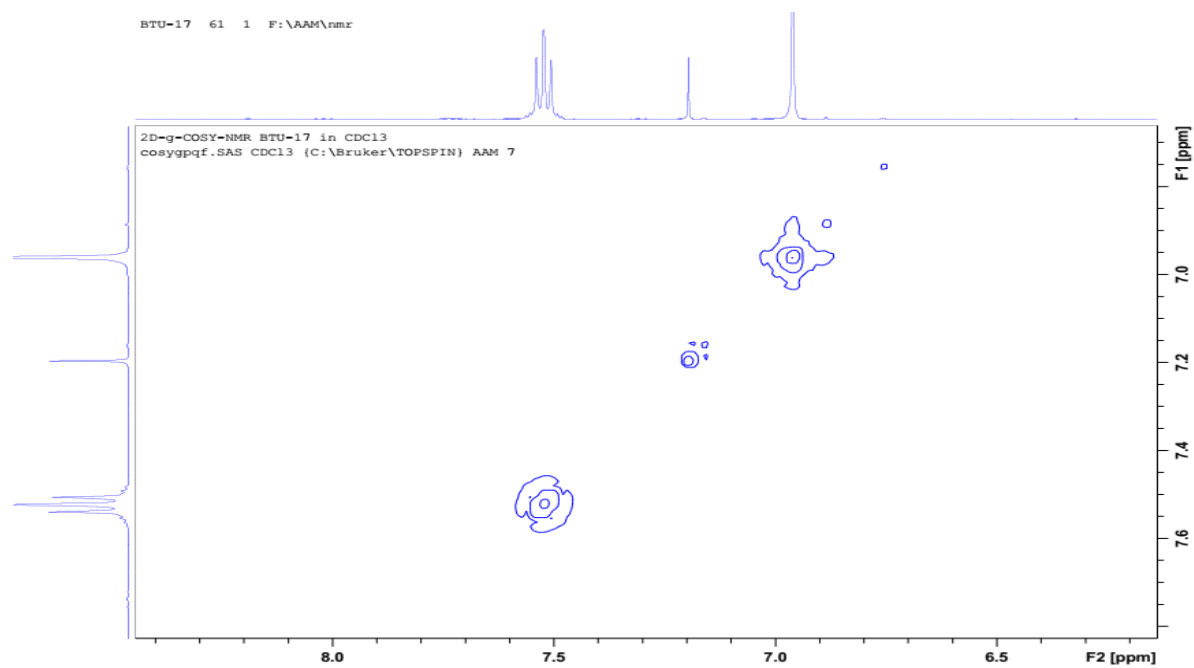
¹H-NMR BTU-17 in CDCl₃
 PROTON64 CDCl₃ (C:\Bruker\TOPSPIN) AAM 7



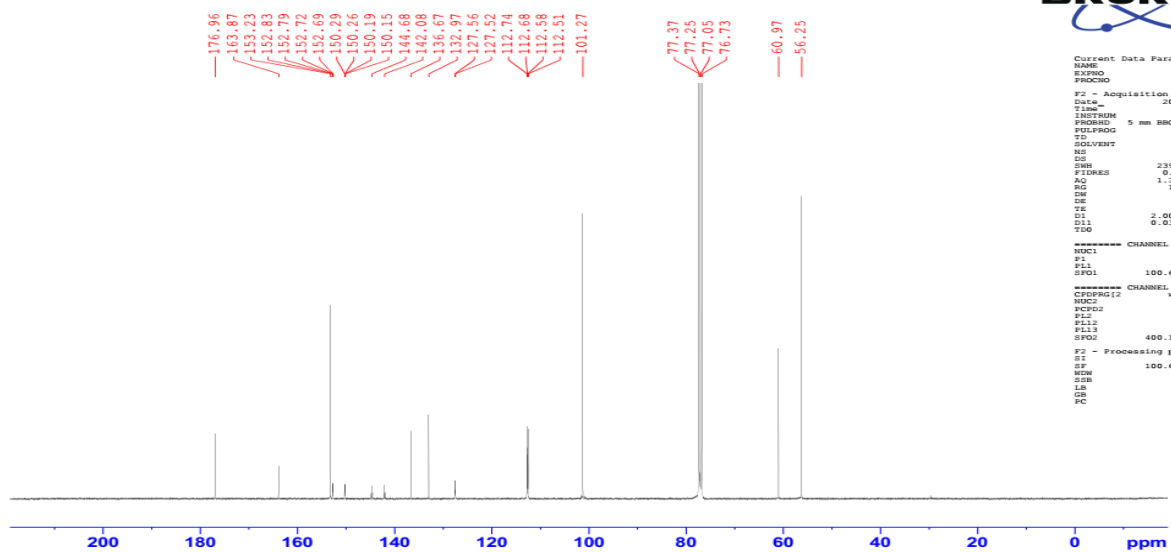
```

Current Data Parameters
NAME: BTU-17
EXPNO: 2
PROCNO: 1
PROCAM: 2
F2 - Acquisition Parameters
Date_UTC: 20100801
Time: 12.12
INSTRUM: spect
PROBHD: 5 mm BBO
PULPROG: zgpg30
TD: 65536
SFO: 400.136350
AQ: 0.589700
RG: 512
AQ: 0.589700
RG: 512
FIDRES: 0.185000
AQRES: 0.185000
SOLVENT: CDCl3
NS: 2048
DS: 4
SWH: 13.000000
F1 - Processing parameters
NAME: BTU-17
EXPNO: 2
PROCNO: 1
PROCAM: 2
F2 - Acquisition Parameters
Date_UTC: 20100801
Time: 12.12
INSTRUM: spect
PROBHD: 5 mm BBO
PULPROG: zgpg30
TD: 65536
SFO: 400.136350
AQ: 0.589700
RG: 512
AQ: 0.589700
RG: 512
FIDRES: 0.185000
AQRES: 0.185000
SOLVENT: CDCl3
NS: 2048
DS: 4
SWH: 13.000000
  
```

BTU-17 61 1 F:\AAM\nmr



13C-NMR BTU-17 in CDCl3
 c13org CDCl3 {C:\Bruker\TOPSPIN} AAM 7



```

Current Data Parameters
NAME      BTU-17
EXPRO    61
PROCNO   1

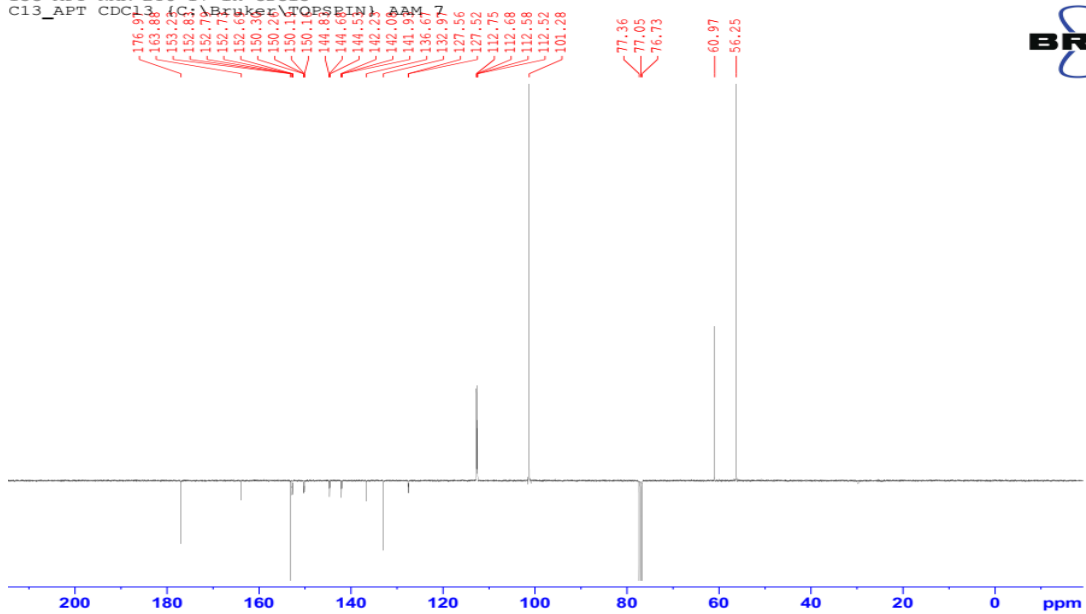
F2 - Acquisition Parameters
Date_    20201009
Time     2.32
INSTRUM spect
PROBHD   5 mm BBO BB-1H
PULPROG zgpg30
TD       65536
SOLVENT  CDCl3
NS       10240
DS       4
SWH      23990.814 Hz
FIDRES   0.365918 Hz
AQ       1.3664256 sec
RG       18390.4
DE       20.810 usec
TE       300.2 K
TE2      300.2 K
D1       2.0000000 sec
D11      0.0300000 sec
TD0      1

----- CHANNEL f1 -----
NUC1     13C
P1       9.00 usec
PL1      -1.00 dB
SFO1     100.627459 MHz

----- CHANNEL f2 -----
CPDPRG12 wait16
NUC2     1H
PCPD2    80.00 usec
PL2      -2.00 dB
PL12     19.00 dB
SFO2     400.131405 MHz

F2 - Processing parameters
SI       32768
SF       100.617760 MHz
WDW      EM
SSB      0
LB       1.00 Hz
GB       0
PC       4.00
  
```

13C-APT-NMR BTU-17 in CDCl3
 C13_APT CDCl3 {C:\Bruker\TOPSPIN} AAM 7



```

Current Data Parameters
NAME      BTU-17
EXPRO    61
PROCNO   1

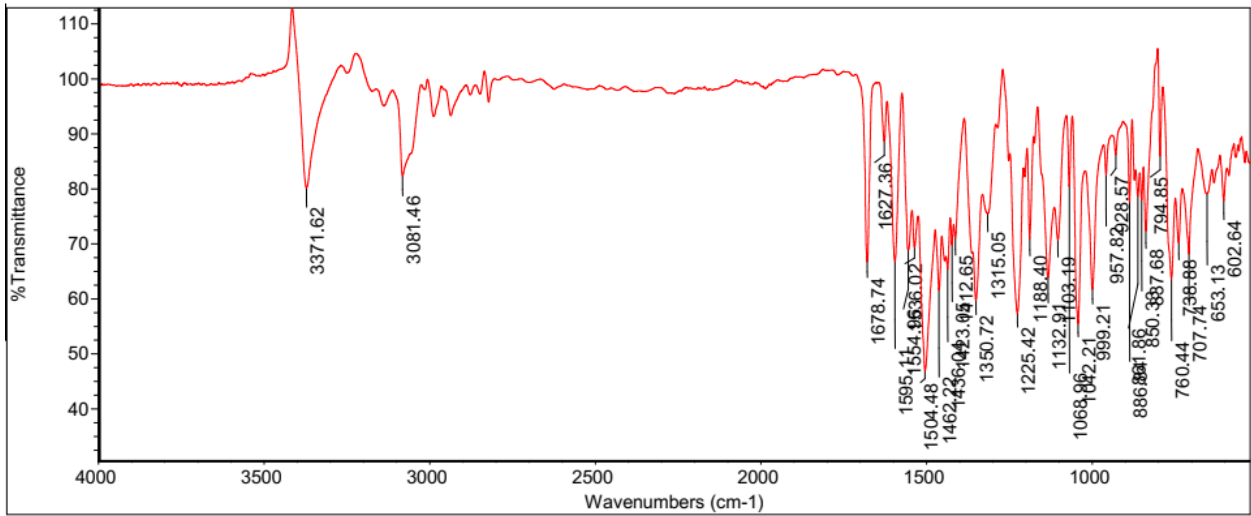
F2 - Acquisition Parameters
Date_    20201009
Time     2.48
INSTRUM spect
PROBHD   5 mm BBO BB-1H
PULPROG zgpg30
TD       65536
SOLVENT  CDCl3
NS       10240
DS       4
SWH      23980.814 Hz
FIDRES   0.365918 Hz
AQ       1.3664256 sec
RG       18384
DE       20.810 usec
TE       300.2 K
TE2      300.2 K
D1       2.0000000 sec
D11      0.0000000 sec
D12      0.00689455 sec
TD0      1

----- CHANNEL f1 -----
NUC1     13C
P1       9.00 usec
PL1      -1.00 dB
SFO1     100.627459 MHz

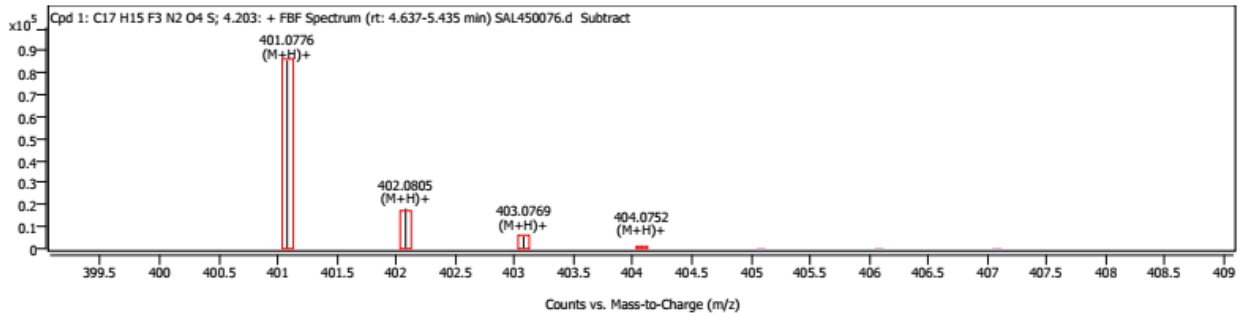
----- CHANNEL f2 -----
CPDPRG12 wait16
NUC2     1H
PCPD2    80.00 usec
PL2      -2.00 dB
PL12     15.00 dB
SFO2     400.131405 MHz

F2 - Processing parameters
SI       32768
SF       100.617760 MHz
WDW      EM
SSB      0
LB       1.00 Hz
GB       0
PC       4.00
  
```


BTU-17-Thu Feb 25 16:41:27 2021 (GMT+00:00)



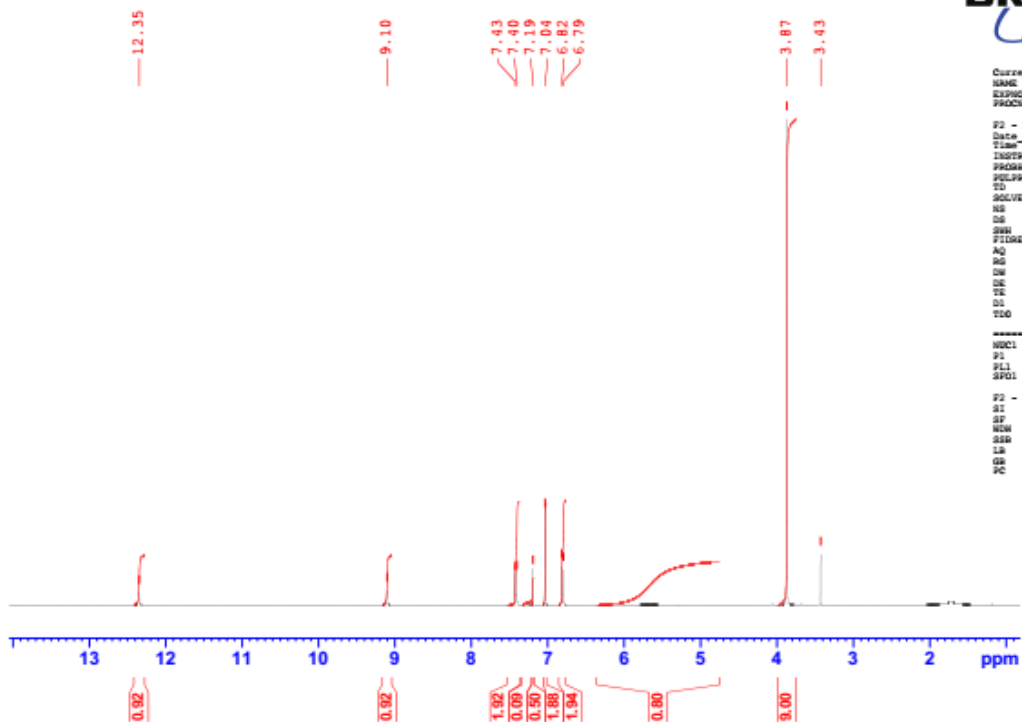
Compound Spectra



Spectrum Peaks							
m/z	m/z (Calc)	Diff (ppm)	Abund	Height %	Height % (Calc)	Ion Species	Z
401.0776	401.0777	-0.35	85776	100.00	100.00	(M+H) ⁺	1
402.0805	402.0807	-0.58	18194	21.21	20.24	(M+H) ⁺	1
403.0769	403.0772	-0.87	5575	6.50	7.24	(M+H) ⁺	1
404.0752	404.0789	-9.29	988	1.15	1.15	(M+H) ⁺	1

BTU-18

¹H-NMR BTU-18 in CDCl₃
 PROTON64 CDCl₃ (C:\Bruker\TOPSPIN) AAM 8



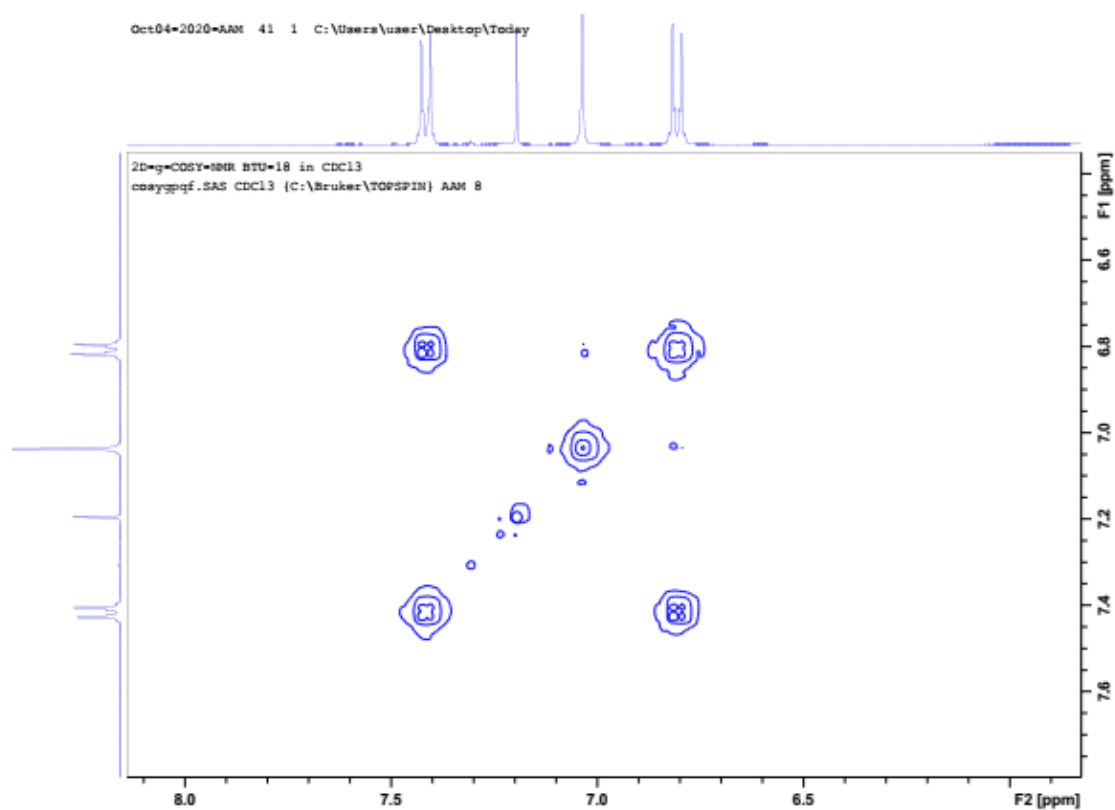
```

Current Data Parameters
NAME      Oct04-2020-AAM2
EXPNO    40
PROCNO   1

F2 - Acquisition Parameters
Date_    20201004
Time     14.16
INSTRUM  spect
PROBHD   5 mm QNP 1H-1
PULPROG  zgpg30
TD        65536
SOLVENT  CDCl3
NS        64
DS        0
SWH       8002.817 Hz
FIDRES    0.156393 Hz
AQ         3.1972721 sec
RG         71.8
CW         56.800 usec
DE         6.50 usec
TE         296.2 K
SI         2.58999990 sec
TD0        1

===== CHANNEL f1 =====
NUC1      1H
P1         10.00 usec
PL1        -2.00 dB
SFO1      400.132326 MHz

F2 - Processing parameters
SI         32768
SF         400.1303265 MHz
WDW        EM
SSB        0
LB         0.30 Hz
GB         0
PC         450.00
    
```

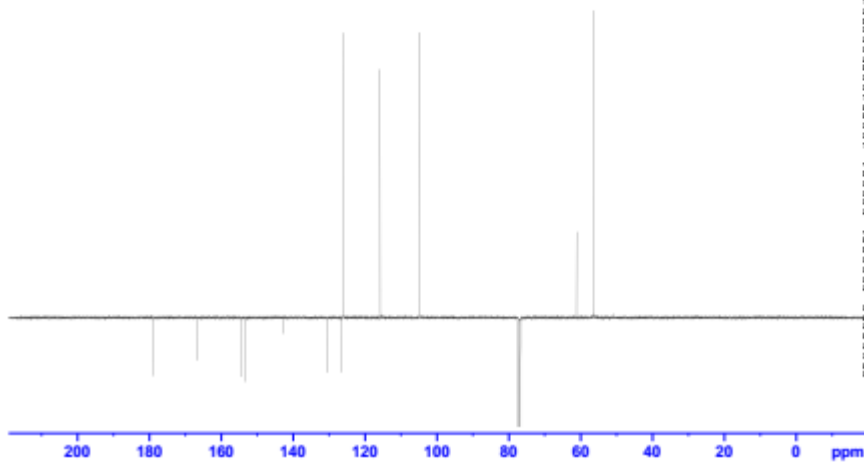


13C-APT-NMR BTU-18 in CDC13
 C13_APT CDC13 (C:\Bruker\TOPSPIN) AAM 8

178.82
 166.77
 154.67
 153.53
 142.89
 130.44
 126.59
 126.14
 115.74
 104.99
 77.36
 77.04
 76.72
 61.08
 56.52

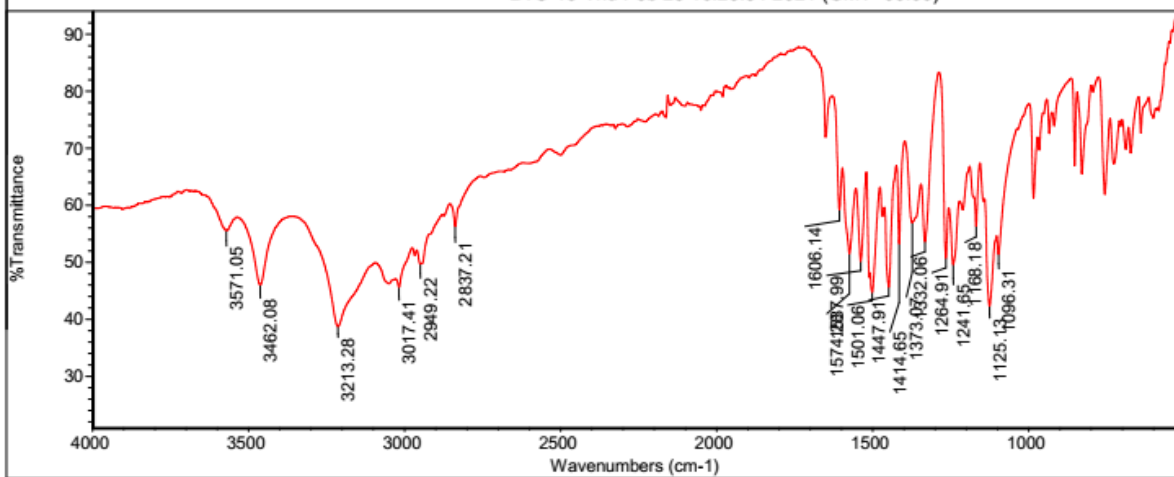


Current Data Parameters
 NAME: C:\13C-APT-NMR
 EXPNO: 1
 PROCNO: 1
 F2 - Acquisition Parameters
 Date_: 20200904
 Time: 6.30
 INSTRUM: spect
 PULPROG: zgpg30
 TO: 60000
 SOLVENT: CDC13
 NS: 610
 DS: 4
 SWH: 23860.810 Hz
 FIDRES: 0.348918 Hz
 AQ: 1.3662766 sec
 RG: 327.68
 SQ: 20.850 sec
 DE: 6.50 sec
 TE: 296.2 K
 CHFT1: 109.000000
 CHFT2: 1.000000
 D1: 2.0000000 sec
 D12: 0.0200000 sec
 TDR: 1
 ===== CHANNEL f1 =====
 NUC1: 13C
 P1: 6.00 sec
 PC: 18.00 sec
 PL1: 0.00 dB
 SFO1: 100.628160 MHz
 ===== CHANNEL f2 =====
 CPDPRG2: waltz16
 NUC2: 1H
 P2: 12.00 sec
 PC2: 82.00 sec
 PL2: -2.00 dB
 PL12: 19.00 dB
 SFO2: 500.136051 MHz
 F2 - Processing parameters
 SI: 32768
 SF: 100.628160 MHz
 SCW: 50
 SW: 0
 LB: 1.00 Hz
 GB: 0
 PC: 6.00

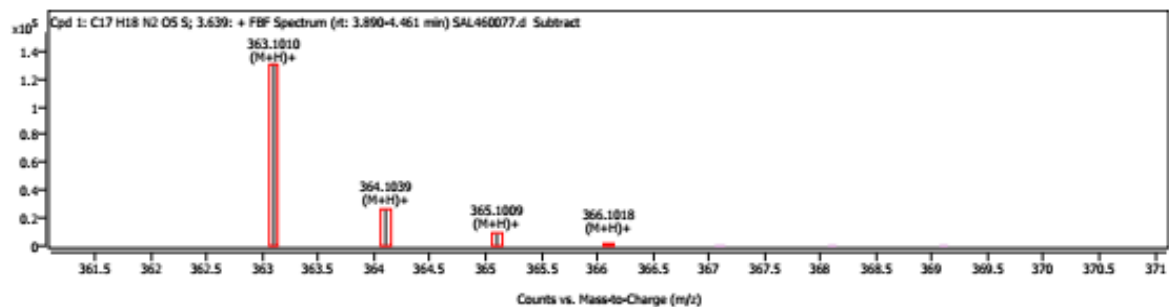


ThermoFisher
 SCIENTIFIC

Thu Jan 20 08:08:00 2022 (C
 BTU-18-Thu Feb 25 16:25:54 2021 (GMT+00:00)

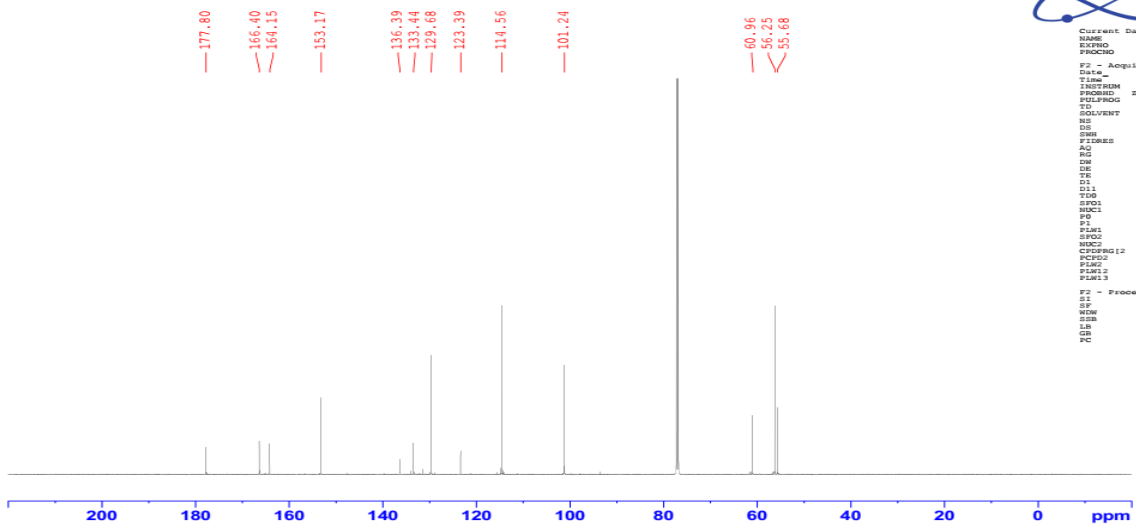


Compound Spectra



Spectrum Peaks							
m/z	m/z (Calc)	Diff (ppm)	Abund	Height %	Height % (Calc)	Ion Species	Z
363.1010	363.1009	0.31	131078	100.00	100.00	(M+H) ⁺	1
364.1039	364.1039	0.00	26431	20.16	20.32	(M+H) ⁺	1
365.1009	365.1006	1.00	9050	6.90	7.46	(M+H) ⁺	1
366.1018	366.1023	-1.37	1537	1.17	1.20	(M+H) ⁺	1

BB H1 Decoupled C13 NMR Spectrum of BTU-19 in CDCL3
 c13org CDC13 {C:\Bruker\TOPSPIN} SAS 19

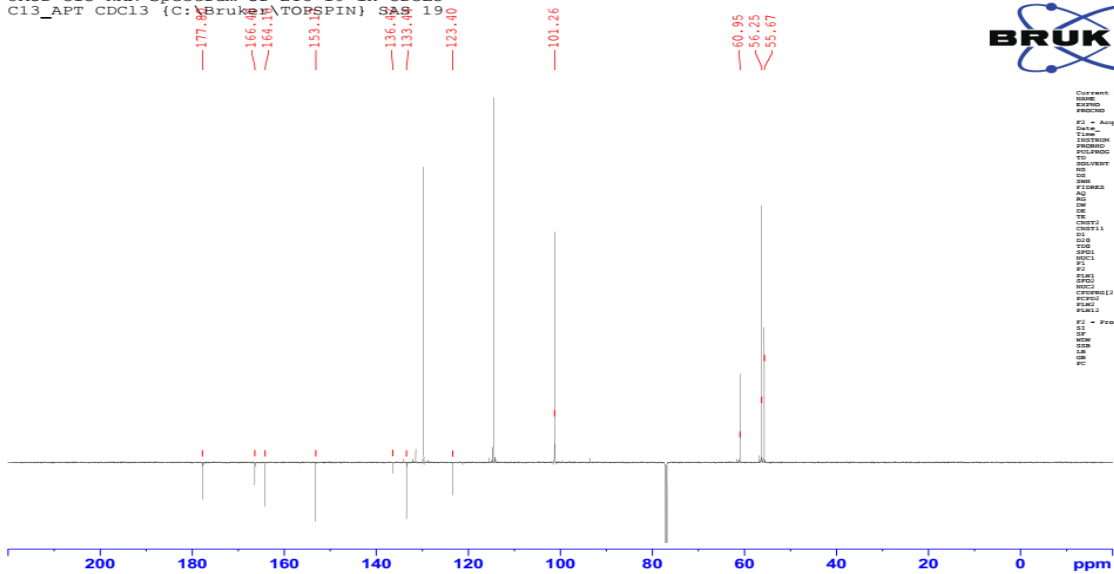


```
Current Data Parameters
NAME      SAC_BTU19
EXPNO     2
PROCNO    1

F2 - Acquisition Parameters
Date_     20100219
Time      7.32 h
INSTRUM   spect
PROBHD    Z114607_0986_0
PULPROG   zgpg30
TD         65536
SOLVENT   CDCl3
NS         1210
DS         4
SFS        36231.887 Hz
FIDRES     1.105709 Hz
AQ         0.3642368 sec
RG         2000
DM         13.800 usec
DE         8.50 usec
TE         298.2 K
D1         2.00000000 sec
d11        0.03000000 sec
SFO1       150.9179718 MHz
F0         150.9179718 MHz
NUC1       13C
NUC2       13C
P1         12.00 usec
PC1        82.95493610 M
SFO2       600.1724007 MHz
PCPD12     441.645
PCPD2      70.00 usec
PL12       24.5889917 M
PLM12     0.50164998 M
PLM13     0.75232001 M

F2 - Processing parameters
SI         32768
SF         150.9128662 MHz
WDW        EM
SSB        0
LB         1.40 Hz
GB         0
PC         1.40
```

JMOD C13 NMR Spectrum of BTU-19 in CDCL3
 C13_APT CDC13 {C:\Bruker\TOPSPIN} SAS 19

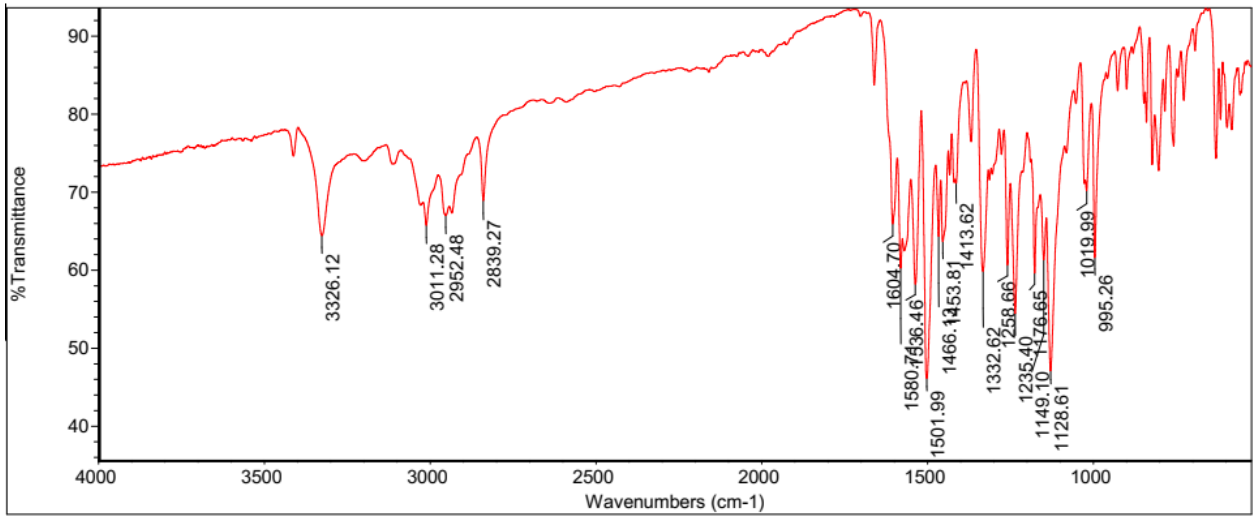


```
Current Data Parameters
NAME      SAC_BTU19
EXPNO     3
PROCNO    1

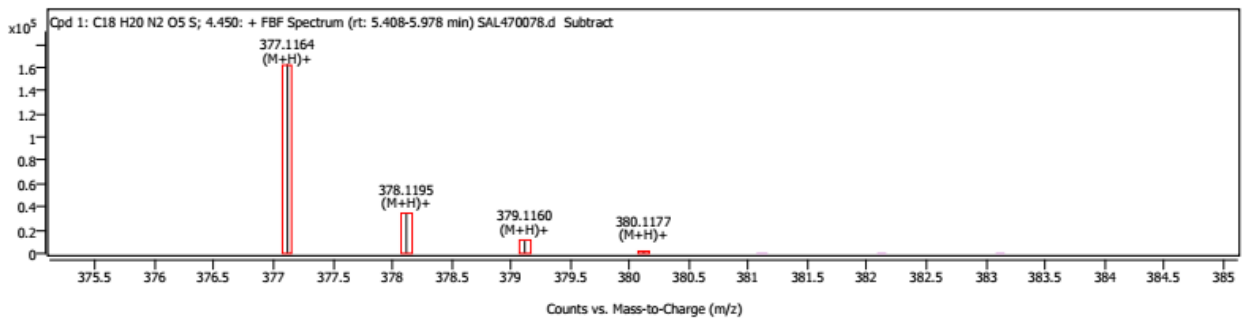
F2 - Acquisition Parameters
Date_     20100219
Time      21.11 h
INSTRUM   spect
PROBHD    Z114607_0986_1
PULPROG   zgpg30
TD         65536
SOLVENT   CDCl3
NS         8192
DS         4
SFS        36231.887 Hz
FIDRES     1.105709 Hz
AQ         0.3642368 sec
RG         2000
DM         13.800 usec
DE         8.50 usec
TE         298.2 K
D1         2.00000000 sec
d11        0.03000000 sec
SFO1       150.9179718 MHz
F0         150.9179718 MHz
NUC1       13C
NUC2       13C
P1         12.00 usec
PC1        82.95493610 M
SFO2       600.1724007 MHz
PCPD12     441.645
PCPD2      70.00 usec
PL12       24.5889917 M
PLM12     0.50164998 M

F2 - Processing parameters
SI         32768
SF         150.9128662 MHz
WDW        EM
SSB        0
LB         1.40 Hz
GB         0
PC         1.40
```

BTU-19-Thu Feb 25 16:53:05 2021 (GMT+00:00)



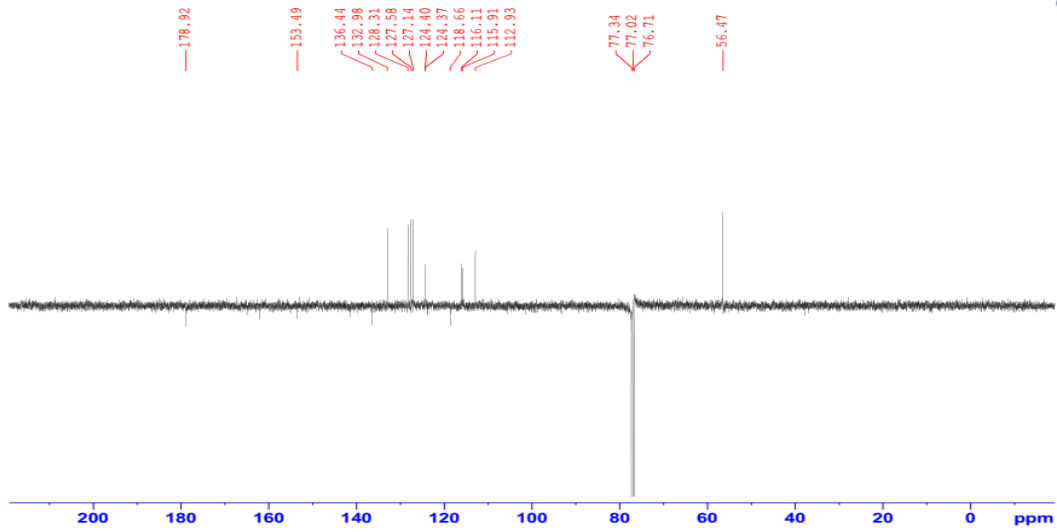
Compound Spectra



Spectrum Peaks

m/z	m/z (Calc)	Diff (ppm)	Abund	Height %	Height % (Calc)	Ion Species	Z
377.1164	377.1166	-0.42	162842	100.00	100.00	(M+H)+	1
378.1195	378.1196	-0.28	34267	21.04	21.42	(M+H)+	1
379.1160	379.1164	-1.08	10568	6.49	7.69	(M+H)+	1
380.1177	380.1181	-1.00	1873	1.15	1.28	(M+H)+	1

13 APT NMR Spectrum of BTU-21 IN CDCl3
 C13_APT CDCl3 (C:\Bruker\TOPSPIN) SAS 14



```

Current Data Parameters
NAME      SAS_BTU-21
EXPNO    1
PROCNO   1

F2 - Acquisition Parameters
Date_    20210203
Time     9.37
INSTRUM spect
PROBHD   5 mm BBO 5-1h
PULPROG  zgpg3
TD       65536
SOLVENT  CDCl3
NS       8500
DS       4
SWH      23980.814 Hz
FIDRES   9.30018 Hz
AQ       1.3664756 sec
RG       14384
DW       20.850 usec
DE       6.50 usec
TE       296.2 K
DICT2    145.000000
CONST11 1.0000000
ZG       2.0000000 sec
TD0      0.00689855 sec
RG0      1

===== CHANNEL F1 =====
NUC1      13C
P1        9.00 usec
PC        18.00 usec
PL1      100.622878 MHz
SFO1      400.1316005 MHz

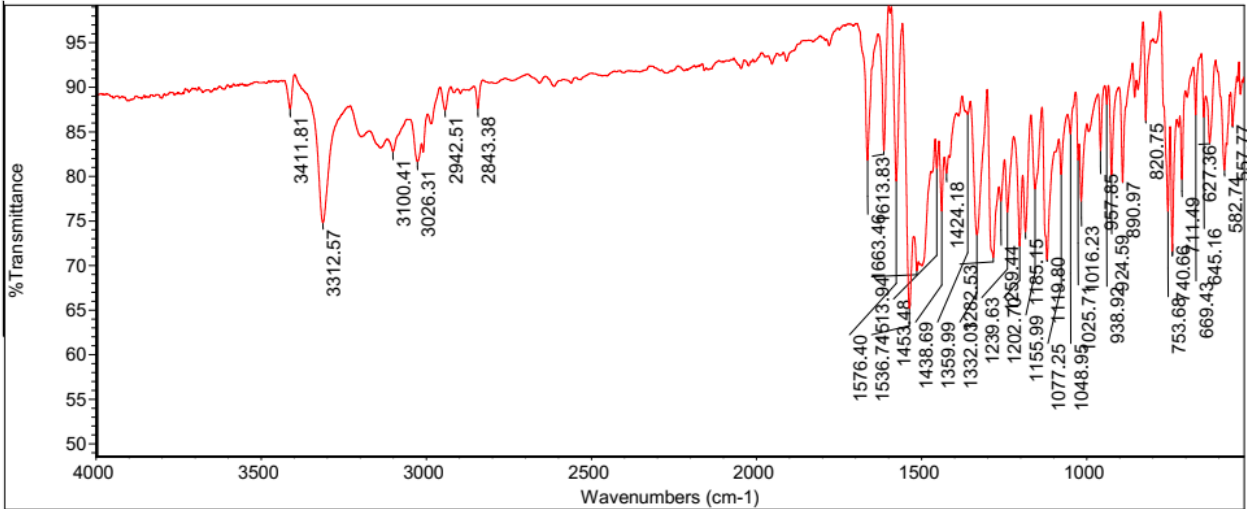
===== CHANNEL F2 =====
DROPT2    wait4
NUC2      13C
P2        9.00 usec
PC        18.00 usec
PL2      100.622878 MHz
SFO2      400.1316005 MHz

F2 - Processing parameters
SI        32768
SF        100.6127830 MHz
WDW       EM
SSB       0
LB        1.00 Hz
GB        0
PC        1.40
  
```

ThermoFisher
 SCIENTIFIC

Tue Dec 14 08:42:33 2021 (

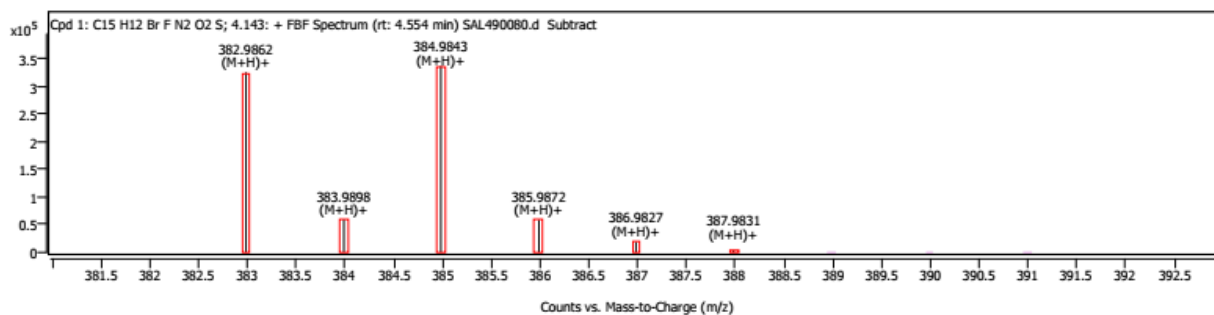
BTU-21-Thu Feb 25 16:49:30 2021 (GMT+00:00)



Spectrum Peaks

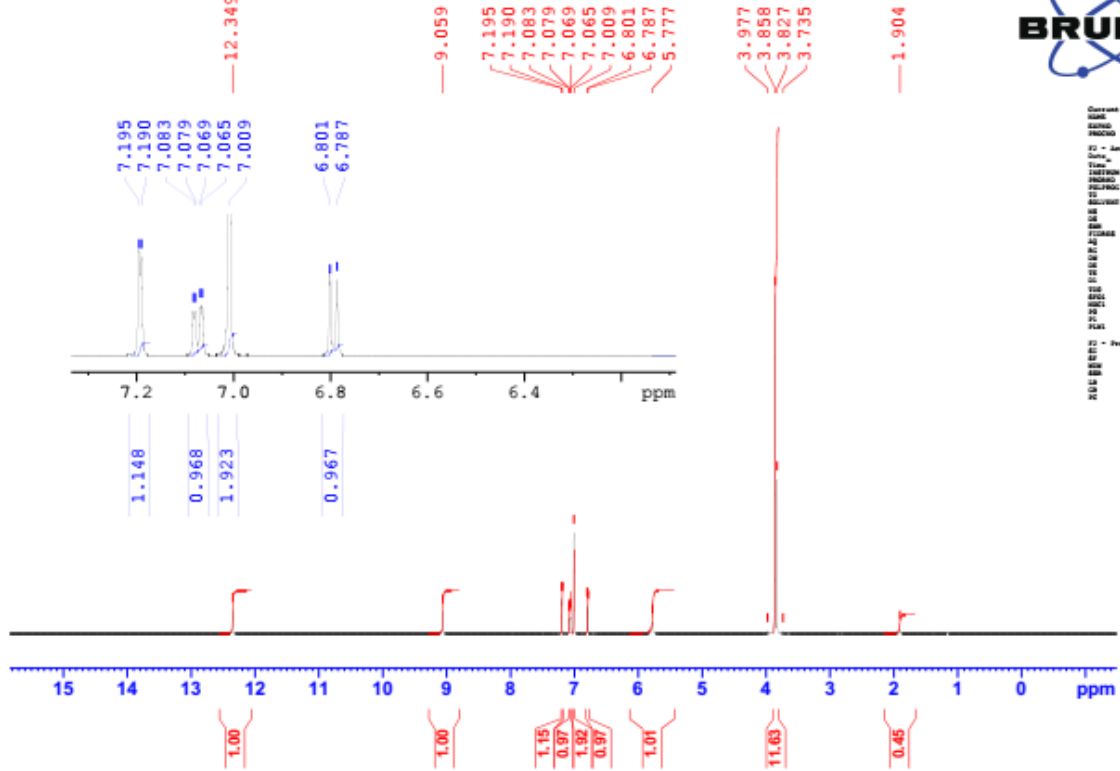
m/z	Z	Abund	Diff (ppm)	Height %	Height % (Calc)	Ion Species	Formula
382.9862	1	325577	0.53	96.66	96.45	(M+H) ⁺	C ₁₅ H ₁₂ BrFN ₂ O ₂ S
383.9898	1	59759	2.27	17.74	17.33	(M+H) ⁺	C ₁₅ H ₁₂ BrFN ₂ O ₂ S
384.9843	1	336822	0.90	100.00	100.00	(M+H) ⁺	C ₁₅ H ₁₂ BrFN ₂ O ₂ S
385.9872	1	58935	0.83	17.50	17.75	(M+H) ⁺	C ₁₅ H ₁₂ BrFN ₂ O ₂ S
386.9827	1	19025	0.01	5.65	6.11	(M+H) ⁺	C ₁₅ H ₁₂ BrFN ₂ O ₂ S
387.9831	1	3475	-3.36	1.03	0.87	(M+H) ⁺	C ₁₅ H ₁₂ BrFN ₂ O ₂ S

Compound Spectra



BTU-22

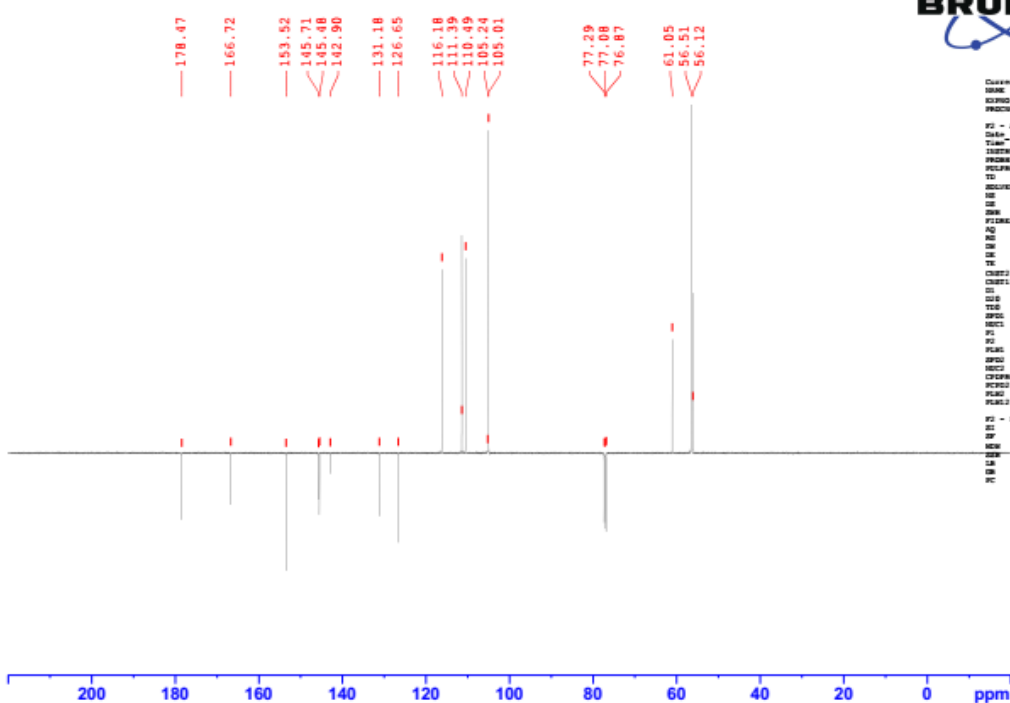
¹H NMR BTU-22 in CDCl₃
 PROTON64 CDC13 (C:\Bruker\TOPSPIN) AAM 11



```

Current Data Parameters
NAME      BTU22-001-AAM
PROCNO    1
F2 - Acquisition Parameters
Date_     20180111
Time      8.28 h
INSTRUM   spect
PROBHD    QNP5M_5MM_1H
PULPROG   zgpg30
TD         65536
SOLVENT   CDCl3
NS         41
DS         4
SWH        12019.200 Hz
FIDRES     0.266798 Hz
AQ         2.741976 sec
RG         382.2
WDW        EM
SSB         0
LB          11.41 Hz
GB          0
PC          0.6000000 sec
SFO        400.1476000 MHz
NUC1       13C
NUC2       1H
PC1         2.00 sec
PC2         0.05 sec
PC3         11.0000000 sec
F2 - Processing parameters
SI         32768
SF          400.1476000 MHz
WDW         EM
SSB          0
LB           0.10 Hz
GB           0
PC           1.00
  
```

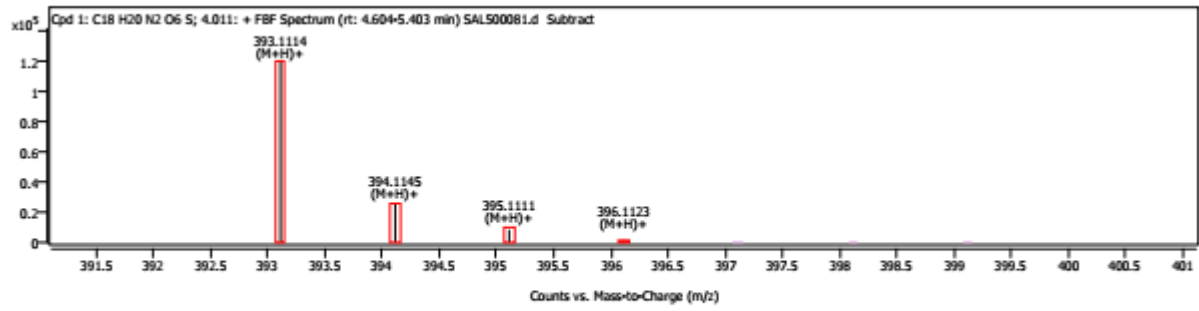
¹³C JMOD NMR BTU-22 in CDCl₃
 C13_APT CDC13 (C:\Bruker\TOPSPIN) AAM 11



```

Current Data Parameters
NAME      BTU22-001-AAM
PROCNO    1
F2 - Acquisition Parameters
Date_     20180111
Time      8.23 h
INSTRUM   spect
PROBHD    QNP5M_5MM_13C
PULPROG   zgpg30
TD         65536
SOLVENT   CDCl3
NS         41
DS         4
SWH        12019.200 Hz
FIDRES     1.289709 Hz
AQ         0.762398 sec
RG         382.2
WDW        EM
SSB         0
LB          11.41 Hz
GB          0
PC          0.6000000 sec
SFO        100.6261260 MHz
NUC1       13C
NUC2       1H
PC1         2.00 sec
PC2         0.05 sec
PC3         11.0000000 sec
F2 - Processing parameters
SI         32768
SF          100.6261260 MHz
WDW         EM
SSB          0
LB           1.00 Hz
GB           0
PC           1.00
  
```

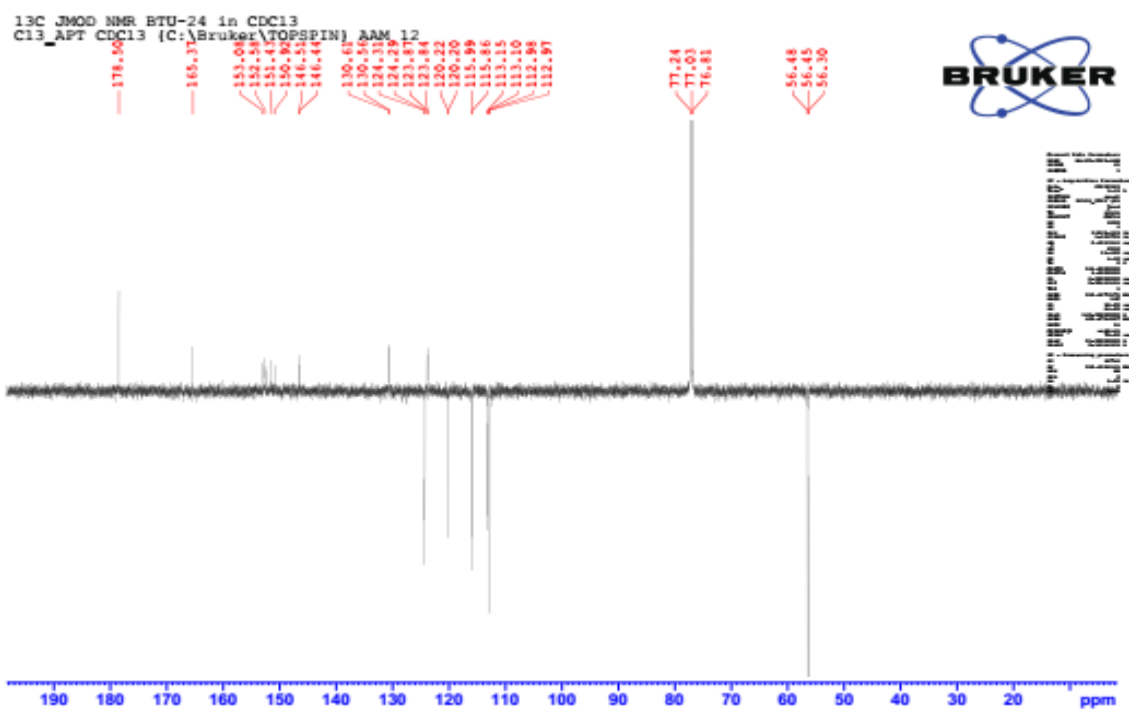
Compound Spectra



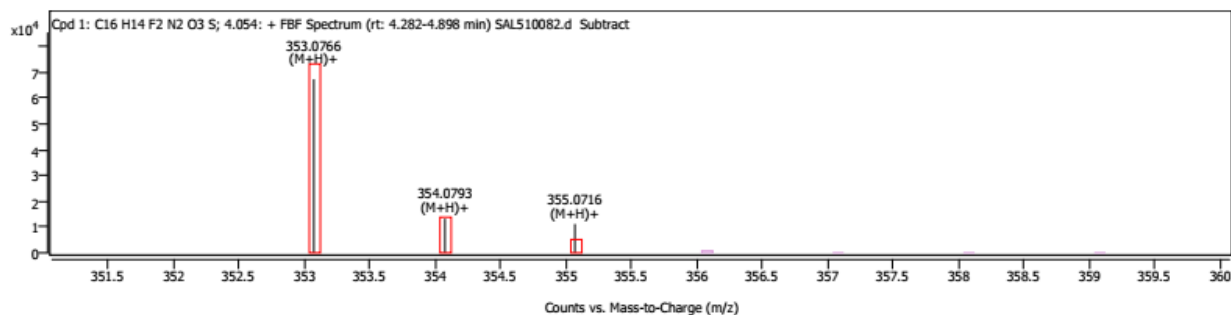
Spectrum Peaks

m/z	m/z (Calc)	Diff (ppm)	Abund	Height %	Height % (Calc)	Ion Species	Z
393.1114	393.1115	-0.14	120197	100.00	100.00	(M+H)+	1
394.1145	394.1145	-0.04	25810	21.47	21.46	(M+H)+	1
395.1111	395.1114	-0.93	8382	6.97	7.90	(M+H)+	1
396.1123	396.1132	-2.30	1425	1.19	1.33	(M+H)+	1

BTU-24



Compound Spectra



Spectrum Peaks

m/z	m/z (Calc)	Diff (ppm)	Abund	Height %	Height % (Calc)	Ion Species	Z
353.0766	353.0766	0.01	67316	100.00	100.00	(M+H)+	1
354.0793	354.0796	-0.73	13229	19.65	19.11	(M+H)+	1
355.0716	355.0757	-11.54	11247	16.71	6.82	(M+H)+	1